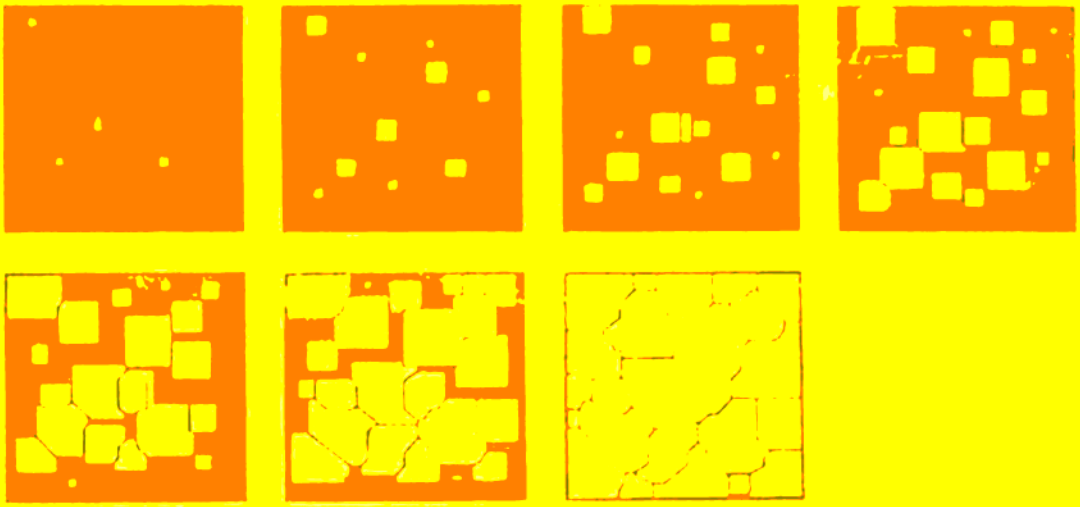

PHYSICAL METALLURGY

A. GULYAEV

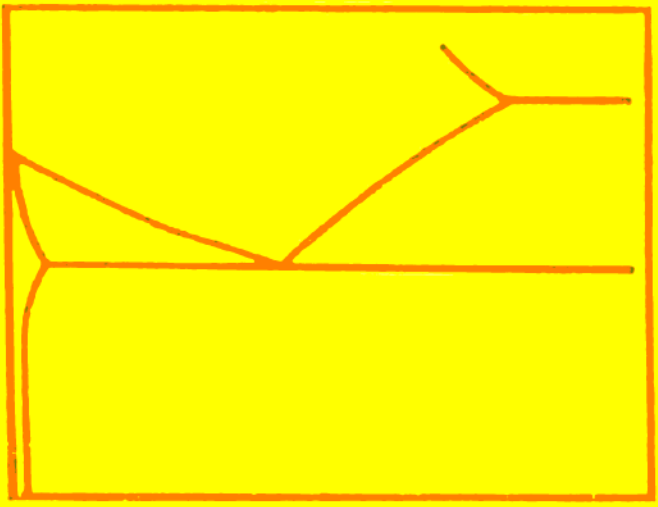

VOLUME 1

MIR PUBLISHERS MOSCOW

PHYSICAL METALLURGY

A. GULYAEV

VOLUME 1

ABOUT THE AUTHOR

Prof. A. P. Gulyaev, Dr. Sc. (Eng.), born in 1908, bears the title of Honoured Scientist of the Russian Federation. He is a prominent authority in physical metallurgy and science of metals and the author of numerous books and articles on the subject, including the present textbook **Physical Metallurgy**, which has run through five editions, and the monograph **Heat Treatment of Steel**.

PHYSICAL METALLURGY

А. П. ГУЛЯЕВ

МЕТАЛЛОВЕДЕНИЕ

Издательство «Металлургия» · Москва

PHYSICAL METALLURGY

A. GULYAEV

VOLUME I

Translated from the Russian
by V. Afanasyev

MIR PUBLISHERS · MOSCOW

First published 1980
Revised from the 1978 (5th) Russian edition

The Russian Alphabet and Transliteration

А а	a	К к	k	Х х	kh
Б б	b	Л л	l	Ц ц	ts
В в	v	М м	m	Ч ч	ch
Г г	g	Н н	n	Ш ш	sh
Д д	d	О о	o	Щ щ	shch
Е е	e	П п	p	ъ	″
Ё ё	e	Р р	r	ы	y
Ж ж	zh	С с	s	ь	′
З з	z	Т т	t	Э э	e
И и	i	У у	u	Ю ю	yu
Й й	y	Ф ф	f	Я я	ya

The Greek Alphabet

Α α	Alpha	Ι ι	Iota	Ρ ρ	Rho
Β β	Beta	Κ κ	Kappa	Σ σ	Sigma
Γ γ	Gamma	Λ λ	Lambda	Τ τ	Tau
Δ δ	Delta	Μ μ	Mu	Υ υ	Upsilon
Ε ε	Epsilon	Ν ν	Nu	Φ φ	Phi
Ζ ζ	Zeta	Ξ ξ	Xi	Χ χ	Chi
Η η	Eta	Ο ο	Omicron	Ψ ψ	Psi
Θ θ ϑ	Theta	Π π	Pi	Ω ω	Omega

На английском языке

© Издательство «Металлургия», 1978

© English translation, Mir Publishers, 1980

Contents

Preface 9

Part One

The Theory of Alloys

Chapter 1. The Crystal Structure of Metals 11

1-1. Metals 11
1-2. Classification of Metals 14
1-3. Crystal Structure of Metals 19
1-4. The Crystal Lattices of Metals 20
1-5. Real Structure of Metallic Crystals 26
1-6. Anisotropy of Properties of Crystals 32
1-7. Methods for Studying the Metal Structure 33
Literature 39

Chapter 2. Crystallization 40

2-1. Three States of Matter 40
2-2. Energy Conditions for Crystallization 41
2-3. The Mechanism of Crystallization 43
2-4. The Shape of Crystal Formations 47
2-5. The Structure of Ingot 49
2-6. Solid-state Transformations. Allotropy 51
2-7. Magnetic Transformations 55
Literature 56

Chapter 3. Mechanical Properties. Strain Hardening and Recrystallization 57

3-1. Metals and Non-metals 57
3-2. Elastic and Plastic Deformations. Lattice Imperfections and Strength of Metals 57
3-3. Fracture 66
3-4. Methods for Testing Mechanical Properties 73
3-5. Strain Hardening 79
3-6. Effect of Heating on the Structure and Properties of Deformed Metal (Recrystallization Processes) 81
Literature 91

Chapter 4. The Structure of Alloys 93

4-1. Mechanical Mixture 93
4-2. Chemical Compound 94

4-3. Solid Solution Based on a Component of an Alloy . . . 96
4-4. A Solid Solution Based on a Chemical Compound 100
4-5. Ordered Solid Solutions 101
4-6. Electronic Compounds (Hume-Rothery Phases) 102
4-7. Laves Phases 103
4-8. Interstitial Phases 103
Literature 104

Chapter 5. Constitutional Diagrams 105

5-1. Gibbs' Phase Rule 105
5-2. General Remarks on the Construction of Constitutional Diagrams 108
5-3. Experimental Construction of Constitutional Diagrams 110
5-4. The Constitutional Diagram of Systems Forming Mechanical Mixtures of Pure Constituents (First-order Systems) 114
5-5. The Lever Rule 117
5-6. The Constitutional Diagram of Systems with Unlimited Solubility of Constituents in the Solid State (Second-order Systems) 119
5-7. The Constitutional Diagram of Systems with Limited Solubility in the Solid State (Third-order Systems) 121
5-8. The Constitutional Diagram of Systems Forming Chemical Compounds (Fourth-order Systems) 126
5-9. The Constitutional Diagram of Systems Undergoing Polymorphous Transformations 130
5-10. Non-equilibrium Crystallization of Alloys 132
5-11. Three-component (Ternary) Systems 139
5-12. Simplified Methods for Analysis of Multi-component Systems 148
5-13. Correlation Between Properties of Alloys and Type of Constitutional Diagram 151
Literature 153

Part Two

Iron-carbon Alloys

Chapter 6. The Iron-carbon Constitutional Diagram 154

6-1. History 154
6-2. Iron 156
6-3. Cementite 160
6-4. The Constitutional Diagram 161
Literature 174

Chapter 7. Carbon Steels 175

7-1. Effect of Carbon 176
7-2. Effect of Permanent Impurities on Steel Properties . . . 178
7-3. Steels Produced by Various Processes. Clean Steel . . . 185
7-4. Plain Carbon Steels 189
7-5. Work-hardened Steel 193
7-6. Steel Sheets for Cold Forming 194
7-7. Machinability of Steels. Automatic Steels 194
Literature 197

Chapter 8. Cast Iron 198

8-1. Graphitization 198
8-2. The Structures of Cast Iron. Forms of Graphite 204

8-3. The Structure and Properties of Cast Iron . . . 207
8-4. Effect of Impurities 209
8-5. Effect of Cooling Rate 210
8-6. Grades of Grey and High-strength Cast Irons . 211
8-7. Malleable Cast Iron 213
Literature 216

Part Three

Heat Treatment

Chapter 9. General Principles of Heat Treatment 217

9-1. Temperature and Time 217
9-2. Classification of Types of Heat Treatment 219
9-3. Heat Treatment and the Constitutional Diagram . . . 221
9-4. Principal Types of Heat Treatment of Steel 223
9-5. Four Principal Transformations in Steel 225
Literature 227

Chapter 10. The Theory of Heat Treatment of Steel 228

10-1. Formation of Austenite 229
10-2. Coarsening of Austenitic Grain 230
10-3. Decomposition of Austenite 236
10-4. Martensitic Transformation 249
10-5. Bainitic Transformation 261
10-6. Transformations on Tempering 264
10-7. Effect of Heat Treatment on Steel Properties 268
10-8. Thermomechanical Treatment 273
Literature 276

Chapter 11. Practice of Heat Treatment of Steel 277

11-1. Hardening Temperature 277
11-2. Heating Time 279
11-3. Chemical Action of the Heating Medium 280
11-4. Quenching Media 282
11-5. Hardenability 284
11-6. Internal Stresses 291
11-7. Methods of Quenching 293
11-8. Sub-zero Treatment of Steel 296
11-9. Defects in Hardened Steel 296
11-10. Annealing and Normalizing 298
Literature 301

hapter 12. Surface Hardening of Steel 302

12-1. General 302
12-2. Induction Hardening 304
Literature 307

Chapter 13. Chemical Heat Treatment of Steel 308

13-1. The Theory of Chemical Heat Treatment 308
13-2. Carburizing 313
13-3. Nitriding 320
13-4. Cyaniding 325
13-5. Metallic Cementation 327
Literature 328

Index 329

Preface

The first edition of *Physical Metallurgy* was published as far back as in 1948, with some chapters being written by M.E. Blanter, S.M. Vinarov, Ya.B. Fridman, Yu.M. Lakhtin, S.Z. Bockstein, and E.F. Trusova. It was essentially a monograph rather than a textbook, though was based on the experience of teaching of science of metals at the Moscow Institute of Aviation Engineering.

An urgent need for a textbook on physical metallurgy impelled the Author to re-work the earlier edition into a textbook which was published in 1951. In the later editions (1956, 1963) much was done to make a book equally useful as a textbook for students studying physical metallurgy and as a monograph and reference book for metallurgical engineers and specialists in the field. It was also his aim to compile a textbook which could be a satisfactory and ample aid in many diverse courses on physical metallurgy, science of metals and heat treatment of metals as taught in various higher technical schools. For instance, the corresponding parts of the book can be used as textbooks on metallography (Parts I, II, and V), theory of heat treatment of metals (Part III) and alloy steels (Part IV) for students of machine-building, polytechnical and metallurgical specialities.

The Author has some evidence that his book is used much as a monograph and reference book by production and research engineers.

The later editions of the book have been revised and enlarged in accordance with the current progress in science and engineering, in particular, in physical metallurgy.

The material of the book is compiled and arranged in full accordance with the latest teaching programme on the science of materials approved by the USSR Ministry of higher and vocational education (1973).

During the long path from the first to the last edition, many prominent metallurgists (A. A. Bochvar, I. A. Oding, Ya.S. Umansky, S.M. Voronov, I.V. Kudryavtsev, Ya.B. Fridman, I.N. Boga-

chev, Yu.M. Lakhtin, I.I. Sidorin, S.V. Grachev) reviewed the manuscript and helped much by their valuable comments. The Author is sincerely thankful to them, as also to his co-workers and pupils who have participated in the preparation of the book.

Part One

THE THEORY OF ALLOYS

Chapter 1

THE CRYSTAL STRUCTURE OF METALS

1-1. METALS

Physical metallurgy is concerned with the physical and mechanical characteristics of metals and alloys and the relations between their composition, structure and properties.

Before going through the subject, we have to answer the principal question: what is the metal?

In chemistry, metals are understood as a particular group of elements which occupy the left-hand part of the Mendeleev Periodic Table (see Table 1-1). When reacting with non-metallic elements, these elements give up their outer (valence) electrons, because these electrons are only weakly bonded with the nucleus; further, the number of valence electrons in atoms of metals is small (only one or two), whereas non-metals have more outer electrons (5 to 8). All the elements located in the Periodic Table to the left of gallium, indium and thallium are metals and those to the right of arsenic, antimony and bismuth are non-metals.

The elements in groups IIIB, IVB and VB are either metals (In, Tl, Sn, Pb, Sb, Bi), or non-metals (C, N, P, As, O, S), or occupy an intermediate position (Ga, Si, Ge, Se, Te).

In engineering, metals are understood as substances possessing a characteristic 'metallic lustre' (all metals are more or less lustrous) and plasticity. In this respect, they are easily distinguishable from non-metals, such as, wood, stone, glass or porcelain.

"Metals are bright bodies which may be forged"—this definition given by Russian scientist M.V. Lomonosov more than 200 years ago still retains its scientific meaning. The above properties are found not only in pure elements, for instance, in aluminium, copper, iron, etc., but also in more complex substances composed of a few metallic elements and sometimes with an admixture of noticeable

Table 1-1. Mendeleev's Periodic

A

	I	II	III	IV	V	VI	VII	
1	1 H Hydrogen 1.008							
2	3 Li Lithium 6.940	4 Be Beryllium 9.013	5 B Boron 10.82					
3	11 Na Sodium 22.997	12 Mg Magnesium 24.32	13 Al Aluminium 26.97					
4	19 K Potassium 39.096	20 Ca Calcium 40.08	21 Sc Scandium 45.10	22 Ti Titanium 47.90	23 V Vanadium 50.95	24 Cr Chromium 52.01	25 Mn Manganese 54.93	26 Fe Iron 55.85
5	37 Rb Rubidium 85.48	38 Sr Strontium 87.63	39 Y Yttrium 88.92	40 Zr Zirconium 91.22	41 Nb Niobium 92.91	42 Mo Molybdenum 95.95	43 Tc Technecium 99	44 Ru Ruthenium 101.7
6	55 Cs Caesium 132.91	56 Ba Barium 137.36	57 La Lanthanum 138.92	72 Hf Hafnium 178.6	73 Ta Tantalum 180.88	74 W Tungsten 183.92	75 Re Rhenium 186.31	76 Os Osmium 190.2
	87 Fr Francium 223	88 Ra Radium 226.05	89 Ac Actinium 227	104 Ku Kurchatovium 264				

Lanthanides

58 Ce Cerium 140.13	59 Pr Praseodymium 140.92	60 Nd Neodymium 144.27	61 Pm Promethium 147	62 Sm Samarium 150.43	63 Eu Europium 152.0	64 Gd Gadolinium 156.9

Acti

90 Th Thorium 232.12	91 Pa Protactinium 231	92 U Uranium 238.07	93 Np Neptunium 237	94 Pu Plutonium 242	95 Am Americium 243	96 Cm Curium 245

Table of the Elements

B

VIII		I	II	III	IV	V	VI	VII	
									2 He Helium 4.003
					6 C Carbon 12.01	7 N Nitrogen 14.008	8 O Oxygen 16.000	9 F Fluorine 19.00	10 Ne Neon 20.183
					14 Si Silicon 28.06	15 P Phosphorus 30.98	16 S Sulphur 32.066	17 Cl Chlorine 35.457	18 Ar Argon 39.994
27 Co Cobalt 58.94	28 Ni Nickel 58.69	29 Cu Copper 63.54	30 Zn Zinc 65.38	31 Ga Gallium 69.72	32 Ge Germanium 72.60	33 As Arsenic 74.91	34 Se Selenium 78.96	35 Br Bromine 79.916	36 Kr Krypton 83.7
45 Rh Rhodium 102.91	46 Pd Palladium 106.7	47 Ag Argentum 107.88	48 Cd Cadmium 112.41	49 In Indium 114.78	50 Sn Tin 118.70	51 Sb Antimony 121.76	52 Te Tellurium 127.61	53 I Iodine 126.92	54 Xe Xenon 131.3
77 Ir Iridium 193.23	78 Pt Platinum 195.23	79 Au Gold 197.2	80 Hg Mercury 200.61	81 Tl Thallium 204.39	82 Pb Lead 207.21	83 Bi Bismuth 209.00	84 Po Polonium 210	85 At Astatine 211	86 Rn Radon 222

(rare earths)

65 Tb Terbium 159.2	66 Dy Dysprosium 162.46	67 Ho Holmium 164.94	68 Er Erbium 167.2	69 Tm Thulium 169.4	70 Yb Ytterbium 173.04	71 Lu Lutecium 174.99

noids

97 Bk Berkelium 249	98 Cf Californium 249	99 Es Einsteinium 253	100 Fm Fermium 255	101 Md Mendelevium 256	102 No Nobelium 253	103 Lr Lowrencium 256

quantities of non-metallic elements. Such substances are called *metallic alloys.* Therefore, metallic alloys can also be called metals in a broader sense.

Apart from metallic lustre and plasticity, all metals possess a high electric and thermal conductivity.

It may be concluded from the foregoing that there is a certain difference between the term 'metal' as a chemical element and 'metal' as a substance, but both definitions are due to the particularities of the internal structure of atoms of metallic substances, which is the same in pure metals and their alloys.

A particular feature of metallic substances is that they all are built up of such atoms whose outer electrons are only weakly bonded with the nucleus. This fact is responsible for the specific nature of chemical interaction between atoms of metals, as also for the specific 'metallic' properties of these substances. Electrons have a negative charge and it suffices to apply even the slightest potential difference to initiate motion of the electrons to the positive pole, i.e. to create electric current. This is why metals are good conductors of electric current, unlike most non-metals.

Typical of all metals is also their property to decrease electric conductivity with increasing temperature.

With chemical interaction between metals and non-metals. the outer electrons of metal atoms pass to the atoms of a non-metal. The metal atom that has given up its outer electron (or electrons) then becomes a positive ion and the non-metal atom that has got these electrons becomes a negative ion.

Thus, the weak bond of outer electrons in atoms is responsible for the specific chemical and physical properties of metals.

In view of the above specifics, the structure of the crystal lattice of metals and their alloys is principally as follows. Positive ions occupy particular places in the crystal lattice, while free outer electrons form in the metal a free-running fluid, as it were, or electronic gas, which moves at random in all directions. Under particular conditions, for instance, upon application of a potential difference, electrons begin to move in a definite direction thus creating electric current.

The theory of metallic structure regards a metal as a substance consisting of positive ions surrounded by negatively charged particles—electrons which are only weakly bonded with the nucleus. These electrons move continuously in the metal and belong to the whole combination of the atoms, rather than to a single atom.

Thus, a particular feature of the crystal structure of metals is the presence of *electronic gas* which is weakly bonded with positive ions. Since electrons in metal are easily movable and are weakly bonded with the atoms, metals possess typical metallic properties (high electric and thermal conductivities, metallic lustre, plasticity).

1-2. CLASSIFICATION OF METALS [1]

Though each metal differs from all other metals in its structure and properties, metals can be classed into groups according to their particular features (Table 1-2).

[1] The proposed classification differs from the common one, according to which iron and iron alloys are classed as ferrous metals and all other metals are regarded non-ferrous.

Table 1-2

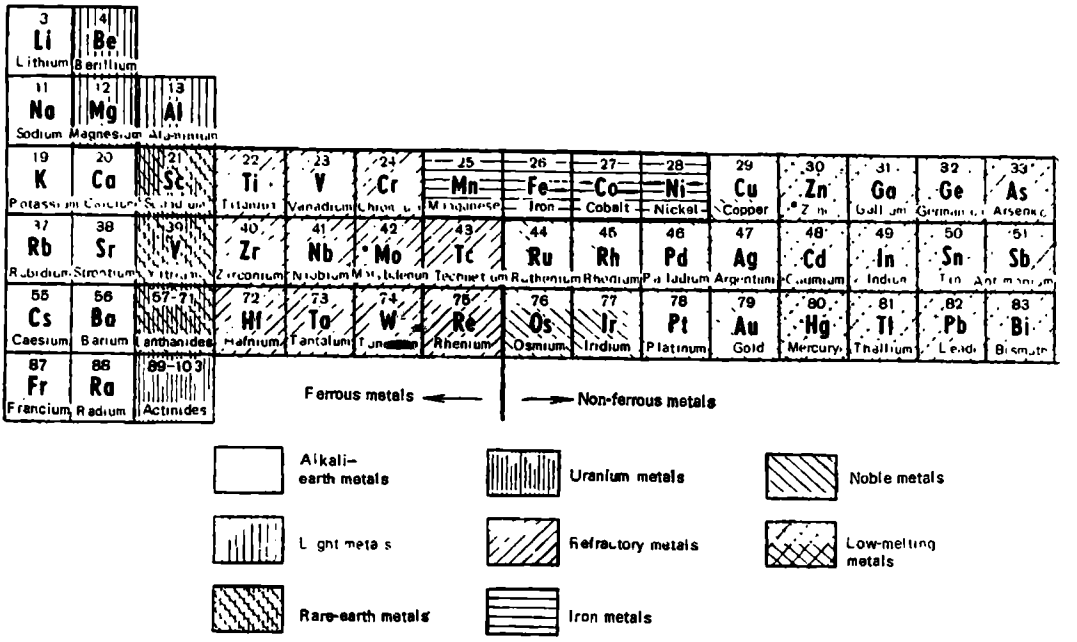

To begin with, all metals can be divided into two large groups, i.e. ferrous and non-ferrous metals.

Ferrous metals are dark-grey in colour, have a high density (except for alkali-earth metals), a high melting point, relatively high hardness, and many of them are polymorphous (see Sec. 2-6, on polymorphism). The most typical metal in this group is iron.

Non-ferrous metals most often have a characteristic colour: red, yellow or white. They have a high plasticity, low hardness, relatively low melting point. They show no polymorphism. The most typical metal in this group is copper.

Ferrous metals can be subdivided as follows:

1. *Iron metals*: iron, cobalt, nickel (called ferromagnets), and also manganese which approaches them in its properties. Cobalt, nickel and manganese are often used as additions in iron alloys and also as the base in certain alloys which are similar to high-alloy steels in their properties.

2. *Refractory*, or *high-melting, metals*, i.e. those whose melting point is higher than that of iron (1539°C). They are used as additions in alloy steels and as the base of some special alloys.

3. *Uranium metals*, or actinides, are used predominantly in alloys for nuclear engineering.

4. *Rare-earth metals*; these include lanthanides, i.e. lanthanum, cerium, neodymium, praseodymium, etc., and also yttrium and scandium whose properties are close to those of lanthanides. These metals possess very similar chemical properties, but differ appre-

Table 1-3. Dates of Discovery and First

Li 1817	Be 1798 1920						
Na 1807	Mg 1755 1920	Al 1827 1895					
K 1807 1955	Ca 1808	Sc 1879	Ti 1789 1945 1930 Fe	V 1830 1950 1905 Fe	Cr 1797 1920 1900 Fe	Mn 1774 1930 1856 Fe	Fe 3rd millenium B. C.
Rb 1861 1955	Sr 1790	Y 1794	Zr 1709 1950 1935 Fe	Nb 1801 1950 1940 Fe	Mo 1782 1910 1910 Fe	Tc 1937	Ru 1844 1900
Cs 1860	Ba 1808	La 1839	Hf 1922 1950	Ta 1802 1940 1920 Fe	W 1783 1910 1900 Fe	Re 1925 1960	Os 1808 1900

ciably in physical properties (melting point, etc.). They are used as additions to alloys of other elements. In nature, these metals occur conjointly and can be separated only with great difficulties; for that reason they are usually added as *misch metal*, i.e. an alloy of 40-45 per cent Ce and 45-50 per cent of other rare-earth elements. Other mixed alloys of rare-earth metals are also known, for instance, *ferrocerium* (an alloy of cerium and iron with noticeable amounts of other rare-earth elements), or *dydimium* (a mixture of neodymium and praseodymium).

5. *Alkali-earth metals* are not employed in free metallic state, except for certain applications as heat carriers in nuclear reactors.

Non-ferrous metals are subdivided into:

1. *Light metals*, i.e. those of a low density; these include beryllium, magnesium, and aluminium.

2. *Noble metals*: silver, gold, platinum-group metals (platinum, palladium, iridium, rhodium, osmium, ruthenium). 'Seminoble' copper can also be related to this group. Metals of this group possess a high corrosion resistance.

3. *Fusible*, or *low-melting-point, metals*: zinc, cadmium, mercury, tin, lead, bismuth, thallium, antimony, and two elements of reduced metallic properties (gallium and germanium).

Application of Various Metals

Co 1735 1910 1910 Fe	Ni 1751 1880 1880 Fe	Cu 6th millenium B.C.	Zn Middle ages	Ga 1875	Ge 1886 1950	As Middle ages
Rh 1803 1890	Pd 1803 1880	Ag 4th millenium B.C.	Cd 1817 1910	In 1863 1940	Sn 4th millenium B.C.	Sb Middle ages
Ir 1803 1890	Pt 1735 1825	Au 1 mln years B.C.	Hg Middle ages	Tl 1861	Pb 5th millenium B.C.	Bi Middle ages

Table 1-4. World Production of Metals, thous. tons

Metal	1850	1900	1929	1964
Iron	4 000	40 000	120 000	437 000
Manganese	0	200	3 500	10 000
Aluminium	0	7	1 000	6 100
Copper	52	560	2 000	5 760
Zinc	80	550	1 450	3 850
Tin	100	850	1 800	3 050
Nickel	0	2	56	400
Magnesium	0	0	2	150
Tungsten	0	0	10	60
Molybdenum	0	0	2	45
Titanium	0	0	0	30
Antimony	10	20	30	60
Cadmium	0	0	0	15
Vanadium	0	0	1	10
Niobium	0	0	0	4
Tantalum	0	0	0	1
Gold	0.4	0.6	0.9	1.2

The applications of a metal are determined by its occurrence in nature and, in the historical aspect, by engineering progress.

Table 1-3, which reproduces the 'metallic' part of the Periodic Table, gives the symbol of an element, the date of its discovery (separation in a more or less pure form in laboratory), and the date of industrial application (for some elements, two dates are given: that of the application in pure form and that in the form of a ferroalloy).

The first metals used by Man were copper, silver and gold. Then followed the metals which can be relatively easily reduced from ores (tin, lead) or occur quite widely in nature (iron).

The majority of metals were discovered in the XIX century, though not all of them found industrial application at that time.

Table 1-4 contains data on the production of various metals in the world. As may be seen, the main portion in the world production of metals falls on iron (in the form of its alloy with carbon—steel). This may be explained by a number of reasons: low cost, high mechanical properties, good possibilities for mass production, and wide occurrence of iron ores in nature.

Steel is produced in larger quantities than all other metals. For instance, of about 600 mln tons of the total production of metals in the world in 1970, over

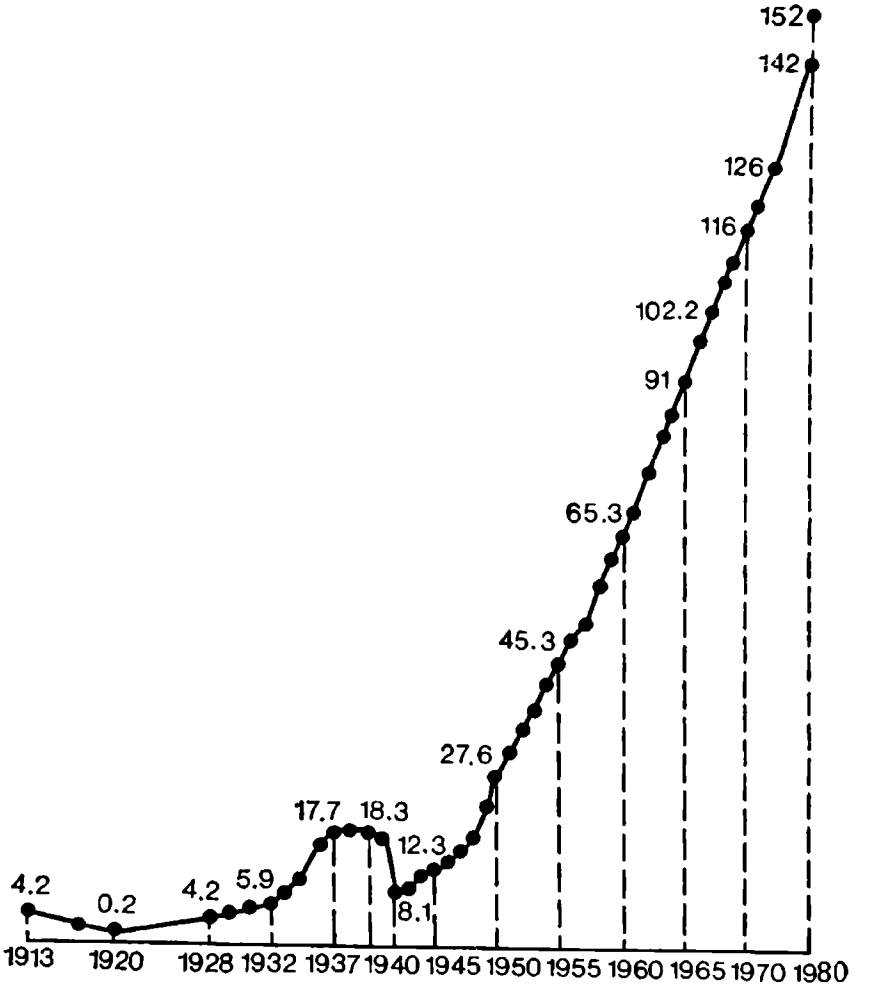

Fig. 1-1. Production of steel in the USSR (mln tons)

550 mln tons were steel (more than 90 per cent), while the production of all other metals was less than 50 mln tons (less than 10 per cent). Fig. 1-1 illustrates the growth of steel production in the USSR.

Steel production is an important index of economic and engineering power of a country. The progress in all branches of industry would be impossible if there were no ample supply of steel.

The cost of a metal is an important factor which determines the possibilities and feasibilities of application of that metal.

1-3. CRYSTAL STRUCTURE OF METALS

Any substance can be in one of the three states of aggregation: solid, liquid, or gaseous[1]. Under the action of gravity, solids retain their shape, while liquids spread over and take the shape of the vessel which they fill. This definition is, however, insufficient to characterize the state of a substance.

For instance, solid glass softens on heating and gradually passes into the liquid state. The reverse transformation also occurs gradually, i.e. liquid glass becomes thicker with decreasing temperature and finally thickens into the solid state. There is no definite temperature ('point') at which glass passes from liquid to solid state and abruptly changes its properties. It is therefore appropriate to regard 'solid' glass as a strongly thickened liquid.

Consequently, the change from solid to liquid state or vice versa (as also from gaseous to liquid state) occurs at a definite temperature and causes an abrupt change in the properties of a substance.

What is then the difference between the gaseous, liquid, and solid states?

In gases, there is no ordered position of particles (atoms and molecules); these particles move chaotically, collide and repulse, and the gas tends to spread over the whole volume available.

In solids, there is a regular order of the position of atoms, the forces of mutual attraction and repulsion are balanced out, and a solid body retains its shape.

In liquids, their particles (atoms and molecules) retain only what is called the *short-range order*, i.e. only a small number of atoms are positioned regularly in the space, but not the atoms in the whole volume, as is the case with solids. The short-range order is unstable; it can appear and disappear under the action of thermal fluctuations.

[1] At very high temperatures (tens of thousands of degrees), gaseous substances pass over to the state of plasma which is characterized by the development of ionization processes up to the complete destruction of electron shells of atoms. It would be incorrect, however, to regard plasma as the fourth state of the matter, though this erroneous standpoint is quite persistent in the scientific literature. If it were so, the change of a substance to the plasma state would proceed to the end at constant (equilibrium) temperature and pressure, according to the phase rule (see Sec. 5-1) for single-component systems. Actually, nothing of the kind is observed experimentally.

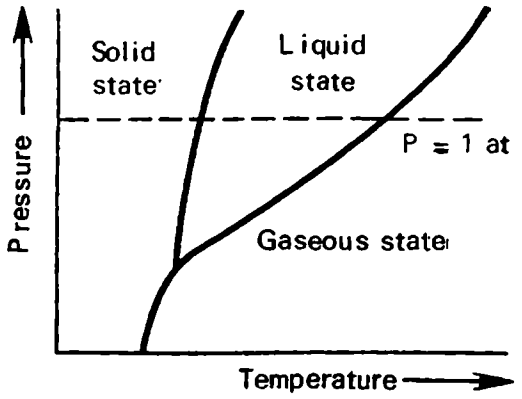

Fig. 1-2. Regions of solid, liquid, and gaseous states, depending on temperature and pressure

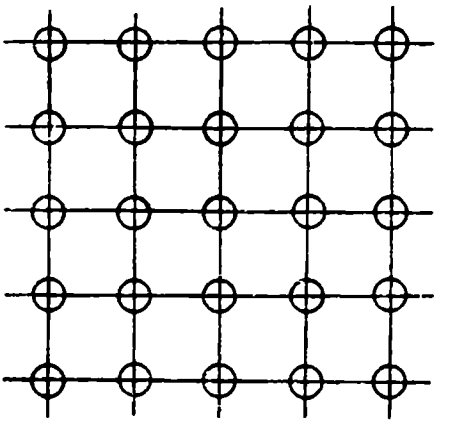

Fig. 1-3. An elementary crystal cell (simple cubic)

Thus, the liquid state is an intermediate one, as it were, between the solid and gaseous states. Under appropriate conditions, some substances can pass over directly from the solid to gaseous state without melting; the phenomenon is called *sublimation* (Fig. 1-2).

An ordered, regular position of particles (atoms, molecules) in space is also characteristic of the *crystalline state* of a substance.

The hypothesis that crystals have an ordered (regular) position of particles (atoms) was suggested very long ago (by E. S. Fedorov in 1860), but has been verified experimentally only after X-rays were discovered (K. von Roentgen, 1895) and applied for study of crystal structures (M. von Laue, 1912). Numerous experiments carried out after that time in many countries have discovered regular arrangement of atoms in crystals of various substances, including metals and alloys.

The crystalline structure of a substance may be imagined as a space lattice with atoms positioned at the sites[1] (Fig. 1-3).

In the next section we shall consider the arrangements of atoms (ions) that are typical of metals, i.e. the types of crystal lattice found in metals.

1-4. THE CRYSTAL LATTICES OF METALS

As has been mentioned, *the crystalline state is characterized primarily by an ordered regular arrangement of atoms in space.* This implies that each atom in a crystal has the same number of nearest atoms—

[1] In metals, the sites of the crystal lattice are occupied by positive ions, rather than by atoms, with free electrons moving in between; it is usually said, however, that the sites of the crystal lattice of metals are occupied by atoms.

neighbours, spaced the same distance apart from the atom considered.

The tendency of atoms (ions) in metal to occupy positions as close as possible to one another, i.e. to arrange themselves as dense as possible[1] results in that there are only a few possible combinations of mutual arrangement of atoms in crystals of metals.

There exist a number of schemes and methods for description of mutual arrangement, or packing, of atoms in crystals. The mutual arrangement of atoms in one of the crystal planes is shown in Fig. 1-3. The imaginary lines drawn through the centres of atoms form a lattice with atoms (positive ions) located in the lattice sites; this is what is called a *crystal plane*. Multiple reproduction of parallel crystal planes forms a *space crystal lattice* whose sites are locations of atoms (ions). The distances between the centres of neighbouring atoms are measured in *angstroms* (1 Å $= 1 \cdot 10^{-8}$ cm) or in *X-units* (1 kX-unit = 1.00202 Å).

Mutual arrangement of atoms in space and interatomic distances are determined by X-ray structural analysis.

The positions of atoms in a crystal can be very conveniently depicted in the form of space arrangements which are called *elementary crystal cells*. An elementary crystal cell is understood as the least combination of atoms which, upon multiple reproduction in space, gives a space crystal lattice.

The simplest type of crystal cell is the *cubic lattice*. In a simple cubic lattice, atoms are arranged (packed) not quite densely.

Atoms tend to occupy positions as close as possible to one another and thus form other types of crystal lattice: *body-centred cubic* (b.c.c., Fig. 1-4*a*), *face-centred cubic* (f.c.c., Fig. 1-4*b*) and *close-packed hexagonal* (c.p.h., Fig. 1-4*c*).

The circles which depict atoms can be located in the centre and at the corners of a cube (body-centred cube), in the centres of cube faces and at the corners (face-centred cube), or in the form of a hexahedron with another hexahedron being half-inserted into it, with the three atoms of the upper plane of the latter hexahedron being inside the hexahedral prism (hexagonal lattice).

The method of depicting the crystal lattice as shown in Fig. 1-4 is only conditional (as any other possible method). It might be more appropriate to depict the atoms of crystal lattices as contacting spheres (as in the left-hand pictures in Fig. 1-4), but this method is often less convenient than the traditional one (right-hand pictures in Fig. 1-4).

The dimensions of crystal lattices are characterized by the lattice *parameters*, or *periods*. A cubic lattice is determined by a single parameter—the length of cube edge *a* (see Fig. 1-4*a*, *b*). The lattice

[1] This is why metals have a higher density than non-metals.

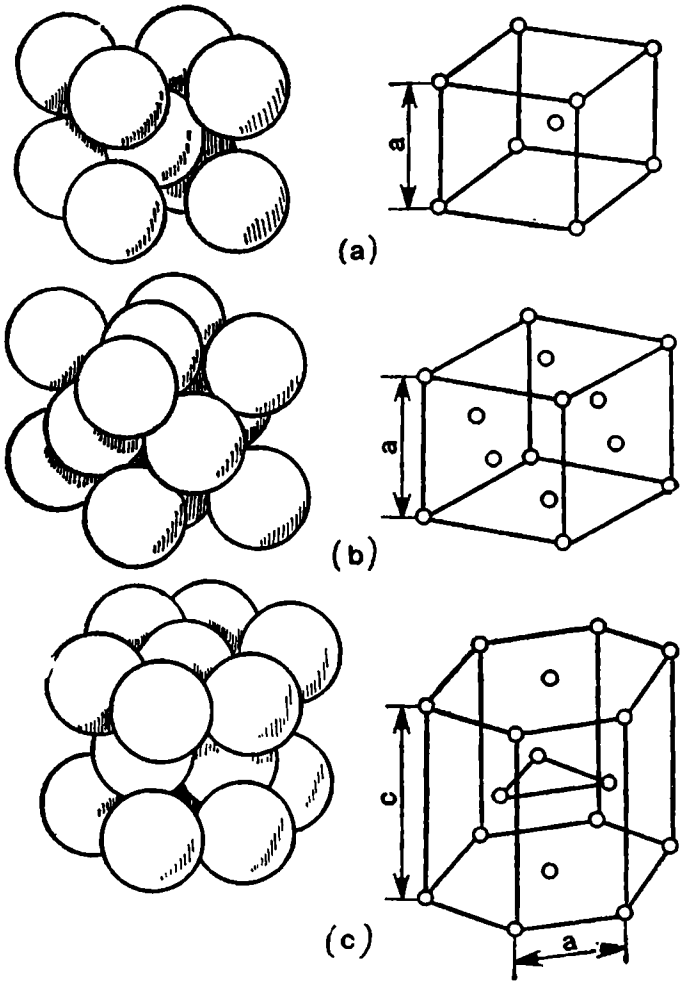

Fig. 1-4. Elementary crystal cells
(*a*) body-centred cubic; (*b*) face-centred cubic; (c) close-packed hexagonal

parameters have magnitudes of an order of the size of atoms and are measured in angstroms.

For instance, the lattice parameter of chromium, which has a body-centred cubic lattice, is 2.878 Å and that of aluminium, which has the structure of face-centred cube, is 4.041 Å.

The lattice parameter is an important characteristic. Modern methods of X-ray analysis enable us to measure the lattice parameters to an accuracy of the fourth or even fifth decimal sign, i.e. one-ten-thousandth or one-hundred-thousandth of angstrom.

Considering the arrangement of crystal lattices (see Fig. 1-4) and assuming that atoms are elastic spheres which touch one another, it may be concluded that there exist simple geometrical relationships between the lattice parameter a and the atomic diameter d.

For a body-centred cube

$$d = a\frac{\sqrt{3}}{2}$$

for a face-centred cube

$$d = a\frac{\sqrt{2}}{3}$$

Assuming that atoms are spheres, it may be calculated that atoms occupy 68 per cent of the volume in a body-centred cubic lattice and 74 per cent, in face-centred cubic and close-packed hexagonal lattices, i.e. atoms in the latter case are packed more closely.

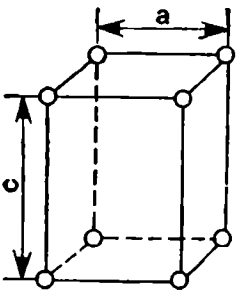

Fig. 1-5. A tetragonal lattice

The hexagonal lattice is typical of many metals (see Fig. 1-4*c*).

If the layers of atoms touch one another, i.e. the three atoms inside the lattice (see Fig. 1-4*c*) touch the atoms on the upper and lower planes, the structure is called the *close-packed hexagonal lattice*.

The dimensions of a close-packed hexagonal lattice are characterized by a constant ratio $c/a = 1.633$. With other values of the c/a ratio the hexagonal lattice is not closely packed.

The face-centred cubic lattice and hexagonal lattice represent the most dense method of packing of spheres of the same diameter.

Some metals exhibit the *tetragonal lattice* (Fig. 1-5), which is characterized by that the edge c is not equal to edge a. The ratio of these parameters characterizes what is called the tetragonality of a lattice. With $c/a = 1$, we have a cubic lattice. A tetragonal lattice (like a cubic lattice) may be simple, body-centred or face-centred, depending on the space arrangement of atoms.

The properties of a particular metal or alloy depend appreciably on the number of 'touching' atoms in the crystal structure. This is determined by the number of nearest equidistant atoms for any atom.

The number of atoms which are at the nearest and equal distance from a given atom is called the *coordination number*. For instance, an atom in a simple cubic lattice has six nearest equidistant neighbours, i.e. the coordination number of the lattice is equal to six.

The central atom in a body-centred lattice has eight nearest equidistant neighbours, i.e. the coordination number is eight. For a face-centred lattice, the coordination number is 12. In a close-packed hexagonal lattice, the coordination number is 12. If $c/a \neq 1.633$, each atom has six atoms at one distance and six at another (the coordination number is 6).

Crystal lattices and coordination numbers are symbolized as follows:

Type of lattice	Abbreviated symbol	Coordination number
Simple cubic	c	C6
Body-centred cubic	b.c.c.	C8
Face-centred cubic	f.c.c.	C12
Close-packed hexagonal* .	c.p.h.	H12
Hexagonal**	h	H6

* $c/a = 1.633$

** $c/a \neq 1.633$

Each metal has a definite crystal lattice[1]. Data on crystal lattices of metallic elements are given in Table 1-5.

Table 1-5. Crystal Lattices of Metallic Elements

3 Li C8	4 Be H12												
11 Na C8	12 Mg H12	13 Al C12											
19 K C8	20 Ca C12 (H12)	21 Sc	22 Ti H12 C8	23 V C8	24 Cr C8	25 Mn	26 Fe C8 C12	27 Co H12 C12	28 Ni C12	29 Cu C12	30 Zn H6	31 Ga tetra- gonal	32 Ge diamond- type
37 Rd C8	38 Sr C12	39 Y H12	40 Zr H12 C8	41 Nb C8	42 Mo C8	43 Tc	44 Ru H12	45 Rh C12	46 Pd C12	47 Ag C12	48 Cd H12	49 In tetra- gonal	50 Sn diamond- type, tetrago- nal
55 Cs C8	56 Ba C8	57-71 rare- earth ele- ments C12 H12	72 Hf H12	73 Ta C8	74 W C8	75 Re H12	76 Os H12	77 Ir H12	78 Pt C12	79 Au C12	80 Hg H6	81 Tl H12, C12	82 Pb C12

Note: Modifications of manganese have complicated crystal lattices.

[1] Some metals exhibit the phenomenon of polymorphism (see later in the book), i.e. undergo transformations at changes in external conditions so that their crystal lattice changes from one type to another.

An essential characteristic of the crystal structure is the number of atoms per elementary cell.

In a b.c.c. lattice, atoms at the cube corner belong to eight unit cells. Therefore, each atom contributes with only one-eighth of its volume to the unit cell. The central atom belongs fully to the given unit cell. Consequently, the number of atoms per unit cell is $1/8 \times 8 + 1 = 2$.

In a face-centred cube, the number of atoms per unit cell is four ($1/8 \times 8 =$ = 1 atom of the number of atoms arranged at the cube corners $+1/2 \times 6 =$ = 3 atoms of the number of atoms at the centres of faces).

Typically, metallic elements, which occupy the left-hand part of the Periodic Table, crystallize into a dense packing, i.e. form simple crystal lattices of a large coordination number. As has been indicated, b.c.c., f.c.c. and c.p.h. lattices are typically metallic. Indeed, almost all metals, beginning with zinc, cadmium and mercury, and further to the left (as may be seen in Table 1-5) in most cases have simple lattices.

Non-metallic elements in the right-hand part of the Periodic Table are characterized by a low coordination number (C4 or even less). Non-metals have a lower density than metals.

The atomic radius of an element, which is determined as the spacing between the nearest atoms, is a periodic property of a substance, as may be seen from Table 1-6.

Table 1-6. Atomic Radii of Metallic Elements, angstrom (for coordination number of 12) (according to G. B. Boky)

3 Li 1.57	4 Be 1.13											
11 Na 1.92	12 Mg 1.60	13 Al 1.43										
19 K 2.36	20 Ca 1.97	21 Sc 1.65	22 Ti 1.45	23 V 1.36	24 Cr 1.28	25 Mn 1.31	26 Fe 1.27	27 Co 1.26	28 Ni 1.24	29 Cu 1.28	30 Zn 1.37	31 Ga 1.39
37 Rb 2.53	38 Sr 2.16	39 Y 1.81	40 Zr 1.60	41 Nb 1.47	42 Mo 1.40	43 Tc 1.34	44 Ru 1.32	45 Rh 1.34	46 Pd 1.37	47 Ag 1.44	48 Cd 1.52	49 In 1.52
55 Cs 2.74	56 Ba 2.25	57-71 La 1.88	72 Hf 1.59	73 Ta 1.46	74 W 1.41	75 Re 1.37	76 Os 1.34	77 Ir 1.35	78 Pt 1.38	79 Au 1.44	80 Hg 1.55	81 Tl 1.71

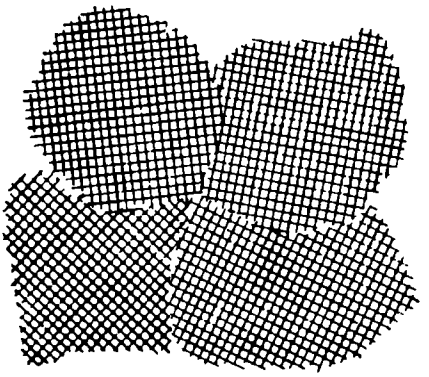

Fig. 1-6. A diagram to illustrate different orientation of crystal lattices in a polycrystalline body

1-5. REAL STRUCTURE OF METALLIC CRYSTALS

Crystals of metals are usually small in size, so that a metallic article consists of a very large number of crystals.

Such a structure is called polycrystalline. For some reasons, which will be discussed in Ch. 2, individual crystals in a polycrystalline aggregate cannot have a regular shape. Such crystals of irregular shape are called *grains*, or *crystallites*.

Individual grains in a metal have different orientation of their crystal lattices (Fig. 1-6). In the general case, crystal lattices of grains are oriented at random, with any orientation in space being equally probable.

Things, however, may be different in some particular cases. Plastic deformation of cold metal (rolling, drawing, etc.) results in that the metal grains are mainly oriented in a particular direction (a *texture* is formed). The degree of primary orientation may be different, with random orientation being at one extreme and the same orientation of all the crystals, at the other.

If a metal is cooled very slowly during solidification, it can solidify into a *single crystal*, or *monocrystal*. There are special methods to grow single crystals. Single crystals of large size (a few hundred grams) are made for scientific studies and are also used in some branches of engineering (semiconductors).

Research has shown that the internal crystalline structure of metal grains is far from being regular.

The nature and degree of irregularities or imperfections in the crystal structure determine to a large extent the properties of a me-

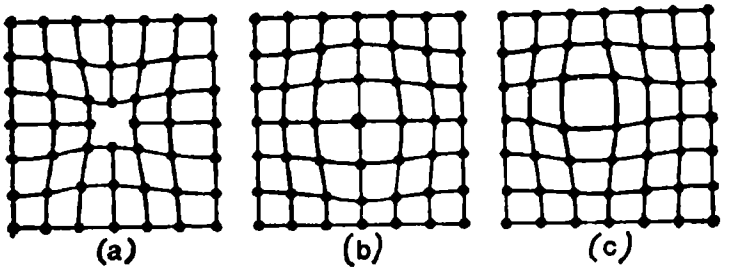

Fig. 1-7. A diagram of point defects
(*a*) vacancy; (*b*) substituted atom; (*c*) interstitial atom

tal. It is, therefore, essential to consider the types of imperfections in the crystal structure of metals or, what is the same thing, the structure of real crystals.

One of the types of imperfections in the crystal structure are non-occupied points in the crystal lattice, in other words, the presence of *vacancies*, or atomic 'holes' (Fig. 1-7*a*). This '*point*' defect of the lattice is of great importance for diffusion processes in metals (for more detail, see Sec. 13-1).

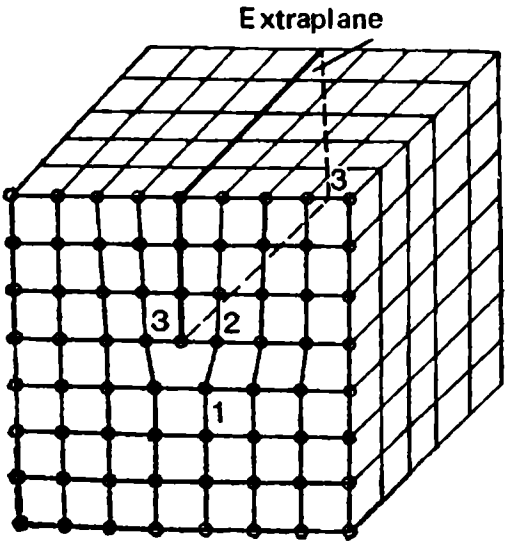

Fig. 1-8. Dislocation in a crystal lattice

At room temperature, the number of vacancies is very small compared with the total number of atoms (roughly one vacancy per 10^{18} atoms), but increases appreciably with temperature, especially near the melting point (one vacancy per 10^4 atoms).

Some external effects (irradiation by radioactive particles, surface friction, etc.) can increase the number of vacancies, i.e. loosen the metal. In certain extreme cases the number of vacancies may be as large as 1 to 3 per 100 atoms.

Another important defect in the crystal structure is *dislocation*. Imagine that an extra incomplete plane of atoms, which is called the *extraplane*, has for some or other reason appeared in a crystal lattice (Fig. 1-8). The edge *3-3* of that plane forms a *linear defect* (imperfection) of the lattice, which is called the *edge dislocation*. An edge dislocation may extend to many thousands of lattice parameters and its Burgers vector (see further in this section) is perpendicular to the extraplane. Another type of dislocation is *screw dislocation* whose Burgers vector is parallel to the extraplane. In real metals, dislocations are mostly of a mixed type: edge dislocations in some portions and screw dislocations in others. A zone of elastic distortion of the lattice forms around a dislocation. The distance from the centre of a defect to the undistorted lattice is taken equal to the width of a dislocation, which is not large (a few atomic distances).

Because of the distortion of the lattice near a dislocation (Fig. 1-9*a*), the latter can easily move from its neutral position, the neighbouring plane passes to an intermediate position (Fig. 1-9*b*), and transforms into an extraplane (Fig. 1-9*c*), and forms a dislocation along the edge atoms. It is clear that a dislocation can move (more strictly, be passed on as the baton in a relay-race) along a certain plane (slip plane) which is normal to the extraplane.

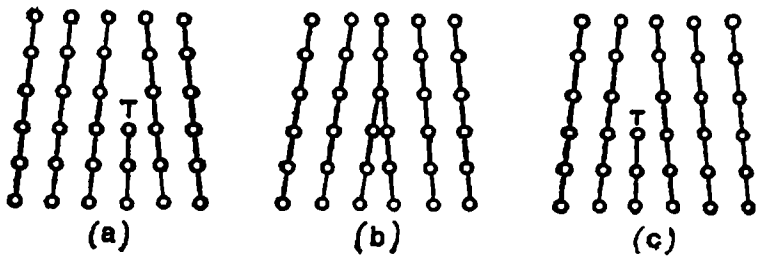

Fig. 1-9. Movement of a dislocation

By modern views, the density of dislocations in common pure metals, i.e. the number of dislocations per unit of surface is 10^8 to 10^9 cm^{-2}. The mechanical properties of a metal depend on the number of dislocations and especially on their capability for motion and multiplication, as will be discussed below.

Figure 1-10 shows microphotographs of metal sections in which dislocations have been revealed by special methods and are seen as individual dots (these are the ends of individual dislocations). In some cases, dislocations are revealed as their traces on the metal surface.

A grain boundary is an obstacle for the motion of dislocations, because of which the dislocation density is greater at grain boundaries (Fig. 1-10*a*). Internal stresses in the metal can concentrate at various inclusions and thus generate dislocations (Fig. 1-10*c*). Dislocations are distributed non-uniformly over the volume of metal and the pattern of their distribution forms what is called the dislocation structure (Fig. 1-10*e*, *g*). Dislocations can often form a network, or, more precisely, a cellular structure (Fig. 1-10*b*).

The structures shown in Fig. 1-10*a-e*, *g* can be revealed by common metallographic techniques and are seen in certain alloys at relatively low magnifications (×1 000). Dislocations in such alloys become visible owing to the decoration effect, i.e. to separation of various particles on them (similar to the case when an aerial conductor becomes visible as a flock of birds has perched on it). Non-decorated dislocations can be revealed only in thin films of metal and are seen only at large magnifications (of an order of × 30 000). Dislocations revealed by such direct methods are shown in Fig. 1-10*d*, *f-h*.

Thus, a regular crystal structure may be distorted by two types of defect: point defects (vacancies) and linear defects (dislocations).

Vacancies move continuously in a lattice when a neighbouring atom passes to a 'hole' and leaves empty its former location. An increase in temperature, i.e. in the thermal mobility of atoms, increases the number of such acts and adds to the number of vacancies.

Unlike vacancies, linear defects cannot move spontaneously and chaotically. A slight stress, however, is sufficient for a dislocation to start motion and form a plane, and in the cross-section, a slip line *C* (Fig. 1-11).

As has been indicated, a field of distorted crystal lattice forms around a dislocation. The energy of distortion of the crystal lattice is characterized by what is called the *Burgers vector*.

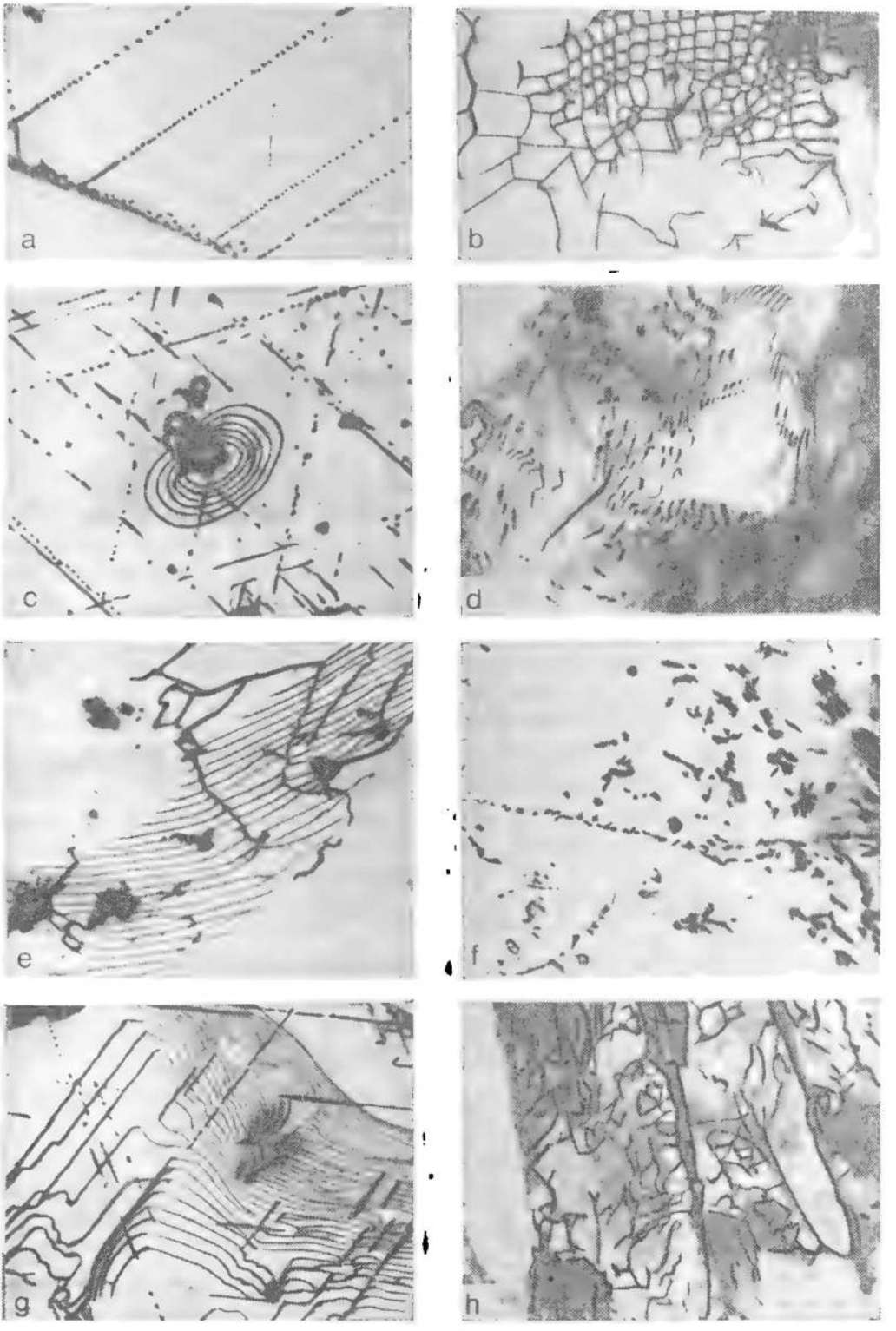

Fig. 1-10. Dislocation structures

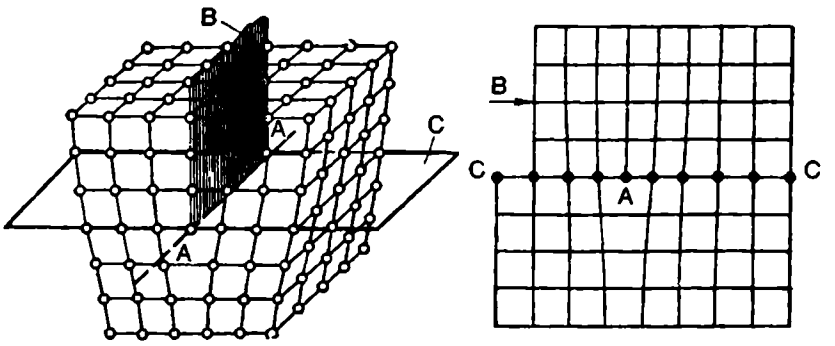

Fig. 1-11. A shear plane (C) as a trace of moving dislocation (A-A); B—extra-plane

If a contour $ABCD$ is drawn around a dislocation $\perp$ (Fig. 1-12), the portion BC will consist of six sections and the portion AD, of five. Their difference is $BC - AD = b$, where b is the magnitude of the Burgers vector. If a contour is drawn around a few dislocations (the distortion zones of the crystal lattice which overlap or merge), the total Burgers vector will be the sum of the Burgers vectors of the individual dislocations. The magnitude of the Burgers vector characterizes the mobility of dislocations.

Apart from the dislocation structure (which may be quite diverse, as shown in Fig. 1-10), of great importance is the total characteristic of the number of dislocations, which is called the dislocation density. This is understood as the total length of dislocations (in centimetres) per cm^3 of metal volume, i.e. the dimension of dislocation density is $\rho = cm/cm^3 = cm^{-2}$. The dislocation density of metals usually varies within 10^8-10^{13} cm^{-2} (a million kilometres per cubic centimetre).

A metallic grain is far from being a monolithic crystal composed of parallel atomic layers. Actually, it consists, as it were, of a mosaic of individual blocks whose size is $1 \cdot 10^{-5}$-$1 \cdot 10^{-3}$ cm (1 000-100 000 Å) and whose crystal planes are turned through a small angle of a few minutes relative to one another. This structure of metal grains is called *mosaic structure* and the blocks that constitute it are called *mosaic blocks*. Various processes of metal treatment can change the sizes of mosaic blocks and their orientation thus changing the properties of the metal. Blocks can often be combined into larger aggregates which are called *fragments*. Each fragment contains a large number of blocks. Frag-

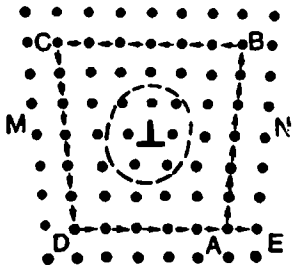

Fig. 1-12. A diagram to determine the Burgers vector for a linear dislocation

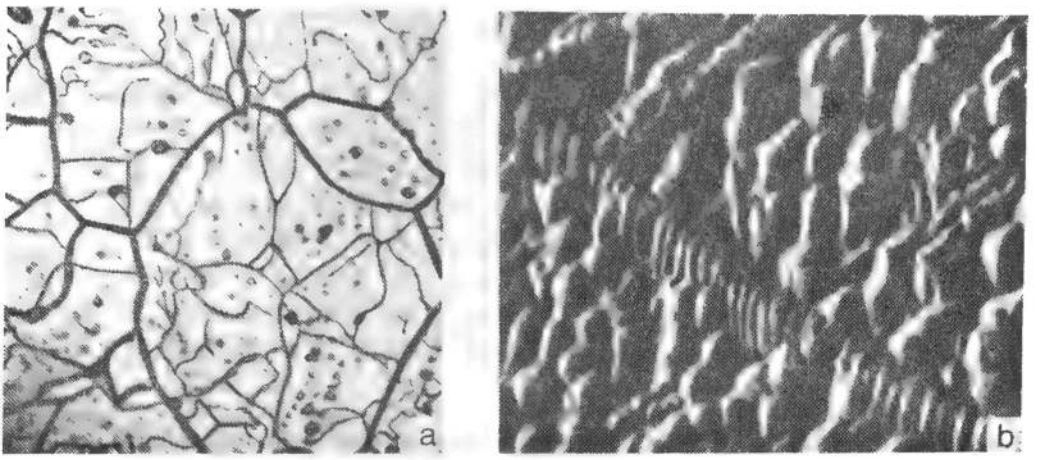

Fig. 1-13. Fine structure of low-carbon steel (B. S. Kasatkina)

(*a*) ferrite grains (thicker boundaries) and fragments (thinner boundaries), ×250;
(*b*) block structure of a ferritic grain (a boundary of a fragment and blocks), ×16 000

ments are also misoriented relative to one another through angles of a few degrees.

Thus, grains in a metal are misoriented relative to one another through angles of a few tens of degrees[1]. Grains can be composed of fragments misoriented only through a few degrees. Finally, fragments can consist of blocks misoriented only through small angles of a few minutes. This three-stage structure is not invariably found in all cases. In some particular cases metal grains may consist of fragments having no block structure, or only of blocks. A thermal process which causes division of grains into fragments is called the *fragmentation*, or *polygonization*.

Mosaic blocks are usually very small and can be seen only in the electron microscope. The size of blocks and their misorientation angles are measured by methods of X-ray structural analysis (see Sec. 1-7).

If fragments are large, they can be easily seen in the optical microscope.

Figure 1-13 shows the microstructure of a metal, which consists of large grains; these in turn consist of fragments and blocks.

Thus, a real metallic crystal contains atomic-crystalline (vacancies and dislocations) and structural (blocks and fragments) imperfections. The former, i.e. vacancies and dislocations, are distributed non-uniformly and concentrate at the boundaries of grains, fragments and blocks.

[1] Grains are separated by what is called high-angle boundaries; neighbouring grains, differing only slightly in their space orientation, are separated by low-angle boundaries and then characterized by a tendency to combination or merging.

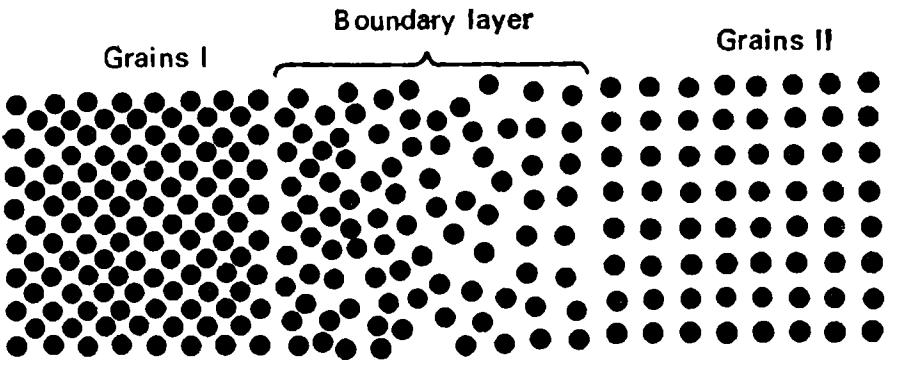

Fig. 1-14. A model of arrangement of atoms in the body and at the boundary of a grain

As has been mentioned earlier, neighbouring grains are strongly misoriented (the misorientation angle being greater than 5°) and between them there is a boundary layer of a strongly distorted structure and a high concentration of atomic-crystalline defects (Fig. 1-14).

Misorientation of blocks is small (less than 1°). Blocks are bonded with one another and retain a regular, though distorted, crystal structure by means of dislocations.

The density of dislocations in that portion of the crystal is higher at a higher angle of misorientation between blocks.

The properties of crystals of a metal are closely associated with many factors of its internal structure: the content (density) of vacancies and dislocations, their location (*dislocation structure*), the size and misorientation of the block structure (*fine structure*).

Modern science possesses numerous experimental means for analysis of fine and dislocation structures of metallic crystals.

It should be also noted that the atoms on a branched so-called *internal surface* (at boundaries of grains, fragments and blocks) possess an elevated energy. Because of this, many of the processes, that will be discussed later, occur predominantly at the boundaries of grains (fragments or blocks).

1-6. ANISOTROPY OF PROPERTIES OF CRYSTALS

Considering various planes, for instance, in a b.c.c. lattice, it may be easily concluded that they are filled with atoms to a different density.

For instance, in the hatched square of a b.c.c. lattice (Fig. 1-15*a*) the centres of atoms are at the corners. Since each of these atoms simultaneously belongs to four squares, each of the squares of area a^2 shares one atom.

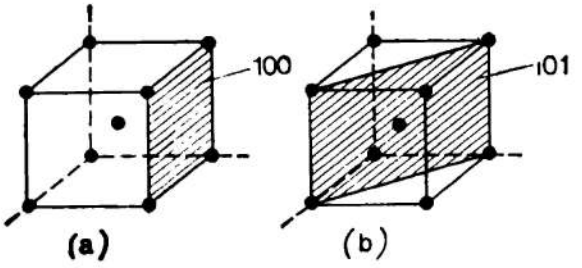

Fig. 1-15. Characteristic planes in a body-centred cubic lattice

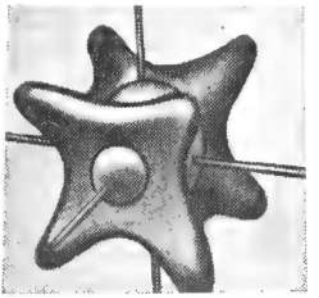

Fig. 1-16. A model to illustrate variations in the ultimate strength of a copper crystal, depending on the direction of applied load

In the hatched rectangle of the same lattice (Fig. 1-15*b*), there are two atoms per area of $a^2\sqrt{2}$, i.e. each of these atoms shares an area of $a^2\sqrt{2}/2$, which is smaller than a^2, therefore, there are more atoms in that plane than in the cube side.

The properties of an individual crystal (single crystal) in a given direction differ from its properties in another direction (Fig. 1-16) and, naturally, depend on how many atoms are met in that direction. The difference in the properties of crystals, depending on the direction of test, is called *anisotropy*. All crystals are anisotropic. Anisotropy is an inherent property of any crystal and is typical of crystalline structure.

A real metal is composed of a plurality of crystals. Individual crystals are only fractions of a millimetre in size, so that many thousands of crystals may be present in 1 cm^3 of metal volume. Since these crystals are randomly oriented, there is roughly the same quantity of differently oriented crystals in any direction. As a result, the properties of this polycrystalline body are the same in all directions, though the properties of every crystal, it is composed of, depend on the crystal orientation. This phenomenon is called ***quasi-isotropy***.

1-7. METHODS FOR STUDYING THE METAL STRUCTURE

There are many methods for studying the crystalline structure of metals. They can be divided into two types: the first type includes the methods for studying the internal structure of crystals and the second, the methods for studying the shape of crystals.

The internal structure of crystals, i.e. the arrangement of atoms in the crystal lattice, is studied by means of *X-ray structural analysis*. X-rays are electromagnetic waves of a quite small length (2 to 0.005 Å)[1].

[1] X-rays are similar to light rays in their nature, though the latter have a greater wavelength (4 000-7 500 Å). X-rays are formed in special apparatus

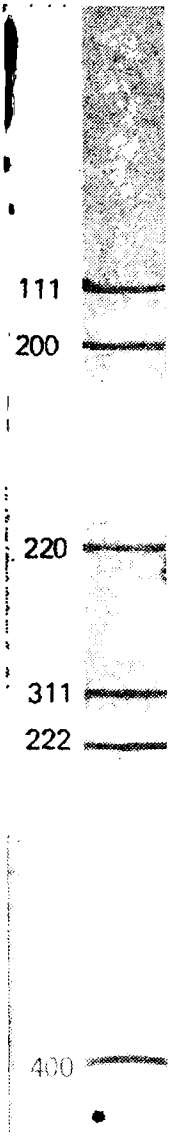

Fig. 1-17. A radiograph of copper

Owing to their small wavelength, X-rays penetrate the body, instead of being reflected from its surface. The electromagnetic field of these rays causes the electrons of atoms to oscillate. The oscillating electrons are sources of electromagnetic waves which are called scattered rays, since they propagate in all directions. It may be assumed that these waves emanate from the atom centre. As atoms are arranged regularly in a crystal, scattered rays interact with one another in a definite pattern, i.e. enhance one another in some directions and attenuate in other directions. If a photographic plate[1] is placed in the path of these rays, rings or spots will be formed on it in places where scattered rays are enhanced.

Yu.V. Vulf (1863-1925) and W.H. and W.L. Bragg have shown in 1913 that this interference pattern, or radiograph, (Fig. 1-17) can be interpreted as the result of interference of the rays reflected from individual parallel atomic planes. This makes it possible to determine the interatomic distances and the pattern of arrangement of atoms in space (i.e. the type of a crystal lattice and its parameter).

More advanced methods of X-ray structural analysis enable us to study crystal structure defects. The width (blurring) of lines on a radiograph is an indication of imperfection of a crystal structure. In particular, the total density of dislocations is proportional to the width of lines:

$$\rho = \gamma \overline{h}$$

where ρ is the dislocation density, and h is the width of lines.

Various techniques of X-ray structural analysis are used for determining structural particularities (the size of blocks and grains, the extent of textured structure, the presence of stresses, etc.).

The size, shape and mutual arrangement of crystals in metal are studied by *metallographic methods.*

Since all metals are opaque (for the visible light), the shape of crystals, their dimensions and arrangement are studied by using specially prepared microsections of a metal. In that case the metal is cut in the plane that is of interest for the examiner. The plane is then ground and polished to make it mirror-like. The structure of a section can be revealed by forming a relief on it or by tinting various structural components; this is usually achieved by chemical etching. The etching acid acts at most on grain boundaries, since these are most imperfect in their structure; grain boundaries appear as recesses on the etched microsection; impinging light rays will be diffusely reflected from them (Fig. 1-18), so that the grain boundaries will be seen dark in the microscope, while the bodies of grains will be bright (Fig. 1-19).

Microstructures of metals are studied by viewing microsections in special metallographic microscopes, in which the beam of light from a light source is

---

in which electrons are decelerated on impinging a target, with the kinetic energy of the electrons being transformed into a variety of electromagnetic oscillations, X-rays. The formation, properties, and use of X-rays are discussed in the courses on physics.

[1] X-rays are invisible, but, like light rays, produce a darkening effect on photographic emulsions, and therefore, can be photographed.

reflected from a microsection and passes through an objective and eye-piece to form an image of a suitable magnification.

Figure 1-19 shows the structure of a metal at a 100-fold magnification, or what is called *microstructure*. In some cases it is essential to study coarser details of a structure, for instance, aggregations of more or less uniform grains. Such structures, upon deep etching, are studied by the naked eye or by using a magnifying glass. The structure thus revealed is called *macrostructure* and the metal section is called macrosection (see Figs. 2-11 and 2-13).

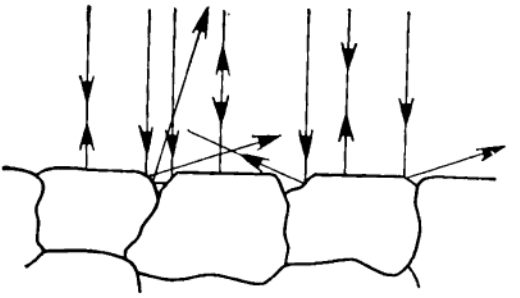

Fig. 1-18. Reflection of light beams by faces and boundaries of grains

The optical microscope is not the proper apparatus for revealing the tiniest crystals. As is known from optics, the microscope resolving power[1] is:

$$d = \frac{\lambda}{n \sin \varphi}$$

where d is the resolving distance; λ is the wavelength; n is the refractive index of the medium in the space between the objective and object; and φ is the aperture angle of the objective. The resolution diminishes with increasing aperture number A ($A = h \sin \varphi$). In modern microscopes, the aperture angle of the objective is roughly 90°. The refractive index of air is unity. Hence

$$d = \lambda$$

and the resolution of an optical microscope is equal to the light wavelength, i.e. 6 000 Å.

If a medium of a greater refractive index is placed between the objective and microsection, for instance, cedar oil ($n = 1.5$), the resolution increases 1.5 times, i.e. up to 4 000 Å.

[1] The least distance between two dots at which they are seen separately and do not merge into a spot.

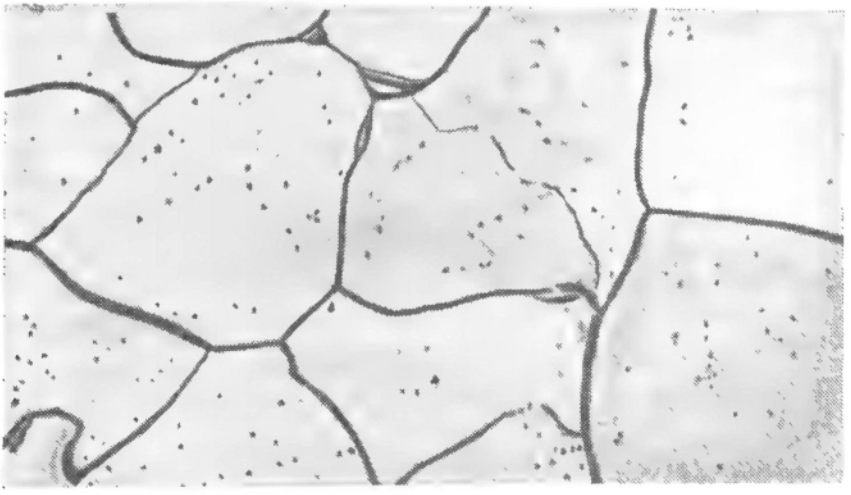

Fig. 1-19. Microstructure of a metal, ×100

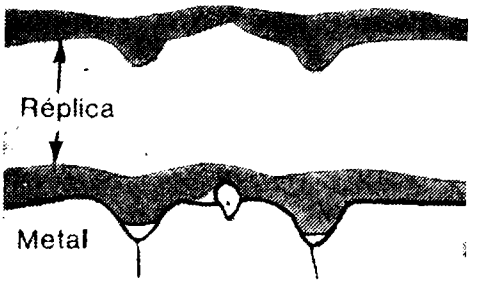

Fig. 1-20. Making a replica of a metal surface for electron diffraction analysis

This analysis shows that crystals of a size less than 0.4-0.6 μm cannot be seen in the optical microscope even if we use the highest magnification[1]. Practically, optical microscopes are used to study and photograph metal structures with magnifications of no more than 1 000-1 500, the tiniest particles that are seen separately having a size of 0.4-0.6 mm in the image. The image thus obtained can be enlarged to make the visible particles greater, but this will reveal no new details in the structure.

Disperse structures and fine details of coarse structures (grain boundaries, block textures, etc.) are studied in metallography by using the *electron microscope*.

The electron microscope uses an electron beam for 'illumination'. As can be seen from the above formula, the resolution of a microscope is determined by the wavelength.

The wavelength of electron beams (λ) depends on the velocity of electrons:

$$\lambda = \frac{h}{mv}$$

where h is Planck's constant; m is the mass of an electron; and v is the velocity of electron, km/s.

In a field of intensity of 50 000 V/m, electrons acquire a velocity of 124 000 km/s, which corresponds to a wavelength of a few hundredths of an angstrom. The resolution of modern electron microscopes is of an order of 5-10 Å (only in cases when the object is studied directly in the electron microscope). Actually, such small details cannot be revealed in electron-microscopic studies of metal structures. The point is that the principle of image formation in the electron microscope is based on placing an object in the form of a thin film in the path of electron beams.

Electron beams will be scattered more in the thicker portions of the film and form dark spots on a fluorescent screen, whereas in thinner places they will be less scattered and form bright fields on the image.

The common technique for preparing objects for electron-microscopic studies is as follows. Upon making a microsection of a metal, a very thin layer of a substance (lacquer, carbon, quartz) is applied to its surface. Thus a replica is formed, which reproduces the relief of the microsection with a high accuracy (Fig. 1-20). The replica is then taken from the microsection and placed into an electron microscope. In thicker portions of the replica (where the metal has been etched more deeply), electrons will be scattered more strongly. Thus, it is possible to reveal the boundaries between structural components of an alloy or the grain boundaries. Owing to surface tension and some other reasons, the substance that is applied to the metal surface does not, however, reproduce the finest details of the metal relief quite accurately, so that the resolving power of the electron microscope, with the use of a quartz replica, for instance, can be roughly estimated at 100 Å.

The useful magnification of the electron microscope is commonly of an order of 5 000 to 20 000, i.e. about 10 times that of the optical microscope.

[1] The resolution of a microscope can be further increased by using ultraviolet rays (of a wavelength of 4 000 Å) instead of white light. Ultraviolet microscopes have found no wide applications, mainly because of certain inconveniences in operation.

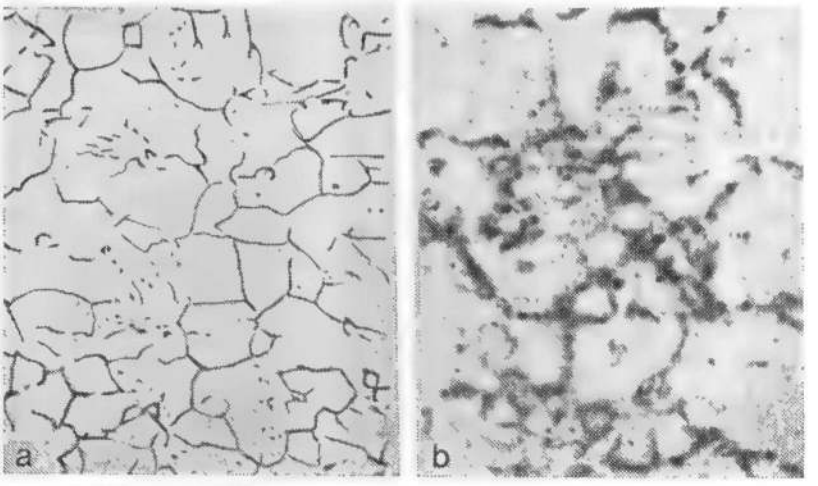

Fig. 1-21. Microstructure of an alloy, ×90
(*a*) as revealed by chemical etching; (*b*) microradiograph

Today, electron-microscopic studies are carried out with the use of thin metal films which are more or less transparent for electron beams. In that case the resolution of the electron microscope is commensurable with interatomic distances.

In the study of metal structures, it should be always kept in mind that the object being studied is a section through a volume of metal. Crystals which are seen round in the cross-section actually are either spherical or cylindrical. A network around crystals which has been revealed in plane actually is a cut through the shells that envelope the crystals.

Microscopic analysis with the use of an optical or electronic microscope can give us much information on the structure of alloys. It fails, however, to detect whether the atoms of the alloy constituents are uniformly distributed in the mixture. For instance, the alloy whose structure is shown in Fig. 1-21*a* seems to be quite homogeneous.

The method of *radiography* has found use recently for studying the structure of metallic alloys. When melting a metal, a definite quantity of radioactive isotope of the element whose distribution is to be studied is given to the melt. A photographic film is applied to a micro- or macrosection of the metal. The film will be darkened by radioactive beams in places where the element being studied has concentrated. The developed film can be photographed under a microscope to obtain a microradiograph of a magnification up to ×150.

Figure 1-21*b* shows a microradiograph of the same metal as in Fig. 1-21*a*. It may be seen that carbon (radioactive carbon has been given to the melt) is distributed non-uniformly, concentrating mainly at grain boundaries.

Apart from the two main methods discussed above, i.e. X-ray structural analysis and metallographic analysis, other more advanced methods are now used by researchers.

In all cases it is essential to know the average composition of the metal being studied; this is achieved by means of *chemical analysis*. The composition of individual phases is determined by *chemical phase analysis* (including *carbide analysis*). A multi-phase object being studied is subjected to electrolysis in which all the phases except for that of interest are dissolved. The phase thus separated is studied by various methods.

The same problems, but on a different, X-ray spectral principle, are solved by the *microprobe*, a new apparatus introduced into the practice of metallurgical

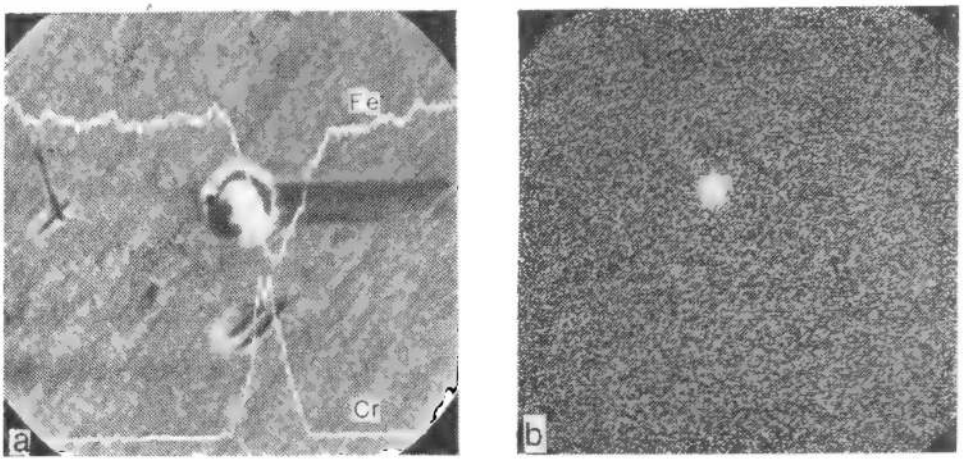

Fig. 1-22. X-ray microanalysis of chromium carbide inclusions in Fe-Cr-C alloy, ×1000

studies. It makes it possible to carry out chemical analysis of the smallest portions in an alloy (a cross-section of 0.5-2 μm^2).

A new type of instrument, the scanning electron microscope, is finding ever increasing use for the purpose.

Inclusions are readily visible in the optical microscope if their size is not less than 0.5-1μm. If an electron beam is directed on such an inclusion and the X-ray spectrum of excited atoms is recorded, it is possible to determine the composition of the inclusion, more strictly, how its composition differs from that of the matrix. An example of such an analysis is given in Fig. 1-22 which shows inclusions in a Fe-Cr-C alloy.

The concentration line passing through the inclusion (Fig. 1-22*a*) shows that the inclusion has a reduced content of iron and an elevated content of carbon, which suggests that the inclusion is chromium carbide (a compound of chromium and carbon). Scanning over the area of inclusion (Fig. 1-22*b*) confirms that the inclusion has an elevated content of chromium compared to that of the matrix.

When studying mechanical properties of metals, it is important to know not only the resistance to fracture, but also the nature of the fracture, i.e. how it has occurred. To do this, the surfaces of fracture are studied. The method is called *fractography* (or *electron fractography*, if fracture surfaces are studied with great magnification in the electron microscope). Fractographic studies enable us to determine unequivocally whether a fracture has been viscous or brittle, i.e. whether the fracture surface has been deformed plastically.

Figure 1-22 shows two typical fractures: a brittle (crystalline) fracture on the left and viscous (fibrous) fracture on the right. The former occurs through detachment of one portion of a crystal from another along the crystal planes (therefore, the fracture is lustrous) and the latter, owing to the formation and coalescence of pores, the process being associated with an appreciable plastic deformation of the surface (the fracture is dull).

This has been confirmed by electron fractographic studies of replica (Fig. 1-23*a*, *c*) or directly of metal surfaces (Fig. 1-23*b*, *d*). The former studies are carried out under an electron microscope and the latter, under a *scanning electron microscope.*

Brittle fracture usually has a *river pattern* (Fig. 1-23*c*, *d*) and viscous fracture, a *cup-shaped* form (Fig. 1-23*a*, *b*).

The methods that have been briefly described here, as also some other methods for studying metal structures, are widely used in scientific research,

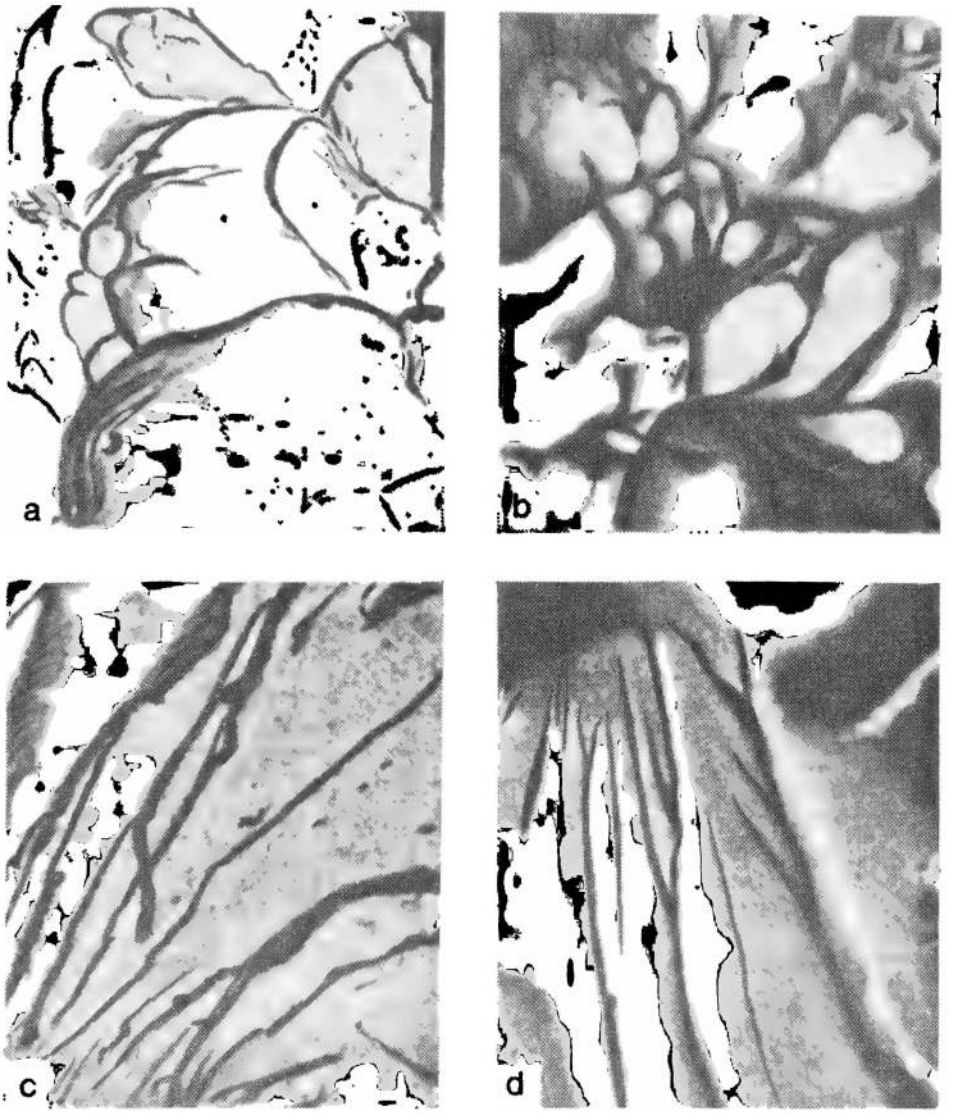

Fig. 1-23. Electron micrographs of metal fractures, ×5 000

(*a*), (*b*) ductile (cup-shaped) fracture; (*c*), (*d*) brittle (river-pattern) fracture; (*a*), (*c*) photographed under an electron microscope; (*b*), (*d*) photographed under a scanning microscope

engineering tests, etc. Every large metallurgical or machine-building works (not to mention research institutes and higher schools) has metallographic and sometimes radiographic and physical laboratories which are equipped with modern instruments.

LITERATURE

Bokstein S. Z., *The Structure and Properties of Metal Alloys.* Moscow, "Metallurgiya", 1971 (in Russian).

Friedel J., *Dislocations.* Oxford, Pergamon Press, 1964.

Physical Metallurgy. Edited by R. W. Cahn. Amsterdam, North-Holland Publishing Co., 1965.

Chapter 2

CRYSTALLIZATION

2-1. THREE STATES OF MATTER

As is known, any substance can be in one of the three *states of aggregation*: gaseous, liquid or solid. In pure metals changes of the state of aggregation occur at definite temperatures: the transformation from solid to liquid state takes place at what is called the melting

Table 2-1. Selected Properties of Metals

Element	Number in Periodic Table	Crystal lattice	Atomic radius, Å	Density (at 20°C), g/cm³	Melting point, °C	Boiling point, °C	Coeff. of expansion (at 20° C), $\alpha \cdot 10^6$	Brinell hardness
Be	4	H12	1.13	1.82	1 284	2 970	12.2	140
Mg	12	H12	1.60	1.74	651	1 110	25.7	30
Al	13	C12	1.43	2.70	660	2 500	23.1	20
Ti	22	H12, C8	1.45	4.50	1 660	3 260	7.14	80
V	23	C8	1.36	5.96	1 700	3 000	8.3	260
Cr	24	C8	1.28	7.14	1 850	2 470	6.2	100
Mn	25	Complex	1.31	7.46	1 244	2 150	22.1	200
Fe	26	C8, C12	1.27	7.86	1 539	2 880	11.5	70
Co	27	H12, C12	1.26	8.9	1 480	3 135	12.5	50
Ni	28	C12	1.24	8.90	1 455	3 080	13.5	60
Cu	29	C12	1.28	8.92	1 083	2 300	16.5	35
Zn	30	H6	1.37	7.14	419	907	32.5	35
Zr	40	H12, C8	1.60	6.52	1 860	3 580	6.23	100
Nb	41	C8	1.47	8.5	2 450	3 700	7.2	80
Mo	42	C8	1.40	10.2	2 625	4 800	4.9	150
Ag	47	C12	1.44	10.5	960	1 950	18.9	25
Sn	50	Diamond-type C4	1.58	7.29	232	2 430	46.6	5
W	74	C8	1.41	19.3	3 410	5 500	4.3	300
Au	79	C12	1.44	19.3	1 063	2 600	14.2	19
Hg	80	H6	1.55	13.51	—38.9	357	—	—
Pb	82	C12	1.75	11.3	327	1 750	28.1	4
U	92	Complex	1.55	19.0	1 133	3 927	23	240

point and the transformation from liquid to gaseous state, at the boiling point. The transformation points depend on pressure (see Fig. 1-2), but are quite definite at a given constant pressure. The transformation points for the most common metals (at a pressure of 1 at) are given in Table 2-1.

The melting point is the most important constant of metal properties. The melting points of various metals range from —38.9°C for mercury which is the most low-melting metal and is liquid at room temperature, up to 3 410°C for tungsten which is the most high-melting among metals.

The low strength (hardness) of low-melting metals (tin, lead, etc.) at room temperature is mainly due to the fact that the melting points of these metals are less distant from room temperature than the melting points of refractory metals. To be able to compare the properties of various metals, they are tested at the so-called *homologous temperatures*, i.e. at absolute temperatures equal to the same fraction of the melting point (for instance, 0.5 of the absolute temperature of melting point of lead is 27°C, and that of iron, 631°C; at these temperatures, the properties of lead are quite close to those of iron).

2-2. ENERGY CONDITIONS FOR CRYSTALLIZATION

Crystallization is the process of transformation of a substance from liquid to solid state in which the crystal lattice forms and crystals appear.

How can it be explained that a substance exists in the liquid state at some temperatures and in the solid state at other temperatures and why does this transformation occur at a definite temperature point?

In nature, all spontaneous transformations and hence crystallization and melting always occur owing to the fact that a new state under new conditions is energetically more stable, i.e. possesses a lower reserve of energy.

This may be explained by the following example.

A heavy ball (Fig. 2-1) tends to roll from position *1* to a stabler position *2*, since its potential energy in position *2* is lower than that in position *1*.

The energy state of a system having an enormous number of particles (atoms, molecules) involved in thermal motion, is characterized by a special thermodynamic function F which is called *free energy*[1] (free energy $F = U - TS$, where U is the internal energy of the system; T is the absolute temperature; and S is the entropy).

It may be said that a system is less stable at a higher free energy and, if there is any possibility, passes to a state with a lower free energy (like the ball in our example, which rolls down from position *1* to position *2* if there is no obstacle on its path).

[1] When a gaseous phase participates in the process, a more complicated term—the *thermodynamic potential* of a system—is used in calculations. The process of crystallization, in which gaseous phases do not participate, can be fully characterized by the free energy.

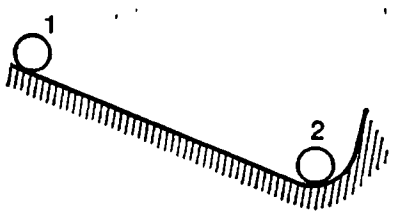

Fig. 2-1.

If the external conditions, such as temperature, are changed, the free energy changes by a complicated law, this law being different for the liquid and crystallized state of a substance. The patterns of temperature variations of the free enegry in the liquid and crystallized states are schematically shown in Fig. 2-2.

Above the temperature T_s, a substance has a lower free energy in the liquid state, while below that temperature its free energy is lower in the solid state. Therefore, the substance should be in the liquid state above the temperature T_s and in the solid (crystallized) state, below that temperature.

It is evident that at a temperature of T_s the free energies of the liquid and solid states are equal and the metal in both states is in equilibrium. This temperature T_s is called the *equilibrium*, or *theoretical, temperature of crystallization.*

Crystallization (or melting) cannot, however, occur at T_s, since at that temperature

$$F_l = F_{cr}$$

For crystallization to begin, it is required that the process should be thermodynamically favourable for the system and that its free energy should decrease. As may be seen in Fig. 2-2, this is possible only when the liquid is undercooled below the point T_s. The temperature at which crystallization practically begins may be called the *actual temperature of crystallization.*

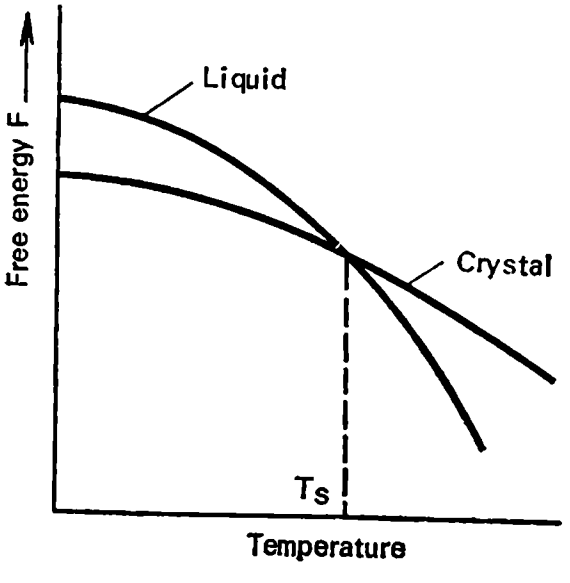

Fig. 2-2. Free energy variations in the liquid and crystalline state versus temperature

Cooling of a liquid below the equilibrium temperature of crystallization is called *undercooling.*

For the same reasons, the inverse transformation from crystallized to liquid state can take place only at a temperature above T_s; the phenomenon is called *superheating.*

The difference between the theoretical and actual tempe-

ratures of crystallization is called the amount, or degree, of undercooling.

For instance, if liquid antimony was undercooled to 590°C before crystallization and crystallized at that temperature, and knowing that the theoretical temperature of crystallization of antimony is 631°C, the degree of undercooling will be found as 631—590 = 41 degrees C.

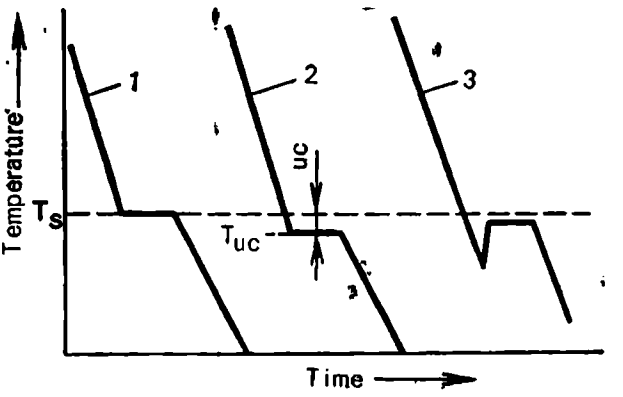

Fig. 2-3. Crystallization cooling curves

The transition of a metal from liquid to crystallized state can be described by curves in time-temperature coordinates (Fig. 2-3).

When liquid metal is cooled, its temperature drops gradually and the process can be called simple cooling, since it involves no change in the state of aggregation.

As the temperature has lowered to the crystallization temperature, a horizontal portion appears on the time-temperature curve, since the removal of heat from the metal is compensated by the *latent heat* liberated during crystallization. Upon full crystallization, i.e. after the metal has transformed completely to solid state, temperature drops again and the solid crystalline substance is cooled. Theoretically, the process of crystallization is described by curve *1*. Curve *2* shows the actual process of crystallization. The liquid is cooled continuously down to the temperature of undercooling T_{uc} which is below the theoretical temperature of crystallization, T_s. Only upon cooling below T_s the energy conditions required for the crystallization to proceed can form in the metal.

In some metals at a deep undercooling, the latent heat of crystallization can be liberated at the initial stage of crystallization so vigorously that the temperature rises jump-wise and approaches the theoretical value (curve *3* in Fig. 2-3). For instance, antimony crystallizes in this manner. With most metals, the degree of undercooling prior to crystallization is usually negligible and even cannot be detected under normal conditions of experiment.

2-3. THE MECHANISM OF CRYSTALLIZATION

As was indicated as far back as in 1878 by D.K. Chernov, who then studied the structure of cast steel, the process of crystallization should consist of two elementary processes. The first process is the formation, or nucleation, of tiniest crystalline particles which were called 'embryos' by Chernov and now are called crystallization *nuclei* or crystallization *centres*. The second process is the growth of crystals from these centres.

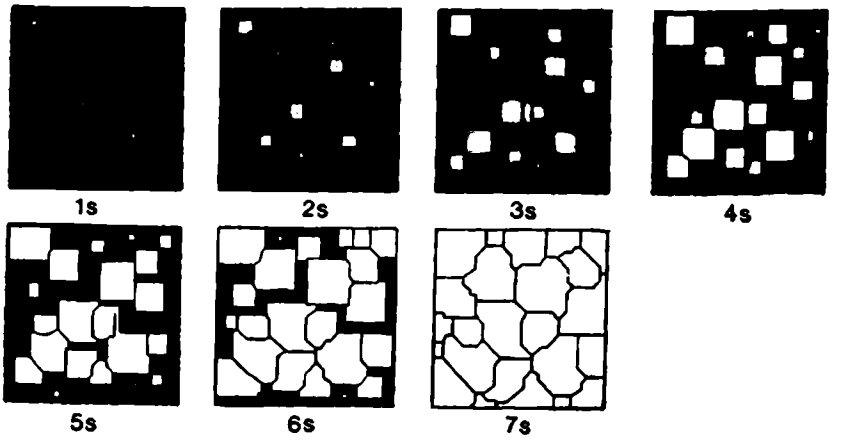

Fig. 2-4. A model of crystallization process (I. L. Mirkin)

A systematic study of the process of formation of crystallization nuclei and their growth, first on transparent organic substances and then on metals, was carried out by G. Tamman. He established a general relationship between the number of crystallization nuclei, rate of growth and degree of undercooling. Later studies of crystallization processes, in particular those made by A. A. Bochvar, K.P. Bunin et al., have shown that Tamman's scheme can have only a limited application to crystallization of real liquid metals. However, many of the regularities found by G. Tamman in his experiments have been verified qualitatively in later studies and are still useful in the analysis of crystallization processes.

The formation of crystals through nucleation and the growth of centres of crystallization can be studied by analysing suitable models (schemes), as has been successfully done by I. L. Mirkin. Such a model of crystallization process is shown in Fig. 2-4. Assume that five nuclei appear each second in the area of Fig. 2-4 and these grow at a definite rate. Thus, five nuclei will be formed at the end of the first second. They will grow up somewhat at the end of the second second and five new nuclei will form to that time. The process of crystallization in the model considered will proceed further in this way, until it is completed at the end of the seventh second.

The qualitative picture of crystallization process as shown in Fig. 2-4 can be described quantitatively by a kinetic curve (Fig. 2-5).

By analysing such crystallization models, we can explain two important aspects:

1. As crystallization proceeds, ever greater number of crystals is involved in it. This is why the process first occurs acceleratedly to a certain moment[1] after which the growing crystals begin to interfere with one another and their growth is slowed down. Another reason for this slowing of crystal growth is that ever less liquid remains for the formation of new crystals.

[1] Usually when roughly 50 per cent of the liquid has crystallized.

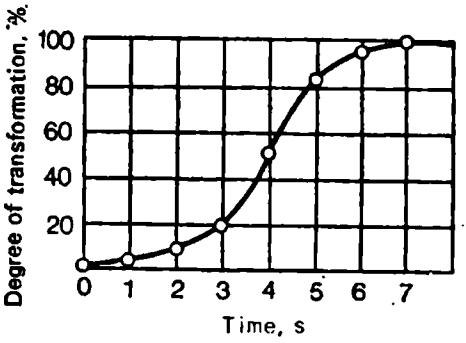

Fig. 2-5. Kinetic curve of crystallization

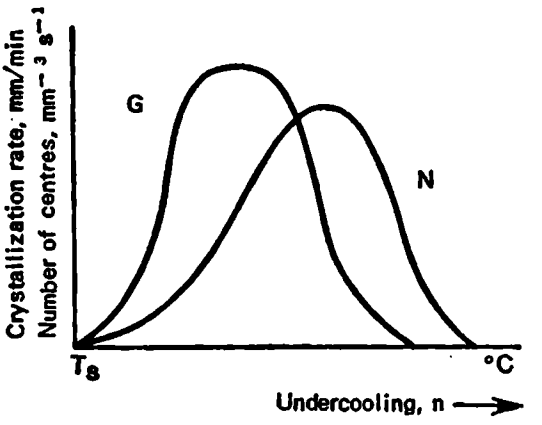

Fig. 2-6. Effect of undercooling on the rate of nucleation, N, and rate of crystal growth, G

2. As long as crystals grow freely in the liquid, their shape is usually regular. As crystals begin to interfere with one another and grow together, their shape becomes irregular and depending on the conditions of contact of growing crystals. This is why grains (crystallites) in metals are irregular in shape, as has been given in Ch. 1.

The rate of the whole crystallization process is determined by two factors: the *rate of nucleation* and the *rate of crystal growth.* Both factors can be measured under various conditions of crystallization.

The number of crystals nucleating per unit time per unit volume, which will be denoted by N, has a dimension of $1/mm^3 \cdot s$. The rate of crystal growth, G, is the rate with which linear size of a crystal increases. Its dimension is mm/s or mm/min.

When studying the crystallization of transparent organic substances at various temperatures, G. Tamman has found that N and G are determined by the degree of undercooling. The dependence of N and G on undercooling is shown graphically in Fig. 2-6. As may be seen, both curves have a maximum. At the theoretical temperature of crystallization ($n = 0$), both N and G are equal to zero and the process of crystallization cannot take place; this fully agrees with the above-mentioned principle that undercooling is indispensable for crystallization to proceed. As the degree of undercooling increases, N and G increase to a maximum and then again diminish; at high degrees of undercooling, they can drop practically to zero.

The growth of N and G at low degrees of undercooling is due to the fact that the mobility of the liquid at temperatures near the equilibrium point (T_s) is high, so that crystallization is speeded up at greater degrees of undercooling owing to an increasing difference between the free energies of the liquid and crystallized states. At

high degrees of undercooling, N and G become equal to zero, since the mobility of atoms is insufficient to rearrange chaotically positioned atoms in the liquid into a regular crystalline structure.

The size of crystals which form through crystallization depends on the ratio between G and N at the temperature of crystallization and given degree of undercooling. At a high value of G and a low value of N (for instance, at a low degree of undercooling, see Fig. 2-6), large crystals are formed, but their number is small; at low G and high N (a high degree of undercooling), a large number of fine crystals will form. Finally, in accordance with Tamman's curves, if we manage to undercool a liquid very deeply without crystallization, G and N will be equal to zero and the liquid will remain untransformed, i.e. uncrystallized. Liquid metals, however, are only slightly liable to undercooling and this state is hardly attainable for them. On the other hand, salts, silicates, and some organic substances are very liable to undercooling. Common transparent 'solid' glass is actually an undercooled thickened liquid. As has been indicated earlier, this state of matter is amorphous and can be characterized by having neither definite melting point nor regular arrangement of atoms in the form of a particular crystal lattice.

A new phase forms through nucleation and crystal growth not only in liquid melts, but also during solid-state transformations; the rate of these processes also depends on undercooling. As distinct from crystallization from a liquid, a transformation in the solid state (recrystallization) usually takes place at an appreciable undercooling, so that the Tamman relationship between G and N is for this case even more acceptable than for primary crystallization.

In view of the foregoing, it may be noted that the transition from one state to another, for instance, from liquid to solid state, is possible only if the solid state is more stable, i.e. has a lower free energy. However, the transition from one state to another requires that an energy be spent to form an interface between the liquid and crystal.

A transformation will occur only if the gain in energy at the transition to a stabler state will be greater than the loss of energy to form an interface.

In other words, the free energy $\Delta\Phi$ of a system is determined as an algebraic sum of two terms which respectively describe the surface energy $S\sigma$ and the volume energy $V\Delta F$:

$$\Delta\Phi = S\sigma - V\Delta F$$

where S is the surface area; σ is the surface tension; V is the volume; and ΔF is the difference of free energies of the liquid and crystalline states (per unit volume).

As a nucleus (a spherical one) is growing, the surface-dependent term increases proportionally to the square of the radius and the volume-dependent term, proportionally to the cube of the radius, i.e., expressing the surface area and

volume of the particle through its radius, we get:

$$\Delta\Phi = 4\pi r^2 n\sigma - \frac{4}{3}\pi r^3 n\Delta F$$

where r is the radius of a particle of the new phase and n is the number of particles.

With increasing size of a nucleating crystal, the free energy first increases (since the volume V is small and the surface area S, relatively large, Fig. 2-7). At a definite critical value, a further increase in the size of nucleus will result in diminishing the value of $\Delta\Phi$[1].

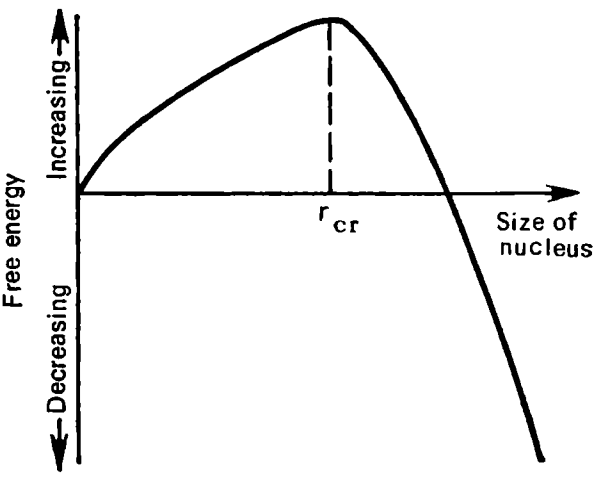

Fig. 2-7. Variations of free energy depending on the size of nucleus

The process of crystallization can take place only if the free energy decreases. Therefore, if a nucleus of a size less than r_{cr} has formed (see Fig. 2-7), it will not grow, since this would increase the energy of the system. With a nucleus of a size of r_{cr} or more, it may grow, since this will diminish the free energy of the system.

The minimal size of a nucleus capable of growing is called the *critical size of nucleus*, and the nucleus proper is called *stable*.

Each temperature of crystallization (degree of undercooling) has a corresponding size of stable nucleus; finer nuclei, should they appear in the liquid, will be dissolved, whereas larger ones will grow and form crystals or grains.

The size of stable nucleus is smaller at a lower temperature (higher degree of undercooling); therefore, a greater number of crystallization centres will then form per unit time and the quicker will be the crystallization process. Thus, the magnitude of N and the total rate of crystallization increase rapidly with increasing degree of undercooling.

2-4. THE SHAPE OF CRYSTAL FORMATIONS

A real process of crystallization is complicated by various factors whose effects may be so strong that the role of undercooling becomes quantitatively subordinate.

The factors that are of prime importance for the rate of crystallization from the liquid state and for the shape of forming crystals

[1] An analysis of the above equation for maximum and minimum should give a curve having a maximum at a definite value of $r = r_{cr}$; $r_{cr} = \frac{2\sigma}{\Delta F}$.

are the rate and direction of heat removal, the presence of undissolved particles which can serve as crystallization centres, the appearance of convective currents in the liquid, etc.

A crystal grows more quickly in the direction of heat removal than in other directions.

If a pimple (a knob) has formed on the side surface of a growing crystal, the latter may be capable of growing in the lateral direction. As a result, a tree-like crystal, or *dendrite*, may form, whose scheme, for the first time depicted by D.K. Chernov, is shown in Fig. 2-8.

Generally speaking, dendritic structure is typical of cast metals. Under favourable conditions, dendrites may sometimes grow to an enormous size. For instance, once a dendrite of a length of 39 cm was found in the pipe of a 100-t steel ingot. A photograph of that dendrite, which is called Chernov's dendrite, is shown in Fig. 2-9.

Dendrites in cast metals are normally much smaller in size: only a few millimetres long.

It should be remembered that dendrites in steel consist of many thousands or even millions of grains of the type shown in Fig. 1-18. All grains within a dendrite should evidently be likely oriented.

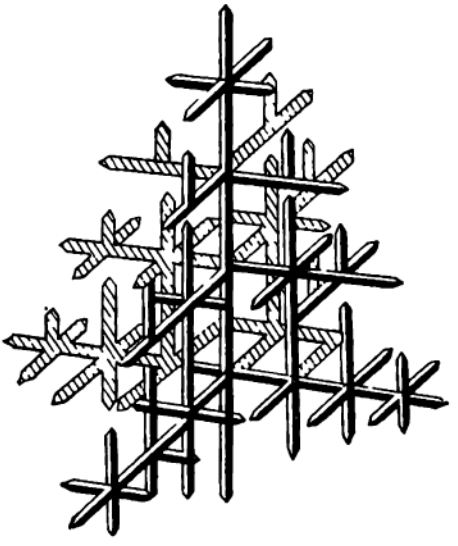

Fig. 2-8. Scheme of a dendrite (D. K. Chernov)

Fig. 2-9. Chernov's dendrite, one-third of full size

The structure shown in Fig. 1-18 is called *polyhedrous*, i.e. consisting of more or less equi-axed grains having roughly the same dimensions in all directions.

2-5. THE STRUCTURE OF INGOT

As has been noted earlier, a real process of crystallization is complicated by the effect of secondary factors (Sec. 2-4). The combined effect of these factors (which often cannot be taken accurately into account) and the general laws of crystallization determine the specific structure of a steel ingot.

The structure of a steel ingot was for the first time described in 1878 by D.K. Chernov. At that time he discovered the principal characteristic features in the structure of cast metal, though numerous new details were found in later studies.

The structure of a cast ingot consists of three principal zones (Fig. 2-10). The first zone is an outer *fine-grained crust 1* composed of misoriented fine crystals—dendrites. At the first contact of the liquid metal with the mould walls, a sharp temperature gradient and the phenomenon of undercooling appear in a thin layer of the metal; this results in the formation of an enormous number of crystallization nuclei and thus the solidified crust has a fine-granular structure.

The second zone of the ingot is that of *columnar crystals 2*. The formation of the solid crust changes the conditions of heat removal (owing to a different thermal resistance, an increased temperature of the mould wall, and some other reasons), the temperature gradient in the adjacent layers of molten metal sharply decreases and hence the degree of undercooling becomes lower. As a result, columnar crystals normally grow to the crust surface (i.e. in the direction opposite

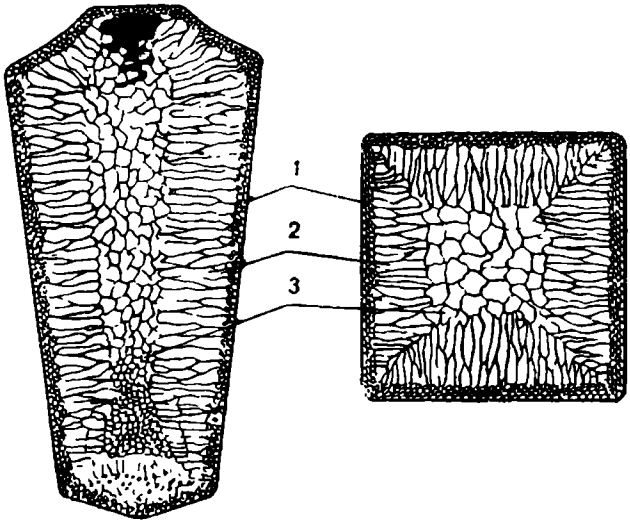

Fig. 2-10. The structure of steel ingot

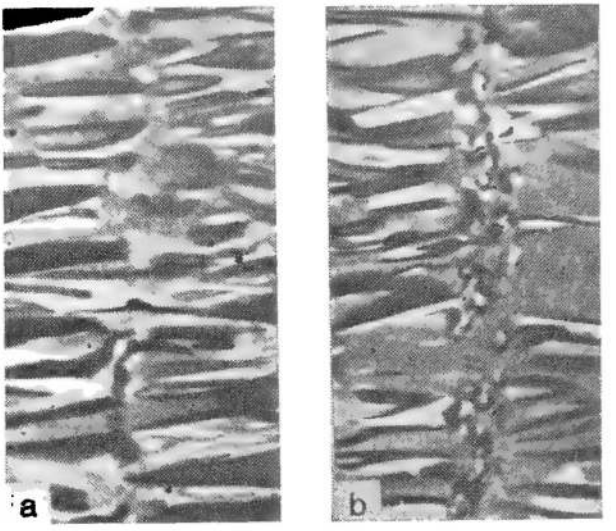

Fig. 2-11. Transcrystallization in an ingot of aluminium bronze

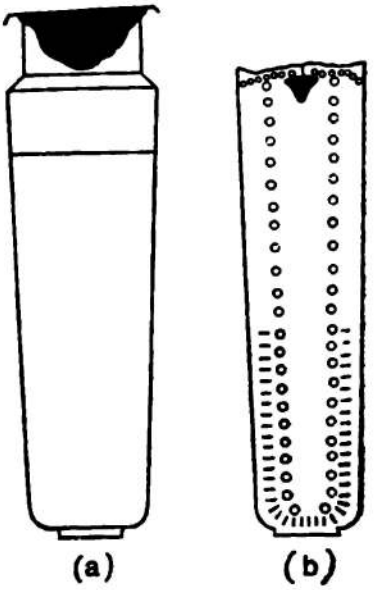

Fig. 2-12. Depth of shrinkage cavity (pipe) in (*a*) killed steel and (*b*) rimming steel

to heat removal) from a relatively small number of crystallization centres.

The third zone, *3*, is that of *equi-axed crystals*. In the central zone of a solidifying ingot, there is no definite direction for heat removal. "The temperature of solidifying metal has time to be equalized in various points and the liquid becomes pasty owing to the formation of crystal embryos in its various points. Further, the embryos develop branches in various directions and begin to interfere with one another" (D. K. Chernov). The process results in the formation of an equi-axed structure. In this zone, various tiniest inclusions which are present in molten steel have been introduced occasionally or remained undissolved (such as refractory constituents) serve as crystallization nuclei.

The relative distribution of columnar and equi-axed crystals in the volume of an ingot is of great importance.

The metal in the zone of columnar crystals is denser and has less cavities and blowholes. However, the strength of the metal at the joints of columnar crystals may be low.

A process of crystallization which results in the junction of columnar-crystal zones is called the *transcrystallization*.

The degree of development of columnar crystals may vary, depending mainly on the composition of the metal, the degree of superheating, the size of ingot, the casting speed, the shape of the mould and the thickness of its walls, and the temperature of mould walls.

These factors can affect the rate of heat removal, the temperature gradients existing in the solidifying steel, etc. An increased degree of superheating and increased rate of ingot cooling increase the content of columnar crystals and may cause complete transcrystallization, as shown in Fig. 2-11*a*; with a somewhat slower cooling, a zone of equi-axed crystals forms in the central portion of the ingot (Fig. 2-11*b*).

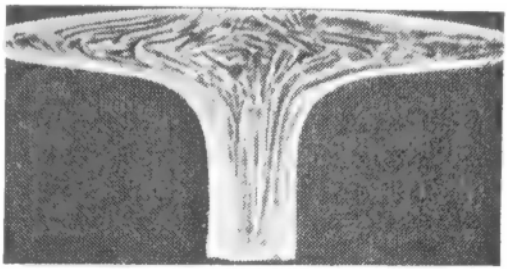

Fig. 2-13. Macrostructure of die-forged valve

A metal in the liquid state occupies a larger volume than upon solidification. A metal cast into a mould, therefore, contracts and *voids*, or *shrinkage cavities*, are formed in it; the shrinkage cavities may be either concentrated in a particular portion of the ingot or distributed over the whole volume of the ingot or in some of its portions. They may be filled with gases which are soluble in molten metal but escape during crystallization. In a well deoxidized (*killed*) steel, if cast into a hot-top mould, shrinkage cavity forms in the top portion only and there are few gas blowholes and voids in the main body of the ingot (Fig. 2-12*a*). A poorly deoxidized steel (called *rimming steel*) has numerous voids and blowholes all over the volume of the ingot (Fig. 2-12*b*).

The shape of primary crystals (dendrites) changes after hot plastic working of the metal (forging, pressing, rolling). Dendrites are stretched in the direction of metal flow and thus form *fibres*. As a result, the properties of rolled metal in the direction of rolling (along fibres) will be not the same as across fibres[1].

Figure 2-13 shows the macrostructure of a die-forged valve, where it is clearly seen that metal fibres follow the valve outline. This is the best orientation of fibres to be obtained in forged parts, if metal fibres are not cut. More precisely, it is desirable that the direction of fibres coincides with that of the principal forces acting in an operating part.

2-6. SOLID-STATE TRANSFORMATIONS. ALLOTROPY

If we proceed from geometrical considerations only, it may be said that the atoms of a given element can form any type of crystal lattice. However, a stable and hence a really existing type of lattice is only that which has the lowest free energy. For instance, lithium,

[1] The anisotropy of properties of deformed metal strongly depends on the presence of non-metallic inclusions; these may form chains along fibres of deformed metal (lineage structure).

sodium, potassium, rubidium, caesium, molybdenum, tungsten and some other metals have a body-centred cubic lattice in the solid state; aluminium, calcium, copper, silver, gold, platinum, etc., a face-centred cubic lattice; beryllium, magnesium, zirconium, hafnium, osmium and some others, a hexagonal lattice.

It has been found for some metals, however, that they change their lattice to a stabler form at variations of temperature or pressure. For instance, iron exists in b.c.c. and f.c.c. forms; cobalt may have either face-centred cubic or hexagonal lattice. Tin, manganese, titanium and some other metals can crystallize in different forms of lattice.

The existence of a metal (substance) in various crystalline forms is called *polymorphism*, or *allotropy*. The various crystalline forms of a substance are called *polymorphic*, or *allotropic modifications*.

Pressure variations that are common in engineering practice, are usually insufficient to cause polymorphic transformations. Therefore, only temperature-induced allotropy is of importance for practical metallurgy.

Table 2-2. Allotropic Forms of Metals

Metal (element)	Allotropic form	Temperature range of stable state, °C	Crystal lattice
Fe	α	< 911	B. c. c. (C8)
	γ	911-1 392	F. c. c. (C12)
	δ	1 392-1 539	B. c. c. (C8)
Co	α	< 450	Hexagonal (H12)
	β	450-1 480	F. c. c. (C12)
Sn	α	< 18	Diamond-type
	β	18-232	Body-centred tetragonal
Mn	α	< 700	Complex cubic multiatomic
	β	700-1 079	Ditto
	γ	1 079-1 143	Face-centred tetragonal
	δ	1 143-1 244	B. c. c. (C8)
Ti	α	< 882	Hexagonal (H12)
	β	882-1 660	B. c. c. (C8)
Zr	α	< 867	Hexagonal (H12)
	β	867-1 860	B. c. c. (C8)
U	α	< 668	Orthorhombic
	β	668-720	Tetragonal
	γ	720-1 132	B. c. c. (C8)

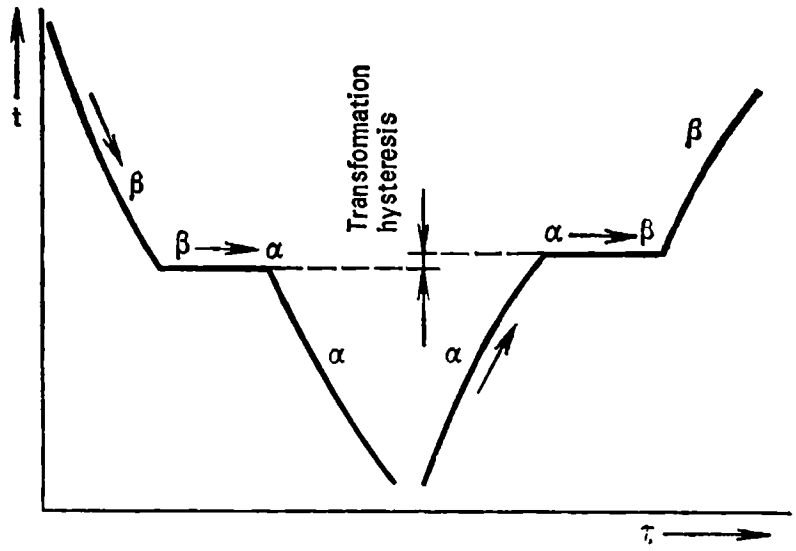

Fig. 2-14. Cooling and heating curves for a metal undergoing allotropic transformations

Table 2-2 gives the temperature ranges in which can exist the allotropic modifications of some metals of practical importance, undergoing temperature allotropy.

Allotropic forms are designated by the Greek letters: α, β, γ, etc. written as subscripts or before the symbol of an element. An allotropic form existing at the lowest temperature is designated by α, the following one by β, etc.

The transformation from one allotropic form to another during heating of pure metal occurs with absorption of heat and at a constant temperature. On a time-temperature curve, the transformation is described by a horizontal line (Fig. 2-14). A transformation in a metal being cooled occurs with evolution of heat (due to evolution of the latent heat of transformation) and theoretically takes place at the same temperature as during heating, but practically at a somewhat lower temperature because of undercooling.

The phenomenon of polymorphism is based on the general law of a stable state having the least free energy, which has been discussed earlier (Sec. 2-2).

The free energy of a system depends on temperature. This is why an α-modification should be stable in one temperature interval, β-modification, in another temperature interval, etc. The temperature at which one modification changes to another is called the *temperature of polymorphic* (allotropic) *transformation*. For instance, iron has two points of polymorphic transformations: at 911°C and 1 392°C.

New allotropic forms appear in a metal owing to nucleation and growth of crystals, i.e. similar to what occurs during crystallization

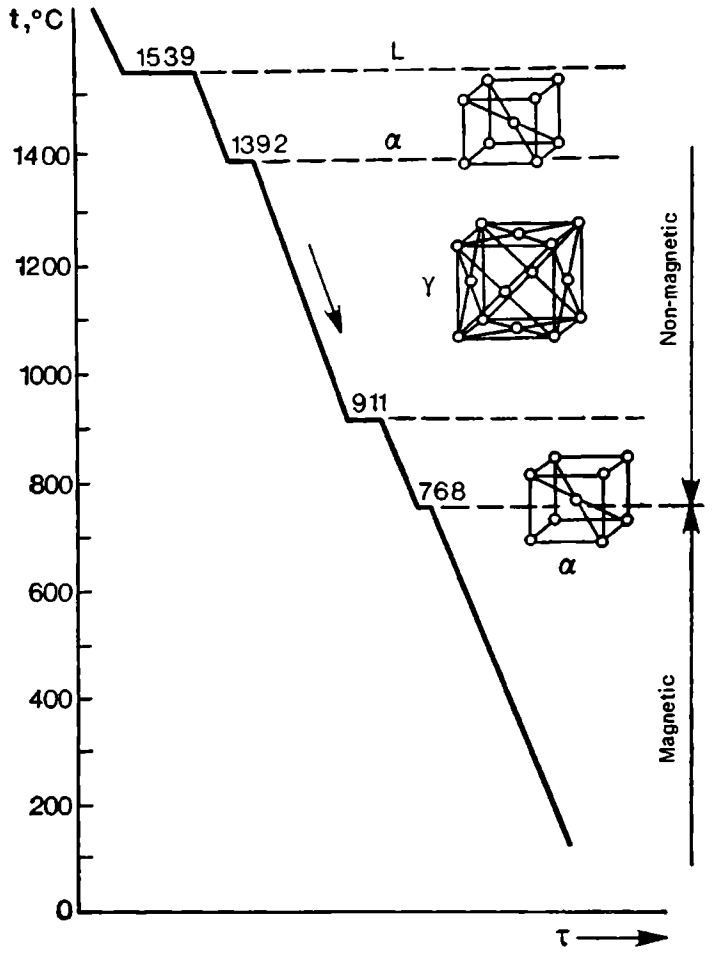

Fig. 2-15. Cooling curve for iron

from the liquid state. Curves of dependence of N and G on undercooling for allotropic transformations are essentially of the same shape as for crystallization from the liquid state (see Fig. 2-6). It should be noted that allotropic transformations in the solid state are associated with a deep undercooling.

It may be stated as a general rule that modifications existing at higher temperatures have a simpler crystal structure and a higher plasticity (E.M. Savitsky).

Allotropic transformations of various metals have certain peculiarities. *Tin.* Tin exists in two modifications. Below +18°C, it is stable as what is called *grey α-tin.* Upon cooling, α-tin appears on common *white tin* (β-modification) in the form of individual knobs on the surface (the phenomenon is called '*tin pest*'). The lattice of white tin (coordination number 6) is by 50 per cent more compact than that of grey tin, which has a diamond-like lattice with the coordination number 4. That is why white-to-grey tin transformation involves an increase in the volume roughly by 25 per cent. Grey tin is a grey

powder possessing no metallic properties. Though the equilibrium temperature of $Sn_\alpha \rightleftarrows Sn_\beta$ transformation is +18°C, the transformation at this or at a slightly lower temperature occurs at a very low speed. The maximum value of G is obtained at an undercooling $n = 50$ degrees C (i.e. at a temperature of −32°C), when the rate G of $\beta \rightarrow \alpha$ transformation is equal to 0.004 mm/h. Owing to the low rate of transformation, β-tin is very liable to undercooling and can remain stable for a long time at temperatures below 18°C.

Iron. Below 911°C, iron exists as α-modification; at 911°C; the body-centred lattice of α-Fe changes to the face-centred lattice of γ-Fe; at 1 392°C, γ-Fe changes again to the body-centred α-lattice (Fig. 2-15). The high-temperature α-modification is sometimes called δ-modification.

Thus, one and the same body-centred cubic lattice of iron is stable within two different temperature intervals. The $\gamma \rightarrow \alpha$ transformation is associated with a change to a lower coordination number and a lower compactness of the crystal lattice. If this reduction were not appreciably compensated by a decrease in atomic radius, the volume of iron upon $\gamma \rightarrow \alpha$ transformation would increase by 9 per cent. Actually (owing to the decrease in atomic radius), the volume of iron increases only by 1 per cent. It should be noted that the structural stresses caused by this insignificant growth in volume are quite appreciable.

The cooling curve of iron has an arrest at 768°C, which is associated with a change in magnetic properties, rather than with lattice rearrangement. Above 768°C, iron is non-magnetic (non-magnetic α-iron is sometimes called β-iron). Below that temperature, it is ferromagnetic.

2-7. MAGNETIC TRANSFORMATIONS

Some metals (such as, iron, cobalt, nickel) exhibit specific magnetic properties, for instance, can be magnetized. These properties are called *ferromagnetic.* However, a metal gradually loses its ferromagnetic properties on heating. As has been demonstrated by P. Curie, iron loses its ferromagnetic properties completely at a definite temperature which is since then called the *Curie point.*

As may be seen in Fig. 2-16, the intensity of magnetization gradually diminishes with increasing temperature and the Curie point corresponds to a full loss of ferromagnetism.

Magnetic transformations have some specifics which distinguish them from allotropic transformations.

Firstly, the magnetic properties gradually vanish on approaching the transformation (Curie) point, i.e. this point does not mark a jump-like change in properties. Secondly, a magnetic transformation exhibits on temperature hysteresis, i.e. an increased rate of cooling cannot lower the transformation temperature. Thirdly, the mechanical and some physical properties are not changed

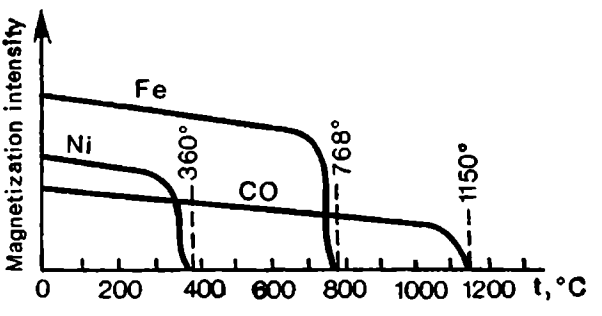

Fig. 2-16. Effect of temperature on the magnetic properties of iron, nickel, and cobalt

on magnetic transformation (though many of the electrical, magnetic and thermal properties are changed). Finally, and what is the most important: a magnetic transformation is not associated with recrystallization, i.e. the formation of new grains or lattice rearrangement.

In these peculiarities, magnetic transformations substantially differ from allotropic ones.

Allotropic transformations are typically associated with crystal lattice rearrangement, recrystallization, and temperature hysteresis. None of these phenomena is observed in magnetic transformations. Therefore, magnetic transformation is a special type of transformation which fundamentally differs from allotropic transformation.

By modern views, magnetic transformations involve changes in the interaction of outer and inner electron shells of atoms. without changes in the crystal structure of metal.

LITERATURE

Steinberg S. S., *Lectures on Physical Metallurgy*. Moscow, GNTI, 1931 (in Russian).

Tamman G., *Lehrbuch der Metallkunde*. Chemie und Physik der Metalle und ihrer Legierungen. Leipzig, 1932.

Chernov D. K., *The Science of Metals*. Ed. by N. T. Gudtsov. Moscow-Leningrad, "Metallurgizdat", 1950 (in Russian).

Umansky Ya. S., Blanter M. S., Finkelstein B. N., *Physical Metallurgy*. Moscow, "Metallurgizdat", 1955 (in Russian).

Bochvar A. A., *Physical Metallurgy*. Moscow, "Metallurgizdat". 1956 (in Russian).

Steinberg S. S., *Physical Metallurgy*. Ed. by I. N. Bogachev and V. D. Sadovsky. Sverdlovsk, GNTI, 1961 (in Russian).

Chalmers B., *Physical Metallurgy*. New York, Wiley, 1960.

Livshits B. G., *Metallography*. Moscow, "Metallurgiya", 1971 (in Russian).

Chapter 3

MECHANICAL PROPERTIES. STRAIN HARDENING AND RECRYSTALLIZATION

3-1. METALS AND NON-METALS

Among numerous properties possessed by materials, their mechanical properties, in the majority of cases, are the most essential and, therefore, they will be given much consideration in the book.

All critical parts and elements, of which a high reliability is required, are made of metals, rather than of glass, plastics or stone.

As has been given in Sec. 1-1, metals are characterized by the metallic bond, where positive ions occupy the sites of the crystal lattice and are surrounded by electron gas.

All non-metals have an ionic or a covalent bond. These types of bond are rigid and are due to electrostatic attraction of two ions of unlike charges.

Because of the metallic bond, metals are capable of plastic deformation and self-strengthening upon plastic deformation. Therefore, if there is a defect in a material or if the shape of an element is such that there are stress concentrators, the stresses in these points may attain a great value and even cause cracking. But since the plasticity of the material is high, the metal is deformed plastically in that point, say, at the tip of a crack, undergoes strengthening, and the process of fracture comes to an arrest.

This does not occur in non-metals. They are uncapable of plastic deformation and self-strengthening, therefore, fracture will occur as soon as the stresses at the tip of a defect exceed a definite value.

These facts explain why metals are reliable structural materials and cannot be excelled by non-metallic materials.

3-2. ELASTIC AND PLASTIC DEFORMATIONS. LATTICE IMPERFECTIONS AND STRENGTH OF METALS

A stress applied to a material causes a deformation, or strain.

The deformation may be either *elastic*, which disappears upon removal of the load, or *plastic*, which remains in tbe material even after the stress has been removed.

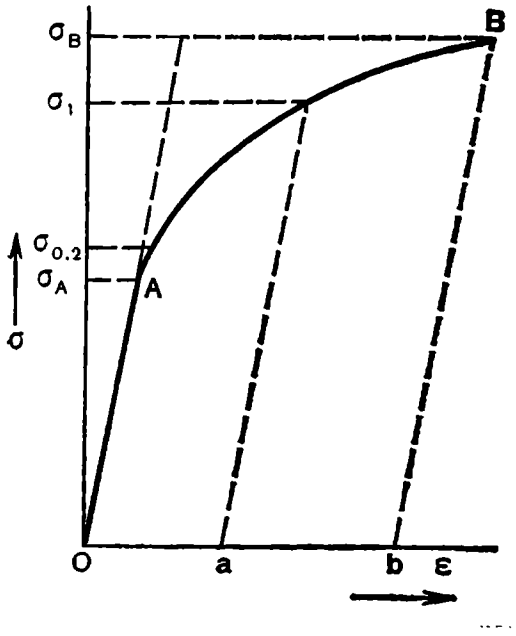

Fig. 3-1. Stress-strain curve

Any stress applied, be it whatever small, causes a deformation. The initial deformations are always elastic and their magnitude is directly dependent on the magnitude of stress.

On the curve shown in Fig. 3-1, elastic deformation is described by line *OA* and its extension (dashed line).

Above point *A*, the proportionality between stress and strain is disturbed. A stress then causes both an elastic and a residual, or plastic, deformation.

Plastic and elastic deformations have been defined above conventionally, but there is a deep physical difference between them.

With elastic deformation, an external force changes the distances between atoms in the crystal lattice. Removal of the load eliminates the cause for changing the interatomic distances, the atoms return to their places, and the deformation disappears.

Plastic deformation is a different and much more complicated process.

With plastic deformation, a portion of a crystal is displaced (sheared) relative to the other portion. If the load is removed, the displaced portion of the crystal will not return to its initial place and the deformation will retain. These displacements can be detected by microstructural analysis, as shown, for instance, in Fig. 3.2.

Besides, plastic deformation is associated with disintegration of mosaic blocks within metal grains and, at appreciable strains, there also may be a noticeable change in the shape of grains and their positions in space, with cracks sometimes appearing between grains (sometimes within them).

It is then clear that the difference between elastic and plastic deformations is quite essential.

The curve *OAB* in Fig. 3-1, which relates the applied external stress (σ) and the relative deformation (ε), characterizes the mechanical properties of a metal:

(a) the slope of the straight line *OA* characterizes the stiffness of the metal, i.e. how an external load can change interatomic distances, which in the first approximation characterizes interatomic attraction forces. The tangent of the straight line *OA* is proportional to the modulus of elasticity (*E*), which is numerically equal to the

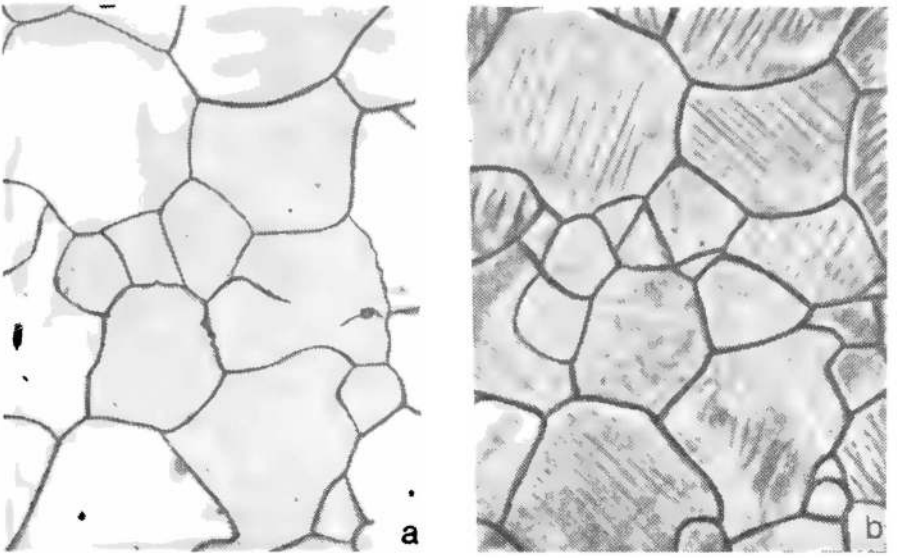

Fig. 3-2. Changes in the structure of iron upon plastic deformation (Rosenhein), ×100

(*a*) prior to deformation; (*b*) upon deformation

quotient of the stress by the relative elastic deformation ($E = \sigma/\varepsilon$); the stress σ_A corresponds to the moment when plastic deformation first appears. The position of point A depends on the accuracy of measurements, being lower when more accurate methods are employed. In engineering measurements, use is commonly made of what is called the *yield limit*, $\sigma_{0.2}$, which is the stress that causes a residual deformation of 0.2 per cent of the length or other size of a specimen or article;

(b) the maximum stress σ_t is the highest stress attained in tension.

The plastic deformation prior to fracture, which is determined as the relative change in the length (or cross-sectional area) of a specimen and expressed as (*relative*) *extension*, or *elongation* δ (or, respectively, relative contraction, or reduction ψ) characterizes the plasticity of a metal; the area under the curve OAB is proportional to work that should be spent to fracture the metal. This parameter, which may be determined by various methods (mainly by impact tests of notched specimens), characterizes the *toughness* of a metal.

Stress-strain curves (see Fig. 3-1) can be different in shape, depending on many factors: the nature of the material being tested, the stressed state, the rate and temperature of the test. Their analysis may provide valuable information. Some typical forms of stress-strain curves (in tension) are shown in Fig. 3-3.

Some soft metals show a *knee* (or *tooth*) on the stress-strain curve (Fig. 3-3*a*). A distinction is made between *physical yield limit* σ_y (when there is a knee on the curve) and *conditional yield limit* $\sigma_{0.2}$ (when there is no knee).

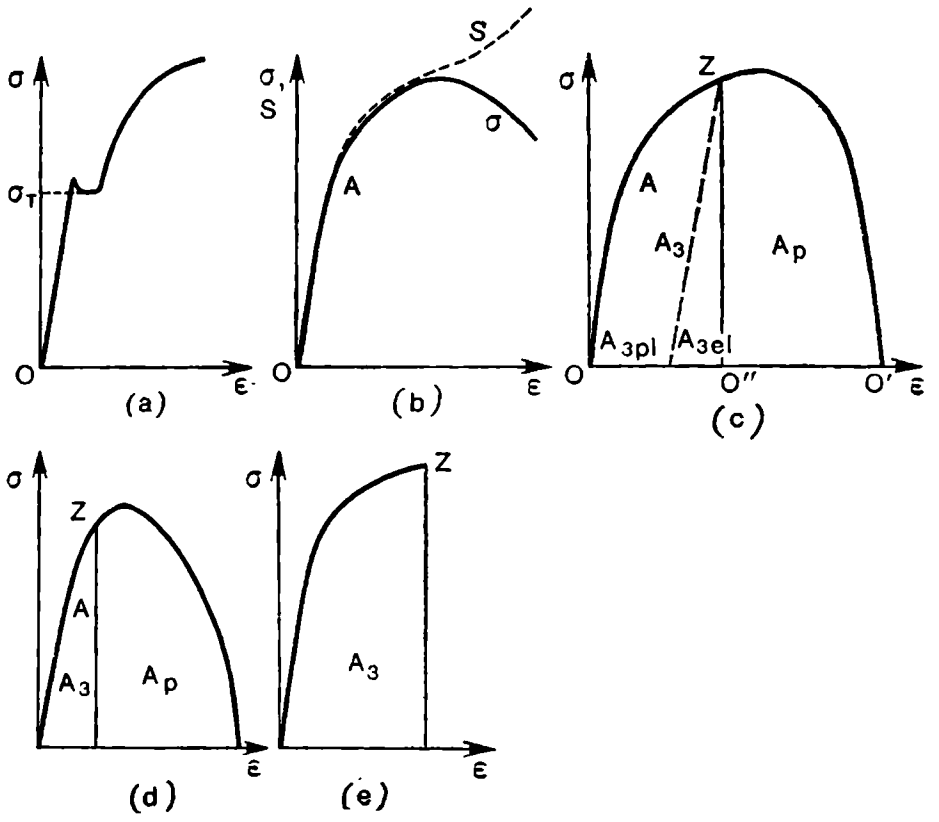

Fig. 3-3. Typical forms of stress-strain curves

The appearance of a local contraction (*necking*) in a tensioned specimen results in a lower conditional stress, $\sigma = P/F_0$ (where F_0 is the initial cross-sectional area of necking), see the solid line in Fig. 3-3*b*, and a higher actual stress $S = P/F_x$ (where F_x is the cross-sectional area of the specimen at the given moment), see the dashed line in Fig. 3-3*b*. The highest point on a σ-ε curve is called the instantaneous strength, or more frequently now, the *ultimate strength* σ_t.

The whole curve from *O* to *O'* can be divided into two sections by point *Z* (Fig. 3-3*c*) which characterizes the moment when a crack appears in the specimen. This crack can develop until fracture, i.e. separation of the specimen into two portions.

Since the area under the curve *OZO'* is proportional to the work of fracture, the area *OZO''* should be proportional to the work required for initiation of a crack (the *work of crack initiation* A_{in}[1]) and

[1] The work of crack initiation is equal to the work of plastic deformation $A_{in.pl}$ plus the work of elastic deformation $A_{in.el}$. The latter is usually small owing to the steep course of the curve *OA*, which is due to the high value of elastic modulus of metals.

the area $O''ZO'$ is the work required to propagate the crack over the whole cross-section of the specimen (the *work of crack propagation* A_p). Thus, the total work is $A_{tot} = A_{in} + A_p$.

Two principally different cases are possible in the behaviour of metals upon passing the Z point. If a certain work is needed to propagate a crack upon its initiation, we have a case of *plastic*, or *ductile*, *fracture* which is characterized by a typical form of the fractured surfaces (see Fig. 1·23*a*) and also by that $A_p \gg 0$ (Fig. 3-3*d*). If, however, the curve is discontinuous at point Z and $A_p \approx 0$, we have what is called *brittle fracture* (Fig. 3-3*e* and Fig. 1·23*c*). An intermediate case is also possible, i.e. when first ductile fracture occurs and then brittle fracture[1].

A stress-strain diagram determines only the strength characteristics (σ_t and $\sigma_{0.2}$). The modulus of normal elasticity (the tangent of curve OA) in such a diagram is appreciably lower than the actual value, since the recorder fixes also the elastic deformations of the elements of the test machine. In order to determine the actual modulus of elasticity, strain gauges are attached to the test specimen; they make it possible to measure very small deformations and thus to plot accurately the OA section of the curve. For the same reasons, the deformation characteristics (δ and ψ) of the material are determined by measuring the specimen before and after the test, rather than by using the diagram.

For some reasons, the area under the curve OAB (see Fig. 3-1) does not precisely correspond to the work of fracture and is not calculated in tensile tests.

The work of fracture and its components (the work of crack initiation and crack propagation) are determined in bending tests (usually by impact tests of notched specimens), which will be discussed in more detail later in the book.

Methods of mechanical tests will be described in a separate section of this chapter.

Let us now consider the mechanisms of elastic and plastic deformations.

Elastic deformation is a change in interatomic distances caused by external forces. Therefore, the stress that causes elastic deformation is also a change in interatomic distances and can be measured by X-ray methods. Evidently, the displaced atoms will return to their places as soon as the stress is removed. In other words, elastic deformation causes no irreversible changes in the material. The smaller the strain caused by a given stress applied, the stiffer is the material. Consequently, the modulus of elasticity characterizes the stiffness of a material. A distinction is made between the *modulus of normal elasticity* (Young's modulus) and the *elastic shear modulus* (Hooke's modulus). In the former case the forces tend to separate atoms from one another and in the latter case, to displace them. Hooke's modulus (E) is 2.5-3 times the Young modulus (G). For iron, in particular, $E = 2 \cdot 10^4$ kgf/mm^2 and $G = 0.8 \cdot 10^4$ kgf/mm^2.

[1] Since it is difficult to accurately determine the position of point Z in tension, our considerations are mainly of a theoretical, rather than applied, nature.

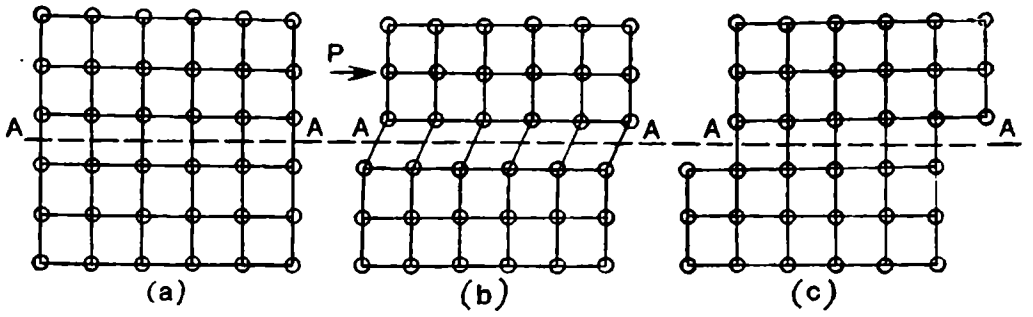

Fig. 3-4. Plastic shear in an ideal crystal lattice (schematically)

The elastic moduli are determined by the forces of atomic interaction and are constants of a material. For instance, the normal elastic modulus for aluminium is $0.8 \cdot 10^4$ kgf/mm^2; for iron, it is $2 \cdot 10^4$ kgf/mm^2, and for molybdenum, $3 \cdot 10^4$ kgf/mm^2. Among all materials, rubber is the least stiff ($E = 0.00007 \cdot 10^4$ kgf/mm^2) and diamond, the stiffest ($E = 12 \cdot 10^4$ kgf/mm^2). This mechanical characteristic is structure insensitive, i.e. the modulus of elasticity can be changed neither by heat treatment nor by other methods which change the structure of a material[1].

On the other hand, an increase in temperature, which changes (increases) the interatomic distances, changes (lowers) the modulus of elasticity.

All other mechanical properties, except for the modulus of elasticity, are structure sensitive and can be changed by heat treatment (which changes the structure) within quite wide limits; this problem will be discussed in more detail later in the book.

As has been noted, plastic deformation is a process of shear of part of a crystal relative to another part. What is then the mechanism of plastic shear?

It is natural to suppose that the process should occur as shown in Fig. 3-4, i.e. all the atoms of the crystal portion above the slip plane AA are displaced simultaneously by a force P from position a successively into positions b and c. The force (σ_{sh}) to be applied to effect this shear can be found theoretically.

The calculation has been done by Ya. I. Frenkel in 1920's and the formula derived by him is

$$\sigma_{sh} = \frac{a}{b} \frac{G}{2\pi}$$

[1] It has been agreed to distinguish between *structure sensitive* and *structure insensitive* properties of materials. The former are dependent on and the latter are independent of structure. This division is only conditional, since all the properties (including the modulus of elasticity) are more or less dependent on structure. Structure insensitive properties are those which practically do not depend on structure; heat treatment should not be used in order to change them.

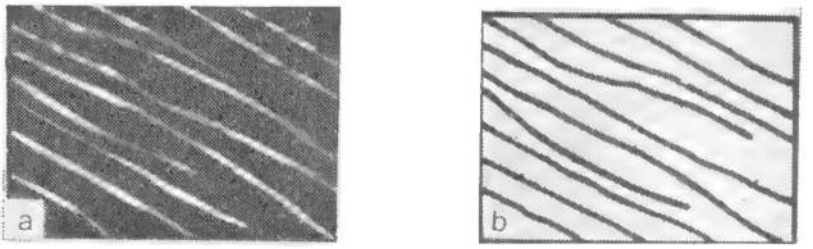

Fig. 3-5. Linear defects in a crystal lattice
(*a*) electron micrograph; (*b*) schematically (D. Mentor)

where G is Hooke's modulus; a is the interatomic distance in the direction of slip (AA in Fig. 3-4); and b is the distance between slip planes.

For close-packed metallic lattices, the fraction a/b is close to unity. Hence, the theoretical force (*theoretical strength*) to effect shear (plastic deformation) is roughly one-sixth of the shear modulus. For iron, the theoretical yield limit should be 1 300 kgf/mm^2, whereas for soft iron it is actually about 15 kgf/mm^2, i.e. roughly one-hundredth.

This difference is so striking that Frenkel's equation and the concept of theoretical strength were considered to be erroneous. The discrepancy has been explained only after the theory of dislocations was developed by G. I. Taylor, E. Orowan, and M. Polanyi.

In Chapter 1, dislocations have been considered as real defects existing in real crystals. Now their existence is disclaimed by nobody, but the problem was much disputed in 1930-50's.

Thus, dislocations were first (in 1920's) invented to explain the discrepancies between the theoretical and actual strength of metals; in 1950's, upon appearance of the electron microscope, they have been discovered metallographically; for instance, Fig. 3-5 shows probably the first electron-microscopic photograph of an extraplane whose edge is a dislocation.

The electron (and optical) microscope more often discloses not a dislocation proper, but its end on a surface, which is seen as a dot (or stroke) surrounded (or, as it is said, decorated) by various defects and impurity atoms, and the end of dislocation on the microsection surface is etched (Fig. 3-6). Thus, the metallographic method has given an evidence that dislocations really exist.

The theory of dislocations, which explained the cause of the low strength of real metals, has been generally recognized only when dislocationless crystals, or so-called whiskers, were obtained. It has turned out that the strength of dislocationless crystals is very close to the theoretical value.

Now, consider a different (dislocation) mechanism of plastic deformation. A simplified diagram of shear caused by a dislocation is shown in Fig. 3-7.

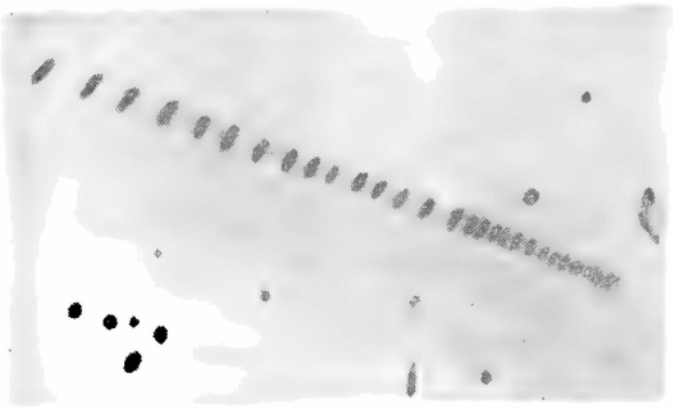

Fig. 3-6. Dislocation pile-up at obstacles

A dislocation (denoted by a sign $\perp$) is moved to the right by force P only owing to the fact that the 'neighbourship' of atoms at both sides of plane AA is being changed. At last, the dislocation will move onto the surface of the crystal (grain boundary or mosaic block) and disappear as shown in Fig. 3-7*c*. The process described occurs much more easily, i.e. at an appreciably lower stress than the simultaneous displacement of all the atoms (see Fig. 3-4), so that plastic deformations actually occur only in this way.

This mechanism of plastic deformation suggests a conclusion that the process of shear in a crystal can take place more easily at a greater number of dislocations in the metal. In a metal free of dislocations, shear is only possible due to simultaneous displacement of a large portion of a crystal, or after new dislocations have formed under the action of elastic deformation. In cases when dislocations are not formed under the action of stresses, the strength of a dislocationless metal should be equal to the theoretical strength.

There exists a different method for strengthening metals. It has turned out that the real strength of metals drops with increasing number of dislocations only at the initial stage. Upon reaching the minimum value at a definite dislocation density, the real strength

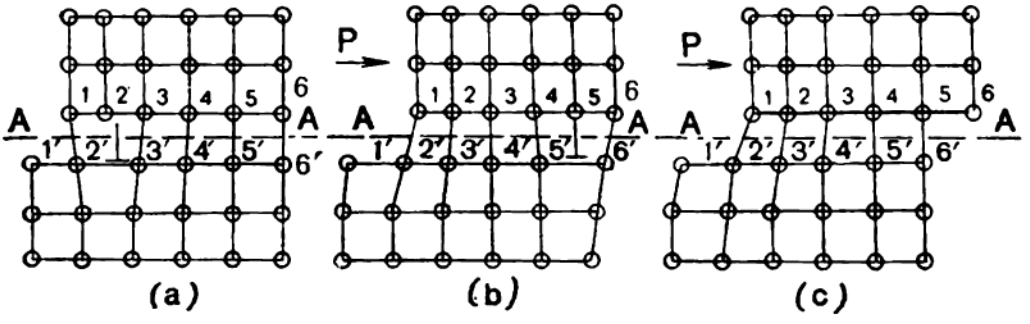

Fig. 3-7. Dislocation diagram of plastic shear

increases again. This type of relationship between the real strength and dislocation density (or other imperfections) is schematically shown in Fig. 3-8. The increase in the real strength with increasing dislocation density may be attributed to the appearance of dislocations in different planes and directions (see Fig. 1-10) and not only of mutually parallel dislocations. These differently oriented dislocations will interfere with one another in their movement and the real strength of the metal will increase.

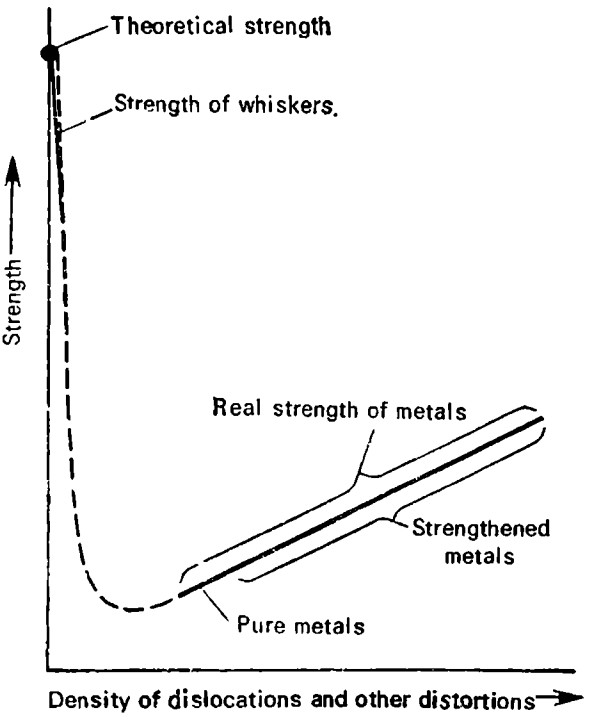

Fig. 3-8. Effect of lattice distortions on the strength of a crystal (according to I. A. Oding and A. A. Bochvar)

Methods for metal strengthening, which are based on increasing the dislocation density, have been known for a long time; these include mechanical strain hardening, refinement of grains and mosaic blocks, heat treatment. Besides, the known methods of alloying (i.e. introducing foreign atoms into the metal lattice), which form various imperfections and distortions of the crystal lattice, are also intended to form obstacles to free movement of dislocations (locking of dislocations). They also include the methods of forming structures with what is called strengthening phases which cause precipitation hardening. All these methods will be discussed in more detail later in the book. In all these methods, however, the strength of metals does not reach the theoretical value. Consequently, the presence of dislocations in a real metal crystal is responsible for the strength of the metal being lower than the theoretical value, but at the same time the metal acquires the capability of plastic deformation.

Is it reasonable in that connection to regard the capability of a metal for plastic deformation as its defect?

Experience shows that the capability of real metals for plastic deformation is the most important and valuable property. It is utilized in various technological processes: wire drawing, bending, upsetting, drawing, stamping, etc. It is of great importance for ensuring the structural strength or reliability of metal structures, machine elements and other metal articles. Experience shows also that if a met-

al is in brittle state, i.e. its capability of plastic deformation is low, it may undergo sudden brittle fracture in structures, in some cases even at reduced loads.

3-3. FRACTURE

It follows from the foregoing that a metal, as a structural material, must have a high resistance to deformation (to elastic deformation which is characterized by the moduli E and G, and to plastic deformation characterized by the yield limit $\sigma_{0.2}$ and ultimate strength σ_t), and a high resistance to fracture.

Today, the resistance to deformation is combined into a complex concept of *strength* and the resistance to fracture, into a concept of *reliability.*

Note that if fracture occurs not at once, but after many acts of loading, each of the acts causing a microfracture[1], the reliability of a material is characterized by the concept of *durability.*

A high-quality structural material should evidently have a high strength, high reliability, and high durability.

How does then fracture occur?

As soon as the stress applied exceeds the yield limit, it causes plastic deformation, i.e. causes the dislocations to move. If there are no obstacles for free movement of dislocations and no new dislocations are formed in the course of deformation, the strain may be whatever great. A tensioned specimen may become tens or hundreds of times longer and resemble wire. This is observed in particular cases (at definite temperatures and definite rates of deformation of certain metals) and is called superplasticity. Naturally, a specimen may elongate in this way only if no local necking forms in it. If a necking forms, deformation is localized at that point and the specimen will break into two pieces, but only after it has contracted in the necking to zero. This is not an infrequent case (Fig. 3-9).

[1] This case covers the processes of gradual fracture, such as wear, fatigue, corrosion, or creep.

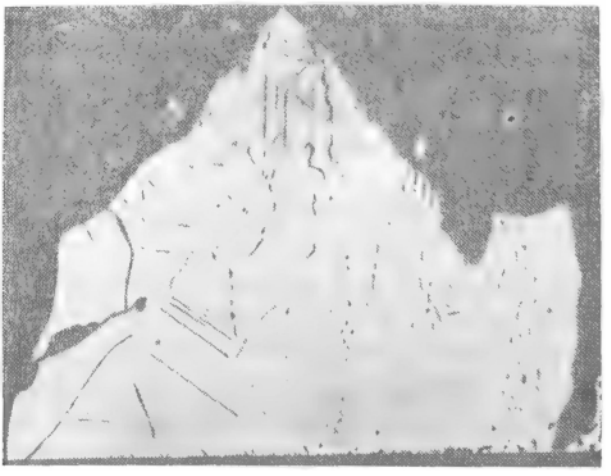

Fig. 3-9. Localized necking on tensioning to zero ($\psi = -100\%$)

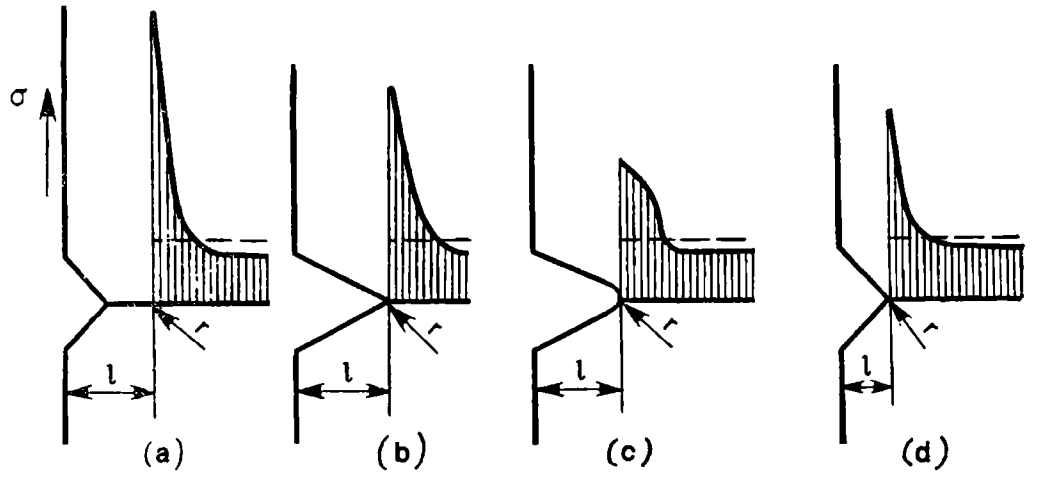

Fig. 3-10. Stress concentration at the tip of a defect. Stress concentrators
(*a*) crack; (*b*), (*d*) sharp notches; (c) 'blunt' notch. Dashed lines show the mean stress σ_m

Therefore, superplasticity can be observed when the plasticity of metal is not decreased in deformation[1] and no necking is formed.

Superplasticity should be understood as the capacity of a metal to uniform plastic deformation without strain hardening. Superplasticity can manifest itself in the following cases:

(a) with a slow deformation of fine-grained materials (alloys) at high temperatures (approximately at 0.7-0.8 of the absolute melting point);

(b) at temperatures near (slightly lower than) the temperature of phase transformations; for instance, at 680-720°C in steel (at temperatures above 720°C, a transformation occurs in steel, see Ch. 6), but not at the temperature of the transformation proper as is sometimes stated in the literature; the plasticity drops abruptly during diffusion-type phase transformations;

(c) at the moment of shear (martensitic) transformations, see Sec. 10-4.

Using the effect of superplasticity, metal can be deformed appreciably without much effort. Superplasticity can, however, take place within a relatively narrow temperature range. For that reason forging under conditions of superplasticity is called in practice isothermal forging, since the dies and material are maintained at a strictly definite temperature.

Nevertheless, this type of ultimate plasticity is typical of very soft pure metals.

In most cases, dislocations are not very mobile, and some of them pile up near certain insuperable obstacles (inclusions, grain boundaries) during the process of deformation.

Piling-up of dislocations may form a discontinuity, i.e. a crack. Such an initial crack is, in itself, an obstacle for movement of dislocations, so that a further piling-up of dislocations (i.e. further plastic deformation) will result in its growth.

Structure defects and discontinuities represent stress concentrators, i.e. the stresses at the edge of a defect may appreciably differ from the mean stress, as shown in Fig. 3-10.

The sharper and longer the defect (compare (*a*) and (*c*), (*b*) and (*d*) in Fig. 3-10) the higher the stress concentration (K), which may be expressed by

[1] There is no strain hardening. For strain hardening, refer to Sec. 3.5.

the formula:

$$K = 2\sqrt{l/r}$$

where l is the half-length of a defect and r is the radius of rounding-off at the tip of the defect.

The value of r may be very small, i.e. a crack may be very sharp, but it cannot be less than 1 angstrom, i.e. the diameter of an atom; it should be assumed that the minimal radius of cracks is around 10 Å. For cracks of this sharpness and various length, the stress concentration K is

l, mm	1	0.1	0.01
K	60	20	6

This means that if a crack of this ultimate sharpness has grown up to 1 mm in length, the stress at its tip is 6 000 times the mean stress.

Taking that the theoretical tensile strength is $\sigma_{th} = E/10 = 2\,100$ kgf/mm² and the mean stress only 10 kgf/mm², the stress at the tip of a crack ($l = 0.1$ mm) will be equal to the theoretical strength and a fracture will occur through separation of some atomic layers from others. The avalanche process of fracture will proceed until the crack separates the metal into two or more pieces, since, as follows from the above equation, the stress required for fracture diminishes with the propagation of a crack.

It follows from the fracture mechanism described that the formation and propagation of a crack to the *critical length* (i.e. the length at which the stress at the tip of crack is equal to the theoretical strength) takes place owing to dislocation movement, whereas crack propagation (above the critical length) occurs without plastic deformation.

This mechanism characterizes what is called *brittle fracture*. Brittle fracture is preceded with plastic deformation until the crack reaches the critical size; after that, brittle dislocationless fracture occurs.

Brittle fracture is a spontaneous process; the energy accumulated in the system sustains the avalanche process of brittle fracture and the expenditure of energy to form new surfaces is less than the elastic energy freed in the process. As has been established by A. A. Griffith there exists a certain critical crack length (let it be called the first critical length and denoted l_{in}) at which crack grows spontaneously and with a decrease of energy in the system. As has been said earlier, a crack can propagate under favourable energy conditions (decreasing energy of the system) and, in addition, after the stress at its tip has reached a definite value, which occurs at the second critical length l_s. Since cracks in metals are not ultimately sharp and $l_s \gg l_{in}$, the brittle strength is determined by the second critical length of a defect; a different picture is found in glass, where $l_s = l_{in}$, or the difference between them is not so large. Thus, there is only a quantitative, but not basic, difference between brittle fracture in glass and metals.

An important, and even principal, aspect of the mechanism of brittle fracture in metals is that the stress at the tip of a crack attains the theoretical strength. This condition can be fulfilled if the propagating crack remains always sharp. If, however, the crack expands and the radius at its tip increases, i.e. both l and r increase and the l/r ratio decreases, ever greater stress will be needed for crack propagation. In that case the crack will never reach the critical size, though it may propagate over the whole cross-section. This type of fracture is called ductile.

What are the principal characteristics of brittle and ductile fracture?

A sharp, often branched-off crack propagating at a high speed and with no plastic deformation is typical of brittle fracture (Fig. 3-11*a*). The crack proceeds owing to the elastic energy accumulated in the system.

Ductile fracture can be characterized by a blunt widening crack (Fig. 3-11*b*) propagating at a low speed and at an appreciable plastic deformation in the metal.

The type of fracture (either brittle or ductile) is determined by fractographic analysis, i.e. by studying the shape of fractured surfaces.

The two types of fracture—ductile 'fibrous' and brittle 'crystalline'—have been shown in Fig. 1-22. The first type of fracture attests that an appreciable work has been spent and that the metal has an appropriate reliability; with the second type, the fracture occurs almost instantaneously and without much work spent, and the metal is unreliable.

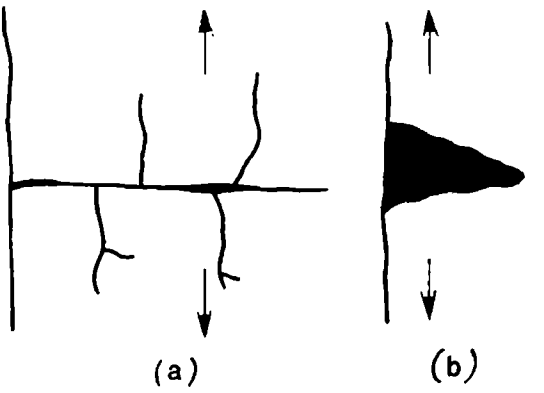

Fig. 3-11. (*a*) brittle and (*b*) ductile cracks

With electron microscopic analysis, ductile fracture has a typical cup-shaped pattern of fractured surfaces (Fig. 1-23). Cup-shaped fracture is the result of the plastic deformation caused by running of a blunt crack. Brittle fracture has a typical river pattern, with plane facets being formed by ruptured crystals.

We have considered the two extreme cases. Actually, neither truly brittle, not truly ductile fracture occurs in metals. Ductile fracture may have traces of brittle fracture (ductile fracture occurs through the formation of pores, but the bridges between pores may undergo brittle fracture, Fig. 3-13). Brittle fracture may have some traces of plastic deformation (jump-over from one rupture plane to another, Fig. 3-12). Therefore, when we speak about ductile or brittle fracture in metals, this means that one of the two fracture mechanisms clearly prevails.

Cases of mixed type of fracture are very frequent. The proportion of each type of fracture can be determined by fractography. For instance, if fibrous fracture occupies 30 per cent of the cross-section of a specimen ($B = 30\%$,) it means that 30 per cent of the cross-section has undergone ductile fracture and 70 per cent, brittle fracture.

The type of fracture depends on many factors: the composition and structural state of the metal, stressing conditions, and especially on temperature.

Many metals, especially those with b.c.c. or c.p.h. lattice, change the fracture mechanism at definite temperatures, i.e. undergo ductile fracture at higher temperature and brittle fracture at lower temperatures.

The temperature interval within which one type of fracture changes for another is called the *ductile-to-brittle transition temperature range.*

As has been noted, ductile fracture is characterized by a fibrous (cup-shaped) pattern and a definite work of crack propagation, whereas brittle fracture has a crystalline (river) pattern and practically zero work of crack propagation.

Consequently, the ductile-to-brittle transition can be characterized by a temperature interval within which the percentage of fibrous fracture changes from 100 per cent to zero (or the work of crack propagation a_γ changes from

Fig. 3-12. Scheme of brittle fracture (section perpendicular to the fracture surface)

Fig. 3-13. Scheme of ductile fracture

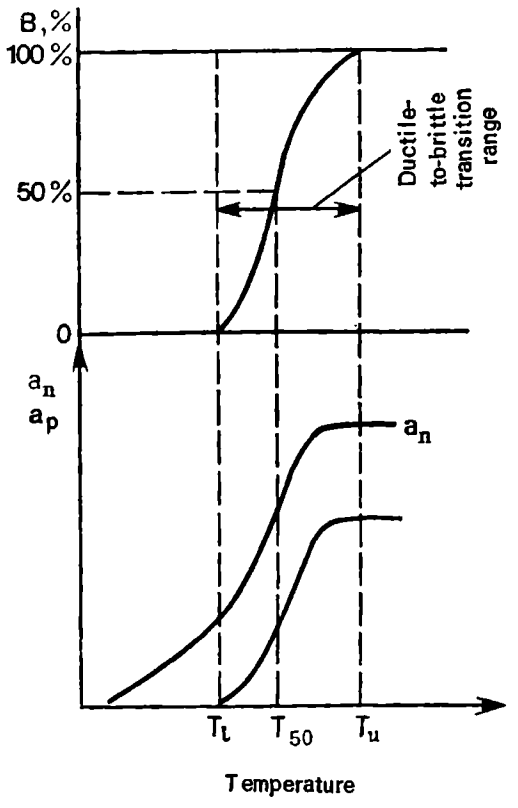

Fig. 3-14. Serial curve

a definite value to zero, Fig. 3-14). A curve like that shown in Fig. 3-14 is called a *serial curve*, since a series of tests at various temperatures is needed to construct it. The ductile-to-brittle transition can evidently be characterized by two temperatures: T_u (above which the fracture is fully ductile) and T_l (below which the fracture is fully brittle and $a_p = 0$).

The ductile-to-brittle transition can also be characterized by a single temperature T_{50}—a temperature at which 50 per cent of a fracture cross-section is fibrous and the work of crack propagation has diminished to one-half of the initial value.

The position of the ductile-to-brittle transition range depends on many factors: (1) the structure and size of grains; in particular, grain refinement lowers it; (2) the composition of the metal; many impurities have an adverse effect on the ductile-to-brittle transition temperature; (3) the rate of deformation; the ductile-to-brittle transition temperature increases at higher rates of deformation; (4) the size of a specimen (part); the ductile-to-brittle transition temperature is higher in specimens of larger cross-sectional area.

It should be noted here that notches (stress concentrators) have no effect on the ductile-to-brittle transition temperature, which may be explained by the fact that a crack first appears at the tip of a notch and, irrespective of the initial concentrator, the stressed state becomes the same all over the cross-section (though it has been essentially different before the appearance of the crack).

As has been said, reliable structural materials are those in which the work of crack propagation is not zero. Therefore, no metal should be used in critical applications at temperatures below its T_l point. A better choice is to employ a material whose T_u point is below the operating temperature. The difference between the operating temperature and T_{50} (since a certain percentage of brittle fracture is tolerable in many cases) may be called the *ductility margin*.

The ductility margin cannot be equal to zero, since certain circumstances during the operation of the material may impair the ductility (increase the ductile-to-brittle transition temperature), i.e. cause embrittlement of the material. In that connection, the position of the ductile-to-brittle transition temperature characterizes the *brittle fracture resistance*. At a lower position of that temperature, the material is more reliable, since the effect of embrittling factors may be insufficient to make it prone to brittle fracture.

A material can be unreliable even above the ductile-to-brittle transition temperature if its work of crack propagation a_p is low in magnitude. It is, therefore, reasonable to increase this characteristic, which determines the resistance to ductile fracture. The magnitude of a_p depends mainly on the level of strength, i.e. is lower at a higher strength (higher values of σ_t and $\sigma_{0.2}$), though some unestablished factors may also be of importance.

It should then be clear that the development of materials of high strength (high values of σ_t and $\sigma_{0.2}$) and high reliability (low position of T_u and T_l and high value of a_p) is an extremely complicated problem.

The ductile-to-brittle transition temperature and the work of crack propagation (and initiation) are determined by impact tests (see the next section), but the values provided by these tests (T_u, T_l, T_{50}, a_p, etc.) cannot be used in strength calculations (in this respect, these values differ from the yield limit and ultimate strength). These characteristics of reliability are easy to be determined. Knowing them, we can decide which of two (or more) materials is better, more reliable, but we cannot use them to design a metal part and determine its dimensions by calculation.

This problem, i.e. the development of characteristics (parameters) of discontinuous materials, which could be used in strength calculations, has been solved recently. Studies of the processes of fracture with a wide mathematical generalization have resulted in a new branch of science—fracture mechanics.

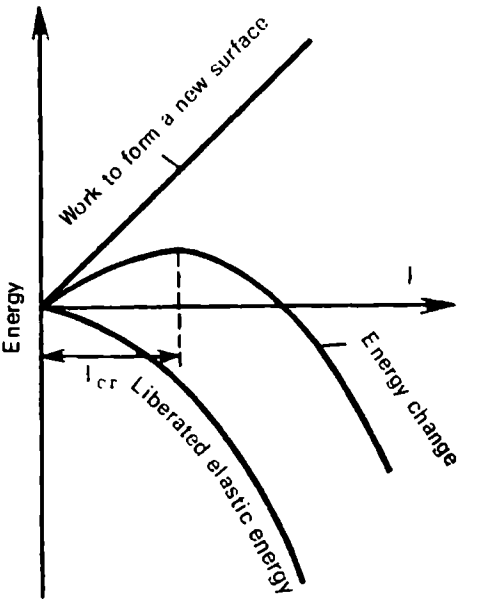

Fig. 3-15. Variation of energy during propagation of a crack (A. Griffith)

The new trend has been initiated by the works of A. A. Griffith (1920's) who has shown that fracture of high-strength materials is due to cracks or similar defects existing in the body, which determine the whole process of fracture. As has been indicated earlier, the stress concentration at the tip of a defect is directly proportional to the square root of the length-to-radius of curvature ratio of that defect. If the stress at the tip of a defect has reached the theoretical strength, brittle fracture occurs and the crack increases in length. This local fracture at the tip of a crack can change to a spontaneous fracture process if the loss in the elastic energy due to crack propagation exceeds the work required to form new surfaces, i.e. the surface energy should be lower than the elastic energy that is freed in the process. This is possible when the length of a crack has reached the critical size (Fig. 3-15).

The force G required to move a crack by 1 cm is in its sense and dimension (kgf/cm or kgf·m/cm^2) analogous to the work of crack propagation (a_p, kgf·m/cm^2). Calculations give the following relationship:

$$G = \pi l \sigma^2 / E$$

where σ is the mean stress.

G reaches its critical value (G_{cr}) when the product (the length of crack times the square of the stress) becomes critical, since the π/E ratio is a constant for a given material.

Thus, the relationship for G links together the stress applied (σ) and the length of the defect (l), which determine the reliability (i.e. fracture resistance) of a material.

A mathematical interpretation of G is what is called the stress intensity K, which is more convenient than G for experimental determination and use in strength calculations:

$$G = K^2/E \quad \text{or} \quad K = \sqrt{GE} = \sigma \sqrt{\pi l}$$

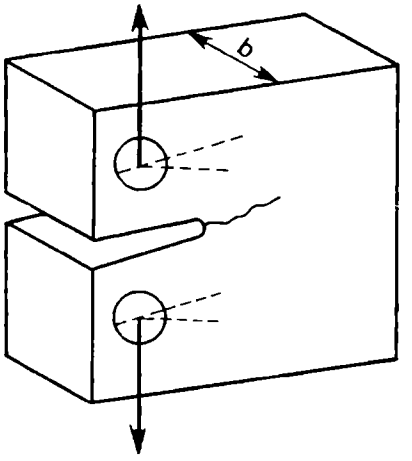

Fig. 3-16. A specimen for testing fracture toughness

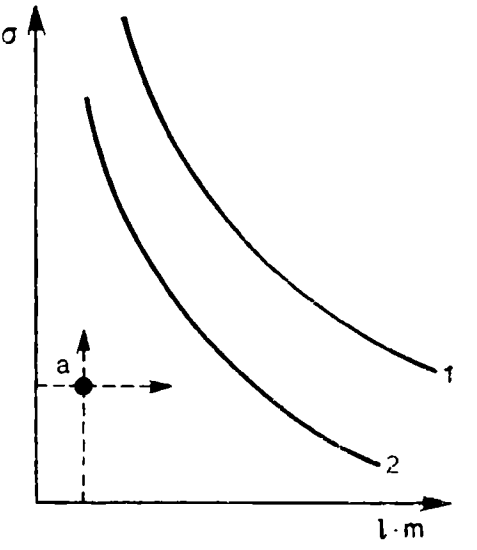

Fig. 3-17. Effect of stress on rupturing defect (lm) at K_{Ic} equal to 200 kgf/mm$^{3/2}$ (*1*) and 100 kgf/mm$^{3/2}$ (*2*)

The dimension of K is kg/mm$^{3/2}$, i.e. is somewhat unusual for characteristics of materials; this shows that K is only a convenient transformation of G which has a definite physical sense.

The stress intensity K at rupture is denoted by K_1 and determined on bulky specimens (Fig. 3-16) under a number of restricting conditions.

Firstly, the tests can be carried out only on materials whose yield limit in smooth specimens is greater than that in specimens with cracks. Thus, this type of test is only applicable to materials undergoing brittle or semi-brittle fracture.

Secondly, the deformation should be plane, i.e. the surface of fracture should be perpendicular to the acting force (without side skews). Only with these requirements fulfilled, the stress intensity as measured in the tests will be stable for a given material and a definite cross-sectional size.

It has been shown practically that the thickness of a specimen (see Fig. 3-15) should satisfy the following relationship

$$b \geqslant 2.5\,(K_{Ic}/\sigma_{0.2})^2$$

This circumstance also lays certain limitations on the application of the method. Indeed, for low-strength high-plastic materials (K_{Ic} = 500 kgf/mm$^{3/2}$ and $\sigma_{0.2}$ = 50 kgf/mm^2), the thickness b of a specimen, as found from the formula, should be 250 mm, which is practically unfeasible. The magnitude of K_{Ic} is usually determined for high-strength steels ($\sigma_{0.2} > 120$ kgf/mm^2) undergoing brittle or semi-brittle fracture.

The practical value of the K_{Ic} parameter is that, if it is known, we can determine the rupturing stress σ (Fig. 3-17) for a given shape and size of a defect ($l \times m$) or, on the contrary, with the known working stress in an element, predict the size of cracks at which fracture will occur.

In the diagram of Fig. 3-17, σ is the working (actual) mean stress, l is the length of a defect, and m is the characteristic of the defect (for defects of the type of cracks, m may be from 0.5 to 2).

If the mechanical state of the material is described by point a in the diagram, a defect at such a stress is not dangerous, but if the working stress will be increased or owing to fatigue fracture (for instance, the length of the defect will increase), fracture will occur at the moment when point a intersects

a curve for K_{Ic}. Evidently, a material having a higher value of K_{Ic} will be more reliable, since fracture will occur at a higher stress or a greater length of crack.

3-4. METHODS FOR TESTING MECHANICAL PROPERTIES

As has been done with the methods for examining the structure of metals, the methods for testing the mechanical properties will be discussed only in principle, without describing the laboratory equipment and testing techniques.

Tensile tests. In these tests, a cylindrical specimen of standard dimensions (with thickened end portions for better gripping in the clamps of the machine) is tensioned. In modern testing machines (Zwick, Instron, MTS), the rate of straining can be controlled within wide range from 0.003 to 3 000 mm/min. At higher rates of deformation, the test is considered to be dynamic (impact test).

Most testing machines are provided with a recorder which automatically plots a stress-strain curve (see Figs. 3-1 and 3-3). The stress-strain curve can be used to determine the parameters of strength and ductility (σ_t, $\sigma_{0.2}$, δ, E), though the deformation characteristics (δ, ψ) and the characteristics associated with small deformations (E, $\sigma_{0.01}$, etc.) should be determined by measurements directly on the specimen (during the test or upon rupture).

The dimensions and shapes of test specimens have been standardized, though a wide variety of non-standard specimens is also allowed.

In metallurgical and industrial tests, use is most often made of a standard specimen with the l/d ratio equal to five (l = 25-30 mm and d = 5-6 mm).

The strength properties of a tested metal in general depend only slightly on the geometrical dimensions of a smooth specimen, so that specimens of different dimensions can be used for determining σ_t and $\sigma_{0.2}$.

On the other hand, the plastic properties (δ, ψ) substantially depend on the dimensions of the specimens tested. For instance, longer specimens (more strictly, those with a greater l/d ratio) give a lower value of relative elongation. The point is that the relative elongation δ consists of two components:

$$\delta_{tot} = \delta_{unif} + \delta_{conc}$$

The first term ('uniform' component) is constant in relative measures and the second term ('concentrated' component) is constant in absolute measures and its contribution to the total relative elongation is smaller with longer specimens.

Let this be explained by a numerical example.

Suppose that a specimen 50 mm long has given δ = 10%, i.e. has elongated at rupture by 5 mm, of which 3 mm are due to δ_{unif} and the remaining 2 mm, to δ_{conc}. A similar specimen, but 100 m long, will elongate at rupture by 6 mm due to δ_{unif} and by the same 2 mm due to δ_{conc}, that is, its total relative elongation will be 8 per cent, but not 10 per cent as would be expected.

On a stress-strain curve, a specimen is stretched uniformly up to σ_t, while beyond that value the elongation is mostly concentrated. This is the principle by which δ_{tot} is considered to be composed of δ_{unif} and δ_{conc} (as in the tests on specimens of different length).

The relative reduction also depends on the absolute dimensions (cross-section) of specimens, being smaller in larger cross-sections.

The data on the mechanical properties of metals, as given in this book or found in the literature, have been obtained on specimens with d = 5-6 mm and l/d = 5 with a testing speed of 0.2 mm/min. At testing speeds appreciably above the given value, plastic strain is inhibited and the tests may give higher values of σ_t and especially of $\sigma_{0.2}$.

Tests of smooth specimens are not always quite indicative. The strength of a smooth specimen most often is not the same as the strength of a real ar-

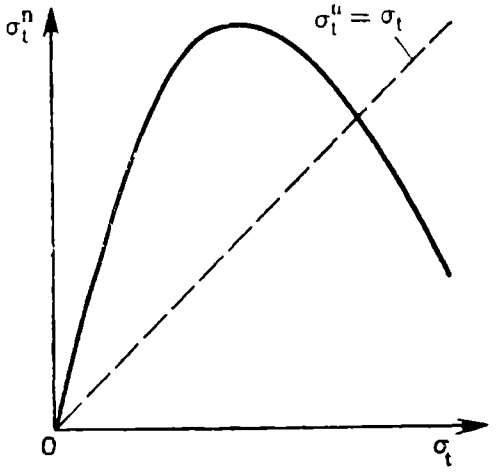

Fig. 3-18. Comparison of strength of smooth (σ_t) and notched (σ_t^n) specimens

ticle though both have been made of the same material; the difference is greater with articles of more intricate shape. For that reason, the results of tests (not only of tensile tests) characterize the properties of a material under the particular test conditions, but by no means the properties of an article, since the latter depend on the article shape as well as on the properties of the material.

In order to bring the test results closer to the real conditions of operation of materials in structures and obtain data characterizing the structural strength, tensile tests of notched specimens (specimens with stress concentrators) have been introduced and are employed quite widely (see Fig. 3-10).

In this case, the strength (σ_n^t) is determined as the rupture stress divided by the net cross-section at the notch.

The relationship obtained by tests of notched specimens is basically as follows (Fig. 3-18).

With ductile fracture, the strength of a notched specimen is always greater than that of a smooth one, owing to the high local plastic deformation and strong local strain hardening.

With brittle fracture, a notched specimen usually shows an appreciably lower and extremely unstable value of strength.

In the region where $\sigma_t^n = \sigma_t$, semi-brittle fracture takes place. Tests of notched specimens for determining the ultimate strength, rather than the fracture toughness, are ineffective, since ductile fracture gives an elevated value of strength, while brittle fracture gives unstable and unreliable values. With such a great effect of stress concentrators (notches) on test results, it has turned out that many factors which are inessential in tests of soft materials are quite important in tests of brittle materials (for instance, the state of the surface, techniques of making specimens, coaxiality of the testing machine grips, etc.). These factors are inessential in tests of materials with the ultimate strength up to 150 kgf/mm² (and at $\psi > 40$ per cent).

With high-strength materials ($\sigma_t > 150$-250 kgf/mm²), much care is needed in preparation of the test machine and specimens and in the tests proper.

The techniques of testing materials of an ultimate strength above 250 kgf/mm² are still imperfect, so that published data on the strength of high-strength materials should be taken with criticism. These materials, which have a low ductility, are most often tested by other, softer methods such as compression, bending, torsion, which give the same strength characteristics ($\sigma_{0.2\,com}$, $\sigma_{t\,com}$), but naturally of a different numerical value (owing to a different stressed state); these tests also give other parameters of ductility, for instance, the deflection in bending or the twist angle in torsion.

The tensile test is the principal one for testing steel and other structural materials and is used more often than other types of test.

The strength of metals is often determined by a simpler non-destructive method—hardness measurement.

The *hardness* of a material is understood as its resistance to the penetration of a foreign body; it is essentially another characteristic of the resistance to deformation. Methods for determining the hardness of materials are numerous. Among them, the one used most often is the *Brinell hardness test* (Fig. 3-19*a*),

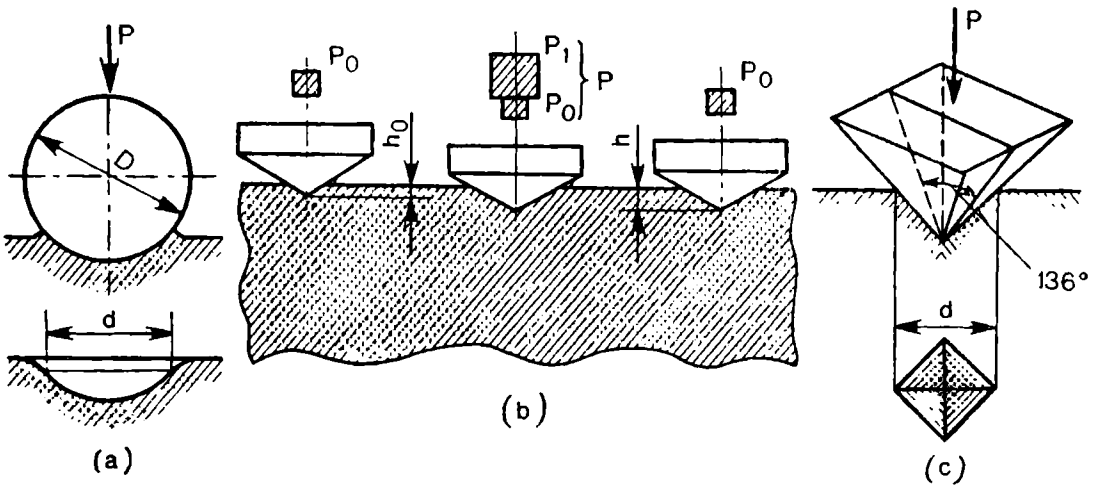

Fig. 3-19. Schemes of hardness tests by various methods
(*a*) Brinell; (*b*) Rockwell; (*c*) Vickers

in which a ball of diameter D is indented into the tested material by force P. The Brinell hardness number *HB* is the load P divided by the area of the spherical surface of the indent (of diameter d). In the *Rockwell hardness test* (Fig. 3-19*b*), the indentor is a diamond cone or sometimes a small steel ball, and the hardness number is an inverse of the depth of indentation (h). There are three scales of Rockwell test: *A*—for indenting a diamond cone by a force P = 60 kgf (*HRA* number); *C*—for indenting a diamond cone with a force P = 150 kgf (*HRC* number), and *B*—for indenting a steel ball with a force P = 100 kgf (*HRB* number).

In the *Vickers test* (Fig. 3-19*c*) a diamond pyramid is indented and the hardness measure (*HV* number) is the diagonal (d) of the indent.

The Brinell and *HRB* tests are used with soft materials, *HRC* with hard ones, and *HRA* and Vickers test, with thin layers (sheets).

There is a definite, though not very accurate, correlation between the various hardness tests. Knowing the hardness number found by one method, it is possible to find a corresponding number by another test through reference to special correlation tables.

The Brinell hardness number is roughly three times the ultimate strength. In other words, if the Brinell hardness number of an alloy is, for instance, 300 *HB*, the ultimate strength of that alloy is approximately 100 kgf/mm². This recalculation is only approximate and is inapplicable to brittle materials, though the discrepancy, only rarely, exceeds 10 per cent of the real strength value.

The hardness tests described characterize the average hardness of an alloy. To determine the hardness of individual structural components of an alloy, the deformation should be localized, i.e. a diamond pyramid should be indented into a definite place found in a microsection at a magnification of 100 to 400 and under a very light load (from 1 to 100 gf), with the diagonal of the indent being measured under the microscope. The value obtained (H) is called the *microhardness* and characterizes the hardness of a definite structural component.

Since the value of hardness in the Brinell test is determined as the ratio of the load P (kgf) to the surface area (mm²) of the indent, its dimension is kgf/mm², i.e. the same as that of strength.

It should be noted, however, that in the hardness tests by indentation, the stress distribution over the tested surface is extremely non-uniform, therefore

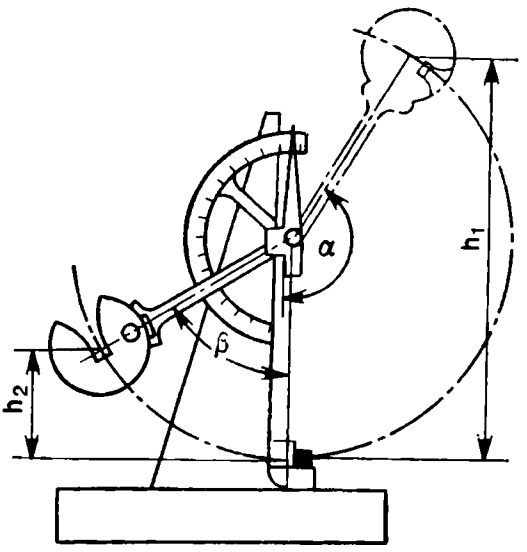

Fig. 3-20. Scheme of an impact testing machine

the division of the load by the surface area of the indent has no clear physical meaning. For that reason, it is better to regard the hardness number as dimen sionless and take that the hardness test is only a technological test which indirectly characterizes the strength of a material.

The ductility (including the technological ductility, or malleability) is tested by numerous tests, which include hammer upsetting, bending on a mandrel, folding test, extrusion (Erichsen test), etc.

Determination of reliability (impact tests). The reliability of a material can be determined by measuring its resistance to fracture, either ductile (a_p) or brittle ($T_u - T_l$ or T_{50}) and the fracture toughness (K_{Ic}). The measurement of KI_c has been briefly discussed earlier in the book. Let us now describe in more detail the determination of fracture resistance by impact tests which have recently found wide application. It has turned out that it is more convenient to break a specimen by a blow at bending and locate the point of fracture with a notch.

It is easier to measure the work of fracture (related to the cross-sectional area of the specimen), rather than the force required for fracturing (though this is quite possible). Relating the spent work to the cross-sectional area, which is the same (0.8 cm²) in all standard specimens, we obtain the unit work of fracture, or impact toughness $a_n = A_n/F_0 = A_n/0.8$ kgf m/cm².

In impact tests, a specimen is laid on two supports and broken by the stroke of a falling pendulum (Fig. 3-20).

The impact test specimens are shown in Fig. 3-21, where the first two are standard and the last, non-standard. They are of the same cross-sectional area (10 × 10 mm) and have a notch 2 mm deep (so that the net cross-section is 8 × 10 mm), but a different radius at the tip of notch: $r = 1$ mm (Fig. 3-21*a*), $r = 0.25$ mm (Fig. 3-21*b*), and $r = 0.0$ mm (Fig. 3-21*c*). In the last case, a notch 1 mm deep is made by machining and after that a fatigue crack 1 mm deep is formed.

The impact toughness measured on these specimens is denoted as follows:

Specimen	Designation
a	a_n,aI,a_1
b	*a*,IV$a_{0.25}$
c	a_p

As has been noted, the work of fracture a_n of a specimen is the sum of two components: the work of crack initiation (a_{in}) and the work of crack propagation (a_p), i.e. $a_n = a_{in} + a_p$. In impact tests, it is more reasonable to measure not the total work of fracture, but the work of crack propagation, since this characterizes the reliability of a material.

The work of crack initiation is understood as the work spent on macrodeformation of a specimen before a crack initiates at the tip of a notch. For a given material, the work of crack initiation a_{in} is proportional to the deformed volume of the material, which in turn is proportional to the sharpness of the notch.

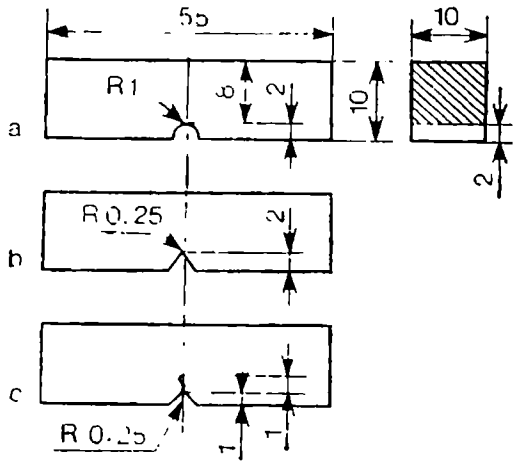

Fig. 3-21. Specimens for impact test

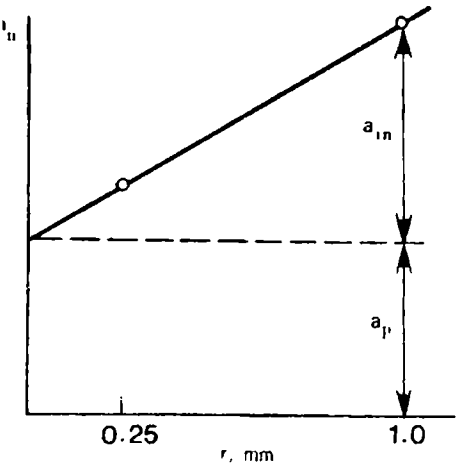

Fig. 3-22. Determining the work of crack propagation by extrapolation

Therefore, by testing a number of specimens with notches of different sharpness and extrapolating the results obtained by a zero notch radius (Fig. 3-22), we can find the impact toughness of a specimen with a notch radius equal to zero, or with a crack; this will be the work of crack propagation (a_p).

The work of crack propagation can also be found by direct tests of specimens with preliminarily formed cracks (according to Ya. B. Fridman and B. A. Drozdovsky, Fig. 3-21*c*). The impact toughness obtained by testing such a specimen is evidently equal to the work of crack propagation, since the crack was formed preliminarily and $a_{in} = 0$. Both methods give essentially the same values of a_p and the selection between the two is decided by practical feasibility.

In impact tests for determining a_p, it is advisable to examine the type of fracture. The fracture must be fully ductile (fibrous or cup-shaped), i.e. the test should be done above the ductile-to-brittle transition temperature (T_{50}). If the tests have been made at temperatures within the transition range, T_u-T_l (see Fig. 3-14), the work of crack propagation will not be fully representative of that characteristic, since it has been spent only to form portions of ductile fracture.

In that case $a_p^t = Ba_p$, where t is the temperature of test, B is the percentage of fibres in the fracture, and a_p is the full work of crack propagation. Above T_u, $B = 1$ and $a_p^t = a$, whereas below T_l, $B = 0$ and $a_p = 0$. Impact tests **below T_l are of no use, since a_p is always zero.**

To determine the resistance to brittle fracture (do not confuse with the resistance to ductile fracture which is characterized by a_p), we have to determine **the ductile-to-brittle transition temperature.**

The construction of serial curves of impact toughness often fails to determine the position of the transition temperature (see Fig. 3-14). The sought-for temperatures: T_u (T_{90}), T_l (T_{10}) or T_{50} can be found by constructing curves characterizing the change of percentage of fibres in fractures. In other words, when constructing a serial curve, it is important to know how the type of fracture (the content of ductile component in it, %) changes from one specimen to another.

Unfortunately, a_p and T_{50} can only be determined by multiple labour-consuming tests. For that reason, mass-production acceptance tests are carried out on a single type of specimen at one or, less frequently, two temperatures. The tests determine only whether a material satisfies the specification. For instance, the specification may require that $a^{-40}{}_n \geqslant 4$ kgf·m/cm². This means

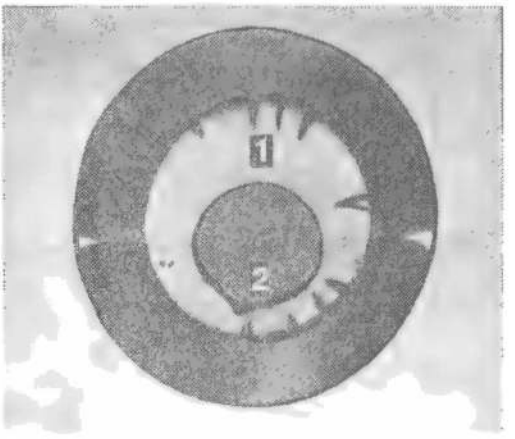

Fig. 3-23. Fatigue fracture
1—fatigue zone; *2*—zone of final fracture

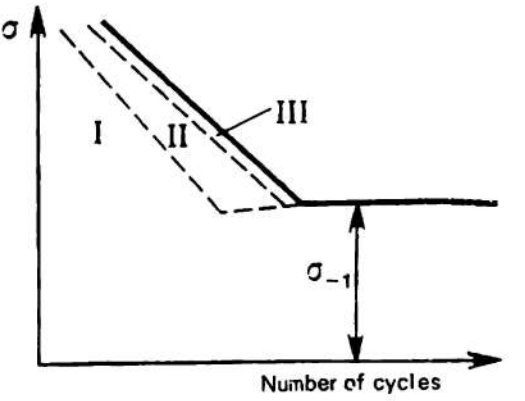

Fig. 3-24. Fatigue curve

that a material is considered suitable for its purpose if its impact toughness at −40°C is above 4 kgf·m/cm² and should be rejected, if otherwise.

Specimens of type *a* with $r = 1$ mm (see Fig. 3-21) are more often used in these tests, though it is more reasonable to use specimens *b* with $r = 0.25$ mm, since they have a sharper notch and, therefore, a lower value of a_{1n}, and thus can better characterize the work of crack propagation.

The *durability* of materials is determined by fatigue, creep, wear, corrosion and other types of test.

With alternating loads, the fracture of a material may occur gradually and at stresses well below the ultimate strength. This process of gradual destruction (fatigue failure) consists essentially in that the external surface of an element is the most heavily stressed portion of its cross-section (in bending or torsion) and therefore undergoes microdeformation. A crack can then appear and spread gradually in this strain-hardened zone. The crack-infected portion of the cross-section can no more support the load applied and the remaining load-carrying portion gradually contracts in size until sudden failure takes place.

Thus, fatigue failure is characterized by a particular type of fracture (Fig. 3-23) which has a fatigue zone *1* and a zone of final fracture *2*.

Fatigue tests are most often carried out on rotating specimens (either smooth or notched) with a constant bending load applied to them. The alternating load (tension-compression) at the external surface of the specimen, and then, as the crack develops, in the depth varies by a sinusoidal or another law. Each test is made at a particular stress and determines the time (number of cycles) to failure. The results of a series of tests are used to plot a fatigue curve such as the solid line in Fig. 3-24. As may be seen from the curve, there exists a stress which can cause no fatigue failure; this is called the *endurance limit* (σ_{-1}, σ_w). At stresses less than σ_{-1}, an element can operate very long. In many cases, however, the allowable stress ($\sigma_w < \sigma_{-1}$) will be too low and the cross-section of the element too large. In such cases the allowable stress is taken to exceed σ_{-1} and it is known in advance that the element will sooner or later break by fatigue (and should be replaced before this occurs). This is the case of what is called *limited endurance*. For instance, railroad rails operate under conditions of limited endurance and it is important to replace old rails by new ones in due time.

Fatigue failure occurs in three stages: gradual accumulation of stresses before a crack appears—zone *I* (Fig. 3-24); crack spreading—zone *II*; and

final sudden failure—zone *III*. For operation under limited endurance conditions, (above σ_{-1}), it is essential that the time to crack initiation be as long as possible (zone *I*) and also that zone *II* be as wide as possible in order to have time to detect the fatigue crack and replace the element.

Compression stresses, when acting in the surface of an element, inhibit the formation of fatigue cracks, thus increasing the fatigue limit and prolonging the time to failure in the zone of limited endurance.

On the other hand, stress concentrators (even roughness of surface) produce tensile stresses and thus lower the endurance limit.

At temperatures below the ductile-to-brittle transition range, fatigue failure takes place very quickly after the appearance of a crack; in other words, in the brittle state of the material, zones *II* and *III* are very narrow, though zone *I* may be quite large and σ_{-1} may be very high.

Another type of gradual fracture is *wear*. It occurs as often as fatigue failure. Wear is the result of friction of two contacting surfaces. A material of a lower wear resistance (which usually, but not always, is also less hard) suffers more from wear in the course of friction. The process of wear consists essentially in detachment of particles from the surface of material. Of great importance for wear is the chemical and physical interaction between the material in a rubbing pair.

In laboratory tests, wear is usually determined by weighing a specimen before and after the wear test, and the wear resistance of the material is characterized by the loss in mass (g/m^2h) per unit area per unit time. Wear resistance depends appreciably on the conditions of friction, so that material *A* may be better than material *B* in some cases and worse, in other cases.

3-5. STRAIN HARDENING

Let us return to the stress-strain relationship (see Fig. 3-1). If the load does not exceed point *A* (conditional yield limit), the metal will have no changes on the load removal. If, however, the load exceeds the yield limit and the stresses in the metal are equal, say, to σ_1, a residual deformation *a* will remain in the metal upon removal of the load. If the metal is then stressed again, its capability of plastic deformation will be lower and its yield limit will increase to σ_1, i.e. a greater stress should be applied to cause plastic deformation. In other words, the metal has become stronger. The strengthening effect produced in metals by plastic deformation is called *strain*, or *work*, *hardening*.

The reader already knows from the foregoing that plastic deformation takes place owing to dislocation movement.

A pair of moving dislocations creates hundreds and hundreds of new dislocations and thus the dislocation density in the metal increases and produces the strengthening effect (increases the ultimate strength, Fig. 3-25).

Variations of the mechanical properties of copper and aluminium versus plastic deformation are shown graphically in Fig. 3-26. As the deformation increases (and the cross-sectional area decreases), the ultimate strength (σ_t) increases and the relative elongation (δ) diminishes. Plastic deformation involves substantial changes in the structure of metal.

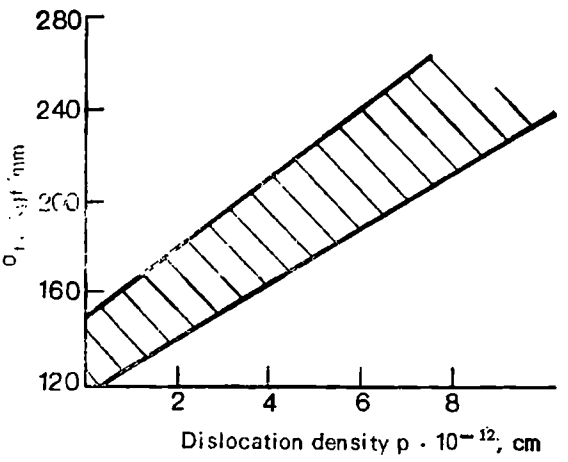

Fig. 3-25. Effect of dislocation density on strength (high-strength steel)

The crystal structure of plastically deformed metal can be characterized by a definite orientation of grains (*grain texture*), as well as by distortion of the crystal lattice.

Plastic deformation of a metal causes disorderly oriented grains to tilt so that their axes of highest strength are oriented along the direction of deformation.

With increasing plastic deformation, the texturing increases and may reach 100 per cent at heavy deformations, i.e. all grains become similarly oriented.

It would be wrong to think that plastic deformation results in grain refinement. Actually, grains are deformed, flattened out and their form changes from equi-axed to nonequi-axed (pancake shape), but their volume remains the same.

Numerous shear planes in metal are indicative of displacement of one portion of a crystal relative to another, which takes place by the dislocation mechanism. Their traces are clearly seen on polished metal (before deformation) and are often called Chernov-Lüders slip lines (see Fig. 3-2).

This pattern of plastic flow causes changes in the intragranular structure: mosaic blocks are disintegrated and their misorientation increases.

Internal stresses localized in small volumes also increase.

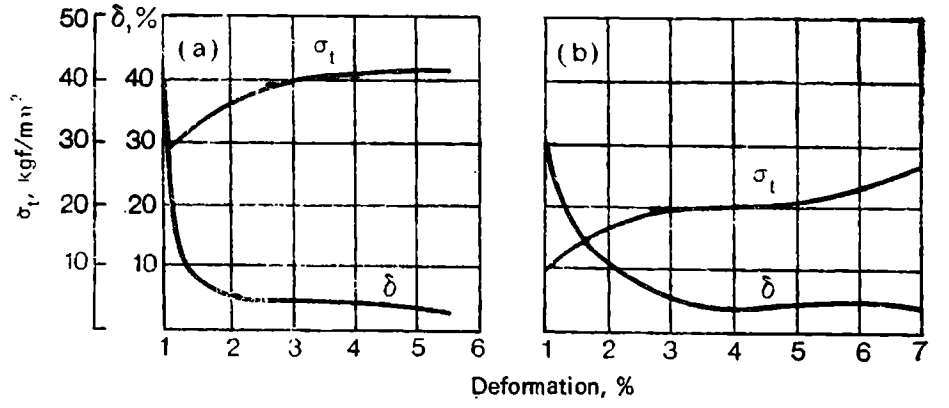

Fig. 3-26. Effect of plastic deformation on the mechanical properties of (*a*) copper and (*b*) aluminium

Because of all these changes, the density of metal decreases with increasing deformation. Figure 3-27 shows the results of tests on determining the density of pure iron in ruptured specimens. The deformation upon rupture was at the maximum at the necking (section *9*) and almost zero at the gripping end (section *1*). Accordingly, the density of the specimen has been found to diminish from section *1* to section *9*.

The effect of decreasing density at heavy deformations may be explained by the formation of voids within grains and between them (which is called *destruction*).

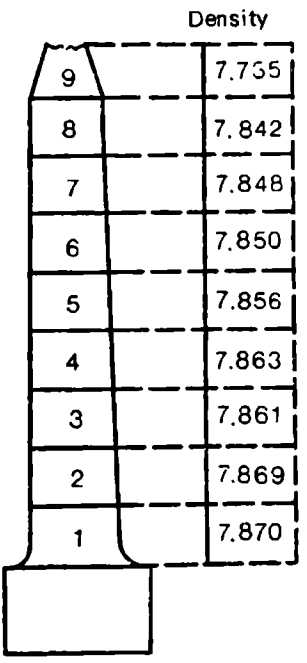

Fig. 3-27. Effect of plastic deformation on the density of tensioned specimen

3-6. EFFECT OF HEATING ON THE STRUCTURE AND PROPERTIES OF DEFORMED METAL (RECRYSTALLIZATION PROCESSES)

Plastic deformation makes metal structurally unstable, and certain phenomena should spontaneously occur in it to establish a stabler structural state.

The spontaneous processes which bring a plastically deformed metal to a stabler state include the elimination of crystal lattice distortions and other intragranular processes and the growth of grains. The first process (elimination of lattice distortion) involves only slight displacement of atoms therefore can take place at relatively low temperatures. Even a slight heating (300-400°C for iron) can eliminate lattice distortions (as a result of numerous submicro-processes: the reduction of the density of dislocations owing to their mutual annihilation, coalescence of blocks, reduction of internal stresses, decrease in the number of vacancies, etc.). In X-ray microphotographs, the lines that have been blurred just upon metal plastic deformation (due to lattice distortions and disturbance of lattice regularity) become clear again. The process of elimination of lattice distortions in a deformed metal during heating is called *recovery*. It results in that the hardness and strength of the metal somewhat decrease (by 20-30 per cent of the original values), and the ductility increases.

Another process possible in deformed metal is what is called *polygonization* which essentially consists in that the randomly arranged dislocations in grains are rearranged into arrays and form a cellular structure (Fig. 3-28). This structure may be stable and inhibit the processes that might develop at a higher temperature. *Recrystallization*, i.e. the formation of new grains, occurs at higher temperatures

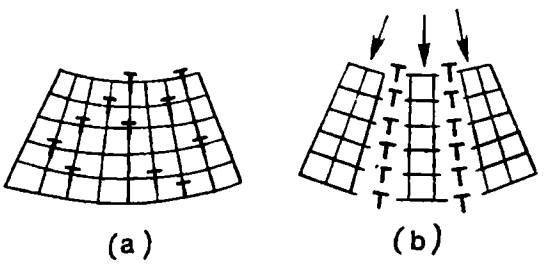

Fig. 3-28. Formation of a dislocation array (polygonization)

than those needed for recovery or polygonization and may commence at a noticeable rate on heating the metal above a definite temperature. Comparison of the recrystallization temperatures for many metals has established that the minimal temperature of recrystallization and the melting point are linked together by a simple relationship: $T_r = aT_{m.p}$, where T_r is the recrystallization temperature, $T_{m.p}$ is the absolute temperature of the melting point, and a is a coefficient dependent on metal purity. The higher the purity of metal, the lower is its recrystallization temperature. For metals of common commercial purity, $a = 0.3$-0.4. The recrystallization temperature of alloys is as a rule higher than that of the respective pure metals and may sometimes be as high as $0.8T_{m.p}$. On the contrary, very pure metals have a very low temperature of recrystallization: 0.2 or even $0.1T_{m.p}$.

As soon as recrystallization (its first stage) is completed, the structure and properties of metal are restored to the original values, i.e. those the metal had prior to deformation. The processes occurring during heating of strain-hardened metal are shown schematically in Fig. 3-29.

The coefficient a makes it possible to easily calculate the recrystallization temperature for conventional-purity metals: it is about 450°C for iron, 270°C for copper and 50°C for aluminium. For light-melting metals, such as zinc, tin or lead, the recrystallization temperature is below room temperature.

Apart from metal purity, the degree of prior deformation also has an effect on the minimum temperature of recrystallization. With a heavier deformation, the structure is distorted more heavily and is less stable, therefore, has a greater tendency to change to a stabler state. Consequently, a heavy degree of plastic deformation facilitates recrystallization and lowers the minimum temperature of this process.

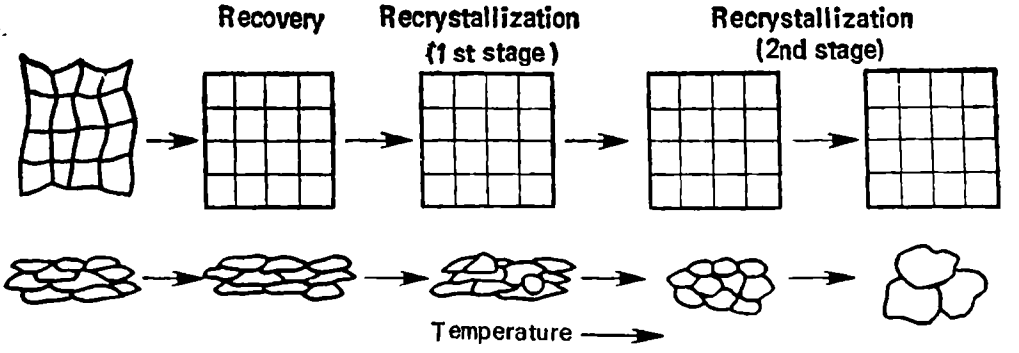

Fig. 3-29. Variations in the structure of strain-hardened metal during heating

Recrystallization temperature is of a high practical importance. When it is needed to restore the structure and properties of strain-hardened metal (for instance, for subsequent rolling, drawing, etc.), it should be heated above its recrystallization temperature. This process of heat treatment is called *recrystallization annealing* (for more detail, see Ch. 11).

Plastic deformation above the recrystallization temperature can also produce a strengthening effect, but this is immediately removed owing to the process of recrystallization occurring in the metal. It should be noted that recrystallization begins not during the deformation, but immediately after it and proceeds more quickly at higher temperatures. At very high temperatures, well above the temperature of recrystallization, it may be completed in a few seconds or even a fraction of a second.

Therefore, with plastic deformation at a temperature above the temperature of recrystallization, the metal may undergo strain hardening, but this is immediately eliminated. This process of metal working, where no strain (work) hardening occurs, is called *hot plastic working*. A process of plastic working (plastic deformation) below the recrystallization temperature is called *cold plastic working*.

Hence, plastic deformation of iron at 600°C should be regarded as hot working and at 400°C, as cold working. For lead and tin, plastic deformation at room temperature is, in essence, hot working, since the recrystallization temperatures of these metals lie below 20°C. In practice, these metals are called non-strain-hardenable, though slip lines can form in them during deformation (this is evidenced, for instance, by crackle of a tin plate when bent).

Hot working of metals is done at temperatures well above the lowest temperature of recrystallization, in order to increase the ductility and prevent the possibility of strain hardening.

Annealing of work-hardened material under industrial conditions is also done at temperatures above the lowest temperature of recrystallization, so as to ensure an appropriate rate of recrystallization processes. Table 3-1 gives the theoretical temperatures of recrystallization, practical temperatures for recrystallization annealing, and the temperatures for hot plastic working for selected metals.

In view of the changes in the structure of work-hardened metal, discussed above, it should be expected that the properties of metal will correspondingly change on heating. Indeed, as the temperature rises, the hardness first slightly diminishes owing to recovery. Upon annealing at a temperature slightly above the temperature of recrystallization, the hardness abruptly drops to the original value (the value the metal had prior to strain hardening). This temperature is exactly the lowest temperature of recrystallization, or *recrystallization threshold* (Fig. 3-30). Other strength characteristics (ultimate strength, yield limit) change in a similar manner. Figure 3-30 shows also the variations of ductility (δ). A low temperature of heating can

Table 3-1. Temperature of Recrystallization and Hot Plastic Working of Metals

Metal	Temperature, °C, of		
	recrystallization (theoretical at $\alpha = 0.4$)	recrystallization annealing	hot plastic working
Iron	450	600-700	1 300-800
Steel	450	600-700	1 300 (1 100)-800
Copper	270	450-500	800-600
Brass	250	400-500	750-600
Aluminium	50	250-350	460-350
Molybdenum	900	1 400-1 600	1 400-2 000

slightly increase the ductility (due to recovery processes), but only recrystallization can restore the original (prior to strain hardening) value of ductility.

Variations in microstructure during heating of work-hardened metal are shown in Fig. 3-31. Figure 3-31*a* illustrates the initial structure of work-hardened brass[1] which is seen to contain stretched grains and a large number of slip planes. A low-temperature heating, which only slightly lowers the hardness (due to recovery), does not change substantially the microstructure (Fig. 3-31*b*). Heating to 350°C causes recrystallization and makes crystals almost equi-axed. This temperature is, evidently, somewhat above the recrystallization threshold of the brass, since the size of grains is still not large. A higher temperature of heating (550-800° C) causes grain coarsening.

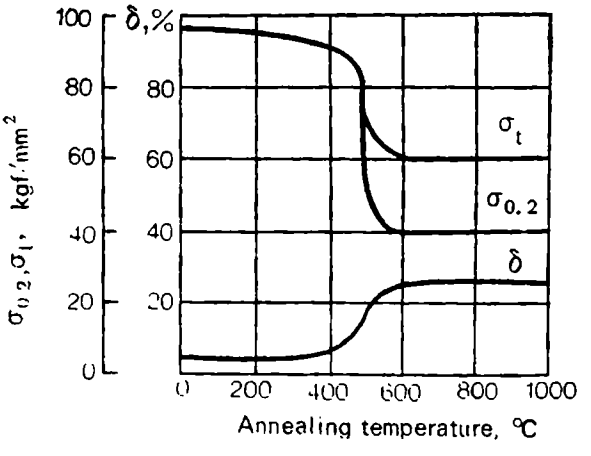

Fig. 3-30. Effect of annealing temperature on mechanical properties of strain-hardened iron (I. A. Oding)

Presenting these results as a temperature-grain size graph, we obtain a curve of the form shown in Fig. 3-32. Thus, recrystallization commences from grain coarsening and the size of final grains is larger at a higher temperature.

The process of recrystallization can be divided into two stages:

[1] Brass is an alloy of copper and zinc; for more detail see Ch. 27.

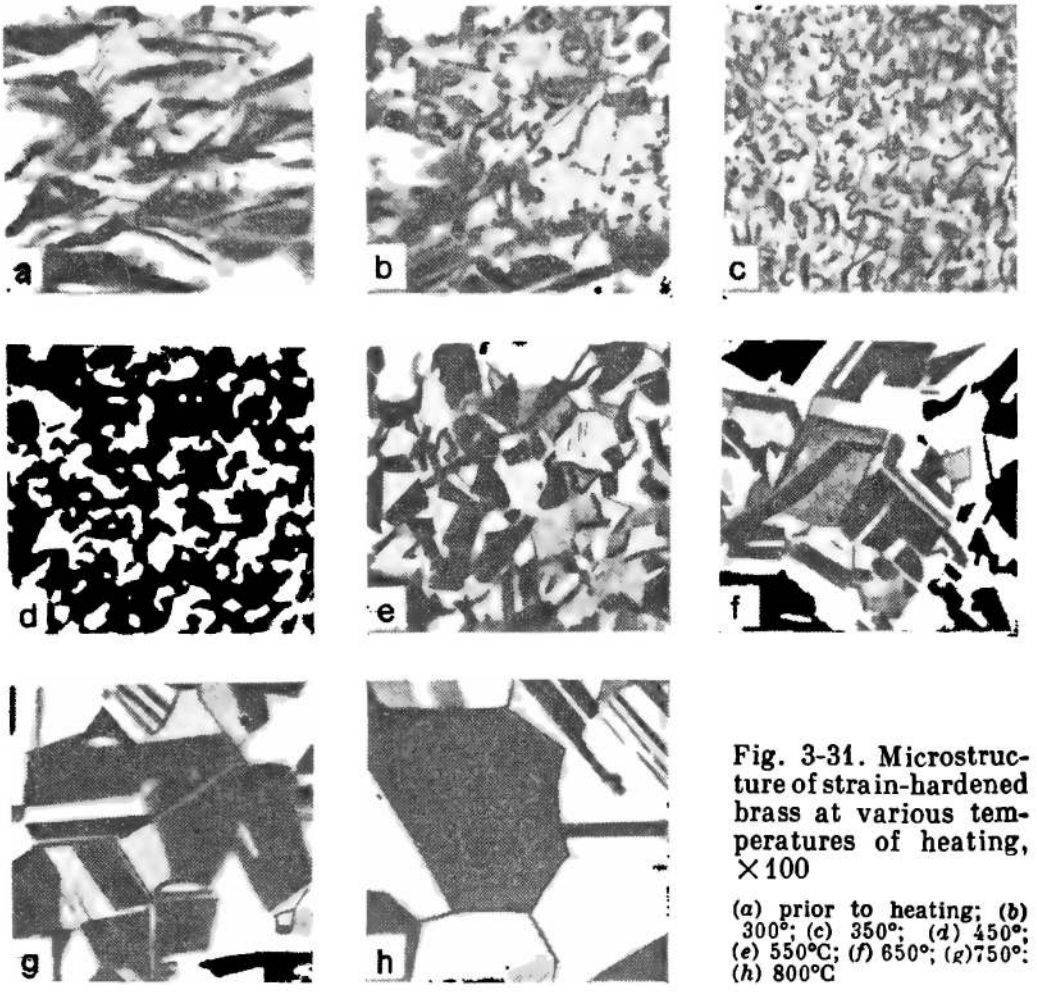

Fig. 3-31. Microstructure of strain-hardened brass at various temperatures of heating, ×100

(*a*) prior to heating; (*b*) 300°; (*c*) 350°; (*d*) 450°; (*e*) 550°C; (*f*) 650°; (*g*) 750°; (*h*) 800°C

(a) primary recrystallization during which elongated grains, that have been deformed by plastic deformation, are transformed into fine rounded-off randomly oriented grains;

(b) secondary recrystallization (grain growth) which essentially consists in enlargement of grain size and takes place at a higher temperature.

The microstructures shown in Fig. 3-33 illustrate the typical process of grain growth. In Fig. 3-33*a*, the structure of an alloy (solid solution of chromium in nickel) is shown just upon primary recrystallization. Fine equi-axed grains are clearly seen in the photograph. At a higher temperature, some grains appreciably grow in size at the expense of others and the structure consists of rare large grains surrounded by finer grains (Fig. 3-33*b*).

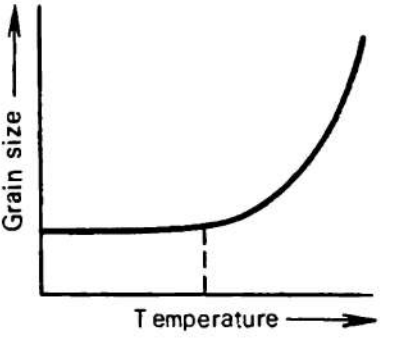

Fig. 3-32. Effect of heating temperature on grain size of strain-hardened metal

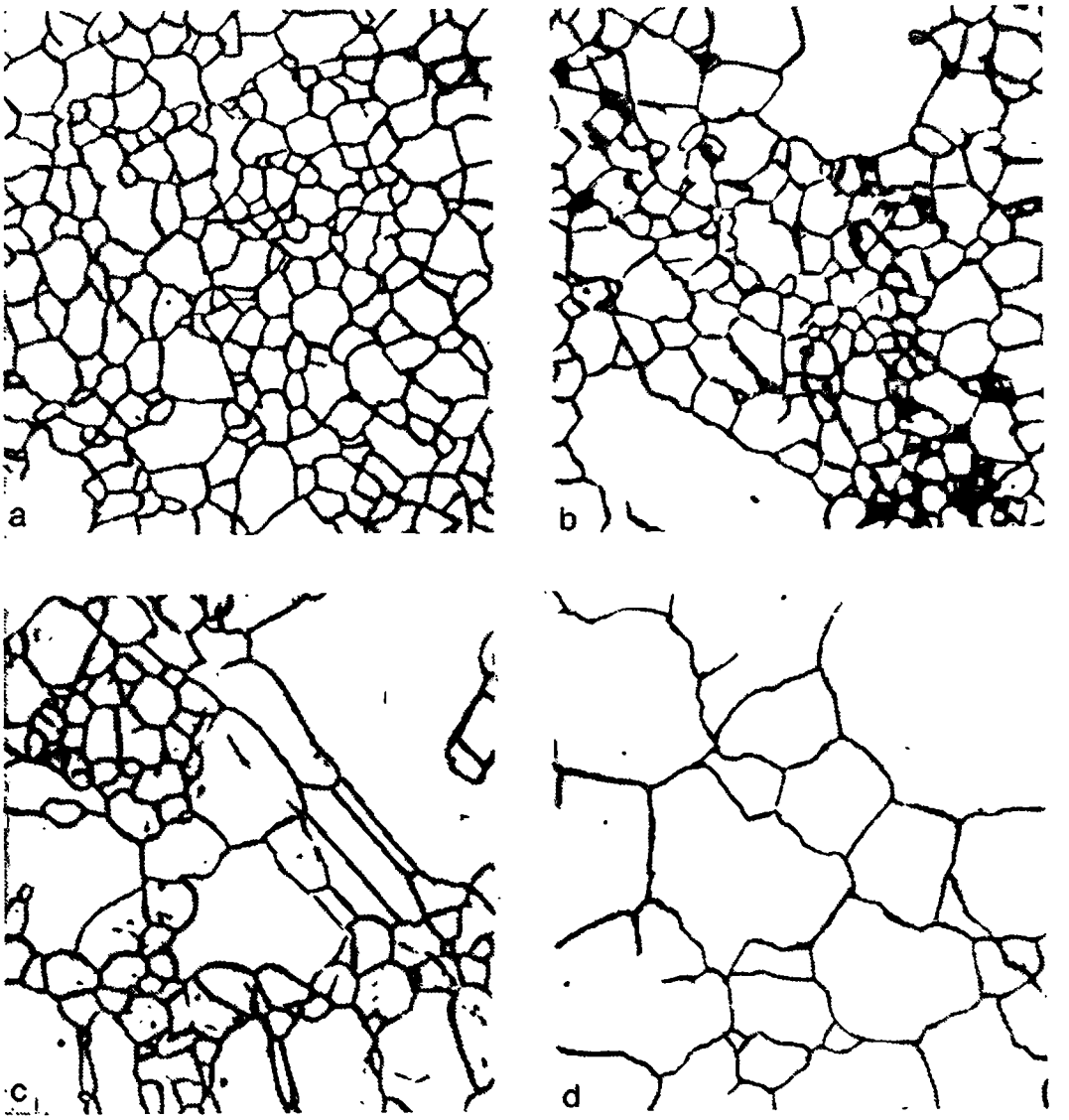

Fig. 3-33. Grain growth during recrystallization, ×100

With a further increase in temperature, the number of large grains increases (Fig. 3-33*c*). Finally, all fine grains are devoured by larger ones and the structure will consist of large grains only (Fig. 3-33*d*).

The processes of primary and secondary recrystallization have certain particularities.

Primary recrystallization consists in the formation of new grains. These are usually fine or, it may be said, extra-fine, and appear at interfaces between large deformed grains. Though certain intragranular processes of elimination of defects (recovery) have taken place during heating, they have not come to full completion and, on the other hand, newly formed grains are free from such defects.

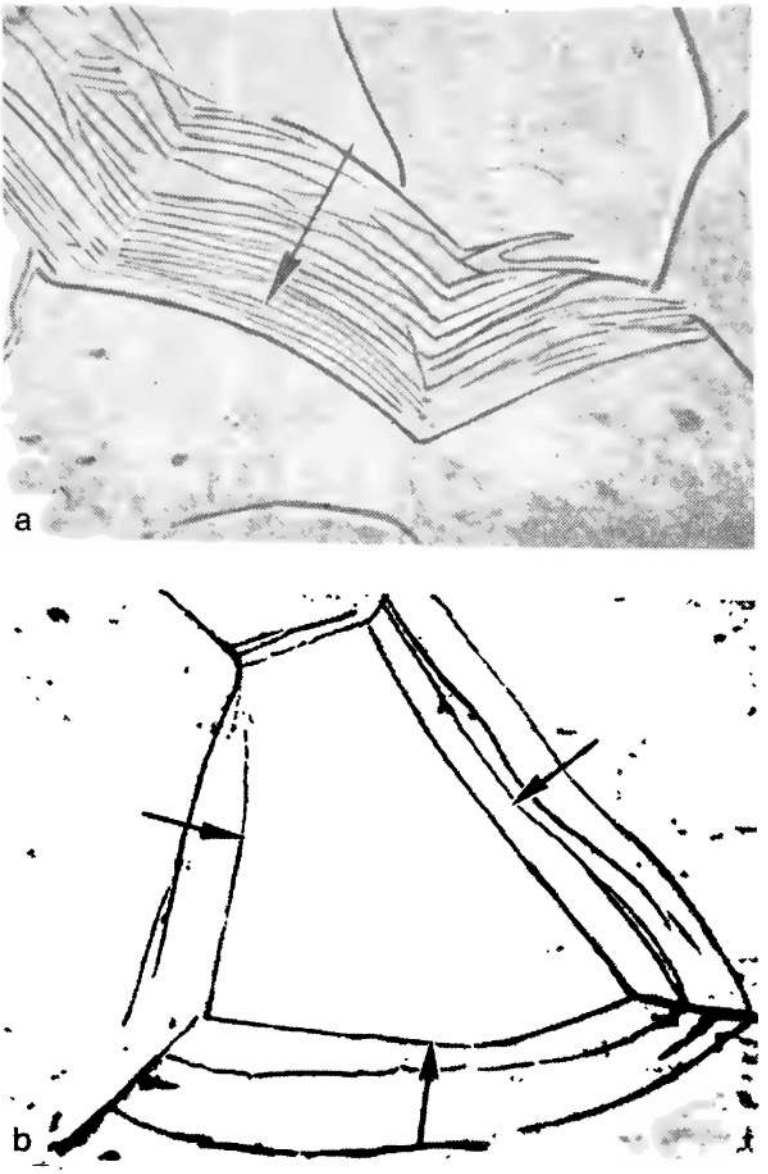

Fig. 3-34. Migration of grain boundaries. Arrows indicate the movement of a grain boundary, which occurs jumpwise
(*a*) tin bronze, ×225; (*b*) tantalum, ×100

At the end of the first recrystallization stage the structure may consist of only such grains, i.e. very fine grains of a few micrometres in size. But at that moment the process of secondary recrystallization begins which, as has been indicated, consists in grain growth.

The growth of crystals is a spontaneous process determined by the tendency of the system to reduce its internal energy.

If we assume that the system possesses a definite surface energy per unit area, the process of grain coarsening, i.e. combination of

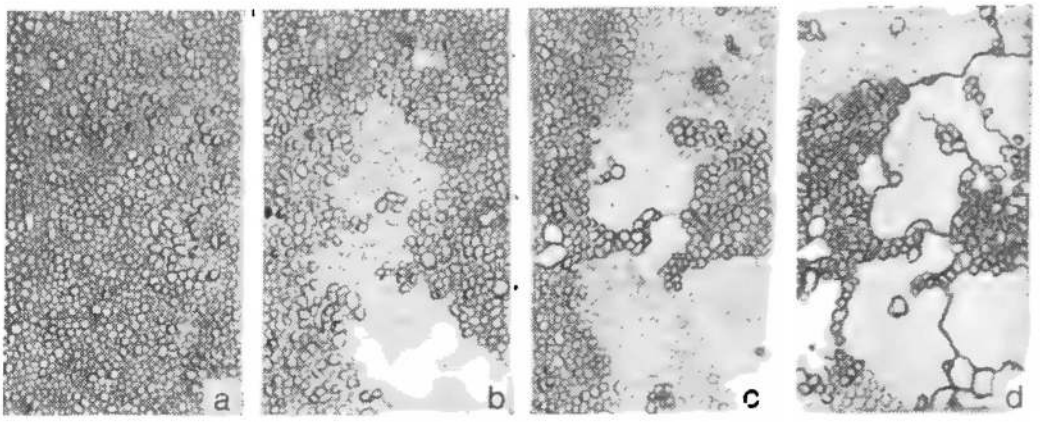

Fig. 3-35. Coalescence of grains
(*a*) initial stage; (*b*) and (*c*) gradual dissolution of boundaries; (*d*) final stage

fine grains into a smaller number of larger grains, will diminish the total surface area of grains ('internal surface'), and hence, diminish the free energy of the system.

It is essential to know the mechanism of grain growth, since the size of grains determines many properties of the metal. Knowing this mechanism, we can control grain size by appropriate heat treatment.

Three various mechanisms may be suggested to explain grain growth:

(1) due to nucleation: primary recrystallization results in nucleation of centres of new crystals and the growth of these crystals results in the appearance of new grains, though their number is less than in the original state of the metal, therefore, they will be larger on the average upon completion of the process;

(2) due to migration: a grain increases in size due to migration of its boundary (Fig. 3-34). Since a large grain is thermodynamically more stable than a fine one (has a lower S/V ratio, where S is the surface area and V is the volume), larger grains grow further by devouring finer grains;

(3) due to grain coalescence, i.e. grain boundaries are gradually dissolved and many fine grains combine into a larger grain (Fig. 3-35).

The first (nucleation) mechanism is evidently realized only rarely (the formation of new grains from recrystallized ones is energetically less probable). Migration of grain boundaries is a diffusion process and its rate is determined by the rate of self-diffusion. Therefore, the process can be of preferable significance at a high temperature, well above the temperature of recrystallization.

Coalescence of grains does not rely on diffusion and, what is most important, the process of coalescence can take place simultaneously over all (or many) grain interfaces. As has been indicated, grain interfaces are places where various defects, primarily dislocations, are concentrated. Annihilation of these

defects is, in essence, annihilation of grain boundaries. Consequently, grain growth through coalescence of grains can occur at a lower temperature than grain growth through migration and, as experience shows, may result in the formation of very large grains.

An incompleted process of coalescence has a typical structure consisting of a few large grains and a high number of fine grains. The properties of a metal having such an uneven grain structure are neither high nor stable.

It may be concluded from the foregoing that coalescence of grains has an adverse effect on the structure, and therefore, on the properties of a metal, since it can result in either coarse grain (on completion of the process) or uneven grain (if the process has not come to its end). Proper measures should be taken to prevent this effect.

Which of the two principal mechanisms of grain growth will be realized in a metal depends on temperature: at lower temperatures grain growth takes place due to coalescence, at higher temperatures due to migration of grain boundaries. The original structural state of the metal, in particular the degree of prior deformation, is also of importance.

With a slight plastic deformation, the density of defects is low, therefore, the formation of new defect-free recrystallized grains will give no appreciable gain in free energy. This is why primary recrystallization in slightly deformed metal proceeds not easily (and only at a high temperature) and secondary recrystallization gives almost no grain coarsening.

At a definite, fairly low, degree of plastic deformation, a relatively low density of dislocations is formed in metal, mainly at grain boundaries, and ensures primary development of grain growth by the coalescence mechanism; with completed process, this results in a very strong coarsening of grain (Fig. 3-36).

The degree of deformation which ensures chiefly the development of coalescence and results upon heating in growth of grains to a gigantic size is called the *critical degree of deformation*, or simply, critical deformation. Its value is not high, usually within 3-8 per cent. If recrystallization annealling will be done after plastic deformation, the critical deformation should be avoided.

With a supercritical deformation, the density of defects is such that the mechanism of grain coalescence is ineffec-

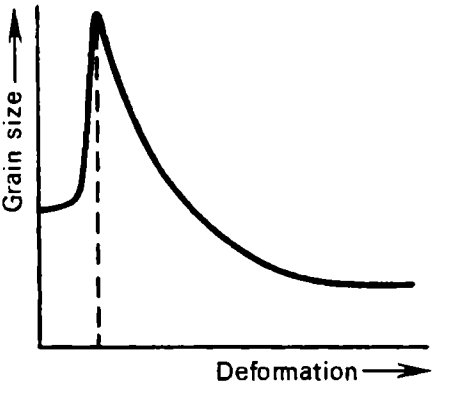

Fig. 3-36. Effect of preliminary deformation on grain size in recrystallized metal (schematically)

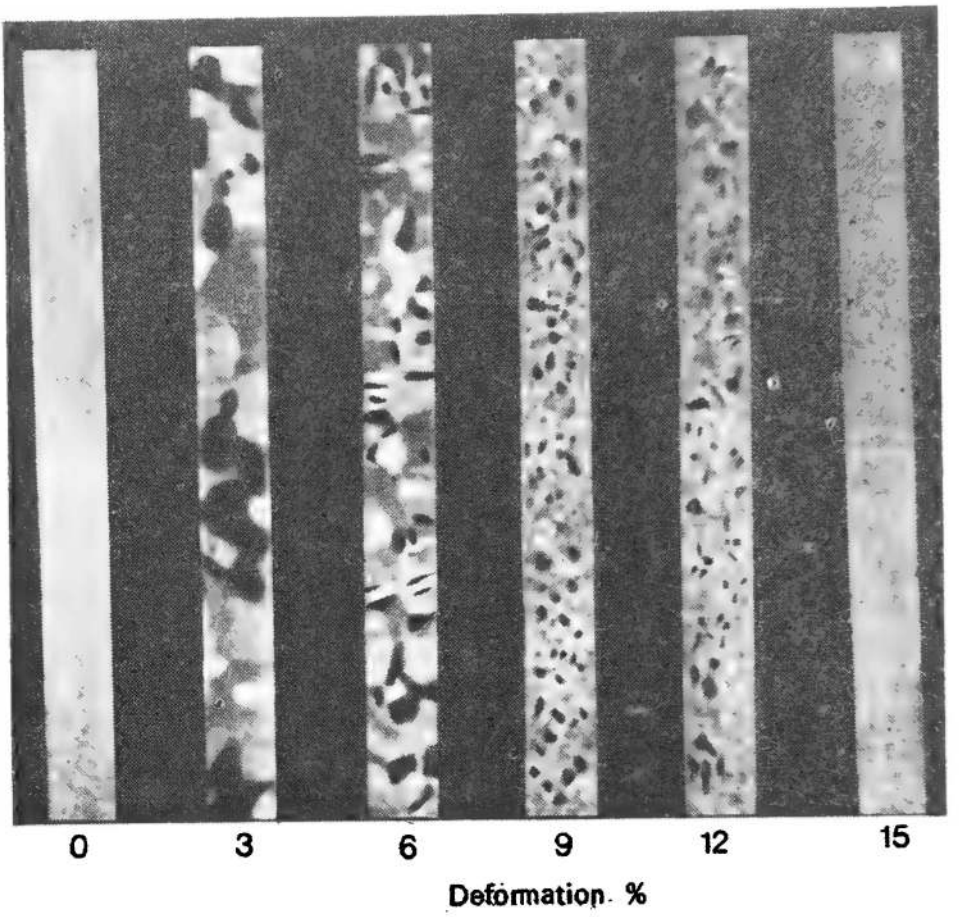

Fig. 3-37. Macrostructure of recrystallized aluminium at various degrees of deformation

tive. Grain growth takes place mainly due to boundary migration and, under comparable conditions, produces a finer grain than that obtained through grain coalescence.

Figure 3-37 shows the structure of work-hardened aluminium. The metal was deformed by tension and then let to recrystallize at 550°C for 30 minutes. In the non-deformed metal (its macrostructure is shown without magnification), the structure is so fine that individual grains are invisible for the naked eye. The coarsest grain was obtained at the minimum deformation (residual elongation 3 per cent) which is evidently close to the critical deformation value. With further increase in the degree of deformation, the size of grains of recrystallized metal decreases. Therefore, the average size of grains upon recrystallization depends on the temperature at which recrystallization has been carried out (see Fig. 3-32) and on the degree of prior deformation (see Fig. 3-36). The dependence of grain size of recrystallized metal on these two factors can be characterized by what is called *full recrystallization diagrams.*

Such a diagram for a nickel alloy is illustrated in Fig. 3-38*a*, where it may be seen that the size of grains diminishes with increasing deformation and decreasing temperature of recrystallization annealing. Grain growth is observed on

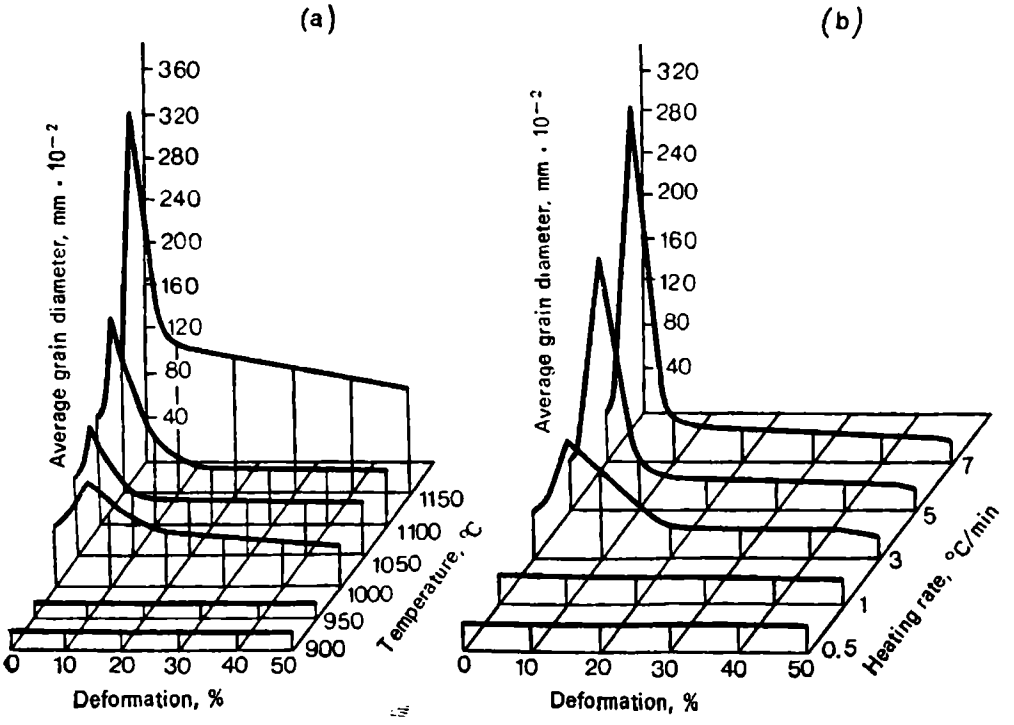

Fig. 3-38. Full recrystallization diagram of heat-resistant nickel alloy (Author)
(*a*) heating rate 7°C/min; (*b*) heating temperature 1080°C

heating above the temperature of recrystallization, in the case considered, above 950°C[1]. Low deformations (about 5 per cent) give an intensive growth of grain, especially at high temperatures of heating. This intensive grain growth in weakly deformed metal is observed only on quick heating. With slow heating (Fig. 3-37*b*), the process of polygonization has enough time for completion, so that grain growth through coalescence of many grains into a large grain does not take place. The process that then takes place in the metal is the common recrystallization, i.e. nucleation of crystal centres and growth of crystals from them, and produces no gigantic grains. Slow heating can be replaced by stepwise heating, with the soaking temperature being 30-50°C below the temperature of recrystallization.

LITERATURE

Read W. T., *Dislocations in Crystals.* New York, McGraw-Hill, 1953.

Cottrell E. H., *Dislocations and Plastic Flow in Crystals.* Oxford, Clarendon Press, 1953.

Steinberg S. S., *Physical Metallurgy.* Vol. 1. Moscow, "Metallurgizdat", 1961 (in Russian).

Fracture. Proceedings of an International Conference on the Atomic Mechanisms of Fracture, held in Swampscott, Massachusetts, April 12-16, 1959. Massachusetts, 1960.

Chalmers B., *Physical Metallurgy.* New York, Wiley, 1959.

[1] The recrystallization threshold for this alloy is 960-980°C.

Gorelik S. S., *Recrystallization in Metals and Alloys.* Moscow, "Metallurgiya", 1966 (in Russian).

The Structure and Mechanical Properties of Metals. Proceedings of a conference. Moscow, "Metallurgiya", 1967.

Gulyaev A. P., *Impact Toughness and Cold Brittleness of Structural Steel.* Moscow, "Mashinostroenie", 1969 (in Russian).

Maclintock F. A., Argon A. S., *Mechanical Behaviour of Materials.* Massachusetts, 1966.

Yokobori T., *An Interdisciplinary Approach to Fracture and Strength of Solids.* Groningen, 1969.

Honeycomb R. W. K., *The Plastic Deformation of Metals.* London, Edward Arnold, 1968.

Fracture Toughness of High-strength Materials: Theory and Practice. ISI Publication 120. London, 1970.

Novikov I. I., *Theory of Heat Treatment of Metals.* Moscow, "Metallurgiya", 1974; English translation: Moscow, Mir Publishers, 1978.

Fridman Ya. M., *Mechanical Properties of Metals.* Moscow, "Mashinostroenie", 1974 (in Russian).

Grabsky M. V., *Structural Superplasticity of Metals.* Moscow, "Metallurgiya", 1975 (in Russian).

Zelenova V. D., *Mechanism of Ductile and Brittle Fracture and Methods for Testing Fracture Resistance of Metals and Alloys.* Moscow, "Mashinostroenie", 1975 (in Russian).

Rauzin Ya. R., Shur E. A., *Structural Strength of Steel.* Moscow, "Mashinostroenie", 1975 (in Russian).

Fracture. An Advanced Treatise. Ed. by H. Lubowicz. Volumes 1-6. New York, London, 1968.

Chapter 4

THE STRUCTURE OF ALLOYS

An alloy is a substance obtained by melting together two or more components.

It is also possible to produce alloys by other methods, such as sintering, electrolysis, sublimation (the products thus obtained are called *pseudo-alloys*), but the most common process is that by melting together various pure elements.

Alloys made predominantly of metallic elements and possessing typical metallic properties are called *metallic alloys.*

Naturally, the structure of metallic alloys (which will be discussed in this chapter) is more complicated than that of pure metal and depends mainly on how their constituents can interact with one another.

In some instances, the simple substances—constituents of an alloy—do not interact chemically with one anotner in the solid state. The structure of such an alloy is essentially a *mechanical mixture* of particles or grains of the two (or more) constituents.

In otner cases, the constituents of an alloy can interact chemically with one another and form *chemical compounds* or can be mutually soluble and form *solutions.* Sometimes, intermediate phases can form in an alloy.

This chapter will deal with interactions of constituents in metallic alloys.

4-1. MECHANICAL MIXTURE

Two constituents, A and B, will form a mechanical mixture in an alloy if they are mutually insoluble in each other in the solid state and cannot form compounds with each other by chemical interaction. These conditions given, an alloy will contain pure crystals of A and B (Fig. 4-1), which may be readily seen in the microstructure (provided that they are large enough).

A radiogram of the alloy will then reveal the presence of two lattices, of A and B. If the properties of A crystals and B crystals in the alloy were tested separately, the results would be fully identical

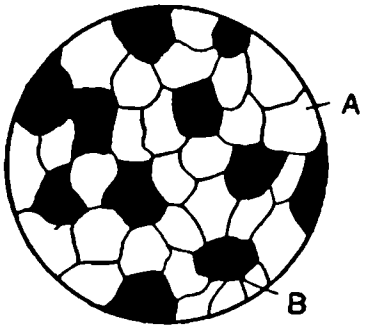

Fig. 4-1. Microstructure of a mechanical mixture (schematically)

with the properties of pure metals A and B.

The mechanical properties of such alloys depend on the relative contents of the constituents, and also on the size and shape of grains and are usually somewhere between the characteristics of the pure constituents (for more detail see Sec. 5-13).

4-2. CHEMICAL COMPOUND

Upon formation of a chemical compound:

(a) the ratio of the number of atoms of the two elements exactly corresponds to the stoichiometric ratio, which may be expressed by a simple formula (in the general case, a chemical compound of two elements may be designated as A_nB_m);

(b) a typical crystal lattice (different from the lattices of the constituents) will form with ordered arrangement of atoms of the two components.

A chemical compound may be also characterized by a definite melting point (or dissociation point) and an ability to change its properties abruptly at a change in composition (the phenomenon is called the *singularity of properties*, for more detail see Sec. 5-13).

For instance, in the crystal lattice of NaCl which is shown in Fig. 4-2*a*, *b*, sodium ions form a face-centred cubic lattice. Chlorine ions form a similar lattice, but displaced by a half-period relative to that of sodium ions.

Naturally, the stoichiometric ratio for this compound is: Na : Cl = 1 : 1. Thus, the crystal lattice of a chemical compound has no molecules[1].

[1] It should be noted, however, that certain crystalline substances are built of molecules with a clearly distinguished structure. Among these molecular crystals are crystals of many organic substances. Molecular crystals, however, do not exist in metallic phases.

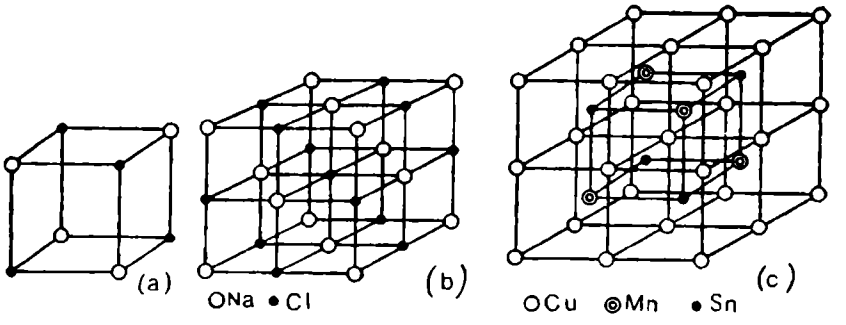

Fig. 4-2. Crystal lattices
(*a*), (*b*) NaCl; (*c*) Gu_2MnSn

The stoichiometry of a compound is determined by an ordered arrangement of atoms. If an atom of A is surrounded by a definite number of atoms of B and each atom of B is surrounded by the same number of the A atoms, the stoichiometric ratio for this compound is AB (as for NaCl).

If the structure of a crystal lattice is such that the number of the A atoms surrounding each of the B atoms is only one-half the number of the B atoms which surround an A atom, the formula of the compound should be AB_2, and so on.

If a chemical compound is formed by metallic elements only, the points of its crystal lattice will be occupied by positive ions which are held in place by electron gas; thus, the lattice will have what is called the metallic bond.

This type of bond is not rigid, so that the proportion of an element under particular conditions may differ from the stoichiometric ratio for a given chemical compound (see Sec. 4-4). For the same reason, the formation of chemical compounds from metallic atoms disobeys the valency laws.

Figure 4-2*c* shows the crystal lattice of a ternary chemical compound Cu_2MnSn whose elementary cell contains 8 copper atoms, 4 manganese atoms, and 4 tin atoms[1].

Formation of a chemical compound of a metal and a non-metal gives an *ionic bond.*

In that case, the elements interact so that an atom of the metal gives up its (valence) electrons and becomes a positive ion, while an atom of the non-metal receives these electrons on its outer electron shell and becomes a negative ion. In chemical compounds of this type, elements are held in the lattice by electrostatic attraction.

The chemical composition of a compound with ionic bond is decided by the valency law, i.e. by the availability of free (valence) electrons and the completeness of the electron shells of the reacting elements.

Compounds of this type possess a rigid bond and have a constant composition exactly corresponding to the stoichiometric ratio, i.e. atoms of any of the elements forming this compound can be neither in excess nor in deficiency.

---

[1] The eight corner atoms of copper belong by 1/8 to this lattice; the six face-centering atoms belong by 1/2; the twelve atoms in the middle of edges, by 1/4; and the single atom in the centre belongs fully to this lattice; therefore, in the elementary cell shown in Fig. 4-2*a*, eight copper atoms, four manganese atoms and four tin atoms are arranged within the lattice and fully belong to it. The stoichiometric ratio of atoms in this compound can be expressed by the formulae $Cu_8Mn_4Sn_4$ or Cu_2MnSn.

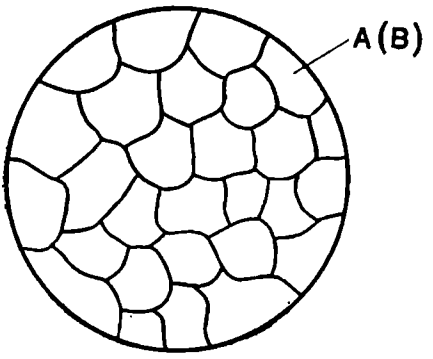

Fig. 4-3. Microstructure of solid solution (schematically)

4-3. SOLID SOLUTION BASED ON A COMPONENT OF AN ALLOY

When molten, most metallic alloys employed in industry are homogeneous liquids, i.e. liquid solutions. On passing to the solid state, many of them retain their homogeneity, and therefore, solubility. The solid phase that forms on crystallization of such an alloy is called *solid solution.*

Chemical and spectral analysis shows that solid solutions contain two or more elements, whereas metallographic analysis of such alloys detects uniform grains in them, as in pure metals (Fig. 4-3). Radiographic analysis reveals in solid solutions only one type of crystal lattice, as in pure metals.

Consequently, in contrast to a mechanical mixture, a *solid solution is a single-phase system consisting of crystals of one type and having a definite type of crystal lattice.* As distinct from chemical compounds, a *solid solution can exist within a definite range of concentrations, rather than at a strictly definite ratio of the constituents.*

The structure of single-component solid solutions is such that the lattice of the base metal (solvent) contains atoms of the other substance (solute). Two principally different cases are possible here:

1. Substitutional solid solutions. For instance, a metal A has the lattice as shown in Fig. 4-4*a*. The dissolution of constituent B in base metal A occurs through partial replacement (substitution) of the A atoms by B atoms in the base metal lattice (Fig. 4-4*b*).

2. Interstitial solid solutions. Atoms of solute C occupy the places between the A atoms, as shown schematically in Fig. 4-4*c*.

With either substitutional or interstitial solutions, atoms of the solute are distributed at random in the lattice of the solvent.

If a solution contains x per cent of constituent B on the average, it may turn out that the concentration of B in a particular portion will be other than x

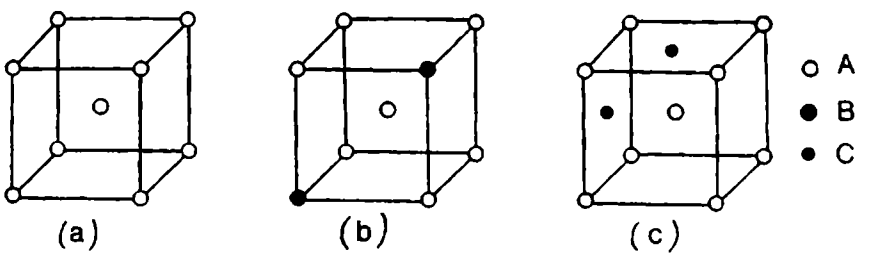

Fig. 4-4. Body-centred cubic lattices

(*a*) pure metal; (*b*) substitutional solid solution; (*c*) interstitial solid solution

(Fig. 4-5). The deviations of the composition of solid solution in rather small portions of the volume from the average composition are called *fluctuations*. The general theory of fluctuations has been developed by Smoluchowski of Poland and is used widely in theoretical metallurgy. The probability of existence of a portion with the concentration of component *B* fluctuating from the average value is lower at a higher magnitude of fluctuation.

If we recall, however, that the number of atoms in a crystal is enormous, it may be expected that in the volume of that crystal there are very many small portions in which the concentration can appreciably fluctuate from the average value.

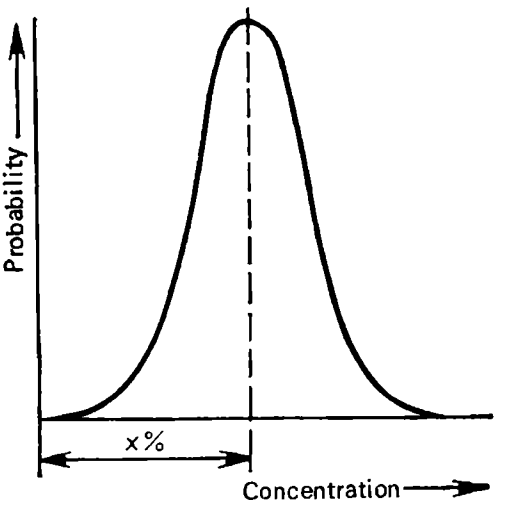

Fig. 4-5. Probability curve

As has been pointed out by S. T. Konobeevsky, the concept of fluctuations is of great importance for understanding the processes of nucleation of crystals of a new phase whose concentration appreciably differs from that of the original phase[1].

When a solid solution forms, the solvent element retains its original crystal lattice. Atoms of the solute element distort the lattice of the solvent element and change the average size of its elementary cell.

With the formation of interstitial solid solutions, the lattice periods are changed, depending on the difference in atomic radii of the solute element and solvent. If the atom of the solute element is larger than that of the solvent, the elementary cell of the lattice increases, and vice versa. In the first approximation, this change is proportional to the concentration of the solute element (at. per cent), though deviations from the linear law may be quite appreciable.

A change in the lattice parameter upon formation of solid solutions is a factor of great importance, which can determine changes in the properties of metal. In general and irrespective of the type of metal, the relative strengthening upon the formation of a solid solution is proportional to the relative change of lattice parameter, and a decrease in the lattice parameter produces a greater strengthening effect than its expansion.

Figure 4-6 shows how the lattice parameter changes in solid solutions based on aluminium, copper and iron.

If we consider how some elements dissolved in iron affect its strength (which should be expected in view of the changes in the lattice parameter, see Fig. 4-6*c*), it may be seen that nickel, chromium and manganese have only a slight strength-

[1] The distribution of dissolved atoms, especially those forming interstitial solutions, appreciably depends on dislocation structure. Dissolved atoms usually accumulate around dislocations forming *Cottrell atmospheres* which impede dislocation movement, or in other words, increase the strength of metal.

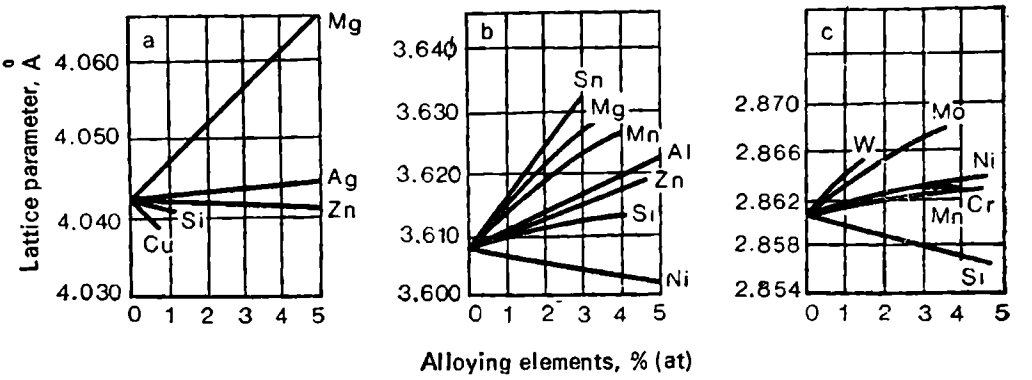

Fig. 4-6. Lattice parameters of solid (substitutional) solutions formed on dissolution of various elements in (*a*) aluminium; (*b*) copper; and (*c*) iron (Author)

ening effect on iron (the probable changes in the structure produced by them are not considered here), whereas tungsten, molybdenum and silicon produce an appreciable strengthening effect. Among the last three elements, silicon produces the greatest effect, since it compresses the iron lattice, whereas tungsten and molybdenum expand it.

In interstitial solid solutions, the lattice periods increase, since the size of atoms (more strictly, of ions) of the dissolved element is larger than the interatomic spaces they occupy, so that atoms of the solvent lattice are moved somewhat apart.

Substitutional solid solutions may be either *limited* or *unlimited*. With unlimited solubility, any quantity of *A* atoms can be substituted by *B* atoms. Therefore, if the concentration of *B* atoms is increased, more and more *B* atoms will occupy lattice sites in place of *A* atoms, until all *A* atoms will be replaced. Thus, the composition of the alloy can change gradually from 100 per cent *A* to 100 per cent *B* (Fig. 4-7). This is possible, however only when the two metals have an identical crystal structure, i.e. both being *isomorphous*.

Consequently, the prime condition for the formation of a continuous series of solid solutions is that the two components have identical crystal lattices, i.e. both are isomorphous[1].

[1] A continuous series of solid solutions can also form when the crystal lattices of the two components are not identical, but close in shape, for instance, a face-centred cubic and a tetragonal lattice.

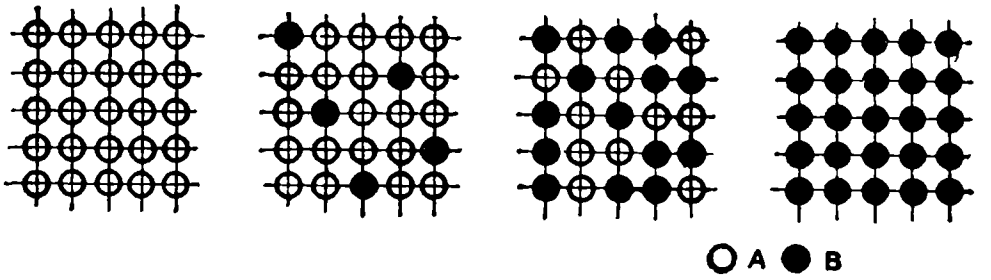

Fig. 4-7. Crystal lattices of a substitutional solid solution with unlimited mutual solubility of components

If two metals with identical crystal lattices strongly differ in atomic radii, the crystal lattice on the formation of a solid solution is severely distorted which brings about an accumulation of elastic energy. When the distortion reaches a definite limit, the crystal lattice becomes unstable and the solubility limit sets in.

Having systematized experimental data, I. I. Kornilov has found that only the elements whose atomic radii differ from that of iron by not more than 8 per cent are unlimitedly soluble in iron. Other metals (such as copper) can form continuous series of solid solutions at a difference between atomic radii up to 10-11 per cent, and low-melting metals which have a low modulus of elasticity (for instance, selenium and tellurium) are unlimitedly soluble in each other at a difference in their atomic radii up to 17 per cent.

Thus, the second condition for the formation of unlimited solid solutions is that the difference in the atomic radii of the constituents should be sufficiently small.

Finally, it has been noted that unlimited solubility is observed predominantly in elements occupying close places in the Periodic Table, i.e. similar to one another in the structure of the valence shell and in the physical nature.

If the metals being melted together belong to two distant groups of the periodic system and thus have a different physical nature, they are often liable to form chemical compounds, rather than solid solutions.

The conditions mentioned above are indispensable for the formation of continuous series of solid solutions. In some cases, however (as for instance in the Au-Ag system), there may be no unlimited solubility, though these conditions are fully met.

If two metals do not conform to the conditions mentioned, they will be limitedly soluble in each other. It has been found that the solubility is lower with a larger difference in the size of atoms and the properties of two components which form the solution. The limited solubility usually diminishes with redueing temperature.

In the further discussion, solid solutions will be designated by the symbol A (B), where A is the solvent (a metal whose lattice is retained in the solid solution) and B is the solute element. For unlimited solid solutions, the symbols A (B) and B (A) are unambiguous, but for limited solid solutions there is an essential difference. For instance, a solution denoted A (B) is the solution of B in A, whereas the designation B (A) implies that A is solved in B. The former solution has the lattice of A and the latter, that of B.

Consider the conditions under which interstitial solid solutions can form. Since in solid solutions of this type, B atoms should be intersticed into the lattice of A, it is evident that the diameter of B atoms cannot be too large and that there should be enough space for B

atoms in the *A* lattice. Indeed, metals form interstitial solid solutions with elements of the periods *I* and *II*, i.e. with those whose atomic dimensions are small (H, N, C, O, B).

4-4. A SOLID SOLUTION BASED ON A CHEMICAL COMPOUND

We have discussed solid solutions based on pure components, i.e. having the lattice of one of the alloy constituents. However, solid solutions can be formed by chemical compounds, as well as by pure elements.

In such cases, the solution retains the lattice of a chemical compound A_nB_m, but the excess of atoms, say, of *B*, is dissolved in the solution and substitutes some quantity of *A* atoms in the lattice. A third element, *C*, can also be dissolved in the solution, with *C* atoms substituting *A* and *B* atoms in the crystal lattice.

Figure 4-2*c* shows the structure of a compound of three metals: copper, manganese and tin. It is most probable that metallic bonds predominantly exist in this compound. Each of the three metals contributes to the common fund by giving up its valence electrons, and one metal can partially substitute another (for instance, copper can substitute manganese if its content in the alloy exceeds the stoichiometric ratio). This is the mechanism of formation of solid solutions on the basis of the lattice of a chemical compound and with an excess of one of the components. The solubility rate may be quite wide, depending on how close the elements of the compound are to each other by their nature.

Evidently, if a solid solution has formed on the basis of a chemical compound, the actual ratio of atoms in it will no more correspond exactly to the chemical formula of that compound.

Chemical compounds capable of dissolving foreign atoms are designated as follows.

For instance, iron boride (Fe_4B_2) is capable of dissolving chromium and carbon, with chromium substituting iron, and carbon substituting boron in the lattice sites. The ratio (Fe + Cr) (B + C) = 4/2 remains in the solution which therefore can be designated as $(Fe, Cr)_4 (B, C)_2$.

In some cases a simplified designation may be used, with metals designated by the *M* letter and non-metals, by *X*. For instance, the same solid solution based on iron boride can be designated as M_4X_2.

Though the formation of solid solutions on the basis of chemical compounds is mainly associated with substitution of atoms in the crystal lattice, it may sometimes turn out that some sites of the lattice remain unoccupied by foreign atoms ('empty').

For instance, the CoAl compound can crystallize with an excess of cobalt and aluminium, compared with the stoichiometric ratio Co:Al = 1:1, aluminium atoms may remain in an excess if cobalt

atoms have not occupied all their places in the crystal lattice sites. Thus, voids are formed in the lattice.

Compound-based solid solutions in which some sites of the crystal lattice have remained unoccupied are called *subtraction solutions.*

It should be noted, however, that not all compounds are capable of dissolving excess amounts of the constituent elements. In other words, there are compounds which form no solid solutions of the constituent elements and, on the other hand, some compounds can exist only as solid solutions and are non-existent as pure chemical compounds at the stoichiometric ratio of atoms. For instance, the exact composition of $CuAl_2$ compound corresponds to 54.1 per cent Cu (by mass). Actually, this compound exists at 53.25 to 53.9 per cent Cu, i.e. only with some copper atoms substituted with aluminium atoms. Without this substitution, the lattice of $CuAl_2$ is non-existent. Such compounds which can exist only as solid solutions and do not exist at the exact stoichiometric ratio are called *berthollides*, in contrast to *daltonides* which can exist at the stoichiometric ratio of the constituents[1].

The existence of berthollides and daltonides was discovered by Acad. N. S. Kurnakov and the names were given after J. Dalton and C. L. Berthollet, two prominent chemists who disputed much at the beginning of the last century on what a chemical compound is. Their dispute is still not settled completely.

4-5. ORDERED SOLID SOLUTIONS

The phenomenon of ordering was discovered by N. S. Kurnakov in 1914. When studying the electrical resistivity of copper-gold alloys, he found that their properties changed without any noticeable changes in the microstructure. Later, it has been demonstrated by X-ray analysis that these changes should be attributed to the redistribution of atoms in the crystal lattice.

As we have noted earlier, atoms of the solute are distributed in common solid solutions at random. Under particular circumstances, however, they occupy definite positions in the lattice sites, i.e. their disordered arrangement changes to an ordered one. The process is called *ordering* and solutions with ordered arrangement of solute atoms, *ordered solid solutions.*

As an example, consider alloys of copper and gold which have identical crystal lattices and are unlimitedly soluble in each other in the solid state. In a common solid solution of copper and gold, there is no strict order in the arrangement of copper and gold atoms at the sites of the face-centred lattice. The probability of occurrence of some or other atom in a given site depends on the alloy concentration. Under definite conditions (slow cooling of very concentrated solid solutions), atoms of copper and gold, however, occupy definite positions in the lattice (Fig. 4-8).

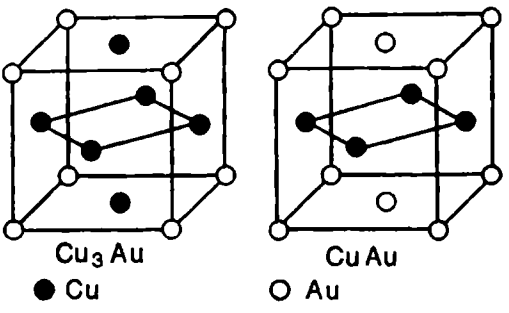

Fig. 4-8. Crystal lattices of ordered solid solutions in the Cu-Au system

[1] This definition of berthollides and daltonides is not generally adopted.

For instance, gold atoms may occupy all corner positions in the face-centred lattice, and copper atoms, all face-centering positions. The atomic ratio of copper to gold will then be 3 to 1, and the phase thus formed may be written as Cu_3Au. If two of the side faces were occupied by copper atoms, the copper-to-gold atomic ratio would be 1 : 1 and the corresponding formula would be CuAu.

The process of ordering may be either complete or incomplete. In the former case, all atoms occupy predetermined positions in an ordered solid solution. In the latter, part of atoms occupy predetermined positions and another part is arranged at random (i.e. a certain 'degree of ordering' exists).

Ordering is a diffusion process (the transformation is associated with displacement of atoms), therefore, can be favoured by slow cooling.

Ordering varies the lattice periods but changes neither the structure nor the type of lattice. Only in rare cases the lattice is slightly distorted. For instance, an ordered solid solution of CuAu has a face-centred tetragonal lattice with the ratio of periods $c/a = 0.935$ and a disordered solution, a face-centred cubic lattice with $c/a = 1$.

Ordered solid solutions can be regarded as intermediate phases between chemical compounds and solid solutions. With complete ordering, these phases resemble chemical compounds, because (a) they contain a definite number of atoms that can be expressed by a formula and (b) atoms are arranged regularly in the lattice. These phases can be related to solid solutions since they retain the original lattice of the solvent metal.

4-6. ELECTRONIC COMPOUNDS (HUME-ROTHERY PHASES)

Compounds of this type can be formed by two metals from the following groups: Cu, Ag, Au, Fe, Co, Ni, Pd, and Pt, on the one hand, and Be, Zn, Cd, Al, Sn, and Si, on the other. As has been found by W. Hume-Rothery, a British metallophysicist, they can be characterized by a definite ratio of valence electrons to the number of atoms (3/2, 21/13 or 7/4), with a particular crystal lattice corresponding to each ratio. For instance, a body-centred cubic lattice (called β-phase) forms at the ratio of 3/2. All compounds with the valence electrons-to-atoms ratio of 21/13 have a complicated cubic lattice with 52 atoms per cell (this is called γ-phase), and finally, with the ratio of 7/4, the lattice is hexagonal (ε-phase).

Electron (Hume-Rothery) phases are found in many alloys of commercial importance: copper-zinc, copper-tin, iron-aluminium, copper-silicon, etc. Usually, all the three phases (β, γ and ε) are present in a system. In the Cu-Zn system, for instance, Cu_5Zn compound forms the β-phase (the ratio of valence electrons to the number of atoms is 3/2)[1], Cu_5Zn_8 forms the γ-phase (the ratio of 21/13)[2], and $CuZn_3$ forms the ε-phase (the ratio of 7/4).

Electron phases have a definite ratio of atoms and a new crystal lattice, not that possessed by the pure elements; these are features characteristic of

[1] Copper has one and zinc two valence electrons. Therefore, the number of atoms in the compound is 2 and the number of valence electrons, 3.

[2] The number of atoms in this compound is $5 + 8 = 13$, and the number of valence electrons, $5 + (8 \times 2) = 21$.

chemical compounds. In these compounds, however, there is no regular arrangement of atoms. At high temperatures, atoms of both elements do not occupy definite points in the lattice, i.e. are arranged statistically. Ordering takes place at a decrease of temperature, but is usually incomplete.

Thus, compounds of this type should be also regarded as intermediate between chemical compounds and solid solutions.

Electron phases existing in commercial copper alloys are given in Table 4-1.

Table 4-1. Electron Phases

Phase	Ratio	Lattice	Electron phases in various systems			
			Cu-Zn	Cu-Sn	Cu-Al	Cu-Si
β	3:2	Body-centred cubic	CuZn	Cu_5Sn	Cu_3Al	Cu_5Si
γ	21/13	Complex cubic	Cu_5Zn_8	$Cu_{31}Sn_8$	Cu_9Al_4	$Cu_{31}Si_8$
ε	7/4	Hexagonal	$CuZn_3$	Cu_3Sn	Cu_5Al_3	Cu_3Si

4-7. LAVES PHASES

Stable chemical compounds with ionic type of bond are predominantly formed by elements of different nature and essentially different atomic radii. If, however, the atomic radii differ only slightly, there is a tendency for the formation of electron phases.

With intermediate differences in atomic radii, the formation of chemical compounds is also possible. Typical examples are so-called *Laves phases* (after Laves, a British physicist). These phases, whose stoichiometric formula is AB_2, can be formed by elements whose atomic radii are in a ratio of approximately 1 : 1.2. Most Laves phases can be related to one of the types as follows: type $MgCu_2$ ($TiCr_2$, UAl_2, $ZrMo_2$, etc.) which crystallizes in a complex cubic lattice; type $MgZn_2$ ($FeBe_2$, WFe_2, $MoFe_2$, etc.) which crystallizes in a complex hexagonal lattice, and type $MgNi_2$ ($ZrFe_2$, $TiCo_2$, etc.), which crystallizes in a complex haxagonal lattice of a different form than that of $MgZn_2$.

Laves phases are found as strengthening intermetallic phases in refractory alloys.

4-8. INTERSTITIAL PHASES

Interstitial phases are formed by transition metals and some metalloids having a small atomic radius (hydrogen, $r_H = 0.46$Å; nitrogen, $r_N = 0.71$Å; carbon $r_C = 0.77$Å). These phases can form when the ratio of the atomic radius of a metalloid to that of a metal is equal to or less than 0.59. In that case the metallic atoms form simple lattices (usually b.c.c., f.c.c. or h.c.p.) and the atoms of the metalloid are intersticed into the voids of the lattice in definite places. This is a particular feature of the lattice structure of interstitial phases.

Interstitial phases satisfy the conditions characteristic of chemical compounds: the ratio of the participating atoms is described by simple formulae, such as M_4X, M_2X, MX, or MX_2 (where M is metal and X, metalloid) and the type of the lattice formed in them is different from the lattices of the original elements. Therefore, interstitial phases can be related to chemical compounds.

Solid solutions based on interstitial phases possess some characteristic properties. It has turned out that solutions with an excess of the metalloid in

equilibrium have been never discovered, but those with an excess of metallic atoms are encountered quite often. In metallic alloys, interstitial phases practically always contain an excess of metal atoms, i.e. the stoichiometric ratio is never observed. Such cases are actually due to a deficiency of metalloid atoms, i.e. to the formation of subtraction solid solutions (see earlier) on the basis of interstitial phases, rather than to the substitution of a metalloid by metallic atoms (which should be considered impossible in view of the large difference in atomic radii).

Examples of interstitial phases are many carbides and nitrides encountered in steels and other alloys.

LITERATURE

Samsonov G. V., Umansky Ya. S., *Solid Compounds of High-melting Metals.* Moscow, "Metallurgizdat", 1957 (in Russian).

Hume-Rothery W., Raynor G. V., *The Structure of Metals and Alloys.* London, Inst. of Metals, 1954.

Cottrell A. H., *Theoretical Structural Metallurgy.* London, 1956.

Steinberg S. S., *Physical Metallurgy.* Vol. 1, Sverdlovsk, "Metallurgizdat", 1961 (in Russian).

Umansky Ya. S., Finkelstein B. N., Blanter M. E., *Physical Principles of Metallurgy.* Moscow, "Metallurgizdat", 1961 (in Russian).

Chalmers B., *Physical Metallurgy.* New York, Wiley, 1959.

Bokstein S. Z., *The Structure and Properties of Metallic Alloys.* Moscow, "Metallurgiya", 1971 (in Russian).

Goldschmidt H. J., *Interstitial Alloys.* London, Butterworths, 1967.

Schultze G., *Metallphysik.* Berlin, Akademie-Verlag, 1967.

Chapter 5

CONSTITUTIONAL DIAGRAMS

5-1. GIBBS' PHASE RULE

The *constitutional diagram* is a graphical representation of the state of an alloy. If the composition of an alloy is changed, its temperature, pressure and state will also change and these changes can be depicted in a constitutional diagram.

The constitutional diagram shows the stable states of an alloy, i.e. those which have the least free energy under given conditions. For that reason, constitutional diagrams are also called *equilibrium diagrams*, since they show the equilibrium phases existing under the given conditions. In that connection, all changes in the state which have been depicted in the diagram relate to equilibrium conditions, i.e. under the provision that the metal is neither superheated nor undercooled. As we have seen earlier, however, equilibrium transformations (i.e. in the absence of either undercooling or superheating) cannot actually take place (see Ch. 2), therefore, a constitutional diagram is a theoretical approximation and can be used practically for analysis of transformations at low rates of heating or cooling.

The general relationships for coexistence of the stable phases which satisfy the theoretical conditions of equilibrium can be expressed mathematically in a form which has been named *Gibbs' phase rule.*

The phase rule establishes a quantitative relationship between the degree of freedom and the number of phases and constituents in a system.

We have already used the terms 'phase' and 'constituent'. Now, before studying Gibbs' phase rule, these terms should be given proper definitions.

A phase is a homogeneous part of a system, which is separated from the other parts (phases) by an interface so that the composition and structure of the substance change jumpwise on a passage through that interface.

Consequently, a homogeneous liquid is a single-phase system, whereas a mechanical mixture of crystals of two types is a two-phase system, since each crystal differs from another in the composition

and structure and crystals are separated from one another by their boundaries (interfaces).

The substances which form a system are called constituents or components. Consequently, a pure metal represents a single-component system, an alloy of two metals, a two-component system, and so on. Chemical compounds can be regarded as components if only they do not dissociate in the temperature range considered.

The number of degrees of freedom (variance) of a system is understood as the number of external and internal factors (temperature, pressure and concentration) which can be changed without changing the number of phases in the system.

If the number of degrees of freedom is zero (*non-variant system*), it is clear that the external and internal factors of the system (temperature, pressure, concentration) cannot be changed without changing the number of phases.

If the number of degrees of freedom is unity (*monovariant system*), the factors mentioned above can be changed within certain limits without causing changes in the number of phases.

Gibbs' phase rule is a mathematical expression of the equilibrium conditions for a system, i.e. the phase rule equation establishes a quantitative relationship between the number of degrees of freedom c and the number of components k and phases f in a system:

$$c = k - f + 2$$

The phase rule equation can be derived by reasoning as follows.

Consider a system of several components which form a number of phases and assume that the system is in equilibrium.

For a system in equilibrium, the thermodynamic potential (level of free energy) of each component is the same in all the phases[1].

With two components and two phases, the thermodynamic potential of a component in the first phase is equal to the thermodynamic potential of that component in the second phase, i.e.

$$Z_1^1 = Z_2^1$$

and the thermodynamic potentials of the second component are also equal in both phases, i.e.

$$Z_1^2 = Z_2^2$$

In these equations, Z is the thermodynamic potential, the superscript is the number of a component, and the subscript is the number of a phase.

The set of these equations is indeterminate, since the two equations contain four variables. The set can be made determinate by arbitrarily assuming the values for any two of the variables. In the case considered, i.e. with two components and two phases, the system has two degrees of freedom (the number of degrees of freedom is the difference between the number of variables and the number of equations).

[1] Otherwise a phase with a component having a higher thermodynamic potential would undergo a transformation.

Assume that a system consists of k components and f phases. If it is in equilibrium, the thermodynamic potentials of the first, second, etc. component should be equal to one another in all the phases, i.e.:

for the first component

$$Z_1^1 = Z_2^1 = Z_3^1 = \ldots = Z_f^1$$

for the second component

$$Z_1^2 = Z_2^2 = Z_3^2 = \ldots = Z_f^2$$

for the k-th component

$$Z_1^k = Z_2^k = Z_3^k = \ldots = Z_f^k$$

How many degrees of freedom has the system considered? Each line above contains $(f - 1)$ equations and there are k lines; therefore, the total number of equations is $(f - 1)\,k$. The variables in our system are temperature, pressure and concentration. Assuming that each phase contains all the components, we find that the concentration of $k - 1$ components can be varied in the system (the concentration of the last component will be found as the balance). Since there are f phases, the number of variables is:

for concentration	$(k+1)\,f$
for temperature	1
for pressure	1
Total:	$(k-1)\,f+2$ variables

Since the number of degrees of freedom c is the difference between the number of variables and the number of equations, we have

$$c = (k - 1)\,f + 2 - (f - 1)\,k$$

or

$$c = kf - f + 2 - kf + k$$

or

$$\boxed{c = k - f + 2}$$

In the above derivation we have assumed that the thermodynamic potential of each component in all coexisting phases is at its minimum, i.e. the system is in equilibrium and does not tend to change its state. Gibbs' phase rule and deductions from it are valid only for the equilibrium state.

In the phase rule equation, concentration, temperature and pressure are independent variables. Assuming that all transformations in metal occur at a constant unvarying pressure, the number of variables can be reduced by one (the pressure is constant) and the phase rule equation will have the form:

$$\boxed{c = k - f + 1}$$

This form of the Gibbs phase rule (under the assumption that pressure is unvariable in all the processes) will be used in the analysis of equilibrium of metallic systems.

Let us see how the degree of freedom of a single-component system ($k = 1$) varies in the case of crystallization of a pure metal. When the metal is liquid, i.e. $f = 1$ (there is only one phase, the liquid), the number of degrees of freedom is unity ($c = k - f - 1 = 1 - - 1 + 1 = 1$).

In that case, the temperature of the metal can be varied without causing a change in the state of aggregation. At the moment of crystallization, $f = 2$ (there are two phases: liquid and solid), $c = k - - f + 1 = 1 - 2 + 1 = 0$. This means that the two phases can be in equilibrium only at a strictly definite temperature (melting point) and that this temperature cannot be changed until one of the phases disappears, i.e. the system becomes monovariant ($c = 1$).

5-2. GENERAL REMARKS ON THE CONSTRUCTION OF CONSTITUTIONAL DIAGRAMS

The constitutional diagram shows how the state of a substance varies depending on temperature and concentration (pressure is assumed to be constant in all cases to be considered).

If a system is single-component, its constitutional diagram will have only one dimension (temperature scale), i.e. will be a straight line, with points on that line marking the equilibrium temperature of a change in the state of aggregation (Fig. 5-1).

For a system of two components, the diagram will have two dimensions, the second dimension determining the concentration of the alloy. Thus, its diagram is constructed in two dimensions (temperature-concentration), see Fig. 5-2.

Temperatures are laid off on the axis of ordinates and concentrations, on abscissa. The total content of both components in the alloy is 100 per cent and every point on the abscissa corresponds to a particular content of each component. For instance, point C gives 40 per cent B and 60 per cent A; point D. 60 per cent B and 40 per cent A; etc. As we move away from point A, the concentration of component B increases up to 100 per cent at point B. Therefore, the extreme ordinates of the diagram correspond to pure components and intermediate ordinates, to binary alloys.

Constitutional diagrams for alloys of three components are tridimensional (two concentration axes and a temperature axis). Systems of four or more components are also depicted as tridimensional diagrams, but with certain simplifications, since they have more than three independent variables.

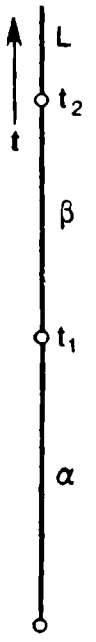

Fig. 5-1. Effect of temperature on changes in the state of aggregation in a single-component system

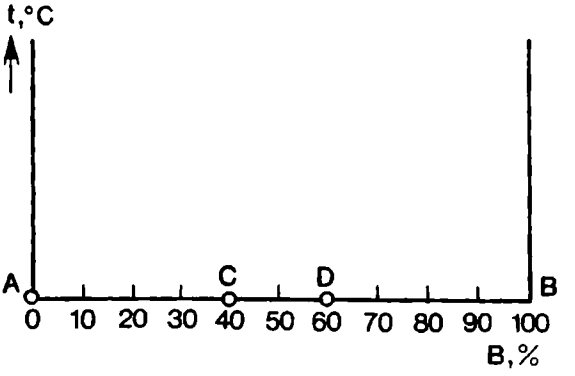

Fig. 5-2. Coordinates to determine the states of a two-component system

Each point on the constitutional diagram shows the state of the alloy of a given concentration and at a given temperature. Each vertical line determines temperature variations for a particular alloy. A change in the phase state of an alloy is marked by a point on the diagram. The lines which connect points of analogous transformations divide the diagram into regions of analogous phase states. The form of a constitutional diagram depends on how the two constituents can react with each other in the solid and liquid states, i.e. whether they are mutually soluble in the liquid and solid states or form chemical compounds.

The existence of a particular phase is determined by its thermodynamic potential. For instance, the α-modification in a single-component system has a lower value of the thermodynamic potential (free energy) than the β-modification at temperatures below t_1, and vice versa. At the temperature of t_1, the free energy of α-modification is equal to that of β-modification. Similarly, the temperature t_2 divides the regions of equilibrium existence of the liquid (L) and solid (β) states.

If temperature dependence for the free energy of a given substance (metal) is known (has been found by calculation), it is then evidently possible to determine the temperature of equal free energies of different states without direct experiments and to determine the temperature of equilibrium crystallization or that of equilibrium transformation of one modification into another.

Using the same principle, but a more complicated technique, we can determine from thermodynamic functions the points of transformations in alloys. So far such a calculation gives less accurate results than direct experiments;

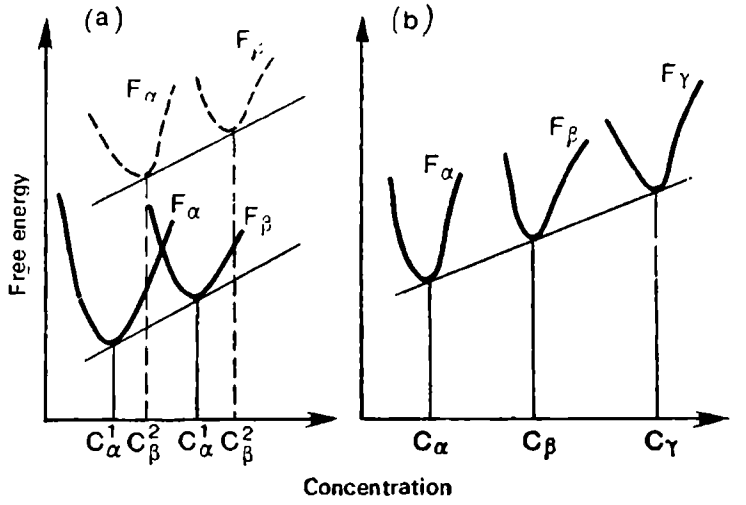

Fig. 5-3. Effect of concentration on free energy F

(*a*) two-phase state; (*b*) three-phase state

this is why real constitutional diagrams have been constructed by using direct experimental methods.

According to Gibbs' phase rule, a two-component system (at a constant pressure) with two phases present in it has one degree of freedom ($c = k - f + 1 = 2 - 2 + 1 = 1$), i.e. the concentration of phases is definite at a given temperature.

If we consider the free energy of two solid solution α and β as a function of concentration, the minimum of free energy for each phase at a given temperature will conform to a definite concentration (Fig. 5-3). In other words, we shall have c^1_α and c^1_β for temperature t_1 (solid lines in Fig. 5-3*a*) and c^2_α and c^2_β for t_2 (dashed lines in the same figure). For multi-component systems (with two or more phases), a tangent can be drawn through the points corresponding to the minima of free energy of a given phase.

For a case of three-phase equilibrium, $c = 0$ ($c = k - f + 1 = 2 - 3 + 1 = 0$), i.e. the system can be in equilibrium only at a definite temperature and a definite phase composition. Since the free energies of phases α, β and γ may vary differently with temperature, there exists only one temperature point at which a common tangent can be drawn through all the three minimum points (Fig. 5-3*b*). This state corresponds to the conditions of non-variant equilibrium ($c = 0$).

5-3. EXPERIMENTAL CONSTRUCTION OF CONSTITUTIONAL DIAGRAMS

Constitutional diagrams are usually constructed by the results of thermal analysis, i.e. cooling curves are obtained for a system, and the arrest and inflection points appeared on the curves due to the thermal effects of transformations are used to determine the points of transformation in the system.

Temperature measurements in metals are commonly made by means of *thermocouples*. The measuring principle is as follows. A thermocouple consists of two wires made of various metals, the wires being welded together at one end (which is called 'hot junction') and by their other ends connected to a galvano-

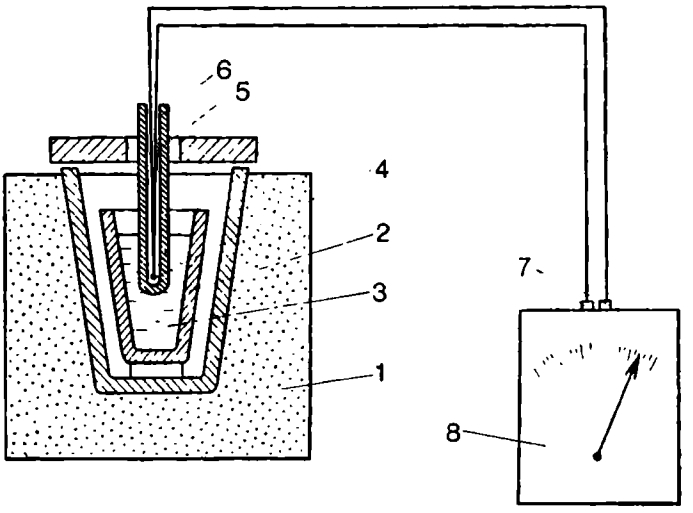

Fig. 5-4. An apparatus for thermal examination of crystallization process (schematically)

1—kiln; *2*—crucible; *3*—molten metal; *4*—hot junction; *5*—thermocouple; *6*—cap; *7*—cold junction; *8*—galvanometer

meter or another sensitive instrument (say, potentiometer) which can measure currents of a very low potential difference[1].

On heating the hot junction, a current appears in the thermocouple and its magnitude will be greater at a higher temperature of the hot junction. With proper calibration of the thermocouple-galvanometer system, the instrument can be used for direct me surements of temperatures in furnaces, molten metals, etc.

The temperature of the point of crystallization is determneid experimentally as follows. An alloy *3* to be analysed is placed in crucible *2* and melted in kiln *1* (Fig. 5-4). Upon melting, the hot junction *4* of thermocouple *5* (protected by a porcelain or quartz cap *6*) is immersed into the molten metal and the kiln is let to cool. The temperature of the metal is measured in regular time intervals during cooling. Any change in the state of aggregation of the metal (due to the evolution of latent heat of transformation) is plotted on the time-temperature curve.

Having made such measurements for a number of alloys and having determined the transformation points for each alloy, we can construct the constitutional diagram of the given system.

In a more accurate construction of constitutional diagrams, the thermal method is assisted by microscopic and *X*-ray analysis of the structure of alloys of various composition and differently heat-treated, by measurements of the physical properties of alloys, etc.

Consider an example. Take a system consisting of two components which neither are mutually soluble in the solid state nor form chemical compounds with each other, but are unlimitedly soluble in the liquid state. It may be taken, with some approximation, that the system considered is that of lead and antimony (actually these two

[1] For higher accuracy of measurements, the cold junction ends are placed into a thermostat (not shown in Fig. 5-4).

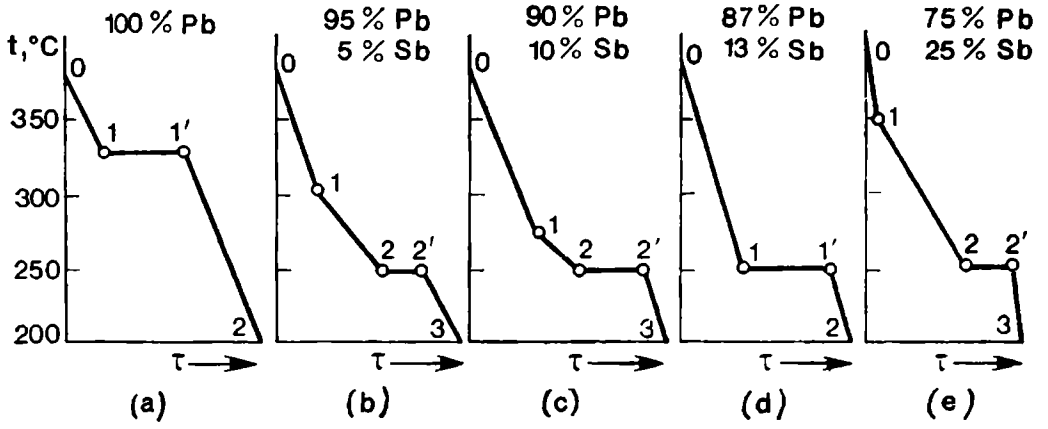

Fig. 5-5. Cooling curves of Pb-Sb alloy

metals are limitedly soluble in the solid state). Assume further that there is a series of alloys of these metals; observations on crystallization of these alloys have given a series of cooling curves (Fig. 5-5).

The curve in Fig. 5-5*a* relates to pure lead which is liquid at temperatures above 327°C, crystallizes at that point, and is in crystalline (solid) state below that temperature. Therefore, the portion *0-1* of the cooling curve for lead represents cooling of liquid, portion *1-1'* represents the crystallization process, and portion *1'-2*, cooling of solid lead.

The curve in Fig. 5-5*b* has been obtained for an alloy of 95 per cent Pb and 5 per cent Sb. Its crystallization begins at a lower temperature than in the previous case (point *1*) and proceeds at varying temperature (from point *1* to point *2*), and then the remaining liquid crystallizes at a constant temperature of 246°C (see portion *2-2'* of the curve). During solidification at a variable temperature (portion *1-2*), crystals of lead separate out from the liquid. This agrees well with Gibbs' phase rule, i.e. the number of degrees of freedom for this case is unity. The system has two components and the number of phases is two (liquid and lead crystals), therefore:

$$c = k - f + 1 = 2 - 2 + 1 = 1$$

Simultaneous crystallization of lead and antimony should proceed at a constant temperature (portion *2-2'*), since three phases exist at that temperature (liquid, antimony crystals and lead crystals) and the number of degrees of freedom is zero ($c = k - f + 1 = 2 - 3 + 1 = 0$).

Since lead separates out continually from the liquid in portion *1-2* of the crystallization curve, the liquid is gradually enriched in antimony. By the time when lead begins to crystallize (at point *1*) the liquid contains 5 per cent Sb, but in point *2*, i.e. by the time of com-

bined crystallization of antimony and lead, it already has, as experience shows, as much as 13 per cent Sb.

Point *1* which corresponds to the beginning of crystallization is called the *liquidus* point, and point *2*, representing the end of crystallization, the *solidus* point.

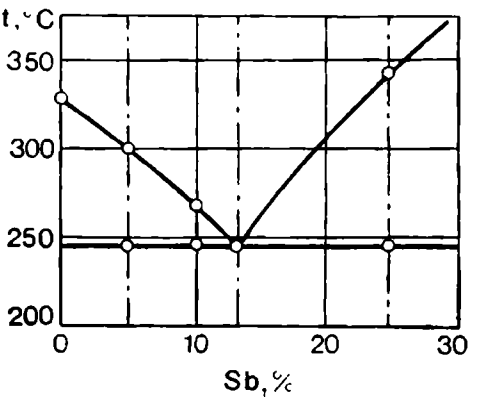

Fig. 5-6. Constitutional diagram of lead-antimony alloys constructed on the basis of cooling curves in Fig. 5-5

In an alloy with 10 per cent Sb (Fig. 5-5*c*), crystallization will occur in the same manner as in that with 5 per cent Sb, but it will start from a lower temperature. Note that the conjoint crystallization of lead and antimony in this alloy will start at the same temperature as in the previous alloy and that the liquid will have by the time of conjoint crystallization the same concentration, i.e. 13 per cent Sb and 87 per cent Pb.

If we take an alloy corresponding to this proportion, i.e. containing 13 per cent Sb and 87 per cent Pb, both types of crystals will evolve simultaneously at a definite temperature and without preliminary crystallization of lead (see Fig. 5-5*d*). Finally, in an alloy with more than 13 per cent Sb, antimony will evolve first (see Fig. 5-5*e*) and the alloy will be gradually enriched in lead; when it cools down to 246°C, the liquid will contain 13 per cent Sb and after that the conjoint crystallization of both types of crystals will proceed at a constant temperature.

For the five alloys considered, the points of the start (t_s) and the finish (t_f) of crystallization are as follows:

Alloy	t_s, °C	t_f, °C
100% Pb	327	327
95% Pb+5% Sb	300	246
90% Pb+10% Sb	260	246
87% Pb+13% Sb	246	246
75% Pb+25% Sb	340	246

Plotting the temperatures obtained on a concentration-temperature diagram and connecting all the liquidus points by a line and all the solidus points by another line, we obtain the constitutional diagram of the Pb-Sb system (Fig. 5-6).

The locus of the liquidus points is called the *liquidus line* and that of solidus points, the *solidus line.*

Evidently. all alloys above the liquidus line are in liquid state and those below the solidus line are solid. In alloys containing less

than 13 per cent Sb, lead crystallizes first. Consequently, these alloys have a liquid phase and crystals of lead in the region confined between the liquidus and solidus lines. Similarly, the alloys with more than 13 per cent Sb contain the liquid and crystals of antimony in the region between the liquidus and solidus lines. Thus, the diagram in Fig. 5-6 shows the constitution of all alloys of a given system, i.e. for a given pair of constituents at any proportion and any temperature. This is why such diagrams are called constitutional. They are used for studying the nature of alloys.

A constitutional diagram makes it possible to determine the structure an alloy will have on slow cooling and also to decide whether the structure of a given alloy can be changed by heat treatment. Since the technological and operating properties of alloys are closely associated with their microstructure, constitutional diagrams are of great importance for practical metallurgy.

The type of diagram is determined by the nature of the interactions which are possible between the constituents in the liquid and solid states. The constitutional diagrams of the most typical metallic systems are discussed in the following sections. In all cases it is assumed that the constituents are unlimitedly soluble in the liquid state, i.e. a homogeneous liquid phase (further designated by L) exists at any concentration of the constituents.

Diagrams for systems with limited or no solubility in the liquid state will not be discussed, as they have no wide application in engineering.

5-4. THE CONSTITUTIONAL DIAGRAM OF SYSTEMS FORMING MECHANICAL MIXTURES OF PURE CONSTITUENTS (FIRST-ORDER SYSTEMS)

In first-order systems, the two constituents are unlimitedly soluble in the liquid state and insoluble in the solid state and do not form chemical compounds. It should be noted that evidently there are no metals which are absolutely insoluble in each other in the solid state; for practical and methodical purposes it is convenient to distinguish a group of alloys whose constituents are badly soluble in each other in the solid state and to take their solubility equal to zero. However, it cannot be stated that all substances are soluble in the solid state, though to some extent. Certain substances, which form molecules with different nature of bond, do not form solid solutions (i.e. are crystallized to the first-order diagram). An example is the crystallization of water solutions of salts.

Let the system considered be composed of substances A and B ($k = 2$). Its phases are: liquid L, crystals of A, and crystals of B (the maximum number of phases is $f = 3$).

The constitutional diagram of this system is shown in Fig. 5-7. *ACB* is the liquidus line and *DCE*, the solidus line. On cooling, *A* crystals begin to crystallize under line *AC* and *B* crystals, under line *CB*. Along line *DCE*, both types of crystal begin to separate out from the liquid when the latter's concentration reaches *C*.

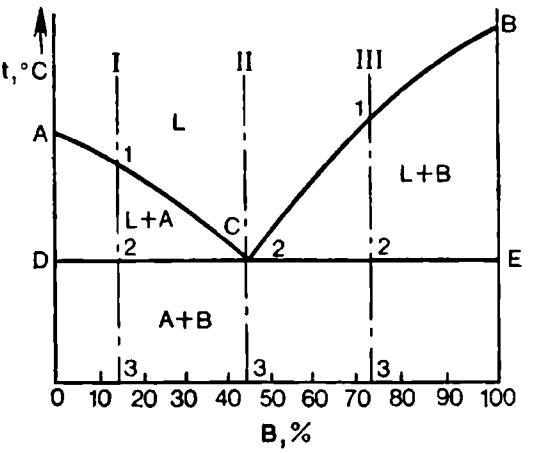

Fig. 5-7. Constitutional diagram to analyse the crystallization of alloys *I-III* in Fig. 5-8

If we take a particular alloy, say *I*, its cooling curve will be as shown in Fig. 5-8*a*. On that curve, portion *0-1* corresponds to cooling of the liquid alloy, portion *1-2* to separation of *A* crystals, portion *2-2'* to conjoint crystallization of *A* and *B*, and portion *2'-3* to cooling of solid metal.

The structures of the alloy at various moments of crystallization are shown schematically under the curve in Fig. 5-8*a*. In the leftmost picture, *A* crystals separate out from the liquid. In the middle

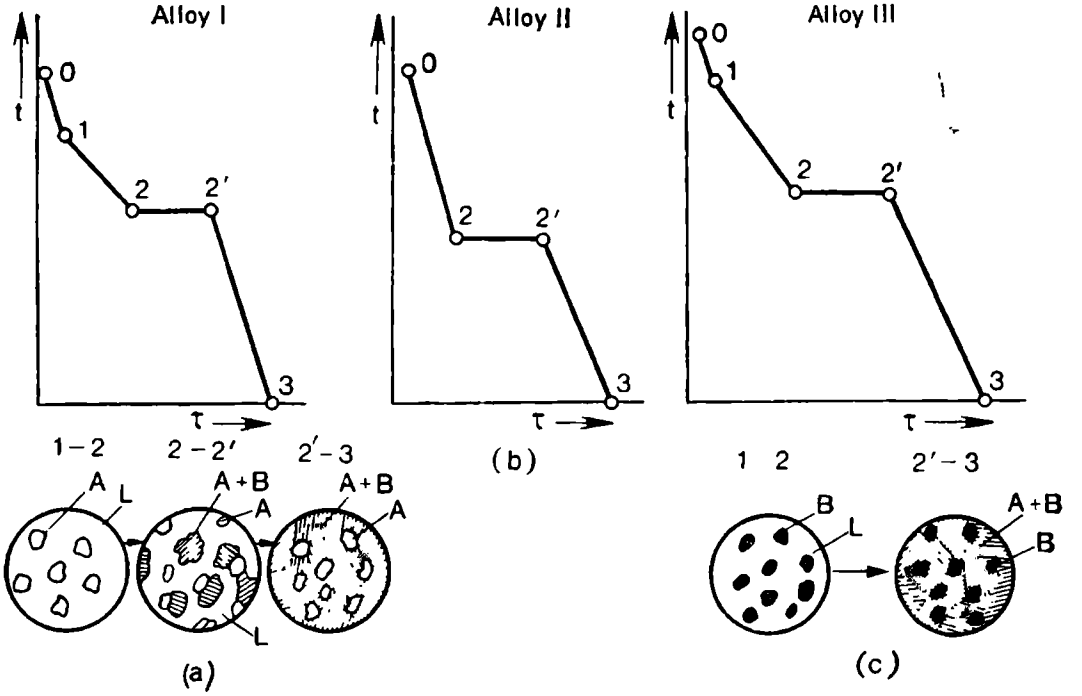

Fig. 5-8. Cooling curves and correspoding structures
(*a*) hypoeutectoid alloy; (*b*) eutectic alloy; (*c*) hypereutectoid alloy

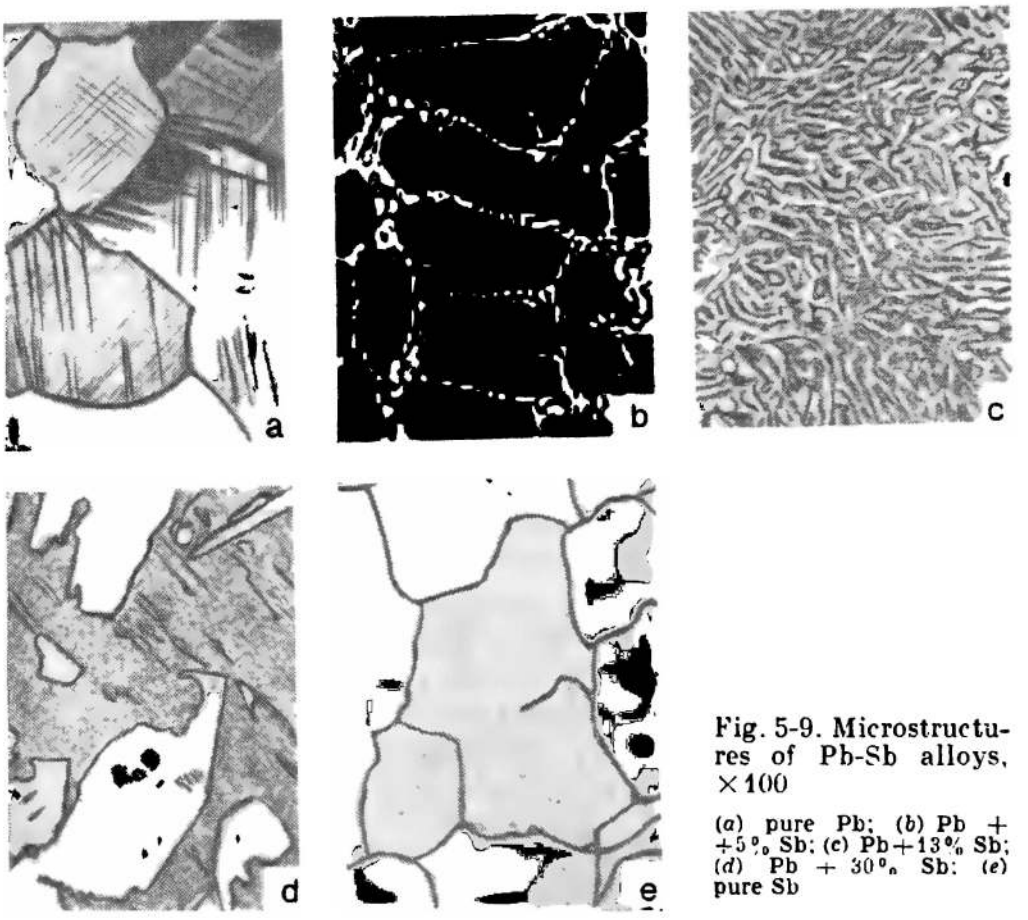

Fig. 5-9. Microstructures of Pb-Sb alloys, ×100

(*a*) pure Pb; (*b*) Pb + +5% Sb; (*c*) Pb+13% Sb; (*d*) Pb + 30% Sb; (*e*) pure Sb

picture, *A* and *B* crystals are formed. The rightmost picture shows the structure of solidified metal, i.e. primary precipitates of *A* crystals and mechanical mixture of crystals of *A* and *B* which have crystallized simultaneously.

The mechanical mixture of two (or more) components which have simultaneously crystallized from the liquid is called the *eutectic*.

The cooling curve for an alloy of eutectic concentration is shown in Fig. 5-8*b*. On this curve, portion *0-2* is cooling of the liquid alloy; *2-2'*, crystallization of eutectic; and *2'-3*, cooling of crystallized solid alloy.

The cooling curve of a hypereutectoid alloy (alloy *III*) is shown in Fig. 5-8*c*, where portion *0-1* is cooling of the liquid, portion *1-2* is precipitation of *B* crystals, *2-2'* is crystallization of eutectic, and *2'-3*, cooling of the solidified metal. The structures of this alloy at various moments of crystallization are shown below the cooling curve. Here, *B* crystals are depicted black to distinguish them from *A* crystals (white) in Fig. 5-8*a*.

Thus, in first order systems, we may distinguish between hypoeutectoid alloy *I*, eutectic alloy *II*, and hypereutectoid alloy *III*.

Figure 5-9 shows microstructures of real alloys in the Pb-Sb system.

The constitutional diagram in Fig. 5-7 shows the regions of existence of various phases. Below the eutectic horizontal line DCE there are two phases: crystals A and B. To the left of the vertical eutectic concentration line (dotted in the figure), A crystals first separate out from the liquid and after that the eutectic crystallizes. Therefore, the structural state of a hypoeutectoid alloy can be described as A + (A + B)-eutectic and that of a hypereutectoid alloy, as B + + (A + B)-eutectic, though in both cases the alloy has only two phases: A and B.

5-5. THE LEVER RULE

The crystallization process involves changes both in concentration of phases, therefore, in the composition of the liquid (for instance, crystals of one of the constituents precipitate from the liquid) and in their proportion (the proportion of a solid phase increases and that of the liquid phase, decreases). When two phases co-exist in a system, the proportion and concentration of both phases can be determined for any point on the constitutional diagram by using what is called the *lever rule*, or the *rule of sections*.

At point a which represents the constitution of alloy K at temperature t_1 (Fig. 5-10), the system consists of B crystals and liquid. Above point l, the system is single-phase and the concentration of the constituents in that phase (i.e. in the liquid) is determined by the projection of point l. During cooling, B crystals precipitate from the system and the composition of the liquid changes towards increasing the proportion of A component. At temperature t_1, the concentration of B in the liquid is determined by the projection of point b; this is the maximum concentration of B that the liquid can contain at t_1. On cooling to the eutectic temperature, the liquid has the eutectic concentration. Therefore, when alloy K is being cooled, the concentration of the liquid varies along the curve lC. The precipitated B crystals have a constant composition (pure B constituent) and the concentration of B in them is represented by the vertical line BB.

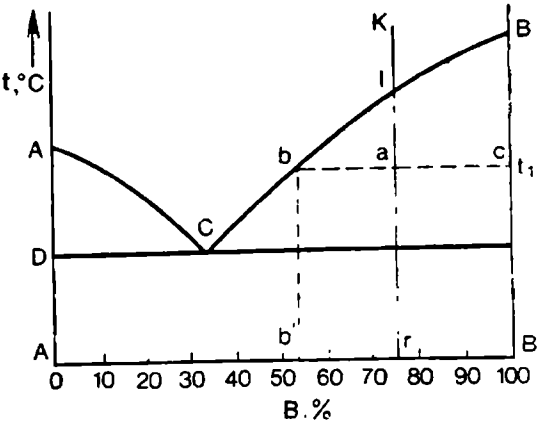

Fig. 5-10. Constitutional diagram (to explain the lever rule)

The first lever rule condition can be formulated as follows: *To determine the concentrations*

of components in the phases, a horizontal line is drawn through the point describing the constitution of a given alloy to intersect the lines confining the given phase region; the projections of the intersection points onto the concentration axis will give the concentrations of the phases.

Consequently, for alloy K at temperature t_1, the concentrations of its phases are determined by the projections of points b and c, since these points are intersections of the horizontal line passing through point a with the curves of the diagram.

The proportion of the phases can be determined by using the second lever rule condition.

Assume that an alloy K is at temperature t_1 and contains r per cent of B and $(100 - r)$ per cent of A. Therefore, if the section AB of the abscissa is 100 per cent, the section rA will determine the proportion of B in the alloy and the section rB, that of A.

At point a, the alloy is composed of B crystals and of the liquid of concentration b. The liquid contains b' per cent of B, i.e. the proportion of B component in it is determined by section Ab'.

Taking that the total mass of the alloy is unity, the sought-for quantity of precipitated crystals is x and the quantity of the remaining liquid, $1 - x$. In that case the quantity of A present in the liquid only is:

$$b'B\,(1 - x) = b'B - xb'B = rB$$

$$xb'B = b'B - rB$$

$$x = \frac{b'B - rB}{b'B}$$

Since

$$b'B - rB = b'r = ba$$

and

$$b'B = bc$$

we have

$$x = \frac{ba}{bc}$$

i.e., if the mass of alloy K is unity and depicted by section bc, the mass of crystals in the state of point a is equal to the ab/bc ratio.

The quantity of the liquid can be found as

$$1 - x = 1 - \frac{ba}{bc} = \frac{bc - ba}{bc} = \frac{ac}{bc}$$

i.e. is determined by the ac/bc ratio.

The proportion of the solid to the liquid phase is found as

$$\frac{x}{1 - x} = \frac{ba \times bc}{bc \times ac} = \frac{ba}{ac}$$

If point a describes the constitution of the alloy, point b, the composition of the liquid phase, and point c, the composition of the so-

lid phase, the total mass of the alloy will be determined by section *bc*, the quantity of liquid in it, by section *ac*, and the quantity of crystals, by section *ba*.

The second lever rule condition can be formulated as follows: *To determine the proportion of phases in an alloy, a horizontal line should be drawn through the point describing the constitution of that alloy in the constitutional diagram. The sections of that line between the given point and the points determining the phase composition are inversely proportional to the quantities of the phases.*

In binary constitutional diagrams, the lever rule is only applicable in two-phase regions. In a single-phase region, there is only one phase and its concentration can be characterized by any point within that region. With three phases co-existing in a binary system, their quantities cannot be determined, since they vary continually during crystallization. For instance, in the diagram of first-order systems, three phases may co-exist at the temperature of eutectic solidification when the three phases are in equilibrium and their concentration points lie on the same horizontal, i.e. there exist the liquid of concentration *C*, *A* crystals of concentration *D* and *B* crystals of concentration *E* (see Fig. 5-7). In the course of crystallization, the concentration of the liquid phase *C* diminishes and the concentrations of the solid phases increase, but the compositions of the phases remain unchanged.

5-6. THE CONSTITUTIONAL DIAGRAM OF SYSTEMS WITH UNLIMITED SOLUBILITY OF CONSTITUENTS IN THE SOLID STATE (SECOND-ORDER SYSTEMS)

The two constituents are unlimitedly soluble in the liquid and solid states and do not form chemical compounds.

The components of the system are *A* and *B* and its phases, *L* and α.

If two components are unlimitedly soluble in the liquid and solid states, only two phases—liquid solution *L* and solid solution α—can exist in the system. Therefore, only two, but not three, phases can co-exist, there will be no crystallization at a constant temperature and no horizontal line in the diagram.

The diagram shown in

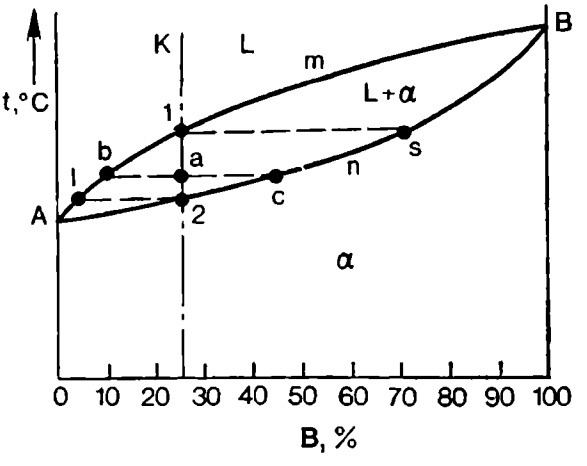

Fig. 5-11. Constitutional diagram of a system with unlimited solubility in the solid state

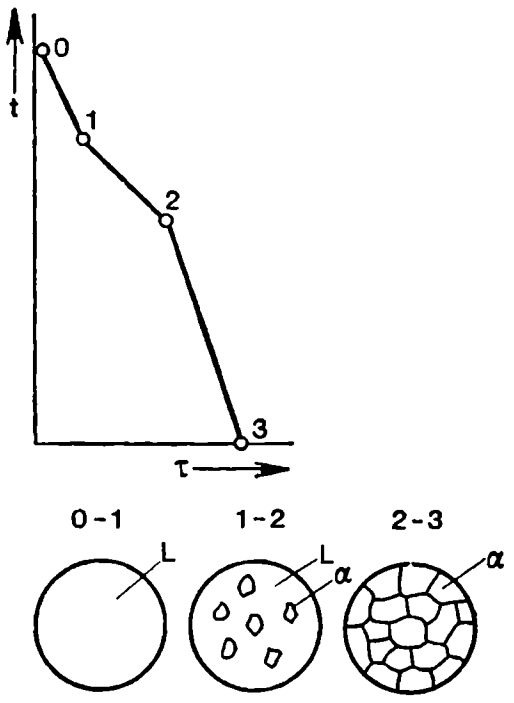

Fig. 5-12. Cooling curve and structures of an alloy forming a solid solution

Fig. 5-11 has three regions: liquid, liquid + solid soluiton, and solid solution.

AmB is the liquidus line, and *AnB*, the solidus line. The crystallization process is described by the cooling curve of the system (Fig. 5-12).

Point *1* corresponds to the beginning of crystallization, point *2*, to the end. An alloy is in a two-phase state between these points (i.e. between the liquidus and solidus lines). Since the system has two constituents and two phases, it is monovariant ($c = k - f - 1 = 2 - 2 - 1 = 1$), i.e. the concentration of the constituents in the phases varies with temperature; each temperature conforms to a strictly definite phase composition. The concentration and quantity of the phases for an alloy between the liquidus and solidus lines can be determined by the lever rule. For instance, an alloy *K* at point *a* (see Fig. 5-11) contains a liquid and a solid phase. The composition of the liquid phase is determined by the projection of point *b* on the liquidus line and that of the solid phase, by the projection of point *c* on the solidus line. The quantities of the liquid and solid phases are determined by the following ratios: that of the liquid phase by *ac/bc* and that of the solid phase by *ba/bc*.

Note that crystals enriched in the higher-melting component precipitate from the liquid melt, whose initial concentration is *K*, in the whole crystallization interval (from point *1* to point *2*). The composition of the first precipitated crystals is determined by point *s*. The crystallization of the alloy *K* should come to its end at point *2*, when the last liquid droplet of composition *l* solidifies. The section which determines the quantity of solid phase is equal to zero at point *1* when crystallization has just started and to the quantity of the whole alloy at point *2* when crystallization come to its end. The composition of the liquid varies along the curve *1-l* and that of crystals, along the curve *s-2*. At the end of crystallization, the composition of crystals is the same as that of the original liquid.

5-7. THE CONSTITUTIONAL DIAGRAM OF SYSTEMS WITH LIMITED SOLUBILITY IN THE SOLID STATE (THIRD-ORDER SYSTEMS)

The two components are unlimitedly soluble in the liquid state, limitedly soluble in the solid state and do not form chemical compounds.

The components in the system are *A* and *B*.

The phases that can co-exist in the system are: the liquid phase (*L*); a solid solution of *B* in *A* (let it be called α-solution); and a solid solution of *A* in *B* (β-solution). Alloys of these systems can be under non-variant equilibrium with three phases (*L*, α, and β) co-existing in them. Two types of diagram are possible: the one with eutectic and that with peritectic, depending on the reaction which takes place when three phases exist.

Diagram with Eutectic

In this system, pure-component phases are not formed, and only solid solutions (α or β) can precipitate from the liquid. Therefore, the regions of existence of solid solutions α and β are located at the vertical lines *A* and *B* corresponding to pure constituents (Fig. 5-13). The ultimate solubility of *B* in *A* is determined by line *DF* and that of *A* in *B*, by line *CG*.

Alloys confined between these two lines are beyond the solubility limit and represent two-phase systems whose composition is α + β.

AEB is the liquidus line in the diagram and *ADCB*, the solidus line. Using the Gibbs phase rule and the lever rule, we can follow the crystallization process of any alloy in the system.

Crystallization of alloy I. Above point *1*, the alloy is liquid. Crystallization starts at that point by precipitation of crystals of α-solid solution whose concentration varies along the curve *a-2*, and the composition of the liquid varies along the curve *1-b*. Crystallization comes to its end at point *2* and the solid solution crystals formed should have (for equilibrium crystallization) the same concentration as that of the original liquid.

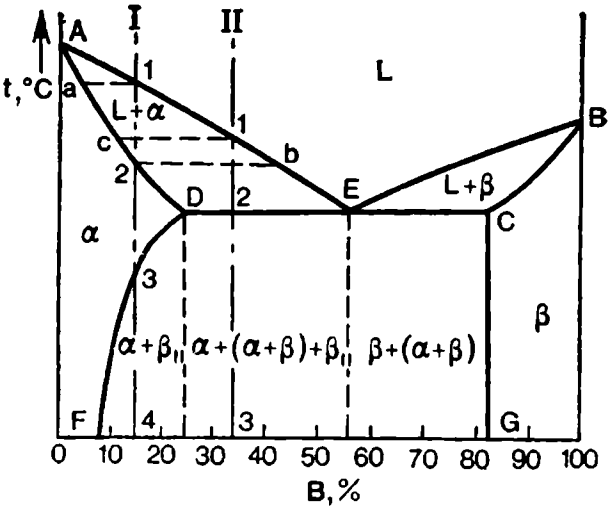

Fig. 5-13. Constitutional diagram of a system with eutectic

These crystals undergo no changes up to point *3* which lies on the ultimate solubility line. Below that point, α-solid solution is supersaturated and separates excess crystals. These are β-solid solution crystals, which can be determined by applying the lever rule to an alloy inside the two-phase region $\alpha + \beta$ (i.e. an alloy below *DF* line).

The composition of α-solid solution varies along the curve *3-F* owing to the precipitation of β-crystals of concentration *G*. The quantity of β-crystals precipitated from alloy *I* increases as cooling proceeds and is characterized by a section confined between curve *3-F* and vertical line *I*.

The cooling curve and structures of that alloy at various temperatures are shown in Fig. 5-14*a*.

The crystals of β which precipitate from solid solution are called *secondary crystals* and are often denoted as β_{II} to distinguish them from primary β-crystals (β_I) which precipitate from the liquid. The process of precipitation of secondary crystals from a solid phase is called *secondary crystallization* (or grain growth), in contrast to *primary crystallization* in which crystals (primary) are formed in the liquid phase.

It should be noted that an alloy, whose concentration is to the left of point *F*, is not capable of precipitating secondary β-crystals.

Since line *CG*, unlike *FD*, is shown vertical in Fig. 5-13, i.e. the solubility of *A* in *B* is independent of temperature, there will be no secondary α-precipitates in the alloy. If, however, line *CG* were inclined to the right, i.e. if the solubility of *A* in *B* decreased with decreasing temperature, the precipitation of secondary α-crystals would be possible.

Point *D* for the α-solid solution gives the maximum solubility of *B* in *A* under the most favourable conditions.

Crystallization of alloy II. As distinct from the previous case, the crystallization of this alloy is associated with a non-variant reaction on reaching the horizontal line *DEC*. Three phases are in equilibrium: liquid *E*, α-crystals of the composition determined by point *D*, and β-crystals of the composition *C*. Let us employ a symbolic notation with subscripts at phase symbols determining the composition of phases. For instance, α_D implies an α-solid solution of the composition described by point *D*. As the temperature reaches the horizontal line *DEC*, a eutectic reaction begins, i.e. crystals of both solid solutions precipitate from the liquid:

$$L_E \rightarrow \alpha_D + \beta_C$$

In a more general form, the eutectic reaction can be written as follows:

$$\boxed{L \rightarrow \alpha + \beta}$$

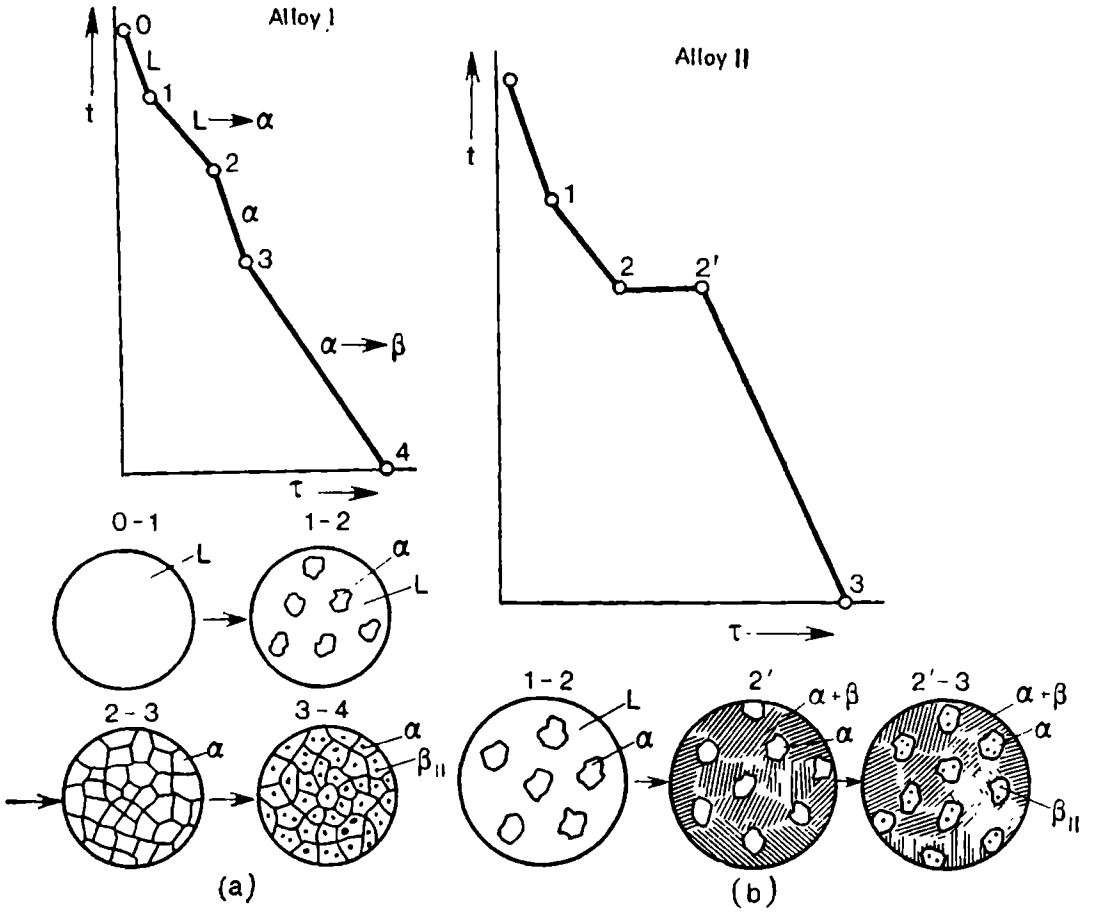

Fig. 5-14. Cooling curves and structures of

(*a*) an alloy which forms a solid solution during crystallization, with subsequent precipitation of a secondary phase; (*b*) a hypoeutectoid alloy

The reaction is non-variant, since two components and three phases participate in it ($c = k - f + 1 = 2 - 3 + 1 = 0$).

Each of the three phases participating in the reaction has definite compositions (determined by the projections of points E, D and C) and a constant temperature of transformation.

Thus, the crystallization of alloy *II* results in the formation of a eutectic $\alpha + \beta$ and of primary α-crystals (which have precipitated during cooling from point *1* to point *2*).

Further cooling varies the solubility, so that secondary β_{II}-crystals precipitate from α-crystals and at room temperature α-crystals (both primary and those contained in the eutectic) will have the composition corresponding to point F.

The cooling curve and structures of alloy *II* are shown in Fig. 5-14*b*.

Secondary crystals precipitated from eutectic components usually cannot be detected microscopically, since secondary precipitates are combined with the like phase of the eutectic.

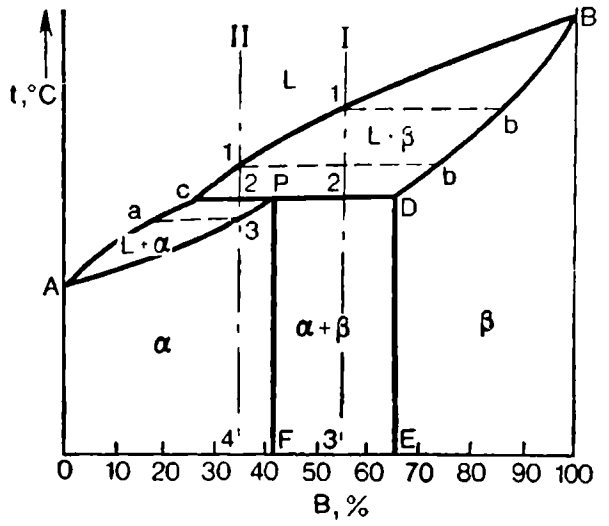

Fig. 5-15. Constitutional diagram of a system with peritectic

Notwithstanding the multitude of structural components[1], an alloy, upon complete cooling, contains only two phases: α and β, so that the lever rule, if applied below line *DE*, will give the total quantity of α- and β-phases irrespective of the structural form in which they are present in the alloy.

Diagram with Peritectic

With eutectic transformation, the liquid crystallizes into two solid phases. A different type of non-variant transformation (three-phase equilibrium) is also possible, where the liquid reacts with the crystals that have precipitated earlier and forms a new type of crystals. Reactions of this type are called *peritectic*.

A diagram with peritectic transformation is shown in Fig. 5-15. It has three single-phase regions: liquid *L* and limited solid solutions α and β.

ACB is the liquidus line and *APDB*, the solidus line.

Crystallization of alloy I. The crystallization begins at point *1* (Fig. 5-16*a*), where β-solution crystals of composition determined by point *b* precipitate from the liquid. As the temperature is lowered further, the concentration of the liquid varies along the liquidus line from point *1* to point *C* and that of β-crystals, along the solidus line from point *b* to point *D*. Upon reaching the peritectic horizontal line *CPD*, the composition of the liquid will correspond to point *C* and that of crystals, to point *D*. These two phases react to form a third phase, α, whose concentration is determined by point *P*, the third point of the horizontal peritectic line. A peritectic reaction can be written as

$$L_C + \beta_D \rightarrow \alpha_P$$

or in a more general form

$$\boxed{L + \beta \rightarrow \alpha}$$

[1] Primary α-solid solution, secondary crystals of β-solid solution, and α + + β-eutectic.

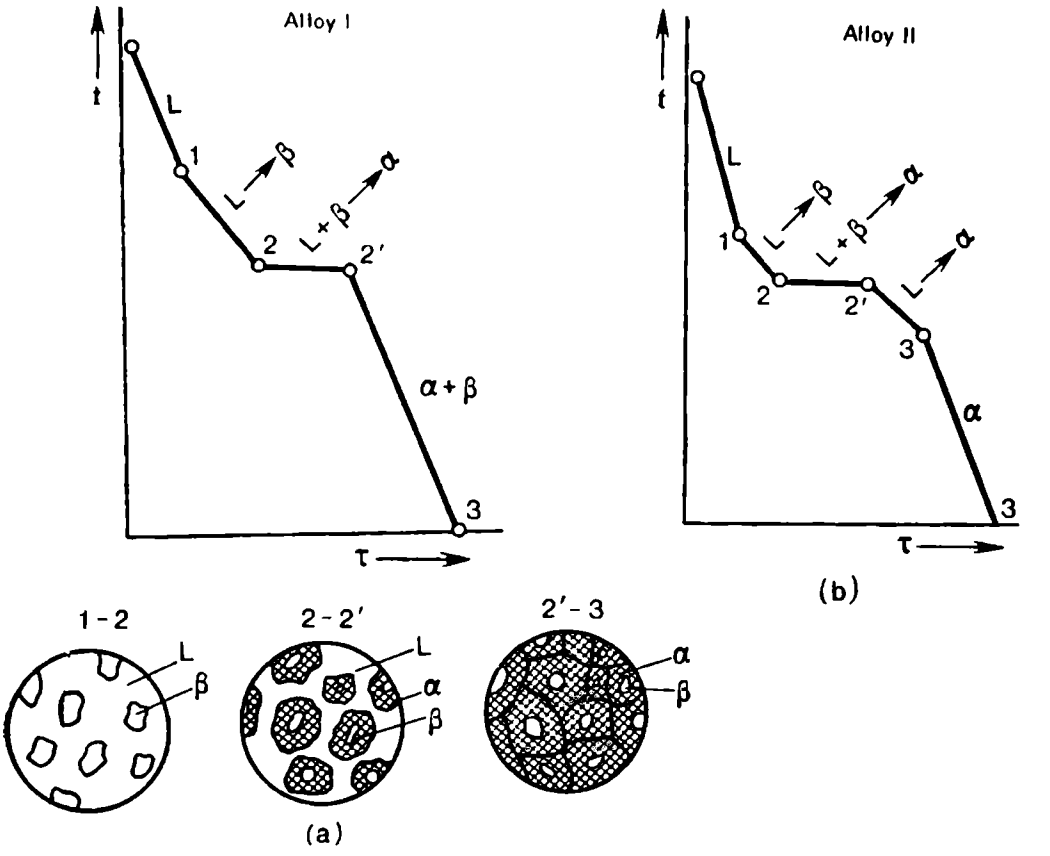

Fig. 5-16. Cooling curves and structures of peritectic alloys

(*a*) with solid solution remained in excess upon peritectic reaction; (*b*) with a liquid phase remained

since points D and P determine the ultimate concentration of β- and α-solid solutions (for simplicity, the ultimate solubility lines are shown vertical in the figure). The ratio of phases in a peritectic reaction that is needed to form an α-phase is determined by the lever rule:

$$\frac{\text{quantity of } \beta}{\text{quantity of } L} = \frac{CP}{PD}$$

For the alloy considered, the quantity of β-crystals and of the liquid participating in the peritectic reaction is determined by the ratio:

$$\frac{\text{quantity of } \beta}{\text{quantity of } L} = \frac{C2}{2D}$$

i.e. there is an excess of β-phase over the quantity required to form α-crystals. This is why β-crystals remain in excess upon the peritectic reaction. Therefore, the structure will contain the products

of the peritectic reaction (α-crystals) and the excess primary β-crystals. The quantity of remaining β-crystals is lower when point *2* is closer to point *P*.

For an alloy of the concentration at point *P*, the ratio of liquid to β-crystals in peritectic transformation is exactly such as needed to form α-crystals of the ultimate concentration.

The cooling curve for alloy *I* and the structures formed at the typical moments of crystallization are shown in Fig. 5-16*a*. Peritectic crystallization (the middle picture) may be characterized by that the new α-phase appears at the interface between the reacting liquid and β-crystals. With alloy *I*, the peritectic reaction completes the crystallization process.

Crystallization of alloy II (Fig. 5-16*b*). This alloy differs from the previous one in that there is an excess of the liquid phase at the peritectic temperature, compared with the quantity required to form α-crystals of concentration *P*. Therefore, the peritectic transformation is finished by exhaustion of the β-solid solution, and the remaining liquid crystallizes within the interval *2'-3* into the α-phase. In this process, the concentration of the liquid varies along the curve *C-a* and that of α-crystals, along *P-3* (see Fig. 5-15).

5-8. THE CONSTITUTIONAL DIAGRAM OF SYSTEMS FORMING CHEMICAL COMPOUNDS (FOURTH-ORDER SYSTEMS)

As has been defined earlier (see Sec. 4-2), a chemical compound is characterized by a definite proportion of its constituent elements, which will plot in the constitutional diagram as a vertical line intersecting the abscissa at a point corresponding exactly to this proportion. If components *A* and *B* form a chemical compound, say A_nB_m, then the $n + m$ molecules of this compound contain *n* atoms of *A* and *m* atoms of *B*. A definite atomic ratio has a corresponding mass ratio.

A chemical compound is considered to be stable if it can be heated to the melting without decomposition; otherwise it is unstable. This circumstance determines two types of constitutional diagram. Besides, two components may form more than one chemical compound or may be soluble in one another; all these are plotted in constitutional diagrams.

Diagram with a Stable Compound

Suppose that two components can form only one stable compound, A_nB_m, and neither the pure components nor the compound can form solid solutions.

In the system considered, A and B are its components and A, A_nB_m and B, solid phases. Of the four phases possible in the system, three phases can co-exist: L, A and A_nB_m or L, B and A_nB_m.

This compound is stable, since it can be heated without decomposition to its melting point (point C). According to Gibbs' phase rule, the melting of a compound occurs at a constant temperature. Thus, the molten compound can be regarded as a single-component system, i.e. $c = k - f + 1 = 1 - 2 + 1 = 0$[1].

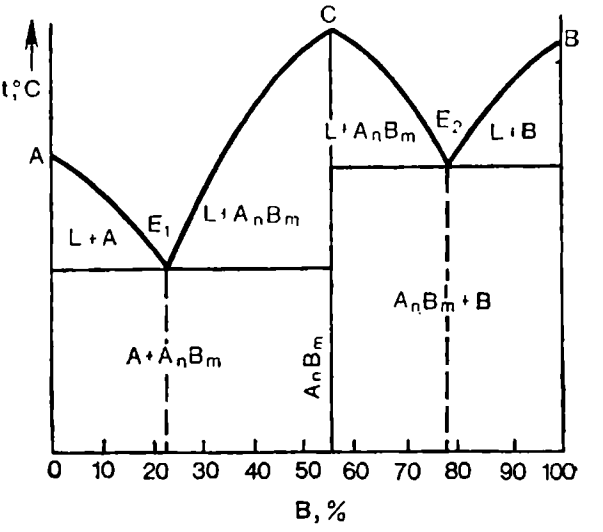

Fig. 5-17. Constitutional diagram of a system with stable chemical compound

Figure 5-17 shows the constitutional diagram of a system with a stable chemical compound A_nB_m[2]. Point C in the diagram is the melting point of this compound. There are two eutectic points: E_1 and E_2. The eutectic E_1 is a mixture of crystals of component A and the compound, and eutectic E_2, a mixture of crystals of B and the compound. The reactions of formation of the eutectic mixtures are respectively as follows:

$$L_{E_1} \rightarrow A + A_nB_m; \quad L_{E_2} \rightarrow B + A_nB_m$$

Primary crystals of the compound precipitate along lines E_1C and CE_2. Therefore, hypereutectoid alloys relative to eutectic E_1 and hypoeutectoid alloys relative to eutectic E_2 are composed in the solid state of primary crystals of A_nB_m and eutectic E_1 or respectively E_2.

[1] The same result is obtained by regarding the compound as a two-component system (with A and B being the system components). Since in that case the concentration of the compound cannot be changed, the '1' in the phase rule equation will be occupied by concentration and we will have: $c = k - f + 0 = 2 - 2 + 0 = 0$.

[2] The vertical line A_nB_m in the diagram corresponds to a simple multiple ratio of the components in atomic per cent, depending on their atomic ratio and atomic weights, i.e. to a definite mass ratio. Usually mass percentages are laid off on the abscissa in constitutional diagrams. Mass percentages a and b can be recalculated into atomic percentages α and β using the following formulae:

$$\alpha = \frac{aB_1}{aB_1 + bA_1} 100, \quad \beta = \frac{bA_1}{bA_1 + aB_1} 100$$

where a and b are the mass percentages of the components A and B, A_1 and B_1 are their atomic weights; and α and β are the sought-for atomic ratios in the alloy.

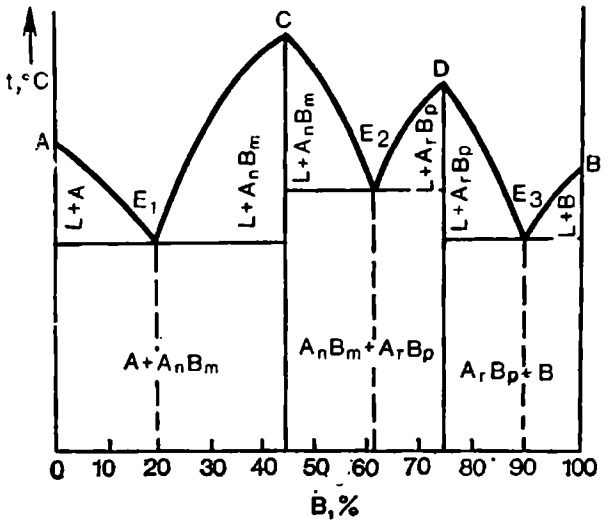

Fig. 5-18. Constitutional diagram of a system with two stable compounds

The solidification of alloys in this diagram occurs exactly in the same way as the solidification of alloys forming mechanical mixtures of crystals of pure components, the only difference being that crystals of the compounds are formed along with crystals of pure components *A* and *B*. Thus, the diagram of a system with a compound can be represented by two simple diagrams attached, as it were, to one another. This diagram may be divided into two portions by a vertical line corresponding to the given compound and each portion may be analysed separately.

If components *A* and *B* can form more than one chemical compound with each other, the constitutional diagram will consist of three, four, etc. simple diagrams for mechanical-mixture alloys (Fig. 5-18).

If the components form limited solid solutions in the solid state and also compound-based solutions, the constitutional diagram will show regions of the existence of the respective solid solutions.

Such a diagram is shown in Fig. 5-19, where α- and β-solid solutions are based on pure components and γ-solid solution, on an A_nB_m compound. It

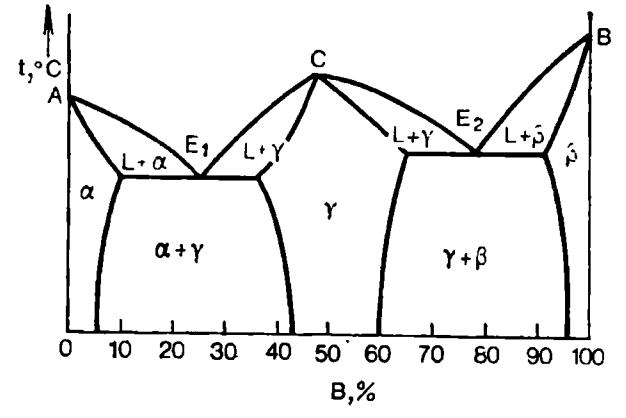

Fig. 5-19. Constitutional diagram of a system with compound-based solid solution

may be easily seen by comparing the constitutional diagrams in Figs. 5-18 and 5-19 that the former is a doubled diagram for alloys composed of mixtures of pure components, and the latter, a doubled diagram for alloys composed of mixtures of solid solutions.

Diagram with an Unstable Compound

Figure 5-20 shows the constitutional diagram for a system in which the two components form an unstable compound. On heating to a definite temperature (t_1), the compound decomposes into liquid and one of the components, i.e. does not melt fully.

On line DCF, three phases are in equilibrium: liquid of concentration D, crystals of component B, and crystals of A_nB_m compound.

When being heated, the compound A_nB_m dissociates into the liquid of concentration D and crystals of B. Therefore, a reverse reaction is likely to proceed on cooling:

$$L_D + B \rightarrow A_nB_m$$

This reaction is similar to a peritectic reaction; the liquid reacts with the crystals which have precipitated earlier, but forms a compound rather than a solid solution, as is the case with peritectic reactions.

The solidification of alloy I under equilibrium conditions will proceed as follows. The process begins at point *1*, where B crystals precipitate and the concentration of the liquid varies along the curve *1-D*. At point *2*, an unstable compound forms at a constant temperature by the reaction given above. Upon completion of the reaction, the liquid remains in excess and solidifies with precipitation of A_nB_m crystals until its concentration reaches point E. At that point, the remaining liquid solidifies into a eutectic composed of crystals of A and A_nB_m. Therefore, the diagram has two horizontal lines: the

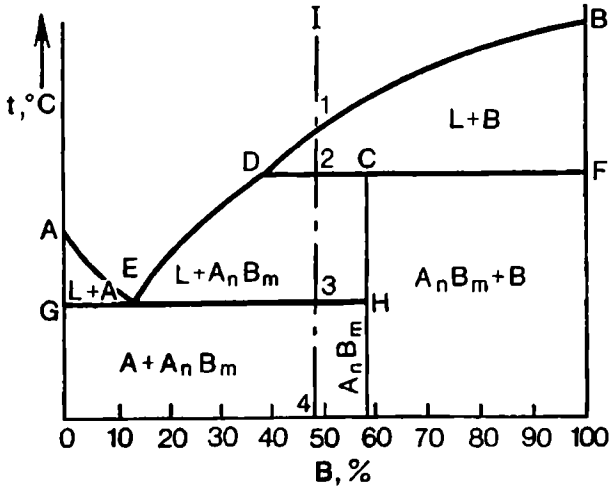

Fig. 5-20. Constitutional diagram of a system with unstable compound

upper on which the unstable compound forms and the lower, which corresponds to the formation of $A + A_nB_m$-eutectic. With fast cooling, the reaction of formation of the compound may be incomplete, so that some primary crystals of B component will have no time to react with the liquid. On further cooling, these crystals will remain untransformed; on reaching the eutectic point, the alloy will contain four phases and its degree of freedom will be negative (which is impossible). This example shows that Gibbs' phase rule is inapplicable to non-equilibrium states. If a system disobeys Gibbs' phase rule (has a greater number of phases than as would be expected), this indicates that it is in a non-equilibrium state.

5-9. THE CONSTITUTIONAL DIAGRAM OF SYSTEMS UNDERGOING POLYMORPHOUS TRANSFORMATIONS

In the discussion above (the diagrams in Figs. 5-13 and 5-20), we have analysed primary transformations associated with solidification of liquid melts.

In secondary crystallization, secondary crystals precipitate due to the temperature variations of the solubility. Secondary crystallization can also be observed in cases where at least one of the components can undergo allotropic transformations. Thus, transformations in the solid state can occur in all cases where at least one of the components is polymorphous (i.e. in systems containing iron, tin, cobalt, manganese, titanium, zirconium or some other elements capable of allotropic transformations).

In all diagrams with polymorphous transformations (Fig. 5-21), the upper portion characterizes the primary crystallization and the lower, the secondary crystallization.

The form of a constitutional diagram is determined by the compounds which can be formed between the allotropic modifications of both components. Let us analyse the most typical cases and the probable forms of constitutional diagram (Fig. 5-21).

Suppose that component A has two modifications: A_α and A_β; the former (which exists at a lower temperature) is isomorphous with component B and can form with B a continuous series of solid solutions (Fig. 5-21*a*); line CDP confines the region of coexistence of two solid solutions: α and β, whose concentrations are determined by curves CD and CP; DPF is the line of peritectic formation of α-solid solution.

If crystals of B component are isomorphous with the high-temperature modification of A, the diagram will have the form shown in Fig. 5-21*b*, where CDF is the region of coexistence of the two solid solutions in equilibrium.

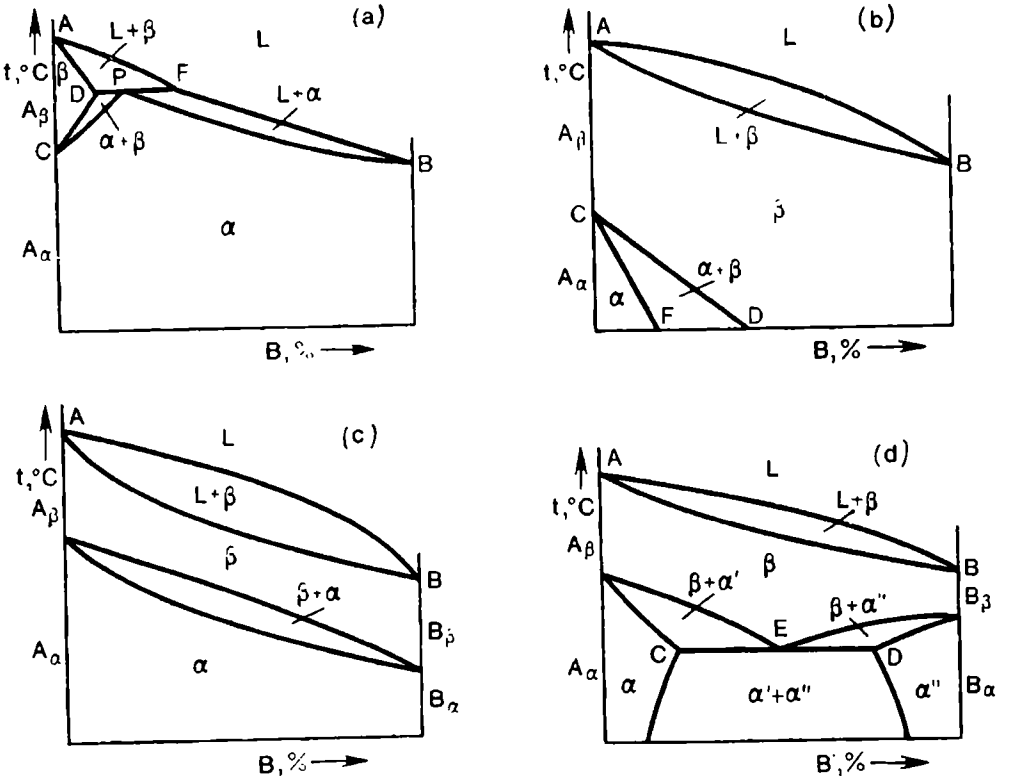

Fig. 5-21. Constitutional diagrams of systems with polymorphic transformation

If both A and B can exist each in two modifications, with A_α being isomorphous with B_α and A_β being isomorphous with B_β and form an unlimited series of solid solutions, the constitutional diagram will have a different form (Fig. 5-21*c*). It will be as if doubled, two-storeyed, for the case when the components are unlimitedly soluble in each other.

If the low-temperature modifications of both components are limitedly soluble in each other and the high-temperature modifications are unlimitedly soluble, we obtain a constitutional diagram which is a combination of the diagrams discussed in Secs. 5-6 and 5-7 (see Fig. 5-21*d*).

At a temperature corresponding to line *CED*, β-solid solution decomposes into two solid solutions:

$$\beta \rightarrow \alpha' + \alpha''$$

The transformation occurs similar to the crystallization of a eutectic, but the original mother solution is the solid solution rather than the liquid. In contrast to the crystallization of eutectic from liquid, this transformation is called the *eutectoid transformation* and the crystal mixture formed, the *eutectoid.*

5-10. NON-EQUILIBRIUM CRYSTALLIZATION OF ALLOYS

It has been stated at the beginning of this chapter that the constitutional diagram describes the equilibrium states of alloys, and its lines determine the temperature-concentration relationships of transformations under equilibrium conditions when the free energies of the old and new phases are equal.

It has been also noted (see Ch. 2) that transformations cannot occur at the temperature of phase equilibrium, since there is no stimulus for a transformation and no gain in free energy. For that reason, the constitutional diagram must be regarded as an extreme case with infinitely low rates of heating or cooling, which gives an infinitely small difference in the free energies of co existing phases, and therefore, an infinitely low rate of transformation. In reality, however, the transformation temperatures in heating at a finite rate are always above the equilibrium ones, and in cooling, below. This is schematically shown in Fig. 5-22, where the $\alpha \rightleftarrows \beta$-transformation at an infinitely low rate of cooling (or heating) has corresponding theoretical equilibrium temperatures: T_0 for non-variant systems (for instance, polymorphous transformation in pure metals) and T_0' and T_0'', for systems with one or two degrees of freedom (transformations in solid solutions). With a finite rate of heating or cooling, the transformation starts and ends above or below the equilibrium temperature. Besides, the diagrams in Fig. 5-22 reflect two more circumstances of importance.

1. The degree of overheating or undercooling is greater at a higher rate of heating or cooling, with the tendency to undercooling being always greater than that to overheating.

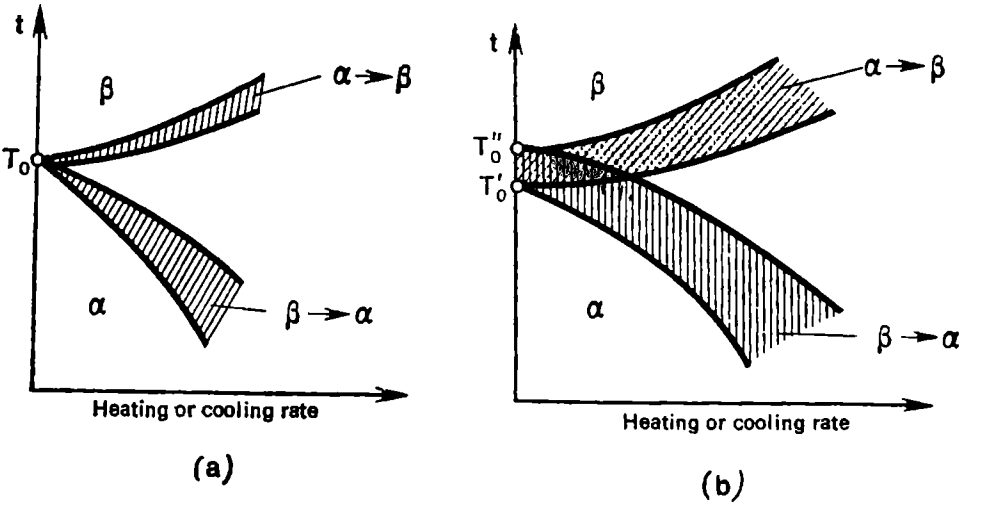

Fig. 5-22. Effect of heating or cooling rate on transformation temperature (*a*) for systems with zero degree of freedom; (*b*) for systems with one or more degrees of freedom

2. Under real conditions, the transformations in all systems occur within a temperature interval which is greater at a higher rate of heating or cooling.

It should be noted that the temperature range of a transformation may be from a few tenths of a degree to many degrees, depending on the nature of alloy, type of transformation and other factors, as well as on the heating (or cooling) rate.

Thus, the transformation states described by the constitutional diagram represent a certain abstraction, since the diagram disregards the necessity of undercooling (or overheating), but this abstraction is essential for studying the real conditions of crystallization.

Having determined how the crystallization might occur theoretically, or more strictly, what phases might form under equilibrium conditions (at an infinitely low rate of temperature variation), we can analyse transformations occurring under non-equilibrium conditions. It should be noted at once that if the rate of temperature variations is not high, i.e. if a transformation occurs at a slight undercooling (the degree of overheating is usually not high), we can neglect this low degree of undercooling and analyse the transformation as if occurring at the temperatures and in the sequence as given by the constitutional diagram. In further discussion, constitutional diagrams will be widely used for analysis of so-called equilibrium structures and transformations occurring with a slow cooling (or heating).

With fast variations of temperature, however, both the temperatures and the conditions of transformation deviate from equilibrium conditions, since the diffusion processes (in undercooled systems) have no time to proceed to completion. In such cases, the equilibrium diagram is invalid, but can be useful as a starting point for understanding the particular structures appearing in non-equilibrium crystallization.

Let us first analyse the primary crystallization and then, secondary crystallization (recrystallization).

Non-equilibrium Crystallization from Liquid Solution

When analysing the crystallization from a solid solution on the diagram in Fig. 5-11, we have established that the compositions of solid solution and liquid vary continuously. The crystals precipitated at an earlier stage of the process are richer in the higher-melting component than those which precipitated later and at a lower temperature. In equilibrium crystallization, the solid phase should be always homogeneous and it is, therefore, assumed that the process of equalization of its composition (commonly by diffusion) does not lag behind the crystallization process proper. In crystallization of solid solutions, however, the initial crystals are usually richer in

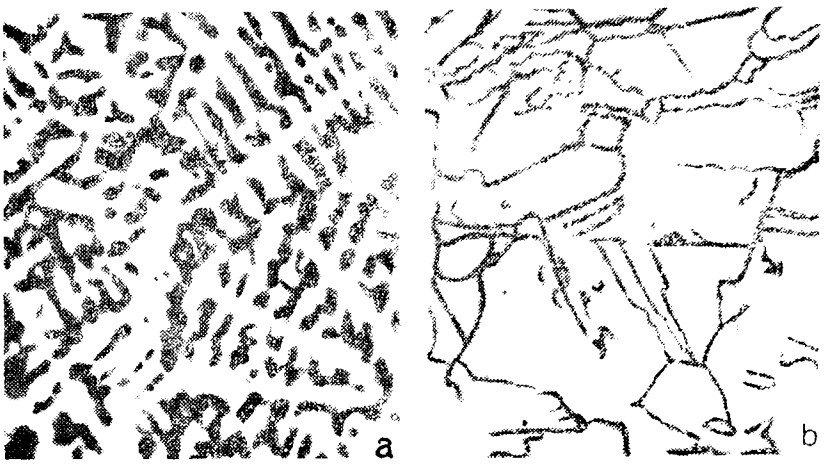

Fig. 5-23. Microstructures of nickel silver alloy (solid solution of zinc and nickel in copper), ×100 (A. A. Bochvar)
(*a*) as cast; (*b*) on diffusion annealing

the high-melting component than those precipitated at later stages. For that reason, the first-order axes of dendrites contain more of the high-melting component than second-order axes do, and so on. Interdendritic spaces, which are last to crystallize, have the highest concentration of the light-melting component and are, therefore, the most light-melting. The phenomenon just described is called *dendritic segregation*. The state of dendritic segregation is non-equilibrium, since a heterogeneous solution has a higher level of free energy than a homogeneous one. With a long heating of an alloy, the dendritic segregation can be eliminated to some or other extent owing to the diffusion which equalizes the concentration in all crystals.

Figure 5-23*a* shows the microstructure of a cast alloy with dendritic segregation and Fig. 5-23*b*, the structure of the same alloy in which the concentration has been equalized through long heating at a high temperature.

Let us now analyse the crystallization of a liquid solution in the constitutional diagram (Fig. 5-24).

In equilibrium crystallization of a solid solution, solid-phase crystals of a definite composition, corresponding to a definite point on the solidus line, precipitate at each particular temperature. The composition of crystals of alloy *I* (see Fig. 5-24) should vary along the curve from point *a* to point *c*, i.e. the first crystals appearing in the liquid (at t') have a concentration *a*, those precipitated at t'', concentration *b*, and so on. The average composition of the solid phase on equilibrium crystallization at this temperature also corresponds to point *b*. Therefore, crystals of varying concentration (from *a* to *b*) precipitate during cooling from t' to t'' and the composition

of the crystals that have precipitated initially and are richer in component A is changed due to diffusion, and they are saturated with component B. In casting, this process usually does not come to its end and the average composition of crystals deviates to the left from the solidus line (point b').

At t''', the theoretical temperature of the end of crystallization, the composition of the liquid (in which the rate of diffusion is much more higher than in the solid state) will be determined by point f and the average composition of crystals, by point c'; the quantity of the liquid that remains at that temperature is determined by the ratio $c'c/c'f$.

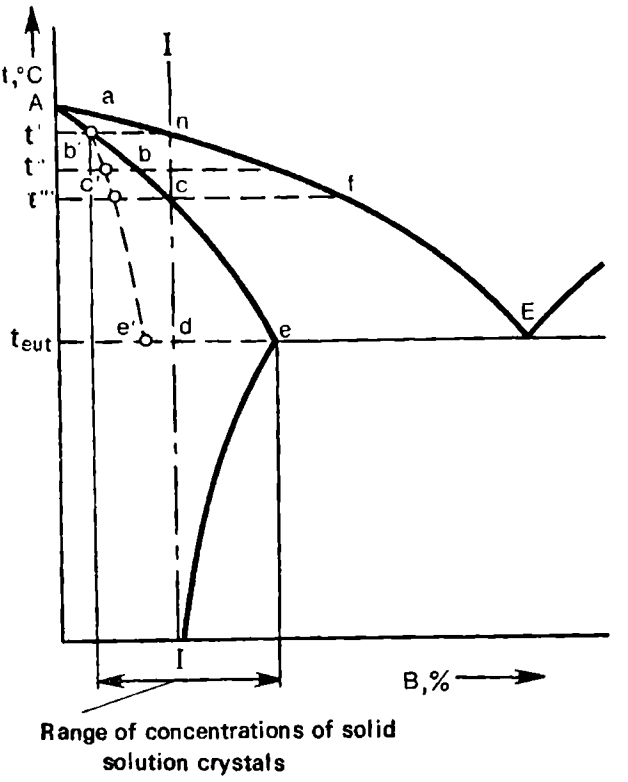

Fig. 5-24. A diagram to illustrate variation in average composition of crystals in non-equilibrium crystallization

Consequently, the process of crystallization under non-equilibrium conditions will be not completed at that temperature (t''), but crystals will continue to precipitate from the remaining liquid; the concentration of these crystals will correspond to the position of line ce and their average composition will be determined by line $c'e'$. If this line ($a'e'$) does not intersect the vertical line I-I, the process will be finished at temperature t_{eu} and the remaining liquid (in a quantity of $e'd\,e'E$ and concentration E) will form a eutectic. The crystals formed are heterogeneous, i.e. have a different concentration: the first crystals have a composition of point a and the last, that of point e.

Thus, equilibrium crystallization takes place without undercooling and the composition of crystals (both precipitated earlier and those precipitating at a given temperature) is the same. This means that diffusion processes occur simultaneously with the precipitation of crystals; these processes equalize the composition of the liquid phase and saturate the earlier precipitated crystals to the concentrations determined by the appropriate points on the liquidus and solidus lines.

In non-equilibrium crystallization, however, the process of diffusion saturation of the precipitated crystals has no time to proceed to completion, and the average composition of the solid phase differs

from the composition of crystals precipitated at a given temperature. This average composition of crystals is described by a dotted line whose position depends on a number of factors (diffusion rate, cooling rate, etc.). As a result, the real structure of the alloy may substantially differ from the equilibrium structure.

Non-equilibrium Crystallization from a Solid Solution

Non-equilibrium crystallization from a liquid solution usually can take place without an appreciable undercooling and the equilibrium conditions are disturbed mainly owing to a lag of the solid-phase diffusion, whereas the diffusion in the liquid phase has enough time to proceed fully. On the contrary, non-equilibrium secondary crystallization may be characterized by an appreciable undercooling and retardation of diffusion in the starting phase and the phases that form.

Let us analyse an important case of decomposition of a solid solution having a limited and temperature-variable solubility.

In accord with the foregoing, in particular with the diagram in Fig. 5-22, decomposition of the solid solution should really start not at the temperature defined by line *FD* (Fig. 5-25), but at a lower temperature, for instance, along line *F'D*. For alloy *I*, an increased rate of cooling will initiate precipitation of the excess phase not at the equilibrium point *1*, but at a lower temperature point, say *1'* and *1''*. As a result, the precipitated crystals of the excess β-phase will be finer and less numerous.

Indeed, the relative quantity of the secondary phase at 20°C for equilibrium crystallization of alloy *I* is determined by section *KF*; for non-equilibrium conditions, it is determined by section *KF'* or *KF''* and the composition of the solid solution is determined by point *F'* or *F''*. These points are to the right of point *F*, therefore, the solid solution formed is *supersaturated*.

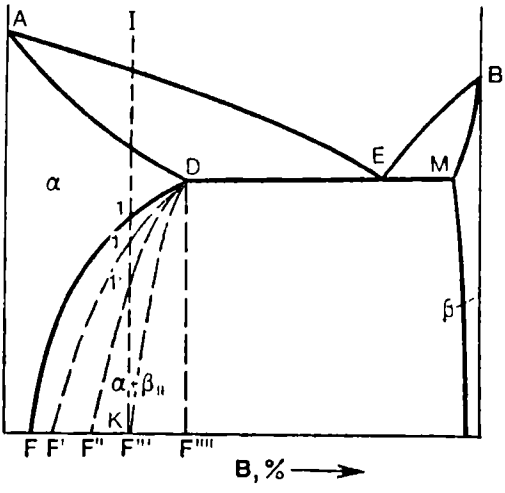

Fig. 5-25. Crystallization from undercooled solid solution

If, with faster cooling, the beginning of precipitation follows curve *F'''D*, no precipitates will be formed in alloy *I*. If the curve of the beginning of precipitation is *F''''D*, this means that any alloy in the system can be undercooled to room temperature under the given cooling conditions without decomposition of the solid solution.

Thus, the degree of decomposition can be varied, up to full suppression, by controlling the cooling rate. Such supersaturated solutions are unstable. If, however, the thermal mobility of atoms in an undercooled solution is inadequate, the state of supersaturation can remain indefinitely long. Otherwise, the supersaturated solution will gradually decompose and an excess phase will precipitate from it. The process can be accelerated by raising the temperature.

Consider the mechanism of nucleation of secondary crystals in two extreme cases: (1) crystallization under conditions very close to equilibrium and (2) the solid solution has been undercooled without decomposition, but its decomposition begins on heating to relatively low temperatures.

In the former case, decomposition begins at a temperature near point *1* (for alloy *I*). Crystals of β-phase form mostly at grain boundaries, since the work of nucleation at a grain boundary is less than that inside the grain. The critical size of a nucleus should be relatively large, since undercooling is small. Further cooling should cause the precipitation of new crystals and the growth of those precipitated earlier. The crystals of β-phase thus formed have no definite orientation relative to the original α-phase and their shape approaches spheroidal (the form of the least free energy). Crystals grow gradually; atoms overcome the energy barrier and at the α-β interface enter, one after another, the lattice of the precipitated phase.

Though the α- and β-phases may substantially differ in the unit volume or the type of lattice, this decomposition causes no stresses, since the appearing stresses are quickly eliminated (*relaxed*) due to the high temperature and the high mobility of atoms.

Things are different in the second case, i.e. in decomposition of a deeply undercooled solid solution.

Since the degree of undercooling is high, crystallization nuclei can appear both inside the grains and at grain boundaries, and the critical size of nuclei of the new phase will be small and their number, large. The growing crystals of β-phase may fail to take a stable spherical shape, since these spheroidal formations might cause appreciable internal stresses in the elastic medium. This is why crystals adapt themselves to this circumstances and acquire a lamellar form, which causes no appreciable stresses in the structure. Indeed, crystals of this new shape, which have precipitated from deeply undercooled solid solutions, are usually very fine. Their thickness is only a few atomic layers and the length, a few tens or hundreds of atomic layers. Such a thin crystal, however, cannot exist individually, but only if attached to a larger crystal (more strictly, inside that crystal).

This can be explained by the diagram in Fig. 5-26. The crystals that have precipitated at a high temperature are not linked orientationally with the mother phase. A layer of atoms belonging to the

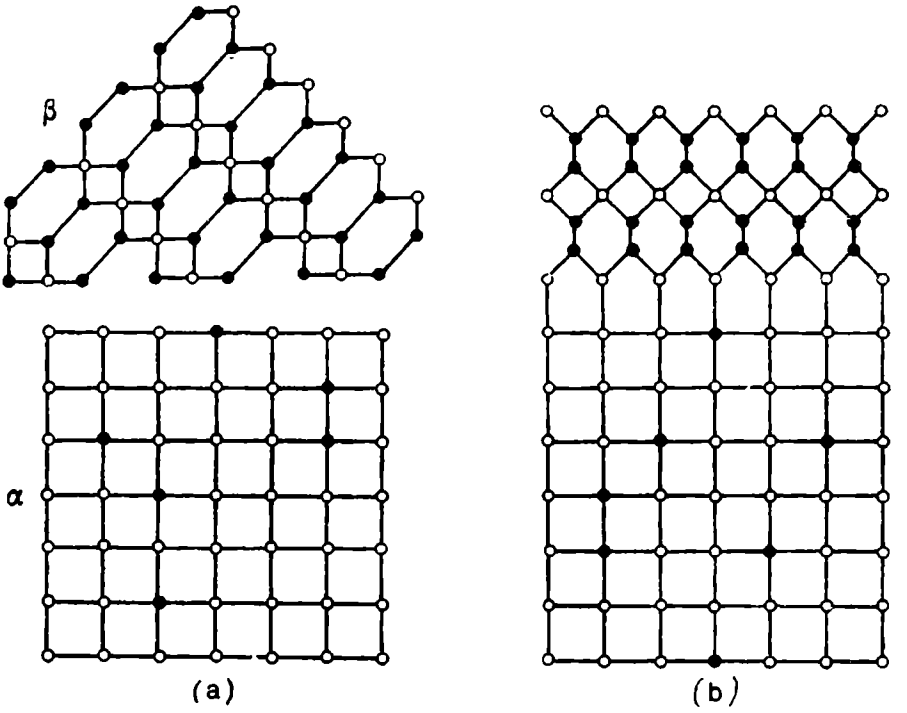

Fig. 5-26. Matching of crystal lattices
(*a*) non-bonded; (*b*) bonded (coherent)

old phase is adjacent to a layer of atoms of the new phase, as shown in Fig. 5-26*a*.

With precipitation at a low temperature, the new β-phase is specifically oriented relative to the old phase, so that a boundary layer of atoms can belong equally to both lattices (Fig. 5-26*b*). This joining of crystal lattices is called *coherent* bond. With coherent bond, stresses can appear and be retained at the interface, the magnitude of these stresses being greater at a greater difference in the structure of the two conjugated lattices (in the division plane).

If the lattice of a β-phase has no plane that might be coherent to the original phase, the transformation will occur in several stages. At the first stage, an intermediate metastable β′-phase forms. The lattice of this intermediate phase has a plane coherent to the initial α-phase. At the second stage, the $\beta' \rightarrow \beta$ transformation will occur, provided that a coherent bond can be effected between these two phases; otherwise, a second intermediate metastable phase should form, and so on.

Therefore, if the conditions of transformation approach the equilibrium, β-phase will precipitate from α-solid solution and the composition of that phase will correspond to the maximum concentration of β-region in the *A-B* diagram (see Fig. 5-25). The precipitated β-crystals are quite large and rounded and have the lattice inherent

in β-phase. If, however, undercooling is deep and the diffusion mobility of atoms is low, the transformation will pass through a number of stages[1].

This is the way in which decomposition of a supersaturated solid solution occurs at sufficiently low temperatures. This process is characterized by the formation of coherent bonds between the phases. If the temperature of an alloy is raised, new processes will develop owing to an increased thermal mobility of atoms and the stresses appearing at the interfaces between the coherent phases. The coherent bond is disrupted (*coherence disruption*), the metastable phases change to a stable β-phase, and crystals of β-phase tend to grow into a spheroidal shape. Upon completion of these processes, the structure and phase composition will be the same as on slow cooling.

The described process of fixing of an unstable state by quick cooling is called *hardening* and the subsequent process of gradual approach to the equilibrium state (by heating and long holding) is called *tempering* and *ageing*. Thus, the structures and properties of alloys can be varied widely by causing their state to deviate more or less from the equilibrium by the methods of *heat treatment* which are extensively employed and are based on the processes of non-equilibrium crystallization discussed in the general outlines above.

The essence of particular processes and the properties obtained will be discussed in more detail later in the book.

5-11. THREE-COMPONENT (TERNARY) SYSTEMS

Modern engineering cannot content itself with the application of pure metals and binary alloys. Most alloys of practical importance are multi-component systems. It is then natural to analyse ternary and more complicated systems.

As we have seen earlier, a single-component system can be represented by points on a straight line (see Fig. 5-1); the constitutional diagram of a two-component (binary) system is plotted in two coordinates (see Fig. 5-2). Ternary systems can be described by tridimensional diagrams, with two of the three axes showing changes in the compositions of two components and the third axis, temperature variations (Fig. 5-27). Given the contents of any two components, the content of the third is found as the balance by the equation $C = 100 - A - B$.

The phase transformations in alloys of a system are marked by points on vertical lines. Having studied a sufficiently large number

[1] Between these two extreme cases, i.e. the transformation practically without undercooling and the transformaton at a low temperature of fully undercooled solid solution, there may exist an infinite number of intermediate cases. Besides, it should be noted that the transformation described, though being most typical, cannot be observed in all cases and all systems.

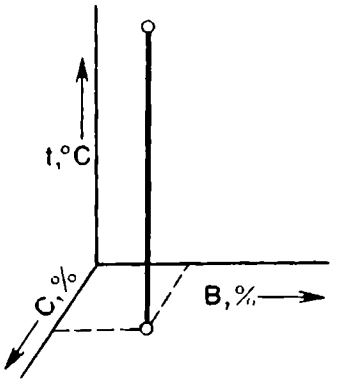

Fig. 5-27. Coordinate axes for a three-component system

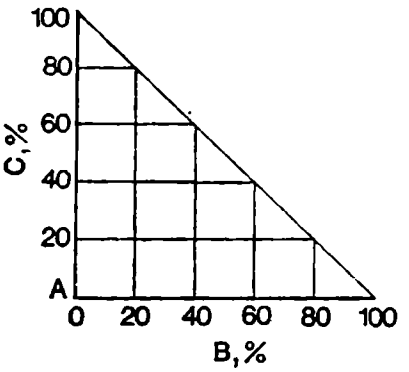

Fig. 5-28. Concentration triangle (rectangular)

of alloys in a system, the points of like transformations can be connected to form transformation surfaces. Thus, a tridimensional model of a constitutional diagram consists of a number of surfaces separating the regions of like phase states. Therefore, the diagram will have a spatial region within which the system exists as a homogeneous liquid. This region is separated by the liquidus surface from an adjacent region in which the liquid and crystals co-exist in equilibrium. Similarly, this region is separated by the solidus surface from the region where only solid crystals exist.

The study of ternary systems may be started from the methods for depicting concentrations. Rectangular coordinates may be used. The origin of coordinates corresponds to pure component *A*. The concentrations of the components *B* and *C* are laid off along the coordinate axes (Fig. 5-28) in the same way as we have done with binary systems (see Fig. 5-2). The extreme points on the axes respectively correspond to pure components *B* and *C*. If the scale is the same for both axes, points *B* and *C* will be equidistant from the origin

Binary alloys *A*-*C* and *A*-*B* are represented by points on the respective coordinate axes; the *B*-*C* binary alloy is represented by points on the hypotenuse of the rectangular triangle.

A shortcoming of this method is that the scales of concentrations of individual components are different. For that reason, the method is used only for depicting a portion of the constitutional diagram of alloys rich in *A* component, rather than for describing the entire system.

An entire ternary system can be depicted to the same scale of concentrations of the components by using oblique coordinates with an angle of 60°. In that case, the base of the tridimensional model will be formed by an equilateral triangle, which is called the *concentration triangle*, since its sides are concentration scales (Fig. 5-29).

To determine the concentrations of components in a ternary alloy, it should be taken that the corners of the triangle correspond to the pure components *A*, *B* and *C*. Side *AB* represents binary (*A* + *B*) alloys; similarly, sides *BC* and *AC* correspond to binary alloys *B* + *C* and *A* + *C*. Points inside the triangle represent ternary alloys.

In each ternary alloy, the sum of the concentrations of three components is constant, i.e. %A + %B + %C = 100% (similar to binary alloys where

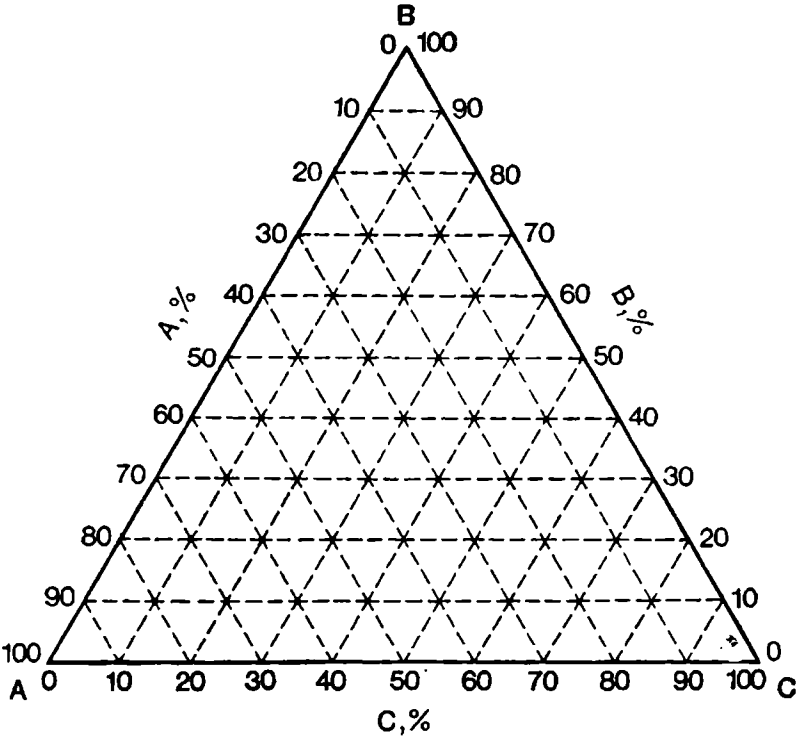

Fig. 5-29. Concentration triangle (equilateral)

%A + %B = 100%), and is equal to concentration axis AB. Therefore, the length of the triangle side is 100 per cent ($AB = BC = AC = 100$ per cent).

If we take a point O within the triangle and pass lines parallel to the triangle sides through it (Fig. 5-30), it may be shown by a simple geometrical construction that the sum of the sections a, b and c formed by these lines is equal to any of the triangle side, i.e. $a + b + c = AB = BC = CA = 100$ per cent.

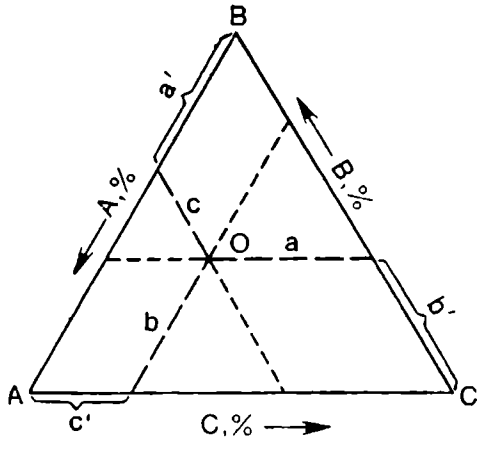

Fig. 5-30. Determining the concentration of an alloy in an equilateral concentration triangle

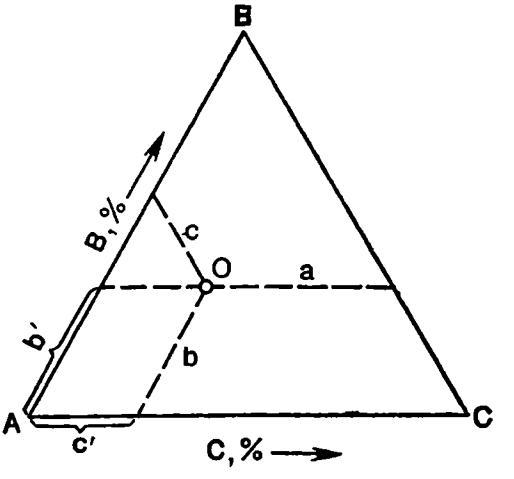

Fig. 5-31. Determining the concentration of an alloy in an equilateral concentration triangle

Since the side of the triangle gives the entire quantity of the alloy, the sum $a + b + c$ should also give the entire quantity of the alloy, and each term in this sum should give the quantity (concentration) of a respective component.

In a binary system, when a concentration point moves closer to the origin of coordinates, for instance, to point A which lies on side AB, the concentration of component A increases and that of B, diminishes. Similarly, if the concentration point within the concentration triangle of a ternary system is moved closer to point A, the section a increases, while sections b and c diminish. As soon as the concentration point touches side AB, the section c becomes zero and the point will represent a binary $(A + B)$ alloy. When the point is made coincident with corner A of the triangle, we will have a pure component A: the sections b and c will be equal to zero, and the section a will be equal to side AC, or 100 per cent.

Therefore, section a shows the concentration of component A in a ternary system; similarly, section b shows the concentration of B and section c, that of C.

Thus, to find the concentrations of the components in a ternary alloy, we have to draw lines parallel to the triangle sides through that point. The length of a section between the given point and a side of the triangle determines the concentration of the component which stands at the opposite corner of the triangle that is, a section brought up to side BC determines the concentration of component A, etc.

For convenience, the concentrations of components A, B and C are laid off on the respective sides of the triangle (clockwise or counter-clockwise). The concentration sections a, b and c are projected onto the sides showing the concentrations of respective components. Sections a', b' and c' on the sides of the triangle are respectively equal to the concentration sections a, b and c and give the composition of the alloy (a' gives the concentration of A, b', that of B and c', that of C).

In many cases it is more convenient to lay off the concentrations of C and B along the sides originating from corner A.

For an alloy of point O, the concentration of B will then be expressed by section b' and the concentration of C, by section c', since it is evident that $b' = b$ and $c' = c$ (Fig. 5-31). The concentration of A is then found as the balance, i.e. $\% A = 100\% - \% B - \% C$.

Considering a series of alloys lying on a straight line parallel to one of the sides of the triangle, say AC (Fig. 5-32), it may be clearly seen that the concentration sections dropped on side AC, i.e. the sections determining the concentration of component B, are equal for all these alloys. Consequently, all alloys belonging to a line parallel to side AC have the same concentration of component B.

Taking a series of alloys on a line passing through a corner of the triangle, say B, it may be found from geometric similarity that the ratio of sections

$$\frac{c'}{a'} = \frac{c''}{a''} = \ldots$$

is constant for all alloys lying on that line, i.e. the ratio of component C to component A is constant for all alloys belonging to a line passing through corner B.

Thus, we have established by analysis of the concentration triangle that:

(1) the corners of the triangle represent pure components A, B and C;

(2) points of binary alloys lie on the sides of the triangle;

(3) points inside the triangle represent ternary alloys;

(4) alloys represented by the points of a line parallel to one of the sides of the triangle have a constant concentration of the component standing at the opposite corner of the triangle;

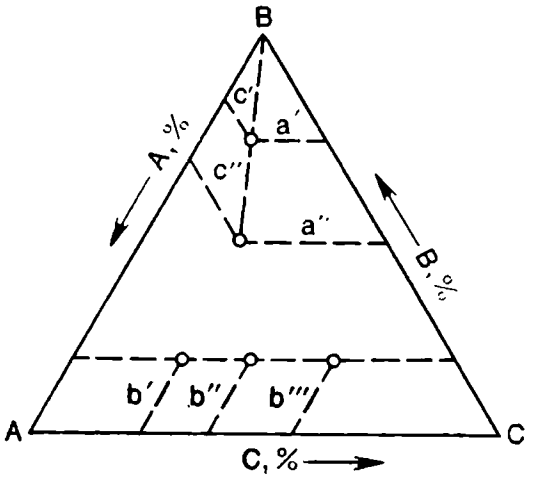

Fig. 5-32. Section through a concentration triangle

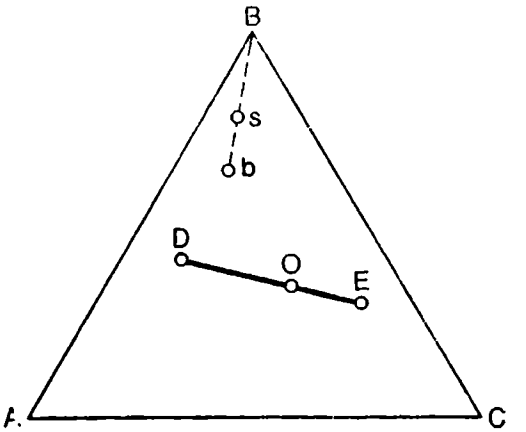

Fig. 5-33. A diagram to illustrate the lever rule as applied to a ternary system

(5) alloys represented by the points of a line passing through a corner of the triangle can be characterized by a constant ratio of concentrations of two components.

Crystallization of ternary alloys obeys principally the same laws as the crystallization of binary alloys, i.e. the Gibbs phase rule and lever rule, but the latter rule cannot be applied as easily, because of the more complicated (tridimensional) geometrical representation of the system.

Let us consider an example to show how the lever rule can be applied to ternary systems.

If we take two binary alloys, say with 60 and 40 per cent B, we can obtain a third binary alloy by melting them together. The concentration of B in the new alloy will be somewhere between 40 and 60 per cent (it cannot be less than 40 per cent or more than 60 per cent), i.e. if we have two alloys, C and D (see Fig. 5-2), the concentration of the third alloy obtained by melting together these two alloys will be at a point lying between points C and D.

Given two ternary alloys, D and E, the point describing a third alloy obtained by melting together these two alloys will lie on the line connecting points D and E (Fig. 5-33).

Point O, which characterizes the composition of the new alloy, will be closer to point E at a greater quantity of alloy E.

Taking n per cent of alloy E and m per cent of alloy D, the position of point O will be determined by the ratio

$$\frac{n}{m}=\frac{OD}{OE},$$

which expresses the familiar lever rule (see Sec. 5-5).

For a reverse process (for instance, the alloy at point O decomposes into two phases, D and E), the concentration points of these phases will lie on the same line DOE and the quantity of phase D will be determined by section OE and that of phase E, by section OD, provided that section ED determines the total quantity of the alloy.

If crystals of pure component B precipitate from liquid S (see Fig. 5-33) the composition of the remaining liquid varies along a straight line which is an extension of line BS. If the concentration of the liquid has come to point b at a certain moment of crystallization, this means that the quantity of crystals

B precipitated from the liquid at that moment relates to the quantity of the remaining liquid as section Sb relates to section SB [in other words, section Sb determines the quantity (mass) of precipitated crystals B].

When applying the phase rule to ternary systems, it should be remembered that $k = 3$ (there are three components in the system). Therefore, the maximum number of co-existing phases (at a constant pressure) in ternary systems is four (non-variant equilibrium):

$$c = k - f + 1 = 3 - 4 + 1 = 0$$

Consequently, crystallization of a binary eutectic ($L \rightarrow A + B$) in ternary systems should occur within a temperature range, with each temperature corresponding to a definite composition of the liquid (monovariant reaction):

$$c = k - f + 1 = 3 - 3 + 1 = 1$$

A ternary eutectic ($L \rightarrow A + B + C$) can also solidify in ternary systems, but only at a constant temperature (since $c = 0$). If we assume that a ternary system is formed by three components, A, B and C, which are soluble in the liquid state and insoluble in the solid state, the crystallization within a temperature interval should start from precipitation of one of the components (say, A, Fig. 5-34); after that, two components will precipitate from the liquid, i.e. a binary eutectic will form also at a variable temperature. At a constant temperature (as a ternary $A + B + C$-eutectic) all the three components will crystallize.

Ternary systems can be classified by the same principle as binary systems, taking into consideration the solubility of the components in the liquid and solid states and the tendency to form chemical compounds. Evidently, types of ternary systems are much more numerous than those of binary systems. The discussion of various ternary constitutional diagrams is beyond the scope of this book and we shall confine ourselves to a general analysis of crystallization processes in a ternary system in which the three components are insoluble in the solid state and do not form chemical compounds.

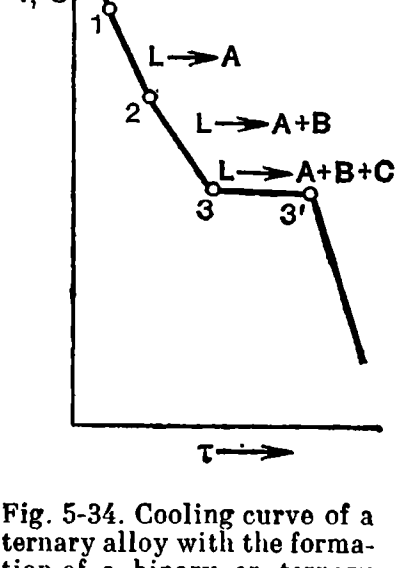

Fig. 5-34. Cooling curve of a ternary alloy with the formation of a binary or ternary eutectic of pure components A, B, and C

Taken in pairs, components A, B and C can form systems with binary eutectics, and taken all together, a system with a ternary eutectic.

The constitutional diagram of a ternary system is shown in a developed form in Fig. 5-35 and its general view in space, in Fig. 5-36.

As may be evident, the section E_1A (see Fig. 5-35) is the projection of the liquidus line of the binary ($A + B$) system at precipitation of A component crystals from the liquid. The section E_3A is the projection of the liquidus line of the binary $A + C$ system at precipitation of the same A component.

Point E_1 is the projection of the eutectic point in the binary ($A + B$) system and line E_1E illustrates the variation of the position of the ($A + B$) binary eutectic point under the effect of the third component. Line E_3E has the same sense relative to ($A + C$) binary eutectic.

Thus, if crystals of A precipitate along line E_1A in the binary ($A + B$) system and along line E_3A in the binary ($A + C$) system, the crystallization in the ternary system will start from precipitation of crystals A for all alloys whose concentration points lie within the area E_1AE_3E.

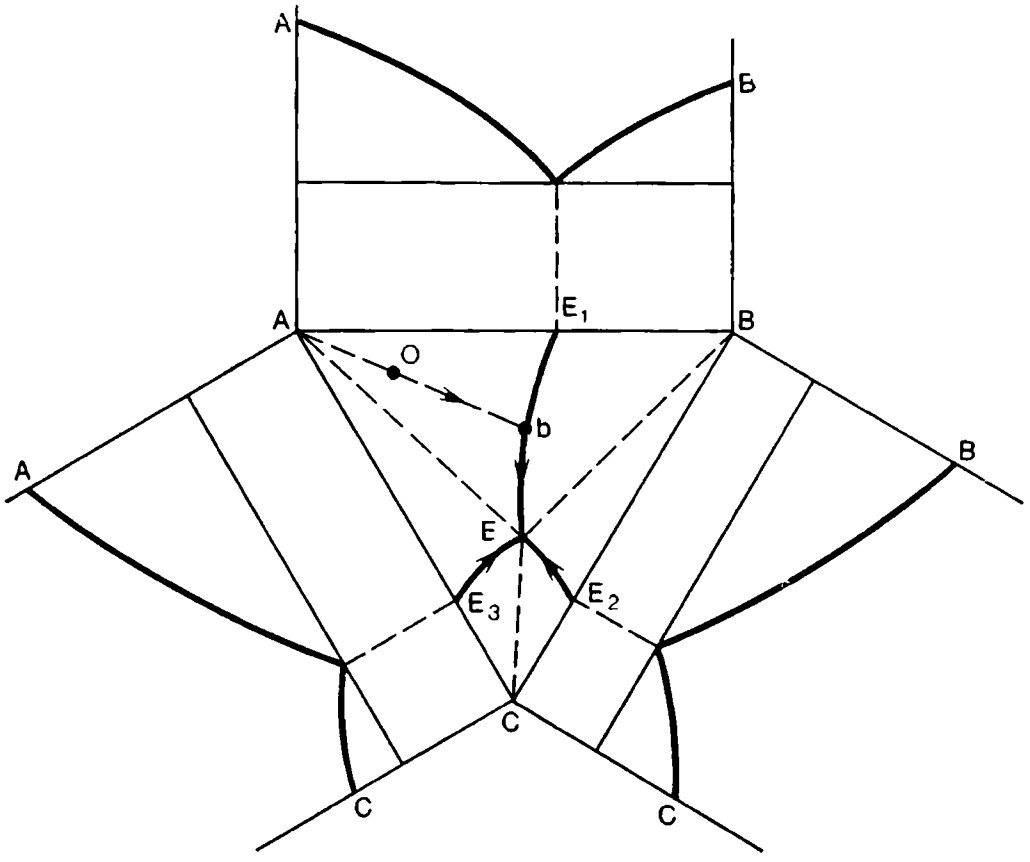

Fig. 5-35. Constitutional diagram of a three-component system. The components are insoluble in the solid state and form a ternary eutectic (developed view)

Consequently, surface E_1AE_3E (see Fig. 5-36) is the liquidus surface of primary crystallization of A crystals. Surface BE_1EE_2 is the liquidus surface of primary crystallization of B and surface CE_2EE_3, the liquidus surface of primary crystallization of C.

Consider the alloy of point O (see Fig. 5-35). On being cooled, A crystals will precipitate from it; according to the lever rule, the composition of the liquid phase will vary along the extension of straight line AO until the point of concentration of the liquid phase coincides with point b on the eutectic line E_1E (line E_1E is the line of crystallization of the binary $(A + B)$-eutectic). At the moment when the crystallization of the components in the liquid comes to point b, the binary $(A + B)$-eutectic begins to crystallize and the composition of the liquid will vary towards increasing concentration of component C until it reaches point E. The liquid of composition E at temperature t' (see Fig. 5-36) crystallizes into the ternary $(A + B + C)$-eutectic, i.e. the following reaction takes place on cooling:

$$L_E \rightarrow A + B + C$$

Connect points E and A by a straight line. The concentration point of alloy O will lie within the area EAE_1. Line E_1E intersects the extension of the straight line connecting the corner A with the point of any alloy lying within that area, i.e. the precipitation of crystals A is followed with precipitation of the binary

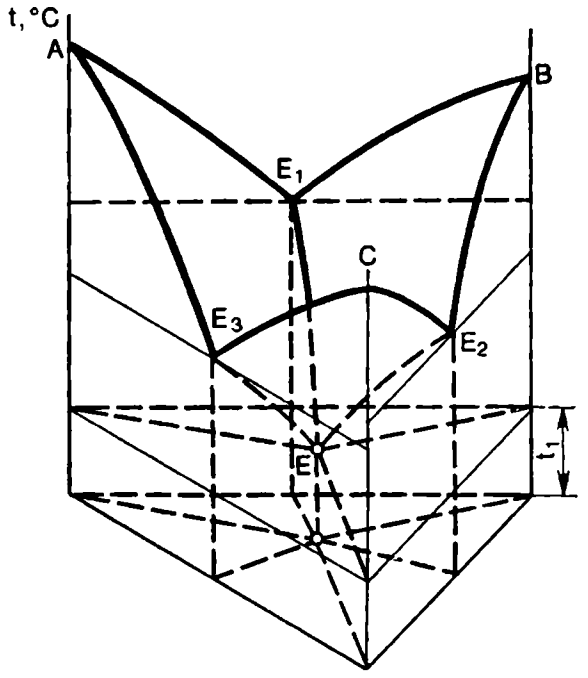

Fig. 5-36. Constitutional diagram of a three-component system. The components are insoluble in the solid state and form a ternary eutectic (space view)

$(A + B)$-eutectic and then with precipitation of the ternary $(A - B + C)$-eutectic. If the concentration point is within the area EAE_3, the $(A + C)$-eutectic will precipitate upon precipitation of A crystals.

Thus, we have established three stages of crystallization in the alloy considered: precipitation of primary crystals (section *1-2*, Fig. 5-34), precipitation of a binary eutectic (section *2-3*), and precipitation of a ternary eutectic (section *3-3'*).

The structure of a ternary alloy (shown schematically in Fig. 5-37) will be composed of primary crystals (A crystals), binary eutectic ($A - B$ crystals), and ternary eutectic $(A + B + C)$.

The ternary eutectic forms in all ternary alloys which crystallize by the mechanism shown in Figs. 5-35 and 5-36. The nature of the primary crystals and binary eutectic depends on the region in the diagram in which the concentration point of the alloy is located (Table 5-1).

Table 5-1. Regions in the Ternary Diagram and Corresponding Structures

Region of concentration point	Structure	Region of concentration point	Structure
EBE_1	$B+(B+A)+(A+B+C)$	ECE_3	$C+(C+A)+(A+B+C)$
EBE_2	$B+(B+C)+(A+B+C)$	EAE_3	$A+(A+C)+(A+B+C)$
ECE_2	$C+(C+B)+(A+B+C)$	EAE_1	$A+(A+B)+(A+B+C)$

Naturally, no ternary eutectic will be in the structure of binary alloys $(A - B, A + C, B - C)$. Equally, no primary crystals of pure components will be in alloys lying on the lines of binary eutectics (E_1E, E_2E, and E_3E), and crystallization in these alloys will start with precipitation of a binary eutectic. Alloys belonging to the lines connecting the ternary eutectic point with the corners of the triangle will have no binary eutectic in their structure,

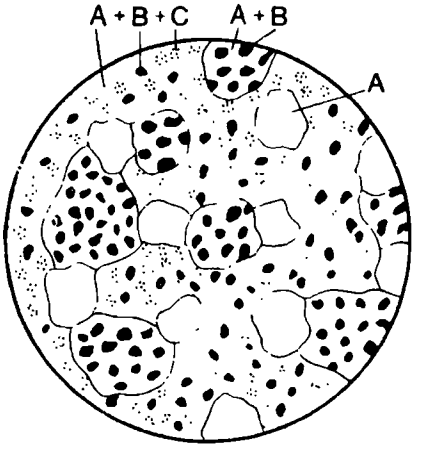

Fig. 5-37. Structure of a three-component alloy with binary and ternary eutectics of pure components

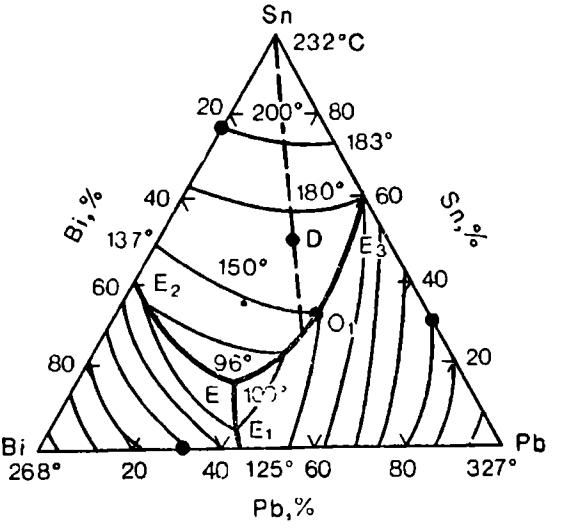

Fig. 5-38. Constitutional diagram of Pb-Sn-Bi alloys

as well. Applying the lever rule, we can conclude that upon precipitation of the pure component in these alloys the liquid will have the concentration of point E, after which crystallization of the ternary eutectic begins.

Finally, the alloy of point E consists of the ternary eutectic only. It is the most light-melting alloy in the system. Its crystallization begins at temperature t' with crystals of all the three components precipitating simultaneously.

In the planar (developed) representation of the diagram (see Fig. 5-35), there is no temperature axis. It may be used for consecutive analysis of the crystallization process, without determining the temperatures at which each of the phases begins crystallizing. If lines of equal temperatures (isotherms) are drawn on the diagram, i.e. lines of intersection of horizontal (isothermal) planes with the surfaces of the diagram, we will be able to judge, to a certain approximation, on the temperatures of transformation in the system.

Figure 5-38 shows the diagram of the Pb-Sn-Bi ternary system, which is a particular case of the diagram in Fig. 5-35 (limited solubility of components in the solid state is not reflected in the diagram).

An alloy of 50 per cent Sn, 30 per cent Pb and 20 per cent Bi (point D in Fig. 5-38) begins to crystallize by precipitation of tin at a temperature between 150° and 180°C (closer to the latter point). When the point describing the composition of the liquid reaches line E_3E (point O_1 which corresponds to a temperature of approximately 145°C), the liquid phase will contain 30 per cent Sn, 42 per cent Pb, and 28 per cent Bi. From that point on, crystallization of the binary Pb + Sn-eutectic begins and the composition of the liquid varies along the curve E_3E up to point E corresponding to 96°C (the liquid at that point contains 16 per cent Sn, 32 per cent Pb and 52 per cent Bi). Crystallization continues at that point at a constant temperature and comes to its end. The alloy of the indicated composition is the most light-melting in the system: the temperature of the beginning and end of its crystallization is 96°C, whereas the melting points of the pure components are substantially higher (268°C for bismuth, 232°C for tin, and 327°C for lead). Of great importance for the study of heat treatment is a variable solubility in the solid state.

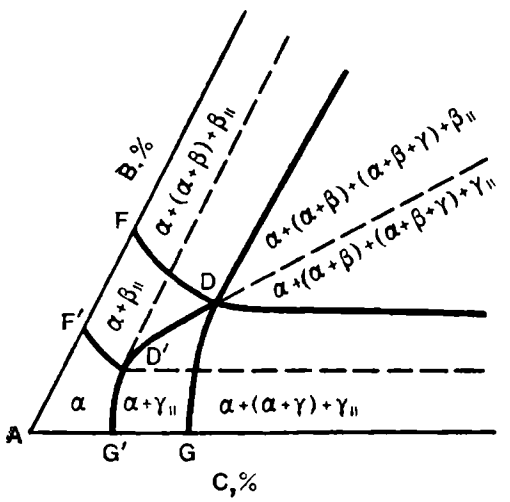

Fig. 5-39. *A*-rich corner of ternary system. All three components form limited solid solutions (α, β, γ) and eutectics (binary and ternary)

In the system considered (see Fig. 5-38), pure components *A*, *B* and *C* can precipitate from the liquid. If these components could form limited solid solutions, α, β and γ, the tridimensional model would have the regions of existence of solid solutions near the vertical edges corresponding to pure components (a portion of the diagram for alloys rich in *A* component is shown in Fig. 5-39).

The ternary eutectic in such an alloy consists of three solid solutions: α, β and γ; the binary eutectics consist respectively of two solid solutions: $\alpha + \beta$, $\alpha + \gamma$ or $\beta + \gamma$.

Line *FDG* shows the maximum saturation of α-solid solution in components *B* and *C*. At room temperature, the solubility of components *B* and *C* in α-solid solution is lower and does not exceed the concentrations determined by line *F'D'G'*. The alloys with the concentration point within the area *AFDG* have a single-phase α-structure upon solidification, but with further cooling, in the alloys whose concentration point lies within the area *F'FDGG'D'* excess secondary crystals from α-solid solution begin to precipitate. The nature of the secondary phases is indicated in Fig. 5-39 and is determined by the composition of an alloy (on line *D'D*, excess β- and γ-phases precipitate simultaneously, which is typical of eutectoid transformations).

The alloys within the area *D'F'AG'* are single-phase (α-solid solution) at all temperatures of alloy existence in the solid state.

5-12. SIMPLIFIED METHODS FOR ANALYSIS OF MULTI-COMPONENT SYSTEMS

The diagram of a ternary system is quite complicated even in the simplest cases when its components form neither solid solutions nor compounds. The diagrams of ternary systems whose components can form limited solid solutions or in which polymorphic transformations occur are too complicated to be represented graphically.

A simpler method for analysis of ternary systems is to use horizontal and vertical sections through tridimensional models. In that case only a portion of a system, rather than the whole system, is analysed. In this method, either all alloys are analysed at a definite temperature (horizontal, i.e. isothermal, sections) or a certain group of alloys at various temperatures (vertical sections).

Suppose that the diagram (see Fig. 5-36) is cut by a horizontal plane above the apex *C* and binary eutectic E_1, but below the corners *A* and *B*. This plane intersects the liquidus surface in which *A* and *B* crystals precipitate along curved lines. Such a horizontal section (Fig. 5-40) has a region of liquid phase *L*

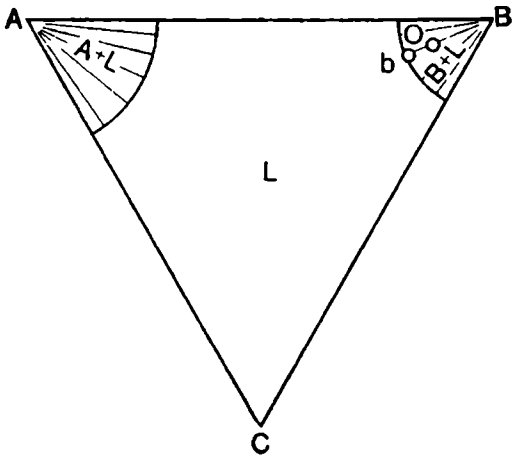

Fig. 5-40. Isothermal section for the ternary system shown in Fig. 5-36 (above the melting temperature of *C* component and *A* + *B*-eutectic)

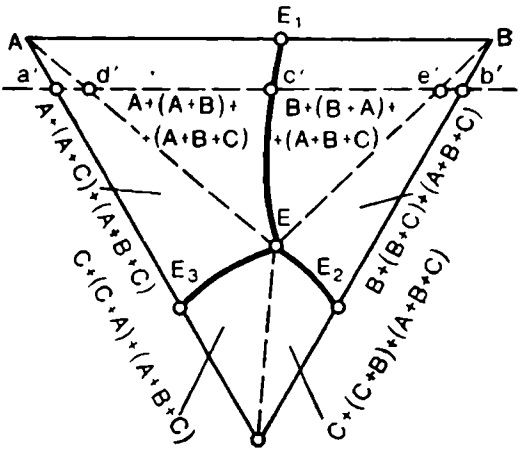

Fig. 5-41. Isothermal section for the ternary system shown in Fig. 5-36 (below the melting temperature of a ternary eutectic)

and two two-phase regions: $A + L$ and $B + L$. An isothermal section enables us to establish the phases that can exist at a given temperature. The compositions of phases in a two-phase region are determined by using the lever rule. For instance, at point *O* there are two phases: the liquid of composition *b* and crystals of component *B*. Their proportion can be determined by the ratio of sections *OB* and *Ob*.

Thus, a horizontal section shows the state of all alloys in a given system at a given temperature. It cannot show, however, what changes will occur in an alloy with a temperature variation.

Of great importance are isothermal sections through tridimensional models at 20°C: they show the phases that exist in equilibrium alloys of a system at room temperature.

An isothermal section at 20°C for the ternary system discussed earlier (Figs. 5-35 and 5-36) is illustrated in Fig. 5-41.

Vertical sections are usually made parallel to a side of the concentration triangle (a constant content of one of the components) or through the apex (constant ratio of concentrations of two components).

If we take a section parallel to side *AB* (Fig. 5-42), i.e. a group of alloys with a constant content of component *C*, the crystallization of these alloys will pass through the following stages:

a'-d' alloys: precipitation of *A* crystals followed with the formation of binary *A* + *C*-eutectic;

d'-c' alloys: precipitation of *A* crystals followed with the formation of binary *A* + *B*-eutectic;

c'-e' alloys: precipitation of *B* crystals followed with the formation of binary *A* + *B*-eutectic;

e'-b' alloys: precipitation of *B* crystals followed with the formation of binary *B* + *C*-eutectic.

After that, all these alloys solidify into a ternary eutectic. Exceptions from this sequence of crystallization are all the alloys that are marked with dots in the diagram: in alloy *c'* primary crystals of pure components do not precipitate; in alloys *d'* and *e'* there is no crystallization of binary eutectics; in alloys *a'* and *b'* there is no crystallization of ternary eutectic.

If we determine the crystallization points of the phases for all the alloys lying in the section *e'-b'*, we can construct a vertical section, such as that shown

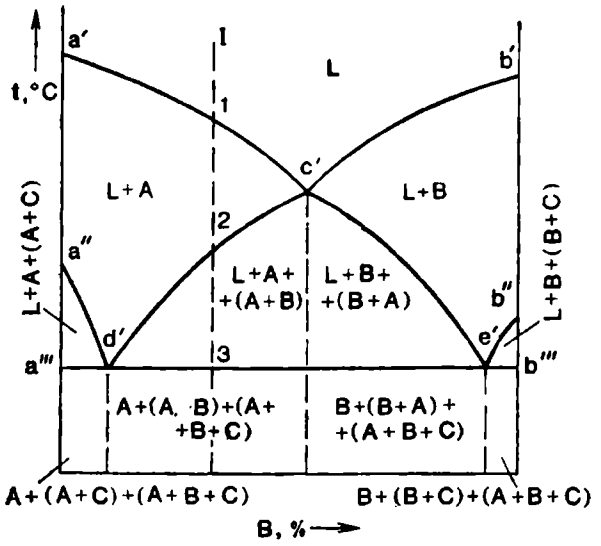

Fig. 5-42. Vertical section (parallel to side AB) through the ternary system shown in Fig. 5-36

in Fig. 5-42. The diagram shows the regions of existence of the phases. The lines in the diagram indicate the temperatures of the following transformations:

Beginning of precipitation of crystals	Lines in the diagram
A	a'-c'
B	b'-c'
Crystallization of binary eutectics	
$A+C$	d''-d'
$A+B$	d'-c'-e'
$B+C$	e'-b''
Crystallization of ternary eutectic	a'''-b'''

Therefore, line a'-c'-b' is the liquidus line and a'''-b''' is the solidus line in the section.

A vertical section through the ternary constitutional diagram can be used to follow the crystallization of the alloys lying in the section plane. Take alloy *1* as an example. At point *1*, crystallization begins by precipitation of crystals of A component. The process continues up to point *2*, where crystals of two types, A and B, begin to precipitate from the liquid, i.e. crystallization of the binary $A+B$-eutectic begins. At point *3*, crystals of three types precipitate from the liquid, i.e. a ternary eutectic forms.

This section is useless, however, if we want to know how the compositions of the phases vary or what the quantities of the phases are, since the lever line (*conode*) does not lie in the section plane. For that reason, such a diagram is not equivalent to a binary diagram, though resembles the latter. A vertical section through a ternary diagram cannot be used to determine the compositions and number of phases. For the reasons mentioned, vertical sections through ternary (and more complicated) diagrams are called *pseudo-binary diagrams*, since they are not the actual and adequate constitutional diagrams. They can be employed for studying the processes of crystallization and transformations for a particular group of alloys (depending on the section selected), without using the lever rule.

How then can we judge on transformations in more complicated systems? A system of four or more components with all possible concentrations and tem-

peratures cannot be represented in a single diagram. This is why, multicomponent systems are analysed by constructing horizontal and vertical sections, most often by constructing pseudo-binary diagrams.

5-13. CORRELATION BETWEEN PROPERTIES OF ALLOYS AND TYPE OF CONSTITUTIONAL DIAGRAM

As is known, the form of constitutional diagram depends on the phases that can be formed by two components. The properties of an alloy are also determined by the compounds or phases formed by the constituents of that alloy. It is then evident that a definite correlation should exist between the form of the constitutional diagram and the properties of the alloy. Figure 5-43 shows four principal types of constitutional diagram and the corresponding tendencies in variations of the properties of alloys at varying concentrations:

1. With the formation of mixtures (Fig. 5-43*a*), the properties of alloys vary by a linear law (additively). Therefore, the properties of alloys are intermediate between the properties of the pure components.

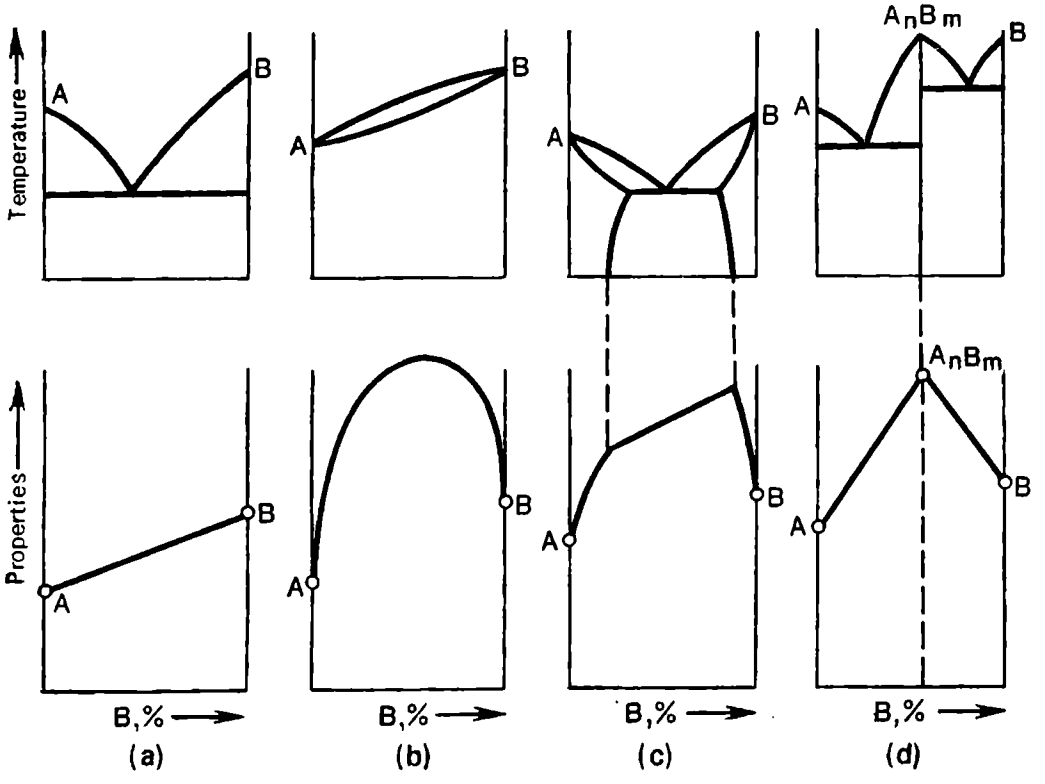

Fig. 5-43. Constitutional diagrams and properties of various types of alloys (N.S. Kurnakov)

2. With the formation of solid solutions (Fig. 5-43*b*), the properties of alloys vary by a curvilinear law and some properties, especially the electrical resistivity, may differ substantially from those in pure components. Therefore, the electrical resistivity of a mechanical mixture may be only slightly greater than in pure components, whereas the resistivity of a solid solution may differ quite substantially. This is why the decomposition of a solid solution into two or more phases usually results in an increase of electric resistivity (*Kurnakov's law*).

3. With the formation of limited solid solutions (Fig. 5-43*c*), the properties in the range of concentrations corresponding to single-phase solid solutions vary by a curvilinear law and in the two-phase region of the diagram, by a linear law, with the extreme points on the line representing the properties of pure phases of maximally saturated solid solutions forming the mixture.

4. With the formation of a compound (Fig. 5-43*d*), the concentration of a chemical compound corresponds to a maximum (or minimum) of a curve (a bend of the straight line in the diagram). This bend point is called the *singular point*. The stoichiometric ratio of components in a given chemical compound can be found in the composition-property diagram by determining the concentration which corresponds to the singular point[1].

Accurate examination of properties of alloys with varying concentrations (i.e. the construction of a composition-property diagram) is an important supplement means for the construction and analysis of a constitutional diagram.

The study of relationships between the composition and properties of alloys by means of composition-property diagrams is the basis of the physico-chemical analysis of alloys, which has been developed by N.S. Kurnakov. At present, the physico-chemical analysis of alloys is one of the principal methods and is widely used in scientific research, studies of structural transformations in novel alloys, and in many other cases.

---

[1] The relationships between the properties of alloys and the form of their constitutional diagram are only schematic and sometimes are not supported experimentally, since they disregard the shape and size of crystals, crystal texture, temperature and some other factors which strongly affect the properties of alloys. The effect of these factors is especially noticeable on the properties of mixture alloys where the additive law may be violated and the properties of an alloy may be above or below the straight line connecting the properties of pure components. For instance, the hardness of an alloy having a disperse two-phase structure is above the additive line. If a mixture alloy consists of two phases, one phase being hard, the other very soft and concentrated at grain boundaries, the hardness of alloys rich in the hard component will be below the additive line. If two components forming a mixture appreciably differ from each other in the temperature of melting point or if their eutectic is very low-melting, the additive relationship for hardness will be observed only at homologous temperatures (for instance, at 0.4 $T_{m.\,p}$).

LITERATURE

Zakharov M. V., Rumyantsev M. V., Turkin V. D., *Constitutional Diagrams of Metallic Systems*. Moscow, "Metallurgizdat", 1940 (in Russian).

Volovik B. E., Zakharov M. V., *Ternary and Quaternary Systems*. Moscow, "Metallurgizdat", 1948 (in Russian).

Petrov D. A., *Ternary Systems*. Moscow, USSR Academy of Sciences, 1953 (in Russian).

Bunin K. P., Malinochka Ya. N., *Introduction to Metallography*. Moscow, "Metallurgizdat", 1954 (in Russian).

Bochvar A. A., *Physical Metallurgy*. Moscow, "Metallurgizdat", 1956 (in Russian).

Vol A. E., *The Structures and Properties of Binary Metallic Systems*. In two volumes. Moscow, "Fizmatgiz", 1959 (in Russian).

Steinberg S. S., *Physical Metallurgy*. Moscow, "Metallurgizdat", 1961 (in Russian).

Hansen M., Anderko K., *Constitution of Binary Alloys*. New York, McGraw-Hill, 1958.

Metallographic Laboratory. Moscow, "Metallurgizdat", 1965. Authors: E. V. Panchenko, Yu. A. Skakov, B. I. Krimer et al. (in Russian).

Livshits B. G., *Metallography*. Moscow, "Metallurgiya", 1971 (in Russian).

Elliot R. P., *Constitution of Binary Alloys*, First Supplement. New York, McGraw-Hill, 1965.

Shunk F. A., *Constitution of Binary Alloys*, Second Supplement. New York, McGraw-Hill, 1969.

Part Two

IRON-CARBON ALLOYS

Chapter 6

THE IRON-CARBON CONSTITUTIONAL DIAGRAM

6-1. HISTORY

Iron-carbon alloys, i.e. steels and cast irons, are the most important metallic alloys used in modern engineering. The production of cast iron and steel exceeds by a factor of more than 10 the production of all other metals.

The iron-carbon constitutional diagram which will be discussed in this chapter can give the principal notion on the structure of iron-carbon alloys: steels and cast irons. It has been generally adopted that alloys of iron and carbon are called steels (with up to 2 per cent C) or cast irons (with more than 2 per cent C). In modern engineering, however, the term 'steels' is also applied to some special iron-base alloys (which we shall discuss later in the book) which contain carbon in small amount or even as a harmful impurity. In order to avoid misunderstanding, the term 'steel' (or 'cast iron') will be applied to alloys with more than 50 per cent iron and the term 'alloys' to those containing less than 50 per cent iron. This division is not strict scientifically, but is clearly defined for engineering purposes.

The study of the iron-carbon constitutional diagram and also of iron-carbon alloys and the processes of their heat treatment was initiated in 1868, when D. K. Chernov published his famous report "Critical Review of Mr. Lavroff's and Mr. Kalakutsky's Articles on Steel and Steel Guns and D. K. Tschernoff's Personal Investigations on the Same Subject"[1] in that year, physical metallurgy became a science.

---

[1] Zapiski Russkogo Tekhnicheskogo Obshchestva, 1868, issue 7, p. 399; full English translation in: Proc. Inst. Mech. Engrs, 1880, pp. 286-307.

D. Chernov was first to suppose in the cited work that certain critical points should exist in steel and that their position should depend on the carbon content. In other words, he gave the first notion on the iron-carbon diagram.

At a later time, Chernov expressed graphically his concepts on the effect of carbon on the position of critical points (Fig. 6-1) and plotted the principal lines of the iron-carbon constitutional diagram.

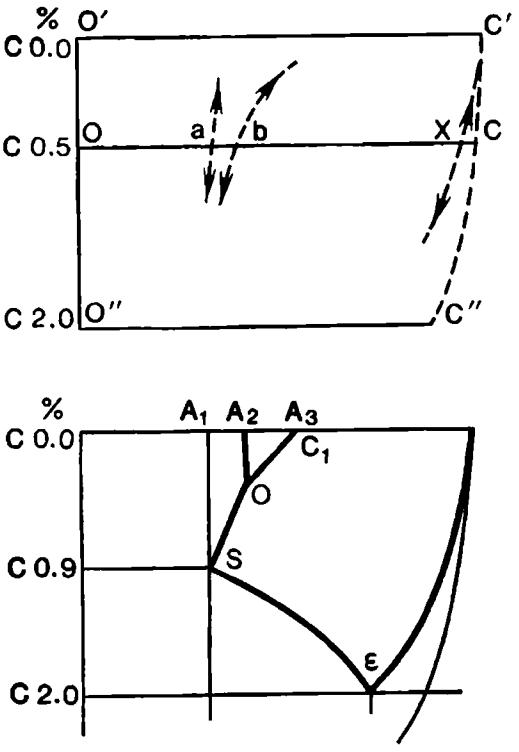

Fig. 6-1. Chernov's drawing of critical points

Works on the study of iron-carbon alloys and the construction of the iron-carbon constitutional diagram are extremely numerous and our knowledge of the structure of these alloys is due to the efforts of many researchers.

The most important studies of the iron-carbon constitutional diagram were made in the last quarter of the last century.

D.K. Chernov determined the position of the critical points in steel by temper colours. In 1886, F. Osmond, a prominent French researcher, used a pyrometer (just invented by H. L. Le Chatelier) to more accurately determine the critical points in steel; he described the microstructural changes occurre don transition through the critical points and gave names to the principal structures in iron-carbon alloys.

The formation of solid solutions in steels on heating was discovered by R. Austen of Great Britian and experimentally verified by direct metallographic analysis by H. L. Le Chatelier of France and by Russian metallurgists A. A. Baikov and N. T. Gudtsov.

Using these data and the theory of phase equilibriums that had been developed by W. Gibbs of Canada, G. Roseboom of the Netherlands and R. Austen worked out the first version of the iron-carbon constitutional diagram. Because of the lack of data, they could not construct a sufficiently full diagram corresponding to the actual phase equilibrium. Only at the end of the last century, P. Gerens of Germany utilized the experience of his precursors and the new results of microstructural and thermal analysis, and published in his book the iron-carbon constitutional diagram that was very close to its modern form. Later improvements in methods of analysis of alloys resulted in substantial, though not fundamental, amendments to the diagram. Studies of the iron-carbon constitutional diagram are still continued, and minor changes are made from time to time in the diagram, in particular in the position of equilibrium lines, owing to the application of purer alloys and more accurate methods of analysis, though no radical changes can be expected in the form of the diagram.

As is clear from its name, the iron-carbon constitutional diagram should extend from 100 per cent iron to 100 per cent carbon. Iron can form with carbon a chemical compound: Fe_3C (iron carbide) called cementite.

In the above analysis of constitutional diagrams with stable compounds, it has been noted that a stable compound can be regarded as a component of an alloy and the diagram can be analysed in parts.

Now we analyse only that part of the iron-carbon diagram which extends from 100 per cent iron to iron carbide (cementite). This not only simplifies our task of examining the system, but is also justified by the fact that iron alloys of practical importance contain not more than 5 per cent carbon.

Therefore, when analysing the iron-carbon constitutional diagram in its portion from iron to cementite, we can take that iron and cementite are the components of this system. It is then essential to study the properties and structures of these components.

6-2. IRON

Methods of mass production of steel have been discovered in the middle of the last century[1] and the first metallographic studies of iron and its alloys can also be dated to that time.

In 1930's, P. P. Amosov, a Russian metallurgist, employed the optical microscope for examination of steel structure and their changes upon forging and heat treatment. In other countries first microscopic examinations were made in 1860's and were associated with the structures of iron meteorites[2].

Later it was established that the structure of meteoritic iron is almost similar to that of common iron (more strictly, of an alloy of iron and nickel) and is mainly due to an extensive heating in its passage through the Earth's atmosphere. Of greater practical importance are metallographic studies of the structure of iron and iron-base alloys, depending on the composition, heat-treatment conditions, etc. P. P. Amosov was first to initiate such studies thirty years ahead of H. C. Sorby and A. Widmanstätten. Sorby used to make very accurate drawings of the structures he saw in the microscope. Figure 6-2 shows the structure of pearlite as drawn by him (compare with the modern microphotograph of pearlite shown in Fig. 6-14). Soon after that, photographs of microstructures of iron-carbon alloys began to appear in the specialist books. At the beginning of this century, first comprehensive monographs on metallography of iron-base alloys were published by A. A. Rzheshotarsky (Russia), A. Martens and Gein (Germany), and H. M. Howe (USA).

As any other metal, iron is never absolutely pure and always contains impurities. Very pure iron with the total content of impurities of around 0.01 per cent or even less can be obtained by modern processes of direct reduction obviating the blast-furnace stage, but commercial iron (often called Armco iron), which is produced in large quantities in open-hearth furnaces, is employed more often. Commercial iron contains on the average 99.8-99.9 per cent iron and 0.1-0.2 per cent impurities, including around 0.02 per cent carbon, around 0.1 per cent copper and thousandths or ten-thousandths of per cent of various other elements.

The data given later in this section refer to commercial-purity iron[3].

---

[1] Up to that time, iron was produced by primitive and rather inefficient methods.

[2] It is no mere chance, because the first metallographers (A. Widmanstätten, H. C. Sorby) were astronomers.

[3] The properties of iron or other metals of high purity may substantially differ from those of commercially pure metals.

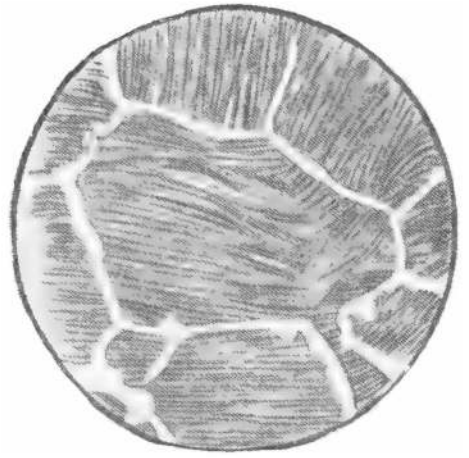

Fig. 6-2. Pearlitic structure drawn by H. C. Sorby (1886)

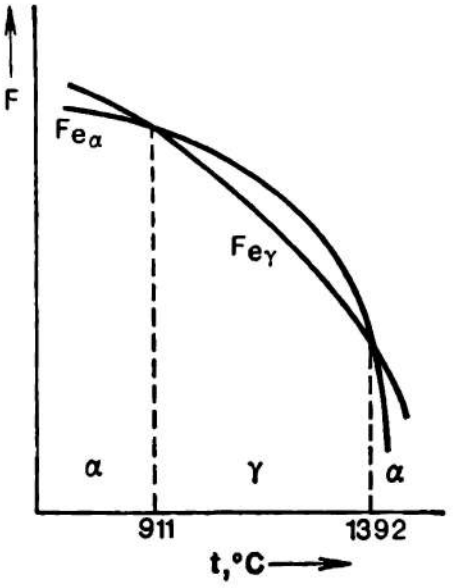

Fig. 6-3. Variations of free energy versus temperature in γ- and α-modifications of iron

The melting point of iron is 1539°C (±5 degrees).

In the solid state, iron has two modifications: α-Fe (b.c.c. lattice) and γ-Fe (f.c.c. lattice).

The crystal lattices of α- and γ-Fe and the temperatures of equilibrium transformations were shown in Fig. 2-15.

A circumstance of principal significance is that α-iron can exist within two temperature ranges: below 911°C and from 1392° to 1539°C. A probable explanation of this fact is that the free energy of the system varies in a definite way, depending on temperature (this is shown schematically in Fig. 6-3).

The free energy of α-iron is less than that of γ-iron at temperatures below 911°C and above 1392°C. In the intermediate range from 911° to 1392°C, the face-centred lattice packing has a lower free energy. This is why the $\alpha \rightarrow \gamma$-transformation takes place on heating at 911°C and the $\gamma \rightarrow \alpha$-transformation, on heating at 1392°C[1]. The high-temperature modification of α-iron (sometimes called δ-iron) is no other allotropic form.

The mechanical properties of iron can be characterized by the following values[2]:

[1] The temperatures of allotropic transformations are given according to the newest data obtained on especially pure alloys. It is quite admissible to use approximate values of 1535, 1400, and 910°C instead of 1539, 1392, and 911°C.

[2] Data on the properties of exceptionally pure iron produced by multiple zone refining have been disclosed in a recent publication (D. S. Kamenetskaya, 1974). It has turned out that the ultimate strength is only 5 kgf/mm² and the yield limit, 2.5 kgf/mm².

	Commercial iron	Direct-reduction iron
Ultimate tensile strength, kgf/mm²	25	20
Yield limit in tension, kgf/mm²	12	10
Elongation, %	50	60
Reduction, %	85	90
Brinell hardness	80	70

The properties of iron may deviate from these values, owing to the effect of various factors (for instance, grain coarsening reduces hardness).

At 768°C, iron undergoes a magnetic transformation and becomes non-magnetic above that temperature (see Sec. 2-7).

Iron can form solutions with many elements: substitutional solutions with metals and interstitial solutions with carbon, nitrogen and hydrogen.

The formation of carbon-in-iron solutions deserves special discussion. The solubility of carbon in iron essentially depends on the crystal form in which iron exists. The solubility of carbon in α-iron is negligible (less than 0.02 per cent) and is hundred times that (up to 2 per cent) in γ-iron. The diameter of carbon atom (in free state) is 1.54 Å.

A body-centred cubic lattice has 12 vacancies at the middle of edges. The diameter of such a vacancy, or void, in the crystal lattice is 0.62 Å, which is evidently insufficient to place an atom (ion) of carbon.

In the face-centred lattice of γ-iron, there is a void, 1.02 Å in diameter, in the centre. A carbon atom can occupy that void, but will cause a certain increase in the lattice size of γ-iron. The carbon atom proper should also diminish in size, since carbon gives up its valence electrons on dissolution. Overlapping of the electron shells of carbon and iron is also probable.

Thus, it is suggested by purely geometric considerations that γ-iron can dissolve carbon and α-iron cannot. There is some indirect evidence, however, that α-iron can dissolve carbon in very small quantities. The data of various researchers on the maximum solubility of carbon in α-iron appreciably disagree, ranging from 0.01 to 0.02, 0.04, 0.1 and even 0.15 per cent. The value of 0.02 per cent is given in a number of works and taken in the further discussion.

It should be assumed that the solubility of carbon in α-iron is due to certain defects in the real lattice of iron, which are especially numerous at grain boundaries.

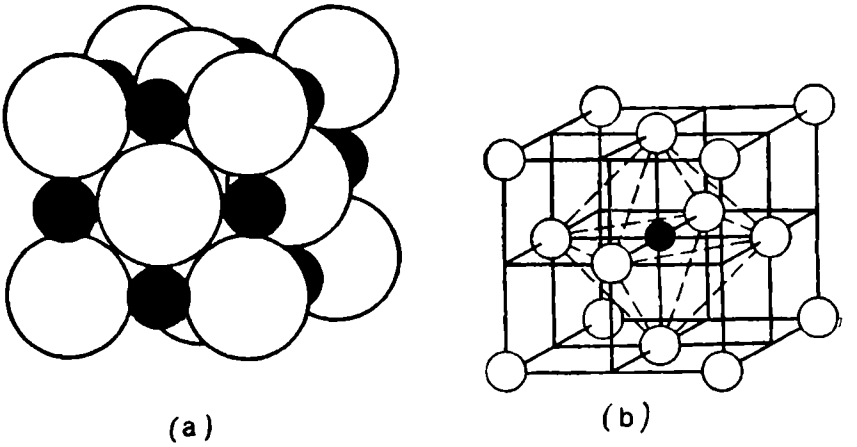

Fig. 6-4. Interstitial solid solution
(*a*) crystal lattice with all voids occupied; (*b*) crystal lattice of austenite

A solid solution of carbon and other elements in α-iron is called *ferrite* and that in γ-iron, *austenite*[1].

The crystal structure of austenite may be imagined as a face-centred cubic lattice consisting of iron atoms, in which smaller carbon atoms are incorporated (intersticed). If all the vacancies (voids) in the f.c.c. lattice were occupied by carbon, the state could be characterized by the scheme shown in Fig. 6-4*a*. But since the size of a carbon atom is larger than the size of a void, the lattice is distorted by an intersticed carbon atom and the other voids become inaccessible for other carbon atoms. The structure of an elementary cell of austenitic lattice in which one carbon atom is dissolved is shown in Fig. 6-4*b*.

The carbon atom positioned in the centre of the elementary γ-cell is surrounded by six iron atoms. These atoms form an octahedron.

The lattice parameter of carbonless α-iron at room temperature is 2.86 Å and that of carbonless γ-iron, 3.56 Å. The latter value is only conditional, since carbonless γ-iron is non-existent at room temperature and the value has been determined by extrapolation.

As is known, the parameter of a lattice increases with temperature and

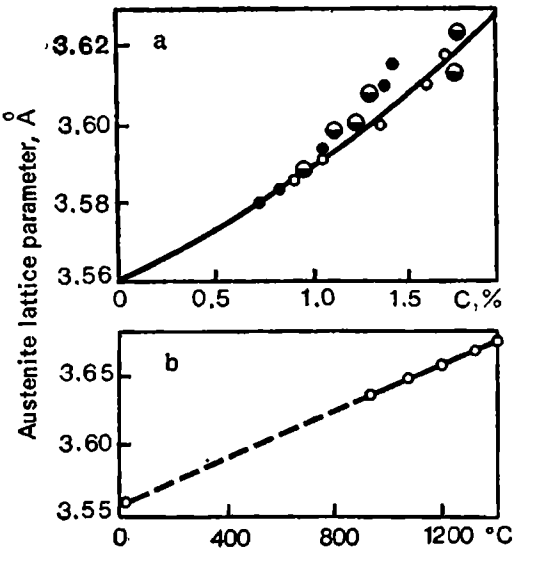

Fig. 6-5. Lattice parameter of austenite
(*a*) effect of carbon; (*b*) effect of temperature

[1] The former from the Latin name of iron (Ferrum) and the latter, after R. Austen. However, the definition of ferrite as a solid solution of carbon in α-iron is only justified for the analysis of the Fe-C diagram. By modern terminology, the purest iron which has only traces of carbon and also various carbonless iron alloys with a b.c.c. lattice are assumed to have the structure of ferrite.

in the presence of dissolved atoms. Experimental measurements have given the lattice parameter of austenite at room temperature in steels with more than 0.6-0.7 per cent carbon (Fig. 6-5*a*) and the lattice parameter of pure γ-iron at higher temperatures (Fig. 6-5*b*). Extrapolating the curves to zero content of carbon (see Fig. 6-5*a*) or to room temperature (see Fig. 6-5*b*) gives the value of 3.56 Å. This parameter would be possessed by pure γ-iron at room temperature if it were possible to obtain γ-iron at that temperature.

The state in which carbon is present in austenite was much disputed by metallurgists, but now it can be taken for certain that carbon is present as twice ionized ions, whereas iron atoms are ionized only once, i.e. carbon contributed two electrons and iron, only one, to the crystal. This fact explains the phenomenon of 'electrolysis' of austenite, which has been discovered by V. I. Prosvirin and co-workers, and consists in that carbon moves to the negative pole (cathode) in austenite under the action of direct current.

6-3. CEMENTITE

Cementite is a compound of carbon and iron, Fe_3C (iron carbide). Since the solubility of carbon in α-iron is low, the structure of steel at room temperature usually contains high-carbon phases in the form of cementite or another carbide.

The crystal structure of cementite is very complicated. There are many methods for depicting it graphically and one of the most apt is shown in Fig. 6-6.

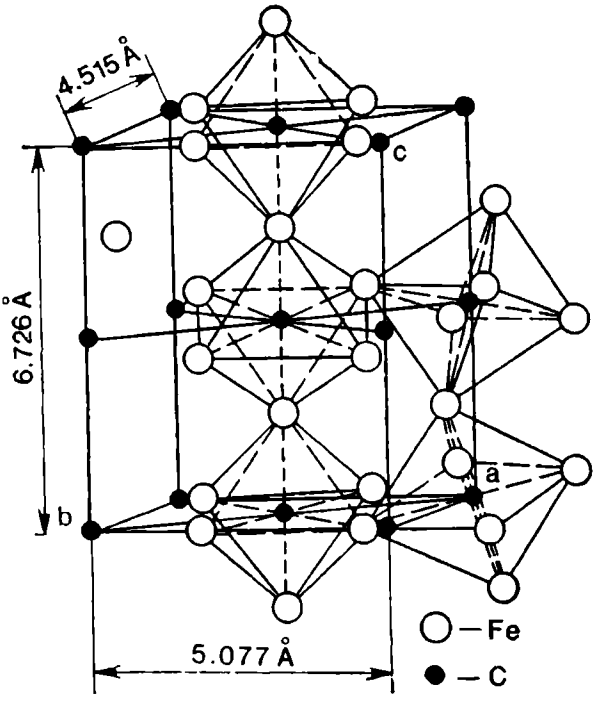

Fig. 6-6. Crystal structure of cementite

As may be seen from the figure, a crystal of cementite consists of a number of octahedrons whose axes are tilted at definite angles to one another (not all of the octahedrons are shown in order not to obscure the figure). The centre of each octahedron is occupied by a carbon atom. Since each iron atom belongs to two octahedrons, the formula of the compound with all the octahedrons occupied by carbon atoms corresponds to the ratio Fe : C = 3 : 1.

The bond between iron atoms is purely metallic. The nature of the bond between carbon and iron atoms in the lattice has not been ascertained. It might be a special type of bond having the features of both metallic and ionic bond (and probably, the nature of this bond is analogous with that between carbon and

iron in austenite). In any case, both carbon and iron in the lattice are ionized positively, i.e. both the metal and carbon behave like metals. This circumstance and the prevalence of metallic bond explain why cementite possesses metallic properties (electric conduction, metallic lustre, etc.).

The melting point of cementite is near 1250°C. Cementite undergoes no allotropic transformations but is slightly ferromagnetic at low temperatures. It loses its magnetic properties on heating to 217°C .Cementite has a high hardness (above 800 *HB* and can easily scratch glass) but an extremely low, practically zero, ductility. These properties are evidently due to the complicated structure of the crystal lattice of cementite.

Cementite is capable of forming substitutional solid solutions. Its carbon atoms can be displaced by atoms of non-metals: nitrogen, oxygen; and its iron atoms, by metals: manganese, chromium, tungsten, etc. Such a solid solution based on cementite lattice is called *alloyed cementite.* It is usually designated as M_3C where M stands for iron and other metals substituting iron in the cementite lattice.

Cementite is an unstable compound and decomposes under certain conditions to form free carbon (graphite). The process is of high practical importance, mainly for high-carbon alloys (cast irons) and will be discussed in more detail in Ch. 8.

6-4. THE CONSTITUTIONAL DIAGRAM

The part of the iron-carbon constitutional diagram in the concentration range from pure iron to cementite is shown in Fig. 6-7. The abscissa (concentration axis) in the figure has two concentration scales: for carbon and for cementite.

A simple rule may be suggested: multiplying the content of carbon by 15 gives the content of cementite in steel or cast iron as percentage by mass and practically as percentage by volume.

ABCD is the liquidus line and *AHJECF*, the solidus line of the system.

Since iron can combine with carbon to Fe_3C and also has two allotropic modifications, α and γ, the following phases can exist in the system:

(a) *liquid* (liquid solution of carbon in iron); it exists above the liquidus line and is designated *L*;

(b) *cementite* Fe_3C; its region is restricted by line *DFKL*; it will be designated as *Cem* in the further discussion;

(c) *ferrite*—a structural component (α-iron) which can only slightly dissolve carbon; will be designated as *F*, α or α-Fe. The region of ferrite in the iron-carbon system is located to the left of lines *GPQ* and *AHN*;

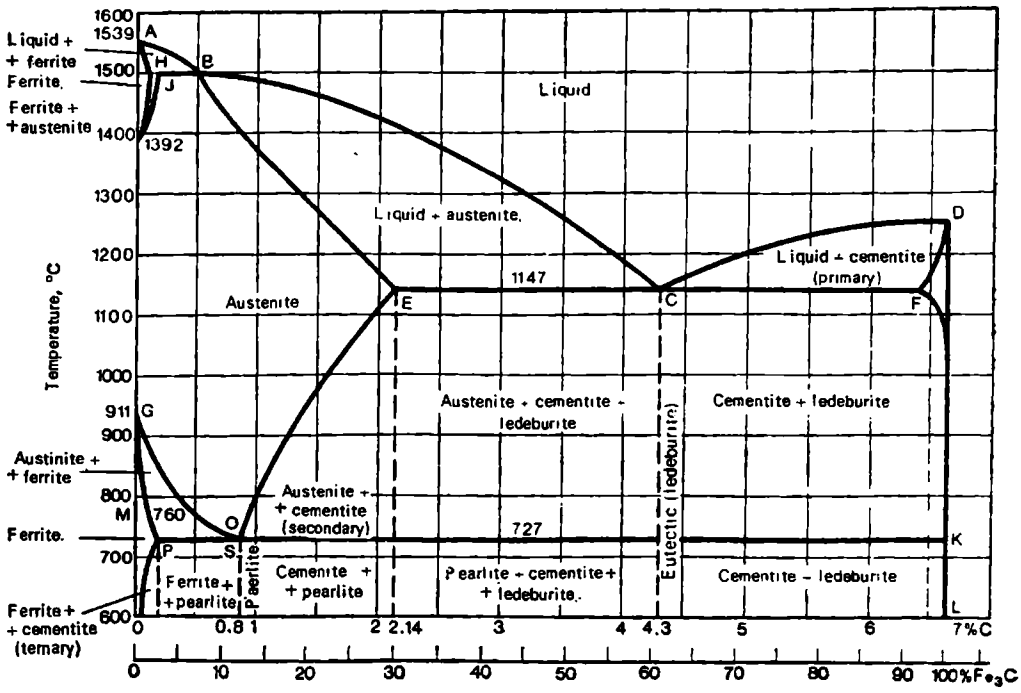

Fig. 6-7. Fe-C constitutional diagram

(d) *austenite*—a solid solution of carbon in γ-iron; its region in the diagram is limited by line *NJESG*; austenite will be designated as *A*, γ or γ-Fe (C).

The three horizontal lines in the diagram (*HJB*, *ECF* and *PSK*) indicate the occurrence of three non-variant reactions.

At 1499°C (line *HJB*), a peritectic reaction occurs:

$$L_B + F_H \rightarrow A_J$$

resulting in the formation of austenite. This reaction is only observed in alloys containing from 0.1 to 0.5 per cent carbon.

At 1147°C (line *ECF*), a eutectic reaction takes place:

$$L_C \rightarrow A_E + Cem$$

resulting in the formation of a eutectic mixture of austenite and cementite which is called *ledeburite*[1]. This reaction can occur in all alloys of the system which contain more than 2.14 per cent carbon.

At 727°C (line *PSK*), a eutectoid reaction takes place

$$A_S \rightarrow F_P + Cem$$

It forms a eutectoid mixture of ferrite and cementite called *pearlite* (the name is due to the pearl-like appearance of the structure).

[1] After A. Ledebur, a German metallurgist.

Pearlitic (eutectoid) transformation can take place in all alloys containing more than 0.02 per cent carbon, i.e. practically in all commercial iron-carbon alloys.

As noted earlier, the form of the iron-carbon constitutional diagram (in its pre-cementite portion), i.e. the position of the characteristic lines on it, is quite established and definite. Only the coordinates (the temperatures and concentrations of the typical points) are or may be corrected from time to time.

The coordinates of the typical points in the iron-carbon constitutional diagram according to the latest experimental data are given in Table 6-1.

Table 6-1. Points in Iron-carbon Diagram

Point	Temperature, °C	Carbon concentration, %	Point	Temperature, °C	Carbon concentration, %	Point	Temperature, °C	Carbon concentration, %
A	1 539	0	*E*	1 147	2.14	*P*	727	0.02
B	1 499	0.5	*C*	1 147	4.3	*S*	727	0.8
H	1 499	0.1	*F*	1 147	6.67	*K*	727	6.67
J	1 499	0.16	*D*	1 250	6.67	*Q*	~ 600	0.01
N	1 392	0	*G*	911	0	*L*	~ 600	6.67

The iron-carbon constitutional diagram is quite complicated and can be divided into portions for more convenient analysis of its structure and of the transformations in iron-carbon alloys. The discussion that follows is basically not new, but is a mere application of the material of Ch. 3 (binary systems) to the particular case of iron-carbon alloys.

Figure 6-8 shows to a larger scale the leftmost upper portion of the iron-carbon diagram (the region of peritectic transformation).

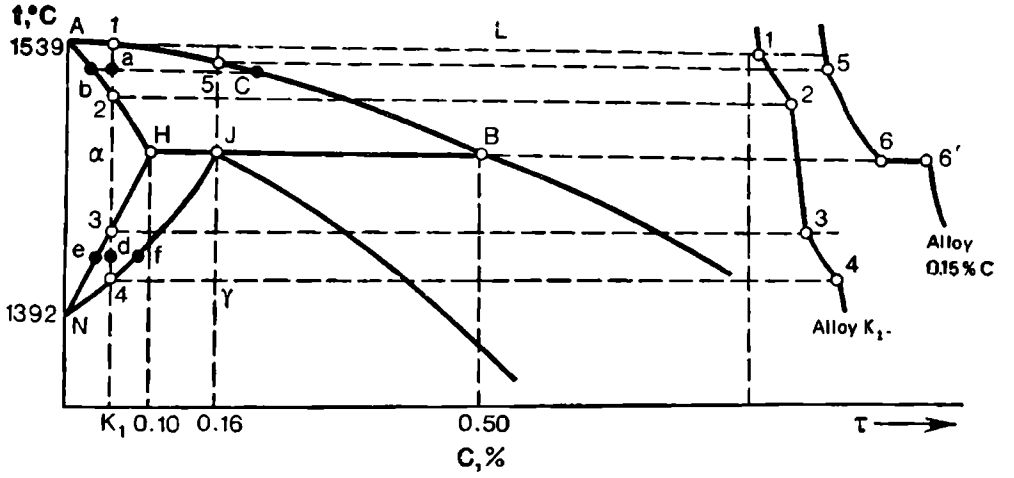

Fig. 6-8. Part of Fe-C diagram. Primary crystallization in low-carbon alloys

Consider the sequence of transformations of an alloy of concentration K_1 with less than 0.1 per cent C (for instance, with 0.05 per cent C).

The alloy begins to solidify at point *1* where crystals of α-solid solution precipitate from the liquid. In the course of solidification, the concentration of the liquid varies along line *AB* (part of the liquidus line) and that of the solid phase, along line *AH* (part of the solidus line). At point *a*, which is within the region of coexistence of the liquid and solid phases, the concentration of the liquid is determined by the projection of point *c* and that of the solid phase by the projection of point *b*; the quantity of the solid phase is determined by the lever rule as the *ac/bc* ratio and that of the liquid phase, as *ba/bc*.

At point *2*, the quantity of the liquid phase becomes zero and the process of solidification is finished by the formation of a homogeneous α-solid solution. The alloy undergoes a new transformation within a temperature range *3-4* where the α-solid solution transforms into γ-solid solution. The concentration of phases changes according to the positions of lines *HN* and *JN*.

At point *d*, the concentration of α-phase is determined by the projection of point *e* and that of γ-phase, by the projection of point *f*; the quantities of the phases can be found from the ratio $\alpha/\gamma = df/ed$.

At point *4*, the structure of the alloy is γ-solid solution.

The temperature curve of the alloy cooling is shown in the right-hand side of Fig. 6-8.

The cooling of an alloy with 0.16 per cent C initially occurs in the same way as that of alloy K_1, i.e. starts from the precipitation of α-phase of varying concentration.

At point *J* at 1499°C, where the concentration of the liquid is *B* and that of the α-phase, *H*, the γ-phase of concentration *J* begins to form. Since three phases co-exist here, the transformation occurs at a constant temperature ($c = k - f + 1 = 2 - 3 + 1 = 0$); section *6-6'* of the cooling curve is horizontal. The process follows the reaction

$$L_B + \alpha_H \rightarrow \gamma_J$$

and forms austenite (γ-phase) of a concentration of 0.16 per cent. If the carbon content is less or more than 0.16 per cent (i.e. to the left or to the right of point *J*), an excess of α-phase or, respectively, an excess of the liquid (which transforms into γ-phase on further cooling) remains upon the peritectic reaction. The transformation will come to its end at lines *VJ* and *JE* (point *E* is not shown in Fig. 6-8) when, finally, a homogeneous structure of γ-phase is formed.

Thus, taken any alloy with less than 0.5 per cent carbon, it will finally solidify into γ-phase (austenite), irrespective of the intermediate formations of α-phase.

Fig. 6-9. Austenitic structure revealed by etching at high temperature, ×500

That austenite is a homogeneous solid solution of carbon in γ-iron has been finally established only by X-ray structural analysis. Before the discovery of X-rays, A. A. Baikov used Le Chatelier's method of etching microsections to examine the structures of metals at high temperatures. Microsections were etched at a high temperature and the structure typical to exist at that temperature was revealed. After that the sections were examined at room temperature; the transformations occurred in the metal on cooling to room temperature had no effect on the structure revealed at high temperature.

Having used this method, A. A. Baikov showed that austenite was actually a homogeneous solid solution.

Figure 6-9 shows the structure of austenite in a steel with 1 per cent C which has been revealed by the method employed by A. A. Baikov. Thus, austenite is a homogeneous solid solution, which fact has been verified by X-ray structural and metallographic analysis.

Now consider the processes of primary crystallization of alloys containing more than 2.14 per cent carbon (Fig. 6-10).

Typically, the primary crystallization in these alloys is finished with a eutectic transformation at 1147°C, when the liquid with 4.3 per cent C crystallizes into two solid phases: austenite (2.14 per cent C) and cementite, i.e. ledeburite is formed.

An alloy having exactly the eutectic concentration of 4.3 per cent C undergoes only the eutectic crystallization which takes place at a constant temperature.

In hypoeutectic alloys, i.e. those containing less than 4.3 per cent C (but more than 2.14 per cent), the eutectic transformation is preceded with the precipitation of primary austenite. An example is the K_1 alloy whose cooling curve is shown in the right-hand part of Fig. 6-10. The beginning of solidification of this alloy is determined by point *1*

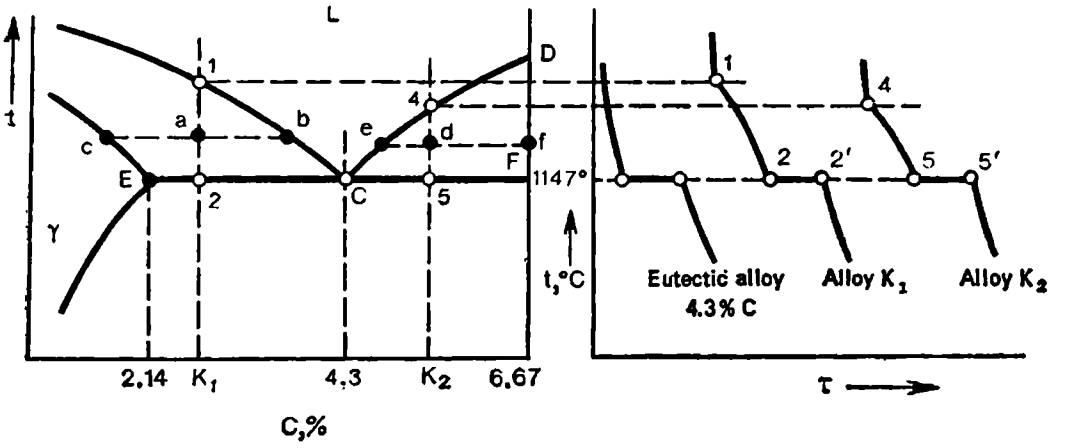

Fig. 6-10. Part of Fe-C constitutional diagram. Primary crystallization of high-carbon alloys

on the liquidus line. On further cooling, crystals of austenite of varying composition (determined by the position of the solidus line) precipitate and the liquid has a concentration corresponding to the position of the liquidus line.

At point *a*, which is in the two-phase region $\gamma + L$, the concentration of the liquid phase is determined by the projection of point *b*, that of the solid phase, by the projection of point *c*. and the quantities of these phases, by the ratio of sections:

$$\frac{\text{quantity of liquid phase}}{\text{quantity of solid phase}} = \frac{ca}{ab}$$

At point *2* at 1147°C, i.e. at the intersection of vertical K_1 and horizontal *ECF* (1147°C), the quantity of the liquid corresponds to section *E-2* and its concentration is determined by point *C* (4.3 per cent C).

At that temperature, the eutectic crystallization takes place

$$L_C \rightarrow \gamma_E + Cem$$

and the primary crystallization in the alloy is completed. The resulting structure upon primary crystallization consists of primary crystals of austenite and ledeburite.

For a hypereutectic alloy, say K_2 (see Fig. 6-10), the initial stage of crystallization begins on the liquidus line *CD* (point *4*) with precipitation of primary cementite.

Precipitation of cementite depletes the liquid of carbon. At point *5* on line *ECF*, the liquid will have the concentration of point *C* and here the process of eutectic crystallization begins. The structure of the alloy upon primary crystallization will consist of crystals of primary cementite and ledeburite.

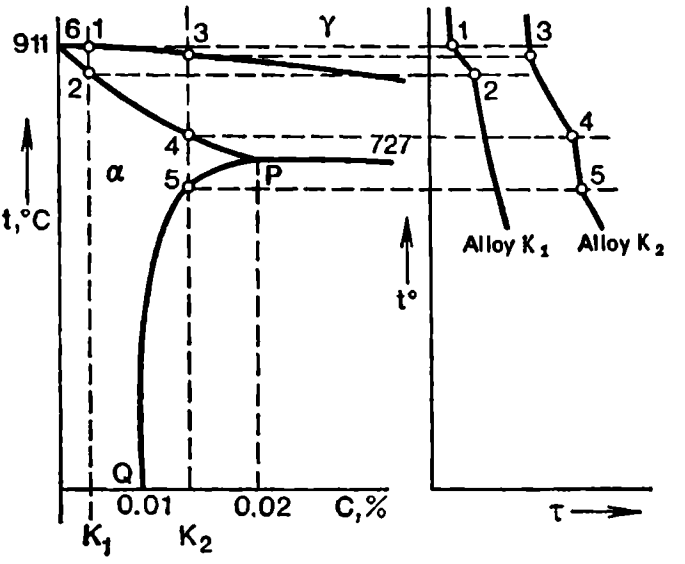

Fig. 6-11. Part of Fe-C constitutional diagram. Secondary crystallization in extra low-carbon alloys

The foregoing discussion suggests the following conclusion of great importance:

In all alloys with less than 2.14 per cent C, the structure upon primary crystallization is austenite; in those with more than 2.14 per cent C, the structure is ledeburite plus excess austenite or cementite.

These different structures at high temperatures determine an appreciable difference in the process and mechanical properties of the two types of alloy. The alloys which contain the eutectic are poorly malleable. On the other hand, high-carbon alloys have a low melting point and are well suitable as casting materials.

Iron-carbon alloys containing less than 2.14 per cent carbon are called steels and those with more than 2.14 per cent carbon, cast irons[1].

Consider the solid state transformations in alloys rather low in carbon.

Figure 6-11 shows the leftmost lower portion of the iron-carbon constitutional diagram in an enlarged scale.

An alloy of concentration K_1, which contains less than 0.01 per cent carbon, has the structure of austenite at temperatures of an order of 1 000°C. Iron can exist only as α-modification at room temperature, therefore, $\gamma \rightarrow \alpha$-transformation, i.e. the transformation of austenite into ferrite, should take place on cooling. With a pure alloy perfectly clean of carbon, this transformation would occur at a constant temperature (911°C) at point *G*. For the alloy of con-

[1] This delimitation between steels and cast irons (2.14 per cent C) relates only to binary iron-carbon alloys or to those containing a low percentage of impurities. The problem on the delimitation between steels and cast irons as related to high-alloyed iron-carbon alloys, i.e. containing also appreciable quantities of other elements, is still disputable.

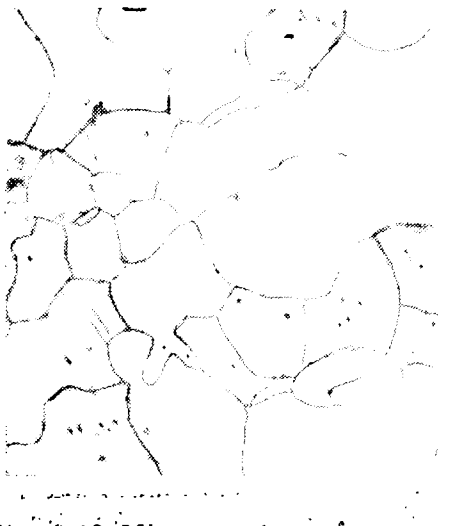

Fig. 6-12. Microstructure of commercial iron. Ferrite. ×400

centration K_1, the transformation takes place within a temperature interval from point *1* to point *2* and will be represented by a bend on the cooling curve of that alloy. The alloy is two-phase in the interval between points *1* and *2*, i.e. consists of α- and γ-phases of varying concentration.

Below point *2*, the alloy is a homogeneous α-solid solution (ferrite) and undergoes no structural changes on further cooling. The structure of ferrite is shown in Fig. 6-12.

The transformation in an alloy containing more than 0.01 but less than 0.02 per cent carbon (K_2 alloy) is shown by a second cooling curve. This alloy differs from the former in that its vertical intersects line *PQ* at point *5* on further cooling after the $\gamma \rightarrow \alpha$-transformation (in the interval *3-4*).

Above point *5*, the alloy is not saturated in carbon. Below that point, it can no more retain the given concentration of carbon in the solution, so that the excess carbon precipitates as a high-carbon phase—cementite. The process occurs continuously during the cooling and causes depletion of the α-solid solution to 0.01 per cent C. The cementite that precipitates from ferrite is called *ternary cementite* (in contrast to *primary cementite* which precipitates from the liquid or to *secondary cementite* which precipitates from austenite).

Let us analyse the transformation of austenite in alloys richer in carbon, in the first place in alloys of the eutectoid concentration (alloy with 0.8 per cent C in Fig. 6-13).

The austenite undergoes no changes on cooling to point *1* (*S*).

Point *S* (727°C) is the lowest temperature at which austenite can exist in equilibrium. From that temperature, eutectoid decomposition of austenite into ferrite and cementite commences.

Neglecting the content of carbon in the ferrite at the moment of transformation (0.02 per cent C), the reaction can be written as follows:

$$Fe_\gamma(C) \rightarrow Fe_\alpha + Fe_3C \quad \text{or} \quad A \rightarrow F + Cem$$

The transformation results in the formation of pearlite, whose structure consists of alternating lamellae of ferrite and cementite (Fig. 6-14).

Alloy K_1, containing, say, 0.5 per cent C, has an excess in iron relative to the eutectoid concentration. This is why the transfor-

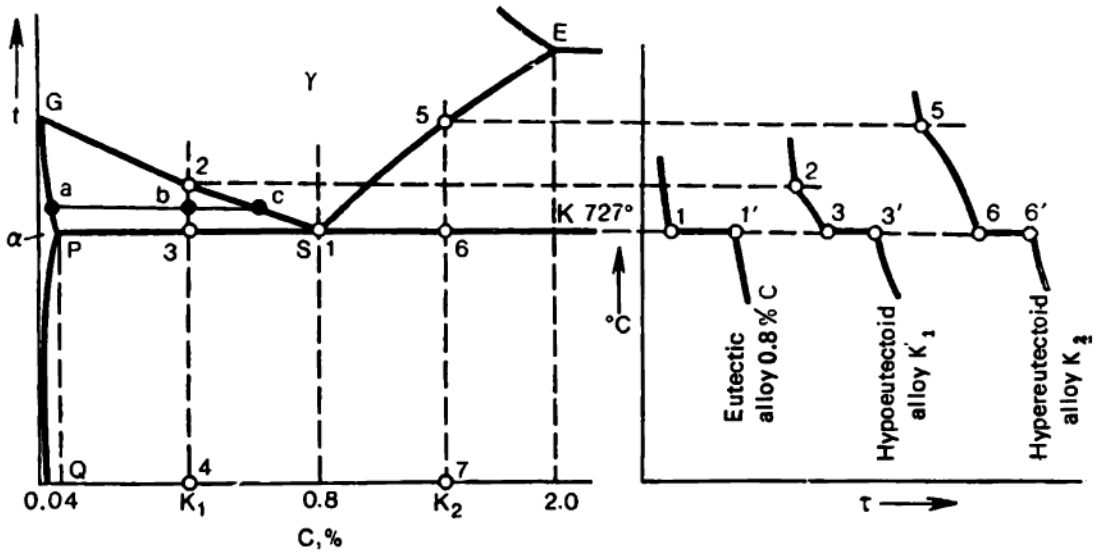

Fig. 6-13. Part of Fe-C constitutional diagram. Secondary crystallization in steels

mation of austenite begins from precipitation of ferrite. Point *2* on line *GS* corresponds to the beginning of that process.

With further cooling, the retained austenite is enriched in carbon owing to the fact that the precipitated ferrite is almost free of carbon. The concentration of austenite varies along curve *GS*.

At point *b*, the structure is ferrite plus austenite, more particularly, ferrite of concentration of point *a* and austenite of concentration

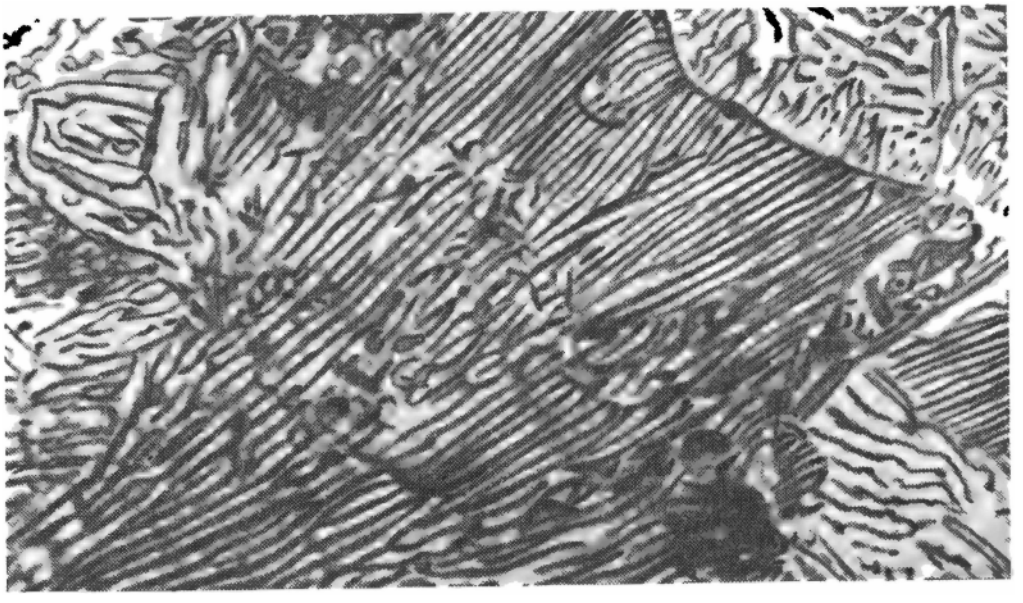

Fig. 6-14. Pearlitic structure, ×1000

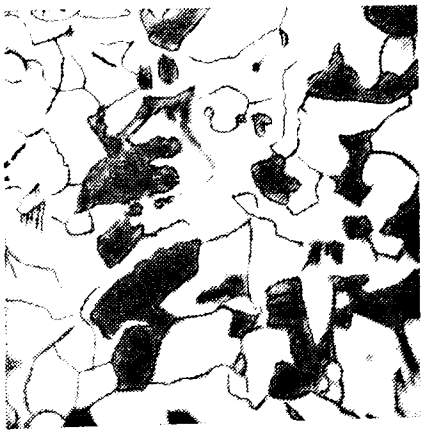

Fig. 6-15. Structure of hypoeutectoid steel (0.4% C). Ferrite + pearlite. ×250

of point *c*. The quantities of these phases are found by the lever rule:

$$\frac{\text{quantity of ferrite}}{\text{quantity of austenite}} = \frac{bc}{ab}$$

On reaching point *3*, austenite will have the eutectoid concentration and will be further transformed into pearlite at a constant temperature (the horizontal portion *3-3'* of the cooling curve). The structure of the steel on completion of the transformation will be ferrite plus pearlite. It is shown in Fig. 6-15.

The quantity of ferrite and pearlite depends on carbon content. With a carbon content of less than 0.02 per cent, the structure consists of ferrite only, with a carbon content of 0.8 per cent, of pearlite only, and at intermediate values, of ferrite and pearlite; the content of pearlite increases with the carbon content of steel. This correlation is illustrated by the micrographs in Fig. 6-16. The method for determining the content of carbon in steel by the relative areas occupied by ferrite and pearlite in the steel structure is widely used in practice along with the chemical analysis[1].

An alloy containing more than 0.8 per cent carbon is shown by vertical line K_2 in Fig. 6-13. The austenitic transformation in it begins at point *5*, i.e. after cementite has precipitated from austenite.

During precipitation of cementite, austenite is depleted of carbon along line *ES* which shows the maximum carbon saturation of austenite.

At point *6*, pearlite begins to form at a constant temperature (horizontal portion *6-6'* of the cooling curve). The resulting structure is pearlite with a network of cementite precipitated at grain boundaries (Fig. 6-17).

A special etcher—sodium picrate—is used to distinguish between cementite and ferrite. It tints cementite black and does not tint ferrite (Fig. 6-17*b*).

Steels are divided into three principal groups:

(a) *eutectoid* steel which contains about 0.8 per cent C and whose structure is pearlite only;

[1] Having measured the relative areas of ferrite and pearlite in the steel structure, the content of carbon in the steel is found as

$$\%C = 0.8\% \ P/100$$

where $\%P$ is the percentage of pearlite in the structure. The method is applicable with annealed carbon steels provided that they are low in manganese.

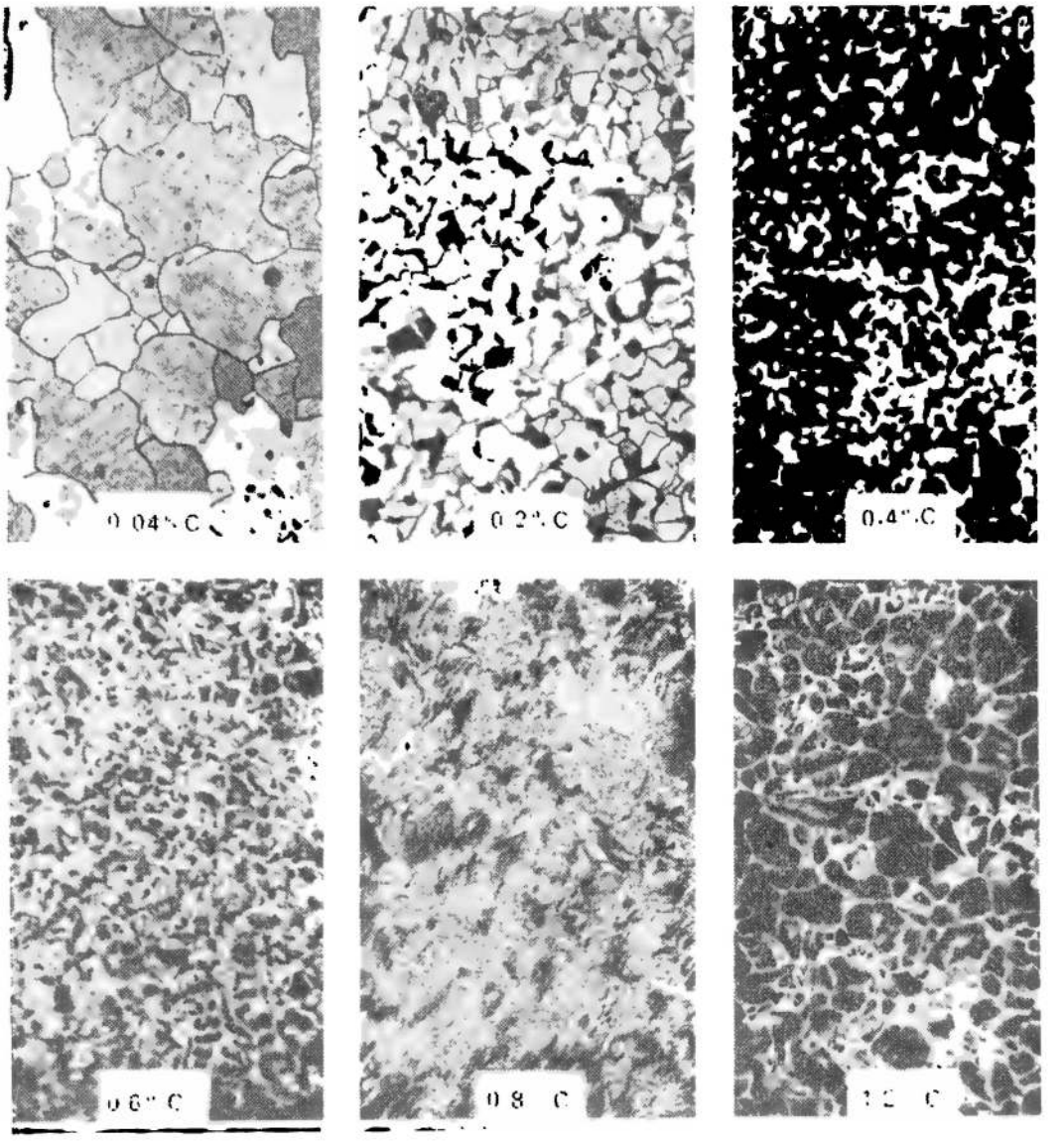

Fig. 6-16. Structures of steel with different content of carbon, ×200

(b) *hypoeutectoid* steel containing less than 0.8 per cent C and having a structure of ferrite plus pearlite; and

(c) *hypereutectoid* steel which contains from 0.8 to 2 per cent C and has a structure of pearlite plus cementite.

Now consider the transformations which take place in high-carbon alloys—cast irons (Fig. 6-18). The structure of these alloys upon primary crystallization consists of ledeburitic eutectic and primary formations of austenite or cementite.

Both the primary austenite and the austenite entering the eutectic have the maximum content of carbon in the solution (2.14 per cent) at the end of crystallization. The solution cannot retain such a large

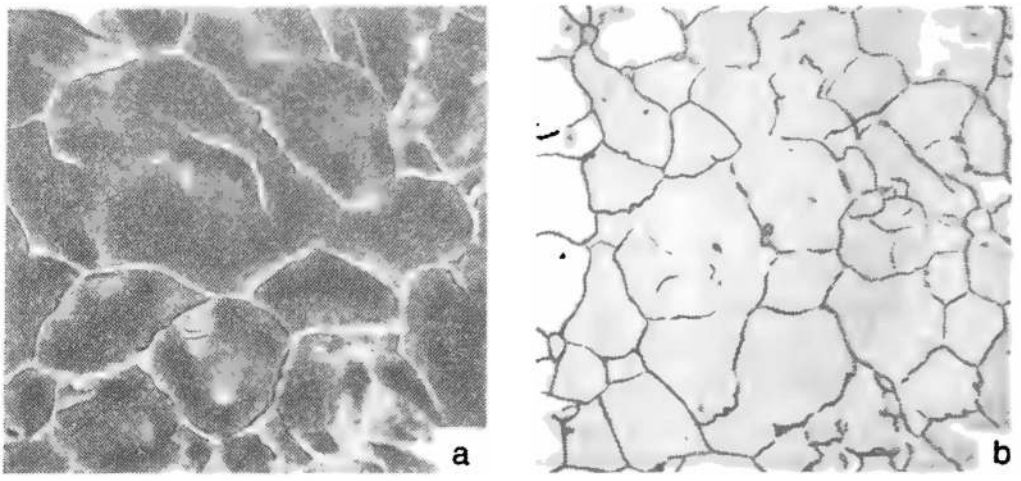

Fig. 6-17. Structure of hypereutectoid steel. Pearlite + cementite network. × 450
(*a*) etched with 4% nitric acid; (*b*) etched with sodium picrate

amount of carbon at lower temperatures, and carbon precipitates from austenite as secondary cementite on cooling from 1 147°C. The concentration of carbon in the austenite varies according to the position of line *ES*. Finally, the austenite undergoes pearlitic transformation on reaching line *PSK*, irrespective of the structural form in which it exists (either excess austenite or eutectic austenite).

Let us consider the particular alloys whose cooling curves are shown in the right-hand portion of Fig. 6-18.

The alloy with 4.3 per cent C has a purely eutectic structure upon crystallization. During cooling from 1 147° to 727°C (from point *1* to point *2*), cementite precipitates from the eutectic austenite: this

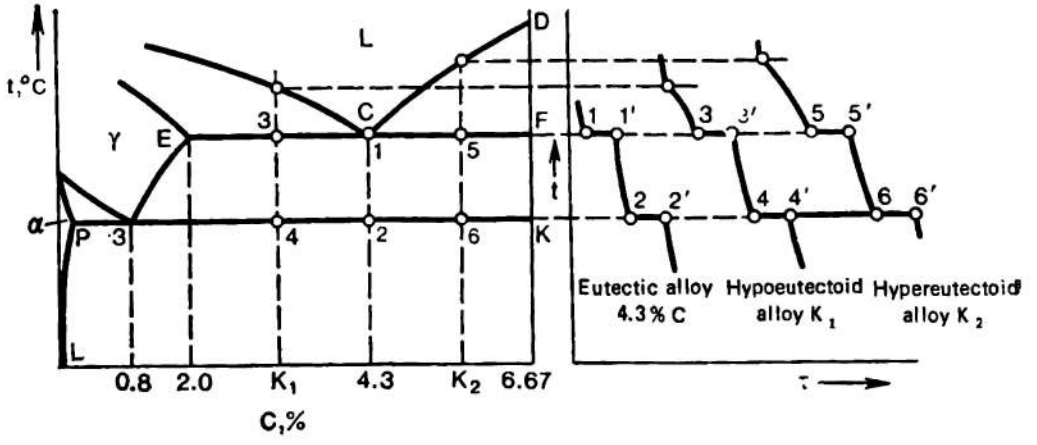

Fig. 6-18. Fe-C constitutional diagram. Secondary transformations in high-carbon alloys (cast irons)

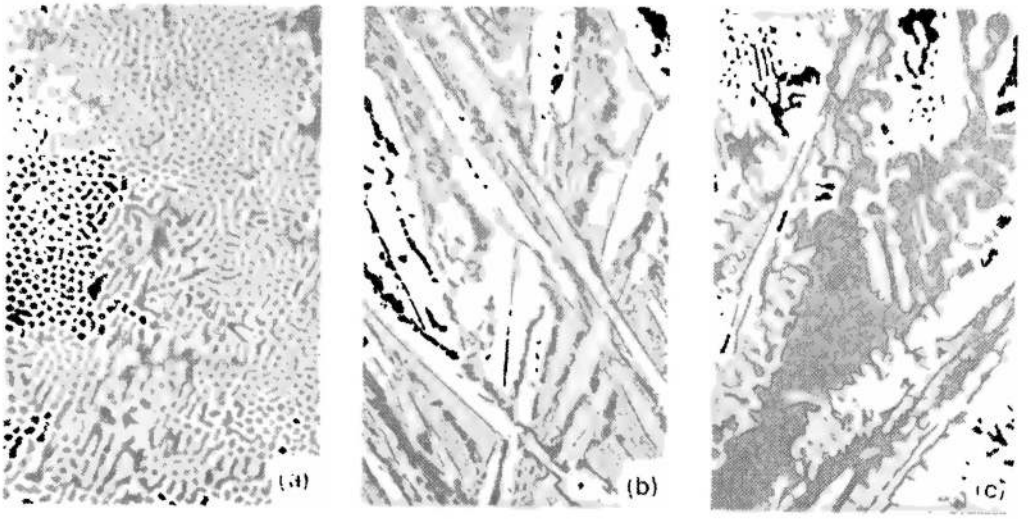

Fig. 6-19. Microstructures of cast iron

(*a*) eutectic (ledeburite), ×450; (*b*) hypereutectic (ledeburite + primary cementite), ×100; (*c*) hypoeutectic (ledeburite + pearlite), ×450

cementite usually cannot be detected structurally, since it is combined with the cementite of eutectic origin.

At point *2*, i.e. at 727°C, the austenite of the eutectic contains 0.8 per cent C and the pearlitic transformation takes place at that temperature.

Therefore, ledeburite below 727°C is a mixture of cementite and pearlite. The structure of ledeburite is shown in Fig. 6-19*a*.

Hypereutectic cast irons undergo the transformations discussed above, since their primary cementite is not prone to transformation.

The structure of a hypereutectic cast iron, which consists of ledeburite and cementite (large elongated bright formations), is shown in Fig. 6-19*b*.

Finally, in hypoeutectic cast irons, the primary austenitic precipitates vary their concentration on cooling from point *3* to point *4* (K_1 alloy) from 2.14 to 0.8 per cent C and at point *4* pearlitic transformation takes place. The structure of such a hypoeutectic cast iron consists of pearlite, ledeburite and secondary cementite. It is shown in Fig. 6-19*c*.

The regions of existence of various structures are marked in the constitutional diagram (see Fig. 6-7). Notwithstanding the apparent complexity of the structural forms, especially in high-carbon alloys, all these regions in the diagram are single- or two-phase.

In particular, region *SEFK* contains two phases: austenite and cementite, region *KPLQ*—ferrite and cementite which can form various structural components as indicated in the diagram.

LITERATURE

Geveling N. V., *Aircraft Metallurgy*. Part I. Metallic alloys. Moscow, ONTI, 1934 (in Russian).

Bunin K. P., *Iron-carbon Alloys*. Moscow, "Mashgiz", 1949 (in Russian).

Hansen M., Anderko K., *Constitution of Binary Alloys*. New York, McGraw-Hill, 1958.

Bolkhovitinov N. F., Bolkhovitinova E. N., *An Atlas of Micro- and Macrostructures of Metals and Alloys*. Moscow, "Mashinostroenie", 1964 (in Russian).

Habraken L., de Brouer J.-L., *De Ferri Metallographia*. Vol. 1. Bruxelles, 1969.

Chapter 7

CARBON STEELS

Steel is the main product of ferrous metallurgy, with roughly 90 per cent being manufactured as carbon steel and 10 per cent, as alloy steel[1]. Thus, carbon steel is the principal metallic material used in industry.

Commercially made carbon steel is an alloy of a complex composition. Apart from the base element, iron (whose content may vary within 97.0-99.5 per cent), it contains many other elements whose presence is due to the specifics of steelmaking process (manganese, silicon), impossibility of complete removal from the metal (sulphur, phosphorus, oxygen, nitrogen, hydrogen) or may be caused by occasional circumstances (chromium, nickel, copper, etc.).

The content of these impurities may be different, depending on the particular steelmaking process (open-hearth, Bessemer). Only one element—carbon—is introduced intentionally into carbon steel.

Carbon can affect the properties of steel even when its content varies insignificantly. With a low content of all other possible impurities, carbon is the principal element affecting the properties of iron alloys. These alloys (with C up to 2 per cent) are, naturally, called *carbon steels.*

As is known, the structure and properties of metallic alloys can be varied within a wide range by heat treatment; this method is especially effective with steels. Not all properties of the metal can, however, be changed by heat treatment. Most properties are structurally sensitive, i.e. depend on the structure of metal, and therefore, can be varied by heat treatment. Others (which are structurally insensitive) do not practically depend on structure. These include rigidity properties (modulus of elasticity E and shear modulus G).

The hardness and strength of carbon steel can be increased by heat treatment three to five times (compared with as-annealed steel, upon slow cooling), whereas its moduli of elasticity will be changed by less than 5 per cent.

In most cases steel parts must have an appropriate rigidity. To attain this, the designer should select a proper area and form of the part cross-section. It then usually turns out that the stresses acting

[1] On alloy steels, see Chapters 14-20.

in the part are appreciably lower than the yield limit. Naturally, in that case heat treatment is not needed, since the metal in 'raw', i.e. not heat-treated, state has quite sufficient strength properties.

In other cases, i.e. when the strength of raw steel is insufficient, heat treatment is employed. The steel to be heat-treated should meet more rigorous requirements, in particular, its carbon content is limited within a narrower range. Such steels are called steels of improved quality.

This chapter will consider the properties of common-quality steels which are mostly employed without heat treatment[1].

Carbon steels of improved quality, high-quality and tool steels will be discussed together with alloy steels in Chapters 16 and 17.

7-1. EFFECT OF CARBON

The structure of steel changes with increasing content of carbon. Steels containing 0.8 per cent C are solely composed of pearlite. Those which contain more than 0.8 per cent C have also secondary cementite; those with less than 0.8 per cent C have the structure of ferrite and pearlite (see Fig. 6-16).

Let us see how variations in the content of carbon, therefore, in the structure of steel, can affect steel properties.

An increase in the carbon content of steel results in increased strength and reduced ductility (Fig. 7-1). The mechanical properties shown in the figure relate to hot-rolled steel articles which have not been heat-treated, i.e. with the structure of pearlite + ferrite (or pearlite + cementite). The diagram has been plotted for average values which may vary within ±10 per cent, depending on the content of impurities, cooling conditions after rolling, etc.[2]. In steel castings, the structure is coarser and gives lower mechanical properties, than it follows from Fig. 7-1 (it mainly affects the ductility properties). The effect of carbon on ductility properties of steel is quite essential. As may be seen from Fig. 7-2, an increased content in carbon raises the ductile-to-brittle transition point and diminishes the impact toughness in the ductile region (at temperatures above the transition point).

The effect of carbon on selected physical properties of steel is shown in Fig. 7-3.

[1] Nowadays common-quality steels are often subjected to heat treatment (to increase their strength). In that case, steels should be selected, i.e. only steel melts of a particular composition are used for the purpose (for instance, common-quality steel Grade Ст5 contains 0.28-0.37 per cent C, but only melts with 0.32-0.37 per cent C may be used for heat treatment).

[2] Recall the symbols of mechanical properties, since they will be often used in the subsequent discussion: σ_t = ultimate strength; σ_y or $\sigma_{0.2}$ = yield limit; a_n = impact toughness; δ = elongation; Ψ = reduction; HB = Brinell hardness number; and HRC = Rockwell hardness number (C scale); for more detail, see Chapter 3.

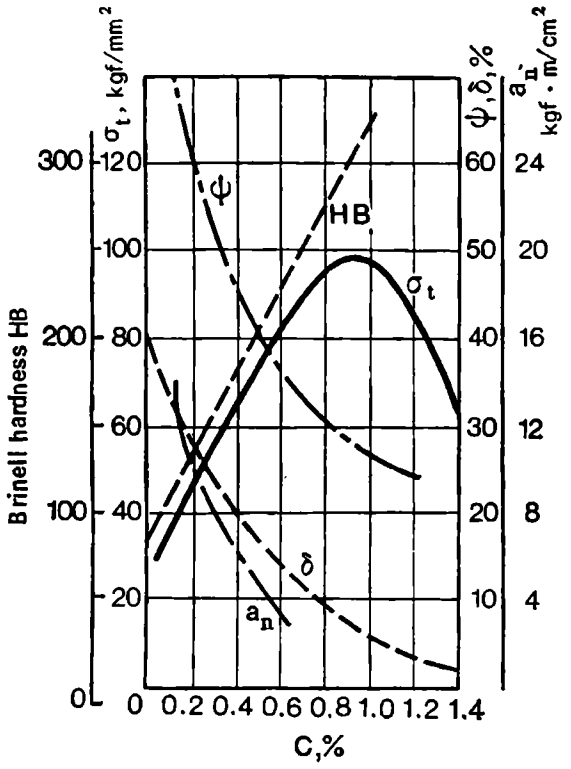

Fig. 7-1. Effect of carbon on mechanical properties of steel

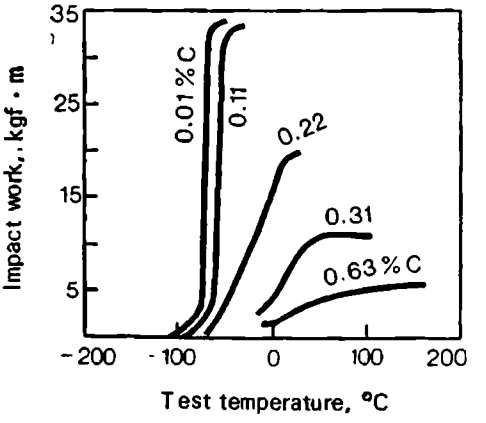

Fig. 7-2. Effect of carbon on cold brittleness of iron

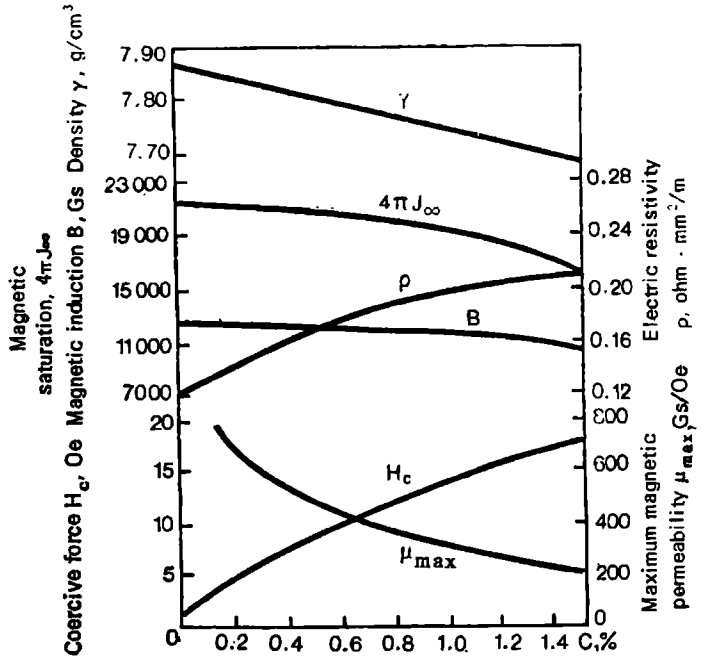

Fig. 7-3. Effect of carbon on physical properties of steel

7-2. EFFECT OF PERMANENT IMPURITIES ON STEEL PROPERTIES

Permanent impurities in steels are manganese, silicon, phosphorus, sulphur and gases (hydrogen, nitrogen and oxygen), since they are always present in all commercial steels.

The upper limits of the content of these elements are as follows: 0.8 per cent Mn, 0.5 per cent Si, 0.05 per cent P, and 0.05 per cent S. With greater contents of these elements, steels should be regarded as alloy grades where these elements are added specially (hence the name alloyed or special steels).

Let us consider the effects of these elements.

Manganese. Manganese is added to any grade of steel for deoxidation by the reaction

$$FeO + Mn \rightarrow MnO + Fe$$

i.e. for removal of harmful ferrous oxide. Manganese can also remove harmful iron sulphides (see later in this section). It is dissolved in ferrite and cementite.

Manganese can appreciably affect the properties of steel. For instance, it increases the strength of hot-rolled steel products. Since the content of manganese is approximately the same in all steels, its effect on various grades of steel is also roughly the same.

Silicon. The effect of silicon, if added at the beginning of heat, is similar to that of manganese. Silicon deoxidizes steel by the reaction

$$2FeO + Si \rightarrow 2Fe + SiO_2$$

Silicon cannot be detected in the steel structure, since it is fully soluble in ferrite (except for the portion of silicon that has not floated up into slag as silica and remained in the metal as silicate inclusions)[1].

Phosphorus. Iron ores, fuel and fluxes contain some phosphorus which remains in manufactured cast iron and then passes into steel.

With the Bessemer converter process, the final steel contains up to 0.07-0.12 per cent P, i.e. the same amount of phosphorus that has been present in the initial cast iron.

With the basic open-hearth process, most of phosphorus is removed from the metal. Steel made in basic open-hearth furnaces or electric furnaces contains little phosphorus (respectively, 0.02-0.04 per cent and less than 0.02 per cent). Further reduction in phosphorus content (down to 0.01 per cent or lower) is difficult to be achieved by metallurgical techniques (though it may be rational from the standpoint of raising the ductile-to-brittle transition point), and can be obtained only by using high-purity charge, for instance, direct-process iron.

[1] See the Fe-Mn and Fe-Si constitutional diagrams in Figs. 14-3 and 14-6.

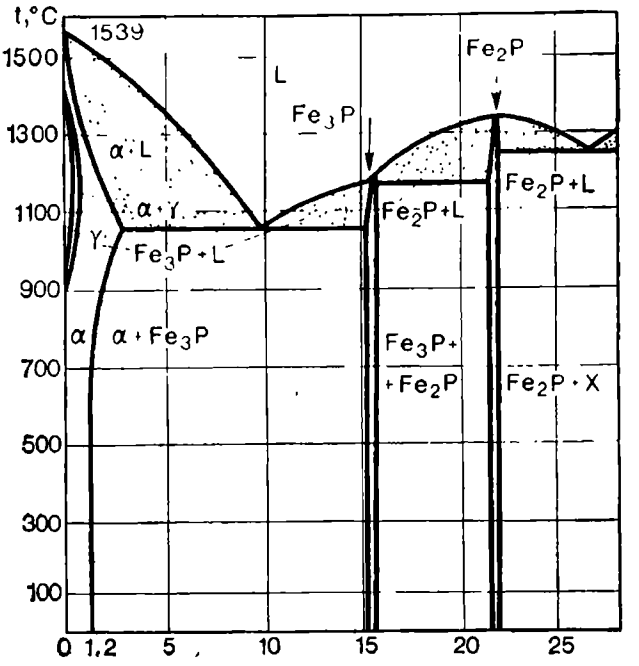

Fig. 7-4. Fe-P constitutional diagram

The iron-phosphorus constitutional diagram is shown in Fig. 7-4. The solubility of phosphorus in α-iron reaches 1.2 per cent. The presence of phosphorus in excess of this value (which diminishes with increasing carbon content) results in the formation of iron phosphide Fe_3P, the phase found in grey cast iron.

Upon dissolution in ferrite, phosphorus sharply raises the ductile-to-brittle transition point, i.e. causes *cold brittleness* of steel (Fig. 7-5).

It should be noted that in some cases phosphorus may be desirable in steel. For instance, it improves machinability of steels and, in the presence of copper, increases corrosion resistance.

Sulphur. Like phosphorus, sulphur can pass to metal from iron ores and from furnace gases as the product of fuel combustion (SO_2). The highest content of sulphur is found in Bessemer converter steels (up to 0.06 per cent). In the basic open-hearth and basic electric processes, sulphur is removed from the metal.

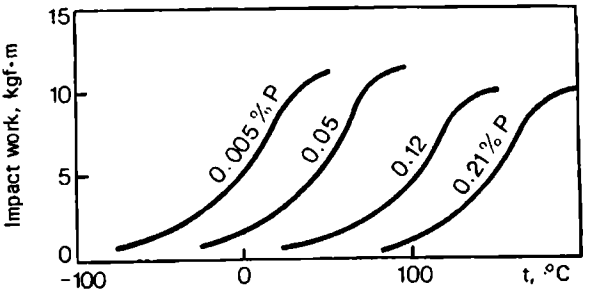

Fig. 7-5. Effect of phosphorus on cold brittleness of steel (0.2% C, 1% Mn)

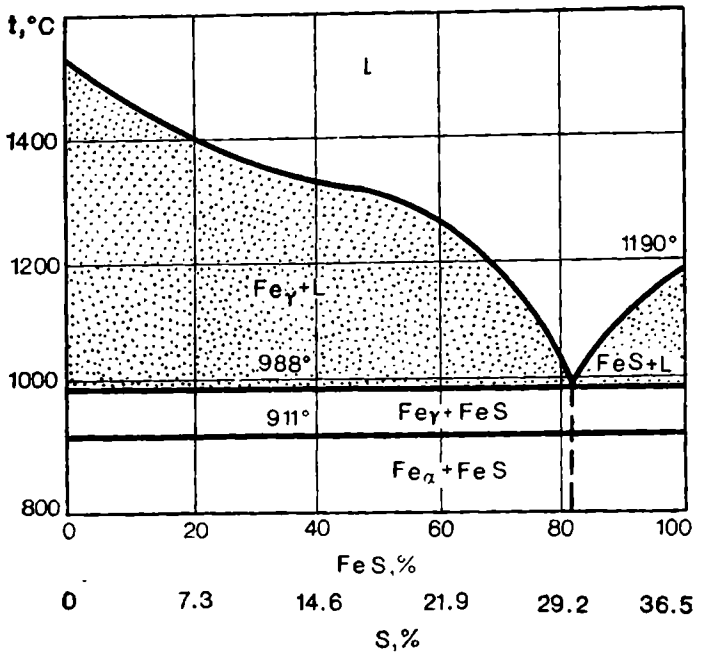

Fig. 7-6. Fe-S constitutional diagram

The content of sulphur in high-quality steels should not usually exceed 0.02-0.03 per cent. In common-quality steels, a higher content (0.03-0.04 per cent) is allowed. The sulphur content of steel can be lowered to 0.005 per cent by treatment with synthetic slags.

Sulphur is insoluble in iron[1] (see the iron-sulphur constitutional diagram in Fig. 7-6). Any amount of sulphur reacts with iron to form *iron sulphide* FeS which enters the composition of the eutectic that is formed at 988°C.

The presence of this fusible and brittle eutectic, which is usually located at grain boundaries, makes a steel brittle at temperatures from 800°C upwards, i.e. in the range of red heat. The phenomenon is called *red shortness*. Because of red shortness, a steel high in sulphur is not suitable for hot plastic working. From that standpoint, **sulphur is a harmful impurity in steel.**

The sulphurous Fe + FeS eutectic, if present in a low amount in steel, usually *coalesces*, i.e. its ferrite is combined with the ferrite of the main metal, so that the FeS compound envelops the metallic grains[2] (Fig. 7-7*a*).

This form of sulphur inclusions is especially detrimental since it is responsible for fractures and fissures in the metal subject to hot

[1] By some data, sulphur is soluble, though verylittle, in both α- and γ-iron.

[2] This phenomenon of coalescence of eutectic is common for all metallic systems in which the eutectic component is present in a small amount. It should also be noted that the term 'coalescence' is not always used in that sense. The coarsening of a second (excess) phase in solids is often called caolescence and the coarsening of a second phase in liquid media (emulsions) is called coagulation.

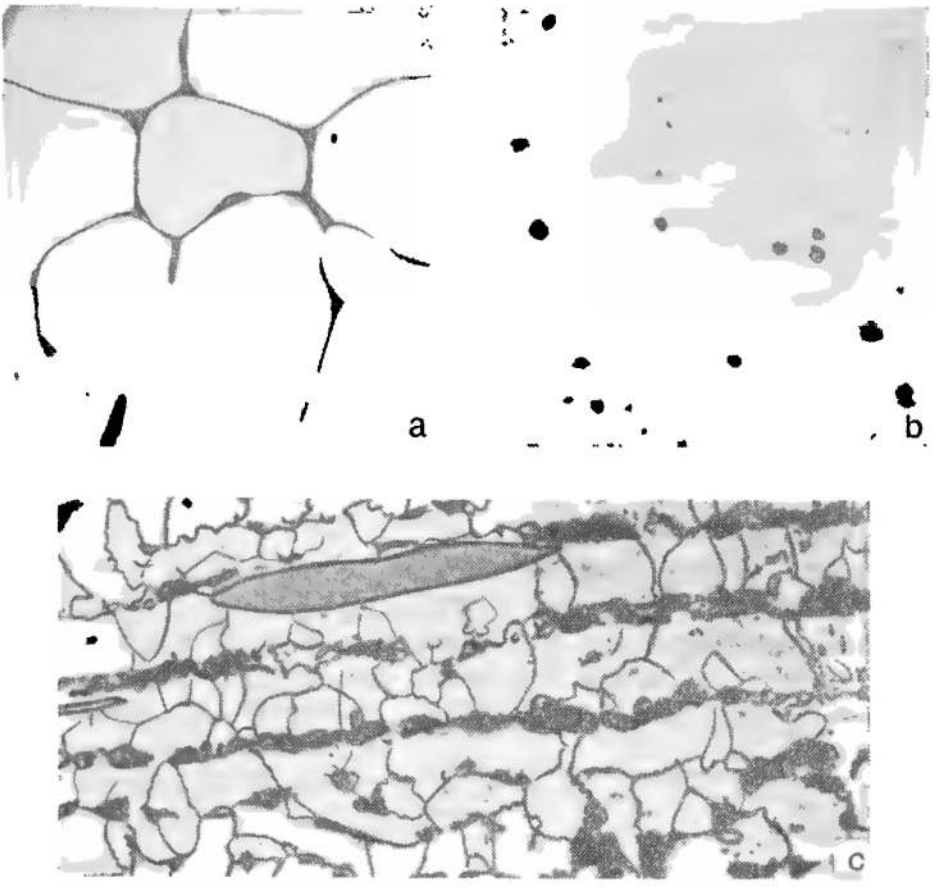

Fig. 7-7. Sulphide inclusions
(*a*) in the form of fringes at grain boundaries, ×100; (*b*) separate inclusions, ×100; (*c*) as manganese sulphide, ×500

plastic working. This is due to the fact that, as the steel is being heated, the metal around iron sulphide inclusions starts to melt down beginning with the temperature of 988°C (a melt is formed according to the diagram in Fig. 7-6). Isolated rounded-off iron sulphide inclusions are less harmful (Fig. 7-7*b*).

The harmful effect of sulphur can be diminished by adding manganese to steel; when added to molten steel, manganese reacts with iron sulphide to form manganous sulphide: $FeS + Mn \rightarrow MnS + Fe$.

Manganous sulphide melts at 1 620°C, i.e. at a temperature well above the common temperatures of hot plastic working. Manganous sulphide is soluble neither in solid nor molten steel, therefore, a fusible eutectic with manganous sulphide phase cannot be formed.

At temperatures of hot working (800-1 200°C), manganous sulphide is plastic and can be stretched into elongated lenses under the action of external forces (Fig. 7-7*c*).

Sulphides are plastic and can be deformed through hot working; in that respect they differ from oxides (FeO, SiO_2, Al_2O_3, etc.) which

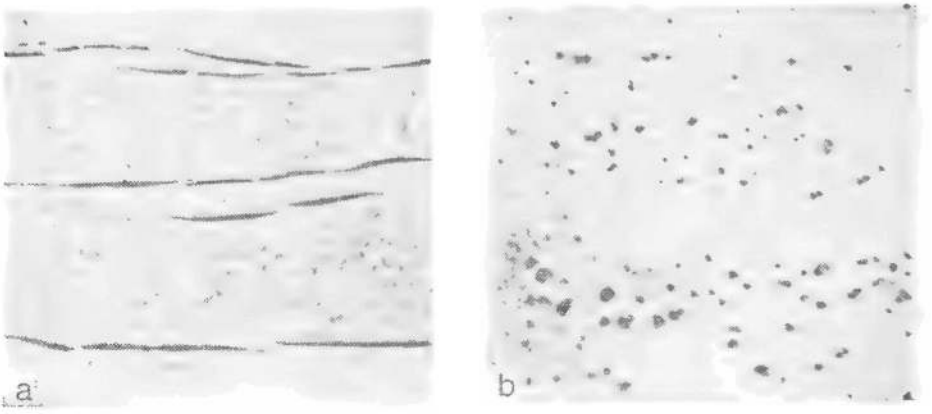

Fig. 7-8. Non-metallic inclusions
(*a*) sulphides (ductile); (*b*) oxides (brittle)

are brittle, easily crushed by mechanical forces, and are arranged in the metal in the form of chains (Fig. 7-8).

Such inclusions are intolerable in critical steel parts. Though they cannot influence the static strength of a steel part[1], these inclusions can lower the fatigue strength and dynamic strength since they act as stress concentrators. With variable loads, these inclusions often provoke fatigue cracks.

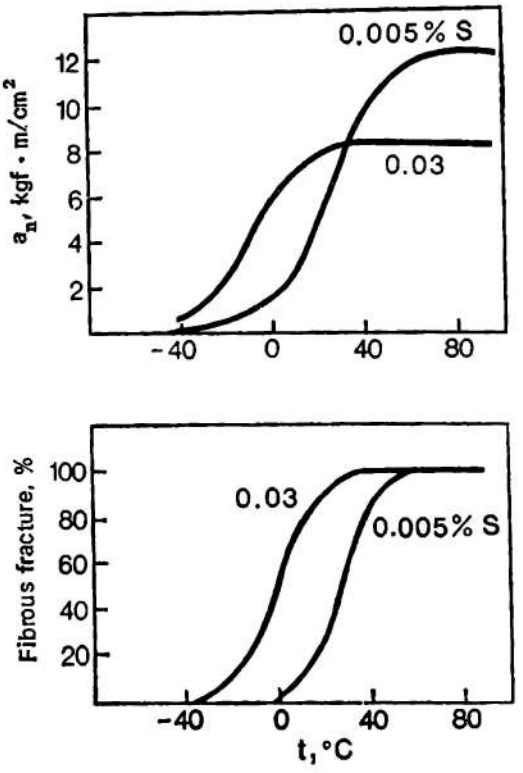

Fig. 7-9. Effect of sulphur on plastic properties of steel

A method of making steel with the slag being prepared in a separate furnace (*synthetic slag*) is finding ever increasing application. The treatment of steel with this slag results in a better removal of sulphur and improved properties of the metal, especially in directions across fibres.

Since sulphur is present in most steel grades as manganous sulphide (see Fig. 7-7), it has a remarkable effect on ductile properties of steel, which is called *sulphide effect*. Unlike other 'harmful' elements, which raise the ductile-to-brittle transition point, sulphur lowers this point, but increases the impact toughness in ductile fracture (Fig. 7-9). In other words, sulphur increases the resistance to ductile fracture and lowers that to brittle fracture.

[1] In tests along fibres, i.e. with sulphide inclusions oriented parallel to the acting forces; in tests across fibres, non-metallic inclusions lower the static characteristics as well.

In the general case, sulphur should be regarded as a harmful impurity in steel.

Like phosphorus, sulphur (see Sec. 7-6 below) improves machinability of steel. In view of this, the content of sulphur in steels for machining should not be excessively low (steels treated with synthetic slags are little suitable for the purpose).

Gases. Hydrogen, nitrogen and oxygen are present in steels in small quantities, depending on the method of steelmaking.

The content of these gases in steels is determined by melting a sample of metal in vacuum and measuring the quantity of gases evolved from the molten metal (Table 7-1).

Table 7-1. Approximate Content of Gases in Steel

Gas	Content of gases, %, in steel produced by			
	electric steelmaking process	basic open-hearth process	oxygen converter process	Bessemer converter process
Hydrogen	0.0004-0.0006 (250)	0.0003-0.0007 (200)	0.0001-0.0003 (150)	0.0004-0.0007 (250)
Nitrogen	0.007-0.010 (300)	0.004-0.006 (200)	0.002-0.005 (100)	0.010-0.015 (500)
Oxygen	0.002-0.004 (150)	0.005-0.008 (350)	0.005-0.008 (350)	0.01-0.03 (1 000)
Total	(700)	(750)	(600)	(1 750)

Note: Numbers in brackets are average values in at. ppm, i.e. the number of atoms of hydrogen, nitrogen or oxygen per 10^6 atoms of iron.

These gases can be present in steel in various forms; they can be present (in gaseous state) in various discontinuities, in α-solid solution or can form various compounds (nitrides, oxides) which are generally called *non-metallic inclusions.*

With much hydrogen present in steel, extremely dangerous internal fractures (flakes, see Sec. 16-11) are very likely to form in the metal.

Brittle non-metallic inclusions formed by nitrogen and oxygen impair the properties of steel.

The solubility of hydrogen, nitrogen, oxygen and carbon in α-iron is not high. Since it diminishes still more with decreasing temperature (Fig. 7-10), under conditions of common (non-equilibrium) cooling of the steel upon rolling or forging there forms a supersaturated solid solution of these elements in α-iron. It is theoretically

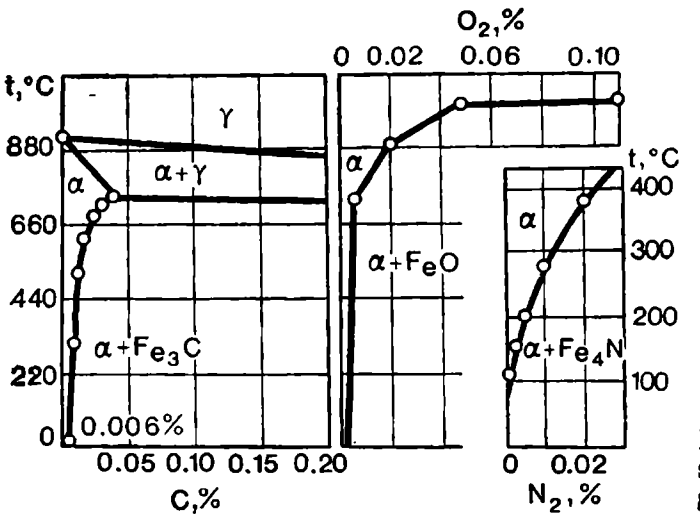

Fig. 7-10. Variations of solubility of carbon, oxygen and nitrogen in iron

more appropriate to call these elements (and carbon) *interstitial impurities*, the more so as their effects on steel properties are specific and alike.

Plastic deformation and subsequent low heating of this supersaturated solution result in a strong embrittlement of the metal owing to ageing processes, the effect being called *strain ageing*. It manifests itself firstly in reduced ductility and a higher ductile-to-brittle transition point. Since the content of these impurities is not high (see Table 7-1), their effect on many other properties of the steel is unnoticeable. Interstitial impurities can. however, strongly affect the ductile properties by diminishing the impact toughness and sharply increasing the ductile-to-brittle transition point (Fig. 7-11*a*, *b*).

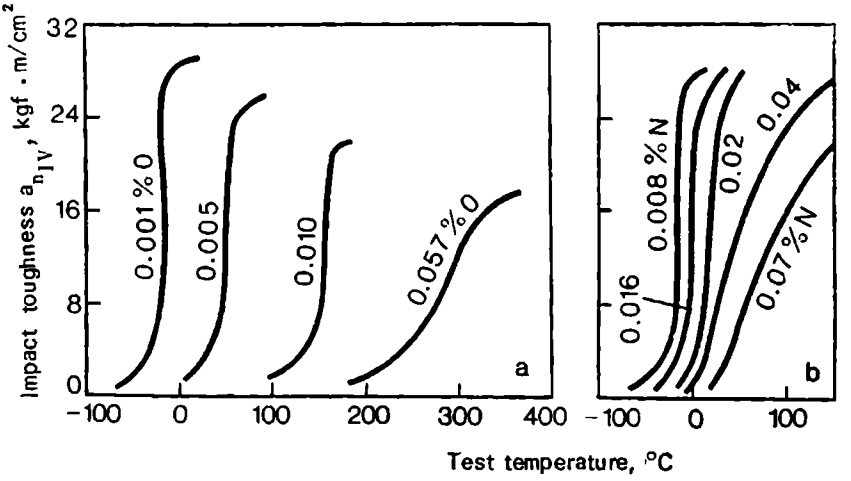

Fig. 7-11. Effect of interstitial impurities of oxygen (*a*) and nitrogen (*b*) on plastic properties of iron

Hydrogen forms no compounds (hybrids) with iron, therefore it can easily evolve from metal. A steel just upon teeming contains a certain amount of hydrogen which afterwards gradually diminishes. The process of evolution of hydrogen from solidified steel can take from a few days to several months, depending on the thickness of steel part. The process also results in gradual improvement of mechanical properties (ductility) of the metal. From this it follows that the presence of hydrogen, nitrogen and oxygen in metal impairs its properties.

Effective methods for diminishing the content of these elements and non-metallic inclusions in steel are vacuum melting and vacuum casting. Vacuumized metal possesses better properties, since it is highly pure from non-metallic inclusions and contains practically no dissolved atoms of hydrogen, nitrogen or oxygen.

In plastically deformed metal, non-metallic inclusions can locate as broken lines (oxides) or elongated lenses (sulphides), see Fig. 7-8, oriented in the direction of rolling. These inclusions serve as nuclei for crystallization of ferrite thus forming a laminated ferrite-pearlitic structure (see Fig. 7-7*c*).

This laminated structure is responsible for an appreciable *anisotropy* of metal properties, i.e. the difference in the properties of specimens cut along and across the rolling direction. This anisotropy is most marked in the characteristics associated with the final stage of deformation (impact toughness, relative reduction), whereas other mechanical properties are less sensitive to laminated structure. The anisotropy of steel properties is characterized by the ratio X_{tr}/X_{long}, where X is a property of metal and subscripts 'tr' and 'long' relate to transverse and longitudinal direction. The impact toughness in transverse direction is usually one half of that in the longitudinal direction (respectively, the coefficient of anisotropy is 0.5). The coefficient of anisotropy of impact toughness can be increased up to 0.7-0.8 by producing metal more pure from sulphur and oxygen, using improved methods of melting, or by diminishing the lineage structure by employing more advanced rolling processes.

These circumstances are taken into consideration in technical specifications and standards for metal products, where the directions of cutting the specimens are specified.

7-3. STEELS PRODUCED BY VARIOUS PROCESSES. CLEAN STEEL

Steels are produced industrially by various processes; accordingly their properties are different. It would be erroneous to think that a particular steelmaking process directly determines this difference. Actually, differences in their properties are due to different contents of permanent impurities (whose effects have been considered earlier), depending on the particular steelmaking

process. Therefore, if we manage to produce a metal of perfectly identical composition by different processes, its properties will also be identical.

As is known, steels are made (melted) in various types of furnace. In that connection, they are classified as Bessemer, open-hearth, oxygen-converter and electric steels.

In the Bessemer converter, molten iron is blown with air and the oxygen of air combines with the impurities present in the iron, including carbon, and thus cast iron is converted to steel. This process is very productive, but cannot remove sulphur and phosphorus as fully as needed (Table 7-2); besides, the metal is saturated with gases, especially with nitrogen.

Table 7-2. Comparison of Steels Produced by Various Processes

Steelmaking process	Content of S and P, % (maximum)		Removed in the process		Order	
	S	P	S	P	of quality	of cost
Basic open-hearth	0.05	0.04	Removed partially	Removed	4	3
Basic oxygen-converter	0.05	0.04	Ditto	Ditto	3	2
Bessemer converter	0.07	0.09	Not removed	Not removed	5	1
Acid open-hearth	0.05	0.05	Ditto	Ditto	2	4
Electric steelmaking	0.03	0.03	Removed	Removed	1	5

As compared with open-hearth steel, Bessemer steel due to higher content of gases, especially of nitrogen, has a higher strength, but a lower ductility, is more liable to ageing, and more contaminated with non-metallic inclusions. Because of the low quality of Bessemer steel, the process is being abandoned in favour of oxygen-converter process in which commercially pure oxygen is used for metal blowing, instead of atmospheric air, and the metal produced is very low in nitrogen (oxygen converters are usually blown from the top with the oxygen jet directed at an angle to the metal surface). Oxygen-converter steel is practically not inferior to open-hearth steel in its properties.

Mainly the common-quality steels are still produced in open-hearth furnaces, though it is economically more favourable to produce them in oxygen converters. It may be expected that the oxygen-converter process will gradually supplant the older open-hearth process. Actually, oxygen-converter plants, rather than open-hearth plants are built at new steelmaking works.

Both with the open-hearth and oxygen-converter process, it is possible to remove an appreciable part of sulphur and part of phosphorus by properly selecting the composition of slags and the conditions of melting. The slags by means of which molten metal is refined from impurities are composed of basic (CaO and MgO) and acid (SiO_2) oxides. Accordingly, the lining of a furnace must be either basic (laid of magnesite or chrome-magnesite) or acid (silica brick), so as to prevent reactions between the lining and slag. If the slag is basic, that is, with an excess of basic oxides MgO and CaO, it can remove most of phosphorus and part of sulphur from the metal. Therefore, even with the starting charge being not quite clean, the metal made in the open-hearth furnace will

be quite free from sulphur and phosphorus, though more saturated with oxygen. With the acid process, the slag has a surplus of silica (SiO_2) in whose presence sulphur and phosphorus cannot be removed from the metal, but the latter is less saturated with oxygen. For that reason the acid process requires that the charge be free from sulphur and phosphorus (i.e. the charge materials are more expensive), but produces metal of a better quality owing to a lower saturation with oxygen.

Open-hearth steels are mostly produced by the basic process, and the acid process is used only for making more expensive grades in which high purity from non-metallic inclusions (oxides) and a low saturation with oxygen are essential.

Sulphur, phosphorus and oxygen are best removed in electric furnaces of arc or induction type. Electric steel is more expensive but has a higher quality. For that reason, electric steelmaking process is predominantly used for making alloyed and high-alloyed steels, heat-resisting alloys, tool steels and the like.

The process of vacuum induction melting is employed for making steels and alloys for most critical applications, since the metal produced by this process is practically free from gases and has the best properties.

Vacuum-melting plants are quite complicated. The same results, as regards the content of gases and non-metallic inclusions, are obtained by melting steel under common conditions and then by placing the ladle with tapped steel into vacuum. This process (steel vacuumizing in the ladle) is less expensive than vacuum melting.

Depending on the method of deoxidation, steel may be either *killed* (deoxidized with manganese, silicon and aluminium) or *rimming* (deoxidized with manganese only). Therefore, rimming steel should differ from killed type in composition: the former is almost free from silicon (Si <0.05 per cent) and the latter can contain 0.12-0.3 per cent Si. Since rimming steel is less thoroughly deoxidized and contains more oxygen, it is inferior to killed steel in its quality.

An intermediate type is what is called *semikilled* steel, which is deoxidized with manganese and aluminium and finds ever increasing use in place of rimming and killed steel (see Table 7-3).

Table 7-3. Comparison of Steels Deoxidized by Various Processes

Steel	Deoxidants	Yield of sound metal, %	Common content of silicon, %	Order of	
				quality	cost
Killed	Mn+Si+Al	85-90	0.15-0.30	3	3
Semikilled	Mn+Al	90-95	0.05-0.10	2	2
Rimming	Mn	95-100	<0.05	1	1

Finally, it should be noted that the composition of metal in an ingot is not uniform. The top and middle portions of the ingot contain more impurities—sulphur, phosphorus, carbon (the phenomenon is called *zonal segregation*). For that reason the metal from the top portion of ingot will differ from that from the bottom portion and both will differ from the average composition. In some cases these deviations may be quite appreciable. The effect of zonal segregation is more pronounced in rimming steel than in killed steel, and also, in large ingots.

Apart from permanent impurities, steels may contain various occasional impurities. For instance, the scrap used in the charge may contain lumps of

chrome-nickel alloy steels. For that reason the steel made by the scrap-and-ore process usually contains certain amounts of the elements with which steels are usually alloyed (chromium, nickel, etc.). Some iron ores contain hardly removable impurities.

Thus, steels of the same grade may differ in the content of impurities (either specified or not specified by State standards and technical specifications) and this can appreciably affect their properties. The strongest effect is produced by interstitial impurities (hydrogen, nitrogen, oxygen and carbon) and by the typical contaminating impurities—sulphur and phosphorus. Many non-ferrous impurities are, without doubt, harmful for the metal.

Various methods of steel melting and processing of molten steel (which have been discussed above) are employed to make sound, and hence, reliable (ductile) steel. Summing up what has been said above, we can draw the following conclusions.

Vacuum processes (in the furnace, ladle, etc.) are mainly aimed at removal of oxygen and employed to help the conventional deoxidation techniques. Slag processes (electroslag remelting, treatment with synthetic slags) produce steel very pure from sulphur.

Phosphorus and some non-ferrous metal impurities can only partially be removed from steel by metallurgical techniques and the degree of purification of the metal from these impurities is not high. Steels very pure from these elements can only be made by using high-purity charge materials, for instance, direct-process iron).

In the future, the conventional process of steel conversion: iron ore → cast iron (from blast furnace) → steel (from open-hearth furnace) will be probably changed for the following: iron ore → metallized pellets (direct-process iron) → → steel (electric furnace) → clean steel (refined by remelting or ladle degassing).

The content of contaminating impurities, when expressed as percentage by mass, is not high and cannot be indicative of impairment of steel quality. Besides, of real value is the content of an element expressed in atomic parts, rather than as percentage by mass (which is determined by the number of neutrons and protons in the nucleus). Many impurity elements have a small atomic weight.

It is, therefore, more appropriate to measure the content of impurities in what is called atomic parts per million (at. ppm), i.e. the number of impurity atoms per million iron atoms.

Table 7-4 gives the typical values of the content of impurities in at. ppm in steels produced by conventional processes, and Table 7-5, in steels refined by modern methods.

Table 7-4. Typical Contents of Impurities, at. ppm, in Steels Produced by Various Processes

Process	Sulphur	Phosphorus	Oxygen	Nitrogen	Hydrogen	Total of all impurities [1]
Bessemer converter	900	1 400	1 000	500	250	6 000
Oxygen converter	500	500	350	100	150	2 000
Open-hearth	500	500	350	200	200	2 100
Electric steelmaking	250	300	150	300	250	1 500

[1] Including non-ferrous metals and other impurities not mentioned in the table.

Table 7-5. Typical Contents of Impurities in Refined Steel, at. ppm

Steelmaking process	Sulphur	Phosphorus	Oxygen	Nitrogen	Hydrogen	Total of all impurities [1]
Open-arc electric	250	300	150	300	250	1 500
Electroslag remelting	100	300	120	250	150	1 000
Vacuum-arc remelting	250	300	90	200	100	1 000
Electron-beam remelting	200	300	50	200	100	1 000
Vacuum-induction remelting	250	300	50	200	100	1 000

[1] Including non-ferrous metals and other impurities not mentioned in the table.

Expressing the composition of steel in at. ppm, makes it possible to sum up the contents of impurities to determine the total contamination of a steel, i.e. the number of atoms of all the impurities per million atoms of the base metal (iron).

Having summed up the contents of all impurities, it may be seen that Bessemer converter steel is the least clean (contains up to 6 000 at. ppm of impurities), whereas open-hearth and oxygen converter steels (roughly 2 000 at. ppm) and especially electric steel (up to 1 500 at. ppm) are appreciably cleaner. Remelting processes can refine steel even more (up to 1 000 at. ppm) and the cleanest steel (up to 500 at. ppm) can be produced by using high-purity charge.

Thus, the properties of steel depend on the steelmaking process, since the latter determines the content of various impurities and their distribution in the metal. In some cases this circumstance is of great importance and should be properly considered.

7-4. PLAIN CARBON STEELS

Hot-rolled steel delivered by steelmaking works as rolled sections (bars, beams, sheets, tubes, etc.) is the most widely used material for manufacture of various machines, machine tools, building structures, consumer goods, etc. Delivered steel should have the properties as specified by State Standards.

In the USSR, plain carbon steels are classified into three groups: A, B and C, depending on their application.

A. If a steel is to be used for making products without hot working (welding, forging, etc.), its structure and properties in the final product will be the same as delivered from the rolling mill. In that case the user requests for a steel of warranted mechanical properties, while the chemical composition is not guaranteed.

B. If a steel is to be subjected to hot working (forging, stamping, etc.), its initial structure and mechanical properties will be changed. In that case the composition of the steel will be of prime importance for the user, since it determines the conditions of hot working and the final mechanical properties of steel products. Now a steel of warranted composition is delivered to the user.

C. If a steel is to be welded, the user wants to know the composition of the steel, since it determines the properties of the metal in the zone subjected to thermal effect of weld. The user is also interested in the initial mechanical properties of the metal, since these properties will remain the same in portions not subjected to welding. In that case the metal is delivered with warranted composition and mechanical properties.

General-purpose plain steels are not alloyed. Some alloying elements may sometimes be present in them occasionally and their content is limited.

The presence of silicon and manganese may be due to the steel-making process (the necessity of deoxidation). Sulphur and phosphorus are harmful impurities in steel (see earlier) and their content should be minimized as it may affect the quality of steel.

Table 7-6. Mechanical Properties of Plain Carbon Steel Group A (GOST 380-71)

Steel grade	σ_t, kgf/mm²	σ_y, kgf/mm² (minimun)	δ, % (minimum)
Ст0	at least 31	—	23
Ст1кп	31-40	—	35
Ст1пс	32-42	—	34
Ст1сп	32-42	—	34
Ст2кп	33-42	22	33
Ст2пс	34-44	23	32
Ст2сп	34-44	23	32
Ст3кп	37-47	24	27
Ст3пс	38-49	25	26
Ст3сп	38-49	25	26
Ст3гпс	38-50	25	26
Ст4кп	41-52	26	25
Ст4пс	42-54	27	24
Ст4сп	42-54	27	24
Ст5пс	50-64	29	20
Ст5сп	50-64	29	20
Ст5гпс	46-60	29	20
Ст6пс	at least 60	32	15
Ст6сп	same	32	15

Notes: 1. A dash implies that the property is not guaranteed.
2. The properties are given for specimens not more than 20 mm thick; in larger pieces, the ultimate strength can be lower by 1-3 kgf/mm² and the elongation, by 1-3 per cent.
3. The angle of bending to cracking on a mandrel of a definite diameter is also specified.

Plain carbon steels are manufactured by open-hearth or converter process (in side-blown converters) and practically are not produced in bottom-blown Bessemer converters.

The principal elements whose content is responsible for the properties (in the first place mechanical) of steels is carbon.

Depending on the method of deoxidation, steels are divided into killed, semi-killed and rimming grades designated respectively by the Russian letters сп, пс, and кп). More deeply deoxidized steels are better in their quality (see earlier).

The mechanical properties (guaranteed) of plain carbon steels of group A are given in Table 7-6.

Steel 0 is only suitable for the least critical applications and the other grades can be employed in various cases, depending on the required strength, cold brittleness, weldability, etc.

Steels of group B are designated with this letter and a digit (1, 2, 3, etc.) determines the carbon content (in contrast to group A where the digit determines the ultimate strength).

The compositions of plain carbon steels of group B are given in Table 7-7.

Steels of group C, as has been indicated earlier, should have the specified values of strength and the specified composition; some other of their properties are also guaranteed.

Actually, steel Grade Ст1 has the same mechanical properties as steel Grade A Ст1 (Table 7-6) and the composition as Grade B Ст1 (Table 7-7); the same relates to steel grades C Ст2, C Ст3, etc.

More detailed data can be found in the USSR State Standard GOST 380-71 and in other standards for particular metallurgical products.

Table 7-7. Composition of Plain Carbon Steels of Group B (GOST 380-71)

Steel grade	C, %	Steel grade	C, %
ВСт0	up to 0.23	ВСт4кп, пс, сп	0.18-0.27
ВСт1кп, пс, сп	0.06-0.12	ВСт5кп, пс, сп	0.28-0.37
ВСт2кп, пс, сп	0.09-0.15	ВСт6кп, пс, сп	0.38-0.49
ВСт3кп, пс, сп	0.14-0.22		

Notes: 1. The content of manganese is 0.25-0.50 per cent in the low-carbon grades (Ст1, Ст2) and increases with the carbon content up to 0.5-0.8 per cent.
2. The content of silicon is up to 0.05 per cent in rimming grades, 0.05-0.17 per cent in semi-killed grades, and 0.12-0.30 per cent in killed grades.
3. The content of phosphorus is not more than 0.04 per cent and that of sulphur, not more than 0.05 per cent (except for Grade Ст0 which can contain up to 0.07 per cent P and 0.06 per cent S).
4. The content of nitrogen is not more than 0.008 per cent.
5. The content of chromium and copper should be not more than 0.3 per cent each and that of arsenic, not more than 0.08 per cent.

At present, extensive construction work is undertaken in the northern regions of the USSR, where the temperature in winter often drops below —40°C. Under such conditions, the cold brittleness of the metal, i.e. its behaviour at low temperatures, becomes very important. Table 7-8 gives ductile-to-brittle transition temperatures for steel Grade Ст3 which is most widely used in building constructions, such as building and bridge frameworks, and in construction machines (excavators, dredges, etc.).

At temperatures above the point of the beginning of transition to brittle state, steel has a high ductility and is quite reliable under any operating conditions. At temperatures below the point of the end of transition, i.e. when the steel has a fully brittle fracture, it should be used under no circumstances.

The data given in Table 7-8 are only approximate, since the point of transition to brittle state depends on many factors (purity of

Table 7-8. Temperatures of Ductile-to-Brittle Transition for Steel Grade Ст3

Steel	Temperature of transition, °C		
	beginning	end	T^*_{50}
Rimming:			
hot-rolled	+100	0	+50
normalized	+40	—20	+10
heat-refined	+20	—40	—10
Killed:			
hot-rolled	+20	—40	—10
normalized	0	—60	—30
heat-refined	—20	—80	—50

Note: The fracture of steel is fully tough at temperatures above the temperature of the beginning of transition and fully brittle at temperatures below that of the end of transition.

* The temperature at which the fracture contains 50 per cent of ductile fibres.

steel, grain size, etc.). It is, however, clear from the table that killed steel is much better in that respect than rimming steel and that the ductile-to-brittle transition point can be lowered appreciably by heat treatment[1].

Usually, T_{50} is the lowest temperature at which a steel can operate. For operation under extremely severe northern conditions (at air

[1] The operation being called thermal refining, see Sec. 10-7.

temperatures below —40°C), it is recommended to employ killed thermally refined steel[2]. Rimming steel should not be used in critical structures if temperature drops below 0°C are probable.

7-5. WORK-HARDENED STEEL

Steel products of thin cross-section, such as wire, thin sheets, strips, seamless tubes, etc. find wide application. These products are made at steelmaking works by rolling, pressing or cold drawing, resulting in work hardening of the metal. The work-hardening effect can be removed by recrystallization annealing. Products of this type may be delivered by steelmaking works in either annealed or work-hardened state.

The mechanical properties of a steel as-annealed are mainly determined by its composition, in the first place by carbon content.

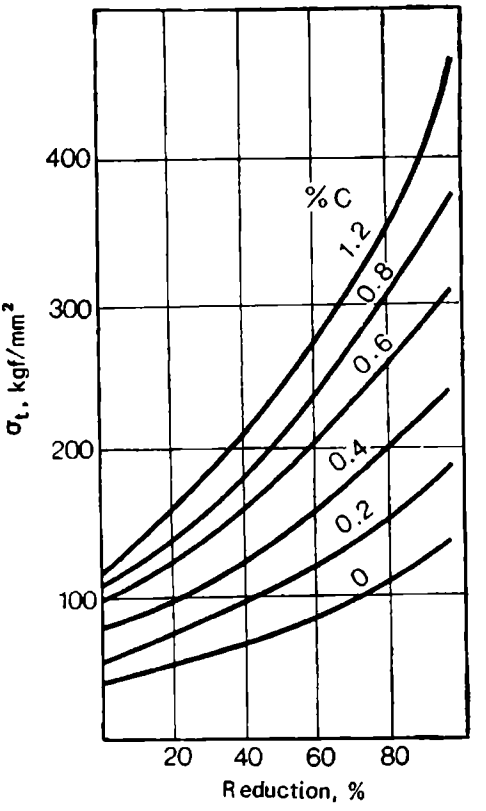

Fig. 7-12. Effect of reduction on the ultimate strength of steel wire with different carbon content

In work-hardened state, the properties of steel depend appreciably on the degree of work hardening (reduction), as can be seen in Fig. 7-12. At the maximum degree of work hardening (reduction of 96-97 per cent), the strength of high-carbon steel (1.2 per cent C) can exceed 400 kgf/mm². Such a high reduction produces a very thin wire. Indeed, the highest values of steel strength (σ_t = 480-500 kgf/mm²) were obtained only for high-carbon steel wire 0.1 mm in diameter produced by a very high reduction (98 per cent).

Work-hardened thin wire produced by great reductions is used for manufacture of ropes and cables. Steels with 0.6-0.8 per cent C are usually employed for the purpose; their strength upon 80- or 90-per cent reduction is 180-300 kgf/mm².

Such high reductions are only possible if the wire material is readily deformable. It has been established that this is possible only if the initial steel structure is fine-lamellar pearlite which can be produced by special treatment in molten-lead or molten-salt baths. The process is called *patenting* and is a variety of isothermal hardening (see later in the book).

[1] In some cases thermal refining can be replaced by a simpler operation of normalizing, but normalized steel cannot be used at temperatures below —40°C.

The composition, properties, size allowances, surface state and other characteristics of wire, sheets, tubes and other products manufactured by cold plastic working are specified in respective technical specifications and standards.

7-6. STEEL SHEETS FOR COLD FORMING

Some steel products, for instance, binding wire or thin sheets for subsequent deep drawing or stamping, must be made of soft low-carbon steel. Of special interest are steel sheets for making car body parts. Steel for deep drawing should have a high ductility, therefore, its carbon content must be as low as possible. The content of carbon in steels for especially complex press forming is limited to 0.08 per cent. Steels with 0.2-0.3 per cent C can be subjected only to bending and slight drawing and those with 0.3-0.4 per cent C, only to bending with small curvature radii. The content of other permanent impurities (manganese, silicon, sulphur, phosphorus) is also limited to low values, since all of them adversely affect ductility. This limitation should not, however, impair the quality of the steel as regards its other characteristics.

The commonest material for deep drawing is low-carbon (low-silicon) rimming steel Grade 08 кп which contains $\leqslant 0.08$ per cent C, 0.25-0.50 per cent Mn, <0.03 per cent Si, <0.03 per cent S, and <0.02 per cent P.

A steel suitable for press forming should have not only a definite composition, but also an appropriate microstructure—fine-granular ferrite with pearlite inclusions at junctions of ferrite grains. Coalescence of pearlite (see Sec. 7-2 on coalescence of sulphide eutectic) results in the appearance of structurally free cementite at grain boundaries; this is extremely harmful for steel formability.

It should be noted that the structure of sheets made of low-carbon rimming steels (including Grade 08 кп) is sometimes non-uniform and has laminations (rolled-off blisters, see Sec. 2-5). They are also liable to ageing at room temperature, owing to their elevated content in oxygen. These drawbacks are not found in respective grades of low-carbon killed and semi-killed steel (deoxidized with aluminium, Grade 08 Ю), which are also used for the purpose, notwithstanding their higher hardness.

7-7. MACHINABILITY OF STEELS. AUTOMATIC STEELS

In most cases steel parts are manufactured by machining, i.e. by cutting steel blanks in machine tools. Naturally, the problem of improving the machinability of steel is of great practical importance.

The problem of how the machinability of steel is associated with the structure and composition has still not been fully studied. The complexity of the problem of machinability by cutting tools lies mainly in the fact that the concept of machinability is indeterminate. Machinability may be estimated in terms of the allowable cutting speed (a factor of extreme importance, which determines the productivity of machine tools), the cutting force or the surface finish of machined elements. Besides, the machinability of a material may

be different in various cutting operations—turning, milling, drilling, grinding, etc.—or in coarse and finish machining.

No satisfactory correlation between mechanical properties and machinability of steel has yet been found, but it can be taken roughly that the machinability (determined in terms of cutting speed) becomes worse with increasing hardness or increasing strength and, in the first approximation, depends only insignificantly on steel composition (Fig. 7-13).

For the same hardness, however, the machinability may appreciably differ in steels having different structure and composition.

Of great importance is the heat conductivity of steels. Steels of austenitic structure possess a low conductivity. The heat evolved during machining is only slightly absorbed by the metal and is mainly concentrated at the point of cutting and heats up the cutting edge of the tool, i.e. lowers the tool durability. This is why austenitic steels are poorly machinable notwithstanding their relatively low hardness.

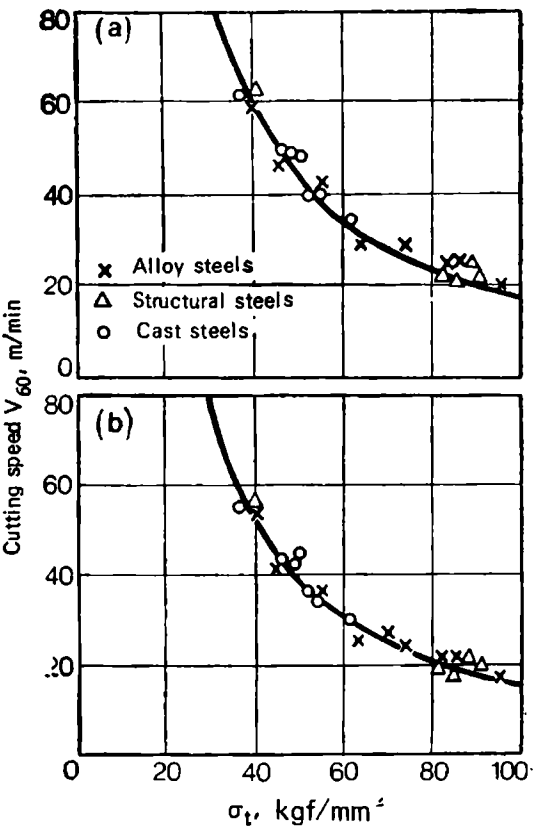

Fig. 7-13. Effect of ultimate strength on machinability (maximum cutting speed at a feed $s = 1$ mm). Cutting depth, mm: (*a*) 2; (*b*) 4

The grain size of steel has no noticeable effect on hardness, but appreciably affects the machinability. Coarse-grained steels have a reduced toughness (see Sec. 3-1 on this subject) and are readily machinable. Because of the reduced toughness, the steel possesses what is called 'machining brittleness', i.e. forms short discontinuous chip in cutting.

The structure of pearlite also has an effect on machinability. Hypoeutectoid steels have a better machinability when their structure is ferrite + lamellar pearlite. Eutectoid and hypereutectoid steels are more easily machinable when their structure consists of granular pearlite. The conditions for forming these structures will be discussed in Secs. 10-3 and 11-10.

As regards the effect of steel composition, it should be noted that, in the general, the machinability becomes worse with an increasing content of carbon which produces a strengthening effect. Steels of

a very low carbon content and commercial iron have, however, a poor machinability, mainly because of their high toughness and plasticity, and they give poorly removable continuous chip in cutting.

Special attention should be given to the effect of phosphorus and sulphur on machinability. These elements increase the durability of cutting tools and help obtain a better finish. For that reason, *automatic steels*, i.e. low-carbon steels with elevated contents of sulphur and phosphorus, have found a wide application for making less critical parts. Among the drawbacks inherent in high-sulphur high-phosphorus steels are lower values of plasticity and toughness and poor corrosion resistance. This fact should be considered when selecting automatic steels for making parts to operate under appreciable mechanical loads, at elevated humidity, etc.

There are some other elements, apart from sulphur, which can improve machinability. These include the analogues of sulphur: selenium and tellurium. These elements are now used to improve the machinability of certain high-alloyed (stainless) steels. The machinability of steel can also be improved by a small (0.1-0.2 per cent) addition of lead which is soluble neither in molten nor in solid steel. In solid steel, lead is present as fine isolated inclusions which make the chip more brittle and produce lubricating effect during cutting. Lead additions have only an insignificant effect on mechanical characteristics of steel. The method of lead alloying has, however, only a limited application, because of the difficulties associated with the introduction of lead into steel and especially with remelting of lead-alloyed steel.

The composition of selected automatic steels is given in Table 7-9. Among them, the sulphur-phosphorous steel Grade A12 has the best machinability. It is used for making less critical parts by machining in mass production.

The other steel grades indicated in Table 7-9 are used for making more critical parts which are then subjected to heat treatment.

Table 7-9. Composition of Free-cutting (Automatic) Steels, %
(GOST 1414-75)

Steel grade	C	Mn	Si	S	P
A12	0.08-0.16	0.7-1.0	0.15-0.35	0.08-0.20	0.08-0.15
A20	0.17-0.24	0.7-1.0	0.15-0.35	0.08-0..5	<0.06
A30	0.27-0.35	0.7-1.0	0.15 0.35	0.08-0.15	<0.06
A40Г	0.37-0.45	1.20-1.55	0.15-0.35	0.18-0.30	<0.50

LITERATURE

Machine-building Materials. A Reference Book. Volume 1. Moscow, "Mashgiz", 1959 (in Russian).

Bolkhovitinov N.F., *Physical Metallurgy and Heat Treatment of Metals.* Moscow, "Mashinostroenie", 1965 (in Russian).

Machine-building Materials. A Reference Book. Volume 2. Moscow, "Mashinostroenie", 1967 (in Russian).

Gulyaev A.P., *Clean Steel.* Moscow, "Metallurgiya", 1975 (in Russian).

Chapter 8

CAST IRON

Cast iron is distinguished from steel by a higher carbon content, better castability, and lower ability to plastic deformation (it is not malleable under common conditions); further, it is cheaper than steel.

The following types of cast iron are distinguished, depending on the state of carbon in the structure:

white cast iron in which all the carbon is combined into carbides (the structures of this type of cast iron have been discussed in Sec. 6-4);

grey cast iron in which all or an appreciable portion of the carbon is present in free state as *lamellar graphite*;

high-strength cast iron in which all or an appreciable portion of carbon is present in free state as *spheroidal graphite*;

malleable cast iron which is obtained by annealing of white cast iron castings; all or an appreciable portion of its carbon is present in free state as *flaky graphite* (temper carbon).

Thus, cast irons (except for white cast iron) differ from steels by the presence of graphite inclusions in the structure and, from one another, by the form of these inclusions.

Naturally, the most principal problem in the theory of cast irons is to establish the conditions for the formation of graphite, i.e. conditions of *graphitization*.

8-1. GRAPHITIZATION

Carbon can exist in two allotropic crystalline forms: as diamond and as graphite. Diamond is a rare form and is not found in alloys.

In iron-carbon alloys, carbon can occur in free state as graphite. Graphite has a lamellar crystal structure (Fig. 8-1).

The distance between carbon atoms in a crystal plane is 1.42 Å and the distance between adjacent planes is 3.40 Å. Of the four valence electrons of carbon atom, only one passes to the electron gas, which fact determines that graphite has certain, though weakly pronounced, metallic properties (for instance, a high electric conductivity).

The strength and plasticity of graphite are rather low.

Another high-carbon phase often present in iron-carbon alloys is cementite; its crystal structure and properties have been discussed in Sec. 6-3.

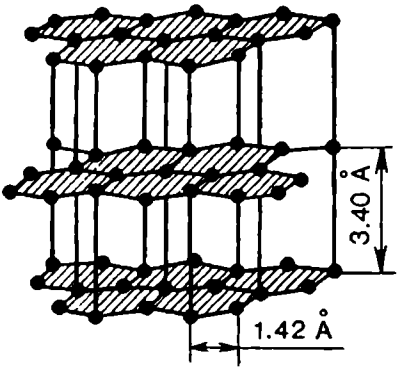

Fig. 8-1. Crystal structure of graphite

Comparison of the crystal structures and compositions of austenite, cementite and graphite may suggest the following conclusion: the crystal structures of austenite and cementite are very similar, whereas the crystal structure of graphite differs substantially from that of austenite (see Figs. 6-4*b*, 6-6, and 8-1). In the composition, austenite is closer to cementite than to graphite (since austenite contains up to 2.14 per cent C, cementite, 6.67 per cent C, and graphite, 100 per cent C). For that reason, cementite forms more easily from austenite or from the liquid and the work of nucleation and the related diffusion changes are lower in the crystallization of cementite than in that of graphite. Therefore, it is more probable kinetically that cementite, and not graphite, will crystallize from a solid solution (austenite) or liquid (more strictly, a mixture of ferrite — cementite or austenite + cementite is more likely to form than a ferrite + graphite or austenite + graphite mixture).

On the other hand, graphite is a stabler phase than cementite; this means that a mixture of ferrite + graphite or austenite + + graphite has a lower free energy than ferrite + cementite or austenite + cementite. Therefore, the thermodynamic factors are favourable for the formation of cementite, but not of graphite.

These two circumstances should be considered when studying the conditions for the formation of graphite. If the kinetic factors allow, graphite-containing structures will form and otherwise, those with cementite, notwithstanding the greater stability of graphite structures; in the latter case the formation of graphite is a secondary reaction and graphite will form due to decomposition of cementite.

As has been given in Ch. 2, a change in the state of aggregation, for instance from liquid to solid, is always due to the fact that the new state is more stable, has a lower free energy. Below the point T_s (see Fig. 2-2), the crystalline state is stabler than the liquid and possesses a lower free energy; this is why crystallization occurs below that temperature point.

The point T_s for the crystallization of the liquid into an austenite + cementite mixture lies at 1 147°C (line *ECF* in the Fe-C constitutional diagram, Fig. 6-7). Therefore, the lines of temperature variation of free energy of the liquid melt and austenite + cementite mixture intersect at the temperature of 1 147°C (Fig. 8-2). Crystallization should take place below that temperature and melting, above it.

As given earlier, an austenite-graphite mixture is thermodynamically more stable than an austenite-cementite mixture. This implies that the line character-

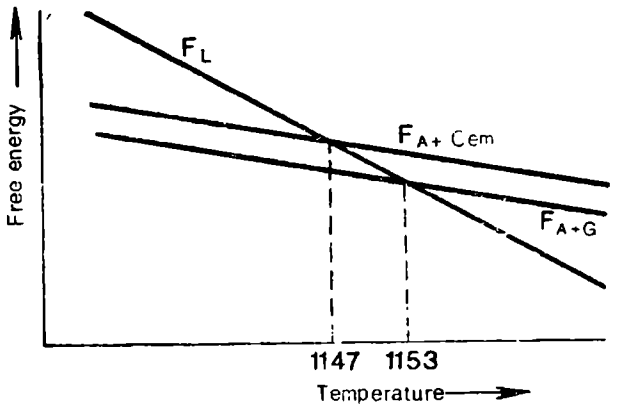

Fig. 8-2. Effect of temperature on free energy of liquid melt (F_L) and of mixtures of austenite + cementite (F_{A+Cem}) and austenite + + graphite (F_{A+G})

izing the free energy of an austenite-graphite temperature (see Fig. 8-2) is at all temperatures below the line corresponding to the free energy of an austenite-cementite mixture. Therefore, the free energy line for austenite + graphite intersects the free energy line of the liquid at a higher temperature than 1 147°C, namely, at 1 153°C.

This suggests the following conclusions.

Below the equilibrium point of the reaction $L \rightleftarrows A + Cem$ (1 147°C), crystallization occurs with the formation of cementite, since this process is kinetically more feasible. Graphite can only form as a secondary product, i.e. due to decomposition of cementite.

Between 1 147° and 1 153°C, the formation of an austenite-cementite mixture from the liquid is impossible in principle and crystallization results in the formation of an austenite-graphite mixture directly from the liquid.

By similar reasoning we can determine when austenite can decompose into ferrite + cementite and when into ferrite + graphite. The temperature of 727°C is the point of phase equilibrium, whereas the equilibrium point of $A \rightleftarrows F + G$ reaction is higher (at 738°C as found experimentally); therefore, in the temperature range from 738 to 727°C austenite can decompose into a ferrite + graphite mixture, but not into ferrite + cementite (pearlite). These thermodynamic considerations should be shown in the phase equilibrium diagram.

The iron-carbon constitutional diagram in Fig. 8-3 corresponds to the formation of austenite + cementite or ferrite + cementite mixtures. For that reason, the diagram is often called the iron-iron carbide ($Fe\text{-}Fe_3C$) constitutional diagram or metastable diagram, since cementite is an unstable phase. The formation of austenite + + graphite and ferrite + graphite mixtures occurs at higher temperatures and the lines of phase equilibrium should lie at higher temperatures. Thus, we obtain a diagram with doubled lines (see Fig. 8-3), the solid lines determining the temperature of austenite (ferrite)-cementite phase equilibrium and dashed lines, the phase equilibrium between austenite (ferrite) and graphite.

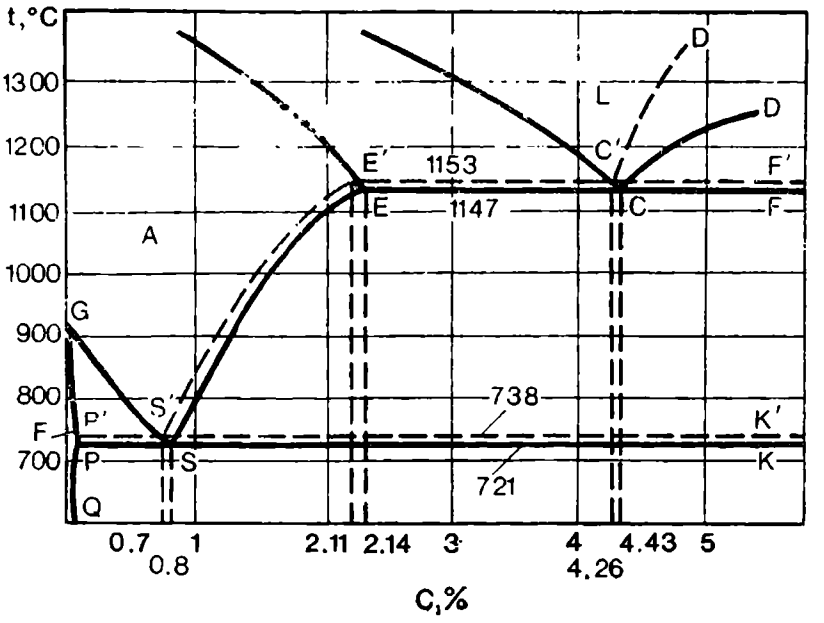

Fig. 8-3. Fe-C constitutional diagram. Solid lines — cementite system; dashed lines—graphite system

In this diagram, line $E'C'F'$ (1 153°C) is the phase equilibrium line for the reaction $L \rightleftarrows A + G$ and line $P'S'K'$ (738°C), the phase equilibrium line for the $A \rightleftarrows F + G$ reaction.

Since both austenite and liquid are less capable than cementite of dissolving graphite, lines $S'E'$ and $C'D'$ pass to the left of the corresponding lines SE and CD.

The formation of graphite from the liquid or austenite takes place in a narrow temperature interval between the stable and metastable lines of the diagram, i.e. under the conditions of slight undercooling, and therefore, a low cooling rate. It then follows, and has been confirmed by experience more than once, that grey cast iron structures form directly from the liquid or austenite on slow cooling and white cast iron structures, on faster cooling.

The formation of graphite from the liquid or austenite is a sluggish process, since the work of nucleation of graphite is great and an appreciable diffusion of carbon atoms is needed to form graphite crystals; also, conditions should be favourable for the removal of iron atoms from the crystallization front of graphite.

The direct formation of graphite from the liquid in pure iron-carbon alloys would be a rare phenomenon, were it not for a circumstance that promotes graphite formation.

The point is that the liquid (melt) of high-carbon alloys (cast irons) is never perfectly pure. Cast iron is usually more or less contaminated on melting, i.e. contains finest particles of various inclusions and impurities, among them finest particles of graphite

These particles serve as centres for initiation of graphite crystallization, i.e. carbon atoms settle on them to form graphite crystals. In that case the work of nucleation of graphite may even be less than the work of nucleation of cementite, because of which the formation of graphite crystals becomes kinetically feasible even at temperatures below the equilibrium point (1 147°C).

Overheating of cast iron well above the melting point causes dissolution of these suspended particles (though probably incomplete), thus inhibiting direct formation of graphite. Various additions to the cast iron can favour the appearance of additional centres for graphite crystallization and in many cases promote the formation of graphite.

Graphite can crystallize into various forms, depending on the conditions of crystallization, which fact is of a great importance (as will be explained later in the book).

Our considerations on the crystallization of graphite from liquid are also applicable to its crystallization from austenite. There is no clear experimental evidence that graphite precipitates directly from homogeneous austenite, though, as follows from the thermodynamic analysis made earlier in this section, this should be possible in a narrow temperature range (between the stable and metastable lines in the diagram). If, however, partial graphitization occurred in heating owing to the decomposition of cementite, carbon can precipitate on the existing graphite inclusions (on cooling below line $P'S'E'$); this has been observed in experiments.

Thus, apart from the transformations into cementite, which we have discussed in the chapter on iron-carbon alloys (Ch. 6), the alloy solutions (liquid melt or austenite) can also decompose to form graphite.

Apart from the formation of graphite directly in crystallization, another process of graphite formation is also possible. As has been noted time and again, cementite is an unstable compound and under particular conditions (temperature) can decompose into austenite + + graphite or ferrite + graphite. This process relies on the diffusion of carbon to crystallization centres and self-diffusion of iron from the points of graphite precipitation.

The process does not practically occur at room temperature but is sharply accelerated with increasing temperature.

At temperatures below line $P'S'K'$, the stable phases in the system are ferrite and graphite; therefore, cementite should decompose into these two phases and the corresponding reaction can be written as

$$Fe_3C \rightarrow Fe_\alpha + C \quad \text{or} \quad Cem \rightarrow F + G$$

Above line $P'S'K'$, austenite and graphite are the stable phases and cementite should decompose by the reaction

$$Fe_3C \rightarrow Fe_\gamma\,(C) + C \quad \text{or} \quad Cem \rightarrow A + G$$

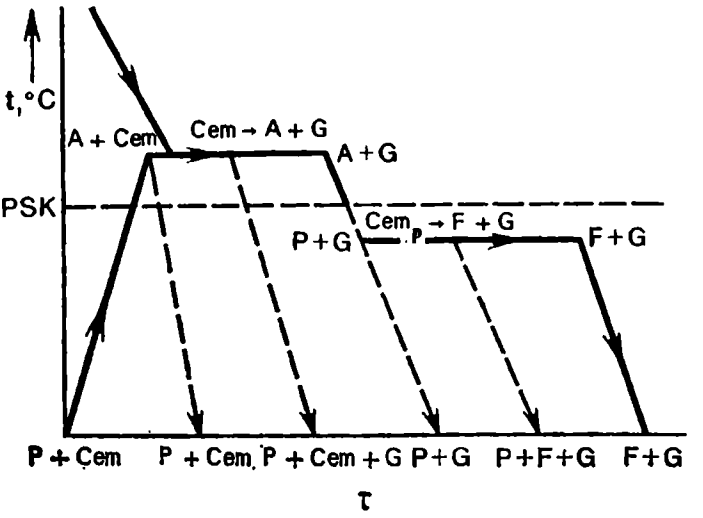

Fig. 8-4. Formation of structures in graphitization

Consequently, graphitization of cementite results in the formation of graphite and ferrite (below line $P'S'K'$) or graphite and austenite (above that line). In the latter case, part of the carbon is present in γ-solid solution and though the process is faster at higher temperatures, it cannot precipitate all the carbon in free state (i.e. as graphite). At temperatures below line $P'S'K'$, the process is slower but can result in complete graphitization, i.e. precipitation of all of the carbon in free state[1].

For better understanding of this complex and practically important process, let us analyse graphitization on another diagram (Fig. 8-4).

Assume that the cooling process has been sufficiently speedy and resulted in the formation of an initial structure of white cast iron (pearlite + cementite). On heating of white cast iron above the PSK line, its pearlite transforms into austenite; holding at this temperature (above 738°C) causes graphitization of the excess (undissolved) cementite. If the process is completed, the structure at a high temperature will be austenite + graphite and that upon cooling, pearlite + graphite. With the primary graphitization not completed (above PSK line), the structure retains some cementite and is essentially austenite + graphite + cementite at a high temperature and pearlite + graphite + cementite at a low temperature.

When passing through the critical point (line PSK), austenite transforms into pearlite, and holding at a temperature near the critical point (slightly below it) can cause decomposition of the cementite of pearlite (second stage of graphitization). If the process is complete, all the cementite of pearlite decomposes and forms a ferrite-graphitic structure; if incomplete, the structure will retain some pearlite.

[1] As has been noted earlier (Sec. 6-4), the solubility of carbon in ferrite is very low and can be neglected in the discussion of graphitization.

The process can occur either isothermally (as shown in the diagram) or on slow cooling. If graphite has partially crystallized into flakes, its further formation will occur by deposition of graphite on these flakes. This determines the various forms of graphite that can appear in cast iron.

8-2. THE STRUCTURES OF CAST IRON. FORMS OF GRAPHITE

White cast iron. Its name is due to the appearance of the fracture which is dull and white. The structure of white cast iron (at room temperature) is cementite and pearlite. Therefore, all the carbon in it is in the form of cementite, and graphitization is zero. White cast iron is hard and brittle and practically cannot be machined by cutting tools.

The structures of white cast iron and the conditions for their formation were discussed in detail in Sec. 6-4.

Grey cast iron. It has been named after the grey colour of its fracture. The structure of grey cast iron contains graphite whose quantity, shape and particle size may vary within a wide range. Thus, grey cast iron contains graphite and white cast iron, does not. An intermediate form is known as *mottled iron*; its structure contains graphite along with secondary cementite or cementite from ledeburite. Mottled iron is not employed in machine-building.

The microstructure of cast iron consists of a metallic matrix and graphite inclusions. According to the type of matrix, cast irons are classified as follows.

Pearlitic grey cast iron (Fig. 8-5*a*). Its structure is pearlite with graphite inclusions (graphite streaks in the figure). As known, pearlite contains 0.8 per cent C, therefore, this quantity of carbon in pearlitic grey cast iron is present in combined state (as Fe_3C) and the remainder, in free state, i.e. as graphite.

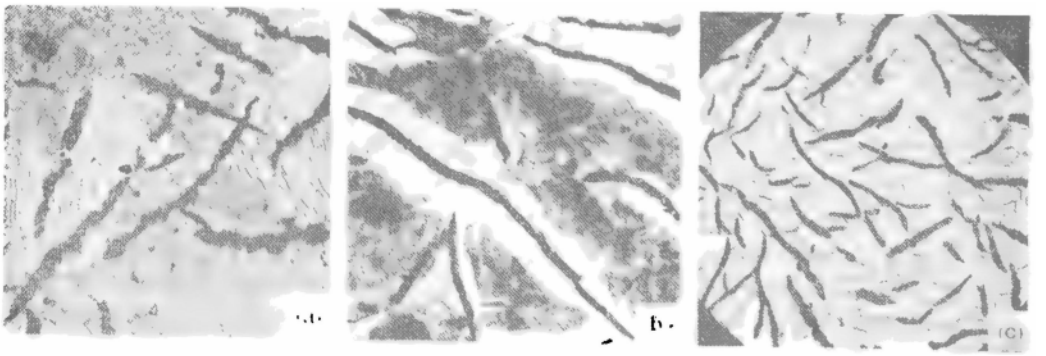

Fig. 8-5. Microstructures of grey iron
(*a*) pearlitic, ×200; (*b*) ferritic-pearlitic, ×100; (*c*) ferritic, ×100

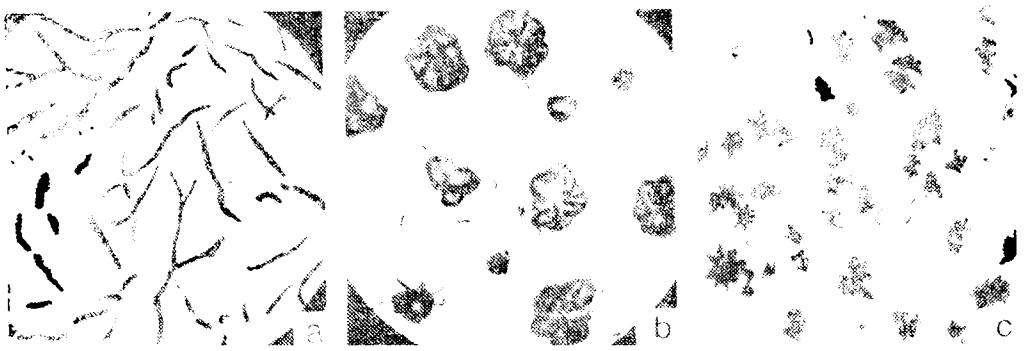

Fig. 8-6. Microstructures of cast iron with different forms of graphite

(*a*) lamellar graphite (common grey cast iron), ×100; (*b*) spheroidal (high-strength cast iron), ×200; (*c*) flaky graphite (malleable cast iron), ×100

Ferrite-pearlitic grey cast iron (Fig. 8-5*b*). Its structure is ferrite + + pearlite with graphite inclusions. In this type of cast iron, the quantity of combined carbon is less than 0.8 per cent C.

Ferritic grey cast iron (Fig. 8-5*c*) in which the metallic matrix is formed by ferrite and all the carbon is present in the form of graphite[1].

It can be concluded from the analysis of these structures that their metallic matrix is similar to the structure of eutectoid steel, hypoeutectoid steel, or iron. Therefore, cast irons differ from steels in their structure only by the presence of graphite inclusions which determine the type and properties of cast iron.

Graphite can be present in cast iron in three basic forms:

Lamellar graphite. In common grey cast iron, graphite forms streaks or lamellae and is accordingly called lamellar graphite. The structure of common ferritic cast iron with graphite streaks is shown in Fig. 8-6*a*; the spatial shape of these inclusions is illustrated in Fig. 8-7*a*.

Spheroidal graphite. In modern high-strength cast irons which are smelted with a small addition of magnesium (or cerium), graphite has a spheroidal shape. The microstructure of grey cast iron with spheroidal graphite is illustrated in Fig. 8-6*b* and the photograph of a single inclusion, in Fig. 8-7*b*.

Flaky graphite. If white cast iron as obtained by casting is annealed, its cementite, being unstable, decomposes and graphite that forms has a compact, almost equi-axed, but not spheroidal, shape of particles. This is what is called *flaky graphite*, or *temper carbon*. The

---

[1] Chemical analysis can determine the total carbon (C_{tot}) and the quantity of carbon combined into carbides (C_{com}); thus it is possible to determine the type of cast iron. If $C_{com} \approx 0.8$ per cent, the cast iron is pearlitic; if $C_{com} < < 0.1$ per cent, we have ferritic iron; intermediate values relate to ferrite-pearlitic cast irons.

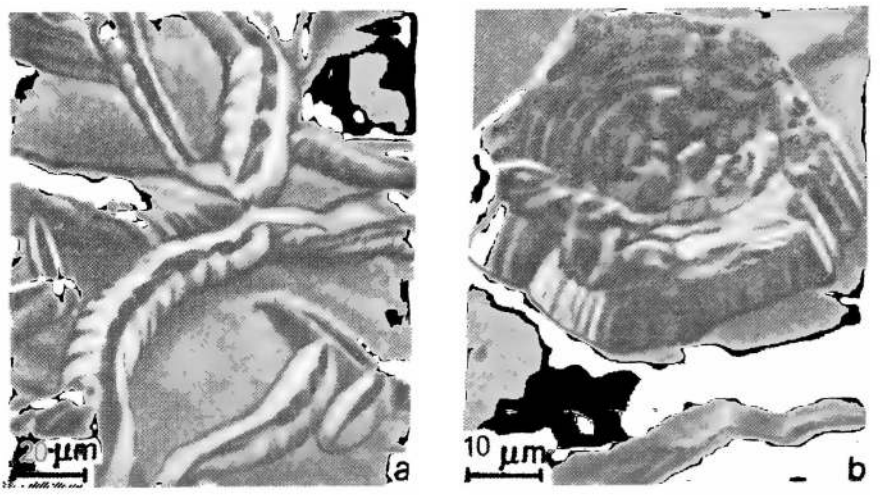

Fig. 8-7. Graphite inclusions in cast iron
(*a*) lamellar; (*b*) spheroidal

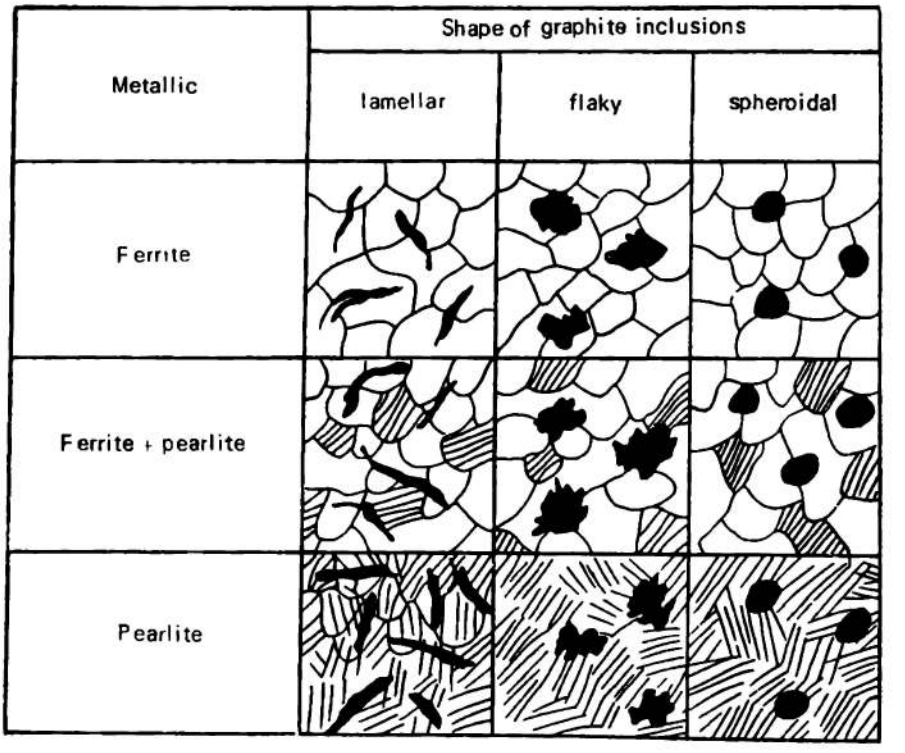

Fig. 8-8. Classification of cast irons by the structure of metallic matrix and the form of graphite inclusions (the structures are shown schematically)

microstructure of a cast iron with flaky graphite is shown in Fig. 8-6*c*. In practice, cast iron with flaky graphite inclusions is called *malleable cast iron.*

Thus, cast iron with lamellar graphite is called common *grey cast iron*, that with spheroidal graphite, *high-strength cast iron*, and that with flaky graphite, *malleable cast iron.*

The classification of cast irons by the structure of metallic matrix and shape of graphite is illustrated in Fig. 8-8.

8-3. THE STRUCTURE AND PROPERTIES OF CAST IRON

Since the structure of cast iron consists of metallic matrix and graphite, its properties will be determined by both the properties of the matrix and the quantity and type of graphite inclusions.

Cast iron has inferior properties relative to steel, and therefore the graphite inclusions in it can be regarded, in the first approximation, as voids or cracks. It then follows that cast iron can be regarded as a steel infected with numerous cracks and voids.

Naturally, the properties of cast iron are lower at a larger volume of voids. For the same volume of voids (i.e. the same quantity of graphite), the properties of cast iron are determined by the shape and distribution of these inclusions. Consequently, the mechanical properties of cast iron are lower at a higher content of graphite; and the coarser these inclusions, the more they disintegrate the metallic matrix. The worst mechanical properties are exhibited by cast irons in which graphite inclusions form a closed network.

What properties are especially sensitive to lamellar graphite inclusions which act as cracks or sharp notches in the metal?

Tensile stresses promote the formation of failure centres at the ends of graphite inclusions. As regards its mechanical properties, cast iron is characterized by a low resistance to crack propagation (nevertheless, it fractures in the ductile mode, has a cup-shaped fracture, but a_p is very low), and therefore, exhibits low mechanical properties in tests where normal tensile stresses prevail.

If tensile stresses are minimum, such as in compression, the mechanical properties of cast iron turn out to be quite high and very close to the properties of a steel of the same composition and structure as that of the cast iron matrix.

This is why the ultimate compression strength and hardness of cast iron depend mainly on the structure of the metallic matrix and only slightly differ from the respective properties of steel.

Some other properties of cast iron, in particular the rupture strength, bending and torsional strength, are mainly determined by the content, shape and size of graphite inclusions and appreciably differ from the respective properties of steel.

These relate mainly to grey cast iron with lamellar graphite inclusions. The effect of graphite inclusions becomes less pronounced as their shape changes from lamellar to spheroidal.

Rounded-off inclusions of spheroidal graphite cannot produce sharp stress concentrations, they are not 'cracks' in the matrix and spheroidized cast iron has an appreciably higher strength in tension and bending than cast iron with lamellar graphite (hence the name—high-strength cast iron). Intermediate values of strength are exhibited by malleable cast iron with flaky graphite.

Thus, the strength of cast iron (resistance to normal stresses) is determined by the structure of the metallic matrix and the shape of graphite inclusions.

The ductility of cast iron with different forms of graphite can be characterized by the following values of relative elongation, per cent:

Graphite	Lamellar	Flaky	Spheroidal
δ, %	0.2-0.5	5-10	10-15

The ductility only slightly depends on the structure of the metallic matrix (lower values are typical of pearlitic cast irons and higher, of ferritic). The Brinell hardness, which is determined by the structure of the matrix, may have the following values:

Cast iron . . .	Ferritic	Ferritic-pearlitic	Pearlitic
HB	150	200	250

The hardness only slightly depends on the shape of graphite.

Apart from the principal structures of ferrite and pearlite, other types of structure[1], possessing higher-strength properties, can be formed in cast iron by heat treatment. However, the properties (ductility, strength) of common grey cast iron are mainly determined by the shape of graphite and this does not change essentially on heat treatment, therefore heat treatment is ineffective with common grey cast iron and is resorted to only seldom.

In spheroidal graphite cast iron there is no lamellar inclusions which might serve as stress concentrators, because of which a change in the structure of the matrix may have an appreciable effect on the properties of the metal. Spheroidal graphite cast iron can be subjected to all methods of heat treatment commonly used with steel and these methods are increasingly employed for improving its properties.

We have noted that graphite inclusions are harmful to cast iron. This view is, however, unilateral and not always correct. In some cases graphite inclusions can produce a useful effect.

[1] They will be discussed in more detail in Part III, *Heat Treatment*.

In a number of cases, cast iron may have an advantage over steel, namely due to the presence of graphite; firstly, the presence of graphite makes the metal more easily machinable (since the chip is brittle, or discontinuous); secondly, cast iron has better antifriction properties owing to the lubricating effect of graphite; thirdly, graphite inclusions can quickly attenuate vibrations and resonance oscillations; fourthly, cast iron is almost insensitive to surface defects, notches, etc.

Indeed, since cast iron contains an enormous quantity of graphite inclusions, which act as notches and voids, it is quite natural that additional surface defects will be only of a minor importance not comparable with their role in a high-strength steel free of non-metallic inclusions.

It is also worth mentioning that cast iron has better casting properties than steel. It is more convenient in casting operations owing to its lower melting point and to the fact that its crystallization stops at a constant temperature (formation of eutectic); further, it has a better fluidity and can better fill in the moulds. These advantages of cast iron make it a valuable structural material which is widely used in machine elements, mainly in those not subjected to high tensile or impact loads.

8-4. EFFECT OF IMPURITIES

Common commercial cast iron is not a binary iron-carbon alloy but contains the same impurities as carbon steel, i.e. manganese, silicon, sulphur and phosphorus, and yet in greater quantities. These impurities can substantially affect the conditions of graphitization, and therefore, the structure and properties of cast iron.

Silicon has an especially strong effect on the structure of cast iron; it enhances graphitization. The content of silicon in cast irons varies quite widely: from 0.3-0.5 to 3-5 per cent. By varying the content in silicon it is possible to produce cast irons with very different properties and structures: from low-silicon white cast iron to high-silicon ferritic (grey iron with lamellar graphite or high-strength iron with spheroidal graphite).

Manganese, unlike silicon, prevents graphitization or, as it is said, favours chilling of cast iron.

Sulphur also has a provoking effect on chilling, but impairs the casting properties (in particular, lowers the fluidity) and its content in cast irons is limited to 0.08 per cent in small castings and 0.1-0.12 per cent in larger castings where a poorer fluidity is tolerable.

Phosphorus has practically no effect on graphitization. Phosphorus, however, is a useful impurity in cast iron, since it improves the fluidity. This may be explained by the formation of a fusible ternary eutectic (m.p. = 950°C). At the moment of solidification, the

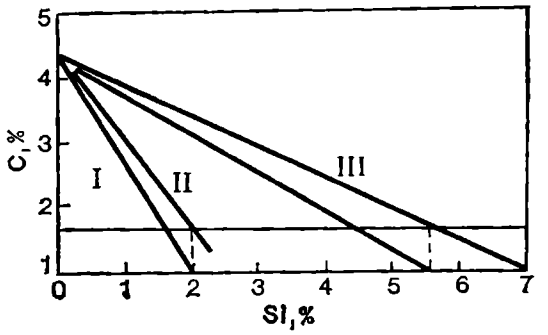

Fig. 8-9. Structural diagram for cast iron to determine the structure to be formed in casting (wall thickness of 50 mm) depending on content of silicon and carbon

I—white iron; *II*—pearlitic grey iron; *III*—ferritic grey iron

eutectic consists of phosphorus-rich austenite, cementite, and iron phosphide (Fe_3P).

Portions of the hard phosphide eutectic increase the total hardness and wear resistance of cast iron.

Apart from these permanent impurities, cast irons often contain other elements which are added intensionally. They are called *alloyed cast irons*. If the impurities were contained in the iron ore from which cast iron has been smelted in blast furnace, the iron produced is called *natural alloy cast iron*. Cast irons are most often alloyed with chromium, nickel, copper, aluminium and titanium. Chromium inhibits graphitization, while copper and nickel have a promoting effect.

At present there is no hypothesis that could satisfactorily explain the effects of alloying elements on graphitization.

In any case, the dissolution of such elements as chromium, manganese, tungsten, molybdenum or vanadium has an inhibiting effect on graphitization. Most of the other elements occurring in cast iron are insoluble in cementite and promote graphitization. This problem has been discussed in many theoretical and experimental reports (M. G. Oknov, K. P. Bunin, I. N. Bogachev and others).

Approximate determinations of the structure of cast iron, depending on the content of impurities, are made by using so-called structural diagrams, such as shown in Fig. 8-9. It may be determined from the diagram what will be the structure of castings with walls 50 mm thick with different contents of carbon and silicon (the content of manganese is constant and equal to 0.5 per cent).

8-5. EFFECT OF COOLING RATE

It has been noticed in the foundry practice that the structure of cast iron may be different in the same casting. In thinner portions and at the surface the degree of graphitization is usually lower than in thicker portions and in the core. In other words, more cementite forms in areas cooled at a higher rate and more graphite in those which are cooled more slowly. The factors that determine the graphitization degree in cast iron are the content of carbon and silicon and the rate of cooling.

The effect of the composition (carbon and silicon content) and cooling rate (wall thickness of castings) on the structure formed in cast iron can be determined by using a structural diagram, such as shown in Fig. 8-10.

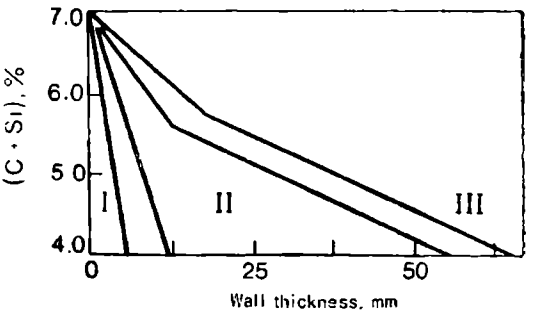

Fig. 8-10. Structural diagram for cast iron to determine the structure to be formed in casting depending on the total content of carbon and silicon and wall thickness

I—white iron; *II*—pearlitic grey iron; *III*—ferritic grey iron

8-6. GRADES OF GREY AND HIGH-STRENGTH CAST IRONS

Grey and high-strength cast irons are classified into grades, according to the values of their mechanical properties.

The mechanical properties of selected grades of grey cast iron are given in Table 8-1.

In the table, grey cast iron is designated by the letters 'СЧ' (an abbreviation of the Russian words 'grey iron') and a four-digit number, the first two digits giving the minimum specified tensile strength and the last two, the minimum bending strength. The strength value of cast iron is taken as the measure of quality.

Table 8-1. Mechanical Properties of Grey Cast Irons (GOST 1412-70)

Iron grade	Ultimate tensile strength, kgf/mm²	Ultimate bending strength, kgf/mm² (lower limit)	Deflection at distance between supports, mm		Brinell hardness
			600	300	
СЧ00	—	—	—	—	—
СЧ12-28	12	28	6	2	143-229
СЧ15-32	15	32	8	2.5	163-229
СЧ18-36	18	36	8	2.5	170-229
СЧ21-40	21	40	9	3	170-241
СЧ24-44	24	44	9	3	170-241
СЧ28-48	28	48	9	3	170-241
СЧ32-52	32	52	9	3	187-255
СЧ35-56	35	56	9	3	197-269
СЧ38-60	38	60	9	3	207-269

The mechanical properties of Grade СЧ00 are not guaranteed; it is employed only in elements subjected to light mechanical loads.

The ultimate bending strength of cast iron is roughly twice and the compressive strength, three to five times the tensile strength, i.e. it may be taken appro-

ximately that

$4\sigma_t = 2\sigma_b = \sigma_c$

As follows from Table 8-1, the best mechanical properties are exhibited by grey cast iron Grade СЧ38-60 (and also by СЧ35-56 and СЧ32-52). These quality-grade cast irons have the structure of pearlite with fine lamellar graphite inclusions.

Cast iron with fine disperse graphite inclusions possesses high mechanical properties, in particular, high hardness and high wear resistance, which are due to the pearlitic structure of the matrix. These grades are used to make piston rings of internal combustion engines and other critical parts.

When casting critical parts, a few specimens are simultaneously cast for making tensile and bending tests in order to determine whether the cast metal satisfies the strength requirements (usually indicated in the drawing).

High-strength cast irons (ВЧ) are also graded according to their mechanical properties, mainly according to the tensile strength and elongation (Table 8-2).

Table 8-2. Mechanical Properties of High-strength Cast Irons (GOST 7293-70)

Iron grade	Ultimate tensile strength, kgf/mm²	Yield strength in tension, kgf/mm²	Relative elongation, %	Impact strength, kgf m/cm²	Brinell hardness
	lower limits				
ВЧ45-0	45	36	—	—	187-255
ВЧ50-1.5	50	38	1.5	1.5	187-255
ВЧ60-2	60	42	2.0	1.5	197-269
ВЧ45-5	45	33	5.0	2.0	170-207
ВЧ40-10	40	30	10	3.0	156-197

Comparing the properties of grey and high-strength cast irons, it may be seen that Grade ВЧ40-10 (see Table 8-2), which is the weakest in its group, is however stronger than the strongest grey cast iron Grade СЧ38-60 (see Table 8-1), but has a lower hardness, which is due to the different form of graphite in these grades.

Grade ВЧ45-0, whose plastic properties (elongation) are not specified, is applicable only in elements operating without dynamic loads.

ВЧ60-2, ВЧ45-5, and ВЧ40-10 are high-quality grades and differ from one another in the structure of the matrix which is pearlitic in Grade ВЧ60-2, ferrite-pearlitic in Grade ВЧ45-5, and ferritic in Grade ВЧ40-10; accordingly, they have different values of ultimate strength.

These grades combine high strength and ductility and are used in critical elements. For instance, the crankshaft of the Volga motor car engine is made of a high-strength cast iron having the following composition: 3.4-3.6 per cent C, 1.8-2.2 per cent Si, 0.96-1.2 per cent Mn, 0.16-0.30 per cent Cr, <0.01 per cent S, <0.06 per cent P, and 0.01-0.03 per cent Mg. This cast iron, which has a very narrow range of alloying elements and low contents of sulphur and phosphorus, is smelted in an electric furnace, rather than in a cupola. This circumstance and the use of heat treatment[1] ensure a high level of properties, higher than those given in Table 8-2, in particular: σ_t = 62-65 kgf/mm², δ =

[1] Normalizing followed with high-temperature tempering to granular pearlite structure.

= 8-12 per cent, and *HB* = 192-240. Though it is inferior to steel in mechanical properties, crankshafts made of it by casting (a cheaper procedure) have a higher structural strength. Thus, cast iron, which possesses better casting properties than steel, can be successfully used for making parts of a complicated shape (with internal cavities, etc.), which will have a higher resistance to various mechanical actions than forged steel parts of a simpler shape. In other words, in some cases parts of a complicated shape made of a less strong material (cast iron) may be structurally stronger than parts of a simpler shape made of a stronger material (steel).

8-7. MALLEABLE CAST IRON[1]

Malleable cast iron which contains flaky graphite is obtained from white cast iron by a special procedure of *graphitizing annealing*, or soaking.

In the manufacture of malleable cast iron, it is quite essential to obtain purely white cast iron on casting, since partial graphitization on casting, and therefore, the formation of lamellar graphite will result in the deposition of graphite on these lamellae in the subsequent graphitization. Such a cast iron will have poorer properties, almost similar to those of common grey cast iron.

Though one tries to obtain white iron in casting, it is not advisable to excessively increase the content of the elements that can inhibit graphitization (for instance, manganese), since this can involve difficulties in graphitizing annealing. For that reason the composition of malleable cast iron is specified within relatively narrow limits.

A typical composition of malleable cast iron is 2.4-2.8 per cent C, 0.8-1.4 per cent Si, <1 per cent Mn, $\leqslant 0.1$ per cent S, and $\leqslant 0.2$ per cent P.

The low content in carbon gives a low quantity of graphite inclusions and improves the quality of cast iron. It is, however, impossible to obtain such a low-carbon cast iron in a cupola furnace, and malleable cast iron is smelted in special furnaces, which naturally increases its cost.

The main expenditures in the manufacture of malleable cast iron parts are, however, associated with the annealing procedure which requires much time and is rather expensive.

Consider the structural changes that occur during white-to-malleable iron annealing.

The process of decomposition of cementite in the annealing to malleable cast iron can be illustrated by the graphitization diagram discussed earlier (see Fig. 8-4).

[1] It would be wrong to think that malleable iron is actually 'malleable', i.e. can be forged by common methods. The name is an old one and characterizes only its better plasticity compared to common grey cast iron (cf. Tables 8-1 and 8-3).

On heating white cast iron above the *PSK* line, there are formed austenite and cementite; cementite decomposes at this temperature and forms graphite flakes (first stage of graphitization). If the cast iron is then cooled below *PSK* line and is let to remain at that temperature for a long time (which is equivalent to very slow cooling), the cementite of the pearlite will also decompose (second stage of graphitization). Upon this procedure, all the carbon will precipitate in the free state and the structure of cast iron will consist of ferrite and flaky inclusions of temper carbon. The cast iron is called *ferritic malleable cast iron.*

When broken, ferritic malleable cast iron is dull and dark in the fracture, owing to numerous graphite inclusions in the ferritic matrix. For that reason it is also called *blackheart malleable cast iron.* The fracture of ferritic malleable cast iron usually has a bright surface rim, since the surface layer is partially decarburized and its structure changes to pearlite without graphite.

If cooling is insufficiently slow (especially in the temperature range slightly below the *PSK* line in the iron-carbon diagram) or the holding time at the second graphitization stage is too short, the graphitization of pearlitic cementite may be incomplete; in that case the cast iron will have the structure of pearlite — ferrite — + temper carbon and is called *ferrite-pearlitic malleable cast iron.*

If cooling below the critical temperature range is done quickly (for instance, castings are cooled in air), the graphitization process will not extend on the cementite of pearlite; the cast iron will then have the structure of pearlite + temper carbon and is called *pearlitic malleable cast iron.*

There is also a method (though rarely used) to produce malleable cast iron by annealing in a decarburizing medium (iron ore, scale, or a special atmosphere). In this process, an appreciable part of the carbon is burned off producing a fully decarburized surface layer 1.5-2.0 mm deep. No holding time is allowed in this method below the critical temperature and the metallic matrix of the core contains much pearlite.

Owing to the decarburizing effect, the fracture is bright and the cast iron thus made is called *whiteheart malleable cast iron*, or, else, *pearlitic malleable cast iron*, since the core is high in pearlite. It should be noted that ferritic malleable cast iron is used more often than other types.

Figure 8-11 shows an annealing schedule for producing ferritic malleable cast iron in large furnaces.

As may be seen from the figure, white cast iron castings are first slowly heated (during 20-25 h) to 950-1000°C; at this temperature the excess cementite is graphitized (the graphitization occurs in 10-15 h), after which the castings are cooled in the furnace to 740°C[1]. Then a second holding time (roughly 30 h) is allowed (isothermal holding is sometimes replaced by slow cooling from 770° to 700°C for approximately 30 h); in the former case the cementite of pearlite

[1] In real cast irons containing 1 to 1.5 per cent Si, A_1 (line *PSK*) lies approximately at 760-770°C, so that the holding at 740°C is the holding below the critical point.

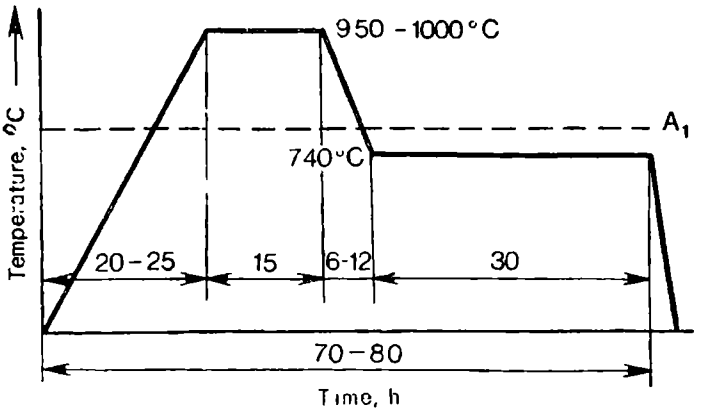

Fig. 8-11. Time and temperature conditions for white-to-malleable iron annealing

is graphitized and in the latter crystallization to a stable system is ensured and all the carbon precipitates in the free state.

The final structure consists of ferrite and clusters of flaky graphite. Upon holding at 740°C, the castings are taken from the furnace and cooled in air; air cooling has no effect on the structure that has already formed. The total time of the procedure is 70-80 h, with 40 h for the graphitization proper and the remaining time for raising and lowering the furnace temperature.

A group of Soviet researchers (S. A. Saltykov, G. I. Troitsky, A. D. Assonov et al.) have developed and applied a process of accelerated annealing of malleable cast iron, in which white cast iron castings are subjected to hardening prior to graphitizing annealing. The fine-granular structure of castings and internal stresses in the metal cause the formation of numerous centres for crystallization of graphite, which accelerates substantially the first and second stages of graphitization and shortens the whole graphitization process to 10-15 h.

Malleable cast iron upon accelerated annealing has a typically fine-grained structure: fine grains of ferrite and fine graphite inclusions.

As other types of cast iron, malleable cast iron is graded according to mechanical properties.

Table 8-3 contains data on mechanical properties of malleable cast irons. The grading of malleable cast irons consists of letters КЧ (for 'malleable cast iron') and two numbers, one giving σ_t, kgf/mm², and the other, δ, %.

Table 8-3. Mechanical Properties of Malleable Cast Iron

Iron grade	Ultimate strength, kgf/mm² (lower limit)	Elongation, % (lower limit)	Brinell hardness (upper limit)
	Blackheart (ferritic)		
КЧ30-6	30	6	163
КЧ33-8	33	8	149
КЧ35-10	35	10	149
КЧ37-12	37	12	149
	Whiteheart (ferrite-pearlitic)		
КЧ45-6	45	6	241
КЧ50-4	50	4	241
КЧ56-4	56	4	269
КЧ60-3	60	3	269
КЧ63-2	63	2	269

As may be seen from the table, ferritic malleable cast iron has a better plasticity than the pearlitic type, but the latter has a higher hardness, therefore, a higher wear resistance.

LITERATURE

Oknov M. G., *Metallography of Cast Iron*. Leningrad-Moscow, GONTI, 1938 (in Russian).

Troitsky G. I., *Properties of Cast Iron*. Moscow, "Metallurgizdat", 1941 (in Russian).

Bogachev I. N., *Metallography of Cast Iron*. Moscow-Sverdlovsk, "Mashgiz", 1952 (in Russian).

Bunin K. P., Ivantsov G. I., Malinochka Ya. N., *The Structure of Cast Iron*. Kiev-Moscow, "Mashgiz", 1952 (in Russian).

Krishtal M. A., Titensky E. G., *The Properties of Malleable Cast Iron*. Moscow, "Metallurgiya", 1967 (in Russian).

Engineering Materials. A reference book. Volume 4. Moscow, "Mashinostroenie", 1969 (in Russian).

Bunin K. P., Taran Yu. N., *The Structure of Cast Iron*. Moscow, "Metallurgiya", 1972 (in Russian).

Part Three

HEAT TREATMENT

Chapter 9

GENERAL PRINCIPLES OF HEAT TREATMENT

The *technology of metals* comprises the three branches: (a) *engineering metallurgy*, i.e. production of metals of desired composition; (b) *mechanical metallurgy*, i.e. shaping of metals and (c) *heat treatment* for obtaining desirable properties.

In metallurgical processes, the metal products are shaped to a required form, such as ingots. The structure of metal (or its surface layers) is changed to some extent in machining, forging or stamping, but this is only an accompanying phenomenon. Equally, changes in the shape of products may occur on heat treatment, though the main objective of this process is to change the structure of metal.

The role of heat treatment in modern mechanical engineering cannot be overestimated. The changes in the properties of metals due to heat treatment are of extremely great significance.

9-1. TEMPERATURE AND TIME

The purpose of any heat treating process is to produce the desired changes in the structure of metal by heating to a specified temperature and by subsequent cooling[1].

Therefore, the main factors acting in heat treatment are temperature and time, so that any process of heat treatment can be represented in temperature-time (t-τ) coordinates (Fig. 9-1).

---

[1] More generally, by changing the temperature of the metal; so the process of subzero treatment starts with cooling to a negative temperature which is followed by heating to room temperature.

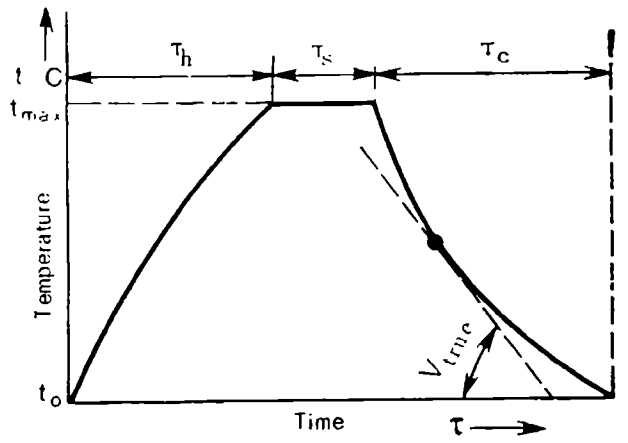

Fig. 9-1. Time-temperature conditions of common heat treatment

Heat treatment conditions are characterized by the following parameters: heating temperature t_{max}, i.e. the maximum temperature to which an alloy metal is heated; time of holding at the heating temperature τ_h; heating rate v_h; and cooling rate v_c.

If heating (or cooling) is made at a constant rate, the temperature-time relationship will be described by a straight line with a respective angle of incline.

With a varying heating (or cooling) rate, the actual rate should be attributed to the given temperature, more strictly, to an infinite change of temperature and time; that is the first derivative of temperature in time: $v_{act} = \partial t/\partial \tau$.

The actual rate is determined graphically by the slope tangent to the heating (or cooling) curve at the given temperature. In practice, average heating (or cooling) rate is used more often, which is calculated for the whole temperature interval or a portion thereof; in the case considered,

$$v_{h.av} = \frac{t_{max}}{\tau_h} \quad \text{and} \quad v_{c.av} = \frac{t_{max}}{\tau_c}$$

Heat treatment may be a complex process, including multiple heating stages, interrupted or stepwise heating (cooling), cooling to subzero temperatures, etc. Any process of heat treatment can be described by a diagram in temperature-time coordinates. Such diagrams are shown in Fig. 9-2*a* and *b*.

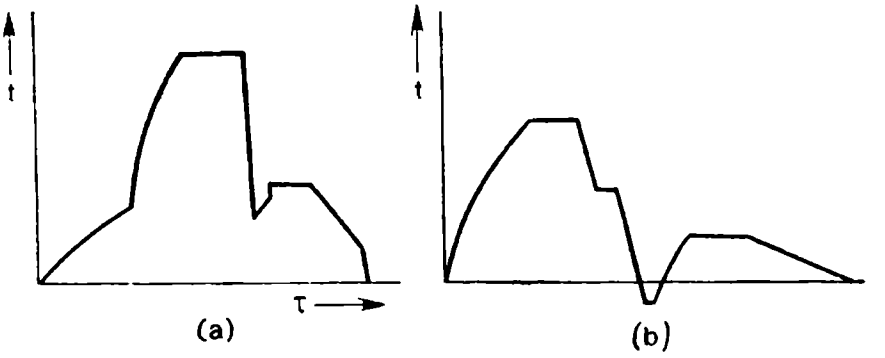

Fig. 9-2. Conditions of complex methods of heat treatment

9-2. CLASSIFICATION OF TYPES OF HEAT TREATMENT

The changes in metal upon heat treatment should be retained, otherwise the heat treatment procedure would be senseless.

To change the properties of an alloy, it is essential that the heat treatment produces certain residual changes in its structure resulting from phase transformations. If metal is in a structurally unstable state (owing to prior treatment), heating can increase the mobility of atoms and the metal will approach the equilibrium state in which heat treatment will be possible without phase transformations.

All types of heat treatment can be classified into four main groups (according to A.A. Bochvar) as follows.

Group I. The metal might be changed to an unstable state by prior treatment. For instance, cold plastic working could produce work hardening, i.e. distortion of the crystal lattice. Diffusion processes have no time to occur during solidification and the composition of the metal is inhomogeneous even within the volume of a single grain. Quick cooling or nonuniform stresses applied cause a nonuniform distribution of elastic strain. An unstable state can remain in the metal for a long time at room temperature, since the thermal mobility of atoms is insufficient for a change to the stable state.

Heating increases the mobility of atoms and thus can noticeably accelerate the processes which can change the metal to the stable state (stress relief, correction of crystal lattice distortions, recrystallization, diffusion).

The heat treatment consisting in the heating of a metal which changes the unstable state (owing to prior treatment) to a stabler state is called *annealing.*

Annealing of plastically deformed metals has been discussed in Sec. 3-6.

Group II. If an alloy undergoes phase transformations (allotropic transformations, dissolution of the second phase, etc.), heating above a definite critical point will change the alloy structure. A reverse transformation will occur on cooling. If cooling is sufficiently slow, the transformation will be complete and the phase composition will correspond to the equilibrium state.

This type of heat treatment is characterized by heating above the point of phase transformation and cooling at a low rate resulting in structural equilibrium of the alloy. This type of heat treatment is also called *annealing.* In order to distinguish between the two types of annealing, the former (in Group I) may be called *first-order annealing* and the latter, *second-order annealing*, or *structural recrystallization.*

Group III. If some phase transformations occur in an alloy on heating, the completeness of the reverse transformation (on cooling) will depend on the rate of cooling. It is theoretically possible to imagine such cooling conditions in which no reverse transformation will occur, i.e. a state typical of high temperatures will be fixed in the alloy by quick cooling to room temperature. This heat-treating procedure is called *hardening*. In many cases, hardening does not fix (or fixes only partially) the state that is stable at higher temperatures. For that reason the extreme case of hardening in which the high-temperature state of an alloy is fixed is called *real hardening*, as distinguished from hardening in a broader sense when the hardening procedure fixes in an alloy an intermediate unstable state of a structural transformation (decomposition), rather than the state the alloy has at the high temperature of hardening.

There is a certain similarity between the heat treatment of the second and the third group. In both cases the metal is heated above the temperature of phase transformation and acquires the final structure, owing to the transformation on subsequent cooling. There is, however, a fundamental difference. In the second-group heat treatment, the purpose of cooling is to approach the equilibrium state of the alloy, and the cooling procedure is, therefore, performed slowly. In the third-group heat treatment, the cooling procedure is done quickly so that the final structural state of the metal can be far from equilibrium.

Group IV. The state of a hardened alloy is typically unstable. Even without temperature actions, some processes may occur in the metal bringing its state nearer to equilibrium. These changes may be favoured by heating which increases the mobility of atoms. A hardened alloy more and more approaches the state of equilibrium as the temperature is being increased. This type of heat treatment, i.e. heating of a hardened alloy to a temperature below the equilibrium phase transformation point is called *tempering*. If the process occurs at room temperature, that is, heat treatment is replaced by holding at room temperature, or at low-temperature heating, it is called *ageing*. Both in the first-order annealing and in tempering, the state of an alloy approaches structural equilibrium. In both cases the initial stage is characterized by an unstable state which, however, results in the first-order annealing from a prior treatment that has caused no phase transformations, and in tempering, from prior hardening. Thus, tempering is a secondary procedure and is always made after hardening.

The above considerations enable us to briefly define the principal types of heat treatment.

Annealing (first-order) is a heat treatment procedure consisting in heating of a metal which is in an unstable state owing to prior treatment; it changes the metal to a state of greater stability.

Annealing (second-order) is a heat treatment procedure in which a metal is heated above the temperature of phase transformation and then cooled slowly to obtain a structurally stable state.

Hardening is a heat treatment procedure in which a metal is heated above the temperature of phase transformation and then cooled quickly to obtain a structurally unstable state.

Tempering is a heat treatment procedure in which a hardened metal is heated below the temperature of phase transformation to obtain a more stable structural state.

Apart from these principal types of heat treatment, there are two other processes in which heat treatment is combined with metallurgical or mechanical methods.

Since metals can dissolve various elements, especially at elevated temperatures, atoms of a substance near the metal surface can diffuse into the bulk of metal and produce a surface layer of a different composition. This processing changes both the composition and the structure of the metal in surface layers and often also in the core and is called *chemical heat treatment* (CHT).

Chemical heat treatment changes directionally both the composition and the structure of a metal and, therefore, belongs simultaneously to two branches of the technology of metals[1].

A type of treatment combining deformation and structural changes is now ever more applied. The metal is deformed to the desired shape and also to produce a strain-hardening effect. The strain-hardened metal is then heat treated. This type of treatment is called *thermomechanical treatment* (THT), or *thermoplastic working*. Evidently, it is a combination of mechanical metallurgy and heat treatment.

Thus, in addition to the basic types of heat treatment (first- and second-order annealing, hardening, and tempering) there are two more complicated types of treatment:

Chemical heat treatment is heating of a metal in suitable chemical reagents to change the composition and structure of the surface layers.

Thermomechanical treatment, or thermoplastic working, is the procedure of straining with subsequent heat treatment which retains, to some or other extent, the effect of strain hardening.

9-3. HEAT TREATMENT AND THE CONSTITUTIONAL DIAGRAM

The constitutional diagram can show what type of heat treatment is applicable to an alloy and in what temperature interval the procedure should be done.

[1] Note that carburization (saturation of steel with carbon) was in the middle of the last century a typically metallurgical process, since it was the sole process for making high-carbon steels.

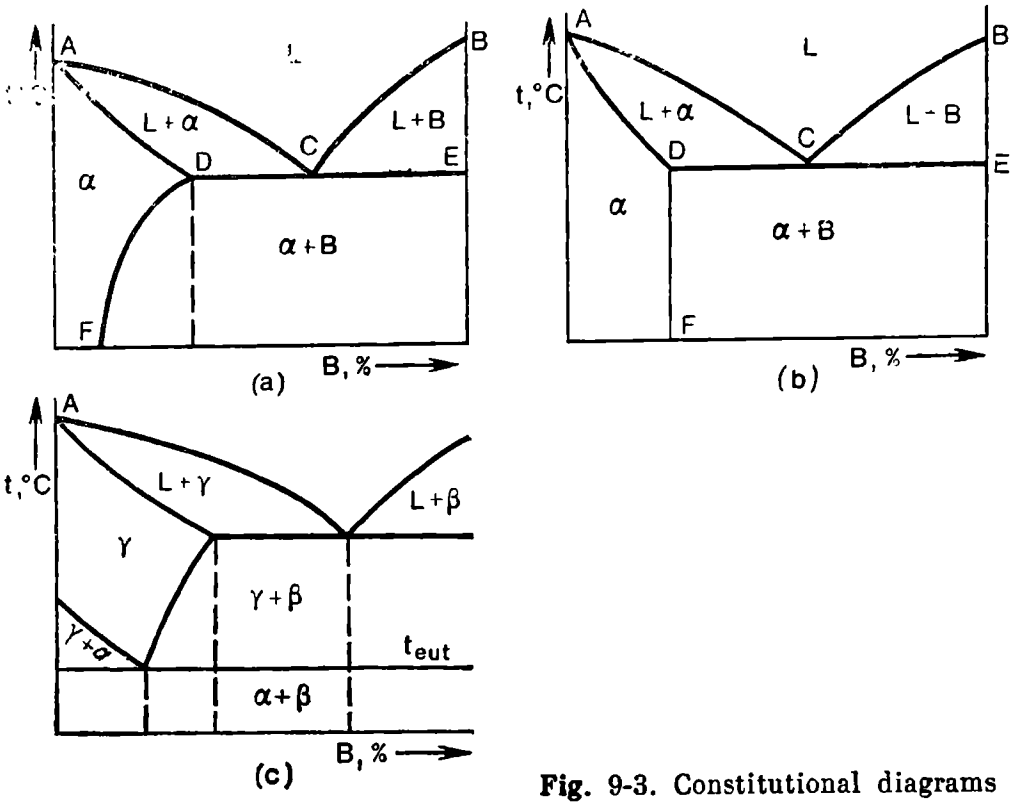

Fig. 9-3. Constitutional diagrams

The procedures of the second, third and fourth groups require that phase transformations in the solid state should occur in the metal, i.e. heating should either cause substantial changes in the solubility or induce allotropic transformations.

All alloys to the left of point *F* (Fig. 9-3*a*) undergo no transformations in the solid state and, therefore, cannot be heat treated by the procedures of the second, third or fourth group[1]. On the other hand, the dissolution of an excess phase *B* in α-solid solution in this case takes place on heating in all alloys to the right of point *F*, so that hardening can fix the supersaturated solid solution (the third group of heat treatment) and the subsequent heating can cause precipitation of the excess phase (the fourth group of heat treatment).

---

[1] This is not quite correct according to modern views. For instance, a change in temperature can cause changes in the number of vacancies and the dislocation structure in a pure metal or in a solid solution undergoing to transformations. Hardening of this alloy can fix at a low temperature the state with an elevated quantity of vacancies, which is typical of the high-temperature state. This will actually be a hardening process, though the constitutional diagram shows no changes with increasing temperature. In that case there will be no noticeable microstructural changes and the properties of the metal will be changed not so radically as upon a process with microstructural changes.

Note that all alloys between points F and D can fully dissolve the excess B-phase and form a homogeneous α solution on heating. Thus, their whole structure will participate in heat treatment. For alloys to the right of point D, a portion of the B-phase remains undissolved on heating and does not participate in heat treatment. The effect of heat treatment will be most pronounced in the alloy of the concentration at point D.

Though the constitutional diagrams in Fig. 9-3*a* and *b* are very similar, no alloy in the latter system can be subjected to second-order annealing, hardening or tempering. In the diagram of Fig. 9-3*b*, line DF passes vertically, which means that the solubility does not change with temperature, therefore, all alloys of this system undergo no phase transformations.

All alloys crystallizing to the constitutional diagram of Fig. 9-3*c* can be heat treated by the procedures of the second, third and fourth groups. All these alloys consist of $\alpha + \beta$ phases at room temperature. At a temperature of t_{eut}, α- and β-phases change to γ-phase. The subsequent cooling determines the type of heat treatment: either annealing (slow cooling) or hardening (quick cooling). Heat treatment by the second and third groups is only possible on heating above the temperature of structural recrystallization, t_{eut}, and the formation of γ-solid solution.

For chemical heat treatment, it is essential that the diffusing elements be soluble in the metal, i.e. the saturated B component and metal A being saturated form a system of alloys with a region of a sufficient solubility of B in A. Alloys of the systems shown in the constitutional diagrams in Fig. 9-3*a* and *b* have the solid solution region at the A-rich end of the diagram, and therefore, chemical heat treatment consisting in the saturation of metal A with component B is possible. For alloys of the system shown in Fig. 9-3*c*, the diffusion of B in A is possible only above t_{eut}, i.e. when component A exists in the system in its high-temperature γ-modification. Below t_{eut}, the A component exists as α-modification which does not dissolve B, and surface saturation through diffusion of B in A is impossible.

Thermomechanical treatment is evidently possible if an alloy has a sufficient plasticity.

9-4. PRINCIPAL TYPES OF HEAT TREATMENT OF STEEL

Since the constitutional diagram is the basis for an analysis of heat treatment of alloys, it is natural that the iron-carbon constitutional diagram is the basis for analysis of heat treatment of steels. As we deal with steels, i.e. alloys with carbon concentration up to 2 per cent (more accurately, up to 2.14 per cent), we shall be interested in that portion of the diagram which extends to 2.14 per cent carbon.

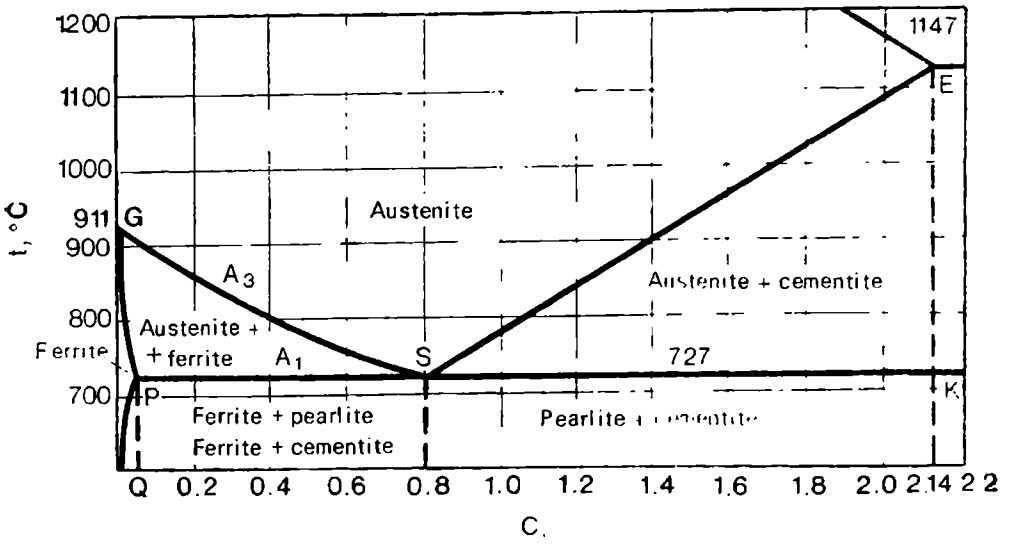

Fig. 9-4. The 'steel' portion of the Fe-C constitutional diagram

The upper temperature limit for heat treatment is the solidus line, therefore, the processes of primary crystallization and the upper portion of the diagram will be of no interest to us in this case.

The portion of the iron-carbon diagram, that will be discussed, is shown in Fig. 9-4.

The critical points in this diagram are designated by A with a subscript.

The lower critical point, A_1, lies on the line PSK and corresponds to austenite $\rightleftarrows$ pearlite transformation. The upper critical point. A_3, is on the line GSE and determines the beginning of precipitation or the end of dissolution of ferrite in hypoeutectoid steels or cementite (secondary) in hypereutectoid steels.

To distinguish between a critical point in heating and that in cooling, the letter c is put in the former case and r in the latter.

Thus, the critical point of the transformation of austenite into pearlite is denoted Ar_1 and that of pearlite into austenite, Ac_1; the beginning of precipitation of ferrite from austenite is denoted Ar_3; the end of dissolution of ferrite in austenite, Ac_3. The beginning of precipitation of secondary cementite from austenite is also denoted as Ar_3, and the end of dissolution of secondary cementite in austenite, Ac_3 (or often as A_{cm}).

The principal types of heat treatment, as given in Sec. 9-2, can be described in the constitutional diagram in the following manner.

Annealing is a structural recrystallization consisting in heating above Ac_3 and subsequent slow cooling. With heating above Ac_1 but below Ac_3, full recrystallization will not occur and the procedure is called *partial annealing*. The state of annealed steel is close to the

state of structural equilibrium and its structure is pearlite + ferrite, pearlite, or pearlite + cementite.

If a steel is heated above Ac_3 and then cooled in air, this will be the first step to change it to a state farther from the structural equilibrium. This type of heat treatment is called *normalizing* and is an intermediate stage between the second-group procedure (annealing) and the third-group procedure (hardening).

Hardening is heating above the critical point, Ac_3, followed by quick cooling. With slow cooling, austenite decomposes into ferrite — cementite at Ar_1. With increasing cooling rate, the transformation occurs at lower temperatures. As the Ar_1 point is lowered, the ferrite-cementite mixture becomes more and more fine-disperse and hard. If the cooling rate is so high and the undercooling so substantial that the precipitation of cementite and ferrite does not take place, there will be no decomposition of the solid solution and austenite (γ-solid solution) will transform into *martensite* (supersaturated solid solution of carbon in α-iron). *Incomplete hardening* is a heat treatment procedure with heating the metal above Ac_1 but below Ac_3, after which the steel structure retains hypoeutectoid ferrite (hypereutectoid cementite).

Tempering is heating a hardened steel to a temperature below Ac_1.

Steels can be subjected to various types of *chemical heat treatment*, depending on the element that diffuses in steel.

The saturation of steel in carbon is called *carburizing*, in nitrogen, *nitriding*, in aluminium, *alitizing*, in chromium, *chromizing*, etc.

Thermomechanical treatment of steel consists in heating the metal to austenitic state, deforming in that state (above Ac_3 in stable state or in unstable undercooled state) and final cooling which is associated with the transformation of the strain-hardened austenite.

9-5. FOUR PRINCIPAL TRANSFORMATIONS IN STEEL

We have seen in the analysis of crystallization (Ch. 2) that this process takes place because one state, say, crystalline, under changed conditions, is more stable than another state, say, liquid.

Phase transformations which occur in steel are also associated with changes in the conditions (for instance, temperature) resulting in that one state turns out to be less stable than the other one.

Before analysing the structural transformations in steel, it should be noted that three types of structure are principal ones and the changes from one to another characterize the basic transformations.

These structures are as follows:

austenite (A), a solid solution of carbon in γ-iron, $Fe_\gamma(C)$;

martensite (M), a solid solution of carbon in α-iron, $Fe_\alpha(C)$;

pearlite (P), a eutectoid mixture of ferrite and carbide which form simultaneously, $Fe_\alpha + Fe_3C$ (the equilibrium solubility of carbon in ferrite is neglected).

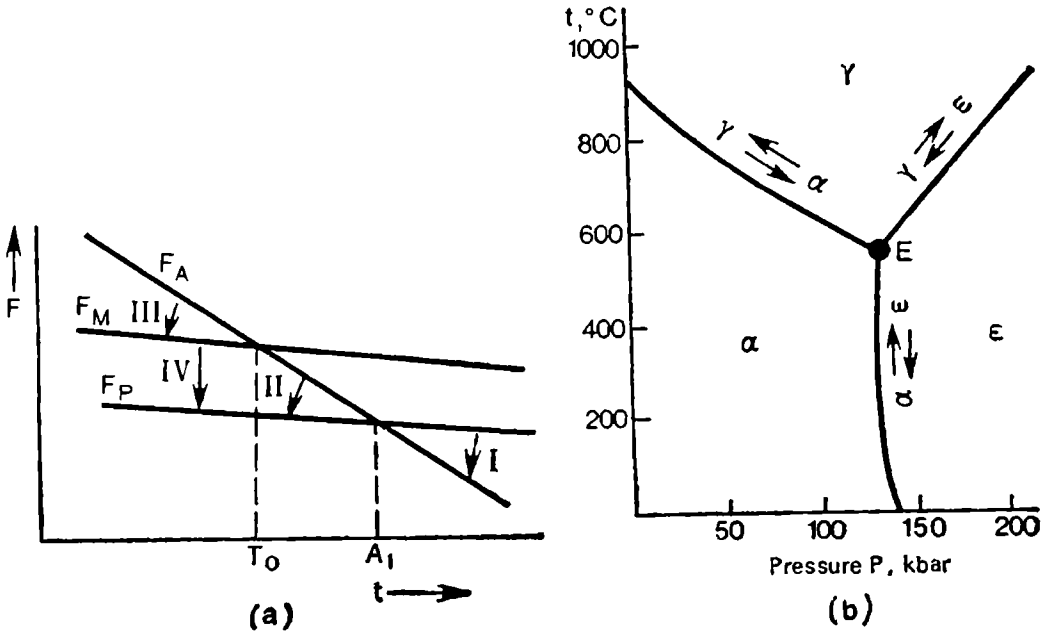

Fig. 9-5. (*a*) Changes in free energy of austenite (F_A), martensite (F_M), and pearlite (F_P) with temperature variations; (*b*) the regions of α-, γ- and ε-iron depending on temperature and pressure

There are four principal types of transformation that occur in heat treatment of steel.

1. The pearlite-to-austenite transformation which occurs above A_1, i.e. above the point of stable equilibrium between austenite and pearlite; at these temperatures, austenite has the least free energy (Fig. 9-5) among the three principal steel structures:

$$Fe_\alpha + Fe_3C \rightarrow Fe_\gamma(C) \quad \text{or} \quad P \rightarrow A$$

2. The austenite-to-pearlite transformation which takes place below A_1:

$$Fe_\gamma(C) \rightarrow Fe_\alpha + Fe_3C \quad \text{or} \quad A \rightarrow P$$

3. The austenite-to-martensite transformation:

$$Fe_\gamma(C) \rightarrow Fe_\alpha(C) \quad \text{or} \quad A \rightarrow M$$

This transformation takes place below the point of metastable austenite-martensite equilibrium (T_0). At this temperature, pearlite is a more stable phase, but the work to transform austenite into martensite is less than that required to form pearlite; for that reason the formation of pearlite (ferrite-carbide mixture) at temperatures below T_0 cannot occur directly, but only by passing through the intermediate stage of austenite-to-martensite transformation.

4. The transformation of martensite into pearlite, more strictly, into a ferrite-carbide mixture:

$$Fe_\alpha(C) \rightarrow Fe_\alpha + Fe_3C \quad \text{or} \quad M \rightarrow P$$

It takes place at any temperature, since the free energy of martensite is always greater than that of pearlite.

A diagram of variations of free energies of the principal steel structures (see Fig. 9-5) shows that the transformation of martensite into austenite is possible above T_0. This transformation has not been, however, discovered experimentally, probably owing to the decomposition of martensite (the martensite-to-pearlite transformation takes place instead).

The transformation of pearlite into austenite is impossible since the free energy of martensite is higher than that of pearlite at all temperatures.

We have discussed the phase transformations which are utilized in heat treatment and are due to temperature changes. Another thermodynamic factor that can be used in heat treatment is pressure. By varying the pressure, it is possible to induce structural transformations which are unfeasible at a constant pressure (1 at).

A diagram of structural equilibrium at independent variables—temperature and pressure—is given in Fig. 9-5*b*. As may be seen, h.c.p. iron (what is called ε-iron) can be formed at a high pressure. The ternary equilibrium point lies at $t = 527°C$ and $P = 130$ kbar. The $\alpha \rightarrow \gamma \rightarrow \varepsilon$ change is possible above the line of 527°C and the $\alpha \rightarrow \varepsilon$ change, below that line.

As has been noted, uniform compression involves technological difficulties and so far is not used for the purpose of structure formation in steels; it is also unclear whether it can be effective for obtaining steels with special properties. Some alloying elements act in the same sense as uniform compression. For instance, the ε-phase can form at normal pressures in steels heavily alloyed with manganese.

LITERATURE

Bochvar A. A., *Fundamentals of Heat Treatment of Alloys.* Moscow-Leningrad, "Metallurgizdat", 1940 (in Russian).

Steinberg S. S., *Heat Treatment of Steel.* Sverdlovsk-Moscow, "Metallurgizdat", 1945 (in Russian).

Gulyaev A. P., *Heat Treatment of Steel.* Moscow, "Mashgiz", 1960 (in Russian).

Novikov I. I., *Theory of Heat Treatment of Metals.* Moscow, "Metallurgiya" 1974 (in Russian); English translation: Mir Publishers, Moscow, 1978.

Lysak L. I., Nikolin B. I., *Physical Principles of Heat Treatment of Steel.* Kiev, "Technika", 1975 (in Russian).

Chapter 10

THE THEORY OF HEAT TREATMENT OF STEEL

Theoretical study of heat treatment of steel was initiated by the discovery of the critical points in steel made by D. K. Chernov in 1868.

Chernov's assumption that the properties of steels are determined by the structure and that the latter depends on the heating temperature and rate of cooling has been generally recognized. During the decades which followed the researchers were engaged in establishing the relationships between the structure and the conditions of its formation (mainly the heating temperature and cooling rate).

The principal achievements in the theory of heat treatment were, however, made in 1920's and 1930's.

Metallurgists have gradually come to the conclusion that the type of structure (its texture, properties, etc.) is determined by the temperature of its formation. It has become clear that the processes occurring in heat treatment can be explained by studying the kinetics of transformations at various temperatures and the factors affecting the kinetics.

These concepts formed the basis of extensive experimental work undertaken by S. S. Steinberg and co-workers in 1930-40. They collected a vast experimental material which upon generalization, has constituted the basis of the modern concepts on transformations in steel and the theory of heat treatment of steel.

Studies in the same direction were started by many researchers in other countries at the same time or somewhat later. Among the pioneers in this field, the names of R. F. Mehl and E. C. Bain (USA), and F. Wever, H. Esser, and H. Hannemann (Germany) should be mentioned first; they carried out numerous and detailed studies into the kinetics of transformations in various steels.

The nature of hardened steel could only be examined by using X-rays and other methods of physical analysis of metals (electron microscopy, internal friction, etc.).

Numerous works of G. V. Kurdyumov and his followers, and also of a number of foreign metallophysicists have revealed important peculiarities in the fine structure of steel.

The theory of heat treatment of steel is understood as the analysis of the processes of structure formation (on transformations) and the particularities of structural state of alloys (in non-equilibrium).

This chapter will deal with the theory of heat treatment of steel, based on the general theory of phase transformations in undercooled systems, which have been briefly discussed in Sec. 5-10. The reader is advised to recall that material before going further.

10-1. FORMATION OF AUSTENITE

The transformation of pearlite into austenite can only take place on a very slow heating, as follows from the Fe-C constitutional diagram. Under common heating conditions, the transformation is retarded and results in overheating, i.e. occurs at temperatures slightly higher than those indicated in the Fe-C diagram.

When overheated above the critical point, pearlite transforms into austenite, the rate of transformation being dependent on the degree of overheating.

Figure 10-1 shows the time of transformation at various temperatures (depending on the degree of overheating). The form of the curves shows that the transformation takes place faster (in a shorter time) at a higher temperature and occurs at a higher temperature on a quicker heating.

For instance, on quick heating and holding at 780°C, the pearlite-to-austenite transformation is completed in 2 minutes and on holding at 740°C, in 8 minutes.

The diagram in Fig. 10-1 is plotted in time-temperature coordinates and, therefore, heating curves can be drawn on it[1].

A pensil in the figure corresponds to the heating of steel at a definite rate, say v_2. It intersects the lines of the beginning and end of transformation in points a'' and b''. Therefore, with continuous heating at a rate of v_2, we shall fix the transformation occurring in the temperature interval from point a'' to b''. With slower heating, say, at a rate of v_1, the curves will be intersected at lower temperatures (points a'

[1] As has been proved, the superposition of heating or cooling curves on the diagram of transformations at constant temperature cannot give accurate quantitative relationships, but may be useful for qualitative analysis of the processes. The method will be widely used in the further discussion.

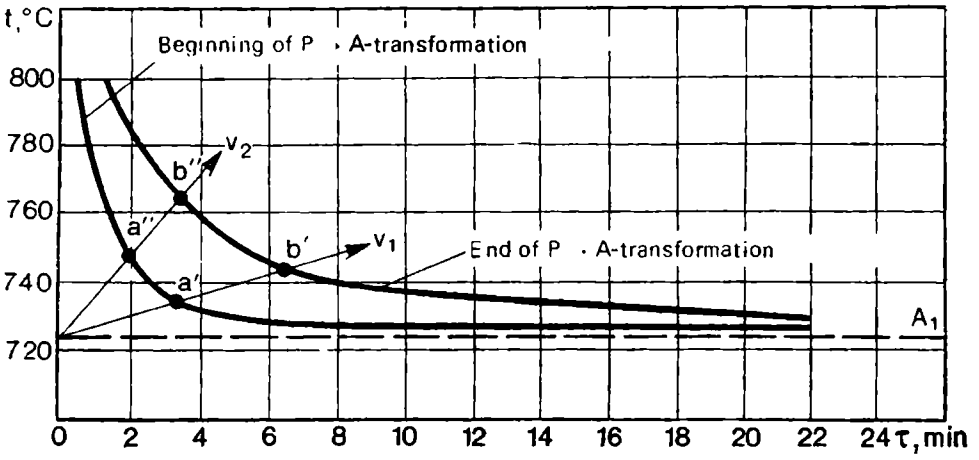

Fig. 10-1. Transformation of pearlite (P) into austenite (A) at constant temperature. Steel with 0.86% C (I. L. Mirkin and M. E. Blanter)

and b') and the transformation will also take place at lower temperatures.

Irrespective of the heating rate, the transformation occurs immediately after the passage through the equilibrium critical point A_1; the temperature interval between a' and b' or between a'' and b'' on heating with a rate of v_1 or v_2 determines not the physical beginning and end of the transformation, but the temperature interval within which the main mass of pearlite changes to austenite. Points a and b are practically determined as the points at which the content of the new (or respectively of the old) phase is 5 (or 1) per cent.

The curves of the beginning and end of transformation asymptotically approach the horizontal line A_1. With heating at an infinitely slow rate, the curves of the beginning and end of the transformation will merge and intersect the horizontal line A_1 in infinity (after an infinitely long time) and the pearlite-to-austenite transformation will occur at a single 'point', i.e. at a constant temperature. This evidently would be the case of equilibrium transformation in the Fe-C constitutional diagram. Unlike equilibrium transformations, real transformations occur at temperatures above A_1 and within a temperature interval, rather than at a fixed constant temperature, this temperature interval lying higher at a higher heating rate.

The end of the transformation is characterized by the formation of austenite and disappearance of pearlite (ferrite + cementite). This austenite is however inhomogeneous even in the volume of a single grain. In places earlier occupied by lamellae (or grains) of pearlitic cementite the content of carbon is greater than in places of ferritic lamellae. This is why the austenite just formed is inhomogeneous.

In order to obtain homogeneous austenite, it is essential in heating not only to pass through the point of the end of pearlite-to-austenite transformation, but also to overheat the steel above that point and to allow a holding time to complete the diffusion processes in austenitic grains.

The rate of homogenization of austenite appreciably depends on the original structure of the steel, in particular on the dispersity and particle shape of cementite. The transformations described occur more quickly when cementite particles are fine and, therefore, have a large total surface area.

10-2. COARSENING OF AUSTENITIC GRAIN

At the beginning of pearlite-to-austenite transformation, the first grains of austenite form at the boundaries between the ferrite and cementite—the two structural constituents of pearlite. Since these

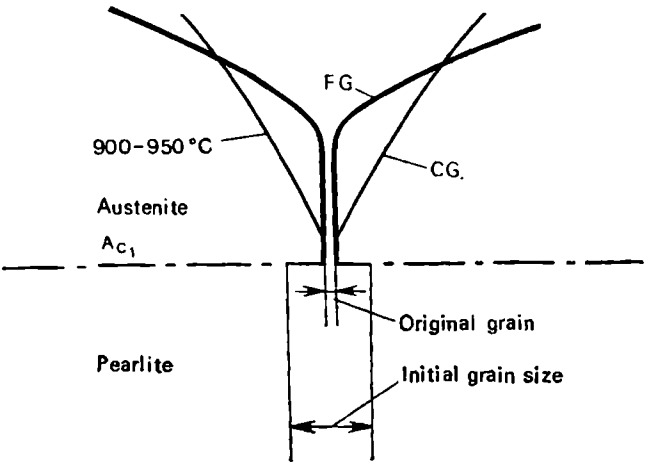

Fig. 10-2. Grain coarsening in inherently coarse-grained (*CG*) and inherently fine-grained (*FG*) steel

boundaries are very developed[1], the transformation starts from formation of a multitude of fine grains. Therefore, at the end of the transformation the austenite will be composed of a great multitude of fine grains whose size characterizes what is called the *original austenitic grain* size.

Further heating (or holding) upon the transformation will cause coarsening of austenitic grains. The process of grain coarsening is spontaneous, since the total surface area of grains diminishes (the surface energy decreases) and a high temperature can only accelerate the rate of this process.

In that connection, two types of steel are distinguished: *inherent fine-grained* and *inherent coarse-grained*, the former being less liable to grain coarsening than the latter.

Figure 10-2 shows how the size of grain varies in these two types of steel which differ from each other in the kinetics of grain coarsening.

The transition through the critical point A_1 is associated with an abrupt refinement of grain. Austenitic grains in fine-grained steel do not grow on subsequent heating up to 950-1 000°C; above that temperature, the factors that prevent grain coarsening are eliminated and the grains rapidly grow in size. In coarse-grained steel, the factors that might prevent grain coarsening are inactive and the process of grain coarsening begins immediately after the transit through the critical point.

As may be seen from Fig. 10-2, the size of grain in inherent fine-grained steel is smaller at temperatures slightly above the critical point (Ac_1), but may be larger at higher temperatures. Therefore, the size of grain in a given piece of metal is not indicative of the inherent grain size.

[1] The area of ferrite-cementite boundaries in 1 cm^3 of pearlite is a few square metres.

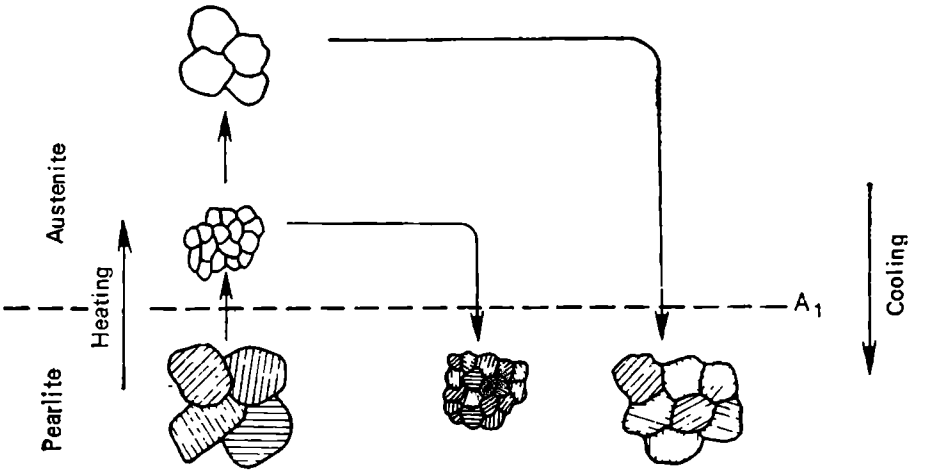

Fig. 10-3. Variations in grain size of pearlite depending on heating in the austenitic range

The size of grains formed in a steel by heat treatment is called the *actual grain size.*

Thus, a distinction should be made between:

(1) original grain, i.e. the size of austenitic grains immediately after the pearlite-to-austenite transformation;

(2) inherent (natural) grain, i.e. the liability of austenite to grain coarsening; and

(3) actual grain, i.e. the size of austenitic grains under the given particular conditions.

The size of pearlitic grains at the same temperature of the austenite-to-pearlite transformation depends on that of the austenitic grains from which they have formed (Fig. 10-3). Austenitic grains grow only during heating (but are not refined in subsequent cooling), because of which the highest temperature a steel is heated to in the austenitic state and the inherent grain size of that steel determine the final grain size.

In the diagrams of Figs. 10-2 and 10-3, pearlitic grains have the same size as the original austenitic grains. This, however, is not quite correct. Pearlite originates at the boundaries of austenitic grains and, evidently, the smaller the austenitic grains, the smaller the pearlitic grains will be. It would be wrong to think, however, that one austenitic grain gives birth to one grain of pearlite; actually, several grains of pearlite may form from one austenitic grain.

The diagrams in Figs. 10-2 and 10-3 describe the most typical cases, but there are some less typical cases which will be briefly discussed below.

If the original steel structure is martensite or bainite, the transformation into austenite will involve no grain refinement (unlike the case in Figs. 10-2 and 10-3), and austenitic grains grow to the same size they had prior to hardening, that is, prior to the austenite-martensitic or austenite-bainitic transformation (Fig. 10-4). This fact can be explained as follows.

With the diffusion mechanism of the austenite-pearlitic transformation, crystals of the new phases displace the structure defects to grain boundaries; in other words, the defects (dislocations, vacancies, impurity atoms) which

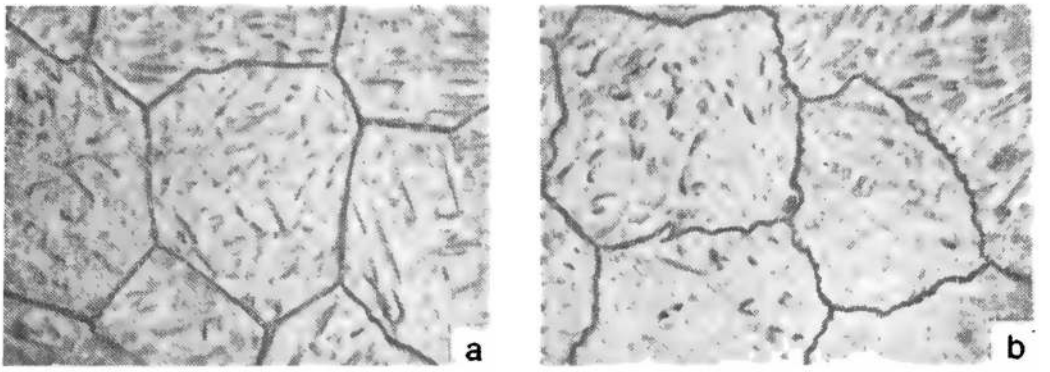

Fig. 10-4. Retention of inherent granularity in hardened steel, ×150 (V. D. Sadovsky)

(*a*) coarse grains of austenite grown by high-temperature heating (at 1 300°C); (*b*) coarse grains of austenite upon reheating at 900°C (no grain-refining effect)

were located at the boundaries of austenitic grains are redistributed at the boundaries of ferritic (pearlitic) grains.

With the martensitic (bainitic) transformation, there is no redistribution of structure defects; they remain in the places they have occupied in the austenite. Fine weakly misoriented austenitic grains that form on the transition through the critical point A_1 have no protective defect layers at their boundaries and are quickly combined into larger grains whose shape and size are predetermined by he prior position of boundary defects; in other words, the former austenitic rains are restored.

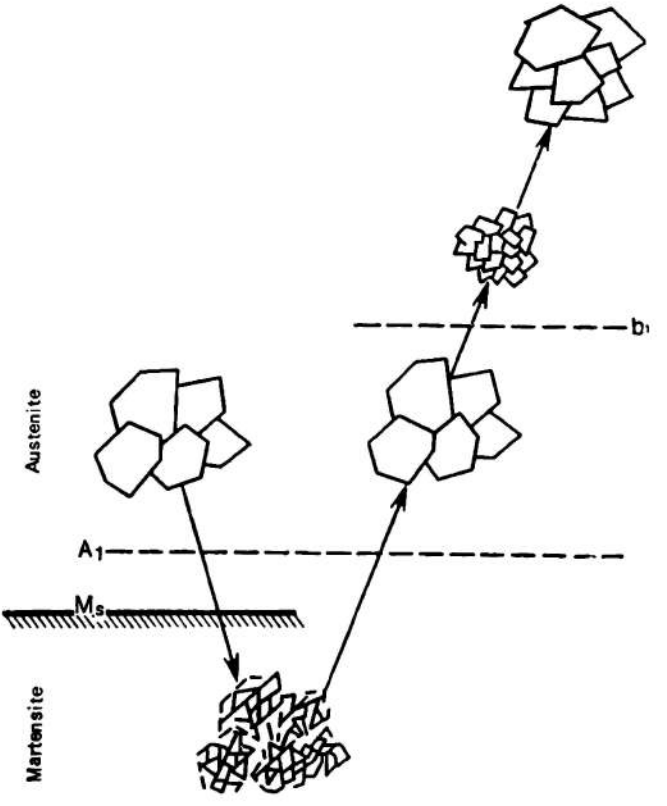

Fig. 10-5. Formation of austenite from the original martensitic (bainitic) structure

A remarkable feature of this austenitic grain is its instability. It can refine abruptly on heating to a higher temperature (Fig. 10-5). This phenomenon was discovered in 1940's by V. D. Sadovsky and co-workers and studied later in more detail. By Sadovsky's view, the martensite-austenitic transformation occurs by a different mechanism (not that of the pearlite-austenitic transformation) and produces the strain-hardening effect (called *structural strain hardening*). The formation of new grains on subsequent heating is the natural process of recrystallization of austenite.

In many cases it is essential to determine the size of prior grains (existed at a higher temperature) of austenite in a different type of steel structure, since this size determines many properties of the steel, especially in the state as-hardened.

There are many methods for determining the size of prior austenitic grains.

The boundaries of austenitic grains can be fixed by various methods: slow cooling which promotes precipitation of excess phases (ferrite, cementite, etc.) at these boundaries; long heating during which oxygen can penetrate inside at grain boundaries and form oxide networks; special methods of etching of martensite; vacuum etching at high temperature which reveals the grain boundaries only.

The actual grain size is determined by measuring the average grain size in a specimen and comparing it with standard scales.

As has been noted, the tendency of austenite to coarsening determines the inherent grain size of steel. To define the size, it is, therefore, essential to know how grain size varies with temperature. In practice, however, it is more convenient to determine the inherent grain size (by checking against standard grain size scales, Fig. 10-6*a*) at a temperature when the grains still do not begin to grow in inherently fine-grained steel (see Fig. 10-2) but have already grown in inherently coarse-grained steel. For common grades of structural steel, this temperature is 930°C. Steels having a grain size index of 1 to 4 at this temperature are considered to be inherently fine-grained and those with an index of 5 to 8, inherently coarse-grained.

The conditional grain size index actually characterizes the average size of grains or the number of grains per mm^2 of the surface of a microsection. For instance, at a grain size index of 6, the average size of grain is 45 μm and 1 mm^2 of the surface contains 500 grains (Fig. 10-6*b*).

Naturally, the tendency to grain coarsening (inherent grain size) depends on the steel composition. Hypereutectoid steels are, as a rule, less sensitive to grain coarsening on heating than eutectoid grades. Many alloying elements added to steel (vanadium, titanium, tungsten, molybdenum, etc.) suppress the tendency to grain coarsening. It has been established, however, that various melts of the same steel grade may have different capacity to grain coarsening, i.e. have different inherent grain size. Here, the process of making steel and the deoxidation method are of importance.

Steels deoxidized only with ferromanganese (rimming steel) or with ferromanganese and ferrosilicon are inherently coarse-grained, while those additionally deoxidized with aluminium are fine-grained.

The most trustworthy explanation to the nature of fine-grained structure can be given by the so-called *theory of barriers*. When added to molten steel shortly before teeming, aluminium combines with the dissolved nitrogen and oxygen into nitrides and oxides (AlN, Al_2O_3). These compounds are soluble in molten steel and precipitate on crystallization and subsequent cooling as finest submicroscopic particles ('non-metallic dust') which are arranged mostly at grain boundaries thus inhibiting grain coarsening.

At a definite temperature, intensive grain coarsening begins even in fine-grained steels (see Fig. 10-2). As has been found experimentally, at high temperatures aluminium nitrides are dissolved in the surface layers of austenitic grains. The barriers that inhibit grain coarsening in austenite are removed and the grain starts growing.

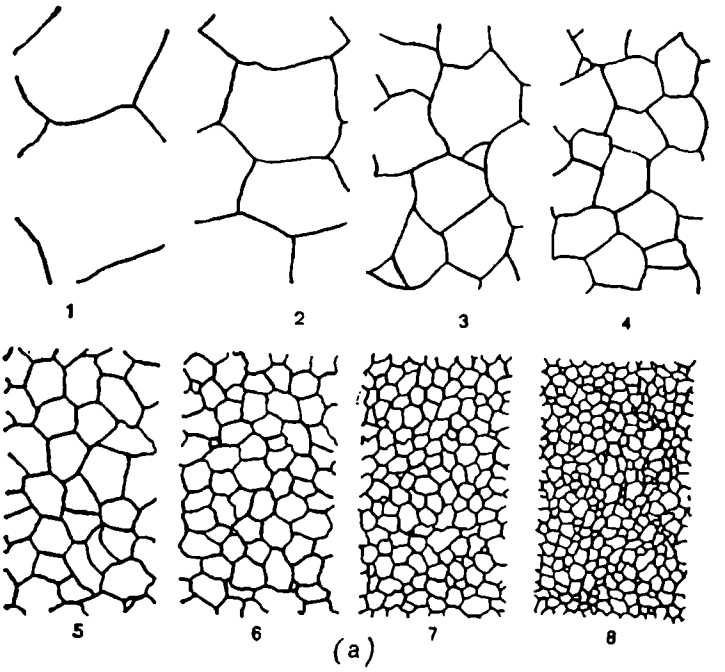

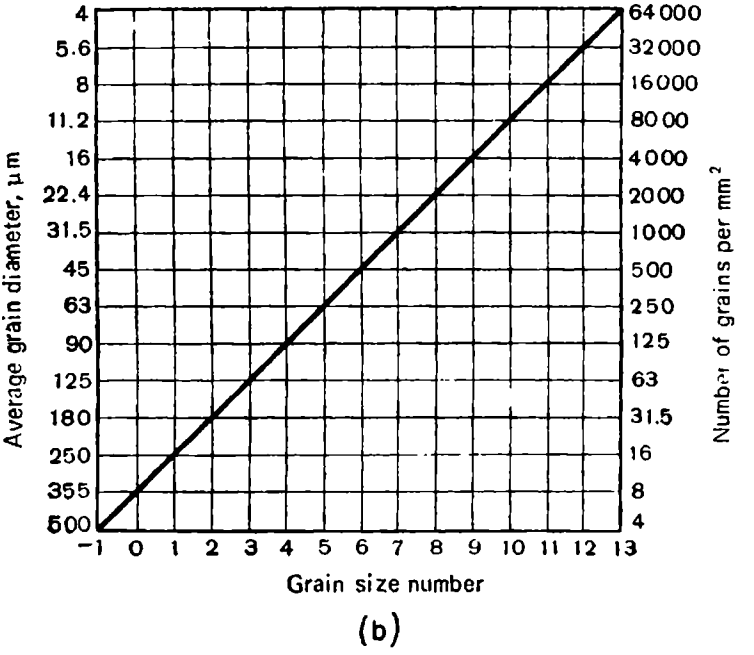

Fig. 10-6. (*a*) Grain-size scales, ×100 and (*b*) nomogram for determining grain size

The properties of a steel are affected only by the actual grain size and not by the inherent grain size. If two steels of the same

grade (one inherently coarse-grained and the other, fine-grained) have the same actual grain size upon heat treatment at different temperatures, their properties will also be the same; if otherwise, many properties of the two steels will also be different.

Coarsening of austenitic grain in steels has almost no effect on the statistic characteristics of mechanical properties (hardness, rupture resistance, yield limit, elongation), but can appreciably reduce the impact toughness, especially at a high hardness (low-temperature tempering). This is due to the fact that grain coarsening raises the ductile-to-brittle transition temperature.

Whereas the actual grain size affects the properties of steel, the inherent grain size is decisive for the processes of hot working.

Inherently fine-grained steel is insensitive to overheating, i.e. intensive grain coarsening begins at appreciably higher temperatures than in a coarse-grained steel. For that reason, the temperature interval of hardening for the former is substantially wider than for the latter.

Inherently fine-grained steel can be rolled (or forged) at higher temperatures and the process (rolling or forging) can be finished at a higher temperature without danger of forming a coarse-grained structure. As a rule, all grades of killed steel are made inherently fine-grained and all rimming steels, inherently coarse-grained.

10-3. DECOMPOSITION OF AUSTENITE

The austenite-to-pearlite transformation is essentially the decomposition of austenite (solid solution of carbon in γ-iron) into almost pure α-iron and cementite:

$$Fe_\gamma (C) \rightarrow Fe_\alpha + Fe_3C$$

At the equilibrium temperature A_1, the transformation is impossible, since the free energy of the original austenite is equal to that of the final product, pearlite.

The transformation can only start at a certain undercooling when the free energy of the ferrite-carbide mixture (pearlite) is lower than that of austenite (see Fig. 9-5).

The lower the transformation temperature, the higher the degree of undercooling and the greater the difference in free energies and the transformation proceeds at a higher rate.

In the pearlitic transformation, the new phases sharply differ in their composition from the initial phase; they are ferrite which is almost free of carbon, and cementite which contains 6.67 per cent C. For that reason the austenite-to-pearlite transformation is accompanied with the diffusion, redistribution of carbon. The rate of diffusion sharply diminishes with decreasing temperature, there-

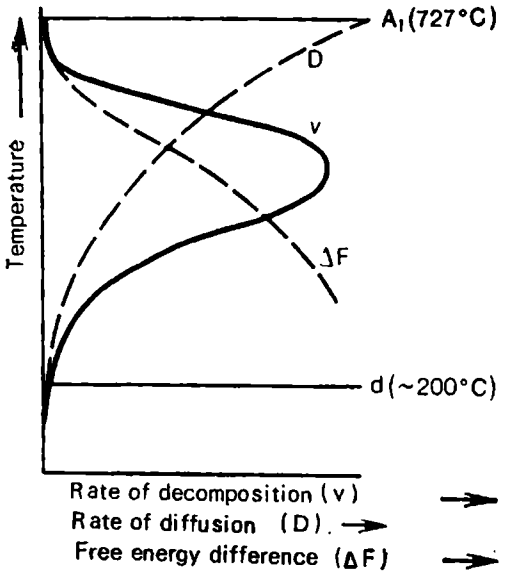

Fig. 10-7. Rate of decomposition of austenite (solid line) depending on degree of undercooling (temperature)

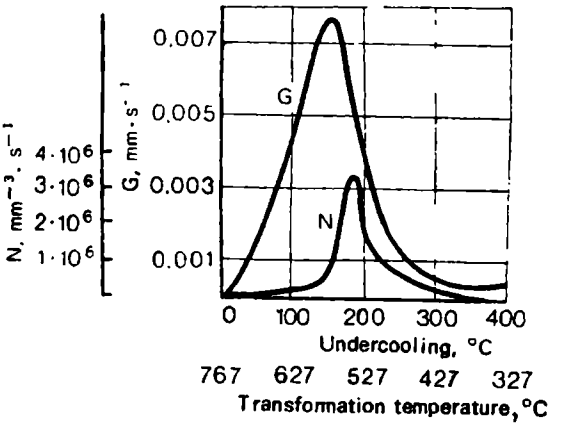

Fig. 10-8. Rate of nucleation (N) and crystal growth (G) of pearlite depending on temperature (degree of undercooling) (I. L. Mirkin)

fore, the transformation should be retarded at a greater undercooling.

Thus, we have come to an important conclusion that undercooling (lowering the transformation temperature) may have two opposite effects on the rate of transformation.

On the one hand, a lower temperature (greater undercooling) gives a greater difference in free energies of austenite and pearlite ($\Delta F = F_A - F_P$), thus accelerating the transformation; on the other hand, it diminishes the rate of carbon diffusion, D, and thus slows down the transformation (Fig. 10-7). The combined effect is that the rate of transformation first increases as undercooling is increased to a certain maximum and then decreases with further undercooling (solid line in Fig. 10-7).

At 727°C (A_1) and below 200°C (d), the rate of transformation is zero, since at 727°C the free energy difference is zero and below 200°C the rate of carbon diffusion is zero (more strictly, too low for the transformation to proceed).

As has been first indicated by I. L. Mirkin in 1939 and then developed by R. F. Mehl (1941), the formation of pearlite is the process of nucleation of pearlite and growth of pearlitic crystals.

Therefore, the different rate of the pearlitic transformation at various degrees of undercooling is due to the fact that undercooling differently affects the rate of nucleation, N, and the rate of crystal growth, G, (Fig. 10-8). At point A_1 and below 200°C, both para-

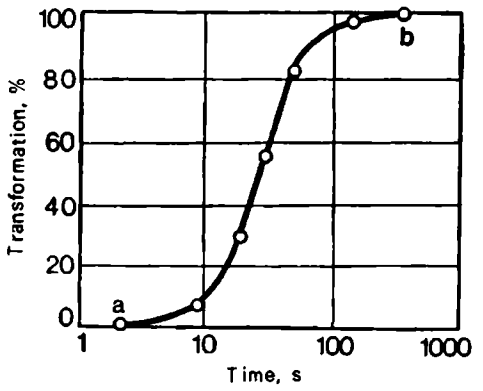

Fig. 10-9. Kinetic curve of austenite-to-pearlite transformation

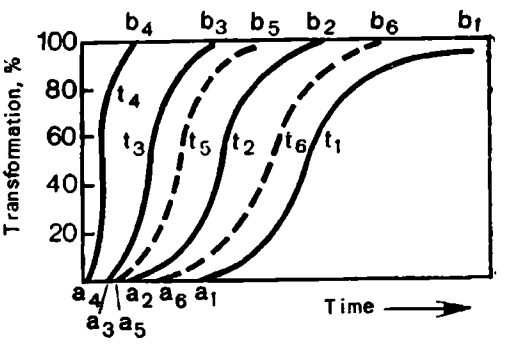

Fig. 10-10. Kinetic curves of austenite-to-pearlite transformation at various temperatures ($t_1 > t_2 > t_3 \ldots$)

meters of crystallization, N and G, are equal to zero and have a maximum at an undercooling of 150-200°C.

It follows from the foregoing that as soon as the conditions are favourable, i.e. austenite is undercooled below A_1, therefore, $F_P < < F_A$ and the diffusion of carbon is not zero, centres of crystallization appear, which give rise to crystals. This process occurs with time and can be represented in the form of so-called kinetic curve of transformation, which shows the quantity of pearlite that has formed during the time elapsed from the beginning of the transformation (Fig. 10-9).

The initial stage is characterized by a very low rate of transformation; this is what is called the *incubation period.* Point *a* of the curve marks the moment when the beginning of the transformation is detected (usually this corresponds to the formation of 1 per cent pearlite). The rate of transformation increases with the progress in the transformation. Its maximum approximately corresponds to the moment when roughly 50 per cent of austenite has transformed into pearlite. The rate of transformation then diminishes and the transformation stops at point *b*.

The rate of transformation depends on undercooling. At low and high degrees of undercooling the transformation proceeds slowly, since N and G are low (see Fig. 10-8); in the former case, owing to a low difference in free energies, and in the latter, due to a low diffusion mobility of atoms. At the maximum rate of transformation the kinetic curves have sharp peaks, and the transformation is finished in a short time interval.

Figure 10-10 shows a series of kinetic curves similar to that in Fig. 10-9 but related to different temperatures (different degrees of undercooling).

At a high temperature, t_1 (slight undercooling), the transformation proceeds slowly and the time of the incubation period (from

the origin of coordinates to point *a*) and the time of the transformation proper (from the origin of coordinates to point *b*) are long. At a lower temperature of the transformation, i.e. a deeper undercooling, the rate of transformation is greater, and the time of the incubation period and of the transformation is shorter. The rate of transformation is at its maximum at temperature t_4 and again decreases at lower temperatures.

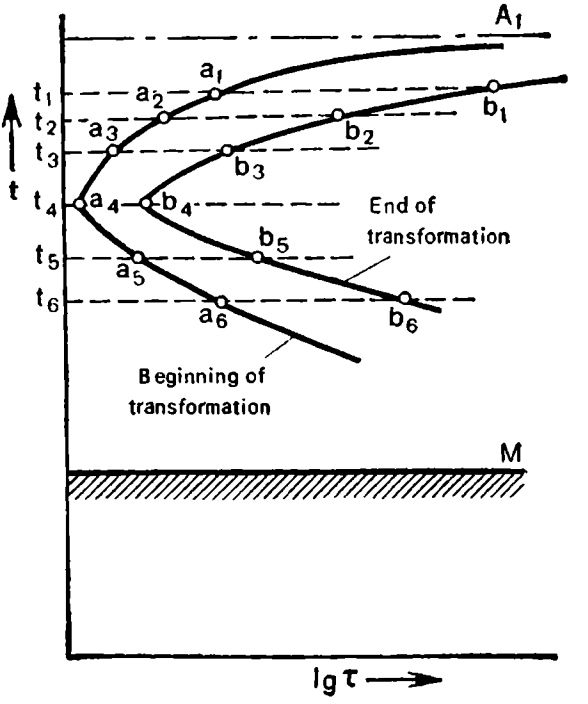

Fig. 10-11. TTT-diagram of austenite-to-pearlite transformation obtained from the kinetic curves in Fig. 10-10

Having determined the time of the beginning of austenite-to-pearlite transformation (incubation period) and the time of the end of transformation at various degrees of undercooling, we can construct a diagram like that shown in Fig. 10-11. The left-hand curve (*a* curve) determines the time of the beginning of the transformation, i.e. the time during which austenite still exists in the undercooled state, and the section arom the axis of ordinates to the *a* curve is the measure of its finstability. This section is the shortest at a temperature of 500-600°C (t_4), i.e. the transformation begins in a shortest time at that temperature.

The right-hand curve (*b* curve) shows the time needed to complete the transformation at a given degree of undercooling. As is seen, this time is the shortest at the same temperature t_4 (500-600°C).

Note that the abscissa of the diagram is logarithmic (log τ). This is done for more convenience, since the rates of formation of pearlite appreciably differ (thousands of seconds near the critical point A_1 and only one or two seconds at the bend of the curve).

The horizontal line *M* in the diagram determines the temperature of the diffusionless martensitic transformation. The martensitic transformation occurs by a different mechanism and will be discussed in the next section.

The diagram in Fig. 10-11 gives the time of austenite-to-pearlite transformation for a given degree of undercooling, i.e. it is assumed that the transformation takes place at a constant temperature. Therefore, it is essentially the *diagram of isothermal austenitic trans-*

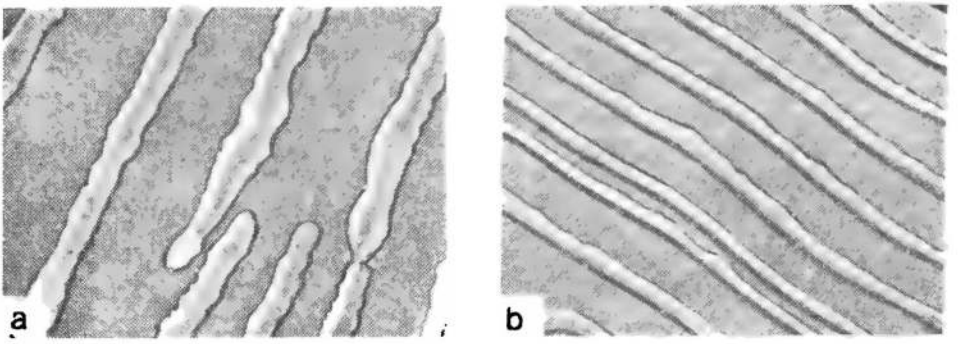

Fig. 10-12. The structure of eutectoid steel obtained at various temperatures of austenitic decomposition

(*a*) pearlite, decomposition at 700°C; (*b*) sorbite, decomposition at 650°C; × 7 500

formation. Diagrams of this type are usually called TTT-diagrams (time-temperature-transformation), or *C*-curves, owing to the specific shape of the curves[1].

The structure and properties of the products of austenite decomposition depend on the temperature at which the transformation has taken place (Fig. 10-12).

At high temperatures, i.e. low degrees of undercooling, a coarse-grained mixture of ferrite and cementite is formed which is easily discernible in the microscope. This structure is called pearlite (Fig. 10-12*a*).

At lower temperatures, and therefore, greater degrees of undercooling, more disperse and harder products are formed. The pearlitic structure of this finer type is called sorbite (Fig. 10-12*b*).

At still lower temperatures (near the bend of the *C*-curve), the transformation products are even more disperse, so that the lamellar structure of the ferrite-cementite mixture is only discernible in the electron microscope (Fig. 10-13). This structure is called troostite.

Thus, pearlite, sorbite and troostite are the structures of the same nature (ferrite + cementite) but a different dispersity of ferrite and cementite.

Pearlitic structures may be of two types: either granular (in which

[1] The first diagrams of isothermal decomposition of austenite were constructed by E. C. Bain and E. S. Davenport in 1930 on the basis of numerous experimental data. This was an essential contribution to the theory of heat treatment. The earlier diagrams were, however, incorrect in the lower portion (in the region of martensitic transformation): they disregarded some errors in experiments and the specifics of the martensitic transformation. For that reason they had the form of *S* and were called *S*-curves. A correct form of the diagram of austenite isothermal decomposition was first obtained by the Author in 1935 (in the form of *C*-curves). Now, this shape of the diagram (and the term *C*-curves) is generally recognized.

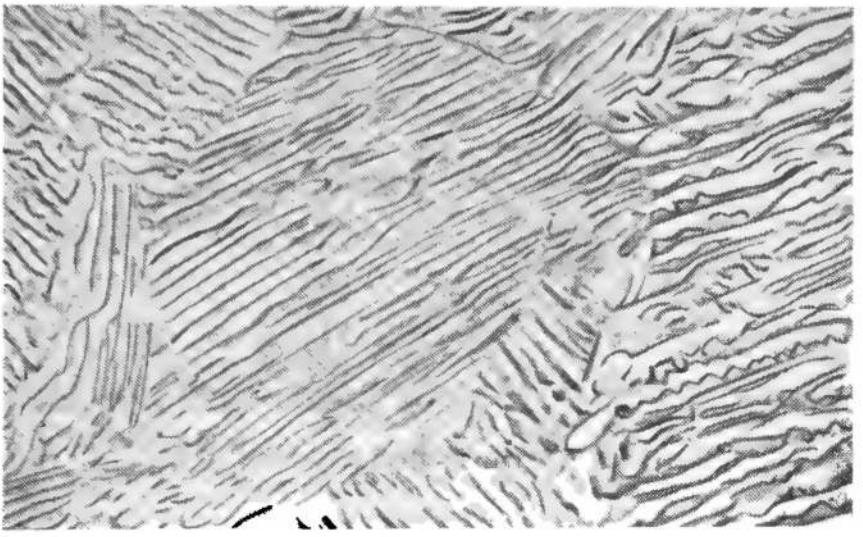

Fig. 10-13. The structure of troostite (electron-microscopic photograph, ×15 000)

cementite is present in the form of grains) or lamellar (with cementite platelets).

Homogeneous austenite always transforms into lamellar pearlite. Therefore, heating to a high temperature sets up favourable conditions for the formation of a more homogeneous structure and thus promotes the appearance of lamellar structures. Inhomogeneous austenite produces granular pearlite at all degrees of undercooling, therefore, heating to a low temperature (below Ac_3 for hypereutectoid steels) results in the formation of granular pearlite on cooling. The formation of granular cementite is probably promoted by the presence of undissolved particles in austenite, which serve as additional crystallization nuclei.

As is shown in Fig. 10-14, initial heating to a temperature up

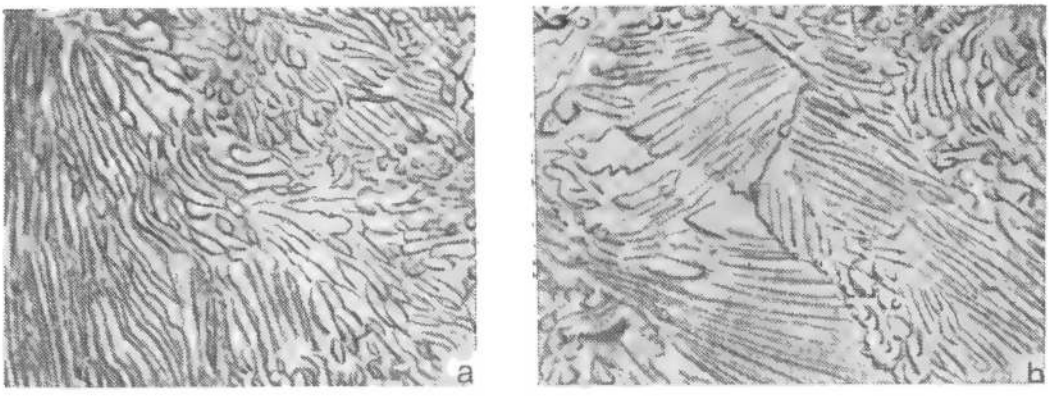

Fig. 10-14. Lamellar pearlite in steel with 1% C obtained by heating at 900°C (i.e. above Ac_3) and isothermal transformation at (*a*) 710°C and (*b*) 670°C; ×800

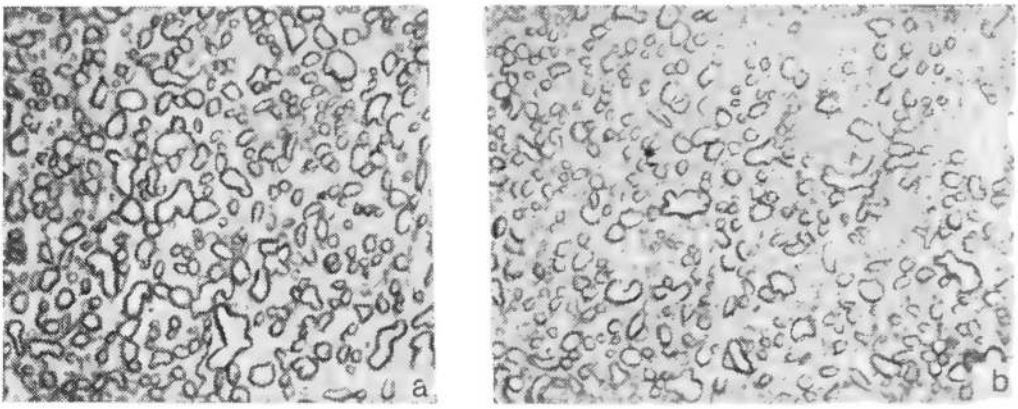

Fig. 10-15. Granular pearlite in steel with 1.2% C obtained by heating at 780°C (i.e. below Ac_3) and isothermal transformation at (*a*) 710°C and (*b*) 670°C; ×800

to 900°C gives lamellar pearlite, with more disperse structures being obtained at lower temperatures.

The structure of the same steel at the same temperature of transformation but upon a low-temperature heating (780°C) is granular pearlite (Fig. 10-15). Cementite grains that are formed in the structure are finer at a lower temperature of transformation.

Consequently, the size of cementite particles depends on the temperature of austenitic transformation and their form depends on the temperature of heating (the temperature of austenitization).

The transformations at temperatures above and below the bend of the *C*-curve differ in the kinetics and the shape of decomposition products.

Above the bend of the *C*-curve, i.e. at small degrees of undercooling, the transformation begins from a few centres and pearlitic crystals freely grow to interference. Below the bend of the *C*-curve there forms an acicular microstructure, since acicular platelets cannot grow freely and the transformation mainly occurs through the formation of new crystals.

The acicular structure that forms below the bend of the *C*-curve is called *bainite*. The transformation of austenite into bainite is in some aspects similar to the pearlitic and martensitic transformations and will be described in more detail upon studying the martensitic transformation (see Sec. 10-5).

As has been given earlier, the rate of isothermal transformation of austenite is determined by the rates of nucleation and crystal growth, N and G.

The rate of crystal growth is quite sensitive to various changes in the steel structure and can be strongly affected by the metallurgical nature of the steel, the degree of deoxidation, the presence of undissolved particles, the homogeneity of austenite, and the size

of austenitic grains. The presence of undissolved particles increases the value of G, since these particles serve as additional nuclei.

The value of G diminishes with increasing size of austenitic grains. Crystallization nuclei appear mainly on grain boundaries, therefore, the conditions for nucleation are worse in coarse-grained steel where the extent of grain boundaries is smaller.

The factors mentioned have, however, no effect on the nucleation rate, N. The value of N depends only on steel composition and, for a steel of a given composition, is a natural characteristic depending only on the degree of undercooling.

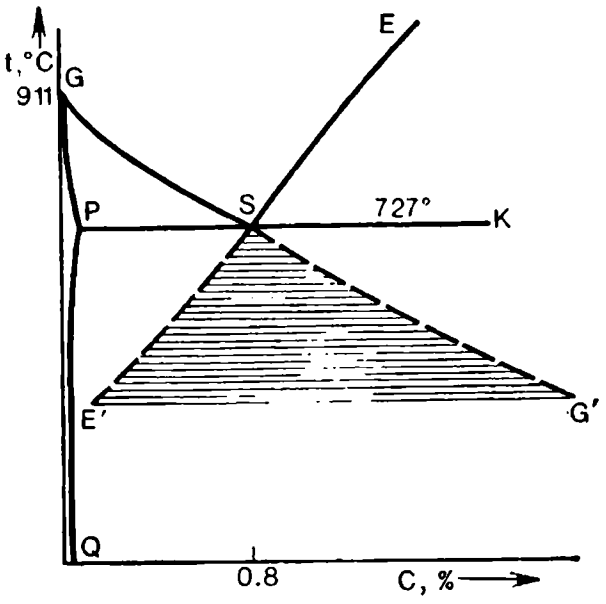

Fig. 10-16. Composition of eutectoid depending on the degree of undercooling below A_1

We have discussed the austenite-to-pearlite transformation in steels whose composition is close to eutectoid. If the content of carbon in a steel differs from the eutectoid value, the pearlitic transformation will be preceded with the precipitation of ferrite or cementite (as follows from the iron-carbon constitutional diagram).

In hypoeutectoid steels, the transformation of austenite begins with the formation of ferrite and the saturation of the remaining γ-solution with carbon, and in hypereutectoid steels, with the precipitation of cementite and depletion of the austenite of carbon. Under equilibrium conditions, the decomposition of austenite into ferrite and cementite (pearlitic transformation) begins when the content of carbon in the austenite, remained upon precipitation of excess ferrite and cementite, corresponds to point S (0.8 per cent).

Consider the transformations under conditions of undercooling. Line SE in the iron-carbon diagram is the boundary of limiting saturation of austenite with cementite; this means that cementite can precipitate from austenite to the right of line SE and, evidently, to the right of the extention of that line downwards into the region of undercooled austenite. Similarly, the extention of line GS is the boundary of saturation of undercooled austenite with ferrite.

If this is so, the simultaneous precipitation of ferrite and cementite from austenite is only possible when the austenite is supersaturated with both components, i.e. to the left of line GG' and to the right

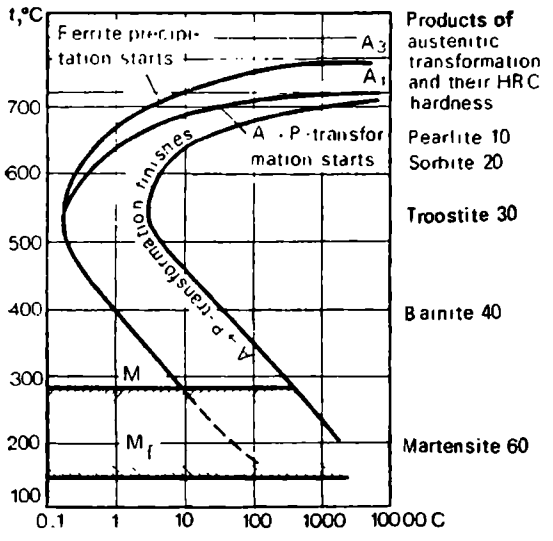

Fig. 10-17. Diagram of isothermal decomposition of austenite in hypoeutectoid steel (0.4% C)

of line EE' (in the shaded triangle of Fig. 10-16). This also means that the eutectoid will have a strictly definite composition only in crystallization without undercooling (at point S), and the composition of eutectoid (pearlite) under real conditions in characterized by a concentration interval between the lines $E'S$ and SG'.

The eutectoid which forms from undercooled austenite and has a concentration differing from the eutectoid value is called *quasi-eutectoid.*

As follows from the diagram in Fig. 10-16, the quasi-eutectoid in hypereutectoid steels contains more than 0.8 per cent carbon and that in hypoeutectoid steels, less than 0.8 per cent, the deviation from this value being greater at a lower temperature of transformation. Therefore, the lower the temperature of transformation, the less the excess ferrite (or cementite) precipitates before the pearlitic transformation begins. At temperatures near the bend of the C-curve and at lower temperatures, decomposition of austenite begins without precipitation of excess phases.

These processes are plotted in the diagram of isothermal decomposition of austenite.

The complete form of the diagram of isothermal austenitic decomposition for a hypoeutectoid steel is shown in Fig. 10-17. The diagram shows the curve of the beginning of ferrite precipitation, the curves of the beginning and finish of the pearlitic transformation, and horizontal lines A_3, A_1, M and M_f. Such a diagram can provide the principal information on isothermal transformation in the given steel for any degree of undercooling. For instance, on undercooling to 650°C, the transformation begins in a definite time with the precipitation of ferrite from the solution. Ferrite precipitates for a certain time, after which the decomposition of austenite into pearlite begins and the process ends on the curve describing the finish of the transformation. If austenite is quickly cooled to 550°C, the transformation will start just with the formation of pearlite. The transformation at 550°C occurs much more rapidly than at 650°C.

If we take a hypereutectoid steel instead of hypoeutectoid, the decomposition of austenite at small degrees of undercooling will be preceded with precipitation of cementite.

The correlation between the nature of isothermal decomposition of austenite, the content of carbon and the temperature can be expressed in a generalized diagram, such as that shown in Fig. 10-18.

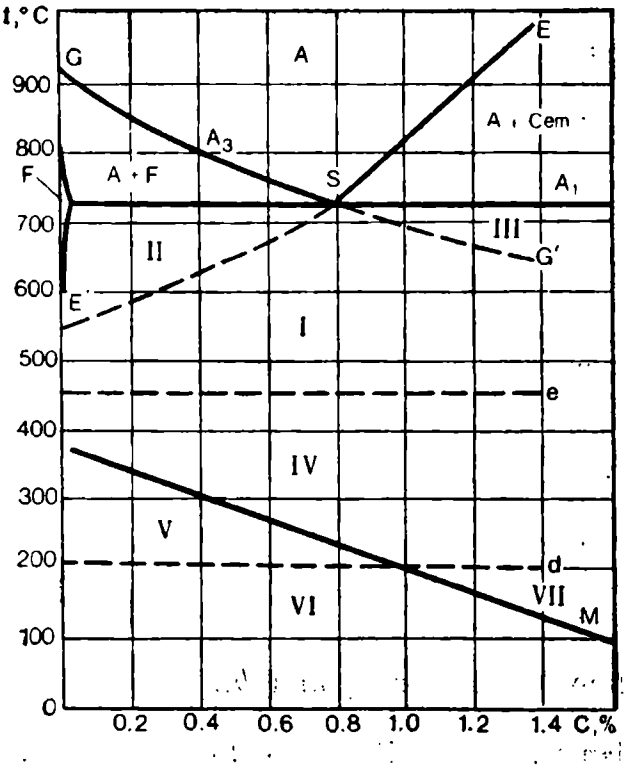

Fig. 10-18. Generalized diagram of transformation of undercooled austenite in carbon steel

In that diagram, the decomposition of austenite takes place in a temperature interval between the horizontal lines A_1 and d. The temperatures corresponding to lines e and d (points of a particular carbon content) and their physical sense were explained by D.K. Chernov. In modern interpretation, the rate of diffusion of iron and alloying elements above point e is sufficient for realizing the appropriate phase transformations, and above point d, only the rate of carbon diffusion is sufficient for the purpose. Therefore, only diffusionless (martensitic) transformations are possible below point d, while the transformations between points e and d occur with the diffusion of carbon but without displacement of metallic atoms. The transformations between the horizontal lines A_1 and e produce lamellar structures and those between e and d, acicular structures. The inclined line M determines the temperature of the beginning of diffusionless martensitic transformation.

The diffusion pearlitic decomposition occurs without precipitation of either ferrite or cementite in region I; to the left of line SE', the process is preceded by the precipitation of ferrite, and to the right of line SG', by the precipitation of cementite.

Consequently, the following regions of austenitic transformation are possible, depending on the content of carbon and the degree of undercooling:

I — austenite-to-pearlite transformation;

II — precipitation of ferrite followed by austenite-to-pearlite transformation;

III — precipitation of cementite followed by austenite-to-pearlite transformation;

IV — austenite-to-bainite transformation;

V — austenite-to-martensite transformation and decomposition of retained austenite into bainite;

VI — austenite-to-martensite transformation;

VII — undercooled austenite remains non-transformed.

Having discussed the transformation of austenite at a constant temperature and various degrees of undercooling, we can now analyse the process of austenitic transformation in continuous cooling, when a steel heated to the austenitic state is cooled at different rates.

The diagrams of isothermal decomposition of austenite are constructed in temperature-time coordinates, as are the cooling curves. Let the cooling curves be superimposed on the isothermal decomposition diagram (Fig. 10-19).

Line v_1, which characterizes slow cooling, intersects the diagram lines at points a_1 and b_1. The transformation will occur at these temperatures (determined by points a_1 and b_1) and will form coarse-lamellar pearlite of a low hardness.

With a quicker cooling (curves v_2 and v_3), the diagram lines are intersected at lower temperatures (points a_2, b_2 or a_3, b_3) and the transformation products will be more disperse.

As follows from this construction, at a greater rate of cooling, the transformation occurs at a lower temperature and forms more disperse and harder products.

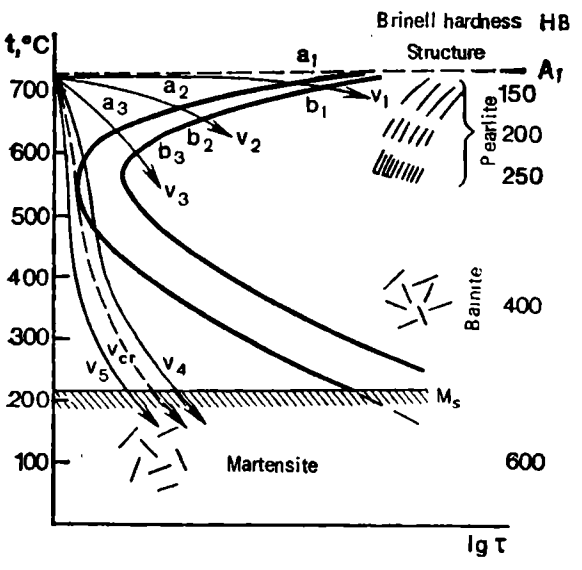

Fig. 10-19. Superposition of cooling curves on *C*-curve of austenite decomposition; the figure also schematically shows the structures formed and their hardness

At a high rate of cooling (v_5), the transformation has no time to proceed in the upper temperature range, the austenite will be undercooled to a low temperature and will transform into martensite, such a cooling will result in hardening.

Therefore, to harden steel, it should be cooled at a high rate so that austenite has no time to decompose in the upper temperature range. As seen from Fig. 10-19, at cooling rates

higher than v_{cr} (v_{cr} is the cooling curve that is tangent to the bend of the *C*-curve) the martensitic transformation takes place and at lower cooling rates, austenite decomposes in the upper temperature range.

The lowest cooling rate needed to undercool austenite up to martensitic transformation is called the *critical rate of hardening*. If a steel is to be hardened, it should be cooled at a rate not less than the critical. The critical rate v_{cr} is lower for steels whose curve of the beginning of transformation passes farther to the right. In other words, with a lower rate of austenite-to-pearlite transformation, it is easier to undercool the austenite to the temperature of martensitic transformation and the critical rate of hardening will be lower.

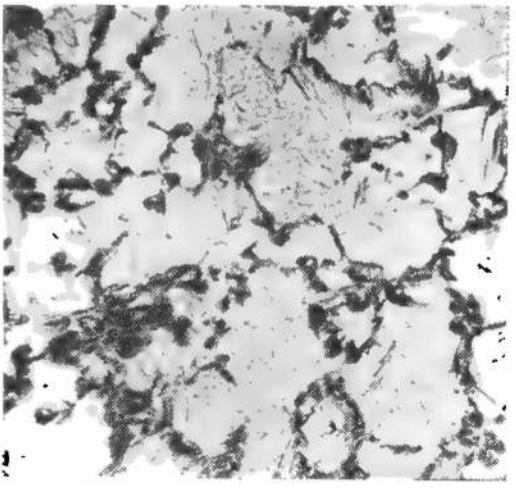

Fig. 10-20. The structure of martensite + troostite, ×350

If cooling is done at a rate slightly below the critical, the austenite will undergo only a partial transformation in the upper temperature range[1] and the structure will consist of the products of transformation in the upper temperature range (troostite) and martensite (Fig. 10-20).

The critical rate of hardening, v_{cr}, can be determined from the diagram of isothermal decomposition of austenite.

Assuming that the temperature drop on hardening is directly proportional to the logarithm of time, the cooling curve in the t-log τ coordinates approximates a straight line and

$$v_{cr} = \frac{A_1 - t_{min}}{\tau_{min}}$$

where A_1 is the temperature of the critical point; t_{min} is the temperature of the minimal stability of austenite; and τ_{min} is the time of the minimal stability of austenite.

The critical hardening rate thus obtained is, however, always greater (usually by a factor of 1.5) than the real v_{cr}. As has been shown by S.S. Steinberg, the discrepancy can be explained as follows.

The time of cooling from A_1 to t_{min}, represented by a straight line, can be imagined as a stepwise cooling with an infinite number of portions of isothermal decomposition at a gradually lowering temperature. The sum of these sections should be equal to τ_{min}. As has been indicated earlier, the transformation processes during the incubation period are not utterly absent, but occur very slowly, their rate being smaller at higher temperatures. In other words, the time section in the incubation period near point A_1 is far from being equivalent to the time section at the temperature of the minimal stability of austenite,

[1] This rate of cooling is represented by curve v_4 in Fig. 10-19.

therefore, the sum (in time) of infinitely small sections in continuous cooling is not equivalent to the time section at the bend of the curve of isothermal austenitic decomposition.

The actual distribution of critical hardening rate can be approximately obtained by introducing the coefficient 1.5. The critical rate of hardening will then be determined as follows:

$$v_{cr} = \frac{A_1 - t_{min}}{1.5\tau_{min}}$$

This analysis shows that a simple superposition of cooling curves on the isothermal diagram of austenitic decomposition can give only an approximate quantitative estimation of a transformation occurring in continuous cooling.

More accurate estimations of the transformations at a continuously varying temperature are made by using the so-called *thermokinetic*, or *anisothermal, diagrams of austenitic transformations*, which characterize the transformation at various cooling rates.

Though isothermal transformation diagrams can give us much knowledge on the nature of transformations, the transformations only seldom can be achieved under isothermal conditions in practice.

With a very quick transformation, the process of decomposition of austenite can and usually does occur as the specified temperature is attained. This is why the isothermal transformation diagrams are quite inaccurate for holding times less than 10 s.

When large sections are heat treated, it is impossible to meet another important condition essential for the construction of a diagram, i.e. quick cooling to the given temperature. Isothermal austenite transformation diagrams are of great theoretical significance but are superseded by anisothermal diagrams in practical cases of selecting heat treatment conditions.

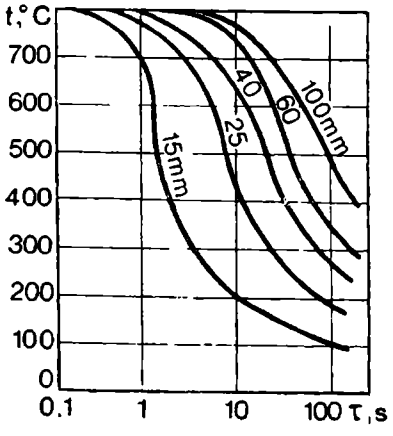

Fig. 10-21. Cooling curves for the centre of cylindrical specimens quenched in water. Numbers at curves are the diameters of specimens

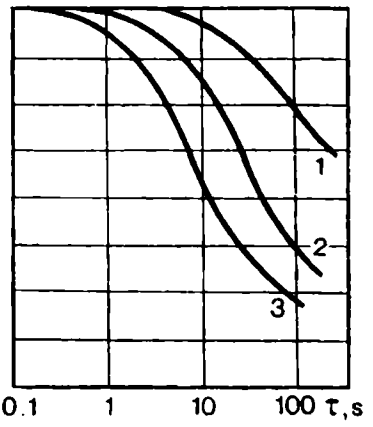

Fig. 10-22. Cooling curves for the centre of cylindrical specimens quenched in various media
1—in air; *2*—in oil; *3*—in water

The cooling conditions have been studied quite thoroughly. It is possible in laboratories to imitate the conditions of cooling large massive articles (Fig. 10-21) and in various quenchant (Fig. 10-22) on small specimens. During cooling of specimens, the points of the beginning and end of transformations are determined by dilatometric (by changes in the dimensions of specimens) or magnetic (austenite is nonmagnetic and its products are magnetic) method. The experimentally found cooling curves and the points of transformation are then plotted in a temperature-time diagram and the sections of like transformations are combined into regions (Fig. 10-23).

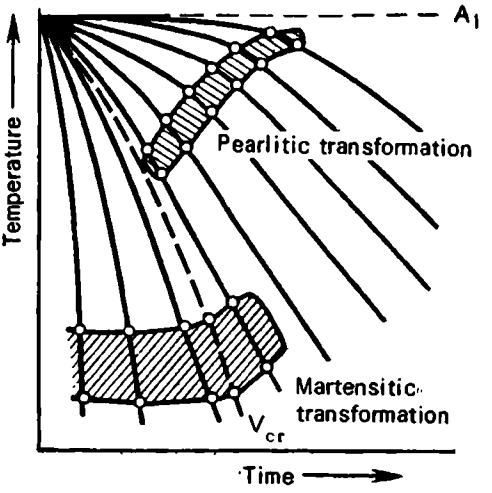

Fig. 10-23. Anisothermal diagram of austenitic transformation

Up to this point, we have considered only schematic diagrams of austenitic transformation. For exhaustive information on the transformation in a particular grade of steel, however, use is made of both types of the diagram and of some additional data: grade and composition of the steel, heating temperature, austenitic grain size, properties (at least hardness) of decomposition products, and proportion of the constituents. All these data are combined as, for instance, is done in Fig. 10-24 which shows the diagrams of isothermal and anisothermal decomposition of austenite in steel Grade 45X.

10-4. MARTENSITIC TRANSFORMATION

If austenite is undercooled to a temperature at which the γ-lattice is unstable, despite the presence of dissolved carbon, but the rate of diffusion of carbon is so small (owing to the low temperature) that can be neglected, then the iron lattice is rearranged without evolution of carbon:

$$Fe_\gamma (C) \rightarrow Fe_\alpha (C)$$

This transformation differs in its mechanism and in the nature of transformation products from the eutectoid decomposition of austenite that has been discussed earlier.

As we recall, the austenite-to-pearlite transformation appreciably relies on diffusion and may be regarded as a diffusion-type transformation.

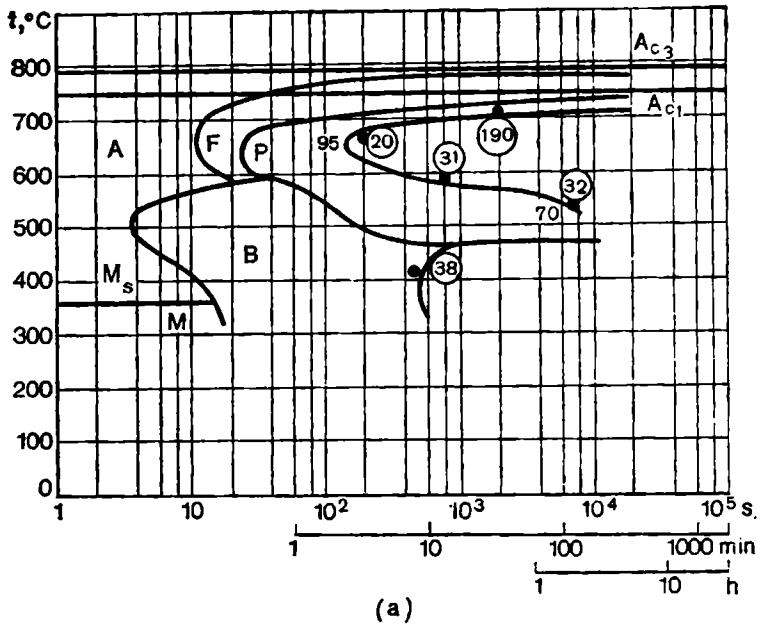

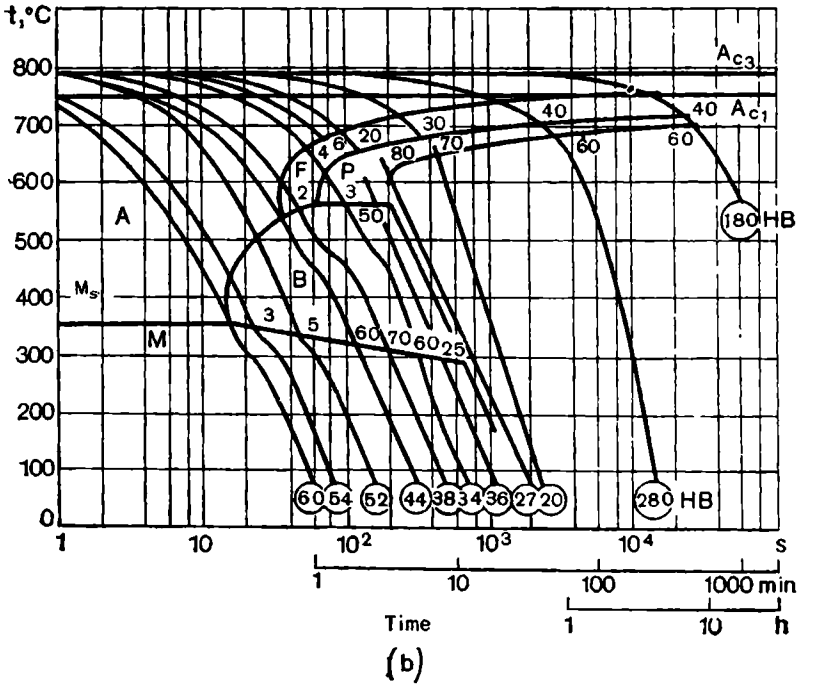

Fig. 10-24. Diagrams of (*a*) isothermal and (*b*) anisothermal (thermokinetic) transformation of austenite in steel 45X (F. Wever). Steel composition: 0.44% C, 0.22% Si, 0.80% Mn, and 1.04% Cr. Numbers at curves are percentages of a structural component upon transformation; circled numbers are *HRC* values of decomposition products

In the austenite-to-martensite transformation, only the crystal lattice undergoes rearrangement, but the concentration of the reacting phases remains the same. Thus, the transformation is diffusionless. *Martensite* in steel is a supersaturated solid solution of carbon in α-iron of the same concentration as in the original austenite. Since the solubility of carbon in α-phase is only 0.01 per cent, martensite is a supersaturated solid solution.

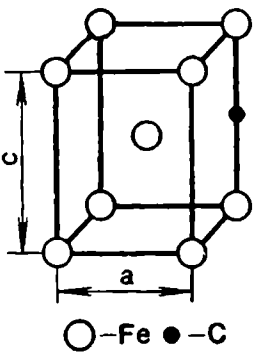

Fig. 10-25. Crystal cell of martensite

Since the transformation is diffusionless, carbon does not precipitate from the solution, and only iron atoms are rearranged from f.c.c. to b.c.c. lattice.

The crystal structure of martensite is characterized by tetragonality, i.e. the c/a ratio in the lattice is greater than unity (Fig. 10-25). This tetragonality of martensite is due to the presence of carbon in the solution.

As seen from the graph in Fig. 10-26, tetragonality of martensitic lattice is directly proportional to the content of carbon[1].

Martensite has a specific microstructure. Its crystals are platelets[2] oriented parallel to one another or tilted at definite angles (60 or 120 degrees, Fig. 10-27).

As has been found, the orientation of martensite platelets is due to the fact that martensite can form only on certain crystal planes and along certain directions in austenite. This oriented transformation can be regarded as a shear or displacement of a volume of metal in a definite plane, which occurs simultaneously with the $\gamma \rightarrow \alpha$-transformation. The transformation is associated with an appreciable displacement of metal atoms in space, though neither the atoms change places nor the distances between them appreciably change. This oriented displacement of atoms during transformation produces a relieved surface in microsections (Fig. 10-28).

Thus, martensitic transformation differs from other phase transformations in the following typical features:

(1) it is diffusionless, i.e. is associated only with lattice rearrangement and the composition of the final phase (martensite) is the same as that of the original phase (austenite);

(2) it is oriented, i.e. the new phase (martensite) is regularly oriented relative to the old phase (austenite); the shearing effect

[1] If a carbon atom occupies the site as shown in Fig. 10-25. A different position of carbon atom changes the tetragonality of the lattice (L.I. Lysak). For high-alloy steels, the dependence of c/a on carbon content may differ from that shown in Fig. 10-26.

[2] Martensite platelets have the form of needles in the plane of microsection and can be properly described by the term 'acicular': coarse-acicular martensite, fine-acicular martensite, etc.

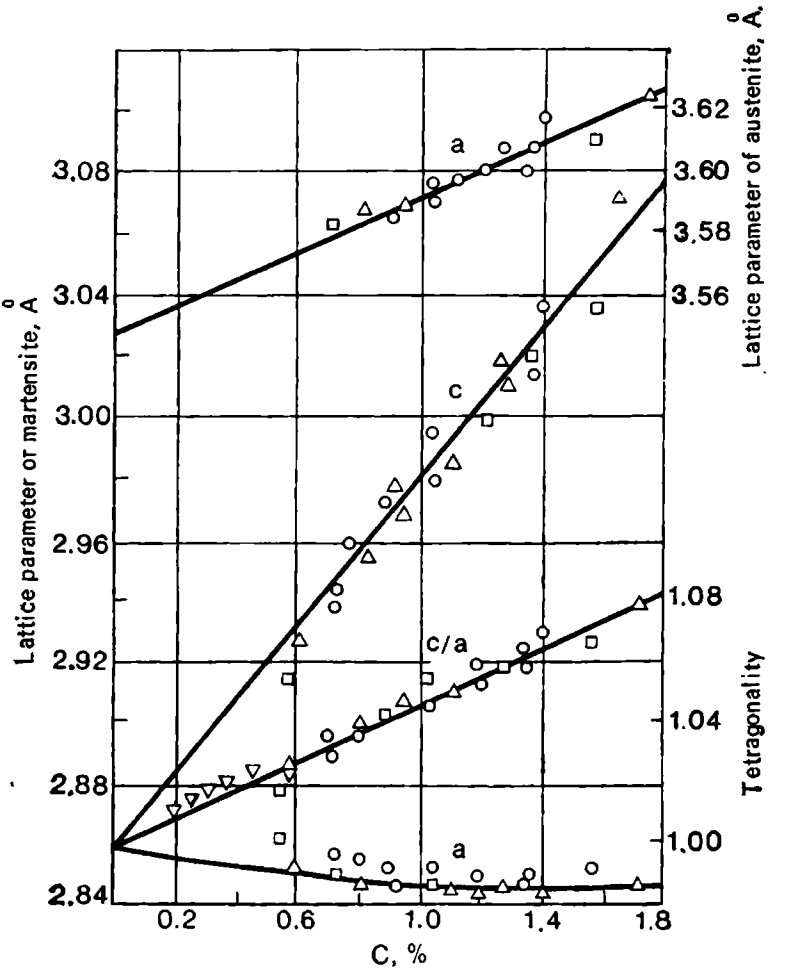

Fig. 10-26. Effect of carbon on lattice parameters of martensite and austenite and *c/a* ratio of martensitic lattice (according to various researchers)

Fig. 10-27. Martensitic needles in a very coarse-grained austenite, ×500

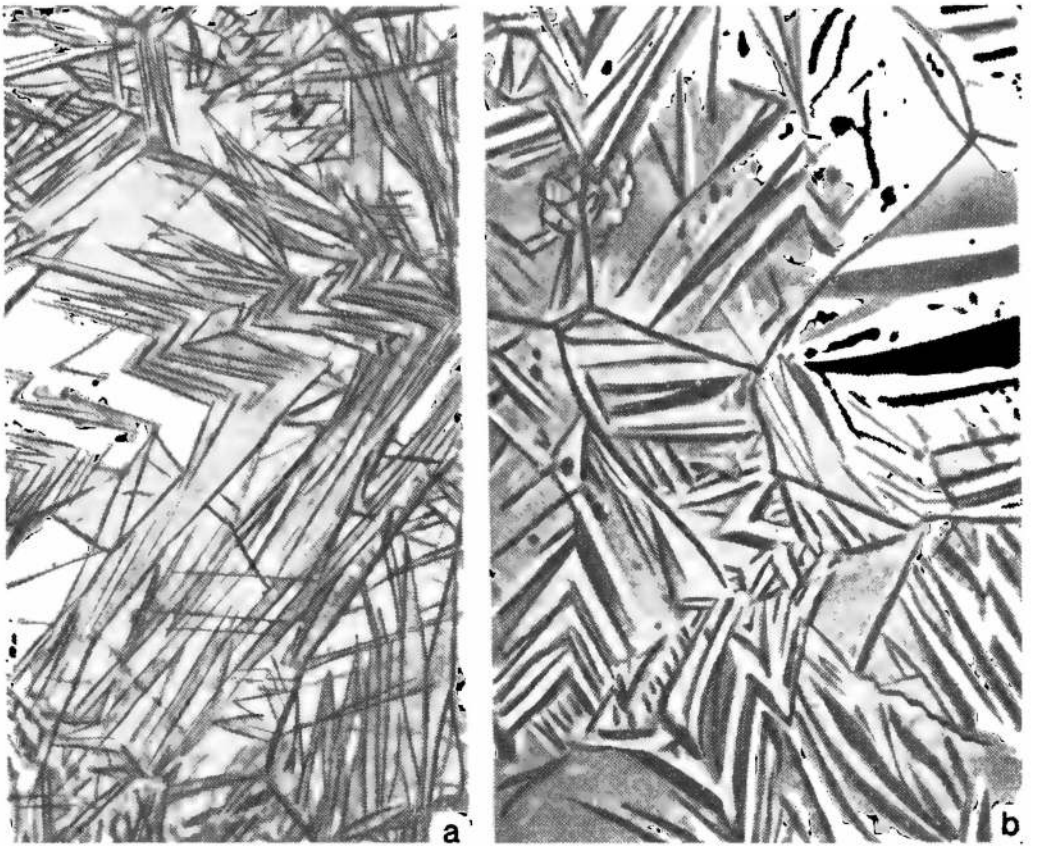

Fig. 10-28. (*a*) Martensitic structure and (*b*) microrelief on the surface of polished specimen of the same steel, ×400

of the transformation produces relieved surface. Transformations characterized by these two particularities are referred to the class of martensitic transformations.

Martensitic transformations have been discovered in many metals and alloys and will be discussed later in the book. In this section we shall discuss only the martensitic transformation in steels.

The martensitic transformation in steel has the two typical features mentioned above and also some other specific features not found in other alloys. In steels, this transformation is irreversible, that is, can only proceed in the direction Fe_γ (C) $\rightarrow$ Fe_α (C), but cannot occur in the reverse direction by the same diffusionless mechanism. Further, martensitic crystals form in steel, irrespective of temperature, in an extremely short time interval (of an order of 10^{-7} s, i.e. practically instantaneously).

It has been established experimentally that the transformation consists in practically instantaneous formation of a portion of martensitic platelets, rather than of a single platelet (each platelet forms in a time interval of approximately $1 \cdot 10^{-7}$ s and the whole

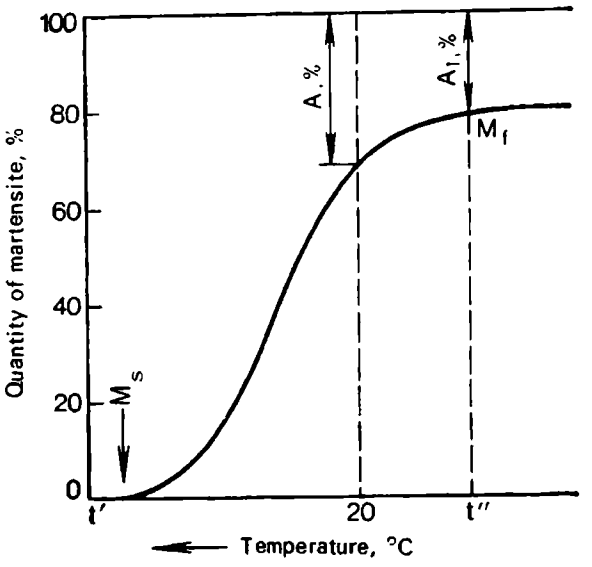

Fig. 10-29. Martensitic curve

portion consisting of hundreds or thousands of crystals, in $1 \cdot 10^{-3}$ s), after which the transformation comes to a stop. With further cooling, the transformation is renewed by the formation of new portions and so on. The process can be represented graphically in the form of a kinetic curve of transformation which is called *martensitic curve*[1]. Such a curve is schematically shown in Fig. 10-29, where the ordinate gives the quantity of martensite that has formed (measured by a magnetic or some other method) and the abscissa is temperature.

As seen from the curve, the transformation in cooling starts at point M_s. This point determines the temperature of the beginning of austenite-to-martensite transformation in a given steel[2].

The quantity of martensite increases as the temperature is lowered. The end of the transformation is determined by point M_f. At this temperature, a certain quantity of retained austenite remains in the structure. Further cooling below M_f causes no transformation nor changes the quantity of retained austenite.

The position of the martensitic points (M_s and M_f) appreciably depends on steel composition. The temperature range of martensitic transformation lowers with increasing content of carbon.

The general effect of some or other factor on the temperatures of martensitic transformation can be represented in the form of so-called *martensitic diagrams*. In particular, the effect of carbon is shown in the diagram in Fig. 10-30.

Carbon appreciably lowers the martensitic points. At a carbon content above 0.5 per cent, the temperature range of martensitic transformation extends to sub-zero temperatures, i.e. such steels

---

[1] As follows from the foregoing, the curve should be broken, each step of the broken line representing the formation of a portion of martensite. Since, however, each transformation act forms a very small portion of martensite and the sensitivity of the instruments which measure the quantity of martensite is not high, the steps of the curve are very small and the latter can be plotted as a smooth curve.

[2] Point M_s is roughly 200°C below T_0 (the temperature of thermodynamic equilibrium between austenite and martensite, see Fig. 9-5).

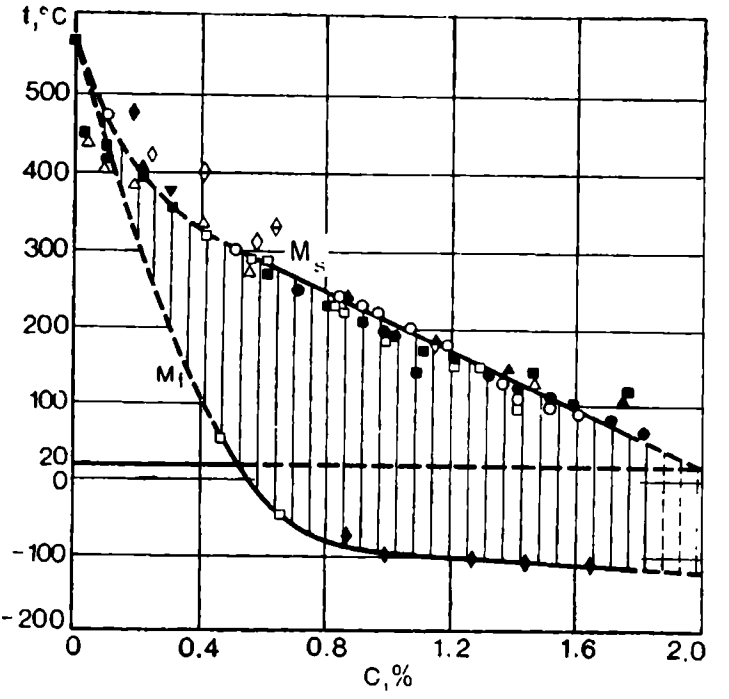

Fig. 10-30. Martensitic diagram (effect of carbon on the martensitic transformation points; according to various researchers)

cannot be made fully martensitic by continuous cooling to room temperature.

Some alloying elements also can lower the martensitic point so that certain grades of alloy steel containing a sufficiently high percentage of carbon and alloying elements have their M_s point below 0°C, and common hardening produces a purely austenitic structure in them (see Sec. 14-6). It then follows that the temperature of martensitic transformation mainly depends on steel composition (composition of austenite).

Let us now discuss some other factors which may affect the martensitic transformation.

In the first place, it should be examined how the temperature of martensitic transformation is affected by cooling rate.

Experiments with continuous cooling of austenite at various rates from v_{cr} (which is roughly 150 °C/s for carbon steel) to approximately 10 000 °C/s failed to lower the temperature of the beginning of martensitic transformation.

It can be concluded therefore that the temperature of martensitic transformation is independent of cooling rate.

Though the cooling rate has no effect on the position of the martensitic point, it can definitely affect the course of the martensitic transformation. At temperatures slightly lower than M_s, a slower cooling gives a greater degree of transformation. This is due to the

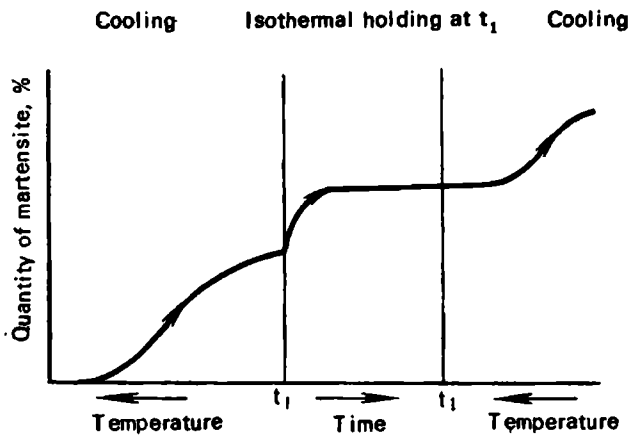

Fig. 10-31. Martensitic curve. Cooling has been interrupted for a certain time at temperature t_1

ability of austenite to isothermally transform into martensite at temperatures slightly less than M_s.

If the cooling is interrupted and an isothermal holding is allowed within the martensitic range (Fig. 10-31), a certain, though small, amount of martensite forms during the holding time. This makes it possible to distinguish between *athermal martensite* which forms in continuous cooling and *isothermal martensite* which forms at a constant temperature. The latter differs from athermal martensite both in the appearance (microstructure) and the properties (the last circumstance has not been thoroughly studied). In common steels, the formation of isothermal martensite quickly comes to a stop, i.e. only a small quantity of isothermal martensite is formed, so that martensite in real steels is mostly of the athermal type. A holding time in the martensitic range (as also at temperatures 100-200°C above M_s) produces the effect of *stabilization of austenite* which essentially consists in that the austenite-to-martensite transformation upon the holding time is renewed not immediately but only after a certain undercooling (Fig. 10-32) and the final structure contains more austenite upon final cooling, i.e. less martensite is formed.

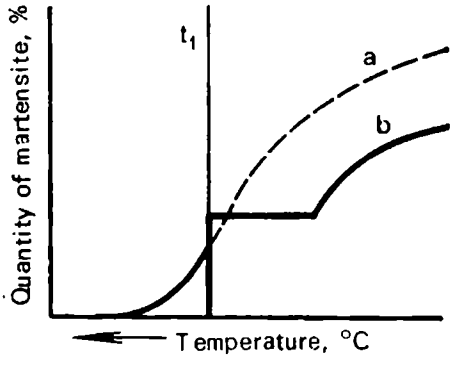

Fig. 10-32. Martensitic curve

a—continuous cooling; *b*—quenching interrupted in the martensitic range (at t_1)

The effect of stabilization can be explained by the relaxation of the stresses which are essential for realization of the martensitic transformation. This is why externally applied stresses cause martensitic transformation but if they are eliminated (for instance, by disintegrating a piece of steel into fine monocrystalline particles), the martensitic transformation will not take place.

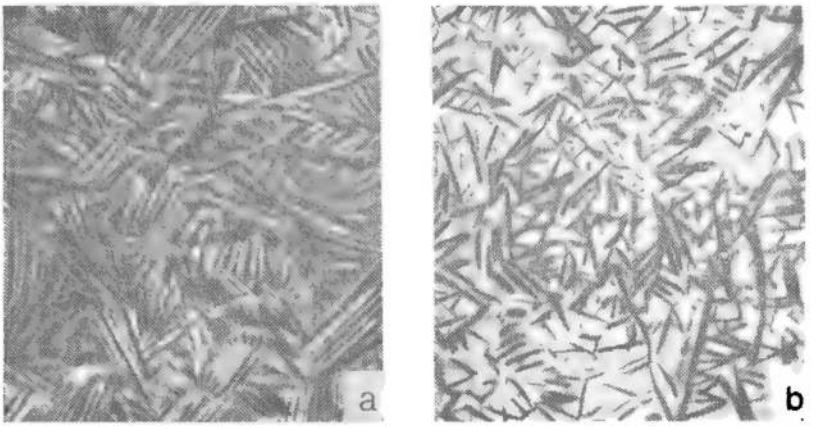

Fig. 10-33. Typical martensitic structures in high-carbon steels, ×500
(*a*) 0.8% C; (*b*) 1.4% C

The structure of martensite in hardened steel is typically acicular (Fig. 10-33). The austenite which can co-exist with martensite at room temperature in the structure is called *retained austenite*. Since the steel structure shown in Fig. 10-33*a* contains little austenite, the whole field is occupied by martensitic needles. With an appreciable quantity of retained austenite (20-30 per cent or more), it is revealed metallographically as bright fields between martensitic needles (Fig. 10-33*b*).

The quantity of retained austenite which can be fixed in a steel by hardening depends on the position of the martensitic point, being greater at a lower position of that point. This is why carbon, which lowers the martensitic point, increases the content of retained austenite (Fig. 10-34).

Hardened low-carbon steels are almost free of retained austenite (the content of retained austenite in steel with less than 0.6 per cent C is 2-3 per cent), but high-carbon grades may contain an appreciable amount of it, depending on the conditions of hardening and the rate of cooling in the martensitic range. This is why the quantity of retained austenite depending on carbon content is represented in diagrams in the form of a band which widens towards increasing content of carbon.

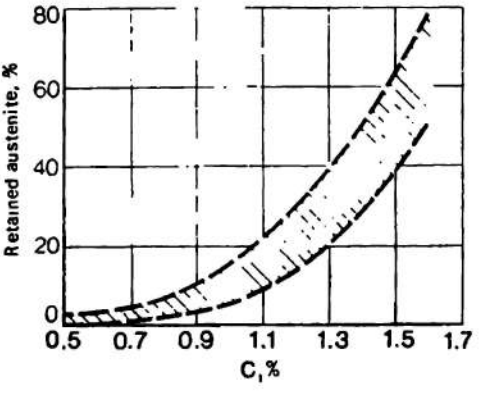

Fig. 10-34. Effect of carbon on the quantity of retained austenite in hardened steel

The martensitic transformation, i.e. the transformation which is typically diffusionless and oriented (see earlier in this section), has been discovered in many (practically all polymorphous) metals and their alloys (titanium, zirconium, cobalt, sodium, tellurium, mercury, lithium), and also in Cu-Sn, Cu-Zn, Cu-Al and other systems undergoing polymorphous transforma-

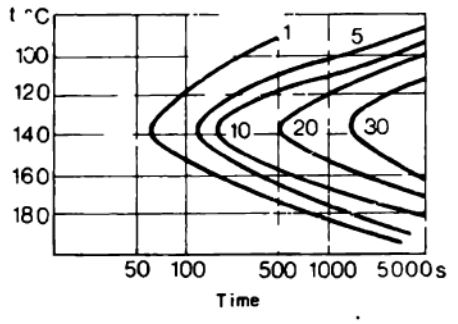

Fig. 10-35. Diagrams of isothermal austenite-to-martensite transformation. Numbers at curves show the degree of transformation. The steel contains 23% Ni, 3.6% Mn, balance iron is practically carbon-free (M. Cohen)

tions in solid solution.

The martensitic transformations in these metals and alloys occur, however, by the isothermal mechanism which substantially differs from the athermal-mechanism that is typical of steels[1].

The athermal transformation, which has been discussed above, occurs mainly in carbon-containing steels. In some carbonless iron-base alloys, the isothermal transformation prevails. For that reason these alloys are a convenient tool for studying the isothermal martensitic transformation (G.V. Kurdyumov, O.P. Maksimova et al.; and also the conditions when one type of martensitic transformation changes to the other (I.Ya. Georgieva).

Though any type of martensitic transformation requires that the original (austenitic) phase be undercooled to a temperature at which diffusion displacements can be regarded to be suppressed, the kinetics of the isothermal martensitic transformation is similar to decomposition by diffusion, which is indicative of (or is a result) the fact that the nucleation of isothermal martensite is a thermally activated process.

In support of the earlier developed concepts (G.V. Kurdyumov), it has been experimentally shown that there exists a temperature interval in which the

[1] At one time (in 1950's), some metallurgists believed that the isothermal mechanism is applicable to all types of martensitic transformation. The problem was sharply disputed and caused confusion of concepts in the field. It has turned out, however, that the kinetics of formation, the morphology, and probably the properties of isothermal and athermal martensite are quite different and should be analysed separately. The theory and kinetics of athermal transformation has been developed by S. S. Steinberg (in 1930's) and that of isothermal transformation, by G.V. Kurdyumov (at the end of 1940's).

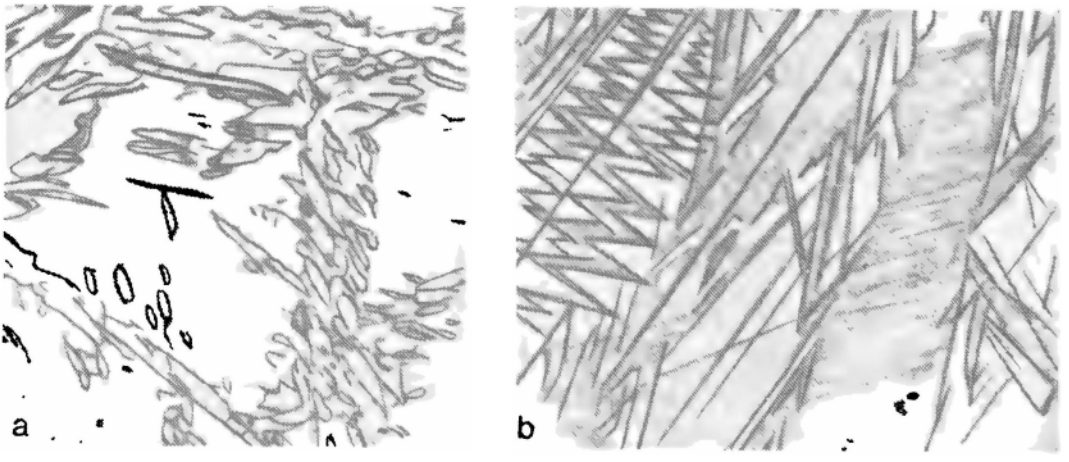

Fig. 10-36. Microstructure of (*a*) isothermal and (*b*) athermal martensite; ×500 (I. Georgieva)

Table 10-1. Effects of Various Factors on Kinetic Characteristics of Athermal and Isothermal Martensitic Transformations

External factors	Affected kinetic characteristic	In athermal martensitic transformation	In isothermal martensitic transformation
Increasing cooling rate	Position of M_s point	Not affected or is raised	Lowered
Decreasing temperature	Rate of growth of martensitic crystal	Not affected or is accelerated	Decelerated
Stresses	Rate (degree) of transformation	Accelerated	Slowed down
Grain coarsening	Position of M_s point	Not affected	Lowered

isothermal martensitic transformation can take place (Fig. 10-35). The rate of this transformation, as in other transformations occurring under isothermal conditions, i.e. activated by thermal oscillations of atoms, first increases with lowering temperature, reaches a maximum (at —140°C for the given alloy) and then decreases. The growth of martensitic crystals for a given type of martensitic transformation depends on temperature and occurs relatively slowly.

According to the theory (G. V. Kurdyumov), the boundary of a growing martensitic crystal remains coherent to the original phase (austenite) until the increasing stress at that boundary disrupts the coherence and stops the transformation. This sharp difference in the kinetics of transformation results in a great difference in the microstructures of the two types of martensite (Fig. 10-36).

The work-hardening effect in the original austenite can suppress the isothermal formation of martensite. Refinement of the austenite grain can slow down the isothermal martensitic transformation.

The effects of various factors on the kinetics of the two types of martensitic transformation are summarized in Table 10-1.

It is still not clear why different types of martensitic transformation can occur in various alloys or even in one and the same alloy; there are even no reasonable propositions on the subject.

As has been noted above, either one or the other type of martensitic transformation can be realized in an alloy, depending on certain conditions. This is decided by the mutual position of the temperature ranges of the two transformations (Fig. 10-37).

If the interval M_s^{ath}-M_f^{ath} lies higher than M_s^{is}[1] (see Fig. 10-37*a*), athermal martensite will form at any cooling rate and only at temperatures below M_s^{ath} the retained austenite can transform into isothermal martensite. The transformation gives few pro-

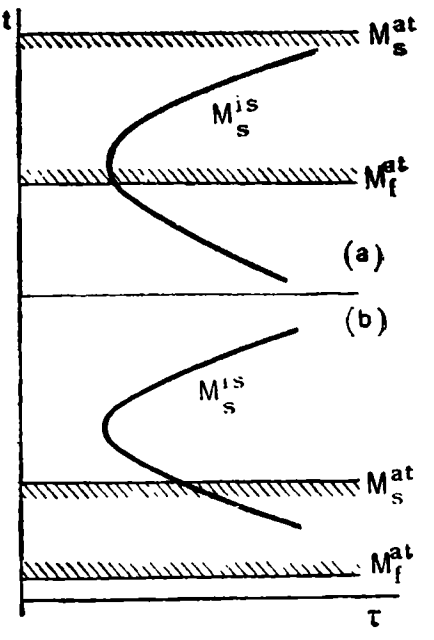

Fig. 10-37. Probable kinetic variants of martensitic transformations

[1] Since the beginning of isothermal transformation depends on cooling rate, the concept of M_s is not quite definite.

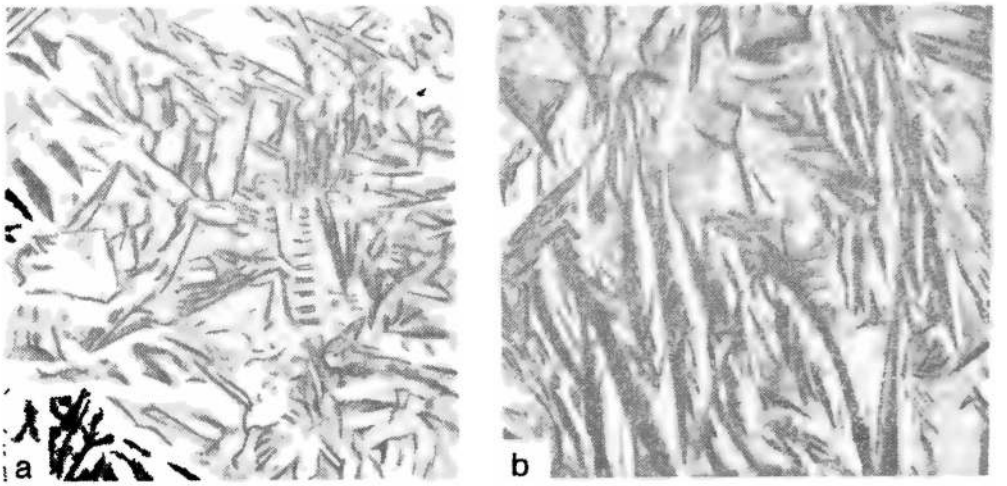

Fig. 10-38. Types of relief obtained in (*a*) direct and (*b*) reverse martensitic transformation; ×200

ducts, since the earlier formed martensite (athermal) produces a suppressing effect. This case is typical of steels and is of the highest practical importance.

If the interval of isothermal martensitic transformation lies above the athermal interval (Fig. 10-36*b*), the isothermal transformation can be initiated by slow cooling or by holding at a temperature below M^{ts}, whereas fast cooling suppresses the isothermal transformation, which results in that the athermal transformation will take place at a lower temperature. Latest studies (L. I. Lysak, B.I. Nikolin) have shown that, apart from the common tetragonal body-centred martensite (formed by the athermal or isothermal $\gamma \rightarrow \alpha$-transformation), other martensitic phases with different crystal lattices can also form in steels, in particular, ε-martensite, which has a hexagonal lattice; ε'-martensite with a rhombohedral structure; and $\varkappa'$-martensite which has a body-centred tetragonal lattice but with a lattice parameter different from that of α-martensite. These phases form in some high-alloy steels of a rare composition, mostly at low temperatures, and can be considered as intermediate phases, i.e. the following chain of transformations is probable:

$$\gamma \rightarrow \varepsilon' \rightarrow \varepsilon \rightarrow \varkappa' \rightarrow \alpha$$

Some links in the chain may be absent and in the limit the direct $\gamma \rightarrow \alpha$-transformation occurs which is the commonest case.

The formation of austenite from martensite, if the latter undergoes no changes on heating, can occur in two ways. The first case is the transformation by the common diffusion kinetics, which is similar to a change from one type of solid solution to another; in that case the compositions of the existing phases (martensite and austenite) may vary within the temperature range of the transformation. The second case is the diffusionless transformation with a constant composition of the phases within its temperature range. This transformation is oriented and produces a reverse relief (Fig. 10-38). Therefore, this change from martensite to austenite has some typical features of martensitic transformation and is called the *reverse martensitic transformation*.

The temperature range of the reverse martensitic transformation (A_s-A_f) depends in the first place on the composition of an alloy and is above the equilibrium temperature T_0 (when the free energies of austenite and martensite are equal, Fig. 10-39). The formation of austenite by the shear mechanism is associated with its hardening (the effect of structural strain hardening).

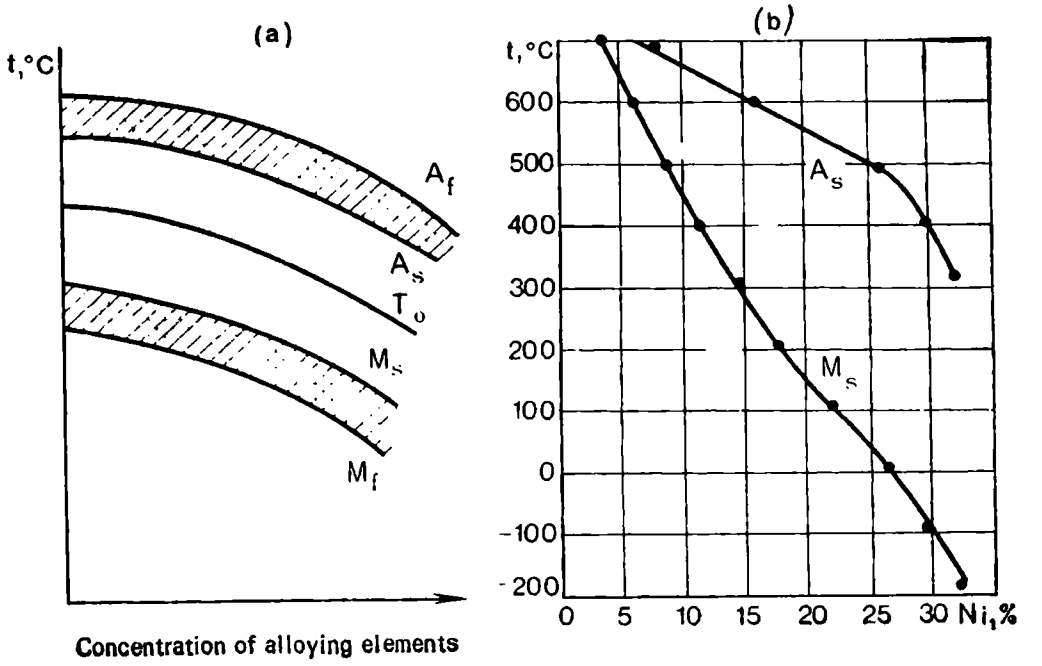

Fig. 10-39. Temperature points of (*a*) direct (M_s-M_f) and (*b*) reverse (A_s-A_f) martensitic transformation in iron-nickel alloys

In 1949, G.V. Kurdyumov and L.G. Khandros discovered a curious effect which they called *thermoelastic martensite*; it consists in that a local deformation which has appeared in the direct transformation fully disappears in the reverse transformation, since the process of $\gamma \rightarrow \alpha$-rearrangement is exactly reproduced in the reverse $\alpha \rightarrow \gamma$-transformation.

This effect turned out to be of practical importance and has been used for the development of a new class of alloys possessing what is called the ***shape memory effect***.

If a piece of such an alloy is deformed (bent or twisted) at a temperature below M_s, i.e. in the martensitic state, and then heated above A_s (i.e. the reverse martensitic transformation is induced), the piece will restore the shape it had prior to the deformation.

The shape memory effect can be utilized, for instance, in the following manner. Suppose that a machine part (say, a car fender) has been deformed by a mechanical action. If the part is made of a material exhibiting the shape memory effect, it can be restored without mechanical trueing, simply by heating it to a temperature above the point of the reverse martensitic transformation.

This is, naturally, only the perspective of a distant future, and the shape memory effect is now employed only in some specific cases. The nearest perspective for its utilization is in machines for direct conversion of heat into mechanical work. The shape memory effect has been discovered in a relatively small number of alloys and compounds (CaCd, AgCd, Fe_3Ni) and is the most pronounced in NiTi intermetallide.

10-5. BAINITIC TRANSFORMATION

The bainitic transformation of undercooled austenite occurs in a temperature range between the pearlitic and the martensitic range and for that reason is often called an intermediate transformation.

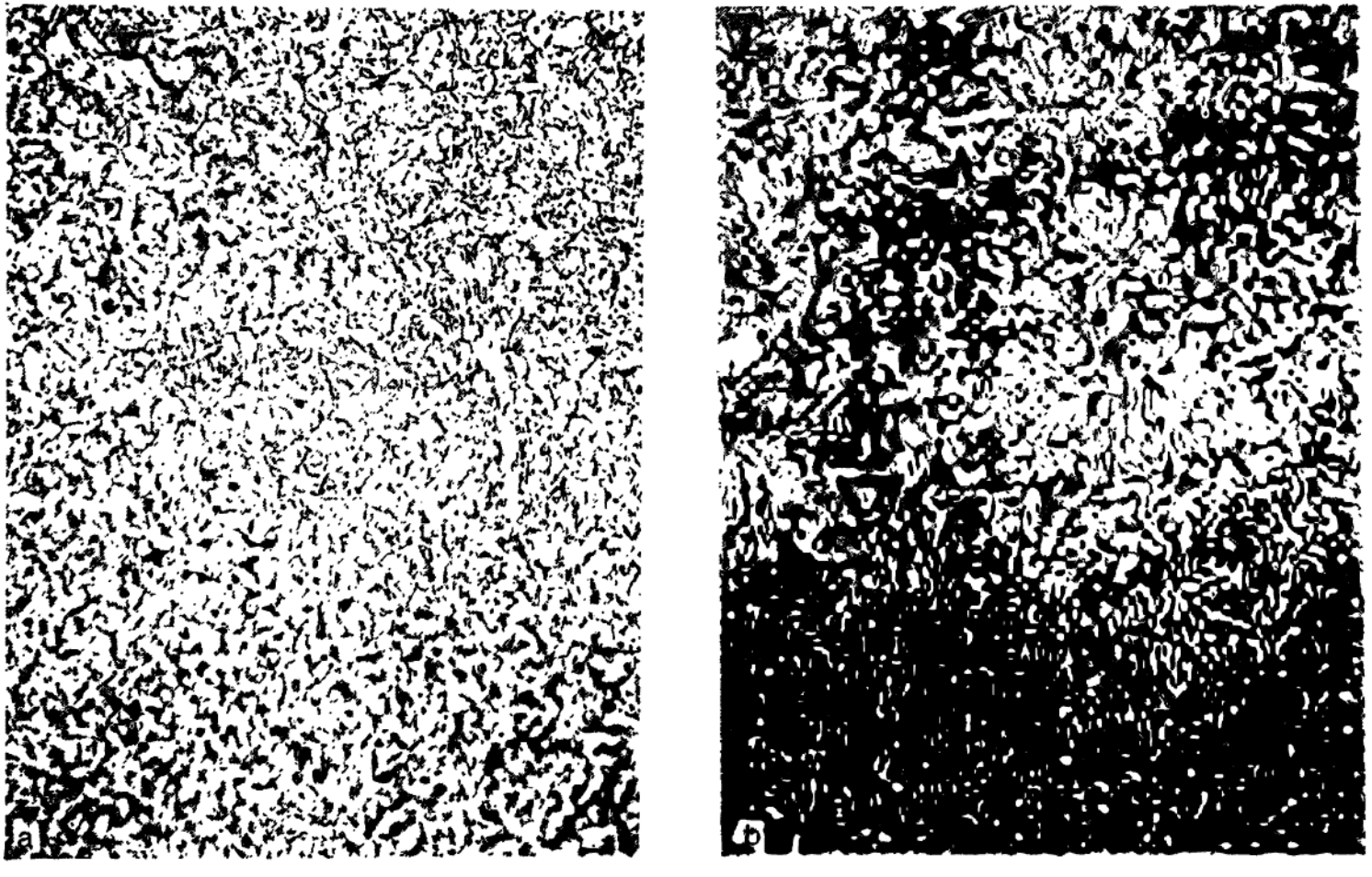

Fig. 10-40. The structure of bainite, ×500
(*a*) upper; (*b*) lower

It has features of both the pearlitic and the martensitic transformation (therefore it should not be related to the principal types of transformation).

The decisive feature of the bainitic transformation is that it occurs in the temperature interval where there is practically no diffusion (self-diffusion) of iron, but the diffusion of carbon is quite intensive, i.e. the interval of bainitic transformation is above Chernov's *d* point but below *e* point (see Fig. 10-18).

Bainitic transformation occurs by a more complicated mechanism than pearlitic or martensitic transformation.

If austenite is undercooled to a suitable temperature (below point *e*), its carbon is redistributed by diffusion so that some portions of austenite are enriched in carbon and the other are depleted. This inhomogeneity of the concentration causes the appearance of stresses and, since the martensitic point of the carbon-depleted portions is above the temperature of the isothermal holding, a plastic deformation will induce the $\gamma \rightarrow \alpha$-transformation by the martensitic reaction. This $\gamma \rightarrow \alpha$-change by the martensitic type is the specific feature of the bainitic transformation, which is confirmed by the fact that bainitic transformation produces a relieved surface on polished microsections.

Thus, though the $\gamma \rightarrow \alpha$-change proper in the bainitic transformation takes place by the diffusionless mechanism, it is prepared by diffusion processes occurring in the austenite; these diffusion processes determine the rate of the bainitic transformation.

The portions of austenite which have been enriched in carbon undergo no changes and remain austenitic upon cooling from the temperature of isothermal holding to room temperature (or they may partially undergo the martensitic transformation).

Carbide particles which are found in the structure of steel upon bainitic transformation precipitate after the $\gamma \rightarrow \alpha$-change, which fact indicates that the redistribution of carbon does not result in full depletion of carbon in individual austenitic portions.

Whereas the described mechanism is valid for the whole temperature range of bainitic transformation, a change of temperature within that range may cause appreciable quantitative differences. At high temperatures (near point *e*), the effect of concentration redistribution is more appreciable than at lower temperatures (near point M_s).

This is why a distinction is made between *upper* and *lower bainite* which differ from one another both in microstructure (Fig. 10-40) and in properties.

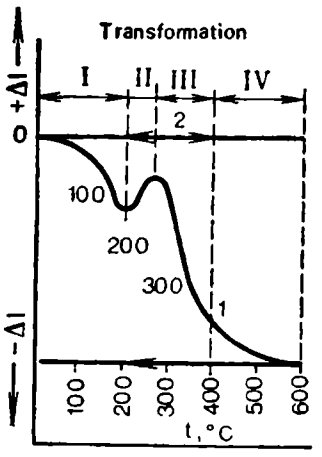

Fig. 10-41. Dilatometric curve of tempering of carbon steel (1.2% C)

1—as-hardened steel; *2*—as-annealed

10-6. TRANSFORMATIONS ON TEMPERING

The transformations occurring during heating of hardened steel have been established quite reliably by studying the microstructure, crystal lattice and the physical and mechanical properties of as-tempered steel and of the variation of these properties in the course of tempering.

The original structure of hardened steel prior to tempering consists of tetragonal martensite and austenite. Since martensite is the structure of the highest specific volume and austenite, the structure of the least specific volume, the transformations on tempering should be associated with volume changes, i.e. the volume of metal will decrease upon martensitic transformation (contraction of specimen) and increase upon austenitic transformation (expansion of specimen). The transformations in tempering can be fixed by means of a dilatometric curve (Fig. 10-41). If an annealed specimen is heated in a dilatometer[1] and there are no transformations in the metal, the instrument will plot a horizontal line[2]. Curve *1* of a hardened steel specimen deviates from horizontal line *2*, which is indicative of certain transformations. As is seen in the dilatometric curve of Fig. 10-41, no transformations occur to a temperature of about 80°C. With further heating to 200°C, the steel specimen contracts in length. This is an indication of what is called the *first transformation on tempering*. As has been detected by X-ray analysis, the *c* parameter of the martensitic lattice gradually diminishes within this temperature interval and the *c*/*a* ratio tends to unity.

The martensite that forms in this low-temperature tempering, in which the *c*/*a* ratio is not equal but very close to unity is called *temper martensite*. Therefore, the first tempering transformation is the transformation of tetragonal martensite into almost cubic temper martensite.

As has been indicated earlier, the sole cause for the tetragonality of martensite is dissolution of carbon; thus, a decrease in tetragonality can be explained by precipitation of carbon from the solution.

---

[1] *Dilatometer* is an instrument for measuring length changes in specimens during heating or cooling; it is employed to determine the critical points, coefficients of linear expansion, etc.

[2] The differential scheme of the instrument compensates for the expansion due to temperature.

The high-carbon phase that precipitates from the solution is extremely fine (a few atomic radii thick) carbide platelets which are coherently bonded with the solid-solution matrix. As has been established by radiographic and magnetothermal analysis, the metastable carbide that forms on low-temperature tempering differs from cementite. It has a hexagonal lattice and a formula close to Fe_2C and is described as ε-carbide in the specialist literature. At higher temperatures of tempering (300-400°C), an $\varepsilon \rightarrow Fe_3C$ carbide transformation takes place (sometimes via an intermediate stage of χ-carbide, i.e. by the reaction $\varepsilon \rightarrow \chi \rightarrow Fe_3C$)[1].

Thus, *the first transformation on tempering produces temper martensite which is a heterogeneous mixture of supersaturated α-solution (of an inhomogeneous concentration) and non-isolated carbide particles.*

It would be erroneous to think that there is no decomposition of martensite below 80°C. At this level of temperatures the same transformations associated with precipitation of carbides take place in the metal, but only at a very slow rate. It was found, for instance, that the content of martensite in a steel with 1.35 per cent C diminished to 1.02 per cent upon holding for 40 months at 20°C. An analysis of transformations at low temperatures (below 150°C), carried out by G. V. Kurdyumov et al., showed that the process was quite specific owing to the low rate of carbon diffusion at these temperatures.

The carbides which precipitate on tempering are formed at the expense of the carbon in the nearest volumes of the metal, whereas more distant volumes retain the initial carbon concentration. The state of the solid solution can thus be characterized by the coexistence of two solid solutions, one with a high (initial) concentration and the other, with a low.

The process of tempering develops by the formation of ever more crystals of the carbide phase in places where the solid solution is high in carbon.

Kurdyumov's studies have shown that thin carbide platelets precipitated at low temperatures of tempering are not fully isolated from α-solid solution. The lattice of martensite (α-solution) is matched with the carbide lattice along a certain crystal plane, i.e. the boundary atomic layer belongs both to martensite and to carbide. This matching (coherence) of the two lattices is disturbed at higher temperatures of tempering, at which carbides separate from martensite and coagulate into carbide particles.

Finally, latest studies by means of special electron-microscopic techniques (Yu. D. Tyapkin) have shown that at the stage prior to lattice separation, the carbide inclusions are regularly distributed in the α-lattice and form, as it were, a *macrolattice* of their own (Fig. 10-42) whose parameters are measured in hundreds of angstroems.

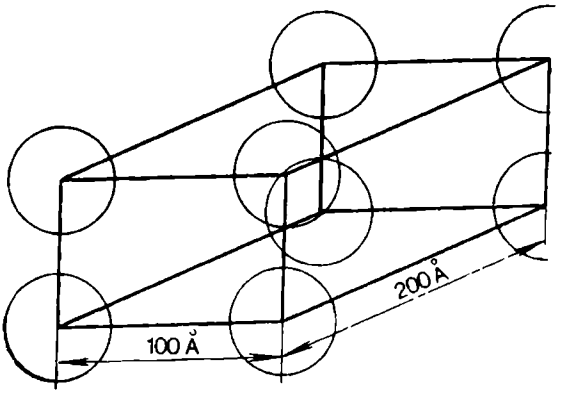

Fig. 10-42. Macrolattice of martensite

[1] The sequence of carbide transformations in tempering has been studied by B. A. Apaev, V. G. Permyakov, and other researchers. There is an opinion that intermediate carbides (ε, χ, etc.) are essentially cementite (Fe_3C) with various defects in the crystal structure.

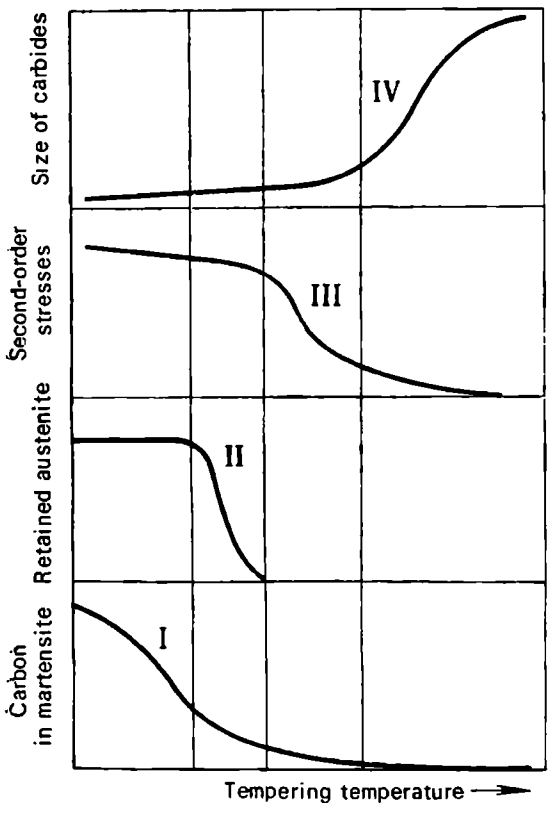

Fig. 10-43. Curves to illustrate the processes occurring in tempering

Heating to a temperature above 200°C will cause a different transformation resulting in expansion of the steel. This is what is called the *second transformation on tempering* which is confined to a temperature range from 200 to 300°C. In this interval, the retained austenite changes to a heterogeneous mixture of supersaturated α-solution and carbide. In other words, retained austenite transforms into temper martensite. This is diffusion transformation and in its nature resembles the bainitic transformation of primary austenite.

At the end of the second transformation, i.e. at 300°C, α-solid solution still contains around 0.15-0.20 per cent C. The contraction that occurs on further heating (see Fig. 10-41) is indicative of the complete precipitation of carbon from the solution and of the relaxation of the internal stresses that have appeared owing to the prior transformations which involved volume changes. At the same time, carbides separate from the matrix and form cementite (Fe_3C). All these changes characterize what is called the *third transformation on tempering*.

In other words, the *third transformation on tempering involves definite changes which result in stress relaxation and transformations of carbides*. The third transformation is finished at 400°C, with the steel structure consisting of ferrite and cementite. A further rise in temperature can cause coagulation of ferrite and cementite particles, which can be readily seen in microstructures at large magnifications.

The transformations occurring on tempering are graphically illustrated in Fig. 10-43, where *I* is the curve of precipitation of carbon from the solution, which occurs mainly at low temperatures (in high-carbon steel), but extends onto a wide temperature range; *II* is the curve of decomposition of retained austenite, which occurs within a limited temperature interval depending on steel composition; *III* is the curve of stress relaxation which develops most intensively at temperatures within 300-400°C; and *IV* is the curve

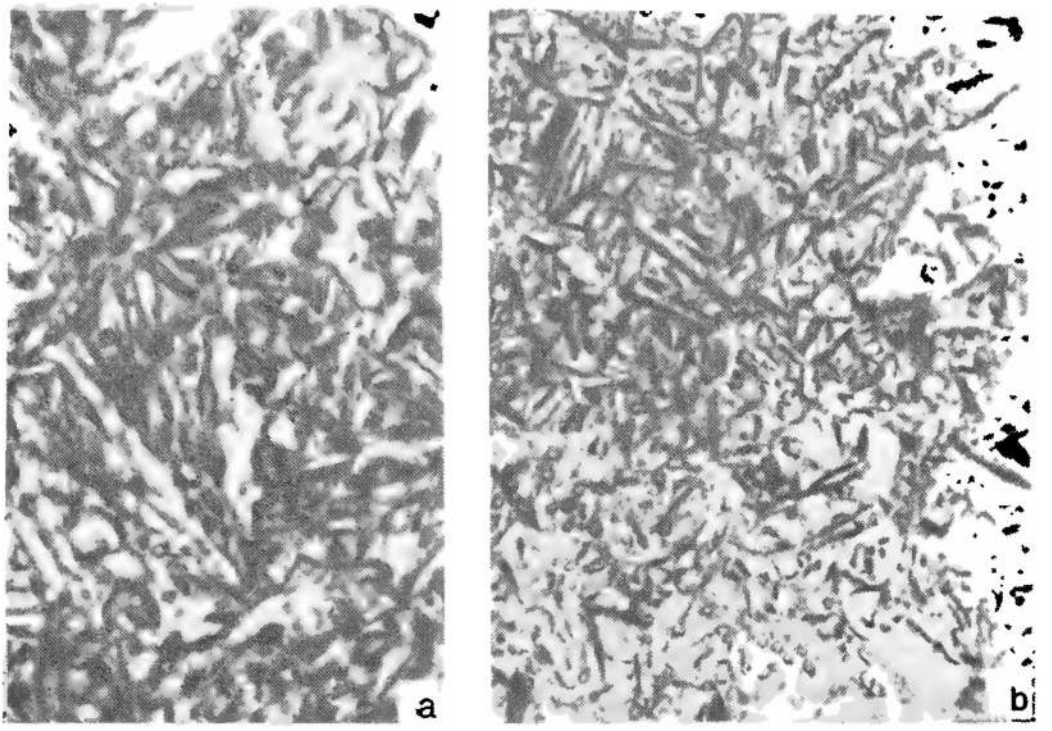

Fig. 10-44. Microstructure of tempered steel (0.45% C), ×500
(*a*) tempered at 400°C, troostite; (*b*) tempered at 550°C, sorbite

of coagulation of carbide particles which begins at low temperatures of tempering (150°C), but proceeds most intensively at temperatures above 400°C.

The indicated temperature ranges relate to tempering of carbon steel with slow heating. With fast heating, the temperatures of these transformations are shifted upwards along the temperature scale.

All the transformations just discussed occur within martensitic platelets, because of which the acicular structure is retained up to quite appreciable temperatures of tempering (Fig. 10-44).

Tempering at temperatures above 400°C forms a mixture of ferrite and cementite; this is why the structures formed on tempering have the same names as those obtained through direct decomposition of austenite into ferrite and cementite.

A steel tempered at 350-500°C has the structure of troostite (Fig. 10-44*a*) and that tempered at 500-600°C, the structure of sorbite (Fig. 10-44*b*). These structures differ in the hardness and dispersity of cementite particles.

It should also be noted that a ferrite-cementite mixture formed by decomposition of austenite substantially differs from a mixture obtained from martensite. The former (hardening troostite or hardening sorbite) contains lamellar cementite and the latter (if formed

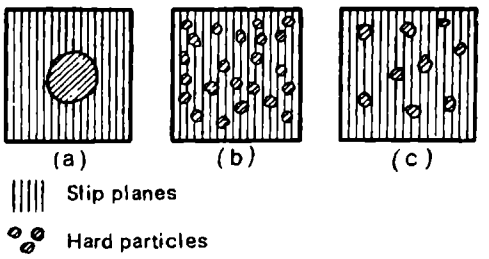

Fig. 10-45. Schemes to illustrate the effect of hard particles on strength and ductility of steel

at temperatures above 400°C) has the granular form of cementite. This difference in the form of cementite determines the difference in the properties of these two mixtures.

10-7. EFFECT OF HEAT TREATMENT ON STEEL PROPERTIES

Heat treatment can appreciably change the properties of a steel, its effect on the mechanical properties being most important.

A steel as annealed, normalized or tempered ($t_{tem} > 400$°C) consists of lamellar ferrite and carbide (cementite) inclusions. Ferrite has a low strength and high ductility, whereas cementite has a high hardness (around 800 *HB*) and zero values of elongation and reduction. The fact that iron-base alloys with more than 0.01 per cent carbon have an elevated strength and reduced plasticity should evidently be attributed to the strengthening effect of carbide inclusions. Since plastic strain (in some or other method of stressing) is possible only in ferrite, the strengthening effect of hard carbide inclusions can be assumed to act as follows.

At a low concentration of cementite inclusions (Fig. 10-45*a*), plastic deformation can develop relatively unobstructedly and the properties of the material are characterized by a low hardness.

With a larger number of cementite particles, for instance, if cementite particles are refined by heat treatment (Fig. 10-45*b*), they will distort the crystal lattice in adjacent grains and impede the movement of dislocations, thus producing a strengthening effect in the steel. On the contrary, if cementite particles are coarsened (Fig. 10-45*c*), certain volumes of ferrite will be freed for dislocation movement and the steel will be more capable of plastic deforming.

Thus, the hardness (strength) of a ferrite-cementite mixture (or any other two-phase mixture) is the sum of the natural hardness of the matrix plus the hardness increment due to metal volumes having a distorted lattice, the latter term being approximately proportional to the area of boundaries between the phases, i.e.

$$H_{al} = H_m + aS$$

where H_{al} is the hardness of the alloy; H_m is the hardness of the matrix of pure iron ($H_m \approx 80$ *HB*); S is the area of phase boundaries; and a is a coefficient.

If hardness is measured in Brinell numbers and the phase boundary area in mm^2/mm^3 (calculated from the average grain size and the number of particles in 1 mm^3 of the metal) $a = 0.004$ for steels with granular cementite inclusions and $a = 0.002$ for those with lamellar inclusions (lamellar pearlite).

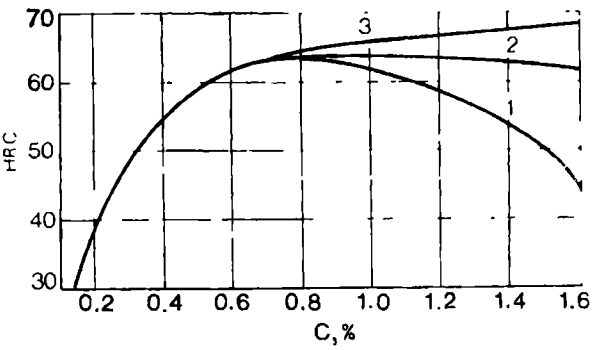

Fig. 10-46. Effect of carbon and hardening temperature on hardness of steel
1—heating above Ac_3; *2*—heating above Ac_1 but below Ac_3 (770°C); *3*—microhardness of martensite

The quantity of carbide particles of a constant size depends on the carbon content in steel (directly proportional to the carbon content in carbon steels). In carbon steel with 0.35 per cent C, cementite occupies approximately 5 per cent of the mass (or volume); steel with 0.7 per cent C contains 10 per cent of cementite, etc. This is why the values of strength in steels increase and the values of ductility diminish with increasing carbon content (as is shown for a normalized steel in Fig. 7-1).

For the same carbon content, the number of carbide particles, and therefore, the area of phase boundaries increase with refinement of carbides. The refining effect is obtained by heat treatment. For instance, the size of particles of the strengthening phase (cementite) in as-normalized steel may be depicted as in Fig. 10-45*a* and their state upon hardening and tempering at various temperatures, as in Fig. 10-45*b*,*c*; the refinement of the carbide component upon this treatment explains why hardened and tempered steel has a higher strength than in normalized state.

A higher temperature of tempering produces coarser cementite particles and thus lowers the strength. The same effect is observed on lowering the cooling rate (in hardening) and on raising the temperature of isothermal decomposition.

Thus, we have explained the variations of hardness in annealed (normalized) and tempered steel which has the structure of ferrite cementite mixture of various dispersity. It is, however, impossible to explain the high hardness of martensite in this manner. The point is that elementary crystal cells in martensite are distorted, shear displacements in its structure are almost impossible, and martensite can be hardly deformed plastically.

At a higher carbon content in steel, the tetragonal lattice of martensite is more distorted and martensite has a higher hardness. The martensite in a steel with 0.1 per cent C has a hardness of approximately 30 *HRC*. With 0.7 per cent C, the hardness of martensite attains the maximum value (64 *HRC*) and does not substantially increase with further increase in the carbon content (curve *2* in Fig. 10-46). However, this curve does not always characterize the hardness of hardened steel since the latter usually contains a certain quantity of retained austenite. If heating for hardening is done

Fig. 10-47. Martensitic needles in austenitic grains of different size, ×500

above point Ac_3 and all the carbon passes into the solid solution, the hardness of hardened steel will diminish with an increase of the carbon content above 0.8 per cent, since the quantity of retained austenite increases quite rapidly (curve *1* in Fig. 10-46; see also Fig. 10-34).

At heating for hardening to a conventional temperature, i.e. to $Ac_1 + 30°C$, the same quantity of carbon in all hypereutectoid steels passes into the solution (in accordance with line *SE* in the Fe-C diagram), therefore, the same quantity of retained austenite is fixed, and all hypereutectoid steels acquire the same hardness upon this heat treatment (curve *2* in Fig. 10-46).

The ductility (toughness) of steel is of no less importance than hardness. The ductility and toughness are usually lower at higher values of hardness. For the same hardness value, however, the values of ductility and toughness may appreciably vary depending on the structure and the size of martensitic platelets.

The mechanism of diffusionless oriented martensitic transformation that has been discussed in Section 10-4 is responsible for the structure of martensite being substantially dependent on the original austenitic structure. Both the displacements on plastic deformation and martensitic platelets develop within austenitic grains from one edge to another. This means that longer martensitic platelets can form in larger austenitic grains. In the structure shown in Fig. 10-47, large martensitic needles have formed in a large grain of austenite and finer needles, in smaller grains. The plastic properties and especially the toughness of martensite and of the products of its decomposition (up to the tempering temperatures at which the microstructure remains acicular) are appreciably impaired with structure coarsening (whereas the hardness is almost independent of the size of martensitic needles). This dependence of the properties of heat-treated steel on the size of martensitic platelets is of great importance.

Thus, in order to obtain the best combination of mechanical properties in hardened steel, it is essential to form a fine-acicular martensitic structure, which is possible only if the original austenitic structure is also fine-grained.

As has been noted, a lower temperature of isothermal decomposition of austenite increases the dispersity of ferrite-cementite particles and thus increases the hardness. This is why pearlite, i.e. the product of transformation of austenite at 650-700°C, has a lower hardness than sorbite which forms on decomposition of austenite at 600-650°C, and so on. Approximate values of the hardness of various structures obtained on decomposition of austenite may be found in Fig. 10-19.

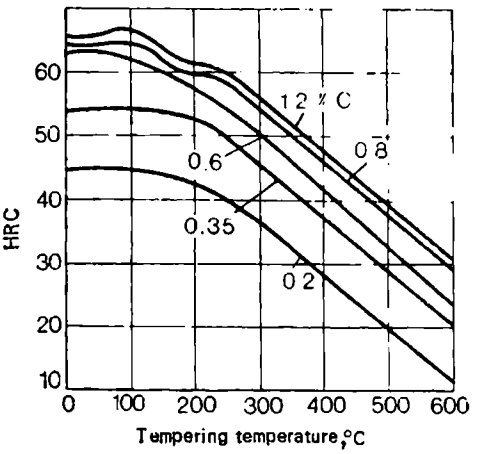

Fig. 10-48. Effect of tempering temperature on hardness of carbon steels with various content of carbon

Tempering is the final operation of heat treatment, which forms the final desired properties in steel parts. For that reason, the properties of tempered steels should be discussed in more detail. The variations of hardness of steels with different carbon contents, depending on the temperature of tempering, are shown in Fig. 10-48.

Hardness changes on tempering owing to certain structural changes. Heating at a temperature up to 100°C gives only a slight (by 1-2 *HRC* numbers) increase in hardness (and only in high-carbon steels), owing to the change from tetragonal martensite to temper martensite. With a further increase of the tempering temperature, the hardness diminishes due to the coarsening of carbide particles and the removal of carbon from α-solid solution. The linear relationship between hardness and temperature is disturbed in the temperature range of 200-250°C, i.e. where retained austenite begins to transform. At these temperatures, the decline in hardness slows down and can even increase somewhat in high-carbon steels where retained austenite transforms into a harder temper martensite. The general trend is, however, that hardness diminishes with increasing temperature of tempering, as also do the other strength characteristics (σ_t, $\sigma_{0.2}$), whereas the ductility indices (δ, ψ) increase (Fig. 10-49). The variations of these properties with tempering temperature are, however, far from being monotonous. The marks on the left-hand scale in Fig. 10-49 correspond to the properties of as-hardened (untempered) steel and those on the right-hand scale, to those of annealed steel.

Tempering at 300°C increases the ultimate strength and the elastic limit. These characteristics are lower in as-hardened steel (owing to the stressed state of the metal) and in that tempered at a lower temperature.

The ductility characteristics (δ, ψ) increase with increasing tem-

perature of tempering. The highest ductility (ψ) is obtained on tempering at 600-650°C, whereas tempering at higher temperatures gives no increase in ψ. Note also that the whole complex of mechanical properties of a steel tempered at 600-650°C is higher than in as-annealed state.

The better mechanical properties of a steel upon hardening and high-temperature tempering compared to the same steel in as-annealed or normalized state (higher values of $\sigma_{0.2}$, ψ, and a_n for the same ultimate strength) can be explained by the different structure of the temper sorbite (pearlite) and the sorbite formed on hardening (as has been noted, the former is granular and the latter, lamellar). A double heat treatment procedure, consisting in hardening followed with high-temperature tempering, appreciably improves the whole complex of mechanical properties of a steel. It is called *improving heat treatment* and is the principal type of heat treatment for structural steels.

The effect of tempering temperature on the impact toughness of steels is as follows. A hardened carbon steel retains a low value of impact toughness (as measured in bending impact tests) up to a tempering temperature of 400°C; at higher temperatures of tempering, the impact toughness intensively increases and attains its maximum at 600°C. In some grades of alloy steel, tempering at a temperature of roughly 300°C can lower the initial value of toughness, which again increases on tempering at temperatures above 450-500°C. This phenomenon will be discussed in Sec. 16-2.

We have considered the effect of tempering temperature on the properties of steels. The tempering temperature is the most essential factor affecting the properties of tempered steel. Tempering

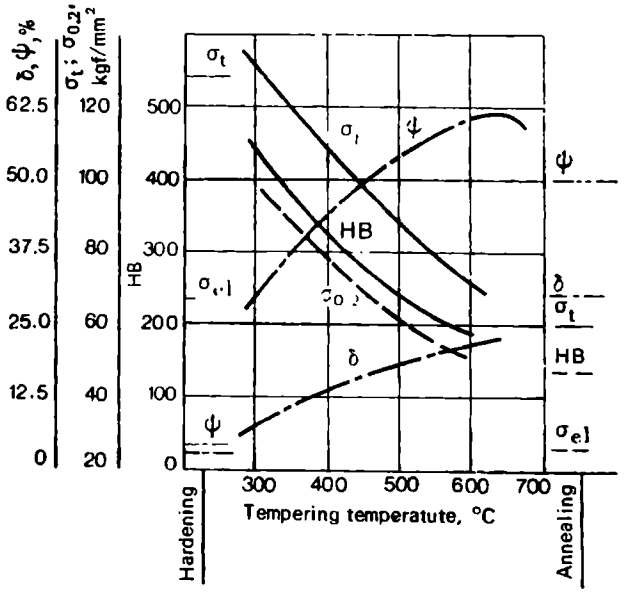

Fig. 10-49. Effect of tempering temperature on mechanical properties of steel Grade 40

is associated with diffusion processes, because of which a sufficient holding time can be favourable for the transformations that occur at a given temperature.

A long tempering can be made shorter but carried out at a higher temperature. If the temperature and time of tempering are balanced so that the tempered steel has the same hardness (*isosklerous tempering*), the other mechanical properties of the steel will be almost the same.

In contrast to some alloy steels, the mechanical properties of carbon steels (and many other types) do not depend on the rate of cooling from the temperature of tempering. The properties of steel on tempering depend only on the temperature and time of tempering.

10-8. THERMOMECHANICAL TREATMENT

As has been noted, thermomechanical treatment (thermoplastic working) is a combination of two methods of strengthening — plastic deformation and phase transformations.

As applied to steels, thermomechanical treatment (THT) consists in strain hardening of austenite followed by the transformation of austenite into another structure.

The most common processes of thermomechanical treatment are as follows (Fig. 10-50):

high-temperature thermomechanical treatment (HTHT), in which austenite is deformed at temperatures above the recrystallization point (t_r in Fig. 10-50), usually above the critical points and then cooled quickly;

low-temperature thermomechanical treatment (LHHT) in which austenite is deformed at a temperature below t_r, i.e. in the unstable state of undercooling below the critical points and then cooled to cause phase transformations;

preliminary thermomechanical treatment[1] (PHT), in which the steel is strain

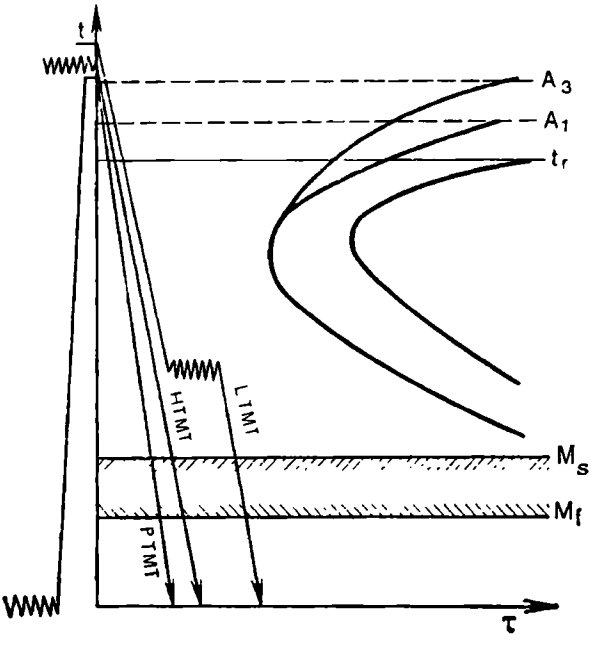

Fig. 10-50. Classification diagram of thermomechanical treatment

[1] Proposed by M. L. Bernstein and A. G. Rachstadt.

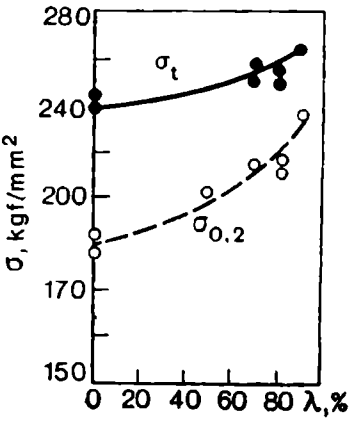

Fig. 10-51. Effect of deformation (λ) in low-temperature thermomechanical treatment on strength of steel (0.3% C, 2.2% Cr, 1.5% Ni, 0.3% V, and 0.3% Mo)

hardened prior to being heat treated and then heated up quickly to the austenitic state and cooled, but so as to retain to some or other extent the strain-hardening effect.

There also are many other varieties of thermomechanical treatment differing in the conditions of heating or cooling, type of deformation and other minor details; the Author has no possibility to describe all of them within the scope of this book.

In all types of thermomechanical treatment the changes that are caused in austenite by plastic deformation are transferred (either partially or completely) to martensite.

Thus, a steel is strengthened due to the martensitic reaction and also due to the structural defects produced in deformed austenite and inherited by martensite[1].

A typical procedure of thermomechanical treatment is low-temperature thermomechanical treatment[2]. Austenite is undercooled to 500-600°C and deformed to cause the strain-hardening effect. A heavier deformation, and therefore, a greater strain-hardening effect, produce a higher strength of martensite (Fig. 10-51). Very heavy deformations (80-90 per cent) are employed to obtain the maximum strength. Since deformation is made at a low temperature (substantially lower than the common temperatures for hot working), the steel retains a high ductility (more strictly, a high resistance to deformation), so that the necessity of a heavy deforming is associated with certain technological difficulties.

Low-temperature thermomechanical treatment has found no wide application which is not surprising if we recall that it increases the strength at the expense of ductility.

HTHT is not a typical procedure of thermomechanical treatment, at least because the strain hardening in austenite is not retained in pure form up to the martensitic transformation. As follows from its definition, HTHT is effected above the point of recrystallization, so that recrystallization processes are likely to occur if the steel is not cooled immediately below t_r (which is difficult to do in practice).

Practically, and this is not so bad, there is a pause, i.e. a time interval from the end of deformation to the beginning of quenching during which recrystallization of austenite takes place. The best results are obtained when the pause

[1] Fine-block twinned structure, lattice distortion by dissolved carbon, etc.

[2] The operation is usually called ausforming in English literature; the name implies that austenite is being deformed.

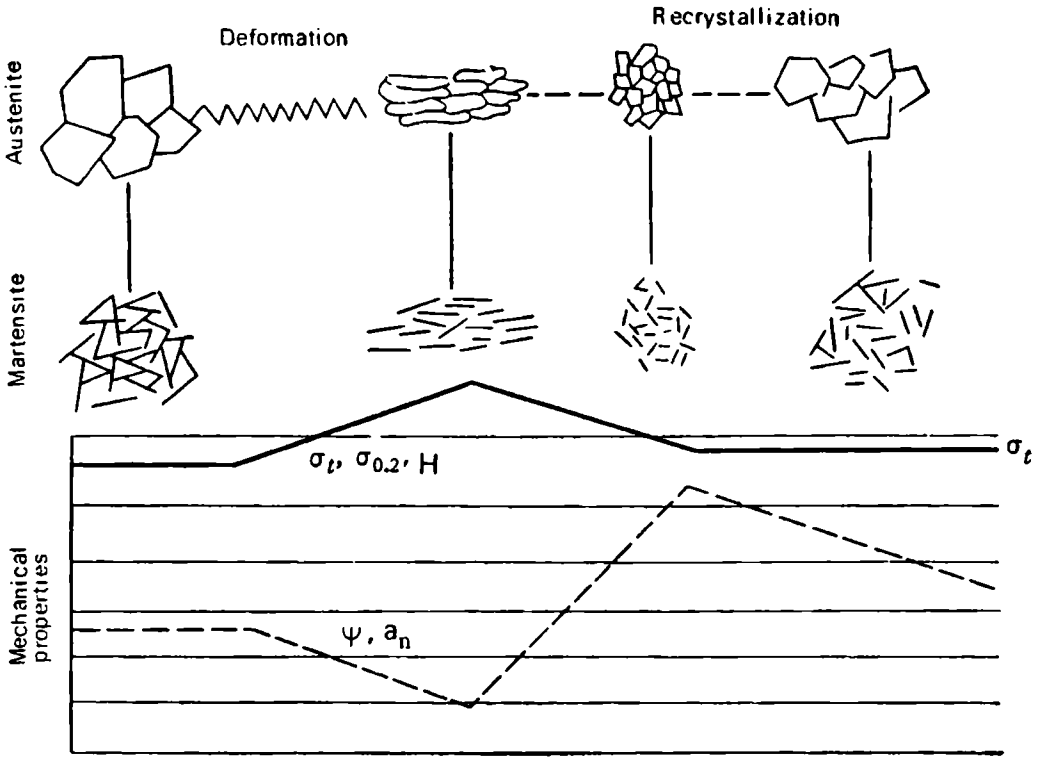

Fig. 10-52. Effect of high-temperature thermomechanical treatment on mechanical properties of steel

is sufficient to complete the first stage of recrystallization, i.e. to remove the strain-hardening effect and form fine grains of recrystallized austenite. A longer pause (holding time) can result in grain coarsening and impairment of steel properties. The time of the pause evidently depends on steel composition, temperature, deformation, and other factors. Since this type of HTHT produces no strain-hardening effect in the deformed metal, there is no strengthening (increasing of σ_t, $\sigma_{0.2}$ and hardness) in the final steel, but the refinement of grain lowers the ductile-to-brittle transition temperature and increases the percentage of ductile component in the fracture in high-strength steels, which results in better indices of ductility (ψ) and toughness (a_n) in conventional tests (Fig. 10-52).

This effect of HTHT can be obtained at a relatively slight deformation (from 20 to 40 per cent).

In all procedures of thermomechanical treatment, the metal is deformed, transforms to martensite and then tempered to a given strength (ductility).

In certain cases, the deformed steel is subjected to isothermal annealing to bainite[1] or even to pearlitic transformation. The latter method, called 'controlled rolling', has found wide application in the manufacture of high-strength low-alloy steels and will be discussed in Sec. 16-7.

[1] The process proposed by L. I. Tushinsky.

In all procedures of thermomechanical treatment, deformation precedes transformation. There is, however, a class of heat treatment procedures based on an inverse order of operations, i.e. transformation followed by strain hardening. They can be combined by a general name *mechanico-thermal treatment.*

If a high strength (martensite) is obtained by hardening, the possibilities for strengthening of this structural state by plastic deformation are not great owing to the low ductility of martensite. Nevertheless, a deformation of 3-5 per cent in martensite can produce an additional strengthening effect of 10-20 per cent. This heat treatment process (hardening to martensite + slight plastic deformation + low-temperature tempering) is also sometimes employed and is called *marforming* (the name implies that martensite is deformed, in contrast to ausforming where deformation is applied to austenite).

A procedure in which the steel is transformed to fine-lamellar pearlite (troostite) and then plastically deformed is called *patenting* (see earlier in the book). In patenting, heavy deformations are essential for obtaining high mechanical properties. It should be noted that patenting of high-carbon steels (1 per cent C) with a heavy deformation (above 95 per cent) can produce the highest value of real ultimate strength obtainable in industrial products: 450 kgf mm^2, or almost one-third of the theoretical ultimate strength. Such a strength, however, is obtained in thin wire only.

LITERATURE

Bochvar A. A., *Fundamentals of Heat Treatment of Alloys.* Moscow-Leningrad, "Metallurgizdat", 1940 (in Russian).

Steinberg S. S., *Heat Treatment of Steels.* Sverdlovsk-Moscow, "Metallurgizdat", 1945 (in Russian).

Kurdyumov G. V., *Hardening and Tempering Phenomena in Steel.* Moscow, "Metallurgizdat", 1960 (in Russian).

Gulyaev A. P., *Heat Treatment of Steel.* Moscow, "Mashgiz", 1960 (in Russian).

Blanter M. E., *Phase Transformations in Heat Treatment of Steel.* Moscow, "Metallurgizdat", 1962 (in Russian).

Sadovsky V. D., *Structural Inheritance in Steel.* Moscow, "Metallurgiya", 1973 (in Russian).

Belous M. V., Cherepin V. T., Vasilyev M. A., *Transformations in Tempered Steel.* Moscow, "Metallurgiya", 1973 (in Russian).

Novikov I. I., *Theory of Heat Treatment of Metals.* Moscow, "Metallurgiya", 1974 (in Russian); English translation: Mir Publishers, Moscow, 1978.

Lysak L. I., Nikolin B. I., *Physical Principles of Heat Treatment of Steel.* Kiev, "Tekhnika", 1975 (in Russian).

Chapter 11

PRACTICE OF HEAT TREATMENT OF STEEL

11-1. HARDENING TEMPERATURE

The temperature of hardening for most steels is determined by the position of the critical points, A_1 and A_3.

For carbon steels, the hardening temperature can be determined by means of the iron-carbon constitutional diagram (Fig. 11-1).

The hardening of a hypoeutectoid steel from a temperature above Ac_1 but below Ac_3 retains a portion of ferrite in the martensitic structure (Fig. 11-2*a*); ferrite lowers the hardness of the hardened steel and impairs the mechanical properties upon tempering. This type of hardening is called incomplete and usually is not employed.

For hypereutectoid steels, the optimum temperature of hardening lies between Ac_1 and Ac_3, i.e. corresponds to the conditions of incomplete hardening (Fig. 11-2*b*).

The presence of excess cementite in the structure of hardened steel is favourable in many respects. For instance, inclusions of excess cementite increase the wear resistance. Heating above Ac_3

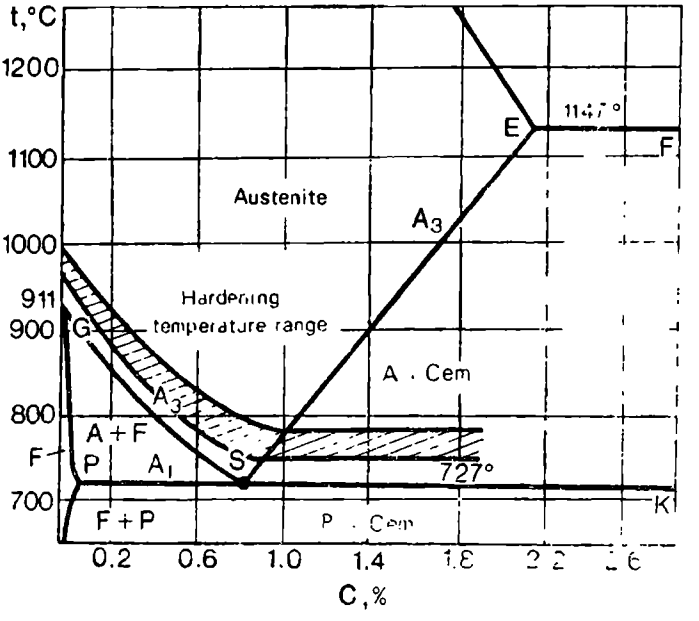

Fig. 11-1. Optimum temperature range for hardening of carbon steel

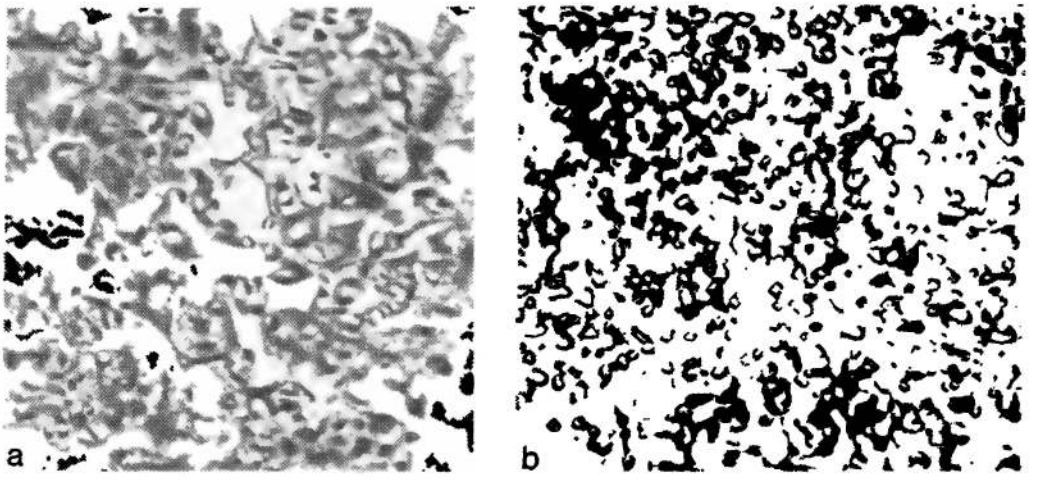

Fig. 11-2. Microstructures of hardened steels

(*a*) hypoeutectoid steel, partial hardening (heating above Ac_1 but below Ac_3); martensite + ferrite; (*b*) hypereutectoid steel, correct hardening (heating above Ac_1 but below Ac_3); martensite + cementite; ×500

is not needed and can even be dangerous, since it dissolves the excess cementite and increases the concentration of retained austenite (see curve *1* in Fig. 10-46) and thus can even somewhat lower the hardness, this heating causes coarsening of austenitic grain, increases the risk of appearance of high hardening stresses, produces a greater surface decarburization.

Thus, the optimum temperature of hardening is 30-50°C above Ac_3 for hypoeutectoid steels and 30-50°C above Ac_1 for hypereutectoid grades.

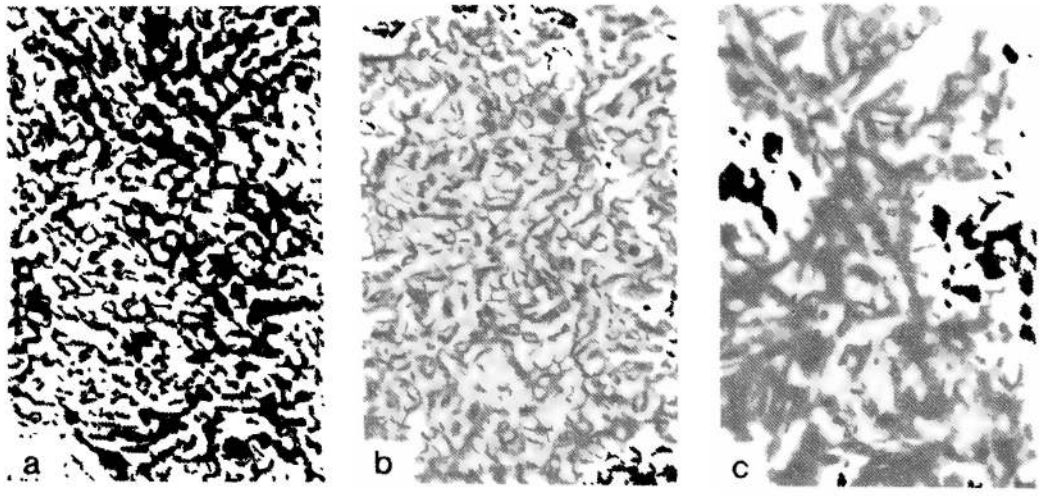

Fig. 11-3. Microstructure of martensite in steel 40, ×500

(*a*) fine-grained structure upon hardening from normal temperature; (*b*) coarse-grained structure upon slight overheating; (*c*) ditto, upon heavy overheating

A higher temperature of hardening coarsens the austenitic grain which is detected in the first place by a coarser acicular structure of martensite (Fig. 11-3) or by a coarse-grained crystalline fracture. A structure of this type has a low toughness.

11-2. HEATING TIME

The total time of heating is the sum of the time for raising the temperature to the specified level (τ_h) and the time of holding (soaking) at that temperature (τ_s):

$$\tau_{tot} = \tau_h + \tau_s$$

The heating time depends on the heating capacity of the medium, the size and shape of heated articles, and their arrangement in the heating furnace; τ_s depends on the rate of phase transformations, which is determined by the degree of overheating above the critical point and by the dispersity of the original structure.

In practice, τ_s can be taken equal to 1 min for carbon steels and 2 min for alloy steels, as in the latter carbides more slowly pass into the solid solution. With heating of large-size parts (when τ_h is appreciably greater than 1-2 minutes), τ_s can be neglected; with small parts (diameter or thickness less than 1 mm), the term τ_h can be neglected.

Heating for hardening is usually done in gaseous media (hot air, fuel combustion products), molten salts or molten metals. The time relation of heating in these media is as follows: 1 in gaseous media, 0.5 in molten salts, and 0.25 in molten metals.

The heating time τ_h is longer for larger parts. If we compare the heating time (τ_h) for a sphere, cylinder, parallelepiped and plate (assuming that $D_{sph} = d_{cyl} = a_{par} = \delta_{pl}$, Fig. 11-4), the relative heating time will be 1 for the sphere, 2.5 for the parallelepiped, 2 for the cylinder, and 4 for the plate.

Finally, if we compare the heating time for parts of the same size and shape, of which the first part is uniformly heated from all sides, the second from three sides (for instance, a parallelepiped placed on the cold bottom of a furnace), and the third is heated from only one side, their heating times will be in a relation of 1 : 1.5 : 4.

Thus, the time of heating depends on many factors and may vary in practice from 1-2 minutes (heating of small parts in a salt bath) to many hours (heating of large parts in a furnace).

The heating time for a given part and particular conditions can be accurately determined only by experiment, but can be calculated approximately. There

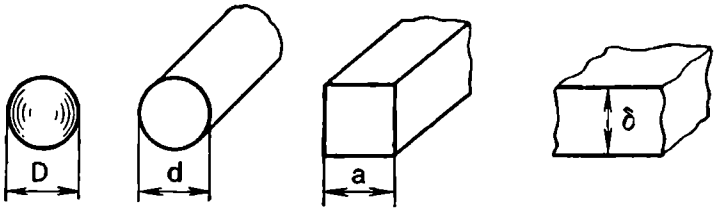

Fig. 11-4

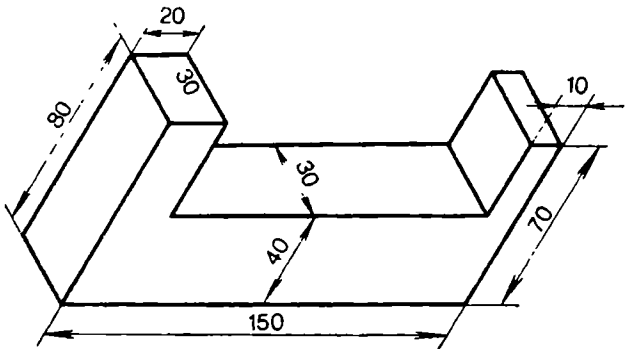

Fig. 11-5

are a number of methods for calculating the time of heating. One of them will be discussed below.

Let the soaking time be 1 or 2 minutes. The time of heating is calculated by the formula:

$$\tau_h = 0.1 D_1 K_1 K_2 K_3$$

where D_1 is the size parameter of the part being heated (mm), i.e. the minimal size of the maximal cross-section (for instance, for a plate it is equal to the thickness δ); K_1 is a coefficient depending on the heating medium (2 for a gaseous medium, 1 for molten salt, and 0.5 for molten metal); K_2 is a shape coefficient (1 for a sphere, 2 for cylinder, 2.5 for parallelepiped, and 4 for plate); and K_3 is a coefficient of uniformity of heating (1 for heating from all sides, 4 for heating from one side).

Example. Determine the time of heating for a part shown in Fig. 11-5. The part is made of an alloy steel and heated from all sides in a furnace.

The maximal cross-section of the part is 30 mm × 40 mm, therefore, $D_1 = 30$. The heating time is calculated by the formula above:

$$\tau_h = 0.1 \times 30 \times 2 \times 2.5 \times 1 = 15 \text{ min}$$

The total time of heating is

$$\tau_{tot} = 15 + 2 = 17 \text{ min}$$

Note that our recommendations relate to heating to 800-900°C, i.e. to common temperatures of heating for hardening, annealing or normalizing for most grades of steel.

The heating time is shorter if heating is to be done to a higher temperature (for instance, heating for hardening of stainless and high-speed steels), since the intensity of radiation rapidly increases with temperature. On the contrary, heating at temperatures below 800-900°C (for instance, annealing heating) proceeds more slowly and requires more time, since heat transfer at low temperatures is mainly effected by convection.

Naturally, it is implied in all the cases considered that the heater (furnace of bath) is sufficiently powerful and cannot be appreciably chilled by placing cold parts into it.

11-3. CHEMICAL ACTION OF HEATING MEDIUM

At high temperatures, the metal surface chemically reacts with the surrounding medium, with two processes being of special importance:

(1) *decarburizing* of steel, which is associated with burning off of carbon in the surface layers ($C + O_2 \rightarrow CO_2$); and

(2) *oxidation* of steel, i.e. formation of iron-oxide scale ($2Fe + O_2 \rightarrow 2FeO$).

The intensity of oxidation and decarburization of steel depends on the temperature and the composition of the steel and surrounding gaseous medium.

Oxidation and decarburization are diffusion processes and are accelerated at higher temperatures.

The furnace atmosphere may consist of various gases, depending on the conditions of combustion and temperature, the commonest furnace gases being CO_2, CO, O_2, H_2, H_2O, N_2, and CH_4.

These gases have a different effect on steel. For instance, H_2 decarburizes, CO_2 oxidizes, O_2 and H_2O oxidize and decarburize, CO and CH_4 carburize.

By analysing the equilibrium laws for these gases, i.e. the laws of their interaction with steel and between one another, it is possible to create such conditions of heat treatment at a given temperature when the oxidizing-reducing and carburizing-decarburizing reactions will proceed at the same rate in both directions, i.e. the metal will not react with the atmosphere and its composition will not change. In that case the atmosphere is said to be inert, or neutral; it has no effect on metal surface.

To form an inert atmosphere in a furnace at a given temperature and for a given steel grade (content of carbon in steel), the carburizing, oxidizing, decarburizing and reducing gases should be present in definite proportions, i.e. definite ratios of

$$\frac{CO_2}{CO}, \quad \frac{H_2O}{H_2} \quad \text{and} \quad \frac{CH_4}{H_2}$$

should be observed.

In modern furnaces for scale-free heating (called controlled-atmosphere furnaces), special means are provided to produce a gaseous medium of a desired composition. Such furnaces are of electric or crucible type (with outside heating of the crucible).

Heating without oxidation and decarburization can also be effected in molten salts.

A salt mixture for a heating bath is prepared so that its melting point be below the desired temperature of heat treatment. It is also essential that salt crusts adhered to the metal surface could be easily dissolved in or washed off by water.

Mixtures of chlorides, nitrates and nitrites of alkali-earth metals and also alkaline mixtures have found use for the purpose. The commonest salt compositions and their applications are given in Table 11-1.

Recently, the process of heating in a fluidized bed has come into use.

If hot air is blown through a layer of fine particles (usually corundum particles 200-250 μm in diameter), the layer is 'fluidized', i.e. resembles a boiling liquid. It can be used as a heating medium provided that its temperature is sufficiently high. Other gases, including inert ones, can be used in place of air. The fluidized bed is a multi-purpose medium and can also be used as a quench (in that case cold air should be blown through the layer). The cooling capacity of a fluidized bed is an intermediate one between water and oil. Using various active media instead of air, the fluidized bed can be employed for various procedures of chemical heat treatment (carburizing, nitriding, etc.)

Table 11-1. Compositions of Salt Baths Used for Heating of Metal

Salt bath	Temperature of complete dissolution, °C	Working temperature, °C	Application
$BaCl_2$	900	1 000-1 300	Heating of high-speed, stainless and other steels
78% $BaCl_2$+22% NaCl	640	750-900	Heating of carbon and low-alloy steels prior to quenching
50% NaCl+50% KCl	670	750-900	
20% KCl+60% NaCl+ +20% Na_2CO_3	700	750-900	
$NaNO_3$	310	400-550	Tempering and interrupted hardening (as chquenant)
50% $NaNO_3$+50% KNO_3	220	300-400	
50% $NaNO_3$+50% KNO_2	150	160-300	
20% NaOH+80% KOH	140	160-300	

11-4. QUENCHING MEDIA

In hardening, the metal should be cooled quickly to undercool austenite to the point of martensitic transformation. Quick cooling is essential not in the whole temperature range (from the temperature of heating to room temperature), but only within 650° to 400°C, i.e. in the range where austenite has the least stability and can be most quickly transformed into a ferrite-cementite mixture. At temperatures above 650°C, the rate of transformation of austenite is low and the steel can be, therefore, cooled at a low rate (of course, not too low, since a very low cooling rate might induce precipitation of ferrite and austenite-to-pearlite transformation). The temperature range from 650 to 400°C should be passed very quickly. In carbon steels, the austenite is again relatively stable at temperatures below 400°C so that cooling below that temperature can be done slowly[1]. Finally, in the martensitic interval, beginning from 200-300°C, slow cooling is especially favourable, since otherwise the appreciable structural stresses might be aggravated by the thermal stresses appearing on quick cooling. An ideal cooling curve in hardening is shown in Fig. 11-6.

[1] In alloy steels, accelerated transformation of austenite is possible at temperatures of 400-300°C, so that these steels should be cooled quickly within that temperature range, in some cases even more quickly than in the range of 600-400°C.

The acting mechanism of quenchants (water, oil) is as follows. When a hot metal part is immersed into a quench bath, a film of superheated vapour forms on the surface of the metal and cooling is effected through that vapour film, i.e. relatively slowly. In a certain time when the temperature of the metal surface rises to a definite value (which is determined by the nature of the quenchant), the vapour film is broken and the liquid begins to boil on the metal surface; in this period, cooling occurs quickly.

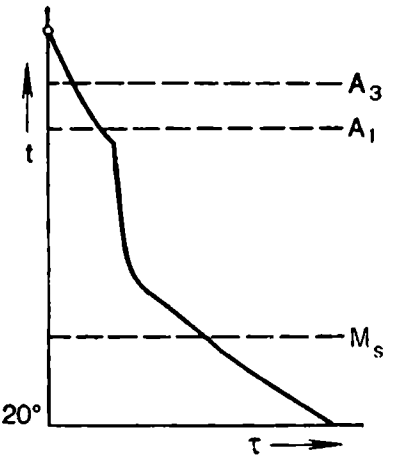

Fig. 11-6. Ideal cooling curve in hardening

The initial stage, at which cooling occurs relatively slowly, is called the *film boiling stage* and the second stage, that of *bubble boiling*. After the temperature of the metal surface has dropped below the boiling point of the liquid, (below 100°C with water quenching), the liquid stops boiling and the cooling process again occurs slowly. This third stage is the stage of *convective heat transfer*.

The cooling effect of a quenchant is much stronger with a wider temperature interval of the second (bubble-boiling) stage, i.e. with a higher temperature of the transition from the first to the second stage and a lower temperature of the transition from the second to the third.

Table 11-2. Characteristics of Selected Quenching Media

Medium	Temperature interval of bubble boiling, °C	Relative cooling intensity in the middle of bubble boiling interval
Water:		
20°C	400-100	1
40°C	350-100	0.7
80°C	250-100	0.2
Distilled water, 20°C	350-100	0.5
Water solutions, at 20°C:		
1% NaCl	500-100	1.5
10% NaCl	650-100	3.0
5-30% NaOH	650-100	2.5
50% NaOH	650-100	2.0
Water solution of 50% NaOH at 96°C	650-100	1.0
Mineral oil, 20-200°C	500-250	0.3

The temperatures (approximate) which delimit various cooling stages and the relative effectiveness of various quenchants are given in Table 11-2. The intensity of cooling also depends on the temperature, physical properties, viscosity and latent heat of vaporization of the quenching liquid.

The following considerations will be of use for the selection of quenchants.

If the stage of quick cooling of a quenching liquid lies, for instance, in the range of 400-100°C (water at 20°C, see Table 11-2), the surface of metal will be cooled quickly as soon as its temperature falls off to that level. Since the temperature at a certain depth below the metal surface is at that moment higher than at the surface, this means that quick cooling actually occurs in this case within a different (higher) temperature interval, say from 500 to 200°C. Therefore, metal parts of larger cross-section require a lower temperature interval of the quick cooling stage in order that the metal in the core be cooled quickly in the temperature range of pearlitic decomposition (650-400°C).

It should be kept in mind, however, that quick cooling in a lower temperature range (400-100°C), though being conductive to deeper hardening, increases the risk of surface cracking, owing to the quick passage through the martensitic interval.

The risk of hardening cracks sharply diminishes if quenching is done in oil which boils at a higher temperature than water and has a higher temperature of transition from bubble boiling to convective heat transfer. But oil has a higher viscosity and lower latent heat of vaporization, therefore, its cooling effect is less intensive than that of water.

The rate of cooling in water can be diminished by heating the water bath, which narrows the temperature interval of bubble boiling. The method is ineffective with oil, since oil at 20°C cools at the same rate as that heated to 150-200°C.

Among shortcomings of oil quenchants are a high flammability[1] and the need for replacement after a relatively short time of use (used oil thickens and loses its quenching capacity). Further, oil burns on the surface of hot metal and forms a burn-on film.

The quenching capacity of water appreciably depends on its purity. Salts, even in a slight concentration, substantially alter the quenching capacity of water. Thus, the cooling rate in distilled or rain water, which is free of salts, is only one-half of that in tap water. The quenching capacity of water is impaired in the presence of dissolved gases, because of which boiled water (or water already used in a quench bath) is a stronger quenchant than unboiled water. The quenching capacity of water can be substantially increased by dissolving alkalis or salts, which widen the temperature interval of bubble boiling and accelerate cooling within that interval. This method is often used in practice.

The quenchants that can be used for stepwise (or isothermal) hardening are given in Table 11-1.

11-5. HARDENABILITY

Hardenability is the property that determines the depth and distribution of hardness induced by quenching[2].

When a piece of metal is being quenched, it is cooled on the surface more quickly than in the core. The distribution of the cooling rate over the cross-section is approximately as shown by the dotted

[1] The flash point of various grades of oil may be from 150° to 320°C.

[2] Not to be confused with the *hardening capacity*; the latter is defined as the maximum hardness acquired by a steel on hardening. Hardening capacity mainly depends on the carbon content in steel (see Fig. 10-46).

line in Fig. 11-7*a*, i.e. the cooling rate is at the maximum on the surface and at the minimum in the core. If the critical cooling rate is equal to that determined by the dotted straight line in the figure, the piece of metal will be hardened not throughout but only to the depth shown hatched in the figure.

Naturally, the depth of hardened layer increases with diminishing critical rate of hardening. If v_{cr} is smaller than the cooling rate in the centre, the piece of metal will be hardened through. If its cross-section is large and the cooling rate on the surface is lower than the critical rate, the piece will not be hardened at all even in the surface in the given process of hardening.

Therefore, the hardenability is greater at lower values of v_{cr}. Both the hardenability and the critical cooling rate are closely associated with the rate of austenite-to-pearlite transformation, and therefore, with the position of the curve of the beginning of transformation in the *C*-curve.

Consider the hardening process in a cylindrical part. The cooling curves for the centre, surface and a circular section of a radius of 1/2 of the cylinder radius can be superimposed on the *C*-curve as shown in Fig. 11-7*b*. Under the given cooling conditions, the structure formed in the cylinder (made of a given grade of steel) will be martensitic in the surface, pearlitic in the core, and martensite-troostitic in the circular section.

If the *C*-curve passes more to the right than as shown in Fig. 11-7*b*, the hardenability will be greater owing to a higher stability of undercooled austenite.

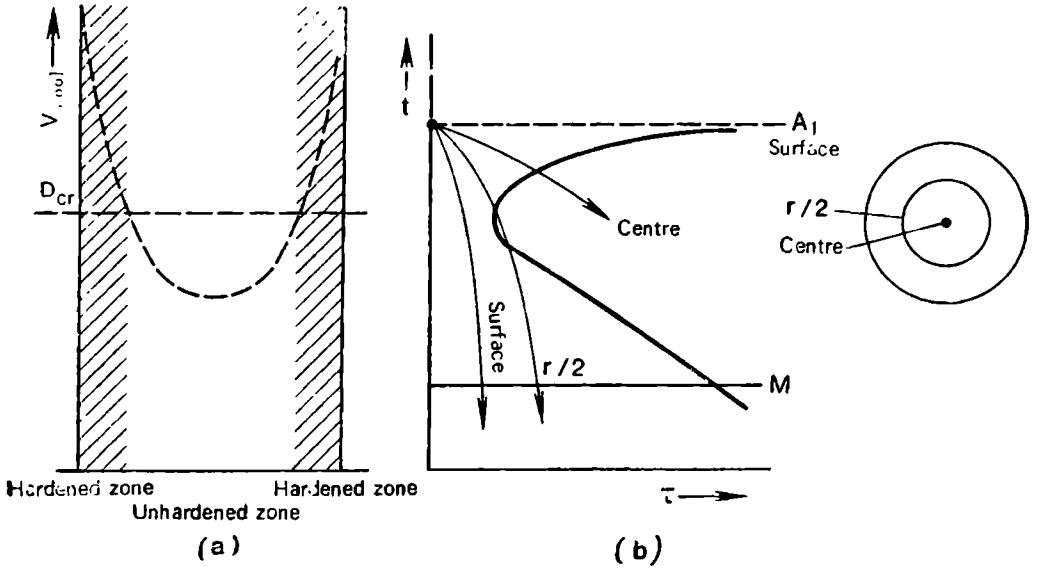

Fig. 11-7. Diagrams illustrating the distribution of cooling rate over the cross-section and its effect on hardening depth

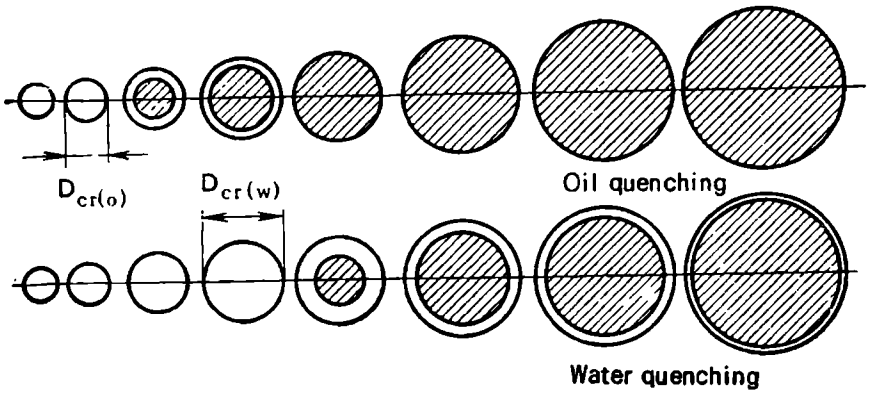

Fig. 11-8. Depth of hardening in rods of different diameter quenched in oil or water. Unhardened core is shown shaded

Therefore, a slower austenite-to-pearlite transformation (the position of lines in the isothermal diagram of decomposition are further to the right) gives a greater hardenability.

The principal factors that can affect the rate of pearlitic crystallization are as follows:

the composition of austenite; all elements soluble in austenite (except for cobalt) retard the transformation;

undissolved particles (carbides, oxides, intermetallic compounds); these particles accelerate the transformation since they serve as additional nuclei and increase the value of N in austenite-pearlitic transformation;

inhomogeneous austenite; it can more quickly transform into pearlite, since the rate of transformation is determined in that case by the less saturated portions of the solid solution;

the size of austenitic grains; the transformation is retarded with grain coarsening, since crystallization nuclei are mainly formed at grain boundaries, therefore, the value of N is lower in a coarser grain where the total length of grain boundaries is less.

Thus, all the factors mentioned lower the rate of austenite-to-pearlite transformation and increase the hardenability.

In practice, the hardenability is estimated in terms of what is called the *critical diameter*, D_{cr}, which is the maximum diameter of a cylindrical rod that can be hardened through in a given quenchant. Therefore, a given steel has its own value of critical diameter in a given quenchant. Naturally, the critical diameter is greater in stronger quenchants.

Figure 11-8 shows the hardening depth (unhatched portion) of specimens of the same steel grade quenched in oil and water. As may be seen, each of the two quenchants has a respective maximal cross-section of through hardening (D_{cr}), with D_{cr} in oil being smaller than D_{cr} in water, since oil cools slower than water.

The concept of *ideal critical diameter* (D_∞) has been introduced in order to eliminate the effect of cooling method on hardenability. This is the diameter of the maximum cross-section of through hardening in an 'ideal' liquid which removes heat from the surface at an infinitely high rate.

The critical diameter is an important and useful parameter for assigning a particular steel grade for a given part.

If an article is to be hardened through on heat treatment, the steel it is made of should satisfy the inequality

$$D_{cr} > D_{art}$$

Steel grades are usually characterized by the critical diameter D_∞, $D_{cr.w}$ (in water) or $D_{cr.o}$ (in oil).

Given one of these critical diameters, we can determine the two other by means of a nomogram such as that shown in Fig. 11-9; for instance, we can determine $D_{cr.w}$ and $D_{cr.o}$ for a known value of D_∞.

Suppose that the ideal critical diameter D_∞ is known and is equal to 48 mm. It is then possible to find in the nomogram (Fig. 11-9) the real critical diameter D_{cr} for quenching in water, oil and air. To do this, we draw a perpendicular from the point of 48 mm in the upper abscissa to the line characterizing 'ideal' quenching ($d = \infty$) and draw a horizontal line through the intersection point.

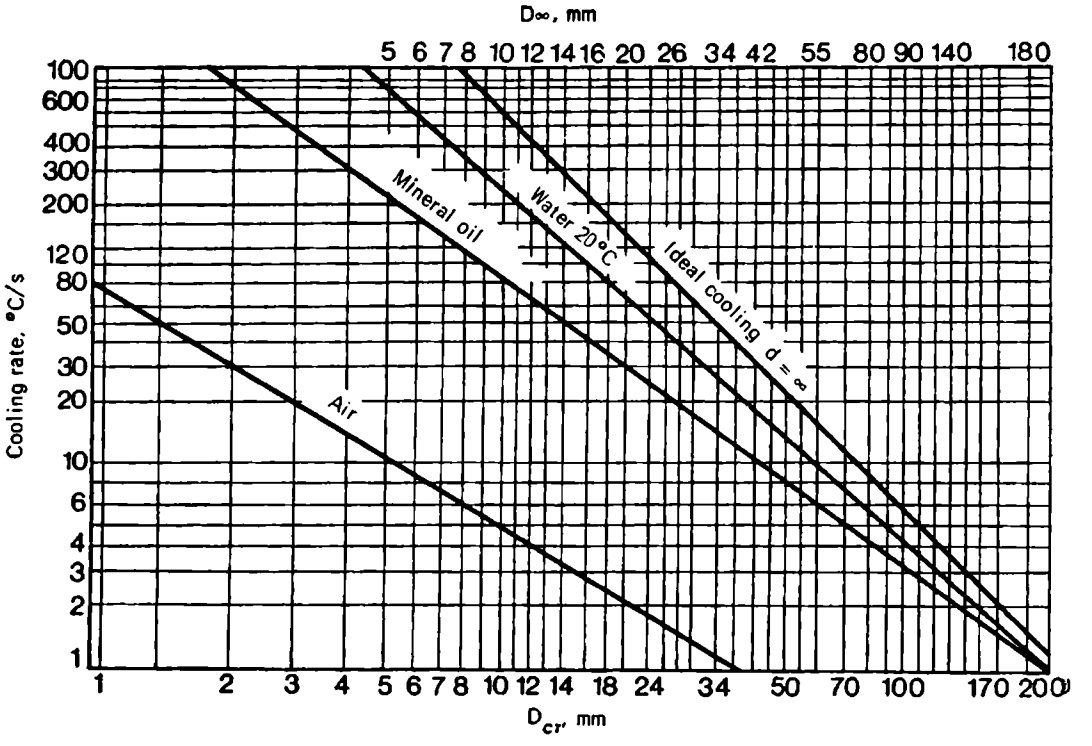

Fig. 11-9. Nomogram to determine the hardenability (M. E. Blanter)

The intersections of this line with the inclined lines characterizing the quenching in water, oil and air will determine the real critical diameters for these quenchants; they will be respectively 38, 26 and 3 mm.

The most simple and convenient method for determining the hardenability, and therefore, the 'ideal' critical diameter, is the end-quench test.

The quenching of a specimen in the end-quench test is shown schematically in Fig. 11-10. In this method, the lower end face of the specimen is cooled at the maximum rate and the cooling rate decreases on moving farther from the end face. Having measured the hardness of the surface along the length of the specimen and represented the results graphically (Fig. 11-11), we can establish that the hardness of a deeply hardenable steel decreases smoothly (curve *2* in Fig. 11-11), whereas that of a less hardenable steel drops off abruptly (curve *1*).

It can be found experimentally what is the cooling rate at various distances from the quench end face. The values are given in the upper portion of the diagram. As may be seen, the cooling rate at a distance of 6 mm from the quench end is 42 °C/s at 18 mm 10 °C/s, and so on.

The curves shown in Fig. 11-11 are the primary curves of hardenability. They can be used to determine what hardness value will be obtained at a given cooling rate and also to determine the ideal (D_∞) and real (D_{cr}) critical diameters.

A lower hardness obtained on decreasing the cooling rate below the critical value is the result of appearance of non-martensitic structures in the hardened metal. The presence of 5-10 per cent of troostite has, however, almost no effect on hardness, because of which it is hardly possible to establish the transition from a martensitic structure to a structure of martensite — a slight amount of troostite in a hardenability curve like that shown in Fig. 11-11. With a higher content of troostite in the structure, the effect on hardness is quite noticeable, so that the boundary between the hardened and unhardened zones is determined by what is called the semimartensitic layer.

The hardness of semimartensitic layer depends on the carbon content in steel (Fig. 11-12). The curves shown in Fig. 11-11 relate to steels with 0.7 per cent C (semimartensitic hardness is equal to 50 *HRC*). Therefore, the semimartensitic layer is at a depth of 3 mm from the surface in steel *1* and at 18 mm

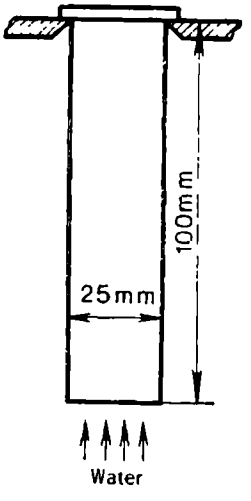

Fig. 11-10. A specimen for end-quench test (schematic)

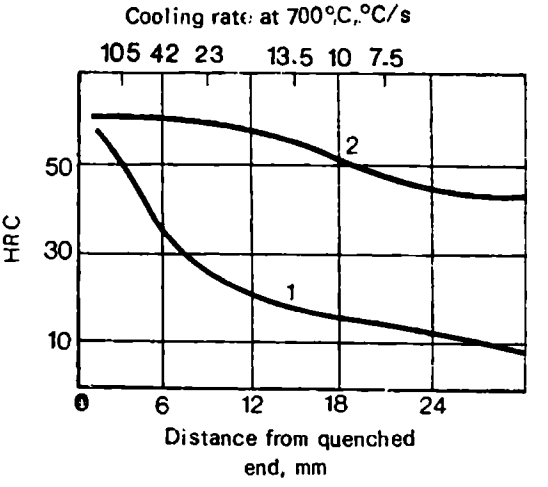

Fig. 11-11. Hardness variation along the length of end-quenched specimen

1—steel of a low hardenability; *2*—steel of a high hardenability

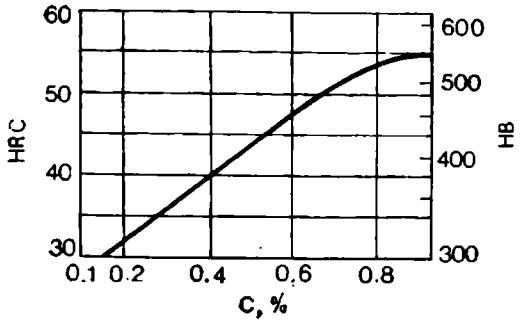

Fig. 11-12. Effect of carbon on hardness of semimartensitic zone

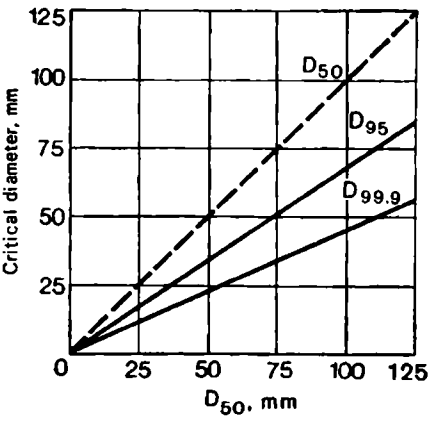

Fig. 11-13. Diagram to determine the depth of through hardening (for semimartensitic zone)

in steel *2*; in other words, steel *1* can be hardened to 50 *HRC* at a cooling rate of 105 °C/s and steel *2*, at 10 °C/s.

To find the critical diameter, we draw horizontal lines from the respective ordinates in Fig. 11-9 to intersection with the inclined lines. The points of intersection give the ideal critical diameter and the real critical diameter for various methods of cooling. In the case considered, D_∞ is equal to 25 mm for steel *1* and 75 mm for steel *2*.

The real critical diameters for steel *1* are: 16 mm for water quenching and 8.5 mm for oil quenching. These are the greatest sections in which a semimartensitic structure can be formed in the core upon quenching, respectively, in water and oil.

The presence of 50 per cent of troostite in the structure impairs the properties of hardened steel, so that the critical diameter as found for the semimartensitic hardness should be regarded as an intermediate stage for determining the critical diameter where the core will be full hardened (95 per cent martensite). To do this, we find D_{50} (for any method of cooling), as has been given earlier, and pass to D_{95}. Referring to the graph in Fig. 11-13, it may be taken approximately that the critical diameter for almost through hardening (95 per cent) is 3/4 of the semimartensitic value. Note also that the critical diameter for the hardenability of 99.9 per cent is one-half of the semimartensitic value.

Steels from various melts of the same grade cannot be characterized by a single line, as shown in Fig. 11-11, or by a single value of ideal critical diameter. Their hardenability appreciably depends on the actual composition, grain size and other factors. They are better characterized by *hardenability bands* which are constructed by the results of tests of a large number of melts. Taken a particular grade of steel, we can expect that its hardenability will be within its hardenability band.

Accordingly, a steel grade is characterized by the maximum and minimum critical diameters which depend on variations in steel composition. Melts with the contents of carbon and alloying elements at the upper limit have a greater hardenability.

The hardenability bands for selected steel grades are shown in Fig. 11-14.

Let us analyse the effect of hardenability on the properties of steel. With through hardening, the properties of hardened steel are uniform all over the cross-section. With incomplete hardening, the

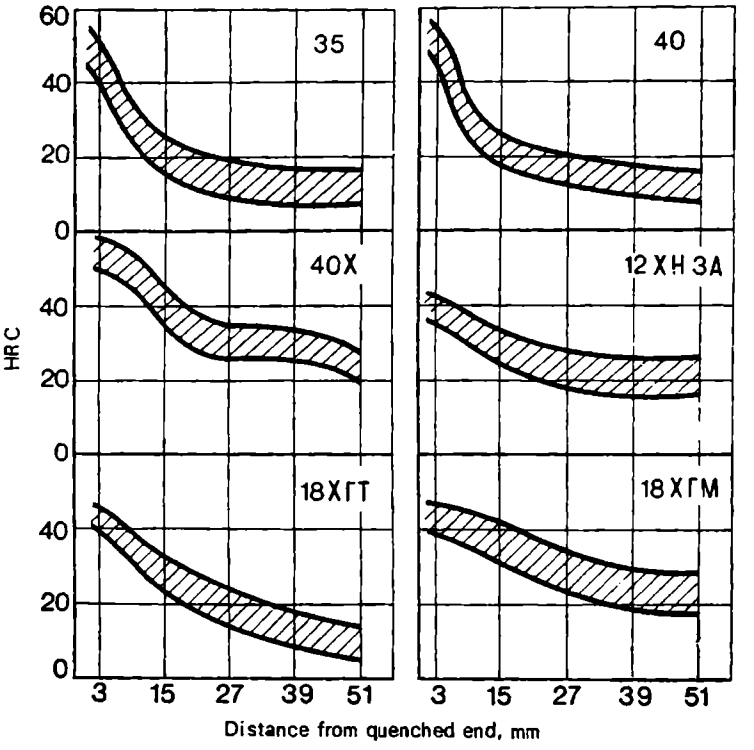

Fig. 11-14. Hardenability bands of selected steels (I. S. Kozlovsky)

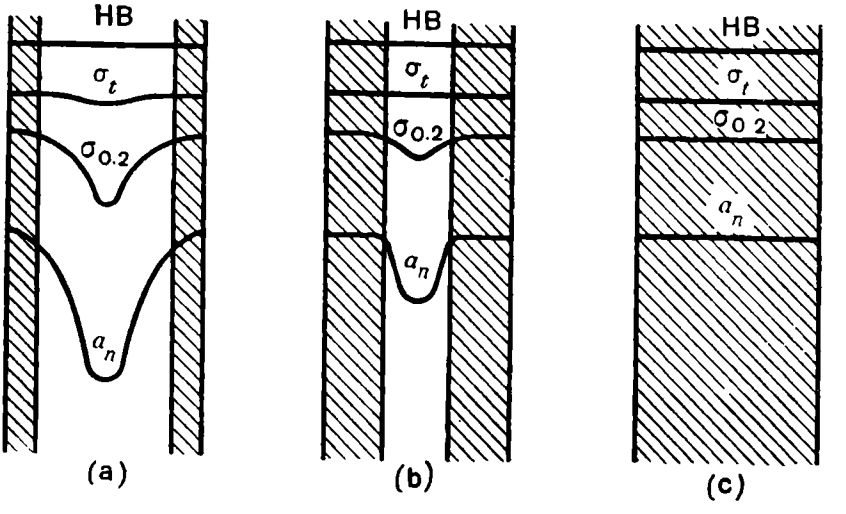

Fig. 11-15. Effect of hardening depth on mechanical properties of hardened and tempered steel (hardened zone shown hatched); the hardenability of steel increases from *a* to *c*

properties vary from the surface to the core in the same manner as in a series of thin specimens quenched at different cooling rates. It is of special interest to analyse how the steels with a different hardenability will differ in their properties if their hardness is equalized over the cross-section by subsequent tempering. It should be recalled here what is the difference between the products of hardening and the products of hardening and tempering, i.e. what is the difference between lamellar and granular structures.

For the same hardness, granular structures possess higher values of $\sigma_{0.2}$, ψ, and a_n (yield limit, reduction, and impact toughness) than lamellar structures. For that reason, a through-hardened section will have a better combination of mechanical properties upon hardening and high-temperature tempering. The distribution of mechanical properties over the cross-section in steels of different hardenability is shown schematically in Fig. 11-15.

An incompletely hardened specimen (Fig. 11-15*a*, *b*) will have lower values of $\sigma_{0.2}$ and a_n in the core; in through-hardened specimens (Fig. 11-15*c*), the properties will be equal all over the cross-section.

Thus, in order to obtain the optimal mechanical properties in a steel upon hardening and tempering, it is essential that granular tempered products be formed all over the cross-section, i.e. throughout hardenability is essential.

11-6. INTERNAL STRESSES

There are three types of internal stresses.

First-order stresses are zonal internal stresses which appear between various zones in a cross-section or between various portions of a part. They are higher at a greater temperature gradient over the cross-section, which appears on heat treatment and depends on the rate and uniformity of cooling, the size of the part and some other factors.

Second-order internal stresses appear within grains or between adjacent grains.

Second-order internal stresses appear between various phases owing to different linear expansion of these phases or due to the formation of new phases having different volumes. These stresses are independent of the factors which influence the first-order stresses, such as cooling rate. Since second-order stresses are formed between individual elements of a structure, they are sometimes called *structural stresses*, whereas first-order stresses are called *thermal stresses*.

Third-order internal stresses appear in smaller volumes, of an order of a few elementary cells of a crystal lattice.

For instance, a foreign atom intersticed into the solid solution elastically distorts the crystal lattice and thus forms third-order internal stresses.

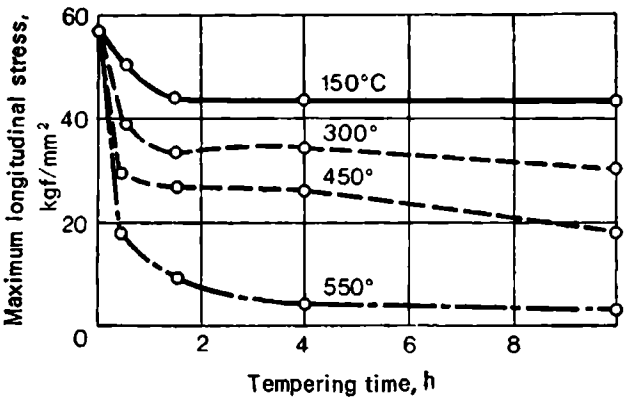

Fig. 11-16. Effect of temperature and time of tempering on residual stresses in steel with 0.3% C

Irrespective of the type of stresses, they always produce the same effect: elastic deformation and distortion of the crystal lattice.

Internal stresses are mainly studied and measured radiographically. For determining first-order stresses a mechanical method can be used, which is based on removal of the surface layer of metal and measuring the strain due to stress redistribution.

First studies of internal stresses in metals were made by N. V. Kalakutsky, a Russian engineer (in 1836-87). In 1920's, G. Sachs of Germany developed a simple mathematical method for calculating internal stresses. Lately numerous studies have been devoted to internal stresses.

First-order internal stresses whose effect is of special importance (since only they are responsible for warpage and cracking in metal parts), depend essentially on the properties of metal, as well as on some external factors (cooling rate, size and shape of parts, etc.). If a metal has a low ductility, the internal stresses formed in it cannot be relieved by plastic deformation and may cause cracking on attaining the ultimate strength value.

Internal stresses vary in heating or cooling. For instance, the surface layers of metal are compressed during heating, since they tend to expand, and this expansion is prevented by the colder internal layers. On the contrary, the surface layers in cooling are subjected to tensile stresses, since they have a lower temperature than the core and internal layers are compressed.

At the end of cooling, the temperature is usually equalized all over the cross-section. Does it mean that this equalization of temperature eliminates all stresses? By no means. After the cooling process is finished, and therefore, the surface layers cease to contract, the core portions of the metal are still being cooled for a certain while and their volume decreases; thus, internal stresses are formed in the metal.

Stresses remaining in metal upon cooling are called *residual stresses.*

Hardened steel is always in a structurally stressed state. An indispensable and radical method for releasing residual internal stresses is tempering.

Heating of a steel during tempering increases the ductility; owing to this, elastic deformations in individual portions of the metal change to plastic deformations and thus the residual stresses are relieved.

The stress-relieving effect is greater at a higher temperature and longer time of tempering (Fig. 11-16). Tempering at 550°C almost fully eliminates hardening stresses (from 60 kgf/mm^2 to 5-10 kgf/mm^2).

11-7. METHODS OF QUENCHING

It is essential to select the best and simplest method of quenching, depending on the composition of steel and the shape and size of the part to be hardened so as to obtain the desired properties upon heat treatment.

Let us consider the existing methods of quenching heated parts, their advantages, shortcomings and applications.

Parts of an intricate shape require a more careful selection of the quenching conditions, since greater internal stresses can form in them on cooling.

More care is also needed in quenching high-carbon steels, since carbon increases the volume changes in transformations, lowers the temperature of austenite-to-martensite transformation, and increases the risk of appearance of deformations, cracks, internal stresses and other quenching defects.

The principal methods of quenching are as follows.

1. *Single quenching* (Fig. 11-17, curve *1*); this is the simplest method. Steel parts heated to a desired temperature are immersed into a quenching liquid and left there to full cooling. This method is employed for hardening simple parts made of carbon or alloy steels. Carbon-steel parts of a diameter 2 to 5 mm are quenched in water, smaller parts and those made of alloy steels are quenched in oil. This method is also applied in mechanized quenching where heated parts are automatically supplied from the furnace to a quench bath.

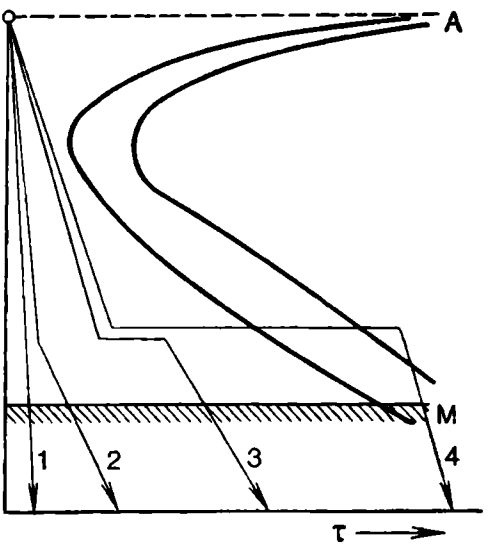

Fig. 11-17. Cooling curves for various methods of hardening, superimposed on TTT-diagram of austenite

For parts of an intricate shape, other methods of quenching should be utilized.

In some cases, heated parts are cooled in air in order to release internal stresses and then quenched.

2. *Double quenching* (Fig. 11-17, curve *2*). Heated parts are first cooled in a rapid quench and then in a slow quench. The first quenching is usually made in water and the second, in oil or air. Thus, the steel is slowly cooled in the martensitic range, which favours relieving of internal stresses. The method is employed for hardening of high-carbon steel tools. A shortcoming of the method is that it is difficult to accurately determine the time of quenching in the first bath, the more so as this time is very short (a few seconds). This requires a high skill of the operator.

3. *Spray quenching*, i.e. spraying of a hot part with water jet, is usually employed when only a portion of a part is to be hardened. This method ensures a deeper hardening than simple water quenching, since no vapour film forms on the metal surface.

4. *Quenching with self-tempering.* A steel part hardened and tempered by common methods has the same values of hardness and toughness all over its surface. This is not expeditious for impact tools, such as chisels, forging tools, etc. In such tools, the hardness should gradually diminish from the working (cutting) portion to the centre and to the shank. This distribution of hardness can be obtained by immersing a hot part into the quench bath according to the temper colours on the surface; though in this case the tempering temperature cannot be checked as accurately as in other methods.

The appearance of temper colours during tempering in the temperature range of 200-300°C is explained by the formation of thin oxide films on the clean (ground or polished) surface of metal. The colour of oxide film is determined by film thickness; a short holding of steel at a temperature of 220°C forms an oxide film 0.04 μm thick which makes the steel surface bright-yellow. As the film grows thicker, its colour changes as follows:

Temper colour	Temperature, °C	Film thickness, μm
Straw-yellow	220-240	0.045
Orange	240-260	0.050
Reddish-violet	260-280	0.065
Blue	280-300	0.070

Tempering by temper colours can be done in either of the two methods. By one method, only the working portion of a tool is immersed into the quench (water) and then taken out. It is then heated by the heat of the remaining portion of the tool and the temperature of heating is checked by the temper colour on the surface. This is what is called quenching with self-tempering. By another method, the whole part is hardened and then its shank portion is tempered in

a salt or lead bath at a high temperature; the working portion is then heated by the heat transferred from the shank. The desired degree of heating is here also determined by the temper colour. The heating is stopped by immersing the whole part into water.

For a given carbon content in the steel, the hardness of the working portion will be determined by its temper colour, increasing from blue to yellow. The old method of quenching with self-tempering has found a very wide application in mechanized flow-line production. In this process, the conditions of hardening (heating time, temperature of quench, time of immersion) are controlled very accurately, which ensures a definite reserve of heat in steel parts and the desired level of self-tempering of hardened layers.

5. *Interrupted quenching* (martempering) (Fig. 11-17, curve *3*). As has been noted, a shortcoming of the double quenching method is that thinner sections are cooled more, i.e. to a lower temperature during the transfer of the part from water to oil. Another drawback is that the process can hardly be controlled, since the time of holding the part in water is very short.

The method of interrupted quenching is free of these drawbacks. The part is cooled in a quench heated to a temperature above the martensitic point of the steel. The part being hardened should be heated to the bath temperature in all its points during holding. After that the part is subjected to final slow cooling during which the hardening occurs, i.e. austenite transforms into martensite. Quenching in two stages diminishes the first-order internal stresses and hence, the hardening deformation.

With this method, parts which are liable to warpage are straightened and trued upon removal from the quench bath, i.e. in the range of martensitic transformation. Metals have an anomalously high plasticity at the moment of martensitic transformation and this effect is utilized for trueing of warped parts.

The application of interrupted quenching is, however, limited by the size of parts. In large sections, it is impossible to attain the critical rate of hardening in a hot quench which cools slowly. For that reason, interrupted quenching of carbon steels can be used only for parts up to 12 mm and for alloy steels, up to 30 mm in diameter.

Quenching is usually carried out in molten salts (saltpetre, alkalis). A particular salt or salt mixture is selected according to the desired temperature of the "step", as may be seen from Table 11-1. The rate of quenching can be appreciably increased by adding 3-5 per cent water to an alkaline or saltpetre bath.

6. *Isothermal quenching* (Fig. 11-17, curve *4*). In contrast to interrupted quenching, the steel hardened by the isothermal quenching method is held in the quench for a time sufficient to complete the isothermal transformation of austenite.

The temperature of isothermal transformation of austenite is usually in the range of 250-350°C. Since austenite decomposes in this temperature range, the steel has a lower hardness but usually a higher toughness than with any other method of hardening.

The time of holding in the quench is determined by the time of

transformation of austenite at a given temperature (the latter is found in the diagram of isothermal decomposition of austenite for a given steel).

11-8. SUB-ZERO TREATMENT OF STEEL

The method of sub-zero treatment, which has been developed in the USSR in 1937-39, and is now widely used, consists in cooling of hardened steel, whose structure contains retained austenite, to a temperature below 0°C. The principles underlying the method are as follows.

Many steels have an elevated content of retained austenite in as-hardened state. If the point of the end of martensitic transformation lies below 0°C (for instance, a carbon steel with more than 0.5 per cent C, see Fig. 10-30), the cooling below 0°C should naturally form an additional quantity of martensite.

An increased content of martensite increases the hardness and volume of the metal, improves the magnetic properties, and stabilizes the dimensions of steel parts.

These variations directly depend on the quantity of martensite that is formed through sub-zero treatment.

The two following circumstances are typical of sub-zero treatment of steels

1. The temperature conditions of sub-zero treatment are determined by the position of the lower martensitic point (M_f). Since the transformation can take place only during the cooling in the martensitic range, the steel should be cooled to point M_f. A deeper cooling is needless since it can cause no further transformation.

The position of point M_f depends on steel composition. For most steels, point M_f lies not lower than —80°C.

2. When assigning the conditions of heat treatment with sub-zero freezing, the effect of stabilization of austenite should be properly considered. The point is that in many grades of commercial steel whose structure contains retained austenite on hardening the quantity of retained austenite diminishes upon a holding time at room temperature, i.e. the austenite is stabilized. Naturally, this stabilization of austenite diminishes the effect of sub-zero treatment. This is why sub-zero treatment should be done immediately after hardening.

Sub-zero treatment is applicable to many parts made of high-carbon steel to obtain the highest hardness (tools, cemented parts, ball bearings, etc.)

The metal volume increases upon sub-zero treatment, so that the method can be used for restoring the dimensions of some very precise parts (such as measuring gauges). The presence of retained austenite in the structure is dangerous for the dimensional stability because of the probable isothermal decomposition of austenite. Thus, sub-zero treatment can stabilize the dimensions of hardened parts by diminishing the quantity of retained austenite.

11-9. DEFECTS IN HARDENED STEEL

Various defects can appear in steel because of improper hardening procedure. The most common are low hardness, soft spots, increased brittleness, decarburization and oxidation of the surface, and finally, warpage, deformation and cracks.

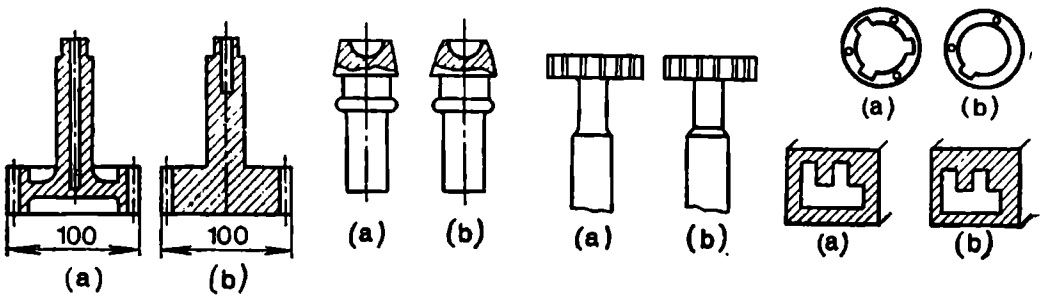

Fig. 11-18. (*a*) Correctly and (*b*) incorrectly designed steel parts

Deformations, warpage and cracks are due to internal stresses which have been discussed earlier.

The most effective method for releasing stresses and preventing defects of this type is to cool the steel slowly in the range of martensitic transformation during hardening. Small-size parts and those of a simple shape (without sharp corners or abrupt changes of cross-section) are less liable to warpage. Therefore, warpage defects can be minimized at the stage of design by a rational selection of the part shape. Examples of correct and incorrect design of steel parts are shown in Fig. 11.18. Parts of a more complicated shape should be preferably made of alloy steels to be quenched in oil.

An *insufficient (low) hardness* of hardened parts can be due to underheating (a low temperature in the furnace or an insufficiently long time of heating at the correct furnace temperature) or to a sluggish cooling. In the former case the martensite has a low hardness (contains too little carbon) and in the latter, the steel is not undercooled to the martensitic range and the structure formed fully or partially consists of the products of austenite-to-pearlite transformation (troostite, sorbite).

In the former case, the desired hardness can be obtained by increasing the furnace temperature or the time of heating. In the latter case, a more intensive cooling should be employed, for this it is advisable to move the part vigorously in the quenching bath or to use salty of acid water.

The *formation of soft spots* is also the result of underheating or sluggish cooling and can be prevented by the same methods as given above.

Soft spots sometimes appear owing to an inhomogeneous initial structure, for instance, to the presence of ferrite clusters. Ferrite may remain in these places on heating to the temperature of hardening or low-carbon austenite may form. Naturally, these portions will have a low hardness even if the hardening procedure is carried out correctly. The defect can be prevented by preliminary heat treatment (normalizing).

An *elevated brittleness* usually occurs on hardening from an excessively high temperature which promotes coarsening of austenitic grain. The defect is revealed in mechanical fracture tests or by examining the microstructure. It can be eliminated by a repeated hardening from the correct temperature.

Oxidation and decarburization of the surface often occur in flame-fired and electric furnaces in which the atmosphere is not controlled. This type of defect necessitates an additional allowance for grinding of parts, which makes the process of manufacture of heat-treated parts more expensive and complicated. A radical method to prevent this defect is to control the atmosphere in heat-treatment furnaces.

Heating in salt baths can also diminish the oxidation and decarburization.

11-10. ANNEALING AND NORMALIZING

Annealing is a procedure of heat treatment in which the steel is heated above Ac_3 (or only above Ac_1 in partial annealing) and then slowly cooled. The heating above Ac_3 provides full recrystallization in steel. The slow cooling in annealing should decompose austenite into pearlitic structures.

Normalizing is a variety of annealing in which the cooling is carried out in still air to effect quicker cooling than in common annealing (Fig. 11-19). Like annealing, normalizing should also cause the transformation of austenite into pearlite in the upper temperature range, but at a somewhat deeper undercooling; the last circumstance determines a certain difference in the properties of annealed and normalized steels.

Annealing and normalizing are usually the starting procedures of heat treatment and their aim is either to eliminate certain defects of the prior operations (casting, forging, etc.) or to prepare the structure to the subsequent process operations (machining, hardening). In many cases, however, annealing and especially normalizing are the final processes of heat treatment. These are the cases when the properties of annealed (normalized) steel are quite satisfactory for the purpose and their improvement by hardening and tempering is obvious.

The main objects of annealing are recrystallization of the steel and elimination of internal stresses. Both objects can be achieved by the common full annealing (Fig. 11-20) in which the steel is

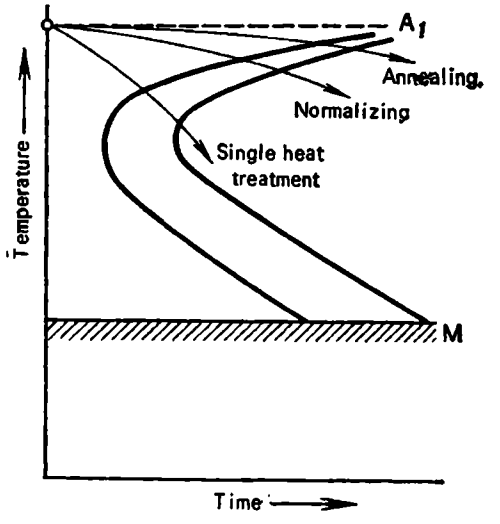

Fig. 11-19. Cooling curves for annealing, normalizing and single heat treatment, superimposed on TTT-diagram of austenite

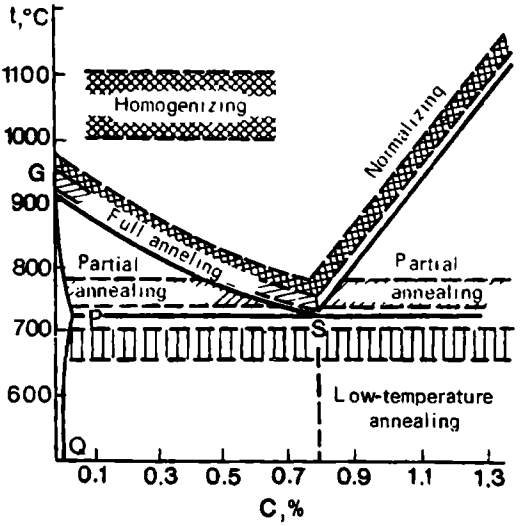

Fig. 11-20. Heating temperatures for various types of annealing

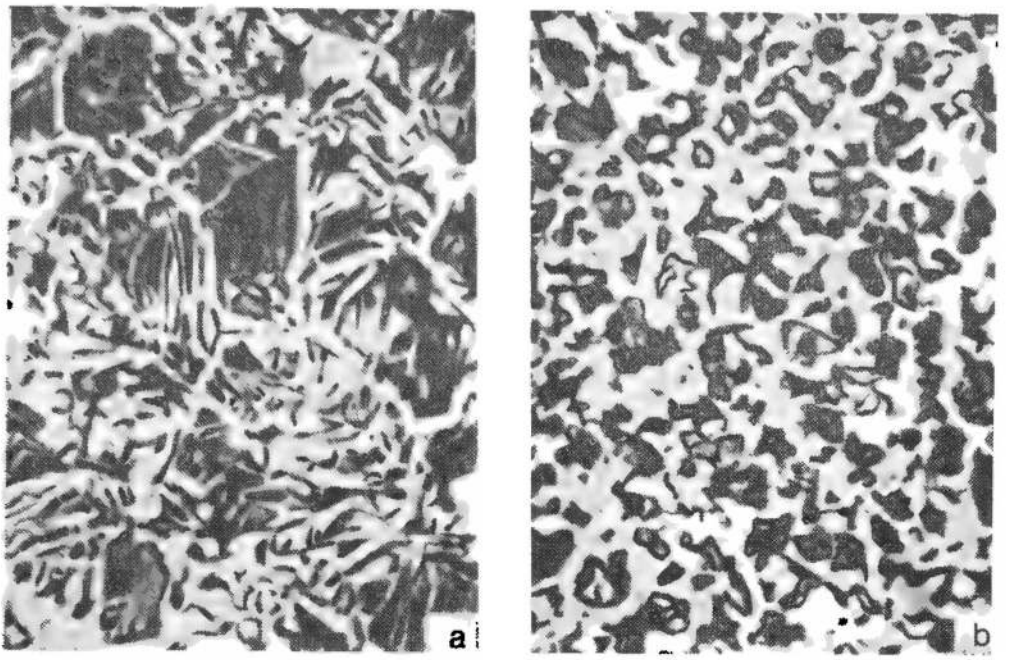

Fig. 11-21. Structure of steel Grade 40, ×100
(*a*) prior to annealing (Widmanstätten structure); (*b*) as-annealed

heated above the upper critical point and then slowly cooled. The heating changes the ferrite-pearlitic structure to austenitic and the austenite retransforms during cooling into ferrite and pearlite, i.e. full recrystallization takes place. Thus, the coarse-grained ferrite-pearlitic structure which often forms on casting or forging is changed by annealing to a finer structure of ferrite and pearlite (Fig. 11-21*a*, *b*). Ferrite precipitates are sometimes acicular and form what is called the *Widmanstätten structure.*

If there is no need to change the position of the ferritic component or if the original structure is not very coarse-grained, it is sufficient to anneal at a lower temperature: above Ac_1 but below Ac_3, which will cause only the pearlitic component to recrystallize. The process is called *partial annealing* (see Fig. 11-20). It is less expensive than full annealing, since heating is done to a lower temperature.

If the original structure is quite satisfactory and there is no need in its recrystallization, but it is desirable to diminish the internal stresses, the temperature of annealing is limited to a lower level, below the critical point. This is what is called *low-temperature*, or simply low, *annealing* (see Fig. 11-21). Evidently, this procedure relates to the first group of heat-treatment processes (first-order annealing), whereas the full and partial annealing relate to the second group (second-order annealing, or structural recrystallization).

The structure of cast steel is usually characterized by inhomogeneous composition and dendritic and zonal segregation. Heating at a high temperature for a sufficiently long time can eliminate or diminish the dendritic inhomogeneity. This procedure is called *homogenizing* or *diffusion annealing*. Heating for a long time at a high temperature (usually at 1 000-1 100°C) can cause an appreciable grain coarsening, i.e. produce a coarse-grained structure, so that an additional heat-treatment operation is needed to refine the structure (common annealing).

If the diffusion annealing has been employed to ingots to be plastically deformed (rolled or forged), the refining annealing becomes obvious, since the coarse-grained structure will be amended by plastic deformation.

Partial annealing of hypereutectoid steels is also called spheroidizing, since it is the sole method for forming the structure of granular pearlite. As has been noted, the heating to form granular pearlite should be done slightly above the critical point Ac_1, otherwise the structure of lamellar pearlite is obtained. Tool steels should be annealed to granular pearlite, since this makes them readily machinable and less sensitive to overheating in hardening.

The rate of cooling in annealing should be such that the austenite can transform at a low degree of undercooling. Practically, the cooling rate should be within 50-100 °C/h, which can be ensured by cooling in the furnace. In practice, the process of *isothermal annealing* is more often in use, since it saves time. The steel heated above the upper (or lower) critical point is then quickly cooled (more strictly, at any rate) to a temperature of 50-100°C below the equilibrium point A_1 and is held at that temperature as long as required for complete decomposition of austenite (Fig. 11-22). Since temperature is easier to control than cooling rate, this annealing process gives more stable results. At present, isothermal annealing is employed more often than annealing with continuous cooling, especially for alloy steels.

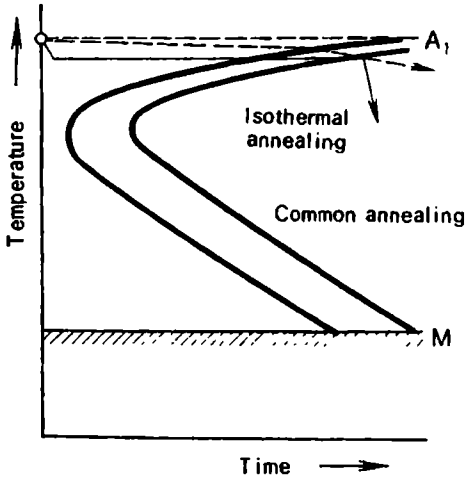

Fig. 11-22. Diagrams of isothermal and common annealing

Normalizing is a less expensive heat-treatment procedure than annealing, since only heating and holding at the normalizing temperature are carried out in the furnace, whereas cooling is done in air, outside the furnace.

Normalizing instead of annealing is recommended for low-carbon

non-alloy steels, since their properties upon both procedures are practically the same. With medium-carbon steels (0.3-0.5 per cent C) the difference in the properties in annealed and normalized state is more substantial and annealing cannot be replaced with normalizing. With these steels, however, normalizing is employed instead of temper hardening (toughening) which consists in hardening + + high-temperature tempering. In that case, normalized steel has a higher strength compared to as-annealed state, but somewhat lower ductility and toughness compared to toughened steel. The mechanical properties of normalized steel are quite satisfactory for non-critical parts; for critical parts, toughening should be preferred.

In normalizing the parts are cooled in still air. If upon heating to the austenitic range the part is cooled by air jet, i.e. at a higher cooling rate which causes the transformation to occur at the bend of the *C*-curve (see Fig. 11-19), the process is called single heat treatment (the term proposed by N. A. Minkevich). It is resorted to in cases when hardening is undesirable but the steel should have a slightly higher hardness than that obtained by normalizing.

LITERATURE

Minkevich N. A., *A Course in Heat Treatment of Steel and Cast Iron*. Moscow-Leningrad, ONTI, 1935 (in Russian).

Malyshev B. V., Shmykov A. A., *Controlled Atmospheres*. Moscow, "Mashgiz", 1953 (in Russian).

Petrash L. V., *Quenching Media*. Moscow-Leningrad, "Mashgiz", 1953 (in Russian).

Sokolov K. N., *Technology of Heat Teatment of Steel*. Moscow, "Mashgiz", 1954 (in Russian).

Gulyaev A. P., *Heat Treatment of Steel*. Moscow, "Mashgiz", 1960 (in Russian).

Popov A. A., Popova A. E., *Isothermal and Thermokinetic Diagrams of Decomposition of Undercooled Austenite*. Sverdlovsk, "Mashgiz", 1961, (in Russian).

Lakhtin Yu. M., *Heat Treatment of Steel*. Principles of the Theory and Technology. Moscow, "Mashinostroenie", 1973 (in Russian).

Chapter 12

SURFACE HARDENING OF STEEL

12-1. GENERAL

Many steel parts are heat treated so as to have a high hardness in the surface and a high toughness in the core, which ensures a high wear resistance and at the same time a high dynamic strength. This is done by methods of surface hardening and chemical heat treatment.

Surface hardening is advantageous over chemical heat treatment as it requires appreciably less time.

Despite the large diversity of methods of surface hardening, all of them essentially consist in heating and hardening of the surface layers only. The heating can be done by various processes: (*a*) in molten metals or salts; (*b*) in the flame of oxy-acetylene or gas burners (called flame hardening); (*c*) in electrolytic solutions; (*d*) by electric currents induced in the surface layers (*induction*, or *high-frequency*, *hardening* in which high-frequency currents are induced in the surface layers of steel parts).

The last process is now increasingly employed in the machine-building industry.

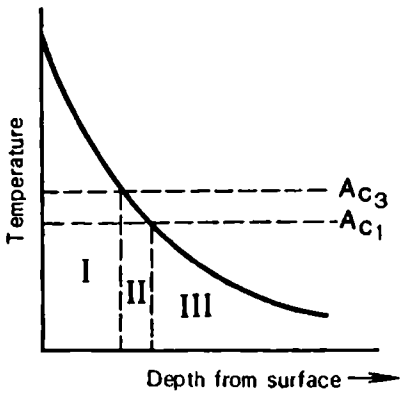

Fig. 12-1. Temperature distribution from surface to depth in surface hardening

The essence of any process of surface hardening consists in rapid heating of the surface layers above the critical points, which forms a sharp temperature gradient across the cross-section (Fig. 12-1). If the heating is interrupted and the part is cooled quickly, the layer that has been heated above Ac_3 (*I*) will be full-hardened; the layer heated above Ac_1 but below Ac_3 (*II*) will be hardened only partially; and the core (*III*) will be not hardened at all, since it is not heated or is heated only below Ac_1.

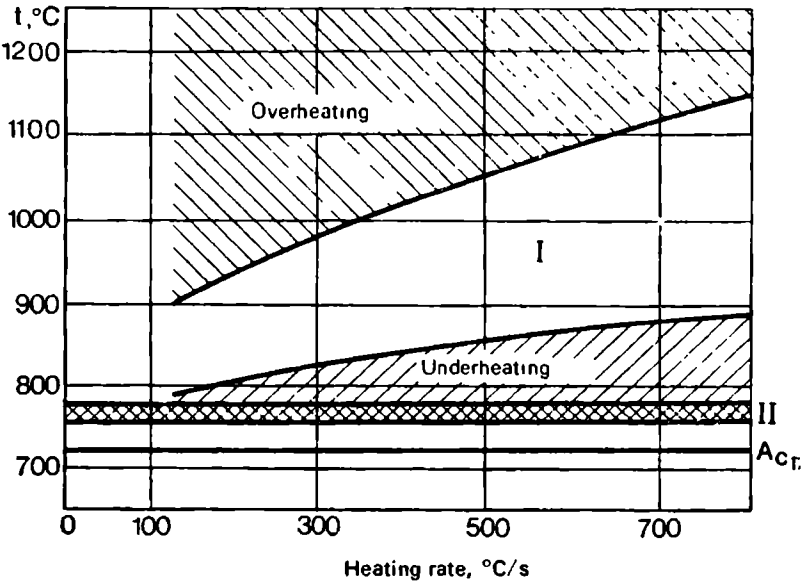

Fig. 12-2. Diagram to select heating temperature. Steel У10 (Author)
I—high-speed electric heating; *II*—slow heating in furnace

Heating of surface layers appreciably above Ac_3 is a common case in all processes of surface hardening, but it does not always means that the metal is overheated and its structure is impaired. When we considered the pearlite-to-austenite transformation (Sec. 10-1), we have noted that with a higher heating rate, the transformation takes place at a higher temperature; since the time of heating is short, the microstructure of the final austenite is less coarsened and the mechanical properties are not worsened much.

Experience shows that each heating rate has a corresponding temperature interval in which a fine-grained structure is obtained.

The diagram in Fig. 12-2 shows the temperature region of correct heating (*I*), depending on heating rate (without holding at the heating temperature). As may be seen, the temperature of heating for hardening increases with the heating rate. Temperatures below the correct temperature interval are insufficient for completion of the austenitic transformation, while higher temperatures cause overheating and intensive grain coarsening. It is also seen from the diagram that the temperature interval of hardening for slow heating in the furnace (*II*) is appreciably lower than that for high-speed heating.

As has been indicated, the temperature of hardening for a particular steel is assigned according to the Fe-C constitutional diagram. This is only true, however, for slow heating in the furnace in which the transformations occur without an appreciable overheating. With high-speed heating, the temperature of hardening should be selected by using diagrams of the type shown in Fig. 12-2.

12-2. INDUCTION HARDENING

Electric current flowing in a metal part encounters resistance and the part gets hot. The quantity of heat Q can be found by the well-known formula:

$$Q = 0.239 I^2 R \tau \text{ cal}$$

By varying the current I, it is possible to obtain any quantity of heat, and therefore, any temperature and any rate of heating. The resistance R of the metallic conductor depends on the type of metal. The time τ during which the current acts may be short so as to increase the productivity of the process.

A typical feature of electric heat treatment is that the heating is done at a very high rate, hundreds or thousands times as much as the heating rate obtainable in furnaces or from external heat sources.

At present, electric heating is preferably effected by high-frequency currents.

With high-frequency heating, the magnetic flux that is formed by an alternating current passing through a conductor (inductor) induces eddy currents in a metal part placed inside the inductor, and the part is heated by these eddy currents.

As is known, the frequency of common electric current in the mains is 50 Hz (industrial frequency); this is what is called low-frequency current. Currents of a higher frequency are called high-frequency currents.

High-frequency currents for induction heating of metals are obtained from frequency converters (for frequencies of 500 to 5 000 and even to 15 000 Hz) or valve oscillators (up to 10 000 000 Hz).

The flowing alternating current is distributed non-uniformly over the cross-section of a conductor, the current density being greater at the surface and lower in the core. It is taken that current flows in a surface layer whose depth (δ) depends on frequency:

$$\delta = 5030 \sqrt{\frac{\rho}{\mu f}}$$

where f is the current frequency, Hz; δ is the depth of current penetration, cm; ρ is the electric resistivity of the conductor, ohm cm; and μ is the magnetic permeability, Gs/Oe.

It follows from the equation that the depth of current penetration (δ) is less at a higher frequency (f). That is why higher frequencies (obtained in valve oscillators) should be used for heating of small parts or when a small depth of heating is required and lower frequencies (obtained in frequency converters) for heating of large parts and when a greater depth (over 3 mm) of heating is essential.

On passage through the magnetic transformation point (A_2), the magnetic permeability μ of steel drops abruptly, resulting in a higher value of δ and lower heating rate (Fig. 12-3). Therefore, the heating rate above the magnetic transformation point is not the same as below that point; this circumstance should be considered when selecting heating conditions.

Each value of heating rate has a corresponding optimum interval of hardening temperatures (see Fig. 12-2). We are mainly interested, however, not in the average heating rate, but in the actual heating rate in the region of phase transformations (above point A_2).

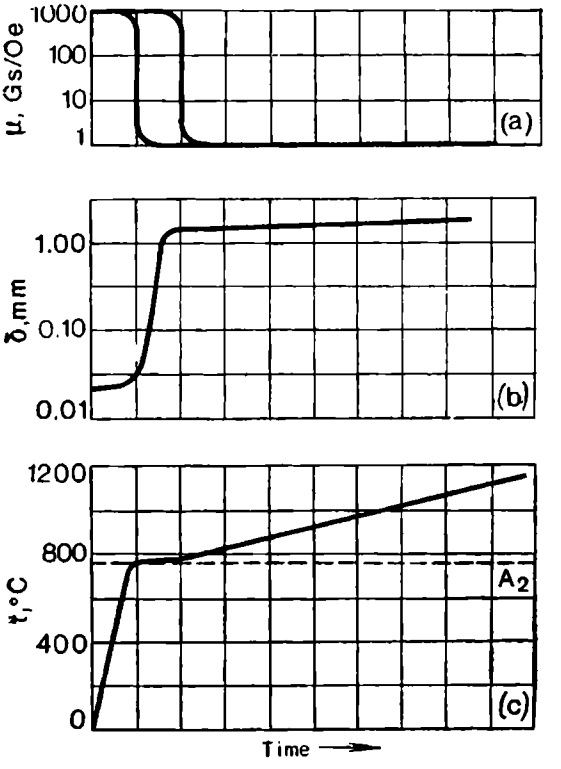

Fig. 12-3. Variations of magnetic permeability (μ) and depth of current penetration (δ) during high-frequency heating

Up to point A_2, i.e. when the steel is magnetic, the heating occurs quickly. Above point A_2, the magnetic permeability decreases abruptly (by a factor of a few thousands) and the depth of current penetration δ sharply increases; this causes a sharp drop in the unit power of heating (per cm^3 of the heated layer) and the rate of heating (see Fig. 12-3).

An arrest in the heating curve at 768°C (A_2) is due to the redistribution of electric current over the cross-section.

The main condition for correct and uniform induction heating is to select an optimum shape and configuration of the inductor for a particular part. The inductor is made of red copper tubes in the form of a loop or coil (Fig. 12-4*a*); the part to be heated is placed inside it (Fig. 12-4*b*); upon proper heating, the part is placed in a sprayer for hardening (Fig. 12-4*c*).

High-frequency heating offers the following advantages: (a) high productivity; (b) no burning of carbon and other elements, as also no noticeable oxidation and scaling; (c) low warpage; (d) accurate control of hardening depth. A convincing example is the macrostructure of an induction-hardened gear wheel shown in Fig. 12-5.

These advantages, as also the ease of automatic control make the process of induction hardening one of the most effective.

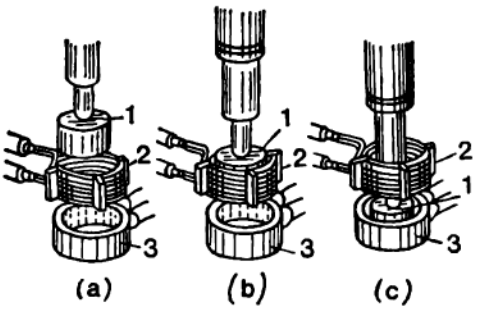

Fig. 12-4. Induction hardening of a cylindrical part
1—part being hardened; *2*—inductor; *3*—sprayer

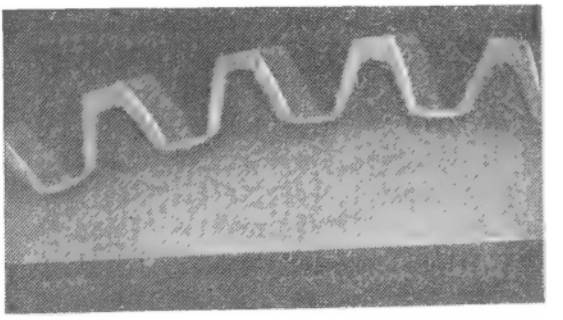

Fig. 12-5. Macrostructure of a gear wheel upon induction hardening

The surface hardening is applicable to common carbon steels with the carbon content of 0.4 per cent or more[1]. It is not recommended for alloy steels, since a high depth of hardening is already achieved by alloying. Besides, steels of reduced hardenability are needed for certain applications. As is known, for instance, it is difficult to heat up gear wheels uniformly to the same depth all over their profile. A wheel will be more heated either in tooth spaces (at a lower current frequency) or in tooth tips (at a higher frequency). A method of deep induction heating of steels of reduced hardenability has been proposed by K. Z. Shepelyakovsky. Figure 12-5 shows the macrostructure of a gear wheel hardened by this method. The whole tooth and a part of root have been heated above the critical point, but since the steel has a reduced hardenability, it has been hardened in the bright surface layer only. As is seen, the depth of hardened layer is the same all over the wheel profile. Steels of reduced hardenability are those carbon steels which have the minimum content of permanent (manganese, silicon) and occasional (chromium, nickel, etc.) impurities (Grades 55ПП, 60ПП, etc.).

The method of induction heating was initially used for surface hardening to depths up to 5 mm. In later studies it has been found, that the process is suitable for through heating as well. This makes induction heating very promising in many branches of industry, in particular for through heating before forging.

The process of induction hardening is too expensive to be used for hardening of individual parts or small series. In mass and large-series production it is very effective.

It should be noted in conclusion that the process of induction hardening is very convenient, since the induction installation can be mounted in any place in the shop and included into the flow pro-

[1] With a lower content of carbon, the required hardness cannot be obtained.

duction line; this offers a great saving of time, production area and transportation.

The process of high-frequency hardening was first employed in the USSR by V. P. Vologdin for heat treatment of automobile parts. The metallurgical problems associated with high-speed heating of steels have been studied by N. V. Geveling, I. N. Kidin, M. G. Lozinsky, and K.Z. Shepelyakovsky.

LITERATURE

Geveling N. V., *Electric Heat Treatment of Surface.* Moscow, ONTI, 1936 (in Russian).

Vologdin V. P., *Induction Surface Hardening.* Moscow, "Oborongiz", 1947 (in Russian).

Kidin I. N., *Heat Treatment of Steel by Induction Heating.* Moscow, "Metallurgizdat", 1950 (in Russian).

Lozinsky M. G., *Industrial Applications of Induction Heating.* Moscow, USSR Academy of Sciences, 1958 (in Russian).

Kidin I. N., *Physical Principles of Electric Heat Treatment of Metals and Alloys.* Moscow, "Metallurgiya", 1969 (in Russian).

Shepelyakovsky K. Z., *Strengthening of Machine Parts by Surface Hardening with Induction Heating.* Moscow, "Mashinostroenie", 1972 (in Russian).

Shepelyakovsky K. Z., *Technology of Heat Treatment of Steel with Induction Heating.* Moscow. "Mashinostroenie", 1973 (in Russian).

Chapter 13

CHEMICAL HEAT TREATMENT OF STEEL

13-1. THE THEORY OF CHEMICAL HEAT TREATMENT

Chemical heat treatment has certain specifics and advantages compared to surface hardening, though is less productive than the latter. The advantages offered by chemical heat treatment may be formulated as follows:

1. The process is independent of the shape of article and produces a hardened layer of a uniform depth over the whole surface of both simple and complicated parts, whereas surface hardening is largely dependent on the shape of article and is inapplicable with many parts of intricate shape.

2. The process produces a greater difference between the properties of the metal in the surface and core as that obtained by surface hardening. Here the properties are determined by the structure and composition of the metal while in surface hardening, by the structure only.

3. The effects of surface overheating can be eliminated by subsequent heat treatment, whereas in surface hardening, which is usually the final procedure, it cannot be eliminated.

In chemical heat treatment, parts are usually placed in a medium rich in the desired element which penetrates the metal by diffusion.

With chemical heat treatment in a gaseous phase (the commonnest case), the treatment is based on the three elementary processes:

(a) *dissociation*; it takes place in the gaseous phase and consists in the decomposition of molecules and formation of active atoms of the diffusing element; for instance, molecules of carbon dioxide or ammonia can dissociate by the reactions

$$2CO \rightarrow CO_2 + C \quad \text{or} \quad NH_3 \rightarrow 3H + N$$

and form active atoms of carbon and nitrogen which are capable of dissolving in the metal; the degree of decomposition of gas molecules is called the *degree of dissociation* and is measured in per cent;

(b) *absorption*; it occurs at the gas-metal interface and consists in dissolution of free atoms in the surface; the process is possible only when the diffusing element B is soluble in the base metal A;

(c) *diffusion*, i.e. penetration of the saturating element into the depth of metal.

All these processes result in the formation of a diffusion layer in which the concentration of the diffusing element varies from the highest value in the surface to zero at a depth y (Fig. 13-1). Such is the case if the diffusing element forms a continuous series of solid solutions with the base metal. If the saturating element B and the base metal A form a system of alloys with limited solubility or with chemical compounds (Fig. 13-2*a*), the structure of the layer will be determined by the isothermal section through the constitutional diagram of that system at the temperature of diffusion saturation.

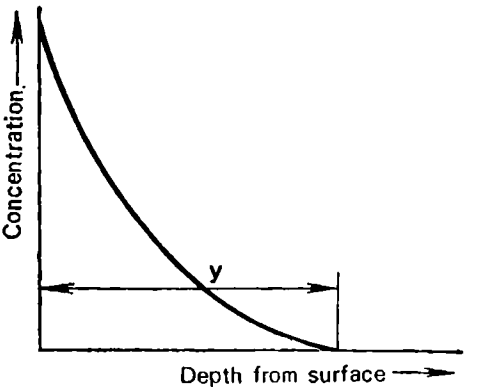

Fig. 13-1. Variation of the concentration of diffusing element in depth

Suppose that the system (metal A and diffusing element B) is described by the constitutional diagram shown in Fig. 13-2 and that the saturation takes place at temperature t_1. If the processes of dissociation, absorption and diffusion have enough time to occur actively, a layer of the B (A) solid solution of a variable concentration will form in the surface (Fig. 13-2*b*); beneath it there will be a layer of the solid solution of A_nB_m compound, also of a variable concentration, and finally, a layer of A (B) solid solution of a concentration

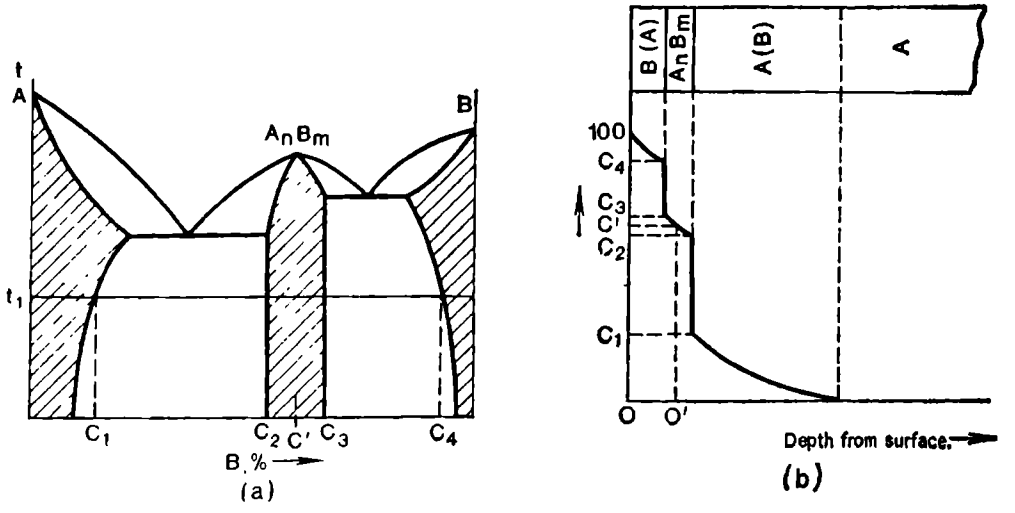

Fig. 13-2. A system of alloys with limited solubility and compounds

(*a*) constitutional diagram (single-phase regions shown hatched); (*b*) distribution of concentration of diffusing element and structure of diffusion layer

diminishing from the saturation limit (at the given temperature) to zero. The concentration at the boundaries between the layers varies jumpwise in accordance with the conditions of equilibrium coexistence of the phases, as follows from the constitutional diagram in Fig. 13-2*a*.

If the process of saturation is not active enough, the concentration in the surface will not reach 100 per cent *B*.

There are two types of diffusion movement of atoms in metals: (a) *self-diffusion*, i.e. the movement of atoms of the base metal in its own crystal lattice and (b) *heterodiffusion*, i.e. the movement of foreign (dissolved) atoms in the base metal crystal lattice.

In the former case, atoms of the base metal are in a chaotic thermal motion and some of them may change places in the crystal lattice by jumping from one site to another. This process of displacement of like atoms occurs continually and chaotically in direction and does not alter the concentration.

In the latter case, the movement of foreign atoms occurs in the direction from places of a high to those of a lower concentration; the process is spontaneous, since a state of a non-uniform concentration has a higher free energy than that having a uniform distribution of solute atoms.

If the concentration of the solution becomes uniform, heterodiffusion, like self-diffusion, is directed chaotically. Cases are known of what is called ascending diffusion in which the atoms move from places of a lower concentration to those of a higher concentration. In each case the process is caused by some factors (usually a non-uniform distribution of a third, slowly diffusing, element or a non-uniform distribution of stresses), and is based on the tendency of the system to diminish its free energy.

How does the diffusion displacement of atoms take place?

As has been given earlier (Ch. 1), all substances undergo thermal fluctuations owing to which some atoms can acquire an appreciably higher energy than the mean energy characteristic of the given temperature of the body. These atoms escape from their equilibrium positions in the lattice sites and move in interstices, thus leaving some lattice points empty.

An atom positioned in a lattice interstice is called a displaced atom (Fig. 13-3) and a crystal lattice site not occupied by an atom is called a vacancy (see Ch. 1). A vacancy or a displaced atom disturbs the regular arrangement of the adjacent atoms (see Fig. 13-3) and thus a field of elastic distortions of the crystal lattice appears around the vacancy or displaced atom.

The hypothetical mechanism of heterodiffusion, which is analogous to the mechanism of self-diffusion, has been described by Ya. I. Frenkel and is now generally recognized. If there is a vacancy (hole) near an atom *A* (Fig. 13-3), the latter can move easily from its place into that hole; an atom *B* will occupy the place of atom *A*,

an atom C, the place of atom B, and so on, i.e. the hole displaces, as it were, together with displacing atoms. The process of heterodiffusion can be more properly described as the displacement of foreign atoms and the process of self-diffusion, as the displacement of 'holes'.

To move from the initial position to a neighbouring 'hole', atom A should first occupy an intermediate position in the interstice. The work required to displace an atom from its equilibrium position is called the *activation energy*, which is the most important characteristic of the capacity of atoms to move. The activation energy is determined by the nature of the substance and is independent of temperature.

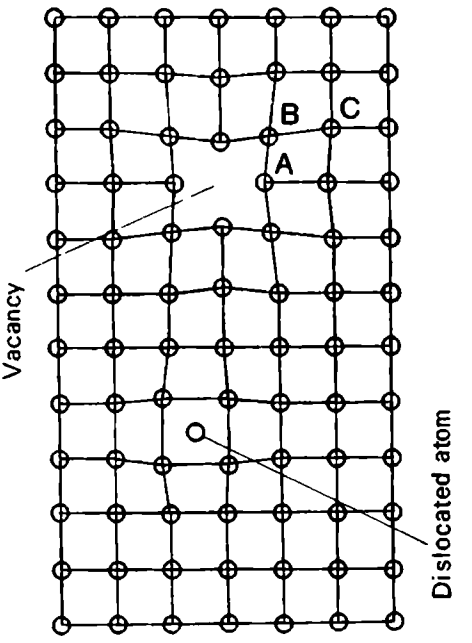

Fig. 13-3

Apart from the 'hole' mechanism, other diffusion processes are also possible, for instance, the motion of a displaced atom from one interstice to another (until it finds a 'hole' and is quieted) or an exchange of places between two neighbouring atoms. The 'hole' mechanism is effected most easily. For instance, calculattions of self-diffusion in copper have given the following values of activation energy: 64 kcal/g-atom for the 'hole' mechanism, 230 kcal/g-atom for the motion of a displaced atom, and 400 kcal/g-atom for the exchange mechanism. Because of these large differences, real diffusion occurs only by the 'hole' mechanism and the role of the other mechanisms is negligible.

The effect of temperature, which is known to appreciably accelerate the diffusion processes, can be explained by the fact that it increases thermal fluctuations and thus forms conditions for appearing more holes in a lattice.

The process of diffusion can be characterized quantitatively by what is called the coefficient of diffusion D which is numerically equal to the quantity of a substance that can diffuse through an area of 1 cm^2 for 1 s at a concentration gradient of unity at the two sides of the area (0 and 100 per cent of substance B); its dimension is cm^2/s.

The effect of temperature on the diffusion coefficient can be described by the formula

$$D = Ae^{-Q/RT}$$

where A is a coefficient depending on the type of crystal lattice; Q is the activation energy; e is the base of natural logarithms; R is the gas constant; and T is the absolute temperature.

Since R and Q are independent of temperature, the diffusion coefficient of a given substance substantially increases with temperature (Fig. 13-4*a*); in the log D-$1/T$ coordinates, this relationship is expressed by a straight line (Fig. 13-4*b*).

As follows from the formula above, the coefficient of diffusion of various substances depends quite appreciably on the activation energy, being substantially lower at greater values of Q.

In interstitial solid solutions, the process of diffusion is facilitated by that it is not needed to displace a solvent atom (ion) into an irregular position, therefore, the activation energy is lower than in the formation of substitutional solid solutions. For instance, the activation energy in the diffusion of carbon in γ-iron is about 30 kcal/g-atom, compared to about 60 kcal/g-atom for the diffusion of some metals (substitutional solid solutions in γ-iron). The coefficient of diffusion in these two cases may differ in magnitude thousands or even tens of thousands of times. Thus, for a steel with 0.2 per cent C at 1 100°C, $D = 6 \times 10^{-7}$ for the diffusion of carbon and $D = 6 \times 10^{-11}$ for the diffusion of molybdenum.

The time of a process of chemical heat treatment is determined by the desired depth of diffusion layer.

With all other parameters of the process (temperature. etc.) being the same, the depth of diffusion layer (y) varies with time (τ) by a parabolic law (Fig. 13-5).

The thicker the layer already obtained, the less it grows in the same period of time.

Some specific features of diffusion in metals can be explained by their crystal structure.

The anisotropy of properties of crystals may have a definite effect on diffusion. For instance, the diffusion of copper in hexagonal zinc in various directions occurs at different rates: more quickly in the base plane and slowly in the direction of the main axis. In lattices

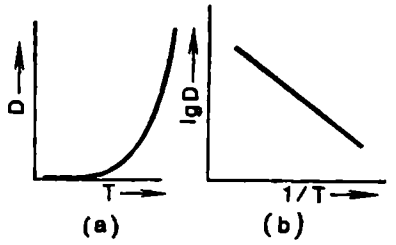

Fig. 13-4. Effect of temperature on diffusion coefficient

D—diffusion coefficient; *T*—absolute temperature

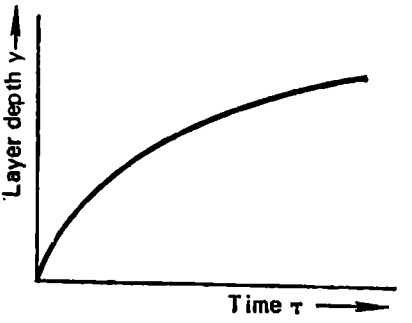

Fig. 13-5. Effect of process time on the depth of diffusion layer

of a larger symmetry (cubic lattices), the rate of diffusion is less dependent on orientation.

The diffusion processes occur more easily at grain boundaries which are places of concentration of crystal lattice defects. If the solubility of a diffusing substance in a metal is low, diffusion can often take place mostly at grain boundaries. The role of boundary layers of increased solubility is less appreciable in cases when the diffusing element is readily soluble in the base metal. Diffusion processes occur more quickly during phase transformations.

13-2. CARBURIZING

The process of carburizing is known from the ancient times. Up to the middle of the last century, this was the sole method for making steel from iron; in recent time, this process, which is widely used for surface hardening, has been developed theoretically.

The carburizing process essentially consists in the saturation of the surface layers of steel with carbon, i.e. the formation of a high-carbon surface layer. Since the original metal is low in carbon, the core remains soft and tough, even after the carburized surface layer is subjected to hardening.

There are two principal types of the process: solid and gaseous carburizing.

With the *solid carburizing*, steel parts are placed in a box filled with a *carburizer* (usually charcoal with various additions). The spaces between charcoal lumps are filled with air whose oxygen combines with carbon at the process temperature of 900-950°C to form carbon monoxide (since oxygen is deficient, CO and not CO_2 is formed).

Carbon monoxide is however unstable at the process temperature and is decomposed upon contacting the iron surface by the reaction:

$$2CO \rightarrow CO_2 + C$$

The atomic carbon is absorbed by the metal surface.

Thus, the process of solid carburizing occurs with the formation of a gaseous phase, i.e. the metal is carburized by the gas produced from a solid carburizer.

The carburizing effect can be enhanced by adding carbonate salts: $BaCO_3$, Na_2CO_3 (soda), K_2CO_3 (potash) to charcoal. The salts decompose and evolve carbon dioxide which reacts with coal ($BaCO_3 \rightarrow$ $\rightarrow BaO + CO_2$; $CO_2 + C \rightarrow 2CO$, etc.). The carburizers (which are used in industry contain 10 to 30 per cent of carbonates.

Solid carburizing is a rather time-consuming procedure, often taking a few tens of hours depending on the desired depth of carburized layer. Even when a thin layer is needed, say, 1 mm, the carburizing time is quite appreciable, a few hours. The long duration of

the process is mainly due to the low rate of heating of the box which is filled with a material of a low thermal conductivity.

Higher speeds can be attained by carburizing in gaseous media.

Gaseous carburizing is carried out in a tightly sealed furnace chamber filled with a carburizing gas. More often, the gas flows through the chamber at a given speed. In this process, no time is spent to heat up the box and the carburizer; the rate of carburizing increases with a smaller depth of the carburized layer needed.

Gaseous carburizing is now the main process of carburizing in mass production, with the simpler solid carburizing being economically effective only in small-series or individual production.

Gaseous carburizing is effected in batch-type or continuous conveyer furnaces. The carburizing gas is prepared outside the furnace and supplied into the carburizing retort.

Carbon monoxide and various hydrocarbons are used as carburizers. They decompose at the process temperature and form atomic carbon:

$$2CO \rightarrow CO_2 + C$$

$$C_nH_{2n} \rightarrow 2nH + nC$$

$$C_nH_{2n+2} \rightarrow (2n + 2)\,H + nC$$

Saturated hydrocarbons (CH_{2n+2}): methane, ethane, propane, butane, etc. are used most often for the purpose; among them, methane is employed as natural gas (92-96 per cent CH_4).

In gaseous carburizing, use is also made of benzene which is supplied dropwise into the carburizing retort; it decomposes into a gas mixture of methane, carbon monoxide and free hydrogen.

As follows from the reactions given above, hydrocarbons decompose with the formation of free carbon. If the steel surface does not absorb all the carbon liberated in the process (absorption lags behind dissociation), the free carbon will crystallize from the gaseous phase and settle as a dense soot film on the metal surface, thus impeding the carburizing process.

For that reason it is very essential to accurately control the composition and flow rate of the carburizing gas.

Carburizing is not done below the critical point Ac_1, since α-iron cannot dissolve carbon and the process would result in the formation of a very thin surface crust of cementite.

The temperature of gaseous carburizing is 900-930°C, but there is a tendency to raise it to 950-970°C or even higher.

As follows from the general concepts of diffusion, a higher temperature of carburizing can appreciably increase the depth of carburized layer.

Figure 13-6 shows the effect of temperature and time of the process on the depth of carburized layer. As may be seen, the rate of

the process is the highest at the beginning and then diminishes gradually, but can be substantially increased by raising the temperature.

At a given temperature of the process, the content of carbon in the carburized layer is determined by the solubility of carbon in austenite (by line *SE* in the Fe-C constitutional diagram). Therefore, a higher temperature of carburizing gives a higher content of carbon in the surface layer (but not more than 2.0 per cent)[1].

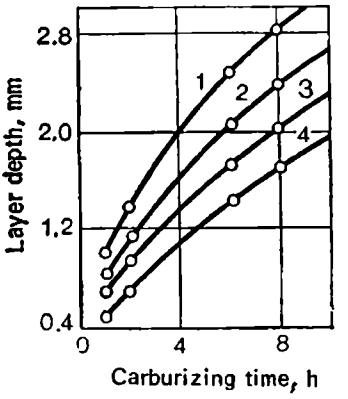

Fig. 13-6. Effect of time of carburizing on the depth of carburized layer at various temperatures
1—1 050°C; *2*—1 000°C; *3*—970°C; *4*—930°C

Thus, the content of carbon in the surface layer is determined by the projection of the point of the *SE* line of the Fe-C diagram at a given temperature and gradually decreases with increasing depth to the original content of carbon in the steel. In other words, the diffusion layer formed at a given process temperature (say, 900°C) is austenite of a carbon concentration varying from 1.2-1.3 per cent in the surface to 0.1-0.15 per cent in the core. On cooling from the process temperature to room temperature, the austenite will transform according to its carbon content in a particular layer.

The structure of a carburized layer obtained on slow cooling from the carburizing temperature is shown in Fig. 13-7. The surface layer which contains more than 0.8-0.9 per cent carbon has the structure of pearlite + cementite; this is what is called the hypereutectoid region; then follows a region having a carbon content of nearly 0.8 per cent; this is the eutectoid region; finally, there is a hypoeutectoid region with less than 0.7 per cent carbon which gradually changes to the original structure in the core.

The carburizing should be carried out so that the carbon content in the outer layer be not more than 1.1-1.2 per cent. A higher content in carbon might result in the formation of an appreciable quantity of secondary cementite and make the surface layer excessively brittle.

This can be done by lowering the carburizing activity of the gaseous medium, i.e. by maintaining the concentration of carbon at the metal surface somewhat below the maximum concentration as determined by the *ES* line of the Fe-C constitutional diagram.

The carburizing ability of a carburizing atmosphere is characterized by what is called the *carbon potential*, i.e. the content of carbon in the metal layer

[1] A higer content of carbon in a thin surface layer, as found experimentally, can be explained by the formation of a thin crust of cementite through the reaction between iron and carbon.

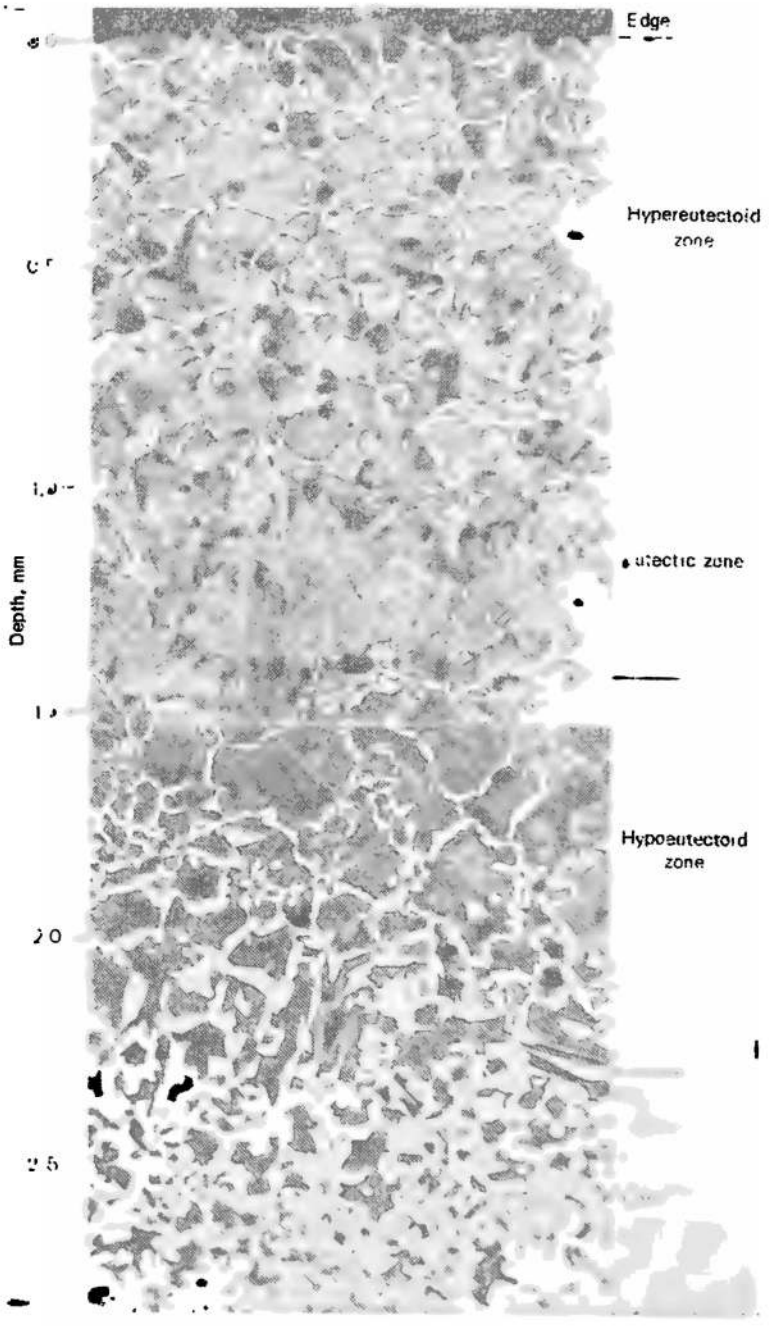

Fig. 13-7. Microstructure of carburized layer upon slow cooling from the carburizing temperature

which is in equilibrium with the gaseous atmosphere. For instance, if the atmosphere has a carbon potential of 0.8 this means that it will carburize steels with a lower content of carbon and that the carbon concentration in the surface layer will not exceed 0.8 per cent; the atmosphere will, however, be decarburizing relative to high-carbon steels (with more than 0.8 per cent C). This is why

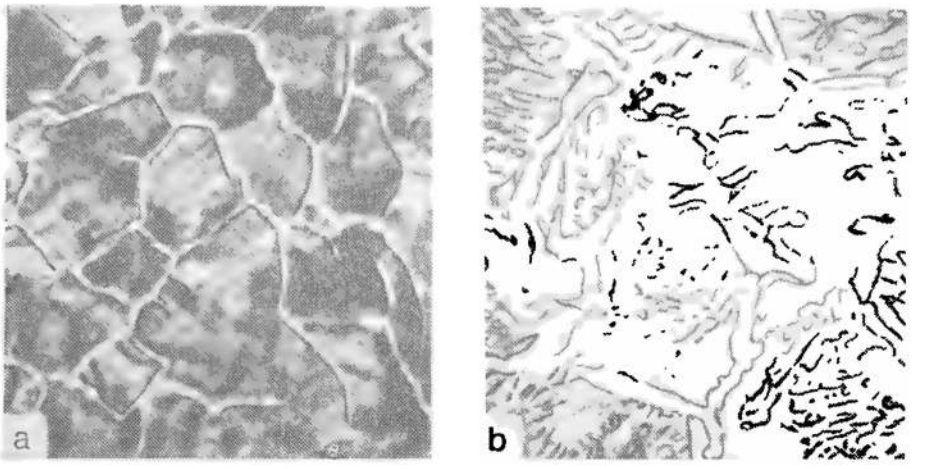

Fig. 13-8. Microstructure of hypereutectoid layer, ×500
(*a*) normal; (*b*) abnormal

the composition of carburizing atmospheres should be accurately controlled to prevent saturation of the carburized steel with carbon, as well as to avoid the formation of soot.

A carburizing gaseous atmosphere is often made by burning natural gases (mostly methane) with an air deficiency in what is called the endothermic gas producer; the *endothermic gas* thus produced has an approximate composition of 20 per cent CO, 40 per cent H_2, and 40 per cent N_2 (carbon potential 0.9 at 900°C).

For a more effective carburization, the process is initially carried out at a higher temperature to produce a higher concentration of carbon (1.3-1.4 per cent), after which the temperature and the carbon potential are reduced so as to attain the desired carbon concentration (0.8 per cent C) owing to diffusion of carbon from the supersaturated surface layers.

Normally the structure of the hypereutectoid region is lamellar pearlite rimmed with a fine network of secondary cementite (Fig. 13-8*a*). In some cases, an *abnormal structure* can form in which the excess cementite is present as massive inclusions (Fig. 13-8*b*) and is often rimmed with free ferrite. On heating, these coarse inclusions of cementite can only hardly pass into the solid solution which is here not saturated with carbon. Steels susceptible to the formation of an abnormal structure can often have soft spotting defects on the surface upon hardening.

The problem of forming a high hardness and high wear resistance in the surface with a tough core cannot be solved by carburizing only. Carburizing gives only a more favourable distribution of carbon over the cross-section. The final desired properties in carburized steel are obtained by subsequent hardening upon which the surface layer has the structure of high-carbon martensite and the core retains a low hardness and a high toughness.

In all cases, carburized and hardened steel parts are tempered at a low temperature (150-200°C) to release internal stresses. Upon this treatment (hardening + low temperature tempering), the surface should have a hardness of 58-62 *HRC* and the core, an appreciab-

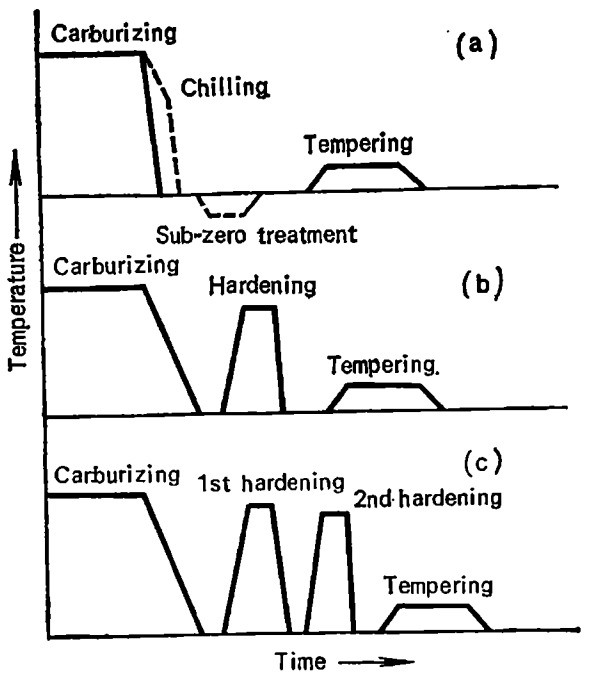

Fig. 13-9. Heat treatment conditions for carburized parts

ly lower hardness, of an order of 25-35 *HRC* for alloy steels and even lower for carbon grades.

Heat treatment of carburized steel parts has some specific features; two of them should be properly considered when assigning the heat treatment conditions. Firstly, the long heating in carburizing might have caused a more or less appreciable grain-coarsening effect. This structural defect should be amended by the subsequent heat treatment. Secondly, carburized parts have a typically non-uniform distribution of carbon over their cross-section. In the first approximation, these parts can be regarded as if consisting of two layers; a high-carbon layer (0.8-1.0 per cent C) in the surface and a low-carbon layer (0.1-0.2 per cent C) in the core. Both these circumstances should be properly considered when selecting the conditions of heat treatment. The following two procedures of heat treatment can be recommended, depending on the purpose of steel parts (Fig. 13-9).

1. For parts in which only a high surface hardness is essential and other mechanical properties are of no great importance, hardening can be effected immediately from carburizing heating, i.e. from 900-950°C (Fig. 13-9*a*). Austenitic grain that has been coarsened in carburizing will form large-acicular martensite in the surface and coarse-grained structure in the core. Owing to some improvements, this method has become applicable to critical steel parts, for instance, gear wheels of automobile transmissions. It also has some indisputable advantages. Other processes of heat treatment, which will be discussed later, are based on heating the carburized parts to a high temperature. These heating procedures can cause warpage of parts and make the whole process of heat treatment more expensive. Hardening immediately from carburizing heating is less expensive and less conducive to warpage of steel parts.

A drawback of this procedure is a coarse-grained structure of the metal and an increased content of retained austenite (therefore, a lower hardness) in the carburized layer owing to hardening from a high temperature.

These drawbacks can be eliminated to a large measure by the following:

(a) using an inherently fine-grained steel (steels delivered to the shop should be regularily checked for grain);

(b) using gaseous carburizing which takes less time than solid carburizing and thus is less conducive to grain coarsening; carburizing with induction heating is most effective; the high temperature of the process (up to 1 100°C) makes it possible to appreciably shorten the time of carburizing;

(c) cooling in hardening, i.e. quenching should be done not immediately from the carburizing temperature, but after cooling to 750-800°C; this method, however, does not refine the structure, but releases internal stresses;

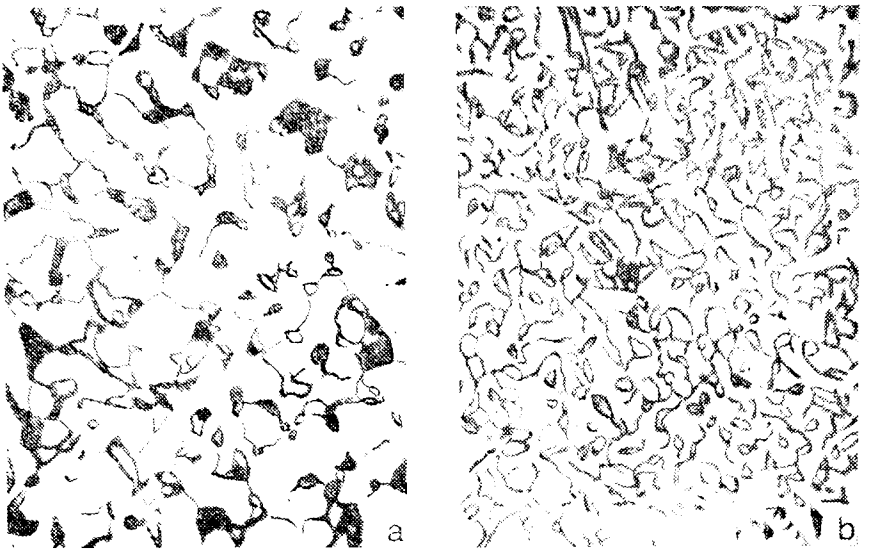

Fig. 13-10. Microstructure in the core of carburized carbon steel; ferrite + + pearlite. ×250
(*a*) hardened immediately after carburizing; (*b*) hardened upon grain regeneration

(d) sub-zero treatment which transforms the retained austenite into martensite and increases the surface hardness.

2. With more rigorous requirements to the structure and properties of carburized steel parts the latter are cooled in air and then hardened from 850-900°C depending on steel grade (Fig. 13-9*b*), i.e. from a temperature above the upper critical point for the core and the surface.

In the core, the metal will recrystallize fully to a finer grain. The surface layers will also undergo recrystallization. Since the heating is done above Ac_3, the cementite network will be dissolved, though the high-carbon surface layers will be somewhat overheated[1]. In that case, tempering at 150-170°C after hardening is essential.

3. Carburized steel parts of which especially high mechanical properties are required are subjected to double hardening with subsequent low-temperature tempering (Fig. 13-9*c*).

The first hardening upon carburizing is done from 850-900°C in order to refine the structure of the core and dissolve the cementite network in the surface (if this has formed on carburizing). This hardening does not form the final hardness, so that quenching can be done in oil or even the hardening can be replaced by normalizing. It is essential to cool the metal quickly to prevent the formation of cementite network in the carburized layer.

Upon the first hardening operation which refines the grain in the core, the metal is hardened from a lower temperature (760-800°C for high-carbon steels). The structure thus formed (fine-acicular martensite with inclusions of excess cementite) ensures a high wear resistance. Since heating is done above Ac_1 but below Ac_3, the core will be hardened only partially.

If a low-carbon steel of a low hardenability is carburized and heated for hardening above Ac_3 or below A_3, practically it cannot be cooled rapidly

[1] As is known, high-carbon steels are normally heated for hardening above Ac_1 but below Ac_3.

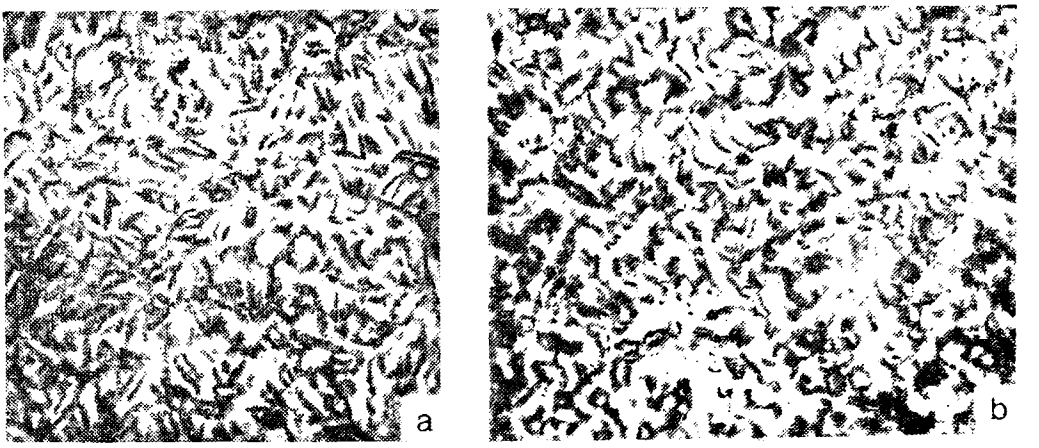

Fig. 13-11. Microstructure in the core of carburized alloy (Cr-Ni) steel. ×500
(*a*) upon ordinary heat treatment, low-carbon martensite; (*b*) upon duplex heat treatment, martensite + ferrite

enough to prevent the pearlitic transformation. Irrespective of the hardening conditions, its structure in the core will consist of pearlite and ferrite and will differ only in grain size (fine-granular upon double hardening and coarser upon single hardening, see Fig. 13-10).

A different structure will be formed in the core of carburized alloy steel. If the hardening is done with heating above Ac_3 (for the core), the structure will be martensitic (Fig. 13-11*a*). Since the martensite is low in carbon, it is not brittle.

If the final hardening is done from a temperature above Ac_1 but below Ac_3, the hardening will be incomplete and the structure will be ferrite + martensite (Fig. 13-11*b*) with a high proportion of ferrite, which ensures a sufficiently high toughness.

Thus, the hardness of the core in carburized carbon steel is not changed by heat treatment and always remains low (of an order of 150 *HB*). On the other hand, the structure in the core of carburized alloy steel can change appreciably. According to some researchers, a higher hardness in the core ensures a higher strength of the part.

There is a trend now to use steels of a higher carbon content for carburizing (with 0.25-0.35 per cent C instead of 0.10-0.20 per cent). Since the core has a higher strength, carburizing can be made to a smaller depth and therefore can be effected in a shorter time.

13-3. NITRIDING

Nitriding is the saturation of steel with nitrogen. The process is not so old as carburizing and has found industrial application only in 1920's.

Since the nitrided layer is in itself very hard (without any subsequent heat treatment) and the dimensions of parts vary only slightly upon nitriding, the process is carried out on steel articles after they have been heat-treated finally (hardening and high-temperature tempering) and ground to the accurate size.

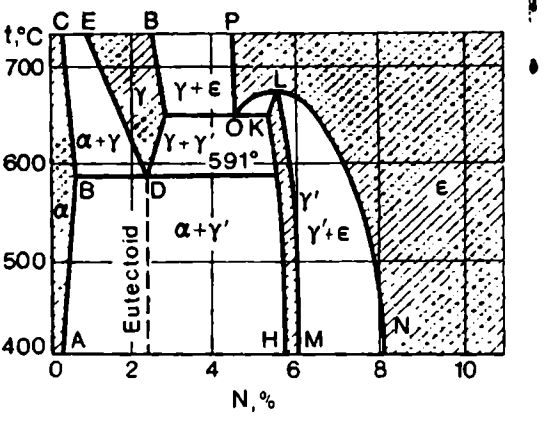

Fig. 13-12. Fe-N constitutional diagram

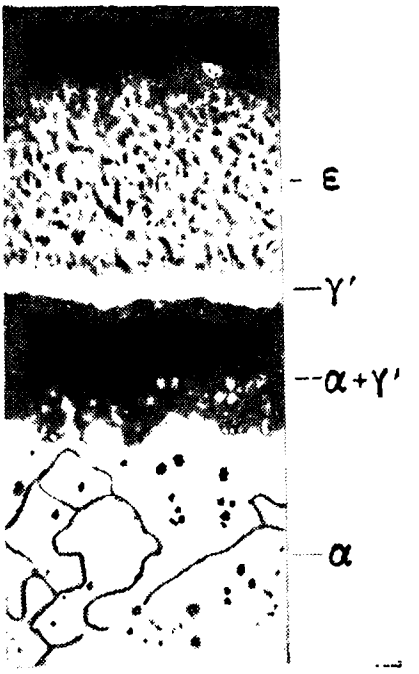

Fig. 13-13. Microstructure of nitrided layer of iron. Nitriding at 650°C with slow cooling. ×500

Nitriding is usually done at 500-600°C. Parts to be nitrided are placed in a tightly closed crucible (retort) which is installed in a heating furnace.

Gaseous ammonia which is supplied to the crucible at a definite flow rate dissociates by the reaction:

$$NH_3 \rightarrow 3H + N$$

and the atomic nitrogen that forms diffuses into the metal.

The processes occurring in nitriding can be explained by reference to the Fe-N constitutional diagram (Fig. 13-12).

The following phases can form in the Fe-N system (single-phase regions are shown shaded in the diagram):

(a) α-nitrous ferrite which contains 0.1 per cent N in the solution at 591°C or roughly 0.01 per cent at room temperature;

(b) γ-nitrous austenite which exists as an equilibrium phase at temperatures above the eutectoid point (591°C);

(c) γ'-nitride Fe_4N, an interstitial phase having a face-centred cubic lattice;

(d) ε-nitride Fe_3N, also an interstitial phase with a hexagonal lattice and a very wide homogeneous region.

Nitrogen can combine with many alloying elements to form nitrides (CrN, Cr_2N, TiN, etc.).

Transition-group metals (iron, chromium, manganese, vanadium, tungsten, molybdenum, titanium) form nitrides. The high hardness of a nitrided layer is due to the large dispersity of nitrides. The dispersity is higher at a higher thermal stability of nitrides, which in turn is higher if the metal has less electrons in the *d*-band and a stronger bond with nitrogen. This theory, which has been developed for carbides, is fully applicable to nitride phases which are very similar to carbides. The problem will be discussed in more detail in Sec. 14-5.

Aluminium, if present in steel, can form an AlN nitride which has a very high thermal stability owing to its covalent bond.

A nitrided layer contains various nitride phases according to the Fe-N diagram and depending on the temperature of the process.

If the temperature of nitriding is below the eutectoid point (591°C), the nitrided layer has three phases: ε, γ' and α.

An isothermal section through the Fe-N diagram at temperatures above the eutectoid point (600-650°C) shows that the nitrided layer obtained at these temperatures can contain four phases: ε, γ', γ and α. With slow cooling from this temperature, the γ-phase (nitrous austenite) decomposes at 591°C into the $\alpha + \gamma'$-eutectoid (the dark layer in Fig. 13-13).

The distribution of nitrogen across the nitrided layer is of a jumpwise nature, since there are no intermediate two-phase layers.

Practically, only alloy steels are subjected to nitriding. The presence of alloying elements and carbon does not affect substantially the kinetics of the formation of nitrided layer.

During the process of nitriding of either pure iron or alloy steel, nitrogen-saturated layers form successively: first α, then $\gamma' - \alpha$, and finally $\varepsilon + \gamma' + \alpha$. At the same time special nitrides (CrN, MoN, AlN, etc.) form in alloy steel. These can also form during cooling from the nitriding temperature, since their solubility in the main nitrous phases diminishes with cooling.

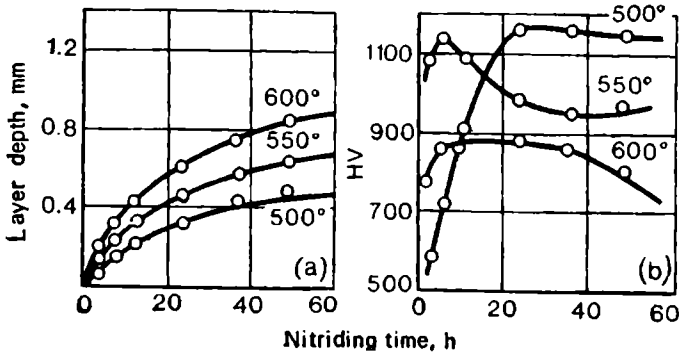

Fig. 13-14. Effect of nitriding time on the depth of nitrided layer (*a*) and surface hardness (*b*) of steel 38XMIOA (Yu. M. Lakhtin)

The surface hardness and the depth of nitrided layer depend on a number of factors among which the principal ones are the temperature of nitriding, the time of the process, and the composition of steel.

The depth of a diffusion layer obeys the general parabolic law $y = K\sqrt{\tau}$, but since the temperature of nitriding is rather low (500-600°C), the coefficient K is small, so that the depth of the layer increases in the nitriding process very slowly, at a rate of approximately one-tenth of that in carburizing.

The dependence of the layer depth on the time of nitriding is shown in Fig. 13-14. As may be seen, the process should be carried out for as long as 40 hours (at 550°C) to form a layer of a depth of, say, 0.6 mm. The rate of the layer growth increases with temperature, but the possibility for increasing temperature is limited by the need to have a high hardness upon nitriding. According to modern views, the high hardness of nitrided layers is due to the formation of very disperse nitrides in the process. Therefore, since coarser nitrides could form at a higher temperature, there might be a loss in hardness (Fig. 13-15).

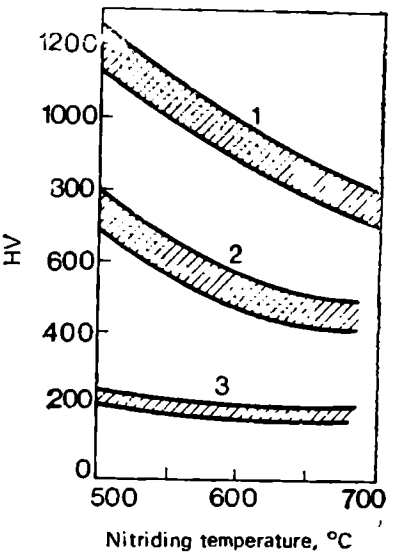

Fig. 13-15. Effect of nitriding temperature on surface hardness

1—nitralloy steel; *2*—structural alloy steels; *3*—carbon steels

The highest hardness of nitrided layer is shown by *nitralloys*, steels containing some elements (aluminium, chromium and molybdenum) which form thermally stable nitrides, not susceptible to coagulation. Common structural steels have a lower hardness upon nitriding, whereas the hardness of nitrided carbon steels is quite low since they do not form special nitrides, while iron nitrides coagulate in them at temperatures above 500°C.

Figure 13-14 shows the depth of nitrided layer in steel Grade 38XMIOA (alloyed with chromium, molybdenum and aluminium) depending on the temperature and time of nitriding. Less alloyed steels can be nitrided more easily, i.e. the desired depth of nitrided layer is obtained in a shorter time at a given temperature. On the contrary, more heavily alloyed steels, such as stainless steels, are less suitable for nitriding, since they can be nitrided only to a depth of 0.20-0.25 mm.

As has been noted, the nitrided layer has a complicated structure and consists, as it were, of a number of layers of different nature.

With nitriding at a temperature below the eutectoid point, the nitrided layer consists of $\varepsilon + \gamma' + \alpha$. The lower α-layer is responsible for hardness (owing to

the precipitation of disperse nitrides); the γ'-layer is very thin and often cannot be detected, and the ε-layer is brittle and has a low strength.

With nitriding at a temperature above the eutectoid point, for instance, at 650°C, the nitrided layer at that temperature consists of $\varepsilon + \gamma' + \gamma + \alpha$; upon cooling, its structure undergoes certain changes, for instance, the γ-phase (nitrous austenite) decomposes during slow cooling into a eutectoid

$$Fe_\gamma (N) \rightarrow Fe_\alpha (N) + Fe_4N$$

On rapid cooling, the γ-phase undergoes the martensitic transformation and the martensitic sublayer has the highest hardness in that case.

As has been noted earlier, the hardness of nitrided layer is independent of the cooling conditions upon nitriding. This is, however, true only for nitriding below the eutectoid temperature. It should be remembered that the temperature of eutectoid decomposition is 591°C only in the Fe-N system and that most of alloying elements raise this point.

Nitriding can be used when it is needed to raise (1) hardness and wear resistance, (2) fatigue strength or (3) corrosion resistance. In each of these cases, the nitriding process has certain peculiarities.

1. *Increasing the hardness and wear resistance* is the principal purpose of the nitriding process. It is applied to special steels (nitralloys) which contain elements forming thermally stable nitrides (CrN, MoN, AlN). In the USSR, the most common grade of nitriding steels is Grade 35XMIO.A (0.30-0.38 per cent C, 1.35-1.65 per cent Cr, 0.4-0.6 per cent Mo, and 0.75-1.1 per cent Al).

Since the steel is rather high in carbon, a carbonitride phase of the type of $Fe_3(C, N)$ or $Fe_3(N, C)$ forms in the surface.

As the nitriding process is aimed here at obtaining a high hardness, the temperature is usually maintained at a level of 500-520°C (the time of nitriding depends on the desired depth).

It should also be taken into account that steel parts deform less at lower temperatures. This circumstance is of great importance, since nitriding is the final operation and the parts are ground to the specified dimensions.

Taking into consideration the effect of the temperature of the process, it may be concluded that a low temperature of nitriding (500-520°C) is essential for obtaining the highest hardness and lowest deformation; the depth of nitrided layer will be however quite small (up to 0.5 mm, more usually 0.2-0.3 mm), but the process takes up a few tens of hours.

If the highest hardness is not very essential, the nitriding process can be carried out at a somewhat higher temperature.

Since nitriding is a very slow process, many attempts have been made to accelerate it. The one that has been successful and is employed practically is the method of stepwise cycles, which consists in carrying out the process in a few stages at various temperatures. The most popular variety in industry is the duplex temperature-raising cycle according to which the nitriding is initially carried out at 500-520°C and the temperature is then raised to 600-620°C. This accelerates the process 1.5 to 2 times and only slightly affects the hardness (which is almost as high as at a low-temperature isothermal cycle).

Comparing the two basic processes of chemical heat treatment of steel, i.e. carburining and nitriding, as applied for increasing the hardness and wear resistance, certain important conclusions can be drawn on their applicability.

Nitriding gives a shallow diffusion layer of an exceptionally high surface hardness, whereas carburizing produces an appreciably deeper layer of a lower hardness and is characterized by a shorter time of the process.

An advantage of nitriding is that it produces a layer of a higher wear resistance. But nitrided parts are more expensive as the process takes more time and, in addition, is only applicable to more expensive alloy steels. Further, the

nitrided layer is thinner than the carburized layer and cannot withstand high unit loads.

2. *Nitriding of structural steels to increase the fatigue strength* (endurance). This method is finding ever wider application in many industries.

The formation of nitride-containing phases in the surface layers is associated with an increase in the metal volume, therefore the surface of the nitrided part is subjected to compression stresses. These stresses increase the endurance limit, since fatigue cracks develop under the action of tensile stresses.

To increase the fatigue strength, use is not made of special steels (such as Grade 35ХМЮА), but of common alloy steels containing nitride-forming elements (mostly common structural Cr-Ni steels, see Sec. 16-4).

3. *Nitriding to increase the corrosion resistance* (sometimes called decorative nitriding) is based on that the nitrided layer having a continuous crust of ε-phase on the surface exhibits a high resistance to corrosion in atmospheric air, mains water and some other media. This method of nitriding essentially consists in the formation of a continuous crust of ε-phase on the surface by the simplest and least expensive process.

Since no other special requirements are placed upon the surface layer, the process is applicable to many types of steel, including plain carbon steels. It is carried out at 600-700°C and takes relatively little time (0.5-1 h).

13-4. CYANIDING

Cyaniding is the process of saturation of steel with carbon and nitrogen at the same time. The process is usually carried out in molten salts and is, therefore, quite efficient.

Cyaniding can be carried out in solid, liquid and gaseous media, and accordingly, is classified into *solid*, *liquid* and *gaseous cyaniding* (the last process is often called *carbonitriding*).

Solid cyaniding is similar to carburizing, with the carburizer containing additionally cyan salts[1]. The process is appreciably less productive than liquid or gaseous cyaniding and cannot be recommended for wide application.

Liquid cyaniding which is made in molten cyan salts is the most popular cyaniding process.

The process is based on the decomposition of cyan salts with the formation of free atoms of carbon and nitrogen which diffuse into the metal depth.

Gaseous cyaniding is effected in a mixture of carburizing and nitriding gases (for instance, a mixture of lighting gas and ammonia).

The effect of cyaniding is determined by the depth of the diffusion layer and the concentration of carbon and nitrogen in the surface layer. The composition and properties of the cyanided layer substantially depend on the temperature of the process: at a higher temperature, the layer becomes richer in carbon and at a lower temperature, in nitrogen (Fig. 13-16).

---

[1] A typical carburizer for the process contains 30-40 per cent $K_4Fe(CN)_6$ (potassium ferrocyanide), 10 per cent Na_2CO_3 (soda), and charcoal is the balance.

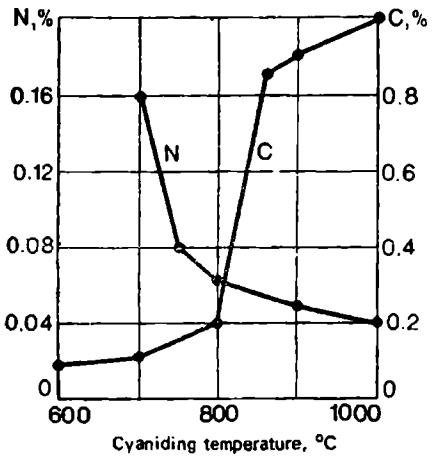

Fig. 13-16. Effect of cyaniding temperature on the content of carbon and nitrogen in surface layer

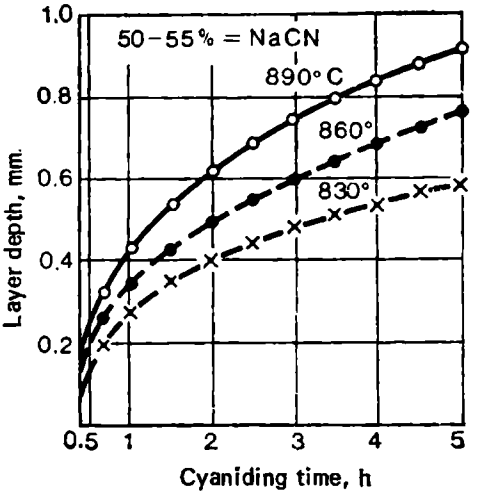

Fig. 13-17. Effect of temperature and time of cyaniding on the depth of cyanided layer

Since cyaniding is the simultaneous saturation of steel with carbon and nitrogen, as if a combined process of carburizing and nitriding, we may say for simplicity that the process approaches carburizing at higher temperatures and nitriding at lower temperatures. This is why a distinction is made between high-temperature cyaniding (at 800-950°C) and low-temperature cyaniding (at 500-600°C).

Low-temperature cyaniding is employed for high-speed tool steels (see Sec. 17-4) and medium-carbon steels. In the latter case the process is known as the *Tenifer process* and consists in the saturation of the steel with nitrogen (and to an appreciably lower extent, with carbon) in cyan salts (40 per cent KCN and 60 per cent NaCN), with dry air being blown through the salt bed. The saturation is carried out for 0.5-3 hours at 570°C.

The process forms a thin (10-15 μm) carbonitride layer Fe_3 (N, C) which has a high wear resistance and is less brittle than pure carbides (Fe_3C) or nitrides (Fe_3N). Below that layer there forms a layer of hard nitrous ferrite (of a hardness of 600-1 000 *HV* in alloy steels) of a thickness of 0.2-0.5 mm.

High-temperature cyaniding (also called *liquid carburizing*) is used with medium- and low-carbon steels and alloy steels.

The process is carried out in a mixture of molten salts of an approximate composition as follows: 40 per cent NaCN, 40 per cent NaCl, and 20 per cent Na_2CO_3 or 6 per cent NaCN, 80 per cent $BaCl_2$, and 14 per cent NaCl (the former is used at 820-850°C and the latter, at 900-950°C).

The main active component in cyan baths is the CN group; increasing the content of CN in a mixture increases the content of carbon and nitrogen in the surface layer but does not increase the layer depth.

The effect of cyaniding in a bath of the given composition, in the first place the depth of the layer, depends on the temperature and time of the process, as may be seen from Fig. 13-17.

The temperature and composition of the bath also determine the structure of the layer metal and its saturation with carbon and nitrogen.

Cyanided steel parts have a bright crust on the surface which is rich in nitrogen and consists of a carbonitride phase of the type of M_3C; then follows a layer of nitrous martensite (if cooling from the cyaniding temperature was made quickly). The presence of a bright surface crust is not always desirable, since it makes the cyanided layer excessively brittle.

As compared to carburized layers, cyanided layers have a higher wear resistance, higher hardness and higher corrosion resistance. Cyaniding also increases the fatigue strength, as any other case-hardening process resulting in the appearance of compressive residual stresses in the surface.

Since cyaniding is carried out at a lower temperature and for a shorter time than carburizing, it causes no grain coarsening. Cyanided steel parts can be immediately hardened to form a high hardness in the surface.

Cyan salts are poisonous; this is an essential drawback of cyaniding. For that reason the process is carried out in special rooms and with strict observance of safety engineering rules.

Cyanided parts have an attractive mat surface and for that reason the cyaniding process is often used to improve the appearance of finished steel parts. To do this, parts are heated in a cyan bath for a short time.

13-5. METALLIC CEMENTATION

Metallic cementation is a general name implying the saturation of the surface of steel with various metals by diffusion. The particular processes are called *chromizing* (saturation with chromium), *alitizing* (saturation with aluminium), *siliconizing* (saturation with silicon), etc. If the steel is simultaneously saturated with two or more metals, the process is accordingly called chrome-alitizing, chrome-tungstenizing, etc.

The processes of diffusion saturation with chromium, aluminium and boron have been studied most thoroughly, whereas those of saturation with molybdenum, beryllium and other elements are known worse.

As other types of chemical heat treatment, metallic cementation can be carried out in solid, liquid and gaseous media.

Solid cementation is performed in a respective ferro-alloy with an addition of ammonium chloride (NH_4Cl). The metallizer reacts with HCl or Cl_2 and forms a volatile metallic chloride ($AlCl_3$, $CrCl_2$, $SiCl_4$, etc.) which dissociates into free atoms on contact with the metal surface.

Liquid cementation is made by immersing steel parts into molten metal, for instance, aluminium.

Gaseous cementation is carried out in gaseous chlorides of various metals.

The diffusion of chromium, aluminium and other metals occurs much more slowly than that of carbon or nitrogen, since the former form substitutional solutions with iron and the latter, interstitial solutions. For the same temperature and time of the process, the saturated layer in cementation is substantially thinner (by a factor of a few tens or hundreds) than a carburized layer.

Because of the low rate of diffusion, cementation processes are expensive and time-consuming and for that reason are not widely used in industry. The process is usually carried out at a high temperature (1 000-1 200°C). They have found application only in special cases when it is needed to form special properties in the surface layer or to save alloying elements.

One of the principal qualities of metal-saturated surfaces (chromized, alitized or siliconized) is a high heat resistance. For that reason steel parts for operation at temperatures to 1 000-1 100°C are made of plain carbon steels with subsequent alitizing, chromizing or siliconizing.

An exceptionally high hardness (up to 2 000 *HV*) and a high resistance to abrasion wear can be obtained by boriding, i.e. by the formation of hard iron borides FeB and Fe_2B in the surface: borided layers are however very brittle.

LITERATURE

Lakhtin Yu. M., *Physical Principles of Nitriding*. Moscow, "Mashgiz", 1948 (in Russian).

Popov A. A., *Theoretical Principles of Chemical Heat Treatment of Steel*. Sverdlovsk, "Metallurgizdat", 1962 (in Russian).

Koretsky Ya., *Carburizing of Steel*. Leningrad, "Sudpromgiz", 1962 (in Russian).

Dubinin G. N., *Chromizing of Alloys*. Moscow, "Mashinostroenie", 1964 (in Russian).

Yurgenson A. A., *Nitriding in Power Engineering*. Moscow, "Mashgiz", 1964 (in Russian).

Minkevich A. N., *Chemical Heat Treatment of Metals and Alloys*. Moscow, "Mashinostroenie" (in Russian).

Lakhtin Yu. M., Leontyeva V. P., *Materials Science*. Moscow, "Mashinostroenie", 1972 (in Russian).

Kalner V. D., *Carburizing and Carbonitriding of Steel*. Moscow, "Mashinostroenie", 1973 (in Russian).

Lakhtin Yu. M., *Physical Metallurgy and Heat Treatment of Metals*. Moscow, "Metallurgiya", 1976; English translation: Mir Publishers, Moscow, 1979.

Lakhtin Yu. M., Kogan Ya. D., *Nitriding of Steel*. Moscow, "Mashinostroenie", 1976 (in Russian).

INDEX

Absorption 308
Activation energy 311
Actual temperature of crystallization 42
Ageing 139, 220
Alitizing 225, 327
Alkali-earth metals 16
Allotropy 51
Alloyed cast iron 210
Alloyed cementite 161
Amosov P. P. 156
Anderko K. 153, 174
Anisotropy in crystals 32
Anisotropy of metal properties 185
Annealing 219, 298
Apaev B. A. 265
Assonov A. D. 215
Athermal martensite 256
Ausforming 274
Austen R. 155, 159
Austenite 159, 225, 229
Automatic steels 196

Baikov A. A. 155, 165
Bain E. C. 228, 240
Bainite 242
Bainitic transformation 261
Belous M. V. 276
Bernstein M. L. 273
Berthollides 101
Bessemer converter 186
Bessemer steel 186
Blackheart malleable cast iron 214
Blanter M. E. 9, 229, 276, 287
Bochvar A. A. 9, 44, 56, 65, 134, 153, 219, 227, 276
Body-centred cubic lattice 21
Bogachev I. N. 9, 210, 216
Bokstein S. Z. 9, 39, 104
Boky G. B. 25
Bolkhovitinov N. F. 174, 197
Bolkhovitinova E. N. 174
Boundary migration 88
Bragg W. H. and W. L. 34
Brinell hardness test 74
Brittle fracture 61, 68
Brittle fracture resistance 70
Brouer J. L. de 174
Bunin K. P. 44, 153, 174, 210, 216
Burgers vector 28

Cahn R. W. 39
Carbide analysis 37
Carbon potential 315
Carbon steels 175
Carburizer 313
Carburizing 225, 313
Cast iron, 198
  microstructures 173
C-curves 240
Cementite 160, 199
Chalmers B. 56, 92, 104
Chemical analysis 37
Chemical heat treatment 221, 308
Cherepin V. T. 276
Chernov D. K. 43, 48, 49, 56, 154, 155, 228, 245
Chernov-Lüders slip lines 80
Chernov's dendrite 48
Chromizing 225
Close-packed hexagonal lattice 21
Coalescence of grains 88
Coefficient of diffusion 311
Cohen M. 258
Coherent bond 138
Cold brittleness 179
Cold plastic working 83
Columnar crystals 49
Concentration triangle 140
Conditional yield limit 59
Conode 150
Constitutional diagrams 105

Coordination number 23
Cottrell A. H. 91, 104
Cottrell atmospheres 97
Covalent bond 57
Critical degree of deformation 89
Critical diameter, for hardening 286
Critical length of crack 68
Critical rate of hardening 247
Crystal lattices of metals 20
Crystal plane 21
Crystal structure of metals 19
Crystalline fracture 69
Crystalline state 20
Crystallites 26
Crystallization nuclei 43
Cubic lattice 21
Curie point 55
Cyaniding 325

Daltonides 101
Davenport E. S. 240
Decarburization of steel 280
Dendrites 48
Dendritic segregation 134
Destruction 81
Diagram of isothermal austenitic transformation 239
Diamond 198
Diffusion 309
Diffusion annealing 300
Dilatometer 264
Dislocations 27
Dislocation density 28
Dislocation pile-up 67
Dislocation structure 32
Dissociation 308
Double quenching 294
Drozdovsky B. A. 77
Dubinin G. N. 328
Ductile fracture 61, 68
Ductile-to-brittle transition temperature range 69
Ductility margin 70
Durability 66, 78
Dydimium 16

Edge dislocation 27
Elastic deformation 57
Elastic shear modulus 61
Electron fractography 38
Electronic compounds 102
Electronic gas 14
Electron microscope 36
Electron phases 102
Elementary crystal cell 21
Elliot R. P. 153
End-quench test 288
Endurance limit 78
Equi-axed crystals 50
Equilibrium diagrams 105
Equilibrium temperature of crystallization 42
Esser H. 228
Eutectic 116
Eutectoid 131
Eutectoid steel 170
Eutectoid transformation 131
Extraplane 27

Face-centred cubic lattice 21
Fatigue curve 78
Fatigue failure 78
Fatigue fracture 78
Fedorov E. S. 20
Ferrite 159
Ferrocerium 16
Ferromagnetic properties 55
Ferrous metals 15
Fibrous fracture 69
Flaky graphite 198, 205
Fractography 38
Fracture 66
Fracture toughness 72
Fragmentation 31
Fragments 30
Free energy 41
Frenkel Ya. I. 62, 310
Fridman Ya. B. 9, 77, 92
Friedel J. 39
Fusible metals 16

Gaseous carburizing 314
Gaseous cementation 328
Gaseous cyaniding 325
Gases, in steel 183
Georgieva I. Ya. 258
Gerens P. 155
Geveling N. V. 174, 307
Gibbs W. 155
Gibbs' phase rule 105
Goldschmidt H. J. 104
Gorelik S. S. 92
Grabsky M. V. 92
Grachev S. V. 10
Grain coalescence 88
Grain coarsening 231
Grain growth 85, 123
Grain-size scales 235
Grain texture 80
Graphite 161

Graphitization 198
Graphitizing annealing 213
Grey cast iron, 198
  ferrite-pearlitic 205
  ferritic 205
  pearlitic 204
Griffith A. A. 68, 71
Gudtsov N. T. 155
Gulyaev A. P. 92, 197, 227, 276, 301

Habraken L. 174
Hannemann H. 228
Hansen M. 153, 174
Hardenability 284
Hardenability bands 289
Hardening 139, 220
Hardening capacity 284
Hardening temperature 277
Hardness 74
Heat treatment 139, 217
Heterodiffusion 310
High-melting metals 15
High-strength cast iron 198, 207
High-temperature cyaniding 326
High-temperature thermomechanical treatment 273
Homogenizing 300
Homologous temperatures 41
Honeycomb R. W. K. 92
Hooke's modulus 61
Hot plastic working 83
Howe H. M. 156
Hume-Rothery W. 102, 104
Hume-Rothery phases 102
Hypereutectoid steel 171
Hypoeutectoid steel 171

Impact testing machine 76
Impact tests 76
Impact toughness 76
Improving heat treatment 272
Incubation period 238
Induction hardening 304
Ingots, structure of 49
Internal stresses 291
Interrupted quenching 295
Interstitial impurities 184
Interstitial phases 103
Interstitial solid solutions 96
Iron 156
Iron carbide 160
Iron-carbon constitutional diagram 154
Iron metals 15
Iron modifications 157
Iron sulphide 180
Isomorphous metals 98
Isosklerous tempering 273
Isothermal annealing 300
Isothermal martensite 256
Isothermal quenching 295
Ivantsov G. I. 216

Kalakutsky N. V. 292
Kalner V. D. 328
Kamenetskaya D. S. 157
Kasatkina B. S. 31
Khandros L. G. 261
Kidin I. N. 307
Killed steel 51, 187
Kinetic curves 238
Kogan Ya. D. 328
Konobeevsky S. T. 97
Koretsky Ya. 328
Kornilov I. I. 99
Kozlovsky I. S. 290
Krimer B. I. 153
Krishtal M. A. 216
Kudryavtsev I. V. 9
Kurdyumov G. V. 228, 258, 259, 261, 265, 276
Kurnakov N. S. 101, 151, 152
Kurnakov's law 152

Lakhtin Yu. M. 9, 10, 301, 322, 328
Lamellar graphite 198, 205
Lamellar pearlite 268
Lanthanides 15
Lattice period 21
Laue M., von 20
Laves phases 103
Le Chatelier H. L. 155
Ledebur A. 162
Ledeburite 162
Leontyeva V. P. 328
Lever rule 117
Light metals 16
Lineage structure 51
Linear defects 27
Liquid carburizing 326
Liquid cementation 328
Liquid cyaniding 325
Liquidus line 113
Livshits B. G. 56, 153
Lomonosov M. V. 11
Lower bainite 263
Low-melting-point metals 16
Low-temperature annealing 299
Low-temperature cyaniding 326

Low-temperature thermomechanical treatment 273
Lozinsky M. G. 307
Lubowicz H. 92
Lysak L. I. 227, 251, 260, 276

Machinability of steels 194
Maclintock F. A. 92
Macrolattice 265
Macrostructure 35
Magnetic transformations 55
Maksimova O. P. 258
Malinochka Ya. N. 153, 216
Malleable cast iron 198, 207
Malyshev B. V. 301
Manganese, in cast iron 209
in steel 178
Manganous sulphide 181
Marforming 276
Martempering 295
Martens A. 156
Martensite 225, 251
Martensitic curve 254
Martensitic diagrams 254
Martensitic transformation 249
Mechanical mixture 93
Mechanico-thermal treatment 276
Mehl R. F. 228, 237
Mendeleev's Periodic Table of the Elements 12-13
Mentor D. 63
Metallic alloys 14
Metallic bond 57
Metallic cementation 327
Metallography 34
Metals, classification 14
dates of discovery 16-17
world production 17
Microhardness 75
Microprobe 37
Microstructure 35
Minkevich N. A. 301, 328
Mirkin I. L. 44, 229, 237
Misch metal 16
Modulus of normal elasticity 61
Monovariant system 106
Mosaic blocks 30
Mottled iron 204

Necking 60, 66
Nikolin B. I. 227, 260, 276
Nitralloys 323
Nitriding 225, 320
Noble metals 16
Non-equilibrium crystallization of alloys 132
Non-ferrous metals 15
Non-metallic inclusions 183
Non-variant system 106
Normalizing 193, 225, 298
Novikov I. I. 92, 227, 276
Nucleation 88

Oding I. A. 9, 65, 84
Oknov M. G. 210, 216
Open-hearth steel 186
Ordered solid solutions 101
Ordering 101
Orowan E. 63
Osmond F. 155
Oxidation of steel 280
Oxygen converter 188

Panchenko E. V. 153
Partial annealing 224, 299
Patenting 193, 276
Pearlite 162, 225, 240
Pearlitic grey cast iron 204
Peritectic 124
Permyakov V. G. 265
Petrash L. V. 301
Petrov D. A. 153
Phosphorus, in cast iron 209
in steel 178
Physical yield limit 59
Plain carbon steels 189
Planck's constant 36
Plastic deformation 57
Plastic fracture 61, 68
Point defects 27
Polanyi M. 63
Polygonization 31, 81
Polyhedrous structure 49
Polymorphism 52
Popov A. A. 301, 328
Popova A. E. 301
Primary cementite 168
Primary recrystallization 85, 123
Prosvirin V. I. 160
Pseudo-alloys 93
Pseudo-binary diagrams 150
Pyrometer 155

Quasi-anisotropy 33
Quasi-eutectoid 244
Quenching media 282

Rachstadt A. G. 273
Radiography 37
Rare-earth metals 15
Rauzin Ya. R. 92
Raynor G. V. 104
Read W. T. 91
Recovery 81
Recrystallization 81, 133
Recrystallization annealing 83
Recrystallization diagrams 90
Recrystallization threshold 83
Red shortness 180
Refractory metals 15
Relative extension 59
Reliability 66, 76
Residual stresses 292
Retained austenite 257
Reverse martensitic transformation 260
Rimming steel 51, 187
River pattern 38
Rockwell hardness test 75
Roentgen K., von 20
Roseboom G. 155
Rule of sections 117
Rumyantsev M. V. 153
Rzheshotarsky A. A. 156

Sachs G. 292
Sadovsky V. D. 233, 276
Saltykov S. A. 215
Samsonov G. V. 104
Savitsky E. M. 54
Scanning electron microscope 38
Schultze G. 39, 104
Screw dislocation 27
Secondary cementite 168
Secondary recrystallization 85, 122
Self-diffusion 88, 310
Semikilled steel 187
Serial curve 70
Shape memory effect 261
Shepelyakovsky K. Z. 306, 307
Shmykov A. A. 301
Short-range order 19
Shrinkage cavity 51
Shunk F. A. 153
Shur E. A. 92
Sidorin I. I. 10
Silicon, in cast iron 209
  in steel 178
Siliconizing 327
Single crystals 26
Single quenching 293
Singularity of properties 94
Singular point 152
Skakov Yu. A. 153
Soaking 213
Soft spots 297
Sokolov K. N. 301
Solid carburizing 313
Solid cementation 327
Solid cyaniding 325
Solid solutions, 96
  interstitial 96
  ordered 101
  substitutional 96
  supersaturated 136
  undercooled 137
Solidus line 113
Sorbite 240
Sorby H. C. 156, 157
Spheroidal graphite 198, 205
Spray quenching 294
Stabilization of austenite 256
States of aggregation 40
Steinberg S. S. 56, 91, 104, 153, 227, 229, 258, 276
Stoichiometric ratio 95
Strain ageing 184
Strain hardening 79
Stress concentrators 67
Stress intensity 71
Stress-strain curve 58
Structural recrystallization 219
Structural stresses 291
Sublimation 20
Substitutional solid solutions 96
Subtraction solutions 101
Sub-zero treatment of steel 296
Sulphide effect 182
Sulphide inclusions 181
Sulphur, in cast iron 209
  in steel 179
Supercritical deformation 89
Superplasticity 67
Supersaturated solid solution 136
Synthetic slag 182

Tamman G. 44, 45, 56
Taran Yu. N. 216
Taylor G. I. 63
Temper carbon 205
Temper colours 294
Tempering 139, 220
Temper martensite 264
Tensile tests 73
Ternary cementite 168
Ternary systems 139
Tetragonal lattice 23
Texture 26
Thermal stresses 291

Thermocouples 110
Thermodynamic potential 41
Thermoelastic martensite 261
Thermomechanical treatment 221, 273
Thermoplastic working 221
Tin pest 54
Titensky E. G. 216
Toughness 59
Transcrystallization 50
Troitsky G. I. 215, 216
Troostite 240
Trusova E. F. 9
TTT-diagrams 239
Turkin V. D. 153
Tushinsky L. I. 275
Tyapkin Yu. D. 265

Ultimate strength 60
Umansky Ya. S. 9, 56
Undercooled solid solutions 137
Undercooling 42
Upper bainite 263
Uranium metals 15

Vacancies 27
Vickers hardness test 75
Vinarov S. M. 9
Vol A. E. 153
Vologdin V. P. 307
Volovik B. E. 153
Voronov S. M. 9
Vulf Yu. V. 34

Wear 79
Wever F. 228, 250
White cast iron 198
Whiteheart malleable cast iron 214
Widmanstätten A. 156
Widmanstätten structure 299
Work of crack initiation 60, 76
Work of crack propagation 61

X-ray structural analysis 33
X-unit 21

Yield limit 59
Yokobori T. 92
Young's modulus 61
Yurgenson A. A. 328

Zakharov M. V. 153
Zelenova V. D. 92
Zinal segregation 187

TO THE READER

Mir Publishers welcome your comments on the content, translation, and design of the book.

We would also be pleased to receive any suggestions you care to make about our future publications.

Our address is:

USSR, 129820,
Moscow, I-110, G-P,
Pervy Rizhsky Pereulok, 2,
Mir Publishers

Printed in the Union of Soviet Socialist Republics

Other Books for Your Library

Engineering Physical Metallurgy and Heat-Treatment by YU. LAKHTIN, D. Sc.

This textbook deals among other aspects of physical metallurgy, with defects in the crystal lattices of metals, and with the thermodynamics of phase transformations. New sections has been added to the chapter on refractory metals. Comprehensively presented are topics on the mechanical properties of metals, with due consideration for the engineering strength and failure mechanism under conditions of static and cyclic loading. Devotes much space to the theory and techniques of heat-treatment and case hardening of steel, description of structural, tool, stainless and heat-resistant steels, alloys with special physical properties and to alloys based on aluminium, copper, titanium, magnesium, etc.

Intended as a textbook for students majoring in metallurgy.

ABOUT THE BOOK

This is a fundamental textbook
on physical metallurgy
as well as on the science
of materials for students
of metallurgical,
machine-building and
polytechnical institutes,
and also for those specializing
in physical metallurgy
and technology of heat
treatment of metals.
The book contains reference
data on practically all types
of metallic materials and can
therefore serve as a monograph
on metals and alloys
for use by process
and research engineers.